LBNL-2001557

Characterizing the Geothermal Lithium Resource at the Salton Sea

A Project Report to the U.S. Department of Energy, Office of Energy Efficiency & Renewable Energy, Geothermal Technologies Office

Submitted by
Lawrence Berkeley National Laboratory

BERKELEY LAB
Bringing Science Solutions to the World

ENERGY.GOV
Office of
ENERGY EFFICIENCY & RENEWABLE ENERGY

This page was left intentionally blank.

Cover Photo: Imperial Valley geothermal power plant near the Salton Sea
Photo Credit: Jeremy Snyder, Lawrence Berkeley National Laboratory

Authors

Patrick Dobson (project lead)
Lawrence Berkeley National Laboratory

Naod Araya
University of Auckland

Maryjo Brounce
University of California, Riverside

Margaret M. Busse
Lawrence Berkeley National Laboratory

Mary Kay Camarillo
University of the Pacific

Lauren English
University of California, Riverside

Jennifer Humphreys
University of California, Riverside

Boriana Kalderon-Asael
Yale University

Michael A. McKibben
University of California, Riverside

Dev Millstein
Lawrence Berkeley National Laboratory

Nori Nakata
Lawrence Berkeley National Laboratory

John O'Sullivan
University of Auckland

Noah Planavsky
Yale University

Joris Popineau
University of Auckland

Theo Renaud
University of Auckland

Jérémy Riffault
University of Auckland

Margaret Slattery
University of California, Davis

Eric Sonnenthal
Lawrence Berkeley National Laboratory

Nicolas Spycher
Lawrence Berkeley National Laboratory

Jennifer Stokes-Draut
Lawrence Berkeley National Laboratory

William T. Stringfellow
Lawrence Berkeley National Laboratory

Malcolm C. A. White
Massachusetts Institute of Technology

Acknowledgments

We thank Berkshire Hathaway Energy Renewables (BHER)/CalEnergy and Controlled Thermal Resources for kindly providing access to the brine and some of the rock samples that were analyzed in this study. We also thank Michael Krahmer from BHER for assistance in sampling drill cuttings; Daniel Alexander, John Garcia, and Luis Navarro from Cyrq Energy; Rod Colwell, Will Osborn, Danny Sims, and Tracy Sizemore from Controlled Thermal Resources; Vince Signorotti, Carmen Rene and Derek Benson from EnergySource Mineral; and Matt Broaddus from Thermochem for assisting with sample collection and giving us tours of their facilities and answering questions from our team. We also appreciate Jon Trujillo, Billy Thomas, and Jonathan Weisgall from BHER/CalEnergy for providing critical data and responding to our many queries. We thank Patrick Muffler (U.S. Geological Survey) for sharing the results of his past studies of the Salton Sea geothermal field with our team. We thank Axel K. Schmidt and Jeffery B. Hulen for providing samples from their 2008 study. We thank Wenming Dong of Lawrence Berkeley National Laboratory (LBNL) for conducting the whole rock lithium analyses. Many thanks to Alexandra Prisjatschew, Andy Adams, and Alexis McKittrick of DOE's Geothermal Technologies Office (GTO) for their level of engagement and enthusiasm for our project. We would especially like to thank Zakary Owens of the Colorado River Basin Regional Water Quality Control Board (RWQCB; Region 7) for his help with gathering and interpreting information on landfills and landfill management.

There are many individuals who were instrumental in our community engagement efforts. Thank you to Efrain Silva and Tisha Nelson for helping us arrange a visit to Imperial Valley College, as well as the instructors and students in the HVAC, welding, building construction, and automotive technology programs for their time, questions, and feedback. Thank you to Mayor Maria Nava-Froelich from the City of Calipatria and Fernanda Vega from Comité Cívico del Valle for providing insight about how to make our community workshop more accessible; Silvia Paz and Nilda Ruiz from Alianza Coachella Valley for contributing questions for our FAQ document, sharing flyers to inform people about our community workshop, and providing valuable feedback; the NorthEnd Alliance 111 for distributing workshop flyers; the Calipatria School District for the use of their facility; and to everyone who attended for your time, questions, and feedback. Thank you to Luis Olmedo and Christian Torres from Comité Cívico del Valle for providing critical feedback. Thank you to Mariela Loera and Rebecca Zaragoza from the Leadership Counsel for Justice and Accountability for providing feedback about community engagement and educating members of our research team about key issues and concerns in the region. We also thank Francisco Parés and Magda Rojas (UC Davis) for their help with our community engagement activities. Thank you to Kelsey Miller from LBNL's Human Subjects Committee for expediting reviews of our community engagement plans and providing helpful suggestions.

We also thank Susan Sprinkle for her work in administering this project, and Peter Nico, Sandy Chin, Helen Prieto, Dan Hawkes, and Dan Mullen for all of their efforts in transforming this report from a series of chapters into a more coherent and integrated document.

This work is supported by the U.S. Department of Energy, Office of Energy Efficiency and Renewable Energy (EERE), Geothermal Technologies Office, under Award Number DE-AC02–05CH11231 to Lawrence Berkeley National Laboratory.

Executive Summary

The energy transition towards a more sustainable and renewable future is a pivotal global endeavor. Central to this shift for the United States is the critical role of domestically sourced lithium, a key mineral in the production of high-performance batteries essential for electric vehicles and renewable energy storage systems. This has driven the United States to invest heavily in a domestic supply chain for battery-grade lithium to enhance energy security, reduce supply chain vulnerabilities, and foster economic growth by tapping into local resources. A notable example is the Biden Administration's "American Battery Materials Initiative," which was included in the $2.8-billion Bipartisan Infrastructure Law (The White House, 2022).

The "Salton Sea Known Geothermal Resource Area" in Imperial County, California has been identified as a potential domestic U.S. resource of lithium due to the brine-hosted lithium in the deep subsurface geothermal reservoir. An analysis funded by the U.S. Department of Energy provides an overview of opportunities and challenges associated with developing the lithium resource in the Salton Sea geothermal reservoir, as well as potential environmental and societal impacts to the county and surrounding region.

The geologic history of the region suggests that lithium in the subsurface brines could have come from multiple sources, including water and sediments from the Colorado River, which have been periodically deposited over the past several million years; rocks from the mountain ranges surrounding the Imperial Valley; and lithium-bearing volcanic rocks and igneous intrusions from past geologic events. Further, several processes may have concentrated lithium in the brine over time, including evaporative concentration of lithium-bearing water that flowed into the basin and leaching of lithium from the sediments and rocks by the circulating geothermal brines.

Geothermal brine production at the Salton Sea Geothermal Field, the area with existing geothermal power plants, has averaged just over 120 million metric tons per year since 2004. Using an approximate lithium brine concentration of 198 parts per million (ppm), the amount of dissolved lithium contained in these produced brines is estimated to be 127,000 metric tons of lithium carbonate equivalent (LCE) per year. The total dissolved lithium content in the well-characterized portion of the Salton Sea Geothermal Reservoir is estimated at 4.1 million metric tons of LCE, and the estimated total resource increases to 18 million metric tons of LCE if assumptions for porosity and total reservoir size are increased to reflect the probable resource extent.

Analysts measured lithium concentrations in the reservoir rocks, which were shown to vary with depth and mineralogy. These data were used to help refine conceptual and computer models of the reservoir; specifically, two complementary computer models of the reservoir were developed. Analysts used the first model to simulate the approximate 30-year history of geothermal power production in the area using historical production and reinjection data, then used that model to simulate a 30-year forecasting period. This forecast assumed continued production and reinjection rates at current levels but removes 95% of the lithium from the produced geothermal brine starting January 1, 2024. The model found that lithium recovery declines by more than half, from 0.8 to 0.3 kilograms per second (kg/s). Forecast scenarios that are optimized to both recover lithium and harness geothermal energy are expected to sustain lithium production rates much more effectively.

The second model included more detailed simulations of the movement of brine and chemical reactivity of lithium within the reservoir. It showed that the reactions of relatively stable lithium-bearing minerals are slow, and that the primary replenishment mechanism for lithium in the brines is the upward flux of convecting lithium-rich brine from below the producing reservoir. However, these replenishment rates are not fast enough to produce significant increases in lithium, which could limit the long-term sustainability of the lithium resource. It is important to note that these models are preliminary and are based on current understanding of fluid replenishment rates, the minerals present in the geothermal system, and their chemical properties and reactivity. Further work should be undertaken to improve them and the associated predictions.

The report also considered potential impacts on regional water resources, air quality, chemical use, and solid waste disposal needs, as well as the seismic risk associated with geothermal power production and lithium extraction activity. These investigations highlighted the need to proceed with good monitoring and verification systems and with appropriate mitigation technologies. However, the analysis illustrates that if these things are done properly, lithium development is not likely to create significant negative environmental impacts.

Specifically, expanding geothermal energy production and lithium extraction will have a modest impact on water availability in the region. Initial estimates suggested that ~3% of historically available water supply for the region would be needed for currently proposed geothermal energy and lithium recovery operations; the majority of current water usage is for agriculture. It is not anticipated that expanding geothermal capacity or lithium production would impact the availability or quality of water used for human consumption and will not directly affect the water quality of the Salton Sea. However, the long-term drought conditions in the western United States may restrict future availability of water to the region, which is sourced from the Colorado River.

In terms of regional air emissions of all pollutants identified in the analysis (particulate matter, hydrogen sulfide, ammonia, and benzene, expanding geothermal energy and adding lithium extraction overall have a small impact. Chemical use involved in geothermal power production and lithium extraction is consistent with chemical use in industrial settings, and the analysis did not identify any persistent organic pollutants or acutely toxic chemicals among those currently being used.

Moving fluids within the subsurface can impact subsurface pressures and stresses, potentially triggering seismic activity. Early in geothermal energy production, increasing seismicity rates in the Salton Sea Geothermal Field correlated strongly with energy production activity; however, that correlation weakened after 1996. Even following the onset of geothermal energy production, seismic hazard in the Salton Sea Geothermal Field has not increased beyond that of the surrounding region.

In addition to technical outcomes from the analysis, the report describes an initial effort to incorporate community engagement into lithium research by understanding the local context and priorities and identifying how to effectively communicate to share information and gather feedback. The report includes information about the social and historical context of the region to enable a more holistic understanding of the resource and its potential impact, and identifies key community questions by observing public meetings, visiting the region, and consulting with local organizations. The report provides

recommendations about how future research efforts can address community concerns and implement more community-engaged practices. These include developing formal partnerships with local organizations and establishing a community advisory board to facilitate ongoing dialogue and opportunities for feedback. The future work will build on and further refine the models and scenarios presented in the report and strive to deepen engagement with local communities.

Table of Contents

List of Figures

List of Tables

List of Abbreviations

ABBREVIATION	MEANING OR DEFINITION
AADTT	Annual Average Daily Truck Traffic
AF	Acre-foot
APFU	Atoms per Formula Unit
AWS	Amazon Web Services
BACT	Best Available Control Technology
BBCSD	Bombay Beach Community Services District
BCH	Bromo-chlorohydantoin
BHER	Berkshire Hathaway Energy Renewables
BSZ	Brawley Seismic Zone
CAAQS	California Ambient Air Quality Standard
CAB	Community Advisory Board
CalEnergy	CalEnergy Resources Limited, is owned by Berkshire Hathaway Energy Company
CalGEM	California Geologic Energy Management Division
CalRecycle	California Department of Resources, Recycling, and Recovery
CARB	California Air Resources Board
CBO	Community-based Organization
CBPR	Community-based Participatory Research
CCV	Comité Cívico del Valle
CDC	California Department of Conservation
CDPH-RHB	California Department of Public Health Radiologic Health Branch
CE	Community Engagement
CEC	California Energy Commission
CPUC	California Public Utilities Commission
CTR	Controlled Thermal Resources
CUSUM	Cumulative Sum
cy	Cubic yards
DBNPA	Dibromopropionamide
DLE	Direct Lithium Extraction
DO	Dissolved Oxygen
DTSC	Department of Toxic Substances Control (California)
eGRID	Emissions and Generation Resource Integrated Database
EIA	Energy Information Administration
EIR	Environmental Impact Report (Federal) Or Economic Impact Report (Some States)
EIS	Emissions Inventory System
EIS	Environmental Impact Statement (Federal)
EJ	Environmental Justice
EOS	Equation of State
ESM	Energy Source Minerals
ESMAP	Energy Sector Management Assistance Program

ABBREVIATION	MEANING OR DEFINITION
ETAS	Epidemic Type Aftershock Sequence
EV	Electric Vehicle
EWASG	Energy, Water, Air, Salt, and Gravity
FAQ	Frequently Asked Questions
Featherstone	The John L. Featherstone geothermal power plant operated by EnergySource (sometimes referred to as the Hudson Ranch Power I plant or facility)
GAMA	Groundwater Ambient Monitoring and Assessment
GLEF	Geothermal Loop Experimental Facility
GTPP	Geothermal Power Plant(s)
HBSL	Health-based Screening Level
HMW	Harvie-Moller-Weare
HR-1	Hudson Ranch Power I plant or facility, also known as the Featherstone GTPP
HWTS	Hazardous Waste Tracking System (California Department of Toxic Substances Control)
ICP-MS	Induced Coupled Plasma Mass Spectrometry
ID	Identification (number)
IFD	Integral Finite Differences
IID	Imperial Irrigation District
IRWMP	Integrated Regional Water Management Plan
IV	Imperial Valley
IVAN	Identifying Violations Affecting Neighborhoods
IVC	Imperial Valley College
IVEJC	Imperial Valley Equity and Justice Coalition
JTD	Joint Technical Document
ka (ky)	Kilo annum (or kilo year), one thousand years
KB	Kelly Bushing (This represents the elevation of the drilling platform, which is above the actual ground surface.)
KGRA	Known Geothermal Resource Area
ktpa	Kilotons per annum
LA-ICP-MS	Laser Ablation Inductively Coupled Plasma Mass Spectrometry
LBNL	Lawrence Berkeley National Laboratory
LCA	Life-cycle Assessment
LCE	Lithium Carbonate Equivalent
LCRS	Leachate Collection and Removal System
LDS	Leak Detection System
LEA	Local Enforcement Agency
Li	Lithium
LVC	Lithium Valley Commission
MAF	Million Acre-feet
MATS	Mercury and Air Toxics Standards
MCL	Maximum Contaminant Levels
MCLG	Maximum Contaminant Level Goals

ABBREVIATION	MEANING OR DEFINITION
MLE	Maximum Likelihood Estimation
MOR	Mid-ocean Ridge
MORB	Mid-ocean Ridge Basalt
MRP	Monitoring and Reporting Program
MT	Magnetotelluric
MT	Metric ton or tonne, one thousand kilograms
MW	Megawatt, one million watts of electricity
MWe	Megawatt Electric, one million watts of electric capacity
MWh	Megawatt-hour, one thousand kilowatt-hours or one million watt-hours
My	Million years
NAWQA	National Water-Quality Assessment Project
NCG	Non-condensable gas(es)
NEA 111	NorthEnd Alliance 111
NEI	National Emissions Inventory
NIEHS	National Institute of Environmental Health Sciences
NIH	National Institutes of Health
NND	Nearest-neighbor Distance
NOD	Notice of Determination
NORM	Naturally Occurring Radioactive Material
NRC	National Research Council
OEHHA	Office of Environmental Health and Hazard Assessment
PHG	Public Health Goals
PM	Particulate Matter
ppb	Parts per billion
ppm	Parts per million
ppmw	Parts per million by weight
PSIG	Pounds per Square Inch Gauge
PTS	Pressure Temperature Spinner
QA/QC	Quality Assurance/Quality Control
RCRA	Resource Conservation and Recovery Act
REE	Rare Earth Elements
RO	Reverse Osmosis
RSA	Reactive Surface Areas
RWQCB	Colorado River Basin Regional Water Quality Control Board
SCLF	Salton City Landfill
SDS	Safety Data Sheets
SEIS	Supplemental Environmental Impact Statement
SEM	Scanning Electron Microscopy (or Microscope)
SS-GF	Salton Sea Geothermal Field
SS-GR	Salton Sea Geothermal Reservoir
SS-KGRA	Salton Sea Known Geothermal Resource Area
STLC	Soluble Threshold Limit Concentration

ABBREVIATION	MEANING OR DEFINITION
SWIS	Solid Waste Information System
SWRCB	State Water Resources Control Board
TCCA	Trichloroisocyanuric Acid
TCLP	Toxicity Characteristic Leaching Procedure
TDS	Total Dissolved Solids
THC	Thermal-hydrological-chemical
TSCA	Toxic Substances Control Act
TSDF	Treatment Storage and/or Disposal Facility
TSS	Total Suspended Solids
TTLC	Total Threshold Limit Concentration
U.S. DOE	United States Department of Energy
U.S. EIA	United States Energy Information Administration
U.S. EPA	United States Environmental Protection Agency
UNDP	United Nations Development Programme
USBR	United States Bureau of Reclamation
USGS	United States Geological Survey
VOC	Volatile Organic Compound
Water Board	California Regional Water Quality Control Board - Region 7
WDR	Waste Discharge Requirements
WET	Waste Extraction Test

Structure of the Report:

The report consists of four major sections and 11 chapters.

- The first section ("Overview") contains two chapters and presents a general introduction and high-level background of the region and its communities (Chapter 1) and the highest-level assessment of the total lithium resource, together with associated uncertainties and assumptions (Chapter 2). The primary contributors to this section are Patrick Dobson, Michael McKibben, and Margaret Slattery.
- The second section ("Lithium and Reservoir Behavior") contains four chapters and presents a deeper dive into the structure and function of the geothermal lithium reservoir. Chapter 3 presents the geologic history of the region, while Chapter 4 presents details on the chemistry of lithium and the rocks from which it is derived. Chapters 5 and 6 discuss the results of two separate but complementary modeling approaches that focus on reservoir function and sustainability under enhanced development for lithium production, and the geochemical processes that created and control the reservoir. The primary contributors to this section are Jennifer Humphreys, Maryjo Brounce, Michael McKibben, Lauren English, Naod Araya, John O'Sullivan, Joris Popineau, Theo Renaud, Jérémy Riffault, Eric Sonnenthal, Nicolas Spycher, Patrick Dobson, Noah Planavsky, and Boriana Kalderon-Asael.
- The third section ("Environmental Considerations") focuses on environmental impacts related to current and potentially expanded geothermal lithium extraction activity in the region. Specifically, four chapters focus on water (Chapter 7), air emissions (Chapter 8), chemical use and solid waste production and disposal (Chapter 9), and induced seismicity behavior (Chapter 10). The primary contributors to this section are William Stringfellow, Margaret Busse, Jennifer Stokes-Draut, Dev Millstein, Mary Kay Camarillo, Nori Nakata, Malcolm White, and Patrick Dobson.
- The fourth section ("Community Outreach") consists of a single chapter (Chapter 11) and presents the results of the community outreach effort described in Chapter 1, as well as takeaways and potential next steps. The primary contributor to this section is Margaret Slattery.

Taken together, the sections and chapters are intended to create a comprehensive understanding of the topic and provide detailed answers to the four key questions identified above. Individual sections and chapters are intended to be largely stand-alone documents, allowing readers to focus on specific areas of interest. By necessity, this structure leads to some material being presented in more than one location.

SECTION ONE: Overview

Chapter 1: Overview and Background

History of the Salton Sea Region

The Salton Sea area is a basin that has periodically filled with water and evaporated throughout history as the Colorado River changes course. Indigenous people have inhabited the region for millennia, with evidence of complex trade networks and settlements dating back at least 10,000 years (Gates and Crawford, 2010; Shackley, 2019). Today, the Torres Martinez Desert Cahuilla Indian Reservation is the closest Indigenous community, but several other tribes share a cultural connection with the Salton Sea and its environs, including the Quechan Indian Nation, the Cocopah Indian Tribe, and the Kumeyaay Nation.

The soil in the region is fertile after millennia of sediment deposits from the Colorado River. The first canals bringing Colorado River water into Imperial Valley were built in 1901, and most of the modern towns in Imperial County were established in the early 1900s to support the growing agricultural industry (Morton, 1977). Niland was formed in an area of citrus plants, Calipatria was established to grow peas and process alfalfa, and Brawley developed to distribute agricultural products. More than a century later, the agriculture industry has the highest economic output and is the second-largest employer in Imperial County (Langholz and DePaolis, 2021).

The modern Salton Sea basin was formed in 1905, when a year of heavy rains caused the Colorado River to breach a canal, dumping water into the Cahuilla basin. In the 1950s, the salinity of the Salton Sea had reached a level similar to that of the ocean, and the California Department of Fish and Wildlife (then known as the Department of Fish and Game) transplanted a variety of fish from the Gulf of California (Walker, 1961). The Salton Sea then became a thriving recreational scene, and the towns of Bombay Beach, North Shore, and Salton City emerged from the resulting tourism industry. The insects, wetlands, and fish species in the Salton Sea became an important stopover point along the Pacific flyway (Jones et al., 2019).

Throughout the 20th century, the Salton Sea's water level was largely maintained by agricultural runoff from the surrounding fields. In 2003, the local water utility, the Imperial Irrigation District, initiated a water transfer of 300,000 acre-feet per year to urban coastal areas, which was enabled by water conservation measures from agriculture (Thrash and Hanlon, 2019). For 15 years, fallow fields provided mitigating inflows to the Salton Sea of 200,000 acre-feet per year, but these expired in 2018. Consequently, lake levels began to drop precipitously in 2018.

With declining lake levels, more of the shoreline is exposed. The exposed lakebed, or "playa," creates serious public health issues due to dust that is kicked up during wind events (Johnston et al., 2019). Air quality is also affected by dust and emissions from agriculture and trucking, particularly around the Calexico/Mexicali border crossing (Mendoza et al., 2010). Estimated asthma rates in Imperial County are around 12% for the total population, and 19% for children under the age of 17, compared to statewide rates of 9% and 10% (California Department of Public Health, n.d.). At the same time, evaporation causes the salinity of the water in the Salton Sea to increase; it is currently 60 parts per thousand, nearly twice as high as the Pacific Ocean (Salton Sea Authority, n.d.). This high salinity has caused many fish species to die, which negatively impacts migratory bird populations. As part of the Salton Sea

Management Plan, California is implementing species habitat conservation and dust suppression projects to mitigate air quality issues and improve the situation for nearby communities and the environment.

Social and Historical Context

"Lithium Valley," as the region is now colloquially known, lies at the center of multiple global trends that are fundamentally reshaping society. On a material level, lithium-ion batteries play a pivotal role in the shift from fossil fuels to a carbon-free transportation and energy system. As EV sales ramp up worldwide, there has been an increased awareness of the critical minerals needed to meet demand (House, 2021). At the same time, regions around the world are seeking to improve supply chain resilience through onshoring more of the value chain, from mineral extraction to manufacturing to recycling (Riofrancos, 2022; Inflation Reduction Act of 2022, 2022). Finally, greater attention is being paid to the Just Transition framework, which recognizes that climate strategies can help create a more equitable future by seeking to repair historical environmental injustice; for example, by creating stable, good-paying jobs and ensuring that benefits accrue to local and disadvantaged communities (Heffron, 2020; McCauley and Heffron, 2018; Newell and Mulvaney, 2013; UNDP Climate Promise, 2022; World Resources Institute, n.d.). These factors converge in Lithium Valley, as a broad coalition of stakeholders attempts to develop a domestic lithium source that will meaningfully benefit the surrounding communities while minimizing environmental harm (CEC, n.d.).

The Salton Sea Known Geothermal Resource Area

A "known geothermal resource area," or KGRA, is a region identified by the U.S. Geological Survey (USGS) as an area in which higher-than-normal temperatures are likely to occur with depth, and in which there is a reasonable possibility of finding reservoir rocks that will yield steam or heated fluids to wells (Geothermal Technologies Office, 2023; Godwin et al., 1971). In a KGRA, subsurface temperatures are high enough at shallow enough depths that they can potentially be used for heat or power generation. The SS-KGRA (Figure 1.1) is one of five known geothermal resource areas located in Imperial County, California (Figure 1.2), and one of many in California and the United States (Energy Information Agency, 2023). This report will use the term SS-KGRA when specifically discussing the surface boundaries designated by the USGS, and Salton Sea Geothermal Reservoir (SS-GR; not to be confused with a groundwater reservoir) when referring to the entire subsurface system containing brine, heat, lithium and potentially other resources, the exact boundaries of which are not fully known. The SS-KGRA (and SS-GR) are named for the nearby lake but are not connected hydraulically to the Salton Sea, and the geothermal industry does not use water from the Salton Sea (Kaspereit et al., 2016; Paz et al., 2022).

The SS-GR brine reservoir is located at depths of approximately 1 to 3 km belowground and contains fluids at temperatures ranging from 250°C to 380°C (482-716°F) (Hulen et al., 2003). The existing geothermal power plants (GTPPs) are located in a subset of the SS-KGRA called the Salton Sea Geothermal Field (SS-GF) (Figure 1.3).

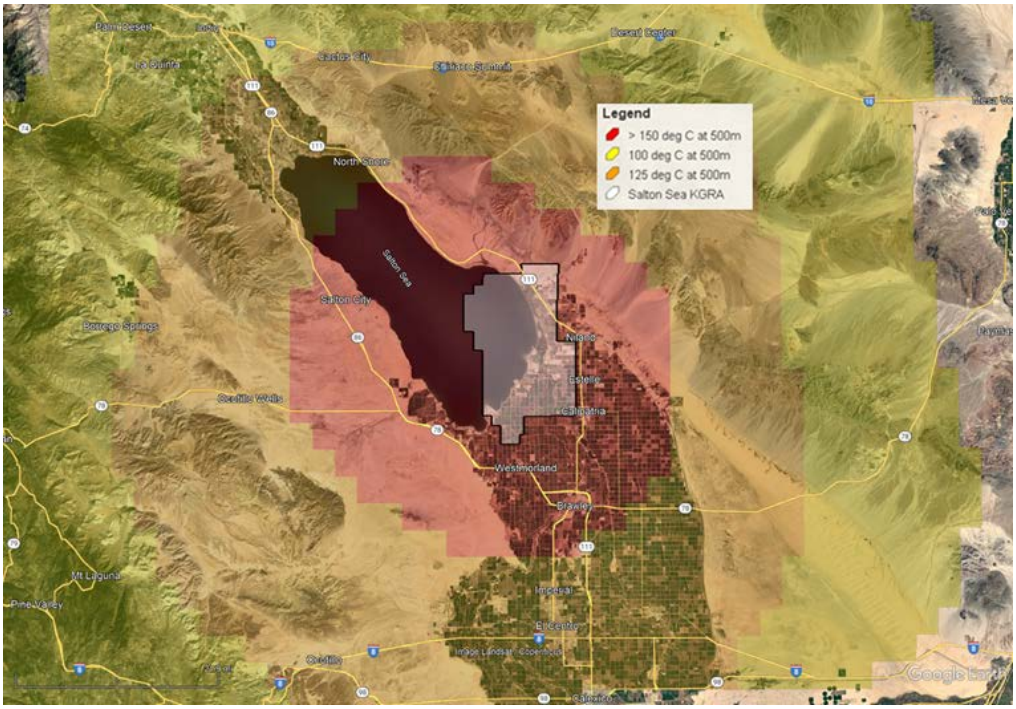

Figure 1.1. Location of the Salton Sea Known Geothermal Resource Area (SS-KGRA), shaded gray and outlined in black. Shading represents subsurface temperatures at 500 meters below ground surface (USGS data). The SS-KGRA is located in Imperial County, California.

In the U.S., there are three basic types of geothermal electricity production: "dry-steam," "flash-steam," and "binary" design (Robins et al., 2021; U.S. DOE, 2023; 2019). Flash-steam processes are used in geothermal areas with liquid brines that are geologically heated deep underground, under pressure, to temperatures above boiling. When these brines are extracted and brought to the surface, the pressure is reduced and the brines are "flashed" to produce steam to run turbines (e.g., BHER, 2023; Hell's Kitchen Power Co., 2021; Moss et al., 1982; Newell et al., 1989).

Although power plants in the SS-GF vary in age and size (Table 1.1), most plants are based on a similar flash-steam design that was developed specifically for extracting energy from the brines of the SS-GF (e.g., BHER, 2023; Hell's Kitchen Power Co., 2021; Moss et al., 1982; Newell et al., 1989). A stylized version of the flash-steam process is presented in Figure 1.4. First, hot brine under pressure is brought to the surface via a production well. At the surface, the brine is put through a series of vessels where the pressure is gradually reduced, and steam is liberated at each step (note the diagram's steam separator and pressure/crystallizers). The steam is cleaned (scrubbed) and used by the turbine to make electricity. The "spent" brine is treated to remove precipitated solids, mainly iron-rich silica, and then reinjected back into the reservoir. Reinjection of the brine is an important part of the process, so that the reservoir pressure can be maintained and there is sufficient fluid to produce more brine. Altogether, the power plants in the SS-GF extract an average of slightly over 120 million metric tons of brine per year, approximately 83% of which is reinjected back into the geothermal reservoir, with some of the geothermal fluid lost to evaporation in the cooling towers.

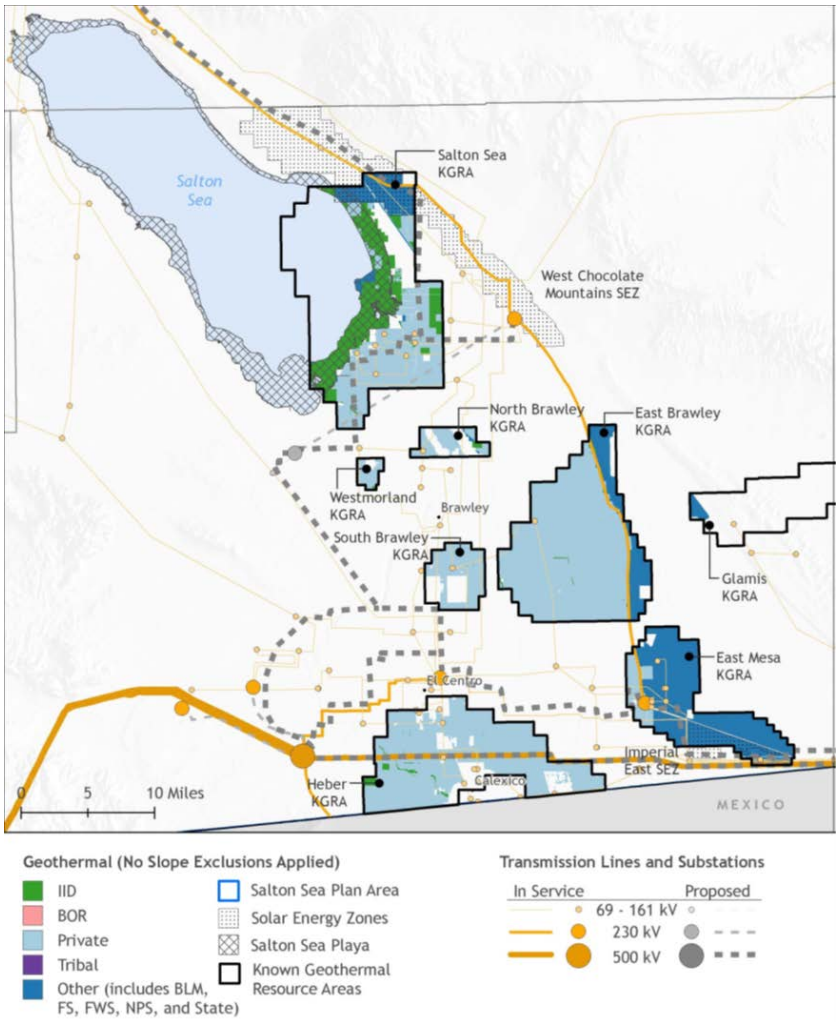

Figure 1.2. Known Geothermal Resource Areas (KGRAs) in Imperial County, California (Gagne et al., 2015).

The SS-GF currently supports 11 power plants (Figure 1.3, Table 1.1) with a combined output of approximately 400 megawatts (MW) of electricity. Geothermal power plants in the SS-KGRA produced approximately three million MWh of net electricity annually between 2014 and 2021. Although this represents only a small percentage of the electricity generated in California, it is an important source of reliable, low-carbon "green" electricity, and expansion of geothermal power production is a key component of California's clean energy goals (CDC, 2023). California has set a goal that at least 60 percent of its electricity must come from eligible renewable energy resources by 2030, and 100 percent by 2045 (Paz et al., 2022). Further, the California Public Utilities Commission has ordered utilities to procure 11,500 MW of new electricity from preferred resources, such as renewables and zero-emitting sources, by 2026 (Richter, 2021b).

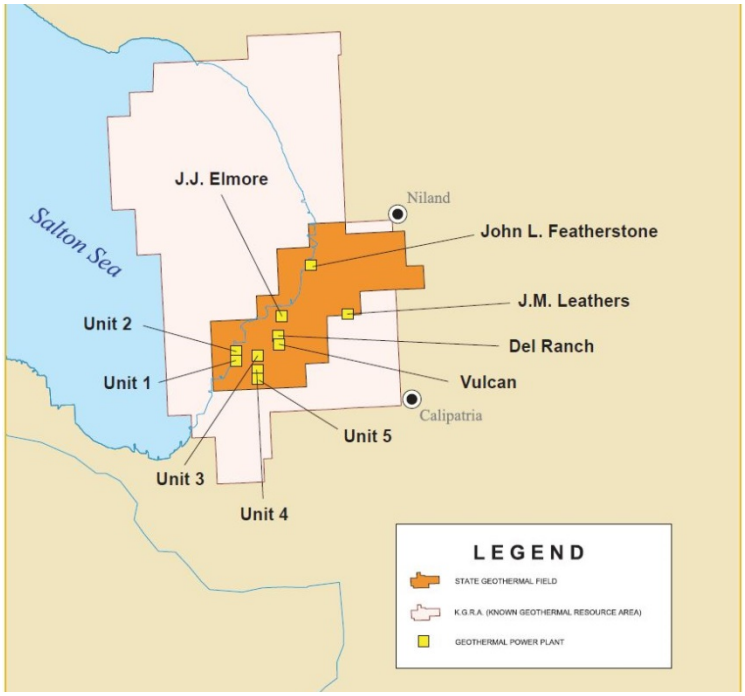

Figure 1.3. Geothermal power plants in the Salton Sea Geothermal Field (SS-GF) (orange) within the Salton Sea Known Geothermal Resource Area (SS-KGRA) in Imperial County, California. (Figure: Imperial Irrigation District.)

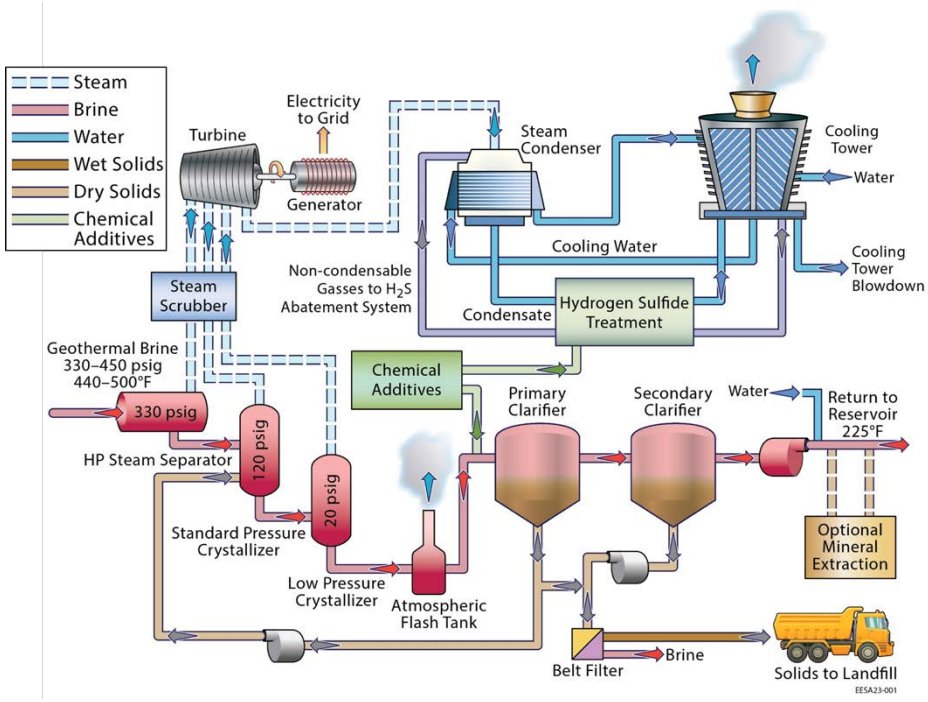

Figure 1.4. Schematic of a typical flash-steam geothermal power plant.

The SS-KGRA is considered underutilized in terms of energy development, suggesting it could become more important in meeting California's clean energy goals. The maximum geothermal capacity of the SS-KGRA is estimated to be over 2,500 MWe (Kaspereit et al., 2016), and it is expected that geothermal

power production in the SS-KGRA will increase by a net output of 357 MW over the next 3-5 years (CEC, 2023a, 2023b, 2023c; County of Imperial Planning & Development Services Department, 2022).

Overview of Geothermal Operators in the SS-GF

Ownership and operation of power plants and associated businesses involves numerous companies. During the period studied in this report (2014-2021), the power plants were managed by two primary entities: Berkshire Hathaway Energy Renewables (BHER) and EnergySource. However, EnergySource transferred the Featherstone power plant to Cyrq Energy (Richter, 2021a) in 2021, while BHER operates power plants and associated operations under the name CalEnergy Resources Limited and other subsidiaries. For simplicity, we will refer to primary operators rather than individual subsidiaries when discussing geothermal field operations.

BHER operates 10 power plants under four management units (Table 1.1). EnergySource is still affiliated with one power plant: the John L. Featherstone plant (Featherstone), operated at the Hudson Ranch Power I location (Table 1.1). As discussed above, Cyrq is now the operator of the Featherstone power plant but has an agreement with EnergySource (as EnergySource Minerals) to provide brine for lithium recovery processes (discussed below). A summary of nameplate capacity by management unit or region is presented in Table 1.1.

Current geothermal power nameplate capacity in the region includes approximately 375 MW from the 10 BHER plants, and 55 MWe from the Featherstone (aka Hudson Ranch I) plant. But as mentioned above, there are plans to increase power production from the SS-GR. BHER plans to build three new power plant complexes, which are to provide an additional 401 MW of nameplate capacity with 357 MW of expected net output (CEC, 2023a, 2023b, 2023c). Another company, Controlled Thermal Resources (CTR), plans to build two new power plants sequentially, the first with 50 MW of capacity and the second with 130 MW (Controlled Thermal Resources, 2023a; Hell's Kitchen Power Co., 2021). CTR operates facilities in the SS-GF under the subsidiary Hell’s Kitchen companies. CTR is proposing to produce both electricity and steam for co-located industrial processes (Sizemore, 2023).

Table 1.1. Existing geothermal power plants

Power Plant Name	Operator or Owner	Operational Unit Name or Management Unit	Year Permitted	Plant Capacity (MW)[d]	Electrical Generation per Month[a] (Mean MWh)	Net Electrical Capacity[b] (MW)	Gross Annual Electricity Generation[c] (MWh)	Net Annual Electricity Generation[c] (MWh)	Gross Efficiency per Nameplate Capacity (%)
Featherstone *(aka Hudson Ranch I)*	Cyrq	Featherstone	2012	55.00	35,928	50	456,856	417,498	95
Elmore	BHER	Elmore	1987	48.49	27,380	49	373,518	333,102	88
Leathers	BHER	Leathers	1988	43.20	28,003	42	378,152	339,083	100
Unit 1	BHER	Region 1	1994	10.25	6,102	10	78,235	72,581	87
Unit 2	BHER	Region 1	1994	19.70	8,741	16	128,072	113,372	74
Unit 3	BHER	Region 1	1994	53.97	27,594	50	385,806	356,379	82
Unit 4	BHER	Region 1	1994	47.50	23,977	42	345,394	311,533	83
Unit 5	BHER	Region 1	2011	58.30	27,263	46	389,120	335,506	76
Vulcan	BHER	Region 2	1991	39.72	22,070	38	329,288	280,827	95
Del Ranch *(aka Hoch)*	BHER	Region 2	1991	43.20	26,647	42	356,262	321,468	94
Turbo	BHER	Region 2	2000	11.50	5,912	10	68,159	66,409	68

[a]Energy Information Agency 2014-2021.

[b]California Energy Commission (CEC, 2023b).

[c]California Energy Commission mean of 2014-2021.

[a]California Energy Commission power plant list (downloaded 3/22/2022).

The SS-GR is unique in that the geothermal brine in this resource area is highly saline and contains relatively high concentrations of lithium (Table 1.2). The three companies that are operating or building power plants in the SS-KGRA – BHER, EnergySource, and CTR – are also developing projects to recover lithium from geothermal brine (Paz et al., 2022). All three companies are planning to apply direct lithium extraction (DLE) technology to produce lithium carbonate, lithium hydroxide, and/or other lithium products required for batteries (Paz et al., 2022; Stringfellow and Dobson, 2021). EnergySource (as EnergySource Minerals) is developing the ATLiS Project, which is expected to produce 17,600 metric tons of LCE per year at full scale (Chambers Group Inc., 2021; EnergySource Minerals, 2021, Paz et al., 2022). BHER, which operates a pilot project, estimates that a full-scale facility could produce 90,000 metric tons of LCE based on their existing GTPP operations, with a potential capacity of 600,000 tons for the entire SS-GR (Besseling, 2018). CTR expects to produce 25,000 metric tons per year of lithium product (reported as either lithium hydroxide monohydrate or lithium carbonate) during initial operations, and plans for an eventual capacity of 300,000 metric tons per year of lithium products (Controlled Thermal Resources, 2023a, 2023b; Hell's Kitchen Power Co., 2021). If successful, lithium production in conjunction with expanded geothermal energy production could transform the economy of Imperial County (Paz et al., 2022).

Frontline Communities

According to the 2020 U.S. census, Imperial County is home to a population of approximately 180,000 people. An estimated 86% of the population is Hispanic or Latino, and nearly 75% speak a language other than English at home (U.S. Census Bureau, n.d.). In reality, these numbers may be higher; Imperial County is considered one of the hardest places to count in California because a high proportion of the population is from demographics that are historically undercounted, many people live in remote housing locations, and there is limited internet access (Thorman et al., 2019). A map of the SS-KGRA and surrounding communities in Imperial County is shown in Figure 1.5.

The SS-KGRA is located on the north end of Imperial County, which has seen a declining population in recent decades as communities have faced extreme challenges related to poverty, unemployment, and public health (Nava-Froelich, 2023). The census tracts in this area (Figure 1.6) are designated as disadvantaged communities by the California Environmental Protection Agency (CalEPA) and federal Justice40 Initiative criteria (CalEnviroScreen 4.0, 2021; Council on Environmental Quality, n.d.). No communities are immediately adjacent to existing geothermal facilities, as the nearest population centers, Niland and Calipatria, are roughly four miles away (Table 1.3). However, several communities can be considered "frontline communities" as they (a) stand to be impacted by infrastructure, traffic, and social changes, (b) share a dependence on the same water source, and/or (c) share the same air basin (U.S. DOE, 2022).

Table 1.2. Characteristic mineral and salt composition of geothermal brines in the SS-GR. Mean of data from published sources, representing post-flash brine chemistry.

Analyte	Average (mg/kg)	Standard Deviation (mg/kg)	Relative Standard Deviation (%)	N
Cl	142,015	18,853	13	13
Na	49,249	5,578	11	13
Ca	25,684	3,050	12	13
K	14,467	3,370	23	13
Fe	1,347	653	48	13
Mn	1,201	393	33	13
Zn	463	169	36	12
Sr	434	67	15	12
SiO2	342	133	39	7
NH4	311	111	36	8
B	298	69	23	11
Ba	205	57	28	11
Li	202	39	20	13
Rb	110	52	47	4
Mg	109	192	176	13
Br	91.4	28.0	31	9
Pb	84	19	23	12
SO4	58.6	37.3	64	9
Cs	19.8	2.9	15	4
I	17.0	3.6	21	3
F	14.7	0.6	4	3
As	9.0	3.6	40	3
Cu	4.1	2.3	57	10
Al	2.4	1.2	51	5
Cd	1.9	0.5	27	7
Ag	1.6	0.7	43	3
TDS (%)	24.3%	2.8%	12	13

(Williams & McKibben, 1989, McKibben & Hardie, 1997, Duyvesteyn, 1992, Featherstone & Powell, 1981, Maimoni, 1982, Blake, 1974, Skinner et al., 1967, Palmer, 1975, Zukin et al., 1987.)

Salton Sea Known Geothermal Resource Area and Surrounding Communities

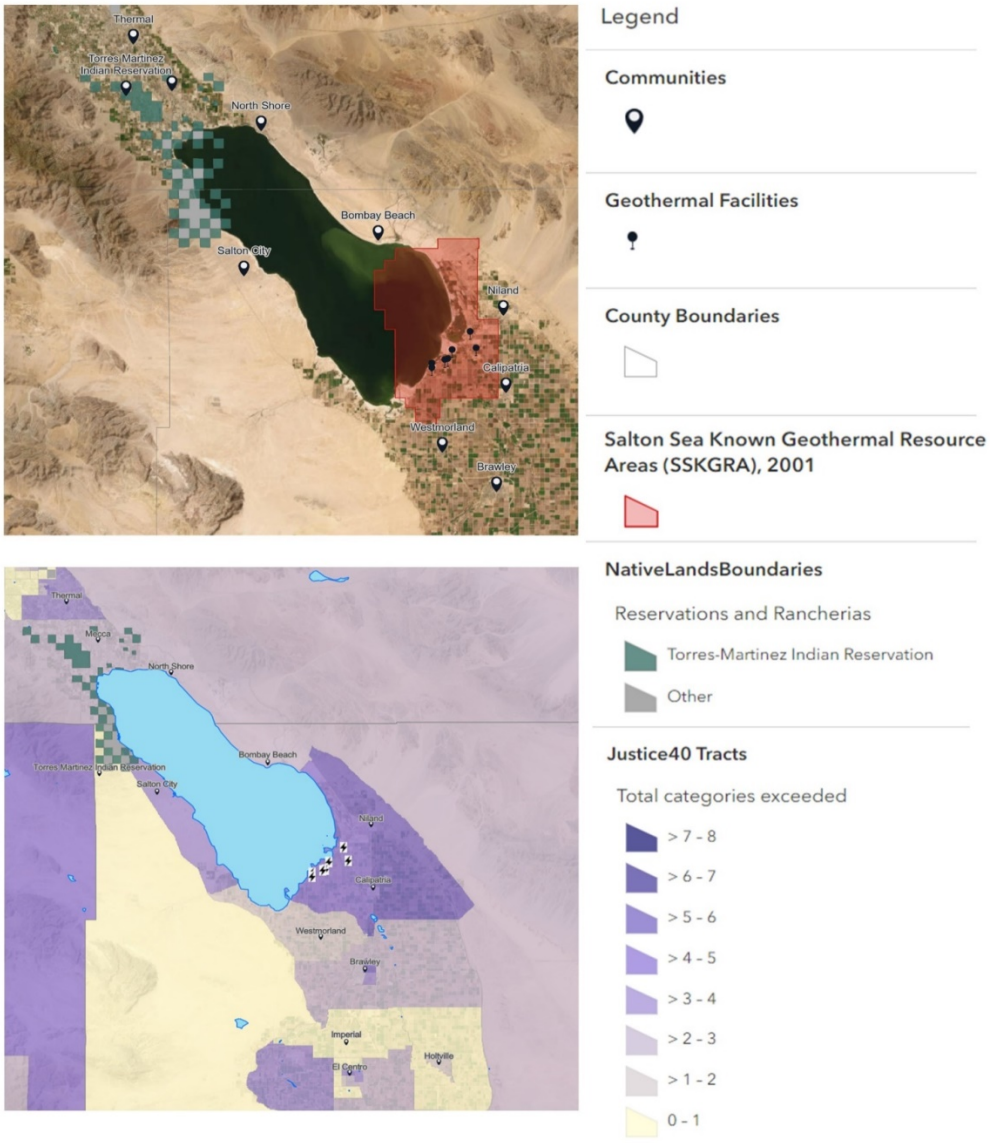

Figure 1.5. Map of the Salton Sea Geothermal Resource Area and surrounding communities (top), with layers showing tribal lands and environmental burden indicators (bottom) according to the Justice40 Initiative criteria (Council on Environmental Quality; California Technology Agency/GIS Unit).

The SS-KGRA is located on the north end of Imperial County, which has seen a declining population in recent decades as communities have faced extreme challenges related to poverty, unemployment, and public health (Nava-Froelich, 2023). The census tracts in this area (Figure 1.6) are designated as disadvantaged communities by the California Environmental Protection Agency (CalEPA) and federal Justice40 Initiative criteria (CalEnviroScreen 4.0, 2021; Council on Environmental Quality, n.d.). No communities are immediately adjacent to existing geothermal facilities, as the nearest population centers, Niland and Calipatria, are roughly four miles away (Table 1.3). However, several communities can be considered "frontline communities" as they (a) stand to be impacted by infrastructure, traffic, and social

changes, (b) share a dependence on the same water source, and/or (c) share the same air basin (U.S. DOE, 2022).

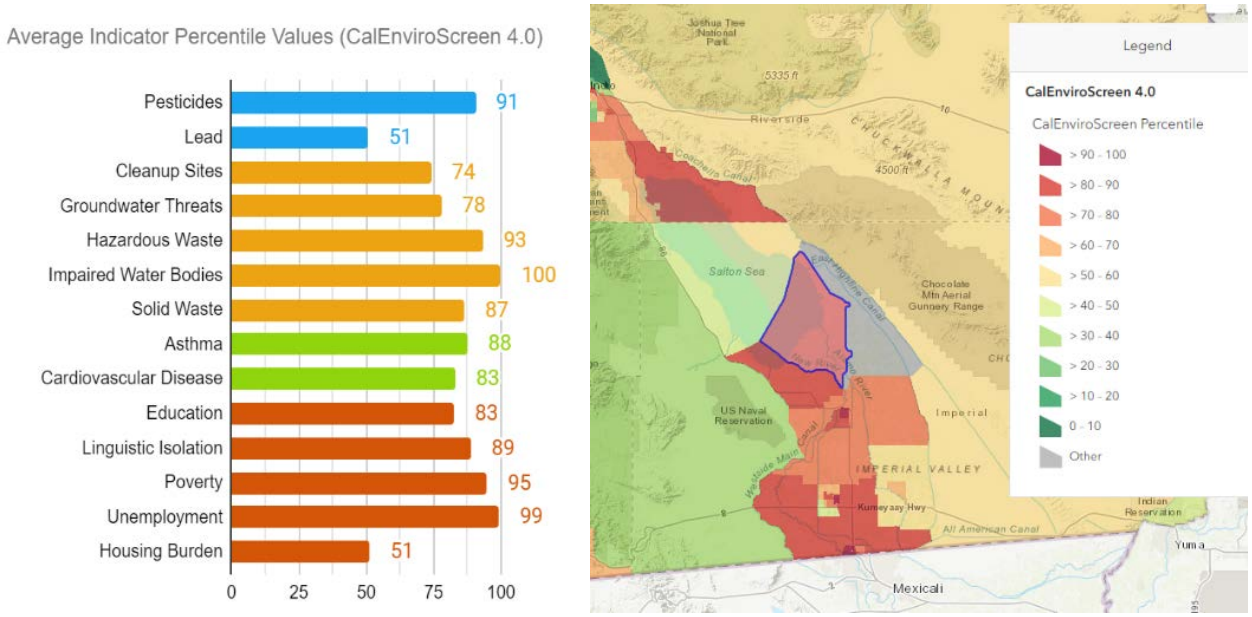

Figure 1.6. Cal EnviroScreen 4.0 results for the census tract surrounding Niland, Calipatria, and Westmorland.

These are also frontline communities in terms of the impacts of climate change. The Georgetown Climate Center offers the following definition: "Frontline communities include people who are both highly exposed to climate risks (because of the places they live and the projected changes expected to occur in those places) and have fewer resources, capacity, safety nets, or political power to respond to those risks" (e.g., these people may lack insurance or savings, hold inflexible jobs, exert low levels of influence over elected officials, etc.) (Georgetown Climate Center, n.d.). The communities surrounding the SS-GF all fit this definition, as they are significantly impacted by high temperatures and drought conditions that are expected to worsen due to climate change in the coming years (Maizlish et al., 2017). Furthermore, with a high proportion of low-income and Latino households, the surrounding communities are particularly vulnerable to environmental burdens and face structural barriers to healthcare, such as language and documentation status (Cheney et al., 2023). At the same time, these statistics do not present a full picture of the area. As one survey respondent commented, "I urge you to analyze the demographics of the Imperial community beyond the scope of 'disenfranchisement' and 'advanced battery supply chain.'" Most people we spoke with expressed a strong commitment to their communities and a desire to stay in the area despite its challenges. Residents mentioned the quiet and peacefulness of Imperial Valley as a reason they want to stay in the area, along with being close to their families. Many young people want to stay but find it difficult to secure reliable employment outside agriculture or correctional services. This motivates a high level of interest and engagement in the development of Lithium Valley, which we observed during our outreach efforts.

Table 1.3. Frontline Communities Near the Salton Sea Known Geothermal Resource Area

Name	Distance to closest geothermal facility*	Distance to SS-KGRA	Justice40 Environmental Burden thresholds exceeded**
Niland	4.04 miles	0.63 miles	Energy, health, legacy pollution, waste and wastewater, workforce development
Calipatria	4.76 miles	0.78 miles	Energy, health, legacy pollution, waste and wastewater, workforce development
Westmorland	7.91 miles	2.65 miles	Housing, workforce development
Brawley	13.45 miles	8.84 miles	Climate change, health, housing, legacy pollution, waste and wastewater, workforce development
Bombay Beach	13.48 miles	1.89 miles	Energy, health, legacy pollution
Salton City	20.7 miles	12.71 miles	Energy, legacy pollution, transportation, workforce development
North Shore	29.4 miles	17.71 miles	Energy, legacy pollution, workforce development
Torres Martinez Reservation	27.85 miles	19.63 miles	Climate change, housing, workforce development

*Refers to straight line distance calculated using ArcGIS, not driving distance.
**See the Justice40 environmental burden methodology for details.[24]

Timeline and Status of "Lithium Valley"

Geologists knew about Imperial County's mineral-rich geothermal brines long before the region's first geothermal power plant was developed. Operators first explored the possibility of extracting minerals in the 1960s (Morton, 1977). Decades later, CalEnergy had a commercial plant operating between 2000 and 2004 to extract zinc from produced brines (Clutter, 2000). These efforts were abandoned because technical challenges prevented the venture from becoming economically viable (Berkshire Hathaway Inc., 2005).

The first company to demonstrate lithium extraction was Simbol, which started operating a demonstration plant in Calipatria in 2011 (Biello, 2011; Simbol Materials, 2011). In 2013, the company announced they successfully produced high-purity lithium carbonate from geothermal brine and planned to build a commercial plant to begin operation in 2015 (Green Car Congress, 2013). Despite this, Simbol abruptly closed down in 2015 (Roth, 2015).

Lithium Valley came into renewed public focus starting in 2019, when California State Assemblymember Eduardo Garcia introduced Assembly Bill 1657 (AB 1657) (Garcia, 2020). AB 1657 required the

California Energy Commission (CEC) to convene a Blue-Ribbon Commission on Lithium Extraction in California, commonly referred to as the Lithium Valley Commission (LVC). The LVC was composed of 14 individuals who represented community organizations, geothermal and lithium extraction companies, tribal councils, state agencies, and environmental organizations. It was tasked to "review, investigate, and analyze" a set of specific issues related to lithium extraction and use in California (Garcia, 2020). The LVC met monthly between February 2021 and January 2023, and released a final report in December 2022 (Paz et al., 2022).

The next important piece of Lithium Valley legislation was Senate Bill 125 (SB 125). SB 125 established the Lithium Extraction Tax Law, which requires producers to pay an excise tax per metric ton of lithium carbonate equivalent for any lithium produced in the state (Senate Budget and Fiscal Review Committee, 2022). Section 47100a specifies that 80% of the tax revenue be disbursed to the county where lithium is produced, with at least 30% of the revenue in Imperial County being disbursed to "communities that are most directly and indirectly impacted by the lithium extraction activities." The remaining 20% of tax revenue is directed to Salton Sea restoration. In addition to the Lithium Extraction Tax Law, SB 125 allocated $5 million to Imperial County to prepare a programmatic environmental impact report and support community outreach and stakeholder engagement.

Imperial County is now preparing a Programmatic Environmental Impact Report, along with a Lithium Valley Specific Plan and Lithium Valley Economic Opportunity Investment Plan (Lithium Valley, 2022). A community workshop report and notes from the Environmental Justice and Technical Advisory Groups are available from the County's Lithium Valley website (Rick Engineering Company, 2023).

Community-Based Organizations (CBOs)

There is a strong network of community-based organizations (CBOs) and non-profits who advocate for disadvantaged communities in Imperial County and the Eastern Coachella Valley (Table 1.4). These range from larger established advocacy organizations like Comité Cívico del Valle, which has operated in Imperial County for decades, to smaller grassroots community groups like NorthEnd Alliance 111 and the Bombay Beach Community Services District, which advocate for basic infrastructure and services in their respective communities. Along with public health, CBOs in this region work on issues related to the U.S./Mexico border, farmworker rights, and housing. The CBOs presented below are organizations that have both engaged with our team directly and are actively involved in initiatives related to Lithium Valley.

CBOs in Imperial County

Comité Cívico del Valle (CCV), based in Brawley and one of the county's most prominent CBOs, is driving much of the community advocacy related to Lithium Valley: its executive director served on the Lithium Valley Commission, and CCV is leading outreach efforts related to the County's Environmental Impact Report and tax revenue investment. In addition to its lithium-related work, CCV oversees several other initiatives to empower the local community and improve public health. For example, the organization operates a network of nearly 70 air quality monitors under its "Identifying Violations Affecting Neighborhoods" (IVAN) program, and it has contributed to numerous research initiatives and publications about public health in the region (Johnston et al., 2019; Madrigal et al., 2020). CCV is also

implementing the "First 40 EV Charger Campaign" to install more EV charging stations in Imperial Valley (Comité Cívico del Valle, n.d.).

Table 1.4. Selection of Community-Based Organizations (CBOs) in the Salton Sea Region

Organization	Website
Comité Cívico del Valle	https://www.ccvhealth.org/
NorthEnd Alliance 111	NA
Bombay Beach Community Services District	https://www.bbcsd.org/
Imperial Valley Equity and Justice	http://ivequityjustice.org/
Los Amigos de la Comunidad IV	https://losamigosdelacomunidad.com/
Alianza Coachella Valley	https://www.alianzacv.org/
Leadership Counsel for Justice and Accountability	https://leadershipcounsel.org/

Closer to the SS-GF, the NorthEnd Alliance 111 (NEA 111) and Bombay Beach Community Services District are smaller grassroots groups that were organized by residents to provide basic needs and services in their communities. NEA 111 is a group of Niland residents who organize monthly food distribution, summer care packages, and blankets and jackets in Niland, Bombay Beach, and Calipatria (Morales, 2022). During the height of the COVID-19 pandemic, it coordinated both testing and vaccinations. NEA 111 also works with the Imperial County Board of Supervisors through its participation in the NorthEnd Action Council (Grant, 2019) and advocates for a fair distribution of benefits for NorthEnd Communities from Lithium Valley development.

The Bombay Beach Community Services District (BBCSD), founded in 1961, is a publicly elected five-member board that performs basic services in Bombay Beach, including streetlight and park maintenance and trash collection. BBCSD is also developing an emergency response unit, as it usually takes at least 45 minutes for first responders to reach the community.

Two other notable CBOs are the Imperial Valley Equity and Justice Coalition (IVEJC) and Los Amigos de la Comunidad IV. IVEJC is a collective that was formed during the COVID-19 pandemic. Its vision is "to eliminate health and social disparities and inequities among the Latinx community in Imperial Valley (IV) and build the next generation of Latinx community leaders" (IVEJC, n.d.). It is part of the Salud Sin Fronteras initiative, which distributed personal protective equipment during COVID to communities in Imperial Valley, particularly at the border crossing in Calexico, and helped farmworker communities get access to vaccines. IVEJC also provides resources about worker safety and rights to farmworkers in Imperial Valley.

Los Amigos de la Comunidad IV's mission is "to increase the capacity of the underserved communities of the Imperial Valley and intertwined regions facing socio-economic and environmental injustices, health care access disparities and institutional discrimination" (Los Amigos de la Comunidad, n.d.). Its initiatives include helping residents apply for Medi-Cal services (Proyecto Accesso!), registering community members to vote, outreach and education about Lithium Valley, and advocating for access to broadband.

In April 2023, the county Board of Supervisors awarded CCV, IVEJC, Los Amigos de la Comunidad IV, Raizes, and the Imperial Valley LGBT Resource Center a total of $720,000 to perform outreach related to the development of Lithium Valley (Morales, 2023). CCV, Los Amigos de la Comunidad IV, and IVEJC are also part of the Lithium Valley Community Coalition, a group of stakeholders comprising local environmental justice (EJ) groups and labor unions that represent disadvantaged communities. According to its website, the Coalition's mission is to "meet the needs of the communities located in Lithium Valley in an equitable, environmentally friendly, and community-conscious manner" (Leadership Counsel, 2016).

CBOs in the Eastern Coachella Valley

Alianza Coachella Valley, or "Alianza," is a grassroots coalition focused on building leadership and supporting thriving communities in Coachella, Thermal, Mecca, Oasis, and North Shore (About Us, 2021). In addition to staff and leadership, its work is guided by a governing body called "La Mesa" that is composed of representatives from partner organizations and community members. Alianza has organized advocacy efforts to improve drinking water, invest in community infrastructure, and increase access to health care for communities in the Eastern Coachella Valley. Its executive director, Silvia Paz, chaired the Lithium Valley Commission.

Leadership Counsel for Justice and Accountability is an environmental justice organization that works with communities in the Eastern Coachella Valley and Central Valley of California (Leadership Counsel, 2016). The Leadership Counsel advocates for policies related to land use, transportation, climate change, safe and affordable drinking water, housing, environmental justice, equitable investment, and governmental accountability. Its strategy focuses on empowering low-income communities of color to participate as equal partners in decision-making processes. While it was not represented on the LVC, the Leadership Counsel did participate by submitting public comments and documents to the docket and sharing information about the LVC with North Shore communities.

The above information was presented to help readers understand the context of the region, including the history, environmental conditions, and socioeconomic characteristics that shape the present situation. The information presented here is based on multiple visits to the region, observations of public and community-meetings (Slattery et al., 2023), analysis of public comments submitted to the Lithium Valley Commission docket (CEC, n.d.), conversations with community members and representatives from local advocacy organizations, and review of the relevant literature, reports, and other publicly available information, including historical archives about the Salton Sea. The format and approach were also informed by the Department of Energy's Guidelines for Creating a Stakeholder Engagement Plan (U.S. DOE, 2022).

Chapter 2: Resource Estimate

Key Takeaways

- The Salton Sea Geothermal System is estimated to contain a proven lithium resource of 4.1 million metric tons of lithium carbonate equivalent (LCE) and a probable lithium resource of 18 million metric tons of LCE.
- Current production wells have brine production rates corresponding to a potential lithium production of 115 kilotons of LCE per annum, sustainable over a lifetime of at least 36 years.
- The region could be a substantial domestic supplier of lithium to the U.S. and help meet its green energy needs over the remainder of the 21st century.

Introduction

This chapter describes an approach to estimating the size of the overall lithium (Li) resource in the Salton Sea geothermal reservoir (SS-GR) and various uncertainties associated with that assessment. This approach uses existing data to construct a simple model to generate a high-level assessment. The material presented in Section 2 builds on this assessment, but with more detailed dynamic modeling to explore different aspects of the reservoir's behavior. This chapter is presented on its own because of the importance of the total lithium resource assessment to multiple stakeholders and the desire that it be clearly presented.

Our lithium resource model is based on a volumetric estimate of the size of the SS-GR along with an average brine lithium concentration, to estimate the total amount of lithium contained within the brine. It is based on the following parameters: areal extent of the SS-GR (surface footprint), thickness of SS-GR, porosity of SS-GR (i.e., fraction of reservoir volume that contains brine), and the lithium concentration of brine. Several studies (e.g., Younker and Kasameyer, 1978; Hulen et al., 2002; Kaspereit et al., 2016) have conducted detailed assessments of the geothermal resource potential of the Salton Sea Geothermal Field (SS-GF) using many of the above parameters. Presented below are relevant details from some studies that relate to each of these parameters.

Areal Extent of the Geothermal System

The extent of the geothermal system has been estimated in several different ways. Wells drilled into the reservoir are the most reliable means of confirming the presence of the geothermal resource. Other methods used to delineate the reservoir's boundaries include shallow temperature measurements (based on data by Newmark et al., 1988) and geophysical measurements that are interpreted to indicate the boundaries of the thermal anomaly. Specifically, these include:

- High temperature (≥ 200°C/km) shallow thermal gradients (based on data by Newmark et al., 1988)
- 1800 and 1775 gamma magnetic contours (Younker and Kasameyer, 1978)

- Magnetotelluric resistivity measurements delineating a resistive heat source for system.

In a previous reservoir model, Younker and Kasameyer (1975) used existing deep wells to delineate a confirmed SS-GR areal extent of 13 km^2 and used measurements of local magnetic contours on land (1800 gamma on land) to indicate a probable larger extent of 28 km^2. Extending this same contour into the Salton Sea, a larger subsurface resource corresponding to 58 km^2 was inferred. Using a different threshold value for the magnetic contour (1775 gamma) resulted in a hypothetical resource footprint of 124 km^2.

That model was updated by Hulen et al. in 2002 using additional field constraints that were not available for the earlier study. Considerably more wells had been drilled and the commercial geothermal field had been developed, resulting in a proven resource footprint. Using the 200°C/km shallow temperature gradient contour, an area of 72.4 km^2 was identified as the likely field areal extent, which included a drilled and proven resource area of 27.9 km^2.

The most recent conceptual model of the field (Figure 2.1) was developed by Kaspereit et al. (2016). This model represents an updated version of the Hulen et al. (2002) model, and uses the shallow thermal anomaly, additional well data, magnetotelluric (MT) data, and structural and seismic data to enlarge the areal footprint of the estimated extent of the resource to 91.9 km^2. The proven resource footprint in this updated evaluation has also been extended to 30.8 km^2. Notably, a significant fraction of the resource is located underneath the Salton Sea. Employing directional drilling, Kaspereit et al. (2016) estimate that 76% (69.8 km^2) of the estimated offshore resource could be reached with wells located onshore.

Reservoir Thickness Estimates

Younker and Kasameyer (1975) indicated that the measured thickness of the SS-GR based on temperature and production data was 1 km, but the inferred thickness could be 2 km based on the depth interval between the 230°C isotherm and zone of intrusion. Klein et al. (2004) used the inputs of Hulen et al. (2002) to inform their assessment of the Salton Sea field and reported a reservoir volume estimate of 25.71 $miles^3$ (107.16 km^3). Using the Hulen et al. (2002) surface area, this equates to an average reservoir thickness of 1.48 km.

Details relating to reservoir depth and thickness can be obtained for the 29 active production wells in the field from the CalGEM database (see Appendix Chapter 2: Salton Sea Geothermal Production Wells). The top of the reservoir can be approximated by the casing shoe depth, which ranges from the shallowest value of 581 m (at Sinclair 10) to 1383 m (at River Ranch 11), with an average value of 908 m, with all values corrected for Kelly bushing (KB) elevation. These values are consistent with the Norton and Hulen (2006) model of the SS-GR (Figure 2.2). A minimum estimate of the reservoir's depth can be estimated by the depth of the production wells, which range in depth from 889 to 2774 m, with an average production well depth of 1878 m.

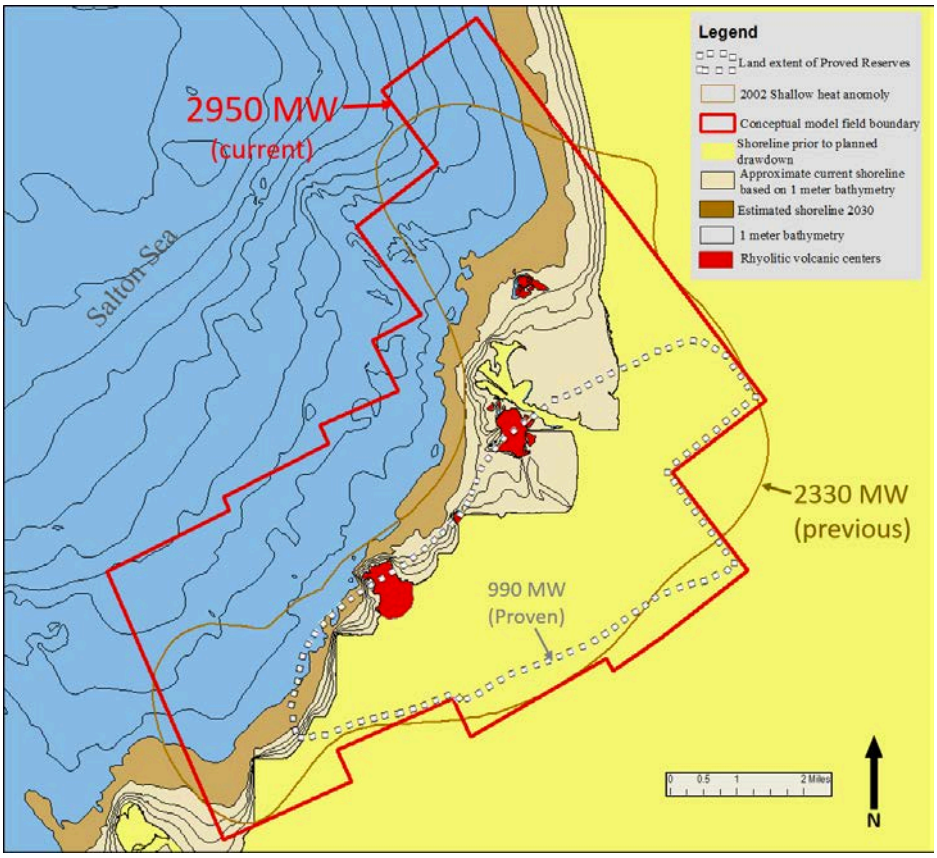

Figure 2.1. Conceptual resource model of Kaspereit et al. (2016) with proven, previous (Hulen et al., 2002), and updated probable resource footprints for the SS-GF.

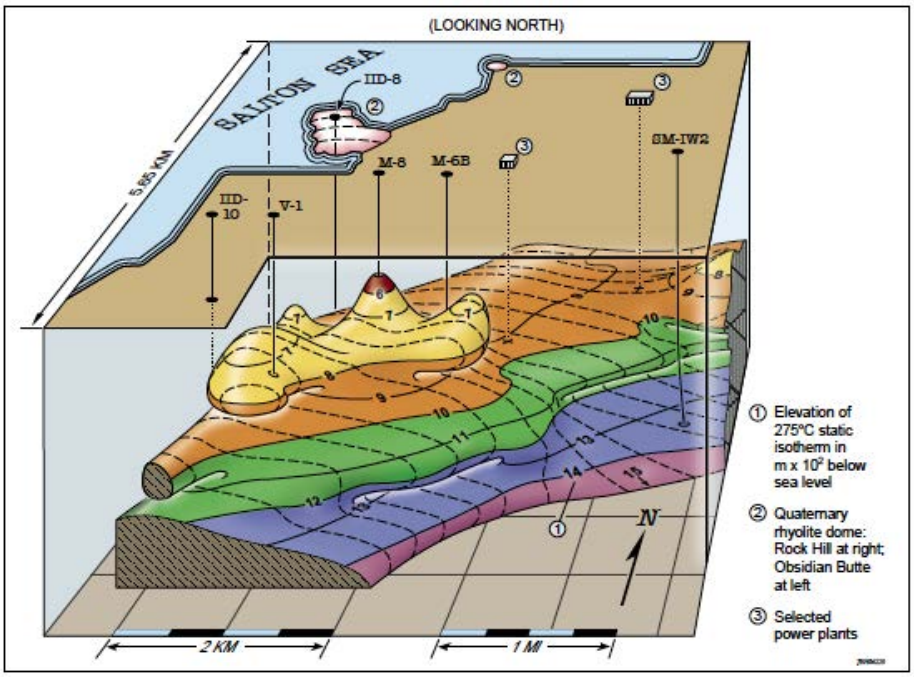

Figure 2.2. 3D model of the 275°C temperature contour of the Salton Sea geothermal system (Norton and Hulen, 2006).

One way of providing a minimum reservoir thickness estimate would be to examine the production-zone interval (i.e., the section of the well within the geothermal reservoir) of each of the production wells at the SS-GF. For the 29 wells currently listed as being in production by CalGEM, this value can be calculated as the distance between the casing shoe (where the casing is set at the top of the reservoir) and the bottom of the well (using the true vertical depth values where available). These values range from 101 m to 1723 m, with an average production zone thickness of 971 m. Four of the wells have a very short production interval (< 300 m), so if these wells are removed from the calculation, the revised average reservoir thickness is 1095 m. This value represents the minimum thickness of the geothermal reservoir, as the reservoir very likely extends below the bottom of the well. However, reservoir porosity declines significantly with depth (see discussion below), so the amount of brine contained in deeper zones is likely negligible.

Porosity Estimates

Again, "porosity" refers to the fraction of reservoir volume that contains brine. There are two types of porosity to consider: matrix porosity, which represents the pore space between the mineral grains, and fracture porosity, which represents the void space in open fractures within the reservoir. In the model of Klein et al. (2004), porosities of 10 to 20% were assigned to the SS-GR. Matrix porosity measurements from a variety of wells were presented by Younker et al. (1982), who noted that fracture porosity is likely an important component of fluid flow within the reservoir. For our study, some 141 core porosity measurements were obtained from five wells using data from Somerton (1973), Somerton et al., (1974), Tewhey (1977), and McDowell (1987). This compilation (Appendix Chapter 2: Salton Sea Rock Property Data) includes most of the well porosity data reported by Younker et al. (1982) but includes many more analyses from the well named "State 2-14." Samples were obtained from depths ranging from 473.4 m to 3020 m. The measured porosity values range from 0.33 to 0, with an average value of 0.112 for the 141 samples; porosity values tend to decrease as a function of depth in a nonlinear fashion. Sandstones generally have higher porosities (average value of 0.155 for 49 samples) compared to siltstones and mudstones (average value of 0.101 for 93 samples). The data were plotted (Figure 2.3) as a function of depth and rock type, and average values were measured for 200 m depth ranges (starting at 450-650 m and continuing down to 2850-3050 m) and then calculated and used to create a best-fit exponential curve to the data. Using the best-fit curve ($y = 3180.6e^{-7.221x}$), we predict the following average matrix porosities with depth (Table 2.1).

Table 2.1. Estimated average matrix porosities based on fit of exponential curve to SS-GF porosity data (see Figure 2.3)

Depth (m)	Predicted porosity
500	0.256
1000	0.160
1500	0.104
2000	0.064
2500	0.033
3000	0.008

Using the information from the CalGEM database, the midpoint depths of the production zones for the 29 production wells (i.e., halfway between the casing shoes and the bottom of the wells) range from 814 to

1929 m, with an average depth of 1393 m (see Appendix Chapter 2). Using the predicted porosity curve, we find that this depth equates to a porosity of 0.114, very close to the measured average porosity value of 0.112 for all core samples.

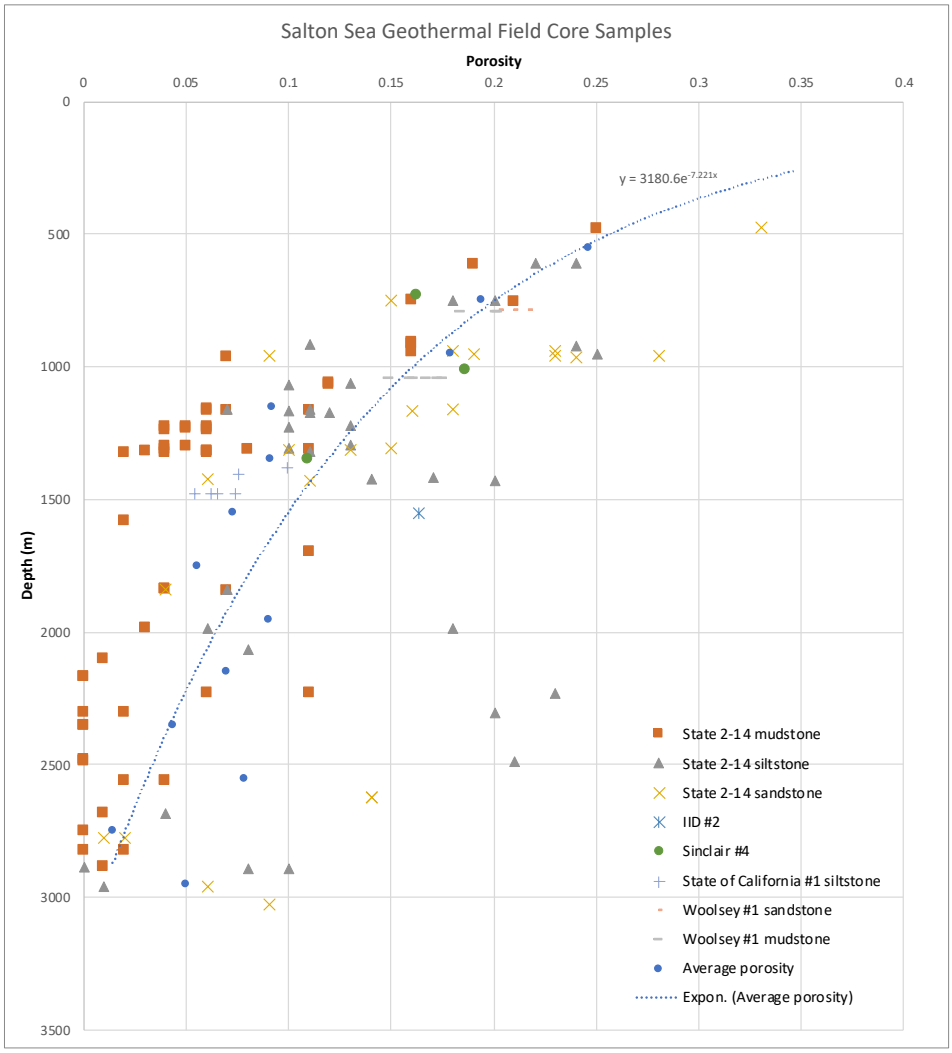

Figure 2.3. Plot of compiled core matrix porosity measurements from the SS-GF, using data from Somerton (1973), Somerton et al., (1974), Tewhey (1977), and McDowell (1987). Average values determined at 200 m intervals were used to fit an exponential curve.

Note that a wide range of porosities are observed, and that while mudstones and siltstones tend to generally have lower porosities than sandstones, their porosity values overlap. Note also that matrix porosity measurements do not include fracture porosity, which becomes increasingly important at depth. A fracture porosity component of 1% has been added to the probable SS-GR resource calculations based on previous estimates of dual porosity at The Geysers geothermal field by Antúnez et al. (1994), who stated "A 1% fracture porosity (secondary porosity) was assumed based on the work of Weber and Bakker (1981). Hulen et al. (1991, 1992) reported fracture porosity values in the order of 1.5% based on porosity and permeability enhancements due to calcite dissolution." The fracture porosity component is not included in the more conservative "proven" estimate of the reservoir volume.

Lithium Concentration of Brine

Published analyses of the Li concentration of Salton Sea geothermal brines (see Appendix Chapter 3: Salton Sea Brine Compositions) range considerably in value, from less than 100 ppm up to 400 ppm (e.g., Skinner et al., 1967; Helgeson, 1968; Muffler and White, 1969; Werner and Olson, 1970; Palmer, 1975; Hoffman, 1975; Featherstone and Powell, 1981; Maimoni, 1982; Michels, 1986; Zukin et al., 1987; Williams and McKibben, 1989; McKibben and Hardie, 1997). However, when using flash-corrected brine compositions with total dissolved solids (TDS) values between 20 and 27 wt.%, the samples have a smaller range of values (141-287 ppm), with an average value of 198 ppm Li.

Lithium Estimates for Brine-in-Place

The combination of resource areal extent, reservoir thickness and porosity, and lithium concentration in the brine can be used to derive estimates for the total brine lithium resource for the proven (drilled) resource (corresponding to the white dashed outline in Figure 2.1), the probable resource (corresponding to the solid red outline in Figure 2.1), and the accessible resource (the portion of the probable resource that is accessible from drilling on land). These estimates are presented in Table 2.2. Note that these estimates do not represent how much lithium can be recovered from this resource; those values will be lower, depending on how low the brine lithium concentration can drop before lithium recovery from the brine becomes uneconomic. Two important equations for calculating lithium estimates are as follows:

- Area (km^2) x Thickness (km) x Porosity = Pore Volume (km^3)
- Pore Volume (km^3) x Brine Density (kg brine/L brine) x Concentration (mg Li/kg brine) = kg of Li in reservoir brines

Table 2.2. Estimates of the lithium brine resource at the SS-GR

	Areal Extent (km^2)	Thickness (km)	Porosity	Pore volume (km^3)	Lithium conc. (ppm)	Lithium (ktons)	Lithium (ktons LCE)
Proven	30.8	1.1	0.114	3.862	198	760	4100
Accessible	69.8	1.5	0.124	12.98	198	2600	13700
Probable	91.9	1.5	0.124	17.09	198	3400	18000

Accessible represents areal extent of probable reservoir that can be accessed from land-based wells. Assumes 1 L brine under reservoir conditions ≈ 1 kg brine (Younker et al., 1982; Williams, 1997). It is important to note the distinction between estimates of lithium metal or ion and lithium carbonate equivalent (LCE). One ton of lithium (Li) is equivalent (i.e., has the same amount of lithium) to 5.32 tons of lithium carbonate (Li_2CO_3).

Available Lithium from Currently Produced Brines at the SS-GR

In addition to the overall brine reservoir at the SS-GR, it is possible to estimate potential lithium production from the existing geothermal wellfield based on current annual brine production rates and lithium concentrations in the brine. Besseling (2018), evaluating the potential for lithium production from the CalEnergy portion of the SS-GF, estimated that 90 thousand metric tons of LCE could be produced annually from the 10 power plants in their existing well field.

The average annual brine production and the concentration of lithium in the brine can be used to estimate the amount of lithium that could potentially be recovered from the existing well field of Berkshire Hathaway Energy Renewables (BHER) and Energy Source Minerals (ESM). Figure 2.4 shows the cumulative annual brine injection and production amounts from all wells in the SS-GF, using monthly production and injection data compiled by CalGEM. Between 2004 and 2022, average annual brine production has been 120,841,748 metric tons, with annual amounts varying between 107,529,379 metric tons in 2011 and 131,674,002 metric tons in 2015.

Using this average production amount and the average brine Li composition of 198 ppm, the amount of Li contained in this amount of brine corresponds to 23.9 thousand metric tons of Li, equivalent to 127 thousand metric tons of LCE. Assuming a recovery factor of 90%, the expected amount of Li that could be produced annually from these wells would be 21.5 thousand metric tons of Li, equivalent to 115 thousand metric tons of LCE. This value is higher than that reported by Besseling (2018), which only represents the CalEnergy portion of the producing field; our estimate also includes the Hudson Ranch area. Note that this initial annual Li production rate is expected to decline over time, as Li-poor brine is reinjected back into the reservoir, slowly diluting and lowering the Li concentration of the brine in the reservoir.

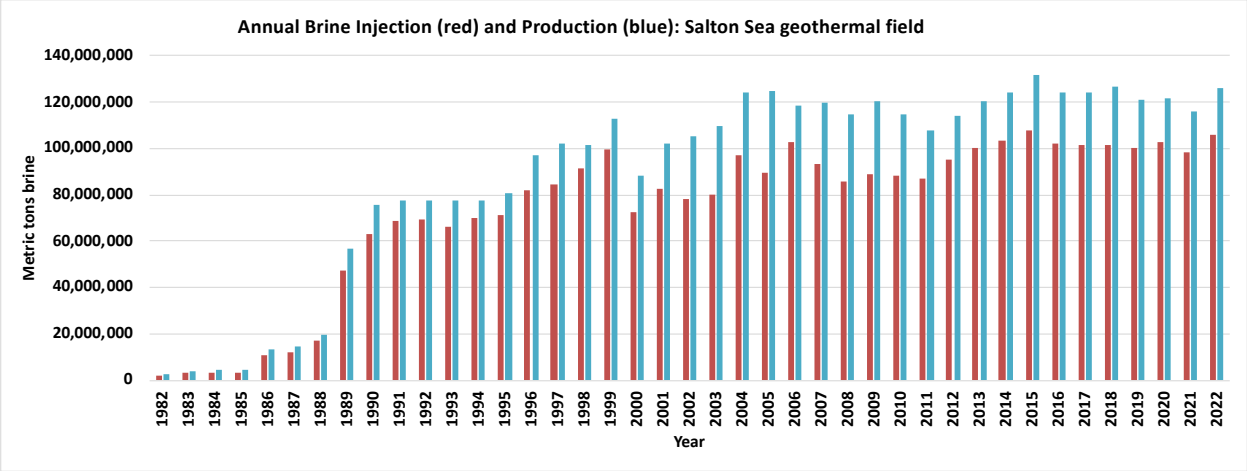

Figure 2.4. Cumulative annual brine production (blue bars) and injection (red bars) at the SS-GF from 1982 to 2022. Data obtained from CalGEM. Injection amounts are less than production due to loss of flashed steam and precipitated filter cake mass during energy generation.

Lithium in the Reservoir Rocks

An important question is how much Li remains in the reservoir rock, as it could potentially supply additional dissolved content by reaction with reinjected, depleted brines. Two data sources can provide insight into this. An unpublished data set consisting of chemical analysis of various elements in Salton Sea geothermal drill cuttings and other rock samples was collected by L.J.P. Muffler and other USGS scientists in the early 1970s. This data set was transmitted to S.D. McDowell in the 1980s and to M.A. McKibben in 2020. Figure 2.5 below shows the Li data for these samples, with a range from 15-80 ppm and an average of 40 ppm. This figure also includes whole-rock Li analyses for core samples from the State 2-14 well that were analyzed as part of this study (see Table 2.3 below).

Berkeley Lab conducted a full chemical analysis (by acid-digestible inductively coupled plasma mass spectrometry, ICP-MS) of outcrop and core samples used by Humphreys et al. (2023) for their laser ablation (LA-ICP-MS) spot analysis of Li in minerals. The data are shown in Table 2.3 below, and the six core samples show a similar Li range (6.7-83.9 ppm) and average (38 ppm) compared to the USGS data set.

These two sets of bulk sample assays give a good indication of the average amount of Li found in the reservoir rocks (~40 ppm). In contrast, Li contents of individual mineral grains can range from a low of 0 ppm to values of over 500 ppm, as seen in chlorites (Humphreys et al., 2023).

Mass Distribution of Lithium between Brine and Rock in the Reservoir

At reservoir temperatures, the brines (198 ppm Li) have a density of about 1.0 g/cm^3 (Younker et al., 1982; Williams, 1997). The reservoir rocks (40 ppm Li) have bulk densities of about 2.7 g/cm^3 (McDowell, 1987). It is easily shown (using Pore Volume x Brine Density x Concentration) that at ~12% reservoir porosity, a given volume of total reservoir (rock plus brine) contains more than four times as much mass of Li in its solid rock than in its brine. This implies that, depending on the kinetics of reactions between Li-depleted reinjected brine and Li-bearing reservoir rocks, some replenishment of dissolved Li to the reinjected brine may be feasible. This discussion is further explored in Chapter 6 on reactive transport.

Lifetime of Lithium Extraction

Given the above estimates of potential rates of Li production and the size of the in-brine Li reservoir, calculations can be made regarding the potential lifetime of Li production from the field. These calculations, derived from dividing the Li resource size by the Li production rate, do not account for the effect of depletion of the reservoir in lithium, which may reduce the lifetime by causing the production to become uneconomic at an earlier date. At a production rate of 115 kilotons per annum (ktpa) LCE, the proven resource (4.1 million metric tons of LCE) could last 35.7 years. Chapter 6 of this report contains a simulation that projects existing production and injection rates, while recovering Li from the brine, which demonstrates that the produced brines will have decreasing Li concentrations over time (see Chapter 6 for details). The current geothermal resource has operated for over four decades (since 1982) with no significant decline in brine production or dissolved metal concentrations. Nonetheless, the cumulative impacts of drilling new production and injection wells and installing new plants on Li concentrations should be carefully monitored, as both thermal and chemical breakthrough will need to be minimized in optimizing the reservoir performance when Li extraction is included as part of the geothermal field operations.

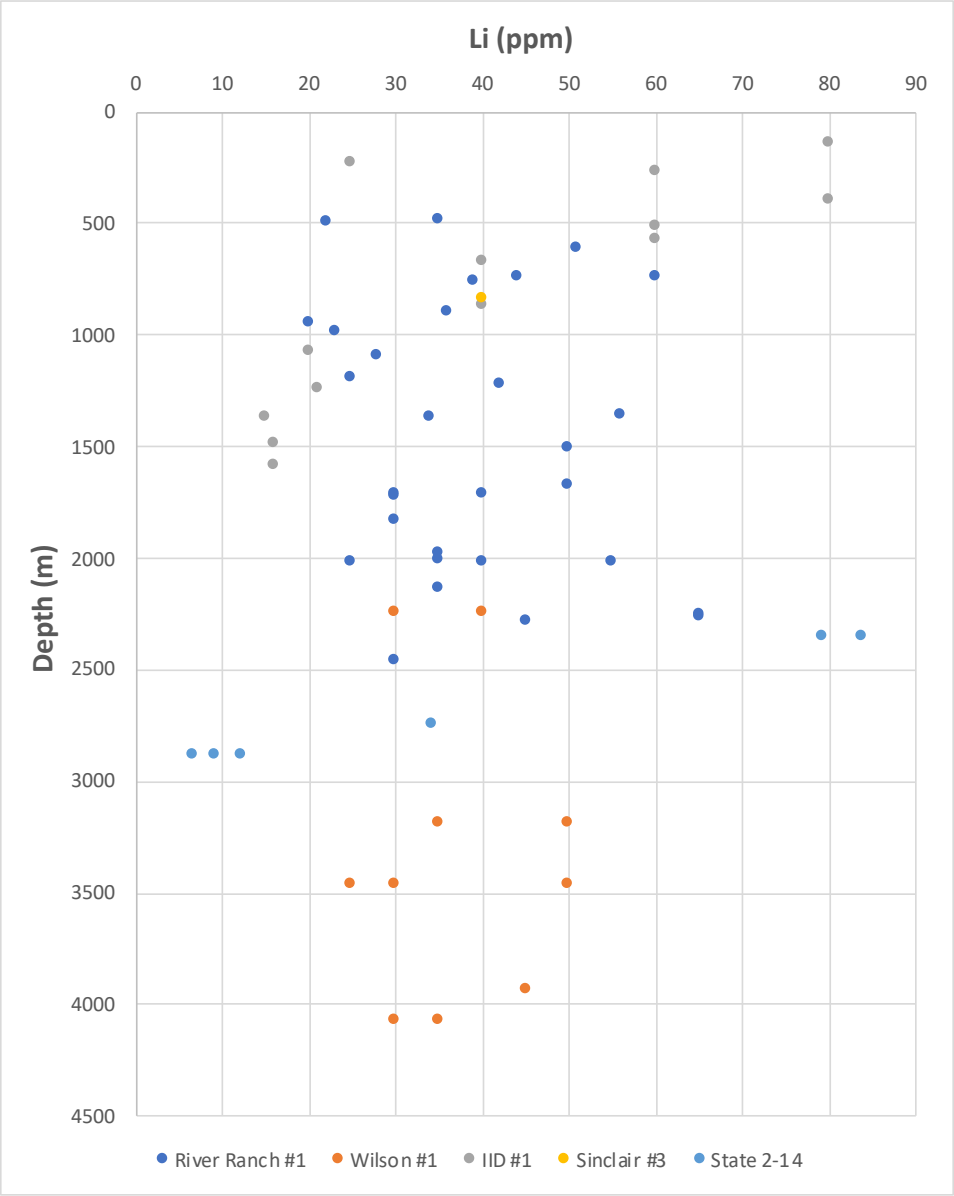

Figure 2.5. Variation of Li metal content in parts per million (ppm) versus depth (m) for cuttings and core from several drill holes in the SS-GF. From McKibben et al., 2021 (courtesy of USGS unpublished data) and this study (State 2-14 samples).

Table 2.3. Results of acids-digestion method (EPA 3051A) and ICP-MS analysis by Berkeley Lab of hand-picked separates of core and outcrop samples used by Humphreys et al. (2023).

Sample ID	Locality and rock type	Li ppm
DH_01a	Durmid Hills mudstone	96.87
DH_01b	Durmid Hills mudstone	114.68
mmAnh_a.b	Anhydrite with mudstone	0.00
mmAnh_b.b	Anhydrite with mudstone	18.65
2881.99m_c.c	State 2-14 well	6.72
2881.99m_c.b	State 2-14 well	12.28
2881.99m_c.a	State 2-14 well	9.16
2744.6m_a	State 2-14 well	34.16
2357.8m_a	State 2-14 well	83.87
2357.8m_b	State 2-14 well	79.15

Summary

The proven minimum footprint of the geothermal resources is 30.8 km^2 with a thickness of 1.1 km, while the accessible footprint from onshore wells is estimated at 69.8 km^2. The probable resource footprint according to structural and geophysical data is 91.9 km^2, with a thickness from thermal anomaly data of 1.5 km. The proven lithium concentration in brine (based on average flash-corrected brine analyses) is 198 ppm. The average measured reservoir matrix porosity is 0.114, but the likelihood of an additional 1% of fracture porosity brings the probable porosity to 0.124.

Using these values and the two equations below, the reservoir is estimated to contain 4 million metric tons of LCE of proven lithium resource and 18 million metric tons of LCE of probable lithium resource.

- Area (km^2) x Thickness (km) x Porosity = Pore Volume (km^3)
- Pore Volume (km^3) x Brine Density (kg brine/L brine) x Concentration (mg Li/kg brine) = kg of Li in reservoir brines

The current production wells have brine production rates corresponding to a potential lithium production of 115 kilotons LCE per annum, sustainable over a lifetime of at least 36 years. Plans for expansion of this field's energy output over the next decade could double or triple this LCE production rate, making the region a substantial domestic supplier of lithium to the U.S. and helping meet the nation's green energy needs throughout the 21st century.

SECTION TWO:
Lithium and Reservoir Behavior

Chapter 3: Brief Geologic History of the Region

Key Takeaways

- The Salton Trough is a continental rift zone filled with more than 6 km of marine, deltaic, alluvial, and lacustrine sediments.
- The area is also characterized by bimodal volcanism (rhyolitic domes and basaltic intrusions) over the past million years; this activity is associated with the rifting.
- Due to crustal thinning and deep magmatic intrusions, the entire Salton Trough experiences an abnormally high heat flux of >100 mW/m^2. This heating yields hot, advecting brine in the subsurface.
- Over the previous thousands to millions of years, the Colorado River has periodically filled the Salton Trough with eroded sediments and water that has evaporated over time, producing sequences of basinal brines amid evaporite and sedimentary deposits.

The Salton Sea Geothermal Reservoir (SS-GR) is located in Southern California, 60 km north of the United States-Mexico border, on the southeastern shore of the Salton Sea (Figure 3.1). This region is shaped by a variety of tectonic processes related to the subduction of the Farallon slab (until ~12 mega-annum [Ma], or million years) and change from subduction to the strike-slip and ongoing extensional motion (e.g., Atwater, 1970; Mammerickx and Klitgord, 1982; Stock and Hodges, 1989). The Salton Trough is a continental rift zone (Figure 3.2) that is characterized by a series of right-stepping dextral faults that link the East Pacific Rise to the San Andreas Fault system (Dorsey, 2006). In the extensional gaps between these step-over faults, there are a series of smaller spreading centers bounded by northwest-trending strike-slip faults and northeast-trending normal faults (Hulen et al., 2002). At present, the Salton Sea is underlain by a series of transform faults and pull-apart basins that formed as a consequence of the rifting associated with the opening of the Gulf of California (e.g., Elders et al., 1972; Han et al., 2016).

Since the onset of subsidence at ca. 8.5-7 Ma, nearly continuous deposition has filled the Trough with more than 6 km of marine, deltaic, alluvial, and lacustrine sediments (Dorsey et al., 2011). The late Miocene was marked by moderate crustal thinning and basin subsidence, which resulted in a deep marine incursion into the Salton Trough. The Imperial Group, a thick marine transgression of fossiliferous claystone and siltstone, was deposited during this time (Dorsey et al., 2011). During a period of increased subsidence in the Pliocene, the nascent Colorado River began depositing a large volume of fluvial sediments into the northern portion of the Trough. The delta plain was characterized by avulsing channels and flood plains that quickly prograded southwards (Dorsey et al., 2011). This period corresponds with the thick arkosic sandstone and intermittent argillaceous intervals of the Palm Springs Formation (Dorsey, 2006). By 2 Ma, right lateral motion on the San Andreas Fault moved the exit point of the Colorado River south of the contemporary Salton Sea (see Figure 3.2.D). The southward migration of the exit point led to the southward expansion of the perirenal Borrego Lake. This changing environment correlates with the thick claystone, siltstone, and fluvial sandstone lens of the Borrego

Formation (Dorsey, 2006). During the early Pleistocene to Holocene, the Colorado River would alternate its flow direction, resulting in repeated flooding and drying cycles of paleolake Cahuilla (McKibben, 1991). This period corresponds with the development of the Brawley Formation of lacustrine mudstone and evaporitic deposits that serves as the impermeable cap to geothermal fluids (Helgeson, 1968).

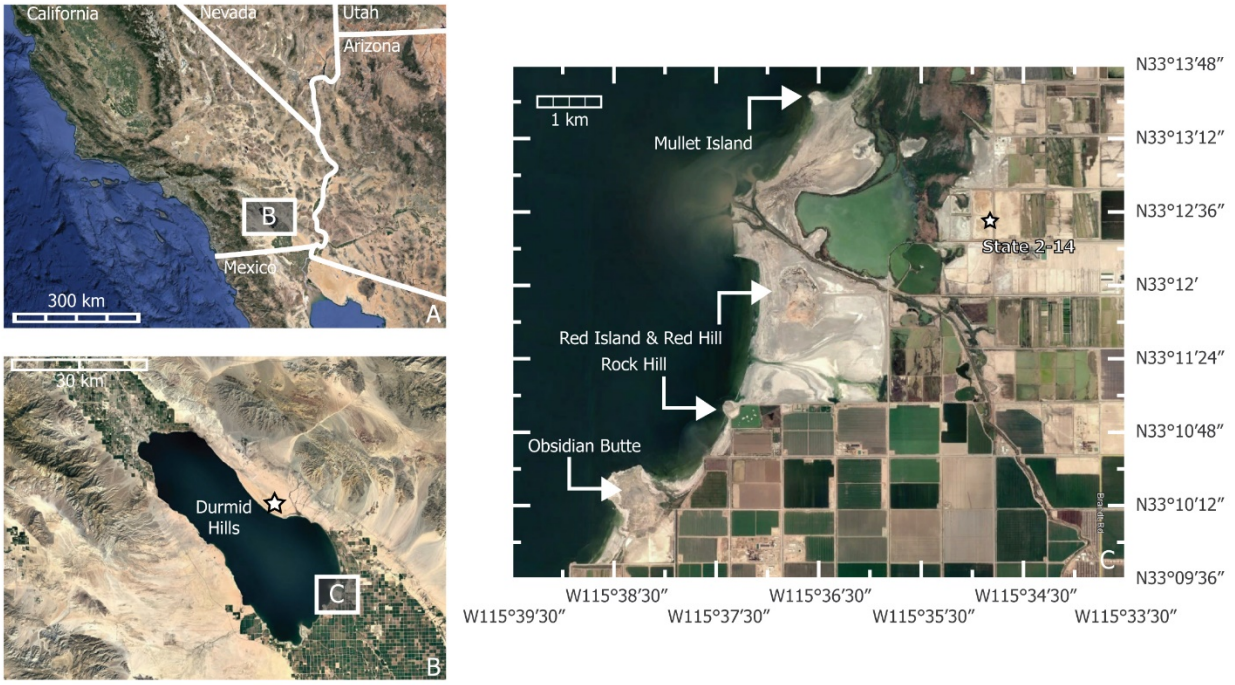

Figure 3.1. A. Regional map of Southern California. B. Map of Salton Sea. The sampling location for the Durmid Hills is labeled with a star. C. Map of the northern part of the SS-GR. Rhyolitic domes are labeled and indicated with arrows. The location of State Well 2-14 is labeled and indicated with a star.

Today, the Colorado River predominately drains southwards into the Gulf of California, but historically it has periodically re-routed northwards, filling the Salton Trough with water and eroded sediments of the Colorado Plateau. This process created repeating instances of lakes in the Salton Trough basin (e.g., Van De Kamp, 1973; Wilke, 1976; Waters, 1983; Philibosian et al., 2011; Tompson, 2016; Rockwell et al., 2022). These ancient evaporative lakes are collectively referred to as "Lake Cahuilla," after the Cahuilla people who live in the Salton Trough (MacDougal, 1914). When the Colorado River would eventually route back to draining southwards into the Gulf of California, Lake Cahuilla would evaporate over the course of ~60 years (Wilke, 1976; Waters, 1983), producing saline lakes and then sequences of evaporite and sedimentary deposits (Van De Kamp, 1973; Rex, 1983). This filling-evaporation cycle took place seven times in the past 2,500 years (Rockwell et al., 2022), and is believed to have been ongoing since ~4 Ma (Winker and Kidwell, 1986). During this time, sedimentation has kept pace with the subsidence caused by rifting beneath the Salton Trough (e.g., Lonsdale, 1989), producing thick sections of sedimentary rocks rich in evaporite minerals (2-4 km thick; e.g., Elders and Sass, 1988).

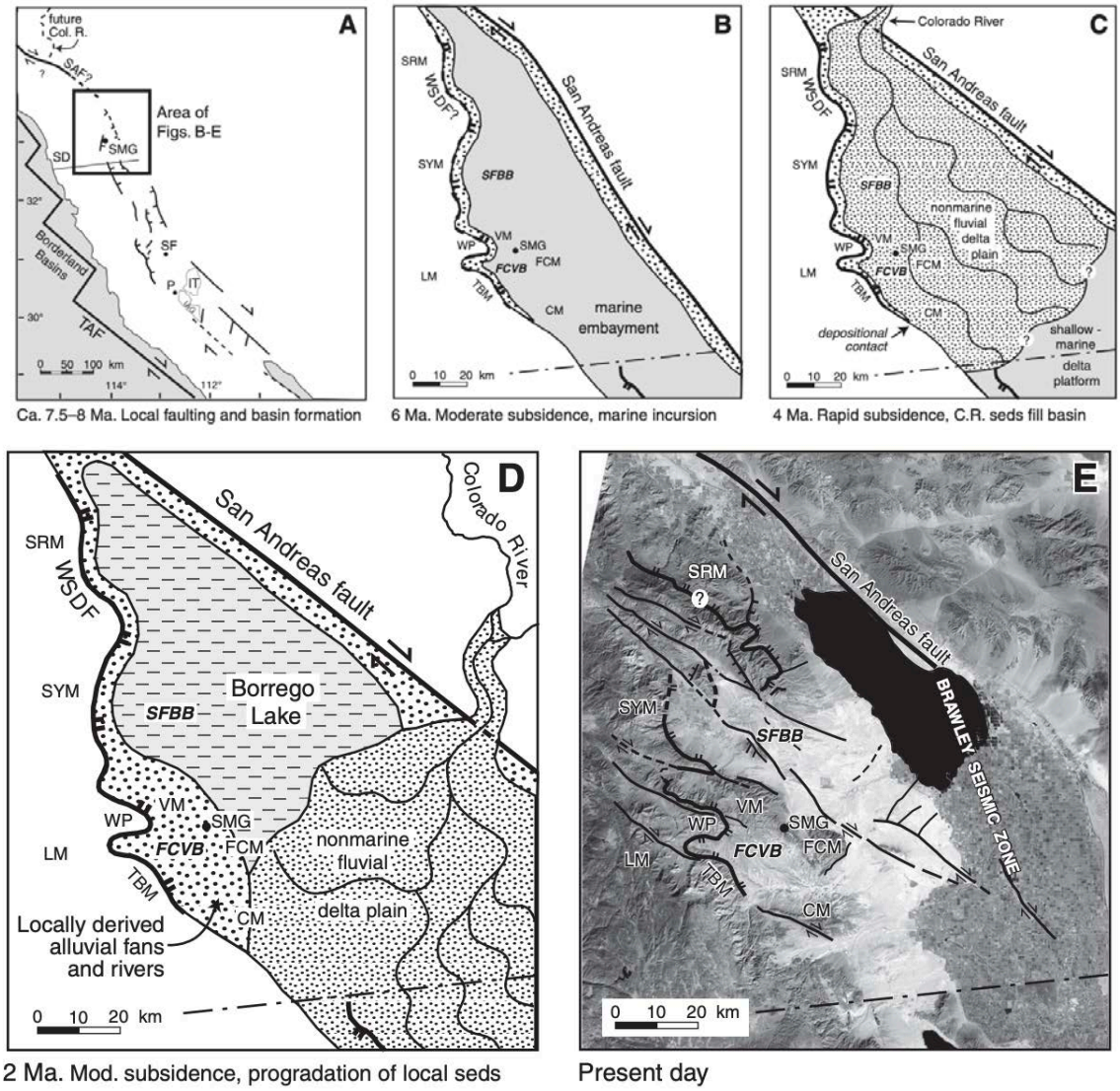

Figure 3.2. Paleogeographic reconstructions of the Salton Trough and surrounding region at 7.5–8, 6, 4, and 2 Ma by Dorsey et al., 2011.

Due to crustal thinning and deep magmatic intrusions, the entire Salton Trough experiences an abnormally high heat flux of >100 mW/m^2 (Lachenbruch et al., 1985). Even higher heat flows of >500 mW/m^2 are concentrated in the area due to localized Quaternary volcanism and upwelling of hydrothermal fluids (Sass et al., 1984). The sedimentary units within the area have been heated from depth due to prolonged rifting in the Trough and associated silicic magmatism (Elders et al., 1972; Han et al., 2016). This heating yields hot, advecting brine and progressive metamorphic-grade rocks. For example, in the State Well 2-14 drill core, these metamorphic grades are a chlorite-calcite zone from ~610-2,480 m depth and from ~180-325°C; a biotite zone from ~2,480-3,000 m depth and from ~325-350°C; and a clinopyroxene zone from ~3,000-3,180 m depth and with temperatures greater than ~350°C, with all zones corresponding to the first appearance of the characteristic minerals for that grade (Cho et al., 1988; Sass et al., 1988). Previous studies on rocks in the Salton Trough have noted that the appearance of chlorite coincides with the disappearance of kaolinite, ankerite, dolomite, calcite, and

quartz (Muffler and White, 1969; Cho et al., 1988), and chlorite has also been observed as replacing plagioclase in thin sections (McDowell and Elders, 1980). These previously observed minerals are similar to the minerals proposed in sodium/lithium (Na/Li) geothermometry to form and break down to equilibrate sodium and lithium concentrations with each other (Sanjuan et al., 2014; Sanjuan et al., 2022).

Surface expressions of this subsurface heating and magmatism can be seen on the southeastern shore of the Salton Sea, where five rhyolitic domes are located (see Figure 3.1.C) that are estimated to be ~2,000-12,000 years old, reflecting uncertainties in dating methods (Robinson et al., 1976; Wright et al., 2015; Schmitt et al., 2019). Beneath these domes, starting at ~1,500 m depth, are a series of buried extrusive and intrusive rhyolites that are ~450,000 years old (Schmitt and Hulen, 2008). The repeated episodes of volcanism in this region are the shallow expression of the long-standing nature of the deep magmatic activity taking place under the region and the associated extensional plate-tectonic-related heat source. This unique focus of tectonic, hydrological, and geomorphological events resulted in the sediments, host rocks, and pore waters that exist at depth beneath the Salton Sea today, including the source of the geothermal brines currently being used to power the SS-GF (e.g., Coplen, 1976; Rex, 1983; Waters, 1983; McKibben et al., 1988; Brothers et al., 2022).

Currently within the SS-GR are two immiscible, density-stratified and distinct fluids: (1) a cooler, lower salinity (<10 wt% total dissolved solids [TDS], ρ = 0.85 g/cm^3) fluid on top; and (2) an underlying hot, hypersaline (>20% TDS, ρ = 1.0 g/cm^3) brine (Williams and McKibben, 1989; Williams, 1997). The interface between the lower salinity fluid and the hypersaline brine approximately follows the depth of the 250°C isotherm in the geothermal field, such that in locations where the 250°C isotherm is shallowest, so too is the depth of the low salinity-hypersaline-brine interface (Williams and McKibben, 1989). This relationship between the brine boundary layer and the 250°C isotherm connects the existence of this hypersaline, geothermal (and Li-bearing) brine to the heat source in this region (Williams and McKibben, 1989). Previous studies of SS-GR hypersaline brines have found that these brines contain on average ~200 ppm Li (Skinner et al., 1967; Helgeson, 1968; Maimoni, 1982; Williams and McKibben, 1989; McKibben and Hardie, 1997).

This brief description of the overall geologic of the region is presented to provide general context for the more detailed investigations and modeling efforts presented in the following chapters.

Chapter 4: Distribution and Isotopic Composition of Lithium in the Salton Sea Geothermal Reservoir

Key Takeaways

- The highest solid state lithium concentrations are found within mudstones and decrease with depth, with surface mudstones containing ~106 ppm lithium, mudstones at 2358 m containing ~82 ppm lithium, and mudstones from 2745 m containing ~34 ppm lithium.
- The mineral chlorite appears to be the main mineral host of lithium in the reservoir rocks, with solid values of over 500 ppm lithium.
- There is less lithium in chlorite grains from regions with higher temperatures.
- The lithium isotope compositions of the Salton Sea geothermal brine exhibit a very narrow range of values (δ^7Li_{avg} = +4.1 ± 0.3 ‰), indicating a well-mixed brine reservoir.

Introduction

This chapter focuses on evaluating potential sources of lithium (Li) by measuring the concentration of lithium in different rocks found above and within the SS-GR, and identifying which minerals contain elevated concentrations of lithium. Also in this chapter are measurements of the lithium isotopic compositions of both sampled geothermal brines and selected rock samples from this area, with the goal of using the isotopic signatures as a way to identify the sources of lithium contained in the geothermal brines. This work relies on analysis of a suite of representative rocks (from outcrops and drill core) and geothermal brine samples. From these were obtained detailed elemental maps using the imaging approach of backscatter scanning electron microscopy (SEM), which were used to identify the minerals in the analyzed rock samples. Laser ablation induced coupled plasma mass spectrometry (LA-ICP-MS) was used to measure the lithium concentrations of different mineral phases within the analyzed rock samples. Selected rock and brine samples were analyzed to determine their lithium isotope compositions. Taken together the data are used to better understand the chemical and physical behavior of lithium in the solids and liquids that make up the SS-GR.

Lithium Contents of Rock and Constituent Mineral Phases

Detailed petrographic descriptions and photographs of the samples studied are included in Appendix Chapter 4, along with descriptions of the analytical methods used. (Appendix Chapter 4 also includes a description of the contributions of two interns, Hoover and Wenzel, to this project; see "Broader Impacts: Mineralogic Investigation Interns.") The remainder of this section describes the results of the analysis of the samples shown contained in Appendix Chapter 4.

Rhyolitic Samples

Surface rhyolitic rocks were collected from Obsidian Butte and Rock Hill (Figures A4.1 and A4.2). Lithium concentrations of these rocks vary, depending on mineralogy (1.1 ± 0.3 – 91 ± 2.3 ppm for the various minerals from Obsidian Butte and 13 ± 0.5 – 90 ± 1.9 ppm for the various minerals from Rock Hill; Humphreys et al., 2023). The highest Li concentrations are found in volcanic glass (Obsidian Butte,

91 ± 2.3 ppm; Humphreys et al., 2023) and plagioclase (Rock Hill, 90 ± 1.9 ppm; Humphreys et al., 2023). Buried, hydrothermally altered rhyolitic rocks from commercial drill wells in the SS-GF at depths from 1573 m (5160 ft) to 2655 m (8710 ft; Schmitt and Hulen, 2008) have Li concentrations ranging from 2 ± 0.9 – 68 ± 2.0 ppm (Humphreys et al., 2023), with quartz having the highest Li concentrations (highest = 68 ± 2.0 ppm with an average = 42 and a standard deviation = 13 ppm; Humphreys et al., 2023).

Sedimentary and Evaporitic Surface Samples

Surface sedimentary and evaporitic rocks were collected from the Durmid Hills (Appendix Chapter 4: Figures A4.3-A4.6; Babcock, 1974), which correspond to unmetamorphosed equivalents of the rock types found in the SS-GR. The Li contents of the Durmid Hills surface sedimentary and evaporitic rocks vary by rock type. Sandstone has low concentrations of Li (0.8 ± 0.3 ppm, Humphreys et al., 2023). The groundmass of the mudstone rock and the mudstone that is interbedded with gypsum has relatively high lithium concentrations (142 ± 2.45 – 177 ± 5.11 ppm, Humphreys et al., 2023). These values are slightly higher than the reported Li concentrations (104 – 136 ppm) measured in the clay-size fraction of near-surface sediments from the Salton Sea (Sturz, 1989) and the whole rock measurements from this study (97 ± 5.1 – 115 ± 4.8 ppm, Humphreys et al., 2023). Lithium contents for the cryptocrystalline gypsum are <1 ± 0.1 ppm (Humphreys et al., 2023).

Subsurface Samples

State Well 2-14 Rock Samples

Like the surface samples, the Li concentrations of the metasedimentary rocks vary according to the mineralogy of the rock and, because mineralogy is tied to metamorphic grade, with depth. Monomineralic epidote ejecta from a flow-test at 1866 m has <1 ppm Li (Humphreys et al., 2023). Interbedded anhydrite and shale have whole-rock Li concentrations of 79.2 ± 2.9 – 83.9 ± 6.6 ppm (Humphreys et al., 2023). Spot analysis Li concentrations for this sample range from <1 ± 0.1 – 581 ± 12.17 ppm (Humphreys et al., 2023) with chlorite grains consistently yielding the highest Li concentrations for this section (269 ± 2.58 – 581 ± 12.17 ppm). An epidote grain from an epidotized metasedimentary rock from ~2485 m depth has 2.7 ± 0.3 ppm Li (Humphreys et al., 2023). Whole rock interbedded anhydrite and mudstone from ~2745 m depth have 34.2 ± 3.2 ppm Li (Humphreys et al., 2023) and a range from <1 ± 0.1 – 87 ± 1.6 ppm Li for spot analyses in the minerals and the heterogeneous, fine-grained matrix. An epidotized mudstone from ~2819 m depth has <1 ± 0.2 – 18 ± 0.7 ppm Li. The deepest rocks studied are recovered from ~2882 m depth and have a whole rock Li concentration of 6.7 ± 1.6 – 12.3 ± 2.5 ppm (Humphreys et al., 2023). Spot analyses of chlorite yield 70 ± 1.3 – 104 ± 22.2 ppm Li, alkali feldspar yield 2 ± 0.4 – 19 ± 0.6 ppm Li, and groundmass yields 3 ± 0.3 – 43 ± 0.8 ppm Li (Humphreys et al., 2023).

Identification of Lithium Host Minerals

State Well 2-14 rock samples in this study come from the chlorite-calcite (~610-2480 m, ~180-325°C) and biotite (~2480-3000 m, ~325-350°C) metamorphic zones (Cho et al., 1988; Sass et al., 1988). The minerals with the highest measured Li concentrations of any phase in this study are relatively large chlorite grains (rims of chlorite range in thickness from ~40-400 μm in diameter) encasing authigenic

pyrite grains from the calcite-chlorite metamorphic zone (269-581 ppm; Humphreys et al., 2023), which are observed encasing skeletal pyrite grains at ~2358 m depth (Figure 4.1). Pyrite grains in the host rocks of the SS-GF are authigenic, formed during diagenetic sulfide mineralization at temperatures <250°C and metamorphic sulfide mineralization at temperatures >250°C. As temperature increases above 250°C with increased depth, porphyroblastic pyrite grows, then decomposes into skeletal aggregates upon reaction with the geothermal brine (McKibben and Elders, 1985). Since the pyrite grains encased by Li-bearing chlorite measured in this study are skeletal, we interpret these pyrites as being in the process of dissolution via reaction with the brine in which Fe is mobilized out of the pyrite (McKibben and Elders, 1985). This dissolution process happens in tandem with hornfelsic recrystallization of the silicate minerals (e.g., quartz and feldspar) at this depth (e.g., McDowell and Elders, 1980; McKibben and Elders, 1985). Additionally, the appearance of chlorite ($(Mg,Fe)_3(Si,Al)_4O_{10}(OH)_2 \cdot (Mg,Fe)_3(OH)_6$) coincides with the disappearance of dolomite-ankerite ($Ca(Fe,Mg,Mn)(CO_3)_2$) and has been observed replacing feldspar ($KNaCa(AlSi)_4O_8$) in the SS-GF (McDowell and Elders, 1980; Cho et al., 1988). The combination of dolomite-ankerite and feldspar dissolution, in conjunction with hydrothermal alteration, would provide the necessary elements for the formation of chlorite in this setting. It is possible that the process of pyrite dissolution and chlorite crystallization also acts as an oxygen buffer between the host rocks and brine at this depth (McKibben and Elders, 1985).

Chlorite-rich groundmasses (where chlorites are <10 μm in diameter; Figure 4.3) in these same metasedimentary rocks (at a depth of ~2358 m) also have elevated Li concentrations relative to non-chlorite minerals (e.g., anhydrite and pyrite) from similar depths (48-252 ppm in the groundmass compared to 0-6 ppm for anhydrite and pyrite; Humphreys et al., 2023). This observation, along with the observation of elevated Li concentrations in larger chlorite clasts, confirms hypotheses based on Na/Li geothermometry involving Li-bearing micas that suggests that chlorite and other octahedral clay minerals are the most likely hosts for Li in the SS-GR rocks (Sanjuan et al., 2022). In both the larger and smaller groundmass chlorite grains, lithium is incorporated into these grains from the brine in trace quantities within the calcite-chlorite metamorphic zone (i.e., Li is not present as a major element). Li is also present in trace quantities in the surface mudstones, which have somewhat higher bulk Li concentrations than the chlorite-bearing rocks in the calcite-chlorite zone (compare 97-115 ppm Li in surface mudstones to 79-84 ppm at ~2358 m depth; Humphreys et al., 2023), suggesting that there is a net loss of Li from the rocks into the brines, and that the Li that remains in the rock is preferentially incorporated into chlorite compared to other mineral indicators of brine-rock reaction. Rocks in the biotite metamorphic zone have even lower Li concentrations than those in the chlorite-calcite zone (7-34 ppm; Humphreys et al., 2023), suggesting that at high temperatures, more Li is lost from rocks into the brines. The extent to which this temperature dependence extends to higher temperatures – e.g., into the pyroxene zone at 3000 m depth in State Well 2-14 (Cho et al., 1988) – is critical to test in a future study.

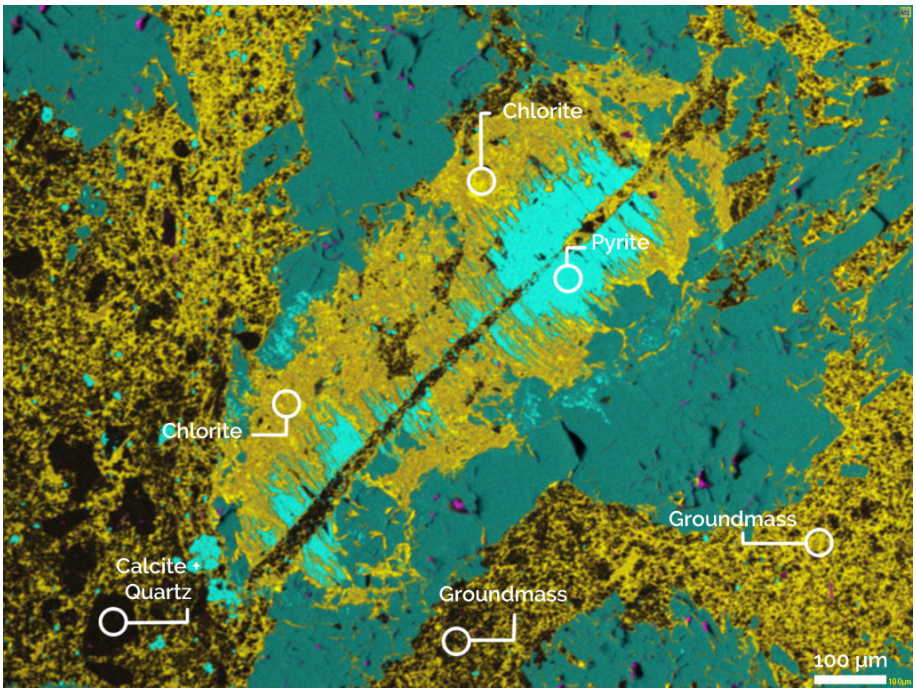

Figure 4.1. Backscatter electron map of metasedimentary anhydrite and mudstone from ~2358 m depth. Relatively aluminum rich regions are represented by magenta, relatively sulfur rich regions are represented by cyan, and relatively magnesium rich regions are represented by yellow. Anhydrite is the dark cyan mineral that is unlabeled on the sample. Relatively large authigenic chlorite surrounds skeletal pyrite.

Correlation with Other Elements

The measured major element chemical compositions of the chlorites in this study overlap with previous measurements of chlorites from the SS-GF (Figure 4.2 A–D; Cho et al., 1988). Chlorite compositions in this study were calculated with $Fe^{3+}/\Sigma Fe = 0.1$, as has been previously observed for chlorites in the SS-GF (Dyar et al., 1992) and on a 14-oxygen basis (Cho et al., 1988). There is a positive correlation between Li and Al ($R^2 = 0.777$; Figure 4.3 A), a moderately positive correlation between Li and Mn ($R^2 = 0.584$, Figure 4.3 C), and a moderately negative correlation between Li and Mg + Fe^{2+} + Fe^{3+} ($R^2 = 0.456$; Figure 4.3 B) in chlorite from the chlorite-calcite zone. In contrast, in the biotite metamorphic zone, there is a negative correlation between Li and Al ($R^2 = 0.491$; Figure 4.3 A) and no other statistically significant relationships between Li and the other major elements in chlorite. In this zone, anhedral chlorite grains are found dispersed among xenoblastic alkali feldspar, epidote, and pyrite grains. There is no correlation between Li and Si in chlorite from either metamorphic zone ($R^2 = 0.092$ at ~2358 m depth and $R^2 = 0.262$ at ~2882 m depth).

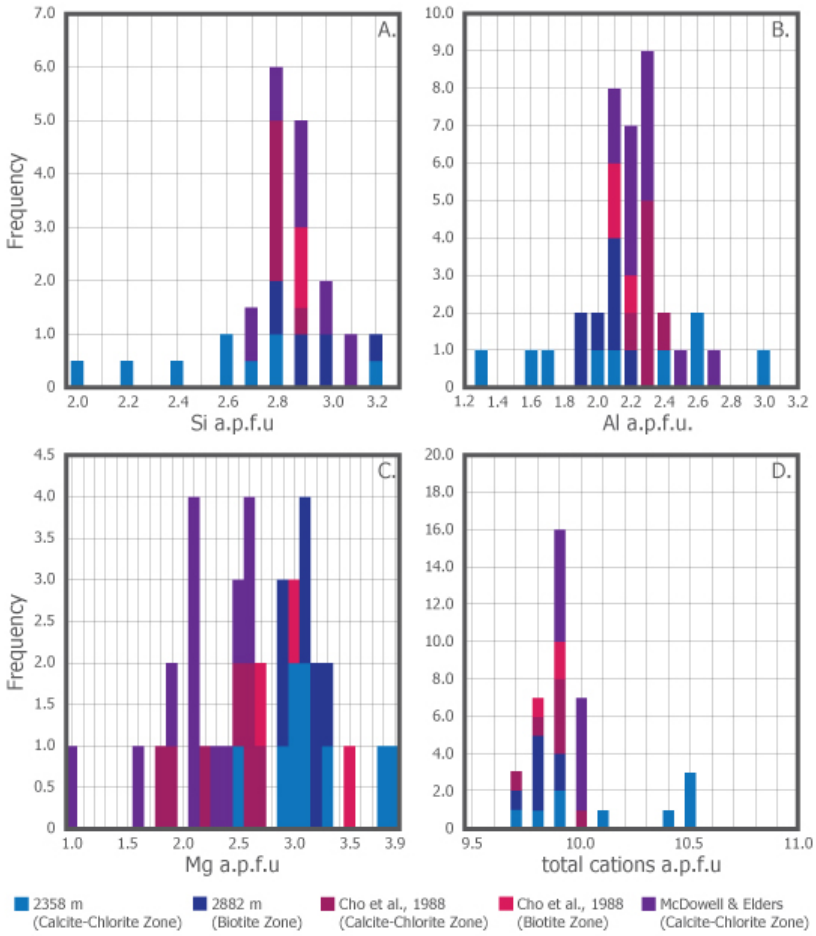

Figure 4.2. Major element comparison of chlorites in this study separated by depth (~2358 m depth, blue; ~2882 m depth, dark blue) with previous studies of the Salton Sea Geothermal Reservoir separated by depth and well (calcite-chlorite zone from State Well 2-14 (Cho et al., 1988), magenta; biotite zone from State Well 2-14 (Cho et al., 1988), pink; calcite-chlorite zone from Elmore 1 (McDowell and Elders, 1980) with equivalent depths to State Well 2-14 calculated from reported temperature (Sass et al., 1988), purple. A. Frequency comparison between samples in this study and previous studies (McDowell and Elders, 1980; Cho et al., 1988) for Si atoms per formula unit (APFU). B. Frequency comparison between samples in this study and previous studies (McDowell and Elders, 1980; Cho et al., 1988) for Al APFU C. Frequency comparison between samples in this study and previous studies (McDowell and Elders, 1980; Cho et al., 1988) for Mg APFU. D. Frequency comparison between samples in this study and previous studies (McDowell and Elders, 1980; Cho et al., 1988) for the sum of all cations (Si + Al + Mg + Fe + Mn + Ti + Na + K + Ca) as APFU.

The strong positive relationship between Li and Al in chlorite from the chlorite-calcite zone indicates that Li substitutes into chlorite together with Al, but the lack of correlation between Li and Si in samples from ~2358 m depth (R^2 = 0.092) indicates that this coupled substitution with Al is not on the tetrahedral Si^{4+} site, as a charge coupled mechanism in the style of $Al^{3+} + Li^{+} = Si^{4+}$. This is supported by the moderately negative correlation between Li and Mg + Fe^{2+} + Fe^{3+} (Figure 4.3. B), the latter of which are two of the other octahedrally coordinated elements in chlorite. The moderately positive relationship between Mn and Li (Figure 4.3. C), further suggests that Li is substituting into an octahedral coordination within chlorite. The partitioning of Li into chlorite is markedly different in the biotite zone: there is no relationship between Si and Al within the calcite-chlorite zone chlorites (R^2 = 0.256); there is a strong negative correlation (R^2 = 0.728) between Si and Al in chlorite grains found in rocks within the biotite

metamorphic zone (Figure 4.3 D). Additionally, there is a weak negative correlation (R^2 = 0.491) between Li and Al within these same rocks (Figure 4.3 A). This suggests that at temperatures >325°C, the incorporation of Al in chlorite occurs in the tetrahedral site, and because these chlorites have lower Li concentrations and display a negative correlation between Li and Al, this substitution is not charge-coupled with Li. The result is that Li may be more incompatible in chlorite at temperatures >325°C in the State Well 2-14 rocks. We caution that the partitioning behavior of Li in chlorite will depend on fluid and mineral compositions and pressure, in addition to temperature, and that these relationships will be important to constrain and/or test with additional measurements.

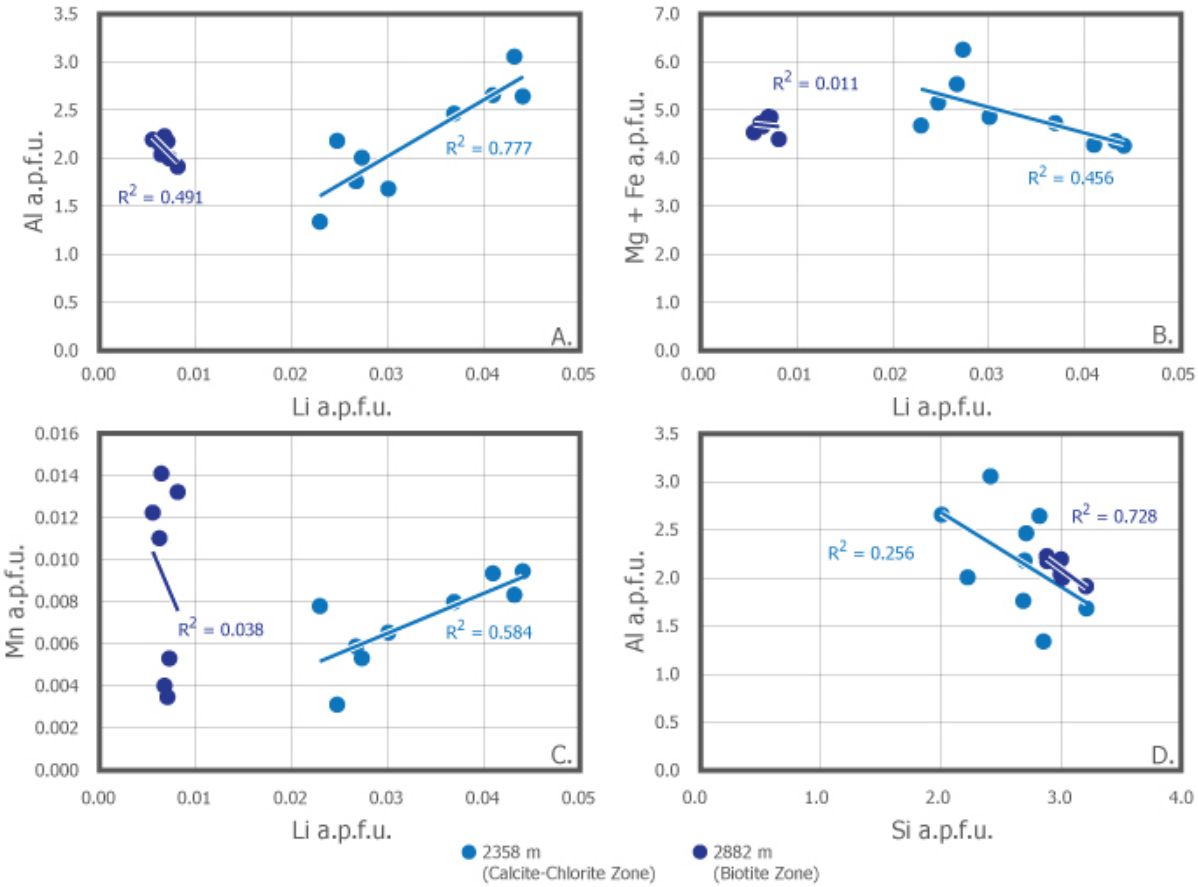

Figure 4.3. Major element comparison of chlorites in this study with Li and Si APFU A. Comparison of Al and Li APFU in chlorites found at ~2358 m depth (blue) and ~2882 m depth (dark blue). B. Comparison of Mg + Fe (Fe^{2+} + Fe^{3+}) and Li APFU in chlorites found at ~2358 m depth (blue) and ~2882 m depth (dark blue). C. Comparison of Mn and Li APFU in chlorites found at ~2358 m depth (blue) and ~2882 m depth (dark blue). D. Comparison of Al and Si APFU in chlorites found at ~2358 m depth (blue) and ~2882 m depth (dark blue).

Lithium Isotope Systematics

Small differences in the concentration of specific isotopes (i.e., atoms of the same element that have different masses) in solids and solutions can be used to trace the source and reactions of those elements. This is done by measuring the concentration of two or more isotopes of a given element in a solid or solution, calculating the measured ratio relative to a known standard ratio for the isotopic system, and then comparing the ratio of those standardized isotopes to the ratio in other standardized solids or

solutions. As chemical reactions move elements back and forth among different solids and solutions, the isotopic ratios for specific elements change and therefore these ratios can be used to understand the behavior of the element. This approach of using isotope ratios was employed as a means of determining the source of Li in the geothermal brines and understanding how the geothermal reservoir functions.

As one of the lightest elements on the periodic table, Li has a large relative difference in the mass between its two stable isotopes, ^{6}Li and ^{7}Li (~17%). This leads to large fractionations (i.e., changes in isotopic ratios) at low temperatures (<250°C; e.g., Chan et al., 1994; Wunder et al., 2007; Millot et al., 2010), such that as the temperature of the fluid decreases, the difference between δ^{7}Li (i.e., the relative increase in the heavier isotope as defined in the following equation: $\delta^{7}Li = [\frac{(^{7Li}/_{6Li})_{sample}}{(^{7Li}/_{6Li})_{standard}} - 1] * 10^{3}$) of the host fluid and the secondary minerals forming from that same fluid increases. For instance, weathering at ambient atmospheric temperatures typically increases the δ^{7}Li of river water ($\delta^{7}Li_{avg}$ = +23‰; Huh et al., 1998) and seawater ($\delta^{7}Li_{avg}$ = +31‰; Millot et al., 2004) compared to both the rocks being weathered (e.g., upper continental crust has a $\delta^{7}Li_{avg}$ = +0.6‰; Sauzéat et al., 2015) and the minerals forming due to weathering (e.g., global average seafloor sediment, also known as GLOSS-II, has a $\delta^{7}Li_{avg}$ = +0.2‰; Plank, 2014).

The fractionation of Li isotopes during fluid-rock interactions occurs because of the preferential incorporation of ^{7}Li into lower coordination environments (e.g., Wunder et al., 2007; Penniston-Dorland et al., 2017 and references therein). Lithium in aqueous fluids is typically in 4-fold, tetrahedral coordination, and many mineral hosts contain Li in a higher 6-fold, octahedral coordination (Figure 4.4). When a fluid containing Li interacts with a rock to precipitate new Li-bearing minerals, ^{6}Li will partition preferentially into the mineral host because of a preference for a higher coordination environment. This process leaves the fluid enriched in ^{7}Li and the new mineral depleted in ^{7}Li. When the fluid and mineral share the same coordination environment (e.g., quartz), the fractionation of Li isotopes is minimized (e.g., Schauble, 2004; Penniston-Dorland et al., 2017 and references therein), as is also the case when fluid-rock interactions occur at progressively higher temperatures (i.e., fractionation is larger at 260°C than it is at 400°C; e.g., Chan et al., 2002; Schauble, 2004; Millot et al., 2010). Lithium isotopes are also susceptible to fractionation due to diffusion on relatively rapid timescales (e.g., Lynton et al., 2005; Marschall and Tang, 2020). For example, Li isotopes between both muscovite and quartz and a chloride-bearing fluid diffusively fractionate between the host fluid and mineral on a timescale of about 30-60 days at high temperatures (400-500°C; Lynton et al., 2005).

Because of these fractionation behaviors, Li isotopes are useful for constraining the extent of interactions between surface and near-surface waters and rocks, such as in the Rhine Graben geothermal brines (Sanjuan et al., 2016), the Qaidam Basin on the northern Tibetan Plateau in China (He et al., 2020), the Central Andes (Godfrey et al., 2013; Munk et al., 2018; Garcia et al., 2020; Godfrey and Álvarez-Amado, 2020), and in the United States (Munk et al., 2011; Araoka et al., 2014). Generally, studies of surface brines compare measured δ^{7}Li and Li concentration of the surface reservoir with surrounding aqueous sources feeding the reservoir to narrow down the potential origins of the Li in the surface brine; these studies also observe other elements and isotopic systems (e.g., Munk et al., 2011; Godfrey et al., 2013; Munk et al., 2018; He et al., 2020). Other studies add to these observations with measurements of brines

at depth (Garcia et al., 2020) or use models to study how fractionation and mixing would change the δ^7Li of the surface Li reservoirs (Araoka et al., 2014; Godfrey and Álvarez-Amado, 2020). Modeling of Li isotopic fractionation of subsurface brines calculated between a solution and solid at a given temperature ($\Delta_{\text{solution - solid}} = 7847/T(K) - 8.093$; Millot et al., 2010) has been used on the hottest Rhine Graben geothermal brines (δ^7Li = +1.0 to +1.7‰) to demonstrate that they are in equilibrium with sedimentary carbonate rocks found within the reservoir, because of the calculated fractionation of Li isotopes between the brine and a rock in equilibrium with the brine, necessitating that the rock have δ^7Li = -6.7 to -6.0‰. This value is too light to be from the granitic rocks in the Rhine Graben reservoir but overlaps with known values for carbonate-bearing sediments (Coplen, 2002), thus indicating that the hottest geothermal brines in the Rhine Graben are from carbonate reservoir rocks (Sanjuan et al., 2016).

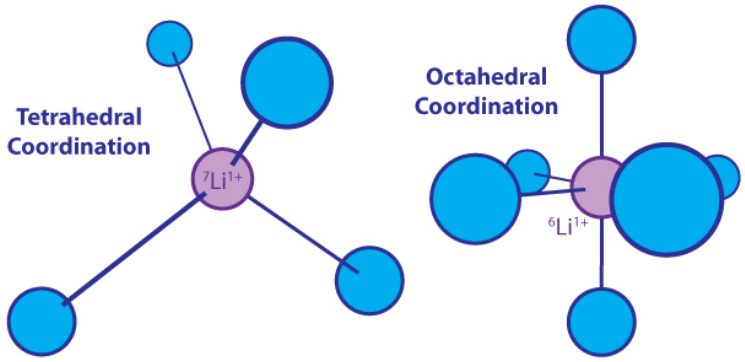

Figure 4.4. Tetrahedral and octahedral coordination of Li. Tetrahedral coordination is preferred by ^{7}Li (e.g., Wunder et al., 2007; Penniston-Dorland et al., 2017 and references therein).

By constraining the behavior of Li isotopic fractionation for the sources and sinks of Li within saline systems, as is the case in the SS-GR, reservoir rocks and brines can (1) provide the record of extent of interactions between surface and near-surface fluids and source rocks in the past, and (2) predict changes in behavior of Li in the future, for example in response to chemical perturbations to the system (as in the case of extracting Li from Li-rich geothermal brine and then reinjecting Li-poor brine back into the geothermal reservoir). This chapter describes the combination of petrography and analytical geochemistry used in identifying the dominant mineral hosts of Li in source rocks in the SS-GR and assessing the extent to which Li may be further recovered from source rocks after reaction with reinjected, Li-poor brines.

Lithium Isotope Compositions of Rocks and Brines from the Salton Trough

Rhyolitic Samples

Whole rock Li isotopic concentrations vary for Holocene rhyolite surface samples (Obsidian Butte has δ^7Li = +3.5 ± 0.04 – +3.8 ± 0.02‰ and Rock Hill has δ^7Li = +8.1 ± 0.03 – +10.3 ± 0.03‰; Humphreys et al., 2023). Buried, hydrothermally altered rhyolitic rocks from commercial drill wells in the SS-GF at depths from 1573 m (5160 ft) to 2655 m (8710 ft; Schmitt and Hulen, 2008) have δ^7Li = +6.4 ± 0.03 – +7.6 ± 0.03‰.

Sedimentary and Evaporitic Surface Samples

The lithium isotopic compositions of the Durmid Hills surface sedimentary and evaporitic rocks vary by rock type. Sandstone has δ^7Li = +5.2 ± 0.08‰, mudstones have δ^7Li = +1.5 ± 0.3‰, while interbedded mudstone and gypsum whole rock samples have δ^7Li = +5.5 ± 0.5 – +6.0 ± 0.06‰ (Humphreys et al., 2023). The cryptocrystalline gypsum has δ^7Li = -9.1 ± 0.06‰ (Humphreys et al., 2023), making it isotopically distinct from the other surface sediment samples.

State Well 2-14 Rock Samples

Like the surface samples, the Li isotopic compositions of the metasedimentary rocks vary according to the mineralogy of the rock and, because mineralogy is tied to metamorphic grade, with depth. Metasedimentary mudstones found at depths from ~1290-1430 m have δ^7Li = 1.8 ± 0.04‰ for the epidotized mudstone (~1290 m depth, Humphreys et al., 2023) and have δ^7Li = +5.7 ± 0.04 – +6.3 ± 0.03‰ for the mudstone with hematite veins (~1430 m depth; see Appendix Chapter 4). Vein material was not analyzed in either of these metasedimentary rocks, and care was taken to sample only the mudstone in these cores. Monomineralic epidote ejecta from a flow-test at 1866 m has δ^7Li = +2.7 ± 0.05 – +3.3 ± 0.03‰ (Humphreys et al., 2023). An epidotized metasedimentary rock from ~2485 m depth has δ^7Li = +2.0 ± 0.03 – 4.3 ± 0.04‰ (Humphreys et al., 2023). An epidotized mudstone from ~2819 m depth has a whole rock δ^7Li = +6.2 ± 0.05 – +7.9 ± 0.04‰ (Humphreys et al., 2023). The deepest rocks studied are recovered from ~2882 m depth and have a whole rock δ^7Li = +4.1 ± 0.03 – +5.1 ± 0.03‰ (Humphreys et al., 2023).

Geothermal Brines

Geothermal brines recovered from multiple geothermal wells in the SS-GF have δ^7Li = +3.7 ± 0.04 – +4.5 ± 0.05‰ (Humphreys et al., 2023).

Comparison to Other Lithium Reservoirs

All but one of the rocks measured in this study have whole rock δ^7Li = +1.5 to +10.3‰; the one outlier has δ^7Li = -9.1‰ (Humphreys et al., 2023). The SS-GR brines in this study have δ^7Li = +3.7 to +4.5‰ (Humphreys et al., 2023), overlapping with that of the rocks, but with less variation. This is consistent with narrow ranges of O and H isotopic measurements of the brine (δ^{18}O = 0 to +3.3‰ and δD = -68 to -75‰), implying that the brine reservoir is internally convecting and well-mixed (Williams and McKibben, 1989). The geothermal brine samples and host rocks in this study overlap in δ^7Li of many potential source materials, including mid-ocean ridge basalt (MORB; δ^7Li = +1.5 to +5.6‰; Moriguti and Nakamura, 1998; Chan et al., 2002; Elliott et al., 2006; Nishio et al., 2007; Tomascak et al., 2008), upper continental crust (δ^7Li = -2.9 to +4.7‰; Teng et al., 2004; Sauzéat et al., 2015), and rivers (suspended and dissolved load, δ^7Li = -5.9 to +43.7‰; Huh et al., 1998; Huh et al., 2001; Kısakűrek et al., 2005; Pogge Von Strandmann et al., 2006; Vigier et al., 2009; Pogge Von Strandmann et al., 2010; Lemarchand et al., 2010; Liu et al., 2015; Pogge Von Strandmann and Henderson, 2015; Dellinger et al., 2015; Pogge Von Strandmann et al., 2020). The samples in this study (brine and rock) also overlap with previous measurements of δ^7Li in Li-rich deposits, including salar brines from the Andes (δ^7Li = +3.7 - +12.6‰; Figure 4.5; Godfrey et al., 2013; Munk et al., 2018; Garcia et al., 2020; Godfrey and Álvarez-Amado, 2020) and Nevada (δ^7Li = -1 - +8‰; Figure 4.5; Araoka et al., 2014) and spodumene Li mines in

Australia, Canada, China, the United States, and Zimbabwe (δ^7Li = -2.83 - +14.7‰; Figure 4.5; Magna et al., 2016; Fan et al., 2020; Desaulty et al., 2022).

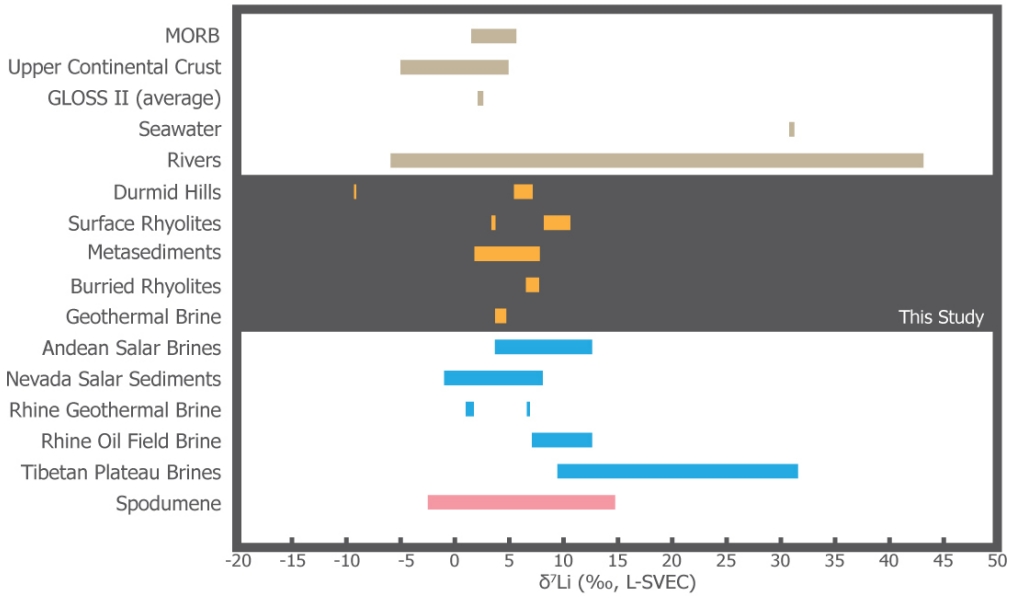

Figure 4.5. The Li isotopic composition for rocks and brines in this study compared to other Li-bearing reservoirs (modified after Penniston-Dorland et al., 2017). Brown bars represent known global ranges for Mid-ocean Ridge Basalt (Moriguti and Nakamura, 1998; Chan et al., 2002; Elliott et al., 2006; Nishio et al., 2007; Tomascak et al., 2008), the upper continental crust (Teng et al., 2004; Sauzéat et al., 2015), seawater (Millot et al., 2004), and rivers (suspended and dissolved load; Huh et al., 1998; Huh et al., 2001; Kısakűrek et al., 2005; Pogge Von Strandmann et al., 2006; Vigier et al., 2009; Pogge Von Strandmann et al., 2010; Lemarchand et al., 2010; Liu et al., 2015; Pogge Von Strandmann and Henderson, 2015; Dellinger et al., 2015). Orange bars represent the rock and brine values measured in this study. Blue bars represent known Li-bearing, location specific isotopic data for the Andean salar brines, Nevada salar sediments, Rhine Graben geothermal brines, Rhine Graben oil field brines (Godfrey et al., 2013; Araoka et al., 2014; Sanjuan et al., 2016; Munk et al., 2018; Garcia et al., 2020; He et al., 2020; Godfrey and Álvarez-Amado, 2020; Desaulty et al., 2022). The Pink bar is for the range in known spodumene isotopic values (Magna et al., 2016; Fan et al., 2020; Desaulty et al., 2022).

The brines in this study are heavier in δ^7Li composition than those reported for Li-bearing geothermal brines from the Rhine Graben (δ^7Li = +1.0 - +1.7‰, 168-190 ppm; Figure 4.5; Sanjuan et al., 2016) and are lighter in δ^7Li composition than oilfield-related brines from the Rhine Graben (δ^7Li = 7.0 - 12.6‰, 6.9 – 72.0 ppm; Figure 4.5; Sanjuan et al., 2016) and the Tibetan Plateau (δ^7Li = 31.3 – 32.‰, 14.4 – 97.5 ppm; Figure 4.5; He et al., 2020). The brine in this study is also lighter isotopically than non-oilfield well brines in the Tibetan Plateau (meteoric: δ^7Li = 31.3 – 32.6‰, 14.4 – 97.5 ppm; ancient brine lake and mountain recharge: δ^7Li = 9.2 – 21.2‰, 8.7 – 408.8 ppm; Figure 4.5; He et al., 2020). The wide range in geologic settings and Li-rich reservoirs that overlap with the isotopic composition of SS-GR rocks and brine in this study necessitates careful quantitative modeling of isotopic fractionation between the brines and the rocks with which the brine is in contact to identify possible source(s) of Li to SS-GR brines.

Changes with Temperature and Depth

Understanding the primary source for the abundance and isotopic compositions of Li in the SS-GR brines is complex, owing to the variety of geologic processes involved in the Salton Trough and the length of

time over which these processes have been affecting the region – from ~4 Ma to present (see Chapter 3; Van De Kamp, 1973; Wilke, 1976; Waters, 1983; Winker and Kidwell, 1986; Lonsdale, 1989; Philibosian et al., 2011; Tompson, 2016; Rockwell et al., 2022). By itself, evaporation of Lake Cahuilla likely had little to no effect on the isotopic composition of the evaporating lake waters, because salt precipitation does not significantly fractionate Li isotopes (e.g., Tomascak et al., 2003; Godfrey et al., 2013). But Li more readily fractionates between fluids and minerals at lower temperatures, and thus fractionation between pore fluid and associated Li-bearing minerals is expected to be greater at shallower to near-surface depths within the SS-GF (e.g., Chan et al., 1994; Chan et al., 2002; Millot et al., 2010). The buried sedimentary and evaporitic rocks are incrementally metamorphosed with increasing depth through hydrothermal interactions until they are in contact with geothermal brines between 330-360°C. Fluid-rock interactions at these and lower temperatures would have driven the recrystallization of clay minerals via reacting with the hot brines at depth (e.g., Helgeson, 1968; Muffler and White, 1969). This process in turn would yield metamorphic mineral assemblages with lighter δ^7Li compositions than the brine, and the brine would become progressively heavier in δ^7Li as the metamorphic mineral assemblage preferentially incorporates ^{6}Li into its crystal structures. Metamorphic minerals forming from brines with progressively heavier δ^7Li compositions would themselves have heavier δ^7Li compositions than minerals formed at earlier stages of this process, though at each stage the metamorphosed clay minerals would be expected to be lighter in δ^7Li than the equilibrium composition's brine. Higher temperatures at depth may have caused the initial release of more Li into the brine from the buried sediments and volcanic rocks as they were hydrothermally altered from the mobilization of Li through interaction with a fluid at a point when the geothermal field was initially forming (e.g., Magenheim et al., 1995; Chan et al., 2002; Millot et al., 2010; Coffey et al., 2021; Ellis et al., 2022), even at low temperatures (< 100°C). However, the rocks in the SS-GR show signs of alteration (Sturz, 1989) and reactive-transport modeling of the SS-GR (Chapter 6) suggests that the interaction between the rock and brine is slower than is necessary to affect the Li concentration of re-injected, Li-poor brines on decadal timescales.

Summary and Recommendations

Lithium concentrations vary with depth and mineralogy within the SS-GR. The highest Li concentrations for rocks and minerals are found within mudstones and decrease with depths, with surface mudstones containing ~106 ppm Li, mudstones at 2358 m containing ~82 ppm Li, and mudstones from 2745 m containing ~34 ppm Li. At depth, chlorite has the highest concentration of Li, with values as high as ~580 ppm found at a depth of ~2358 m. Chlorites from deeper in State Well 2-14 contain less Li, with a maximum measured concentration of ~104 ppm. While chlorite has been observed to be the primary mineral host of Li at depth, further analysis on rocks from deeper (hotter) and shallower (cooler) in the SS-GR should be undertaken to test whether the mineral hosts of Li change with changes in temperature and to determine how whole-rock quantities of Li evolve with depth in the SS-GR.

Lithium isotopic compositions for the rocks vary above depths of 1.5 km and temperatures below ~300°C (Sass et al., 1988), but are consistently lighter than the hypersaline geothermal brine they are in contact with at depths exceeding 1,500 m in the chlorite-calcite zone, and heavier than the hypersaline geothermal brine within the biotite metamorphic zone (> 2,480 m depth and > 325°C). Much like previous hydrogen and oxygen isotopic work done on SS-GR brines (Williams and McKibben, 1989), the δ^7Li composition is narrowly confined (δ^7Li_{avg} = +4.1 ± 0.3‰), indicating a well-mixed brine reservoir.

This study has revealed a temperature dependence for the incorporation of Li into the crystal structure of chlorite in the SS-GR, with a change in Li behavior taking place around 325°C, the transition temperature between the calcite-chlorite and biotite metamorphic zones (Cho et al., 1988; Sass et al., 1988). The clinopyroxene metamorphic zone lies below the biotite metamorphic zone, at even higher temperatures (>350°C; Cho et al., 1988; Sass et al., 1988) but was not sampled during this study. To fully constrain the temperature-dependent behavior of Li within the rocks in the SS-GR, rocks from greater depths and temperatures should be sampled to test whether Li partitioning in chlorite changes at higher temperatures and pressure and/or if there are other mineral hosts of Li in these conditions. Similarly, the mineralogic hosts of Li at shallower depths and lower temperatures have not been identified in this study. What are the Li-bearing minerals prior to the formation of chlorite?

Additionally, contained within the dataset gathered through the study of Li, but unexamined to date, are determinations for the abundance of other major and trace elements, including USGS-designated critical minerals Co, Ni, Zn, Mn, and the rare earth elements (REEs). As is the case for Li described in this study, this unexplored dataset will provide currently unknown but first-order constraints on the mineralogical hosts of these elements, as well as describe the behaviors of these elements during brine-rock interactions in the SS-GR. Continued examination of the existing data set can answer the questions: What are the primary mineralogical hosts of Mn, Zn, Co, Ni, and the REEs in the SS-GR source rocks, and what constraints do the observed mineralogical reaction textures place on the nature of Mn, Zn, Co, Ni, and REE mobility during brine-rock reaction at elevated temperatures and depth?

Chapter 5: Geothermal Reservoir Modeling of the Salton Sea Geothermal Reservoir for Lithium Extraction

Key Takeaways

- Numerical model simulations show that lithium production rates are forecast to decline as a result of chemical breakthrough of reinjection fluid with a low concentration of lithium.
- The rates of decline are dependent on the connectivity between production and reinjection wells and can be optimized through careful planning of reinjection strategies.
- The forecast recovery of lithium from the system declined from 0.8 kg/s to 0.3 kg/s over 30 years using a representative, naïve "business-as-usual" forecast.
- Forecast scenarios optimized to recover lithium and geothermal energy are expected to be able to sustain lithium production rates much more effectively.

Introduction

This chapter seeks to characterize and forecast the recoverable lithium potential of the Salton Sea Geothermal Reservoir (SS-GR) by building upon the existing 3-D conceptual and numerical model by Araya and O'Sullivan (2022). The fundamental research questions that must be answered to assess the sustainable extraction of lithium and energy from the SS-GF are as follows:

- How do the hot geothermal plume and hypersaline zone interact?
- What are the likely permeability controls on the geothermal plume and hypersaline zone?
- How can the permeability/porosity distribution of the system be exploited to maximize extraction of lithium and energy?

Answering these fundamental research questions requires the development of an integrated and robust numerical model. The model needs to fully represent the latest geoscientific understanding of the system and be capable of making detailed forecasts of production and injection of chloride and lithium-rich geothermal brine. Modeling concepts and workflows described by O'Sullivan et al. (2000), O'Sullivan et al. (2016), and Popineau et al. (2018), as well as Leapfrog Geothermal software, were used to create a combined geology, alteration, and structural model that was tightly coupled to the numerical model. Geothermal reservoir modeling best practice was then used to calibrate the numerical model, ensuring that it matched the available field data as well as the conceptual model. The calibrated numerical model can be used to forecast energy and lithium extraction. Details about its development are given in the following sections.

Conceptual Model and Design

Based on previous work by Wagoner (1980), Dorsey (2006), Dorsey et al. (2011), Kirby et al. (2007), and Hulen et al. (2003), the following seven geologic units were modeled chronologically from oldest to youngest: Crystalline Basement, Imperial Group, Palm Springs Formation, Lower Borrego, Upper

Borrego, Brawley Formation, and Alluvium. Regional stratigraphic cross sections from these studies were used to establish the general thickness of each formation. The Borrego Formation was split to capture the dramatic metamorphic and seismic velocity changes that occur at ~1.5 km depths beneath the center of the SS-GF. The crystalline basement surface contact was traced using a regional geological map (CDC, 2015).

The Salton Sea sub-basin is dominated by a complex network of blind right-stepping dextral faults and R' Riedel shear faults. The modeled dextral faults include the left strand of the Brawley Fault Zone (fault I), the right strand of the BFZ (fault B), Red Hill (fault R), Calipatria (fault P), Wister (fault W), Southern San Andreas (fault A) and fault C, which was inferred from the alignment of old CO_2 fumaroles and wells (e.g., Svensen et al., 2007; Mazzini et al., 2011; Rao, 2016). These faults were all modeled as having near-vertical dips. They were digitized from maps provided by Kaspereit et al. (2016), Marshall et al. (2022), and Lynch and Hudnut (2008). Some liberties were taken with their ultimate placement and orientation (Figure 5.1).

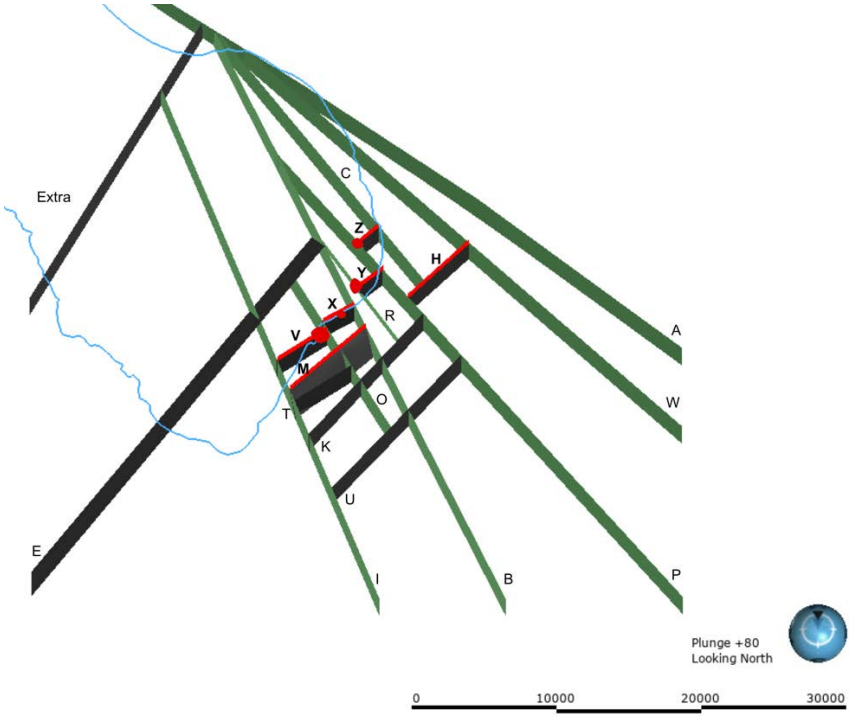

Figure 5.1. Faults included in the numerical model. Salton Sea (light blue) and volcanic buttes (red) shown as reference. Green faults are near vertical dextral faults. Black faults are R' faults with little to no upwelling. The black faults with red traces represent R' faults with significant upwelling.

The previously mentioned fault maps, in addition to one from McGuire et al. (2015), were used to digitize the R' Riedel shear faults. These faults include the Elmore Ranch (fault E), Main Central Fault Zone (fault M), Kalin (fault K), Hudson (fault H), Southern boundary (fault U), fault T, Butte 1 (fault V), Butte 2 (fault X), Butte 3 (fault Y), and Butte 4 (fault Z).

Four 2-D land and offshore resistivity profiles by Nichols (2009) were used to digitally construct the clay cap in the conceptual model (Figure 5.2). The clay cap was defined as the extremely conductive zone (0.2

to 0.4 Ohm-M). Some uncertainty in the location of the clay cap exists because the combination of high temperature, high salinity, and high porosity can also produce very low resistivity values (Nichols, 2009). Thus, some of the low resistivity anomalies may not actually be part of the clay cap. The landward lateral extent of the clay cap was further refined by resistivity and density maps from Younker et al. (1981). Due to the lack of 3-D MT data, modeler discretion was used, thereby increasing the potential uncertainty in model parameters.

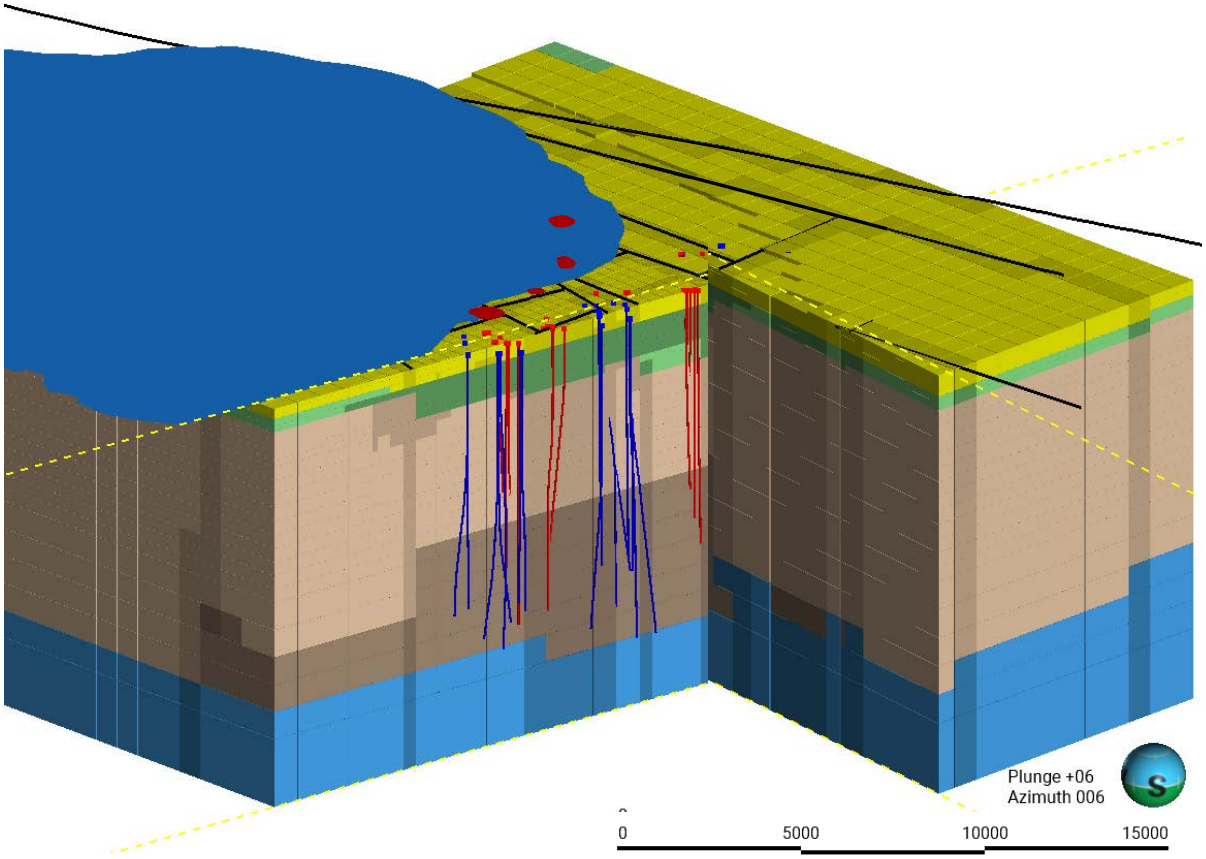

Figure 5.2. Discretized conceptual model of the SS-GR. Salton Sea (lake in blue). Faults are the black lines on the surface and shaded blocks. Active production well tracks (red). Active injection well tracks (dark blue). Volcanic buttes (red surfaces).

Numerical Model Design

Numerical models are used to simulate the natural pre-production state of hydrothermal systems, as well as their current and future behavior in response to utilization. Physical laws such as conservation of mass and energy (as well as Darcy's Law) are used to mathematically simulate hydrothermal flow through a fractured and heterogeneous subsurface. Numerical simulation is a powerful instrument that allows for a robust 3-D characterization of subsurface permeability, porosity, heat, and mass input parameters. This study followed the modeling framework established by O'Sullivan et al. (2023).

The 3-D conceptual model was discretized into a block model for applying mass- and energy-balance calculations using the Waiwera geothermal simulator (Croucher et al., 2020). The model was run in the Cloud using 96 core high-performance compute nodes with Amazon Web Services (AWS).

A grid extending 24 x 24 x 3.5 km and oriented along the NE trending axis of the Main Central Fault Zone was created in Leapfrog Geothermal. The grid has a 400 x 400 m lateral refinement within the SS-GF boundary and an 800 x 800 m refinement on the periphery. The grid was designed with a vertical refinement of 25 m near the surface, 50 m at the water table, 100 m in the upper reservoir, 200 m in the lower reservoir, and 500 m at the greatest depths (Figure 5.3). This allows the model to accurately capture the steep temperature gradients close to the surface while maintaining a good resolution in the production reservoir. The final numerical grid consisted of 37,688 blocks.

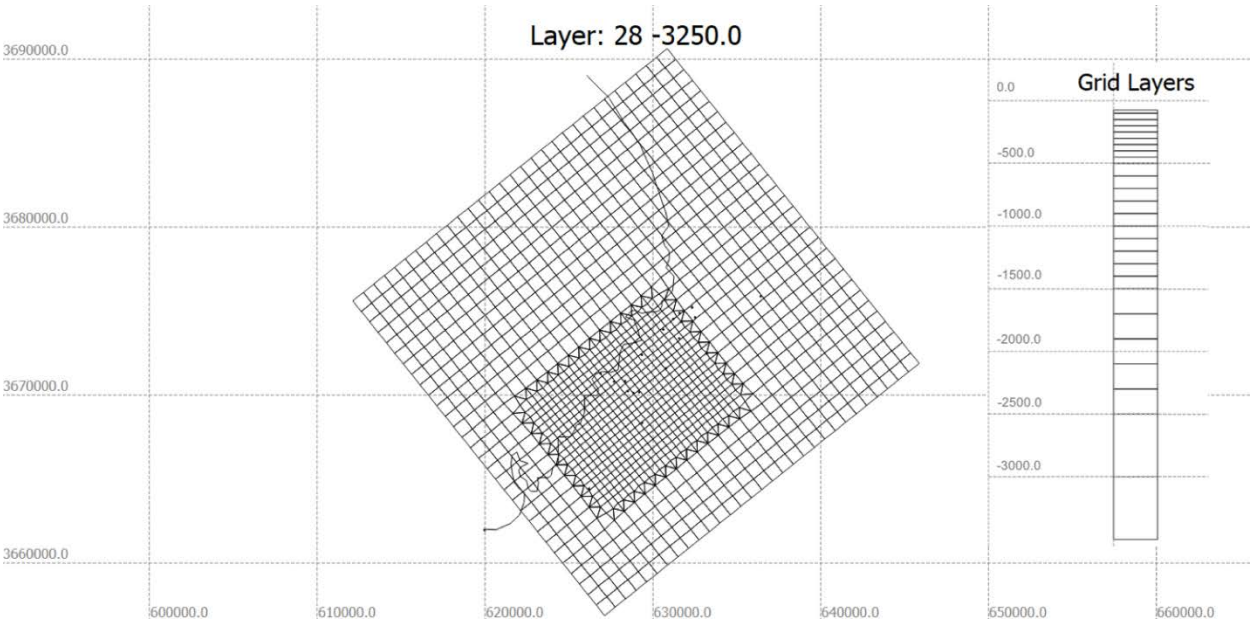

Figure 5.3. Map view of the TOUGH2 grid with the black line representing the Salton Sea shoreline. The cell size in the refined area of the grid is 400 m x 400 m, and in the coarser area it is 800 m x 800 m. The thickness of the grid layers increases with depth.

Waiwera's energy, water, air, salt, and gravity (EWASG) equation of state was used to include salinity and CO_2 in the thermodynamic calculations, and Li was included in the model as a passive tracer. The top of the model was assigned dry atmospheric conditions of 1 bar, a mean temperature of 23°C on land and a wet atmosphere for the Salton Sea with a temperature of 23°C, and a pressure determined by the depth of the sea. The chloride concentration of the Salton Sea was set to a mass fraction of 50,000 ppm. The side boundaries of the grid are located past all bounding faults, allowing no-flow lateral boundary conditions to be applied following best practice suggested by O'Sullivan et al. (2000). At the base of the model, a background heat flux 150 mW/ m^2 was applied with an additional 136 MW applied as heat and mass inputs under the SS-GF, representing the deep geothermal upflow. Chloride was included in the deep upflow at a mass-fraction equivalent to 152,000 ppm and Li at a concentration of 220 ppm, a ratio of 682:1. The CO_2 concentrations were fixed at negligible values for all boundary conditions during this stage of the project.

The model used 561 rock types covering the combinations of lithology, fault zone, fault zone intersections, and alteration that resulted from tightly coupling the numerical model to the conceptual model. This tight coupling ensured that the numerical model lithology, alteration, and structural controls mirror the current geoscientific understanding of the SS-GR as represented in the conceptual model. Many rock-type

classifications share common permeability and porosity values, but the large number of combinations allows a high level of heterogeneity in the permeability and porosity distributions as required. Other secondary rock properties (e.g., density, heat conductivity, and rock grain-specific) were held constant across all rock-type classifications.

During production and future scenario runs, a dual-porosity model was used to capture reinjection returns more accurately. The dual-porosity parameters are given in Table 5.1 below.

Table 5.1. Dual porosity parameters used in the production history model

Parameter	Value
Number of matrix blocks	2 (20% and 77.5%)
Volume fraction of fracture blocks	2.5%
Fracture spacing	25 m
Fracture planes	3
Permeability of matrix	1.0E-16 m^2
Permeability of fractures	variable
Porosity of fractures	80 %

Calibration Data

Exploration Wells

Static temperature and brine-chemistry data from exploration wells drilled prior to the start of 1980s commercial production were compiled from studies by Helgeson (1968), Palmer (1975), and Sass et al. (1988). Helgeson (1968) obtained temperature measurements over a three-year period for the following eight wells: IID 1, IID 2, IID 3, River Ranch 1, Sinclair 3, Sportsman 1, Elmore 1, and State 1. Palmer (1975) compiled temperature and brine chemistry data from MagMaMax 1, MagMaMax 2, MagMaMax 3, and Woolsey 1. Lastly, Sass et al. (1988) analyzed temperature data from State Well 2-14 to construct an equilibrated static temperature profile.

Static temperature surveys for Lander 2, Elmore IW-4, River Ranch 17, Fee 5, and Vonderahe 1 were collected from CalGEM's GeoSteam data repository. Most of these temperature profiles exhibit a change from a conductive to a convective gradient between depths of 600 to 900 m. This break corresponds well with the average depth of the impermeable clay cap (Sass et al., 1988).

Examples of the downhole temperature data are shown in the plots in Figure 5.4.

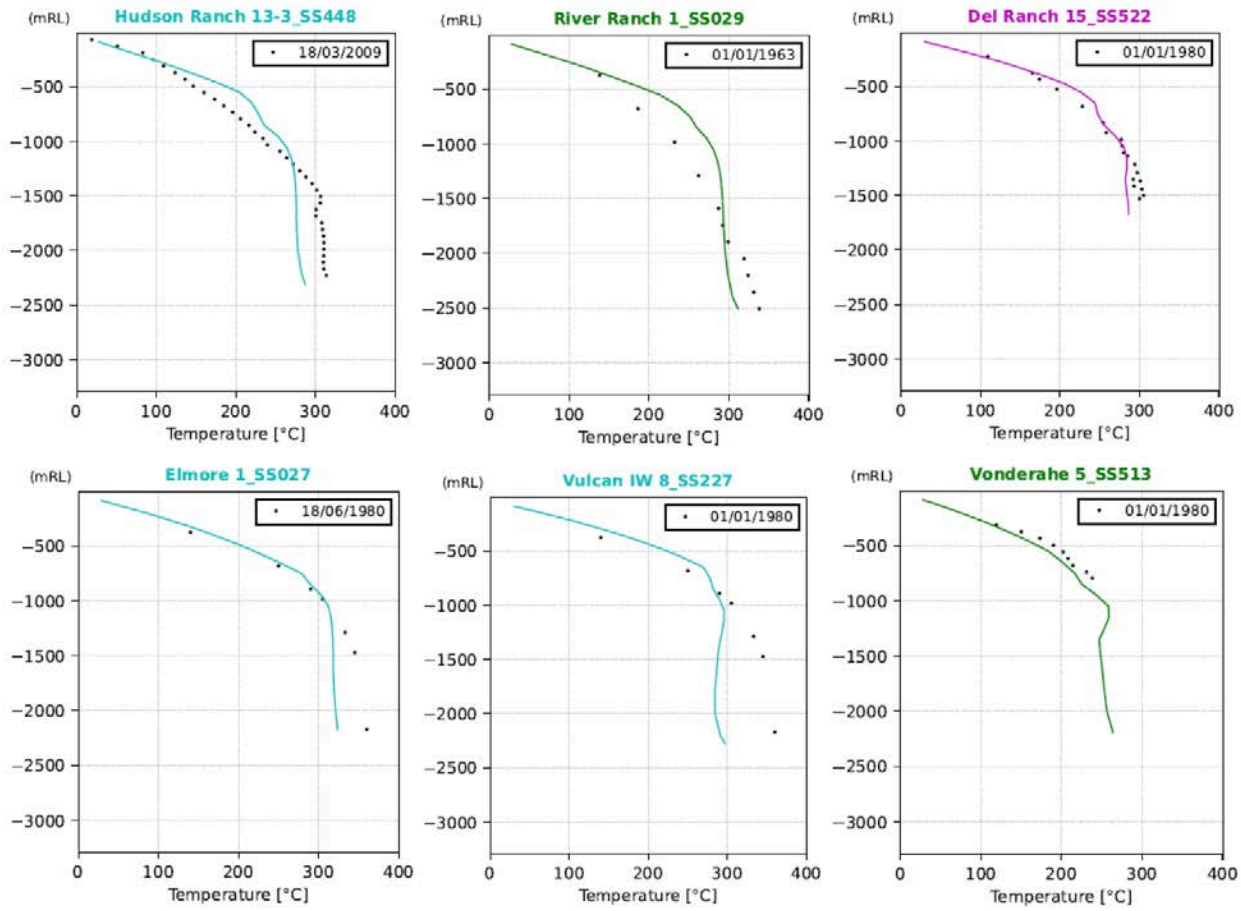

Figure 5.4. Natural state downhole temperatures for selected wells. Model results are shown as lines and measured data as points.

Active Production and Injection Wells

CalGEM's GeoSteam database was used to obtain monthly production and injection data for all active production and injection wells in the SS-GF. These monthly production/injection reports document the average monthly total dissolved solids (TDS), discharge temperature, wellhead pressure, steam mass rate, and brine mass rate. The GeoSteam database was also used to get well schematics, directional surveys, mud logs, static pressure temperature spinner (PTS) logs, and well history reports for all the active production and injection wells. Well schematics provided wellhead coordinates, Kelly bushing (KB) elevations, ground level, and total measured depth. Total and/or partial circulation zones that were noted in the mud logs were used to infer feed zones. This was the best approach given the lack of proprietary well-testing and feed zone data. (Later in this chapter, examples of the production and injection data are shown in the plots of Figures 5.8 and 5.9.)

Figure 5.5 below shows a comparison of the modeled 275°C natural state isosurface with the same isosurface generated by Norton and Hulen (2006) from measured data. The isosurface compares quite well with the high temperature zones rising close to the surface near Del Ranch.

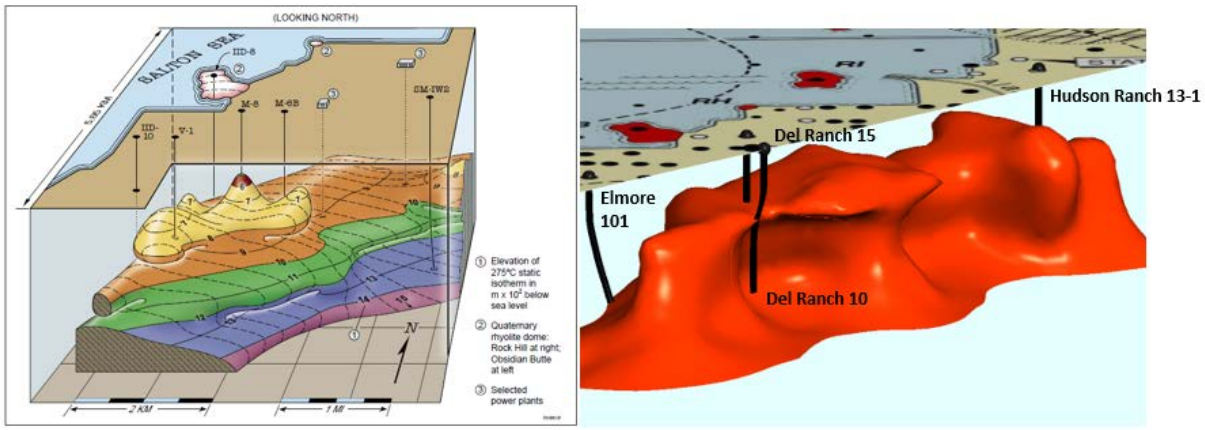

Figure 5.5. Comparison of the natural state model estimated 275°C isosurface (right) with the isosurface from observations (left, adapted from Norton and Hulen, 2006).

As well as calibrating the temperature distribution, the model permeability distribution was adjusted to produce a chloride distribution consistent with the measured data. In particular, the aim was to reproduce the deep hypersaline reservoir overlaid with an intermediate mixing zone and a low-chloride shallow zone. Figure 5.6 shows the 140,000-ppm chloride isosurface from the natural state model. Overall, it captures the deep hypersaline reservoir and the intermediate mixing zone. However, in the model, the deep hypersaline fluid penetrates the shallow zone over a much larger area than has been observed. More model calibration is required, reducing permeabilities in the vertical pathways between the deep reservoir and the shallow system to lessen the upflow of hypersaline fluid. Because lithium is included in the natural state model as a passive tracer, the Li distribution estimated by the natural state model closely follows the chloride distribution, as can be seen in Figure 5.7.

Production Model

The production model was set up using our standardized framework for including production and reinjection wells (O'Sullivan et al., 2023). This approach adds wells as time-dependent source and sink terms in the model blocks corresponding to the feed zones of the production and reinjection wells. The model was then run for the corresponding production history time period and calibrated to match measured transient data for production enthalpies and chloride mass fractions. For the reinjection wells, the enthalpy of the reinjected fluid and its chloride concentration are model inputs taken from measured data. The lithium concentration for the reinjection fluid was assumed to remain constant at a ratio of 682:1 to the measured chloride, therefore assuming that no lithium is currently being extracted from the brine.

Examples of measured data and production model results for selected production and reinjection wells are shown in Figures 5.8 and 5.9. Each figure has a map in the upper left showing the location of the well. The results for the production well are typical, with the measured chloride concentration increasing over time and a gentle decline in production enthalpy.

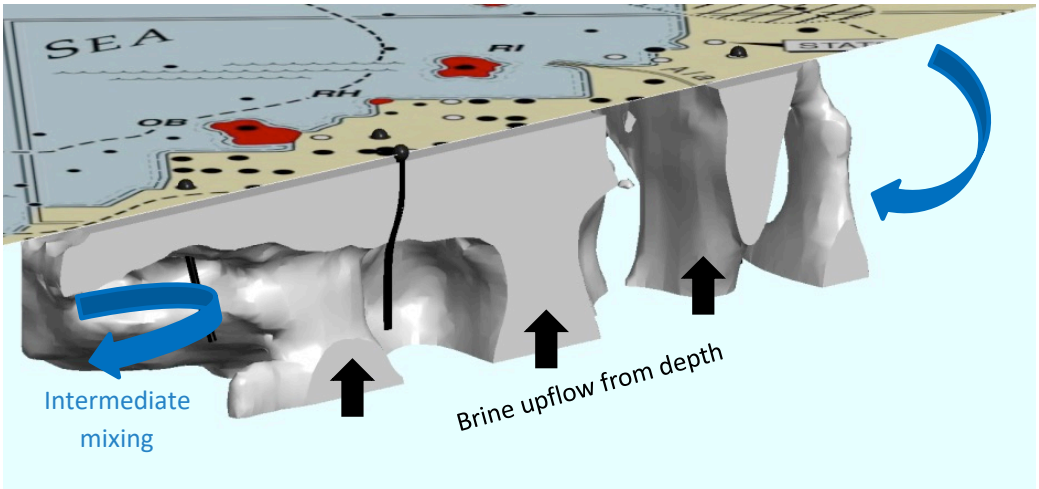

Figure 5.6. Natural state model estimated 140,000-ppm chloride isosurface.

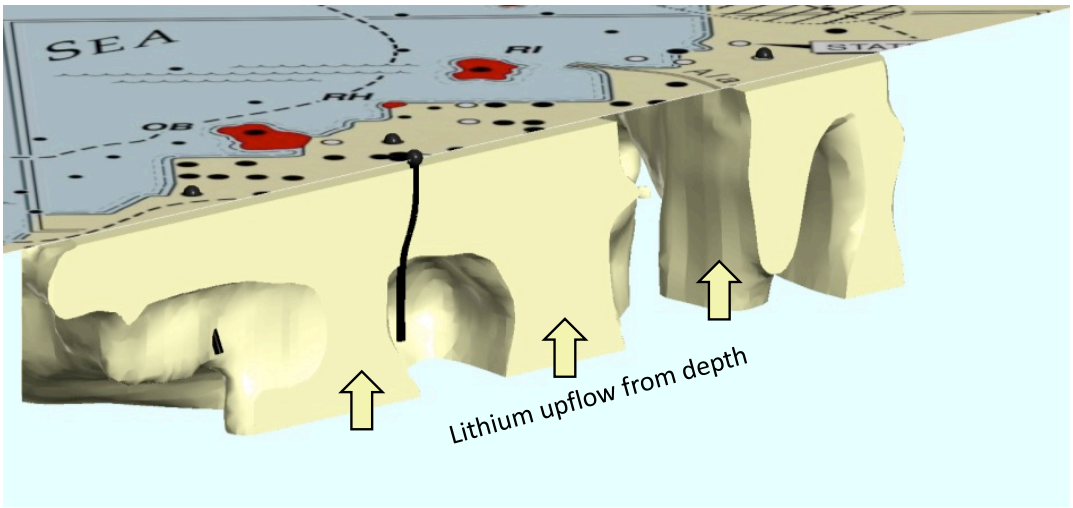

Figure 5.7. Natural state model estimated 170-ppm lithium isosurface.

The plots in Figure 5.9 indicate breakthrough of the higher chloride concentration and lower enthalpy reinjection fluid. The model results for the selected production well match the measured data very well; they show that the model forecasts an increasing lithium production concentration, due to a higher lithium concentration in the reinjected fluid than in the reservoir. The good match with the measured data was achieved by calibrating the model's permeability and porosity distribution and the distribution of the upflow of deep, chloride- and lithium-rich geothermal brine. That this good match is also achieved for the production enthalpy further demonstrates that the model calibration represents the permeability and porosity distribution well. Further calibration could still improve the model's match to the data for the well shown in Figure 5.8, reducing the enthalpy decline in the model slightly by reducing the connectivity between this well and nearby injectors. Similarly, the match to other production wells can be improved with more calibration, though the current calibration is sufficient to draw preliminary conclusions given uncertainty in the available data.

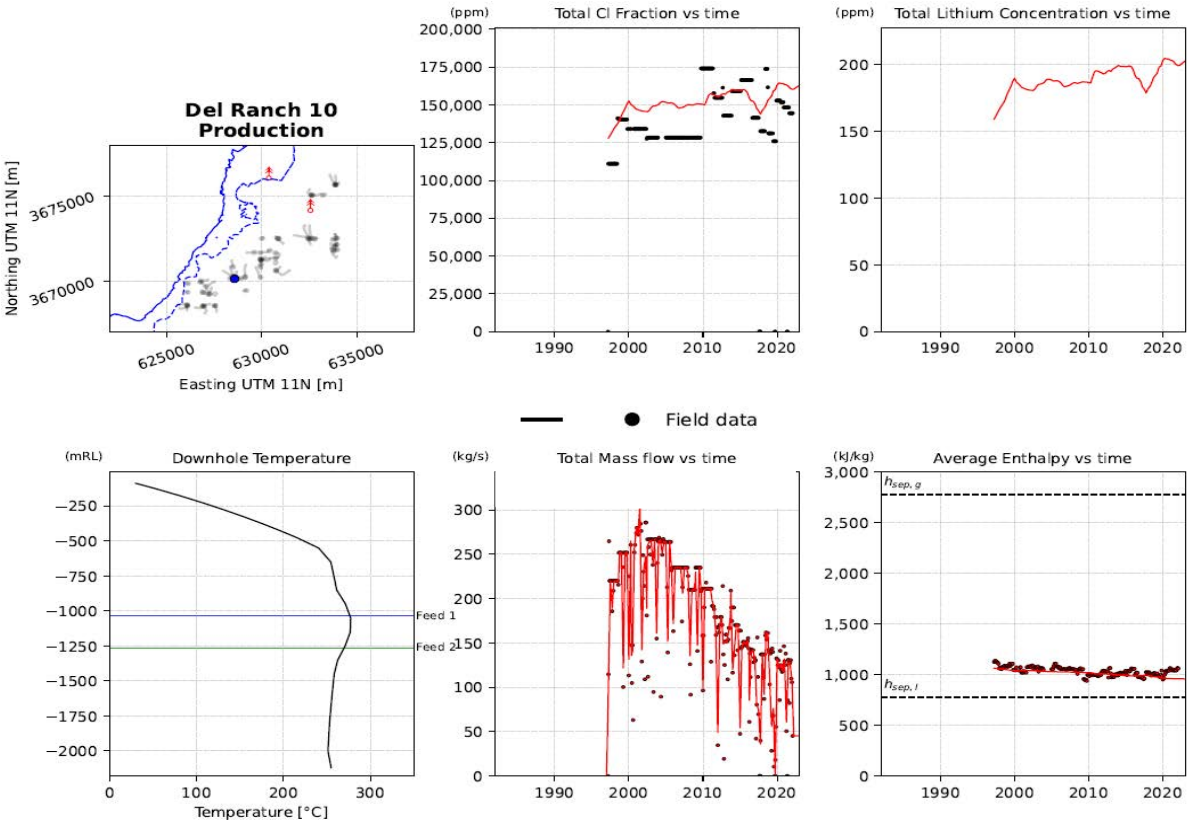

Figure 5.8. Production model results (solid lines) and measured data (points) for the Del Ranch 10 production well. The location of the Del Ranch 10 well is shown in blue in the map (top left) with the Salton Sea coastline (original as solid line, current as a dashed line) and surface features locations indicated by red markers.

The rate of thermal and chemical breakthrough as a result of reinjection is dependent on the permeability and porosity distributions, the location of the production and the reinjection wells and their feedzones, and the rates of production and reinjection. Figure 5.10 shows the model representation of the chloride distribution in 2023 after 40 years of geothermal production and reinjection. Its shows that the increased chloride concentrations are distributed heterogeneously across the field as a result of faults, formations, and differences in production and reinjection elevations. The current model does a good job of matching the overall behavior of the SS-GF, and the dual-porosity approach allows a good representation for the reinjection returns. However, more calibration, more detailed calibration data, and a more refined model grid would allow for more accurate representation of the historic changes in the chloride and lithium concentrations.

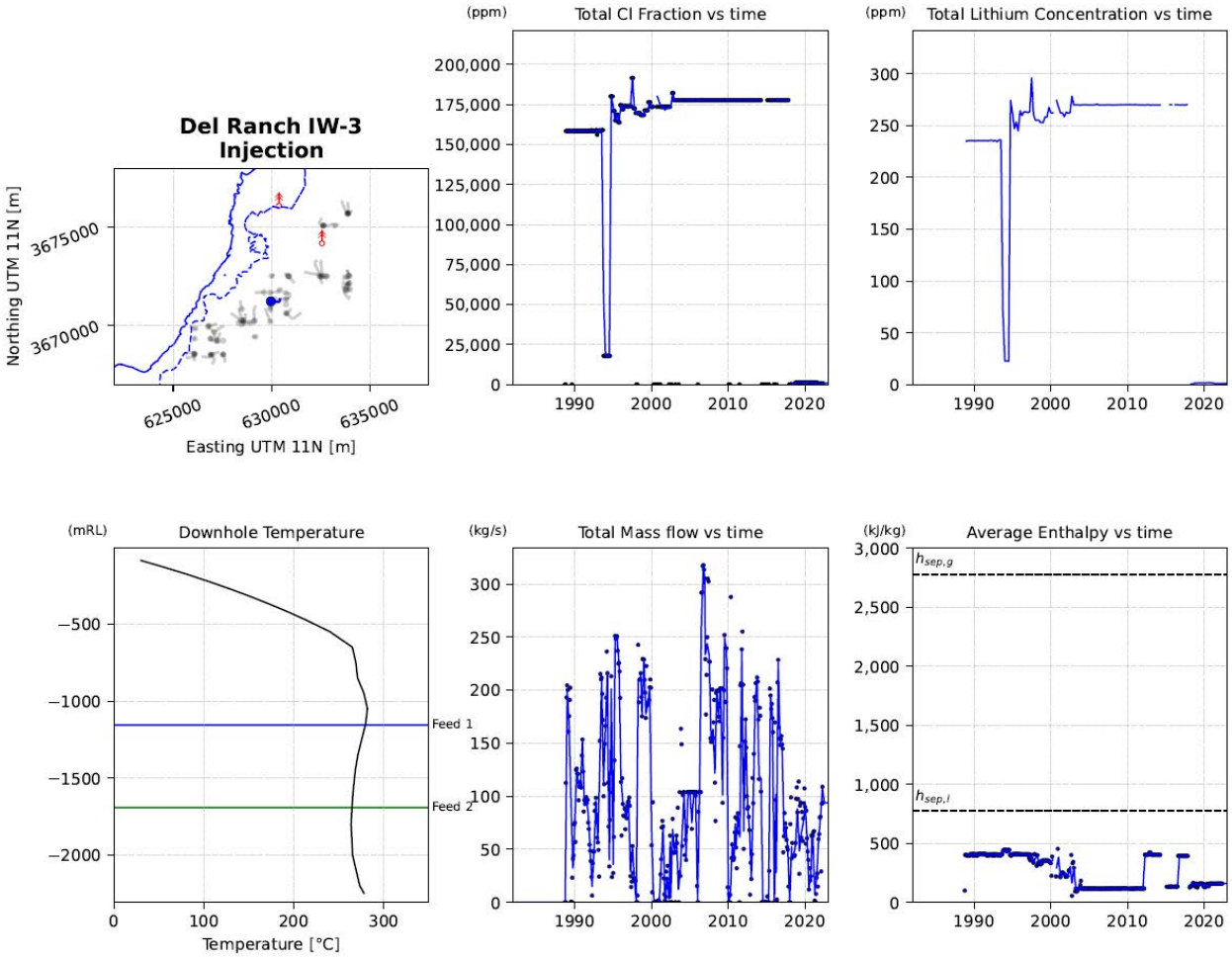

Figure 5.9. Production model results (solid lines) and measured data (points) for the Del Ranch IW-3 reinjection well. The location of the Del Ranch IW-3 well is shown in blue in the map (top left) with the Salton Sea coastline (original as solid line, current as a dashed line) and surface features locations indicated by red markers.

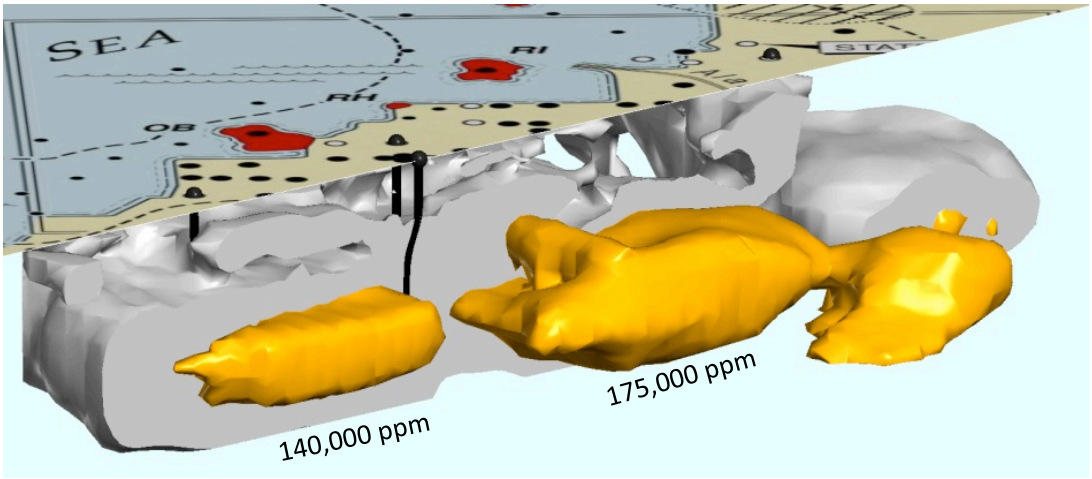

Figure 5.10. Chloride isosurfaces in 2023 estimated from the production model. The 140,000-ppm isosurface is cut away to reveal the 175,000-ppm isosurface.

Future Scenarios

At this stage of the project, a simple future scenario was defined to investigate the broad effect of lithium extraction on lithium production rates. The scenario assumed that all current production and reinjection rates remain constant for all wells for the next 20 years. The reinjected chloride concentrations also remain constant over the full period. However, from January 1, 2024, the lithium concentration for all reinjection wells was reduced by 95%, representative of a future scenario where technology allows the extraction of 95% of lithium from brine before reinjection. An example of the input data for a selected reinjection well is shown in Figure 5.11.

Production concentrations of lithium for all production wells were calculated, with examples shown for two selected wells in Figure 5.12. The total amounts of production and reinjection, as well and the total amount of lithium produced and reinjected, are shown in Figure 5.13. These figures show a general decline in forecasted lithium production because of chemical breakthrough from the reinjected fluid with a low lithium concentration. The plot in Figure 5.14 shows the final distribution of lithium as projected in 2043, with the lower 100 ppm concentration isosurface forming a bubble around the central production and reinjection wells. Bear in mind that the results in Figure 5.12 show that the effect can be quite different depending on which production well is considered. For example, the Del Ranch 10 production well is forecast to experience rapid decline in lithium production due to its proximity and connectivity to nearby reinjection wells, whereas PW Hudson Ranch 13 is forecast to have relatively stable lithium concentrations throughout the 20-year scenario.

These results show that details about connectivity between production and reinjection wells are important for determining lithium production rates. This has two noteworthy implications. First, it is important to model the connectivity between production and reinjection wells as accurately as possible and account for uncertainty in model forecasts. Second, lithium production rates can be manipulated and optimized by planning targeted reinjection.

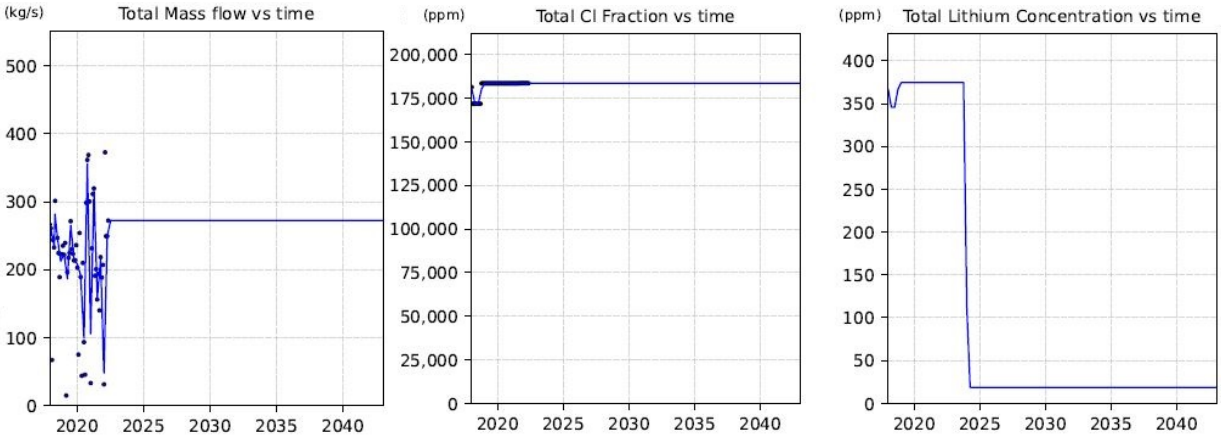

Figure 5.11. Future scenario model results (solid lines) and measured data (points) for a selected reinjection well.

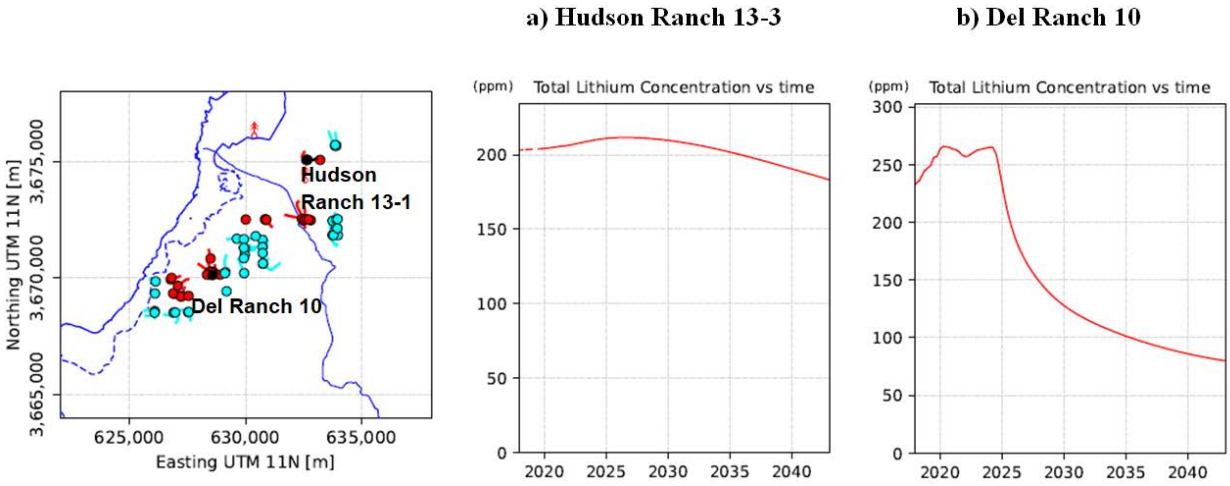

Figure 5.12. Future scenario model results for two selected production wells. Well locations shown on map (left) in black. Other production well locations shown in red, and reinjection wells in cyan.

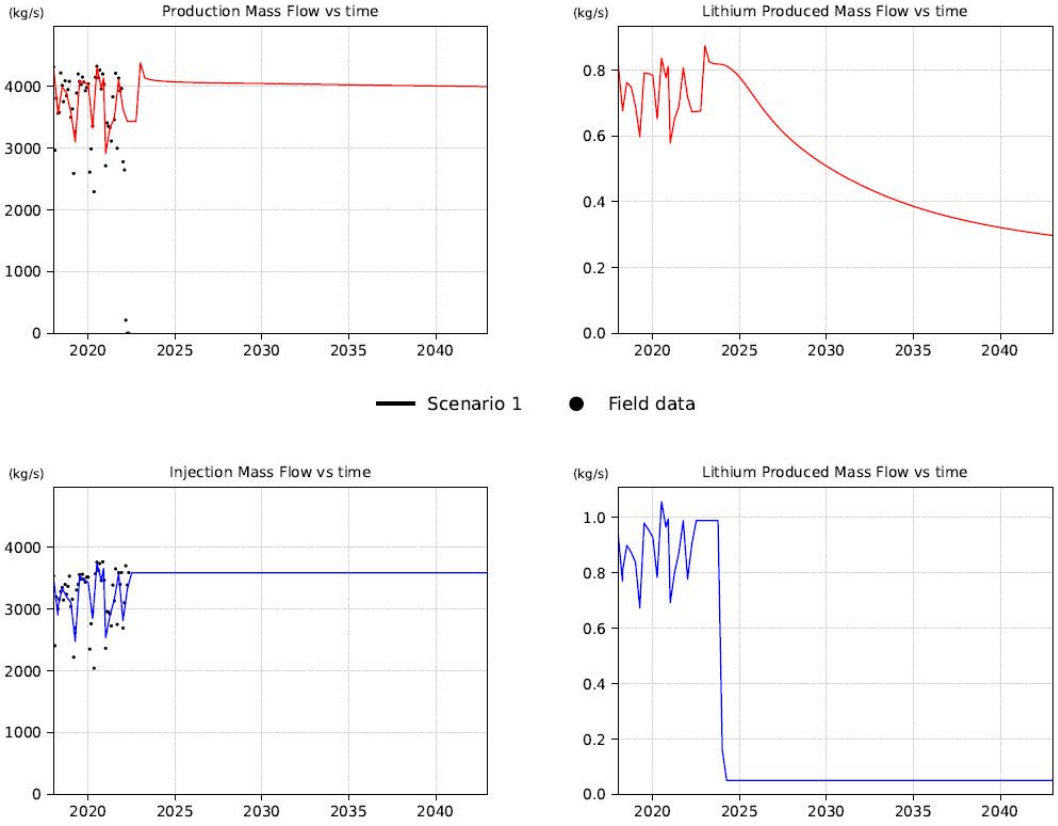

Figure 5.13. Future scenario model results of totals for all production and reinjection wells.

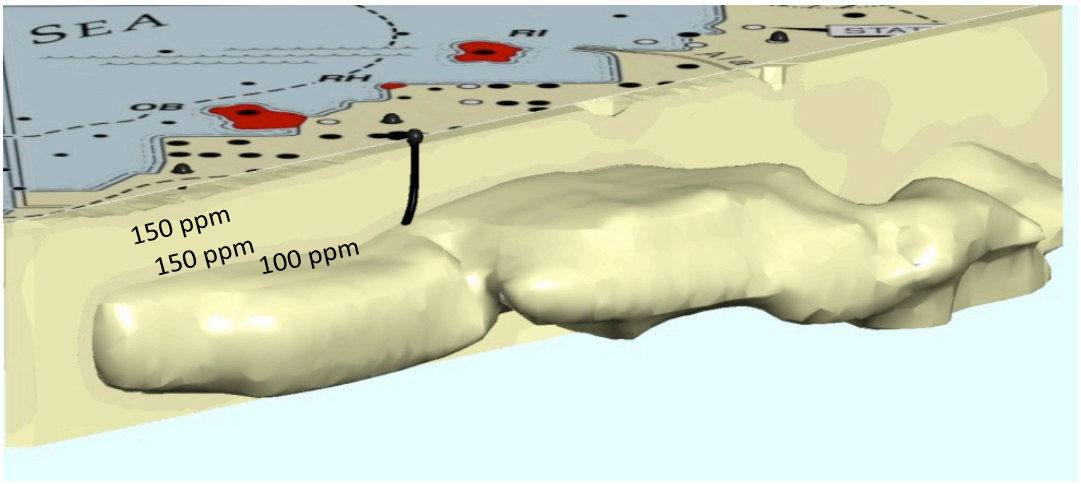

Figure 5.14. Future scenario model estimated lithium isosurfaces in 2043. The 150-ppm isosurface is cut away to reveal the 100-ppm isosurface.

Summary and Recommendations

This modeling study shows that our model of the SS-GR is capable of making realistic forecasts of lithium extraction from the system. The model has been developed using best practices to closely align with the conceptual understanding of the system's behavior and calibrated to broadly match a range of observed data. However, several aspects of the model can be improved to increase the accuracy and robustness of the model forecasts. Specifically, the existing model is relatively coarse at 400 m x 400 in the production zone. This could be reduced to 200 m x 200 m, or even 100 m x 100 m. Model resolution in the production zone affects the accuracy of model forecasts, particularly for reinjection returns, which are a key driver for forecasting lithium production rates over time. A higher-resolution model would also allow better representation of structural controls on the SS-GR, improving the quality of forecasts. Additionally, the shallow part of the reservoir zone in the current model could have more calibration to improve the match to measured chloride (and therefore lithium) concentrations. Improved model calibration improves the quality of the model forecasts and gives stakeholders more confidence in modelling results.

The conclusions derived from any modeling results depends on the scenarios run. Therefore, more informative scenarios must be developed and tested. These should include but not be limited to a staged approach to lithium removal; increased geothermal production (as planned); and targeted reinjection accounting for connectivity between well locations to extract Li more efficiently. A key issue with geothermal reservoir model forecasts is uncertainty arising from model parameters and in the measured data used for model calibration. This issue is particularly problematic when there is not access to a full set of measured data, as is the case for the SS-GF. By far the best approach for addressing this problem is carrying out a formal uncertainty quantification of the geothermal model forecasts. This approach has been successfully applied to several commercial projects and described in several studies (e.g., de Beer et al., 2023; Dekkers et al., 2022; Omagbon et al., 2021). Producing forecasts of lithium production from the SS-GR that include uncertainty quantification would not only account for limitations in the measured data but would also provide much better support for long-term decision making.

Finally, it would be beneficial to improve thermodynamics in the model by calibrating CO_2 content and extending the model to higher temperatures. Both improvements would allow for more accurate representation of thermodynamics of the SS-GR. However, these are longer-term objectives, as simulator development is required to enhance the temperature range of Waiwera's EWASG equation-of-state. Access to detailed CO_2 data, combined with calibration, will be needed to incorporate CO_2 thermodynamics accurately.

Chapter 6: Constraints on Lithium Evolution and Reservoir Sustainability from Reactive-Transport Modeling

Key Takeaways

- A new reactive-transport model that shares information with the reservoir model and includes chemical reactions controlling lithium was developed.
- The primary replenishment mechanism for lithium is the upward flux of convecting lithium-rich brine from below the producing reservoir, along with unexploited brines in the reservoir.
- The upwelling brine with lithium concentrations of about 200 ppm from below the production zone modestly increases lithium in depleted brines by 10-40 ppm over 100 years, depending on depth.
- Reactions of relatively stable lithium-bearing metamorphic minerals are slow even at high temperatures, and injection of a lithium-depleted brine is not significantly enriched by mineral-water reactions over time periods of hundreds of years.

Introduction

Assessing the extent and sustainability of the lithium (Li) resource in the Salton Sea Geothermal Field (SS-GF) is aided by an understanding of the processes that led to the development of lithium-rich brines. Although there is extensive literature over the past 50 years on the origin, geologic history, and geochemistry of the SS-GF, lacking are quantitative models that can be used to assess the rates at which Li concentrations evolve and are transported through the field. For the timescale of exploitation of the Li resource (10-100 years), the rates at which mineral-water reactions and transport processes (advection-diffusion) take place is essential to constraining the lifetime of the resource. The purpose of this work is to examine the rates and extent of water-rock reactions involving Li in the SS-GF, the rates of Li-rich brine replenishment into the reservoir, and the effects of water-rock reactions on Li-depleted brine (+/- condensate) that are re-injected into the reservoir.

The origin of Li-rich geothermal brines (200-400 ppm) produced in the SS-GF has been attributed to deep circulation of evaporated near-surface Li-rich brines, hydrothermal alteration of buried volcanic and sedimentary rocks, magmatic fluid contributions, and/or interaction of hydrothermal fluids with evaporites and/or mudstones (Helgeson, 1968; McKibben et al., 1988; McKibben and Hardie, 1997). The SS-GF has undergone a complex tectonic history, magmatism, rapid sedimentation/burial, metamorphism, and climatic changes with concomitant formation/disappearance of large surface water bodies over tens of thousands to 0.5 million years (Cullen et al., 2021). Lithium concentrations in the unaltered rhyolites are relatively low (~40 ppm), suggesting that the magma body is not likely Li-enriched. The primary source of Li may be from brines formed through repeated evaporation events following Pleistocene high lake levels, supported by Li-rich surface mudstones from the Durmid Hills (Humphreys et al., 2023). To evaluate the roles of hydrothermal circulation, water-rock interaction, and surface evaporative concentration in the SS-GF lithium evolution, reactive-transport models were developed for

Salton Sea evaporation and hydrothermal alteration, using a 3-D calibrated SS-GF reservoir model (Araya and O'Sullivan, 2022), as well as surface evaporation and 1-D reactive-transport models.

Description of the Modeling Approach

Simulations were performed using an updated version of the reactive-transport simulator TOUGHREACT V4.13-OMP (Sonnenthal et al., 2021; Xu et al., 2006; 2011), which is based on the TOUGH2 multiphase flow simulator (Pruess et al., 1999). TOUGHREACT V4.13 is a parallel simulator for 3-D (as well as 0-, 1-, and 2-D) non-isothermal multiphase reactive transport in porous and fractured rock. The temperature (T) and pressure (P) limits are controlled by the applicable range of the chemical thermodynamic database, and the limits of the equation of state (EOS) module are employed. TOUGHREACT has been used to simulate many geological, environmental, and subsurface engineering problems, including diagenetic-weathering processes, geological carbon sequestration, subsurface nuclear waste emplacement, geothermal reservoir management, hydrothermal system exploration, hydrocarbon reservoir engineering and exploration, acid mine drainage, contaminant transport, and groundwater quality.

The major processes for fluid and heat flow (in the modified TOUGH2 core) are: (1) fluid flow in both liquid and gas phases under pressure, viscous, and gravity forces; (2) interactions between flowing phases, represented by characteristic curves (relative permeability and capillary pressure); (3) heat flow by conduction and advection with effects of boiling/evaporation; and (4) diffusion of water vapor, air, or other gas components (e.g., CO_2). Thermophysical properties, such as fluid (gas and liquid) density and viscosity, are calculated as a function of temperature and pressure. Space discretization is employed by means of integral finite differences (IFD; Narasimhan and Witherspoon, 1976). For 3-D and 1-D reservoir simulations, we used the EOS1sc module (supercritical water equation-of-state) derived from inverse TOUGH2 (iTOUGH2; Magnusdottir and Finsterle, 2015). For evaporation of the Salton Sea, we used the modified EOS4 module (water-air with vapor pressure lowering) based on Pruess et al. (1999).

The transport equations are written in terms of total dissolved concentrations of chemical components, which are the concentrations of the basis species plus their associated aqueous secondary species (Yeh and Tripathi, 1991; Steefel and Lasaga, 1994; Walter et al., 1994; Lichtner, 1996; Xu and Pruess, 2001). Because the chemical transport equations (derived from mass conservation) have the same structure as the fluid and heat flow equations, the transport equations can be solved by the same numerical method. Transport of aqueous and gaseous species by advection and molecular diffusion are considered in both liquid and gas phases. Any number of chemical species in the liquid, gas, and solid phases can be considered.

Aqueous and surface complexation, acid-base, redox, gas dissolution/exsolution, and multi-site cation exchange are treated under the local equilibrium assumption. Mineral dissolution and precipitation proceed under either equilibrium or kinetic constraints (Xu et al., 1999), with modifications for boiling systems (Sonnenthal et al., 2005). Thermodynamic and kinetic data for mineral-water-gas reactions are input as a function of temperature, pressure, and solution composition (e.g., pH effects, interaction terms, etc.).

After solution of the fluid/heat flow, the aqueous/gaseous species transport, and the mineral-water-gas reactions, changes in porosity (owing to mineral dissolution/precipitation), permeability, and capillary pressure (for multiphase flow) are considered, which can be coupled back to the multiphase fluid/flow and transport equations. (For these simulations, we used the sequential noniterative method that modifies properties for the following time step.) The flowchart for TOUGHREACT (and the TReactMech simulator, which also solves geomechanics) is shown in Figure 6.1.

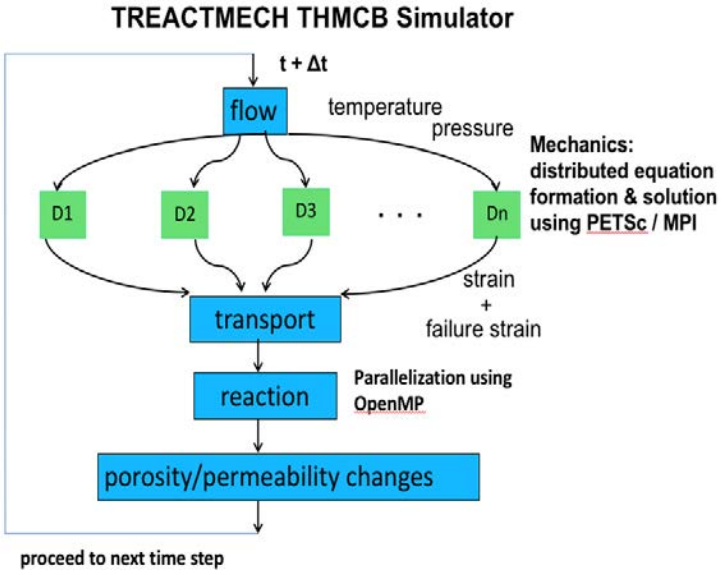

Figure 6.1. Flow chart for TReactMech (TOUGHREACT + geomechanics).

Simulations employ a parallel Pitzer implementation in TOUGHREACT v4.13-OMP (Spycher et al., 2021; Sonnenthal et al., 2021; Zhang et al., 2008). The main extensions over the typical Debye-Huckel approach include: (1) Pitzer ion-interaction model (Pitzer and Mayorga, 1973; Pitzer, 1991) for ionic activity calculation of solutions over a broad range of concentrations; and (2) the coupling of the vapor-pressure-lowering effect of salinity to phase partitioning. The Pitzer formalism was implemented into TOUGHREACT using the Harvie-Moller-Weare (HMW) formulation (Harvie et al., 1984). The HMW formulation was developed from Pitzer's ion-interaction theoretical model and is equivalent to Pitzer's original model (Pitzer, 1973; Pitzer and Mayorga, 1973). The only difference is in the definition of interaction terms, interaction coefficients, and mathematical expressions (Rard and Wijesinghe, 2003).

Hydrological and Thermal Properties

The 3-D and 1-D thermal-hydrological-chemical (THC) reactive-transport models are based on the Araya and O'Sullivan (2022) 3-D reservoir model of the SS-GF (pure water). Details of the calibrated porosities, permeabilities, and thermal properties are described in the latter paper. The 1-D evaporation model for the Salton Sea was developed specifically to account for "drying" of the Salton Sea mediated by an atmosphere having a constant relative humidity and fixed partial pressures of O_2 and CO_2. This model is meant to capture the chemistry of a possible evolving (time-independent) surface brine and associated evaporite minerals, but it is not a physically realistic model of the water body.

Geochemical Data

Water Chemistry

The aqueous geochemical system was simplified into two endmember water compositions: the present-day Salton Sea (Holdren and Montaño, 2002) and the reservoir fluid (Table 6.1). The reservoir fluid was taken from one of the hotter, deeper wells (State Well 2-14) with relatively high Li concentrations as characteristic of the deep brine convecting into the reservoir (McKibben and Hardie, 1997). Some species were determined through mineral equilibration (e.g., Al^{+3}). Lithium concentrations in the Salton Sea were estimated to be 3 ppm based on analyses reported by Werner and Olson (1970) and Sturz (1989).

Thermodynamic Data for Minerals, Aqueous Species, and Gases

The thermodynamic databases (see simulation input files submitted to the Geothermal Data Repository) used in the simulations are based on a conversion of the EQ3/6 *data0.ypf* Pitzer database (after Wolery et al., 2004; Alai et al., 2005), suitable for ionic strengths up to ~40 molal for some systems and temperatures ~150°C at solution vapor saturation pressures (see Spycher et al., 2021). Several modifications were made to the database (see notes in database and Spycher et al., 2021) prior to the additions made to simulate water-rock reactions involving Li. Additions for Li reactions included adding Li Pitzer ion interaction parameters from Lassin et al. (2015), taken after converting the PHREEQC Pitzer database mmc4.dat obtained in the supplemental information of Boschetti (2022a), as well as Li mineral data from the PHREEQC formatted file in the supplemental information of Boschetti (2022b). These data were then corrected for consistency with SiO_2(aq) and Al^{+3}.

Two ideal endmember solid solutions (Li-albite-albite and Li-K-feldspar-K-feldspar) were added to treat minor substitutions of Li in albite and K-feldspar in both primary and potential secondary minerals, similar to the approach used in Wanner et al. (2014), which also included isotopic fractionation of Li isotopes.

One complicating factor is that most hydrothermal minerals are solid solutions potentially with several endmembers and substituting ions. Thermodynamics of solid solutions can be highly nonideal, and data are lacking for many highly complex minerals. Li-bearing chlorite may be considered as a solid solution between Mg-rich clinochlore, Fe-rich daphnite, cookeite, and potentially other substituting cations such as Mn and Sr.

Table 6.1. Initial Salton Sea and State Well 2-14 chemistry and speciated compositions

	Salton Sea[1]	Salton Sea (speciated)	S2-14[2]	S2-14 Speciated
T (C)	25	25	330	349.565
pH	8.12	6.9842	-	4.000
I_STR	-	0.88983	-	4.797
aH_2O	-	0.98101	-	0.904
osmo_P	-	26.403	-	291.48

	Salton Sea[1]	Salton Sea (speciated)	S2-14[2]	S2-14 Speciated
EC(uS_cm)	-	55.101	-	3508.52
Component	ppm/ppb	mol/kg H2O	ppm	mol/kg H2O
Na^{+}	12369.93	5.381E-01	54800	2.382E+00
K^{+}	258.00	6.599E-03	17700	4.524E-01
Li^{+}	3.00[3]	4.322E-04	209	3.009E-02
Ca^{+2}	944.00	2.355E-02	28500	7.107E-01
Mg^{+2}	1399.99	5.760E-02	49	2.015E-03
Ba^{+2}	0.07	5.097E-07	210	1.528E-03
Sr^{+2}	22.00	2.511E-04	421	4.802E-03
Mn^{+2}	0.03	5.461E-07	1500	2.729E-02
Fe^{+2}	0.07	1.253E-06	1710	3.060E-02
Zn^{+2}	0.02	3.059E-07	507	7.749E-03
Al^{+3}	0.06	2.039E-09	0.1	3.704E-06
Cl^{-}	17239.92	4.863E-01	157500	4.440E+00
Br^{-}	13.00	1.627E-04	111	1.388E-03
F^{-}	2.10	1.105E-04	2.1	1.105E-04
HCO_3^{-}	245.00	4.015E-03	1580 (CO_2)	3.588E-02
SO_4^{-2}	10499.93	1.093E-01	53.00	5.514E-04
HS^{-}	na	3.594e-18	10 (H_2S)	2.844E-17
HPO_4^{-2}	0.05	5.209E-07	0.05	5.206E-07
SiO_2(aq)	9.87	1.643E-04	588.00	2.824E-02 (equilibrium with quartz)
$B(OH)_3$(aq)	63.50	1.027E-03	1550.00	2.505E-02

[1]Holdren and Montaño, 2002
[2]McKibben and Hardie, 1997
[3]Synthesis of analyses from Werner and Olson (1970) and Sturz (1989).

Kinetic Data

Kinetic data were derived from a variety of sources, many based originally on Palandri and Kharaka (2004), and many estimated based on similar mineral structures (Table 6.2). Because the reactive surface area is a major factor in the effective rate and can vary by many orders of magnitude, uncertainties in the rate constants are combined into the effective rate. Thermodynamic data are generally much more impactful in the system evolution because they control mineral stability, i.e., whether the mineral tends to dissolve or precipitate. Determining the effective rate generally is best done by "calibration" of reactive surface areas (RSA), and sometimes by modifications to kinetic parameters/rate laws. Where the ages of

the rocks and their geologic histories are known at least approximately, calibration can be done by running forward-looking "native-state" models and comparing to observed secondary mineral abundances and measured present-day water chemistry.

To simulate the native-state evolution, the model considered the initial unaltered mineral abundances to be the same everywhere. Because primary minerals are generally not reacted completely in the SS-GF, the mineral kinetics and initial water chemistry are the dominant factors. The proportions of the minerals only affect the reactive surface slightly if they are reasonably close. For example, 30% vs. 40% feldspar only affects the rate (through the surface area) by a factor of 0.75, whereas rate constants and reactive surface areas have uncertainties of at least a few orders of magnitude, and the latter must be calibrated in a natural system. Initial mineral volume fractions are given in Table 6.2.

Table 6.2. Mineral kinetic parameters, reactive surface areas, and Li contents in minerals, and bulk rock for the low-reactivity base-case

Mineral	$k_{0,25C}$ (1/s)	Ea (J/mol K)	RSA (cm^2/g)	Li (mol)	Li (ppm)	Initial Vol Frac	Li in Rock (ppm)
hectorite-1	1.6596e-13	35.	1.e-4	0.002	36.60	-	-
hectorite-2	1.6596e-13	35.	1.e-4	0.0115	210.43	-	-
cookeite	1.6596e-13	35.	1.e-4	1.0	13292.7	-	-
ephesite	2.5119E-15	66.2	1.e-4	1.0	17887.2	-	-
lepidolite	1.6596e-13	35.	1.e-4	-	-	-	-
taeniolite	2.5119E-15	66.2	1.e-4	-	-	-	-
elbaite	2.37e-13	58.	1.e-4	-	-	-	-
Li-mica	1.6596e-13	35.	1.e-4	0.5	8912.54	1.9e-4	1.78
Li-albite (ss)	2.75e-13	69.8	1.e-5	0.001	26.47	0.237	6.41
albite (ss)	2.75e-13	69.8	1.e-5	-	-	-	-
Li-K-feldspar (ss)	3.8905e-13	38.	1.e-5	0.002	49.88	0.275	13.70
K-feldspar (ss)	3.8905e-13	38.	1.e-5	-	-	-	-
quartz	6.4E-14 3.2E-12	77. 50.	1.e-5	-	-	0.474	-
halite	equilibrium	-	-	-	-	-	-
barite	equilibrium	-	-	-	-	-	-
gypsum	equilibrium	-	-	-	-	-	-
anhydrite	6.4565e-04	14.3	1.e-4	-	-	-	-
calcite	1.6E-6/1.8E-7	24./66.	1.e-4	-	-	-	-
magnesite	4.571E-10	23.5	1.e-4	-	-	-	-
dolomite	2.9512e-08	52.2	1.e-4	-	-	-	-
ankerite	2.24e-09	48.	1.e-4	-	-	-	-

Mineral	$k_{0,25C}$ (1/s)	Ea (J/mol K)	RSA (cm^2/g)	Li (mol)	Li (ppm)	Initial Vol Frac	Li in Rock (ppm)
strontianite	1.2598e-09	62.76	1.e-4	-	-	-	-
talc	1.00e-12	42.0	1.e-4	-	-	-	-
kaolinite	6.9183e-14	22.2	1.e-4	-	-	-	-
illite	1.6596e-13	35.	1.e-4	-	-	-	-
clinochl-30	1.6596e-13	35.	1.e-4	-	-	-	-
Ca-montmor	1.6596e-13	35.	1.e-4	-	-	-	-
Na-montmor	1.6596e-13	35.	1.e-4	-	-	-	-
K-montmor	1.6596e-13	35.	1.e-4	-	-	-	-
Mg-montmor	1.6596e-13	35.	1.e-4	-	-	-	-
smectite-FeMg	1.6596e-13	35.	1.e-4	-	-	-	-
hematite	2.5119E-15	66.2	1.e-4	-	-	-	-
magnetite	3.98e-14	90.9	1.e-4	-	-	0.0095	-
fluorapatite	2.37e-13	58.	1.e-4	-	-	0.0047	-
sphalerite	1.e-15	50.	1.e-4	-	-	-	-
pyrite	H^+: 3.02E-08 O_2(aq): 2.8184E-05	56.9	1.e-4	-	-	-	-
pyrrhotite	1.4e-09	100.	1.e-4	-	-	-	-
Bulk Rock	-	-		-	-	1.0	21.89

Results of Model Simulation

Model 1: Lithium Evolution Through 3-D Reactive-Transport Native-State Reservoir Model

The native-state geochemical evolution of the SS-GF is approximated by starting with a steady-state EOS1sc fluid and heat flow simulation run for over one million years (My) without considering reactive transport. Water and heat are injected into the base of the reservoir, and the fluxes determined through calibration of the initial EOS1 model from Araya and O'Sullivan (2022) to wellbore temperatures and pressures. Note that this was a pure water EOS, which differs in density and viscosity from a saline brine. However, because the fluid is injected into the base of the reservoir, rather than allowing it to convect above the deeper magma body, it is closer to a forced convection system than a naturally convecting system. As a forced convection system, the flow rates are boundary conditions that are not affected as much by the density and viscosity of the fluid as a buoyancy-driven system. As discussed earlier, we used the supercritical module EOS1Sc, which gives similar results to EOS1, but has updated fluid properties and better transitions near the supercritical point (above 350°C).

For the native-state reactive-transport model, the simulation is then restarted after introducing the chemistry of the brine and Salton Sea (at the surface), using the final temperatures and pressures from the

steady-state simulation. Note that while the fluid densities and viscosities are approximated as pure water, the geochemistry and activities of the fluids behave as a complex saline brine with the initial compositions shown in Table 6.1.

Because the rocks and fluid are already at high temperatures, minerals begin to react immediately, particularly at temperatures over 300°C, but also near the surface (Figure 6.2). Figure 6.2 shows the evolution of secondary minerals formed over 200 years of reaction for the low-reactivity case. Lithium is introduced only in the brine injected at the base of the model, and therefore slowly replaces the fluids in the reservoir, reacting with the rock over time. Figure 6.2 also shows the evolution of the lowest temperature minerals in the cooler region and near the surface (barite), trending to hydrothermal dolomite at moderate temperatures, then anhydrite over a wide temperature range, followed by hectorite-1, cookeite, and then hectorite-2 at the highest temperatures. This order is a little different for the high-reactivity case over longer time periods (see below), where cookeite is more dominant at the highest temperatures. This is expected given that it is a chlorite, rather than a smectite.

Figure 6.3 shows the vertical distribution of Li abundances in brine, mineral changes, and temperatures up to 1000 years for the low reactivity case in the high temperature core of the upflow zone. Note the large amount of hydrothermal anhydrite forming a cap at the top of the reservoir. As brine advects from the base of the reservoir, Li increases from about 10-20 ppm per 100 years in the upper parts of the reservoir, and close to 40 ppm per 100 years at 3 km. Where hectorite and cookeite are precipitating at about 950 m depth, there is a sharp inflection in Li in the brine where it is being removed from the fluid.

Figure 6.5 shows the vertical distribution of Li abundances in brine, changes in the bulk rock Li concentrations, and temperatures up to 4000 years for the low reactivity case in the high temperature core of the upflow zone. Curves for changes in the bulk rock Li concentration illustrate the “extraction” of Li from the brine through much of the reservoir, but only significantly affecting the brine composition shallower than about 1400 m. Below 1500 m depth, Li in the reservoir has attained the maximum value injected and has not increased or decreased noticeably due to water-rock reactions. Two regions show very small net removals of Li from the rock: between about 200 m and 400 m depth, and at the very base of the model where brine is injected. The base of the model involves more uncertainty because the injection temperature is fixed while the bottom temperatures vary, so minor thermal disequilibria may be the cause of the Li removal. However, the trend toward less Li removal from the rock with depth is smoothly varying and is not an effect of the boundary temperature disequilibrium.

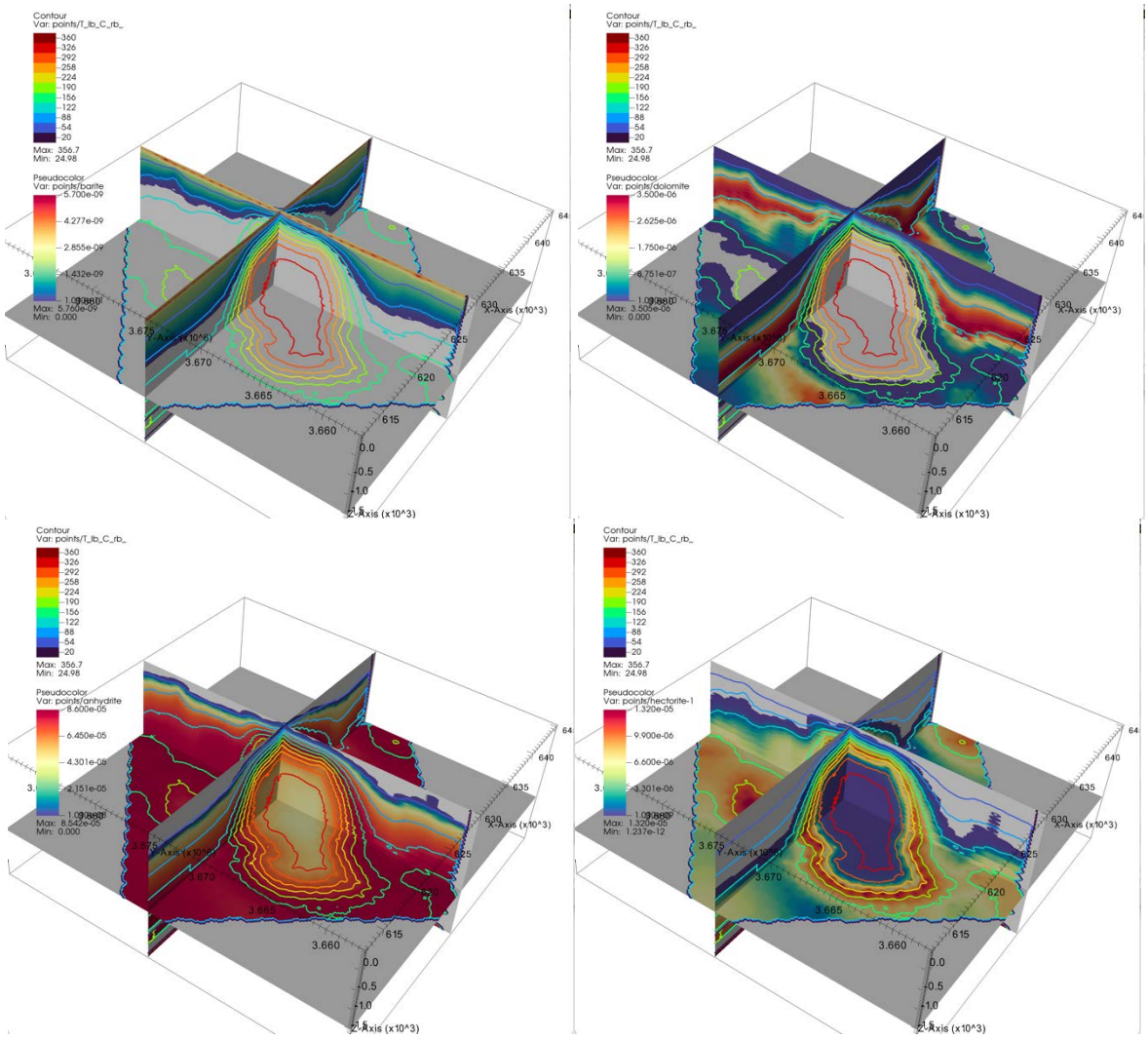

Figure 6.4 shows the vertical distribution of Li abundances in brine, mineral changes, and temperatures up to 2000 years for the low reactivity case in the high temperature core of the upflow zone. Note the large amount of gypsum forming at the surface, and continued precipitation of hydrothermal anhydrite below. At depth, Li in the reservoir is getting close to the maximum value injected and is not increasing or decreasing significantly due to water-rock reactions.

Because the reaction rates for the first case (Figure 6.3) seemed low, another simulation was run using reactive surface areas that are 10 times higher. Distributions of individual mineral changes with depth are shown in Figure 6.6. The dissolution of K-feldspar and albite are quite pronounced at 900 to 1100 m depth, along with precipitation of hectorite and cookeite, leading to greater removal from the brine. The small pink bars at the left (upper scale) show where Li on the order of ppm is being added to the rock.

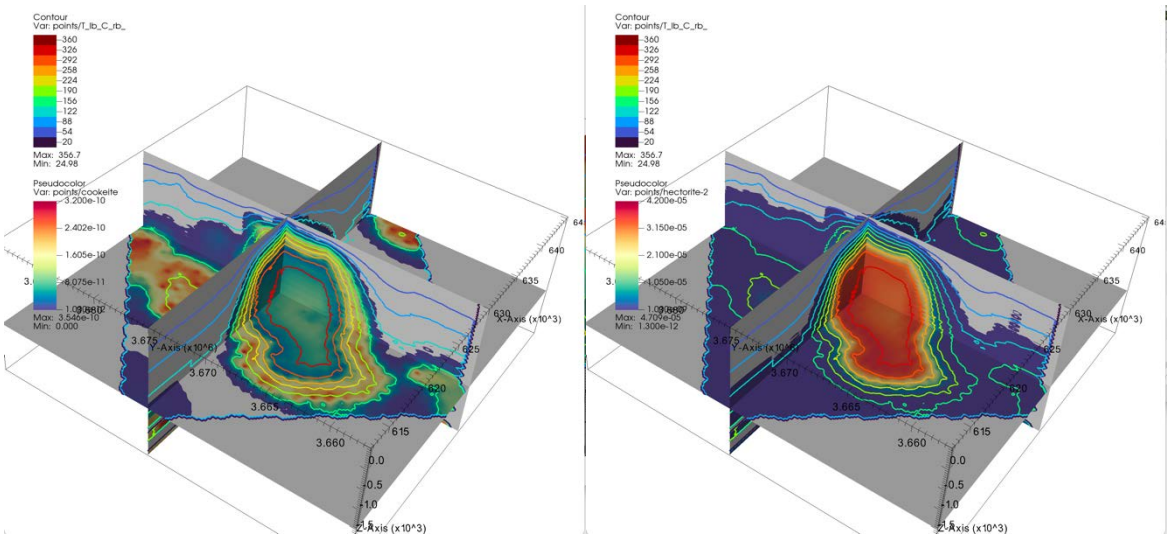

Figure 6.2. Distribution of mineral changes over 200 years; brine convection and reaction for the low reactivity case. In order (left to right, top down): Barite, dolomite, anhydrite, hectorite-1, cookeite, and hectorite-2.

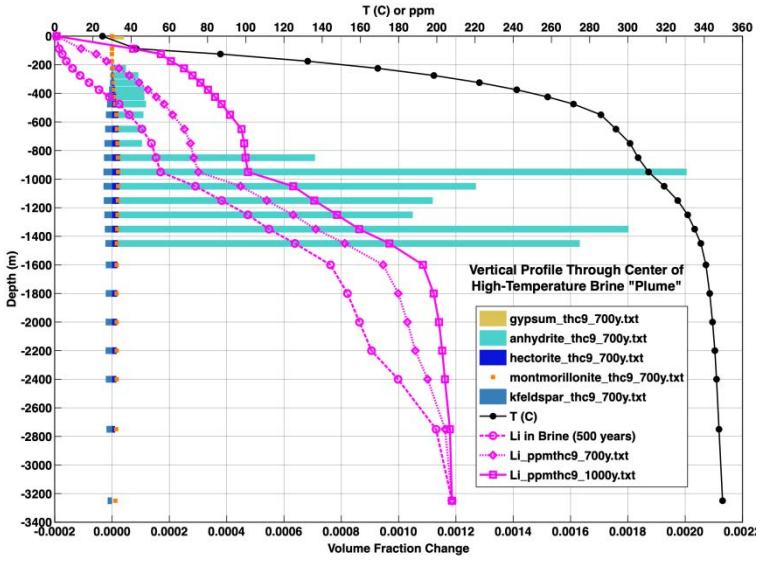

Figure 6.3. Distribution of Li abundances in brine, mineral changes, and temperatures up to 1000 years for the low reactivity case.

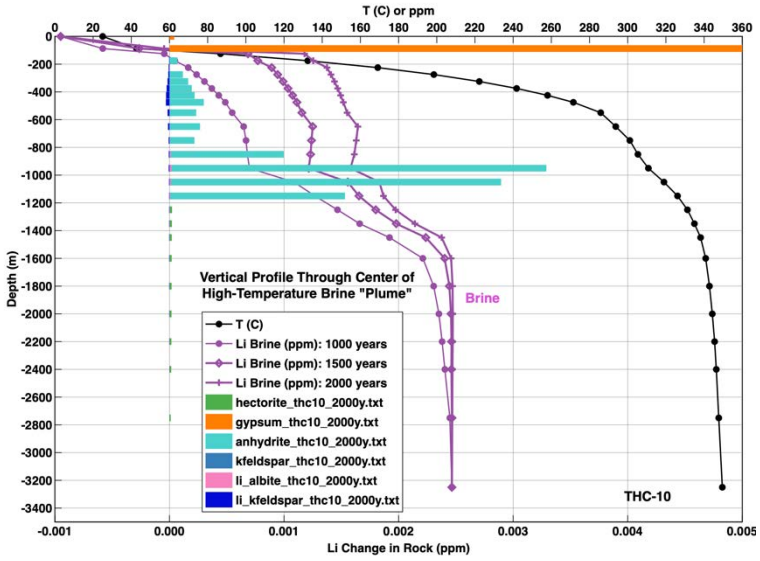

Figure 6.4. Vertical profile of Li abundances in brine, mineral changes, and temperatures up to 2000 years for the low reactivity case.

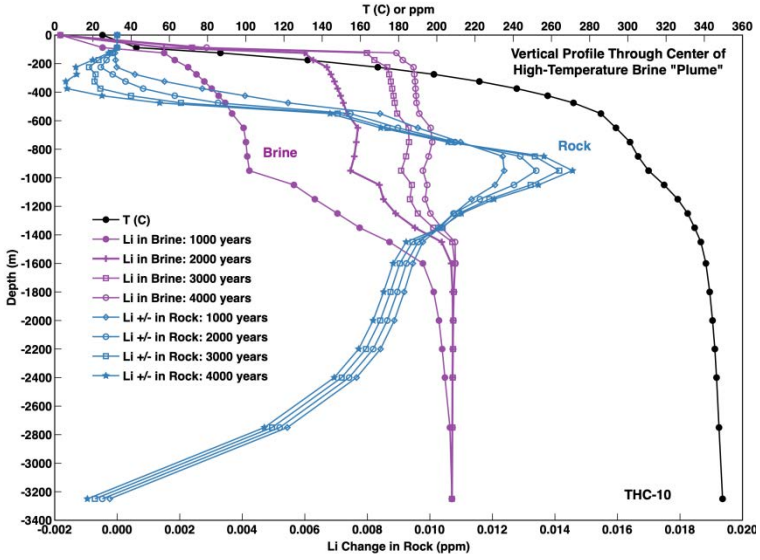

Figure 6.5. Vertical profile of Li abundances in brine and rock up to 4000 years for the low reactivity case.

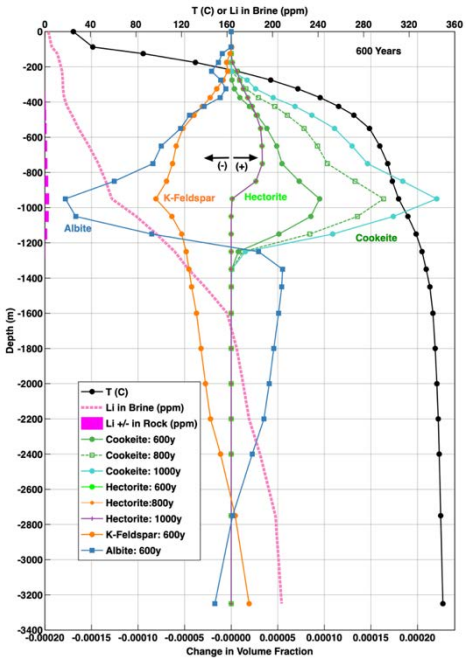

Figure 6.6. Vertical profile of Li abundances in brine and minerals up to 1000 years for the high reactivity case.

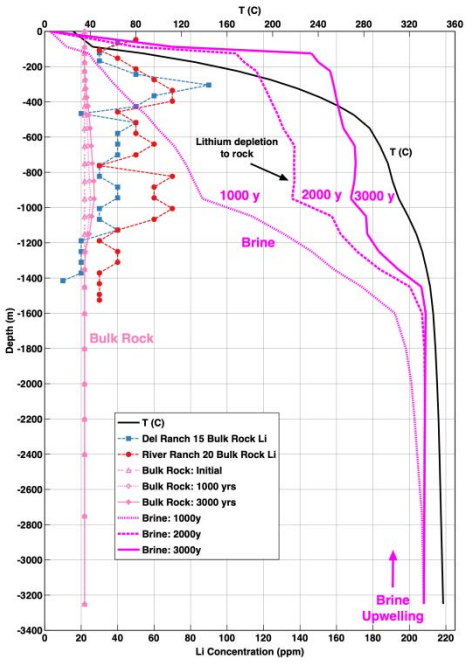

Figure 6.7. Vertical profile of Li abundances in brine and bulk rock up to 3000 years for the high reactivity case. Measured Li abundances in cores/sediments are shown for a few wells.

Distributions of bulk rock Li changes and brine compositions with depth are shown in Figure 6.7 up to 3000 years for the high reactivity case. Also plotted are measured bulk rock Li concentrations. Whereas measured Li concentrations do not span the entire depth range, they clearly show enrichment in the zone predicted by the model. Maximum simulated enrichments of about 10 ppm (starting from 22 ppm) over

3000 years are seen at 950 m depth, with measured concentrations of about 120 ppm. If 40,000 years is an approximate time for the reaction, and Li is added at the same rate, that corresponds to an increase of 133 ppm (total=155 ppm), which is roughly consistent with observed values.

In summary, the 3-D results show that Li in brine is not replenished by Li-bearing minerals within the reservoir footprint. Specifically:

- Li-rich smectite (hectorite) forms at lower temperatures, and Li-rich chlorite (cookeite) at slightly higher temperatures.
- Although dissolution of Li-bearing albite and K-feldspar drives hectorite and cookeite formation, most Li is derived from the hot upwelling Li-rich brine.
- Li is extracted from brine into minerals above 1200 m depth.

Constraints on Reaction Rates

The rates of reaction of minerals interacting with brine are a key factor in predicting the potential for Li to be "extracted" from Li-bearing minerals. Whereas the input parameters and reactive surface areas are consistent with those determined in the much better constrained mid-ocean ridge (MOR) system, it is the effective rates of reaction that require validation. While the high-reactivity case seems more consistent with the observed changes in the rock, it needs further validation.

From the high reactivity case we can sum the maximum volume fractions of primary minerals (Li-albite, albite, Li-K-feldspar, K-feldspar, Li-mica, and quartz) dissolved (at around 950 m depth and 300°C) over 1000 years of brine convection in the highest temperature upflow zone. This yields approximately 1.42 x 10^{-6} volume fraction of primary minerals dissolved per year. An estimated observed reaction rate can be deduced as follows.

Helgeson (1968) noted that about 25% of the rock in the SS-GF geothermal reservoir is hydrothermally altered. Ages of rhyolites at depths ranging from 1600-2700 m are from 420-479 thousand years ago (ka), with a 770 ka age for the Bishop Tuff in State Well 2-14 (Schmitt and Hulen, 2008). These ages and depths give subsidence rates of roughly 3-6 mm/yr. Subsidence rates over the last 40,000 years have been estimated at 10-20 mm/yr (Brothers et al., 2009); which, assuming 15 mm/yr for 40,000 years, gives 600 m subsidence. If repeated intrusions below the Salton Sea took place over at least the last 40,000 years, then these rocks have been above approximately 300°C for 40,000 years, since a depth of 600 meters is still in the hot geothermal reservoir. Assuming a volume fraction reacted of 0.25 over 40,000 years, the reaction rate of the bulk rock is 6.25 x 10^{-6} volume fraction/year. Extrapolating to a depth of 950 m and assuming the same subsidence rate increases the time above 300°C to 63.3 ky and reduces the reaction rate to 3.95 x 10^{-6} volume fraction per year. Certainly, water-rock reactions were taking place at temperatures below 300°C for a longer time period, albeit at a lower rate, so this value is certainly an overestimate of the true rate. The approximate minimum rate can be estimated using the time period for reaction of about 400 ky, which reduces the reaction rate to 6.25 x 10^{-7} volume fraction/year.

Given that the high-reactivity simulation case yields a value of 1.42 x 10^{-6} volume fraction of rock per year, it is in the range of the minimum and maximum estimates. It is possible that the simulated rate is

slightly low, but it is not likely to be an order of magnitude higher. If the simulated rates were much higher, Li concentrations in the brine would be significantly depleted in the reservoir over a few thousand years.

How do these effective rates compare to the MOR system? Simulated rates using TOUGHREACT (DePaolo et al., 2022) give dissolution rates of about 5 x 10^{-4} volume fraction per year, using reactive surface areas for dissolving primary minerals that are four times higher than the high-reactivity case (4 x 10^{-4} vs. 1 x 10^{-4} cm^2/g). These are very similar to experimental rates based on oxygen isotopic exchange (Figure 6.8) and are roughly two orders of magnitude higher than that estimated for the SS-GF. There are at least three major factors for the higher effective rates in the MOR system: (1) higher fluid fluxes maintaining disequilibria – MOR fluxes are about 1 to 5 x 10^{-4} kg/s (DePaolo et al., 2022) compared to maximum upflow rates in the SS-GF of roughly 5 x 10^{-6} kg/s, i.e., two orders of magnitude smaller; (2) potentially greater disequilibria between the convecting seawater and basalt than the convecting brine in the SS-GF; (3) much younger and likely more reactive basaltic rocks compared to sediments and silicic volcanic rocks in the SS-GF. Hence, whereas the rate parameters for the MOR system are similar to those used for the SS-GF, the effective rates are expectedly higher, at least because of the much higher upflow rates.

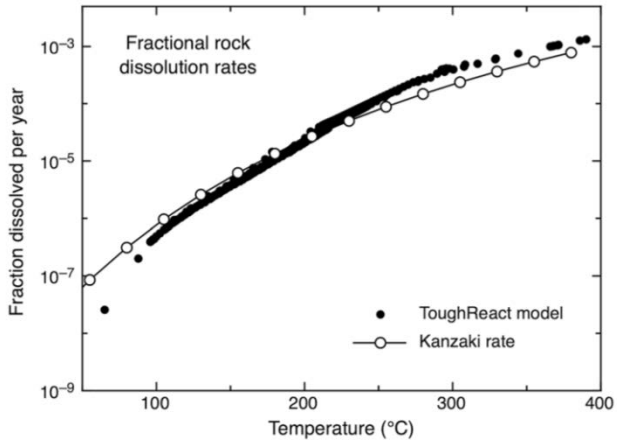

Figure 6.8. Comparison of effective dissolution rates calculated using TOUGHREACT for Mid-ocean Ridge basalts to experimental rates based on oxygen exchange (DePaolo et al., 2022).

Model 2: Lithium Origin Evaluated: Surface Brine Evaporation Reactive-Transport Model

The Salton Sea Evaporation Model is based on the observation that Lake Cahuilla has repeatedly filled and evaporated over at least the past 40,000 years. The Salton Sea water chemistry (Table 6.1; based on Holdren and Montano, 2002) was used as the starting composition. The 1-D model (Figure 6.9, left) assumes an atmosphere with the following initial and boundary conditions:

$$T = 25°C$$

$$RH = 20\%$$

$$P_{CO2} = 0.0004 \text{ bars (400 ppm)}$$

$$P_{O2} = 0.21 \text{ bars (~21\%)}$$

The low relative humidity in the atmosphere drives evaporation, while the atmospheric gas composition is fixed and "communicates" with the water via gas diffusion and equilibration. The model considered equilibrium/kinetic mineral precipitation (Table 6.2), but with no starting minerals. The model was run to near dryness and well past halite saturation (Figure 6.9, right).

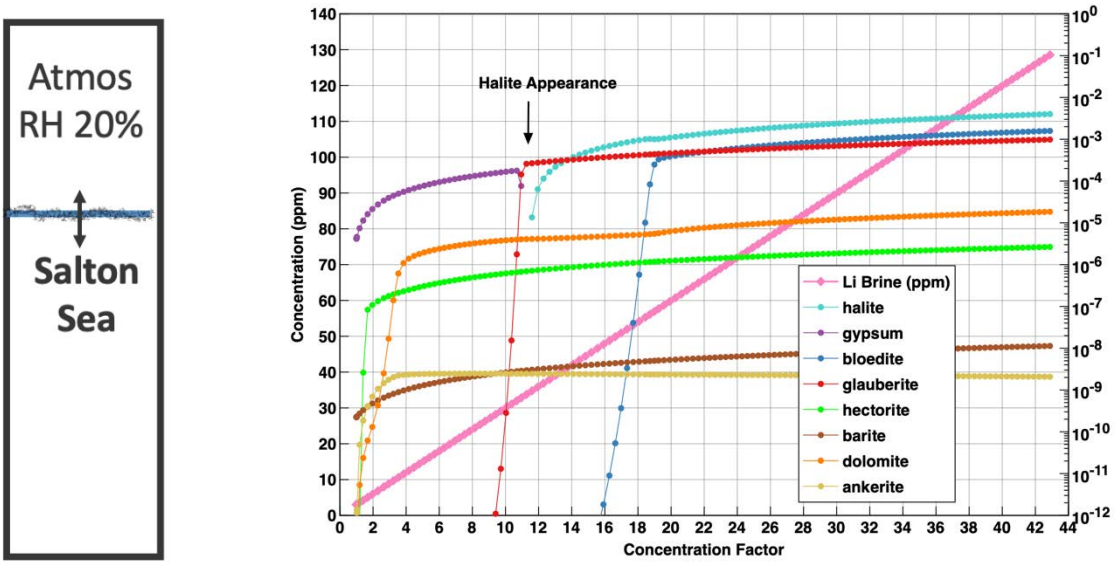

Figure 6.9. Schematic diagram of the 1-D evaporation model for the Salton Sea (left). Simulation using EOS4, showing the onset of precipitation of evaporite minerals, and the Li concentration in the evolving brine (right).

Results of the evaporation model showed:

- Predicted salt minerals are seen in surface evaporites (halite, gypsum, bloedite, glauberite).
- Hectorite (Li-clay) forms (observed in lake deposits) but does not noticeably affect Li concentration in brine.
- Lithium increases to 120 ppm with ~40X brine concentration by evaporation.

After this much evaporation, however, just slightly more than 2% brine is left. The model is consistent with the evaporation of Salton Sea water leading to Li enrichment and observed salt phases, as well as Li-bearing hectorite. However, the amounts of brine are quite small, and under these conditions would be trapped in the evaporite assemblage, as is observed in many playa deposits.

As a simple calculation, we assume a 1 m wide column 2 km high in the geothermal reservoir that has an average porosity of 0.10 and a Li concentration of 200 ppm. If we assume that ancient Lake Cahuilla had an average depth of 40 m, that would correspond to an evaporation down to 1 m of water to get 40X evaporation and 120 ppm Li. To obtain 200 ppm would leave only 0.6 m of brine. To obtain 2 km of 200

ppm brine from a 40 m lake stand would then require 2000/0.6 m or 3333 lakes. Over 40,000 years, that would be a lake filled and evaporated every 12 years, which is highly unlikely. Over 400,000 years, that corresponds to every 120 years, which is still unlikely. The other possibility is that as the lake evaporates, it gets smaller in areal extent, so much of the Li is concentrated in a much smaller volume of brine than just the vertical column would predict. Because the Bishop Tuff is 770 ky old, it is also possible that evaporites and brines started forming at least 800 ky ago.

The following plots (Figures 6.10 and 6.11) show the evolution of Cl and Li in the evaporation model compared to all the values extracted from the 3-D THC reservoir model. The evaporation curve of Cl vs. Li in Figure 6.10 shows the changes in Cl and Li as halite and bloedite precipitate from the brine, and Li reaches about 250 ppm (run about twice as long as the prior simulation). The Salton Sea and deep brine compositions are shown, as well the mixing line. The red cloud of points from the 3-D model are all on the Cl-rich side of the line, indicating Li removal from the fluid. The distribution gets wider towards the Salton Sea composition, indicating greater loss of Li at lower temperatures. One could relate the evaporated composition to the deep brine by simple mixing and reaction of a brine slightly richer in Li than the reservoir. Reactions would also have to involve halite dissolution because the brines are lower than the halite saturation curve (at 25°C at least).

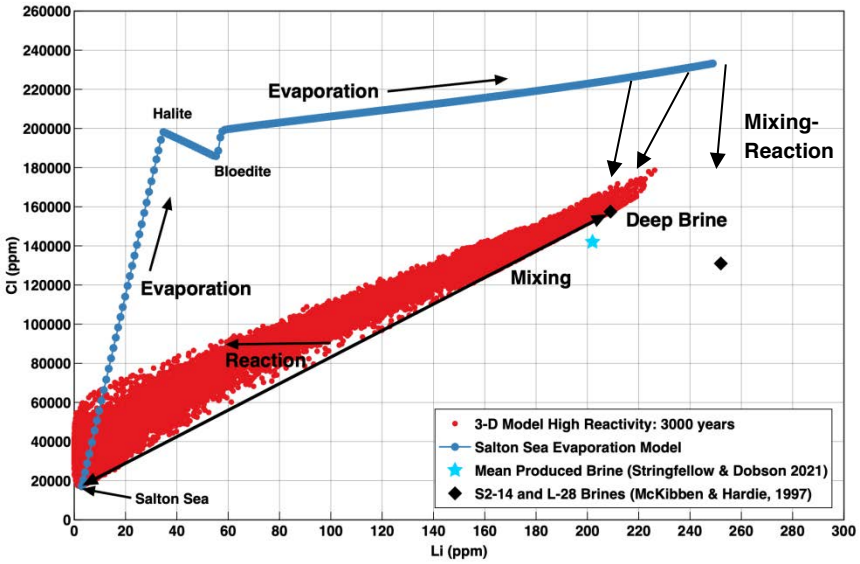

Figure 6.10. Simulation Cl and Li concentrations from the 1-D evaporation model (blue), and all the values from the 3-D SS-GF high-reactivity case after 3000 years.

Figure 6.11 shows the same data plotted on a Li vs Cl/Li plot, further accentuating the lower Li concentrations at a given Cl/Li ratio. For comparison, thermal waters and rhyolites from Yellowstone Caldera are shown (Cullen et al., 2021). Note the moderate Li concentrations in the rhyolites of about 50 ppm, with the hydrothermal fluids only having less than 10 ppm Li. Mono Lake waters also show some enrichment from geothermal fluids, but also at relatively low concentrations of about 10-12 ppm (Tomascak et al., 2003). Isotopic evidence suggests that the source of much of the Li in the playas in the Western U.S. are derived from hydrothermal fluids; however, high Li concentrations must be related to

evaporation, which does not cause Li isotopic fractionation unless an Li-rich mineral is formed (Araoka et al., 2014).

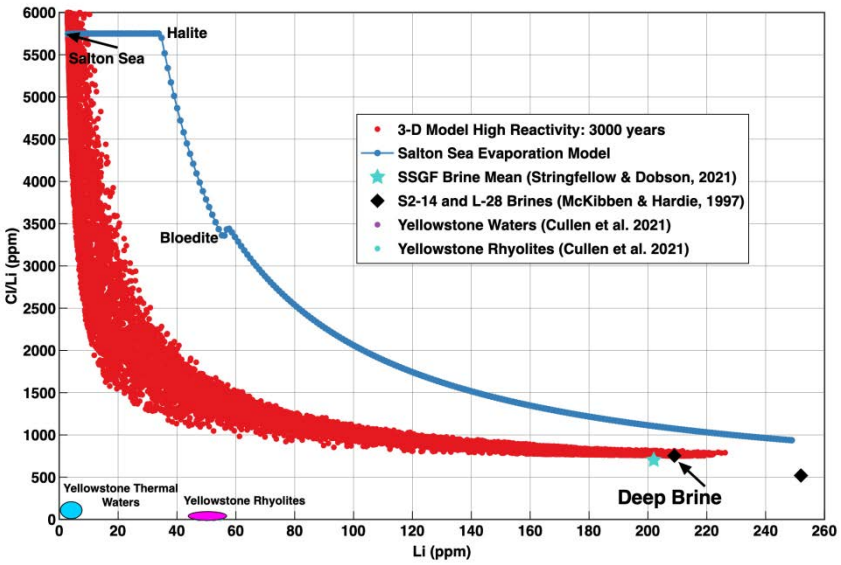

Figure 6.11. Simulated Cl/Li vs Li concentrations from the 1-D evaporation model (blue), and all the values from the 3-D SS-GF high-reactivity case after 3000 years. Also shown are water and rock compositions from the Yellowstone hydrothermal system (Cullen et al., 2021).

Model 3: 1-D Injection-Production Well Reactive-Transport Model

The lithium resource in the SS-GF is controlled by three main sources, with differing timescales of enrichment/depletion: (1) the existing brine in the accessible reservoir; (2) Li-rich brine convecting from the deeper (as yet) inaccessible hydrothermal system; and (3) minerals containing Li. In this section, we evaluate the potential for Li to be added to depleted brine and depleted brine-plus-steam-condensate as it migrates from an injection well to a producing well.

Model 3 Set-up

A 1-D, 400 m long model was built with a grid spacing of 10 m, fine enough to capture the brine advection-reaction front and typical injector-producer well separations of several hundred meters (Figure 6.12). Because the well completions vary in depth and length, the system does not conform to a typical radial well pattern. Therefore, the model represents a flow path for a fluid parcel as it moves through the reservoir and reacts with the rock. The initial conditions (P = 24 MPa, T = 346°C) for the model were derived from the 3-D THC model at a depth of 2450 m. At these depths, less Li was observed to be removed from the naturally convecting brine to the rock in the native-state simulations, and therefore more Li could potentially be mobilized (as a result of more thermodynamically favorable dissolution reactions and greater reaction rates at higher temperatures). Because the producer is simulated using an infinite volume grid block at fixed reservoir pressure, an observation point at 350 meters was chosen to evaluate the lithium breakthrough curve over time.

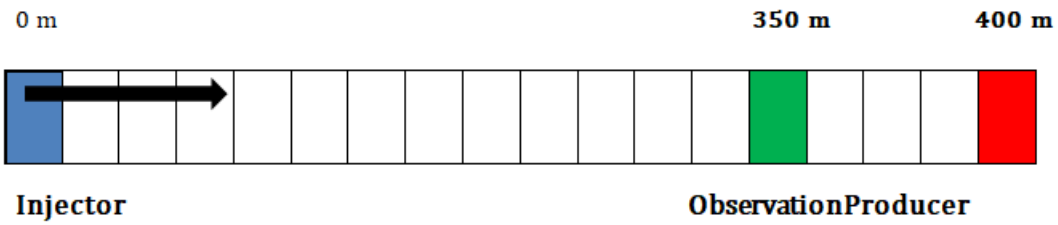

Figure 6.12. Schematic diagram of the 1-D injector-producer reactive-transport model. Note that the simulation grid has 40 grid blocks for a spacing of 10 m.

Two injection chemistries were evaluated: (1) a Li-depleted brine (State Well 2-14 composition with reduced Li); and (2) a diluted brine, equivalent to 90% pure steam condensate mixed with 10% Li-depleted brine. The mineral reactive surface areas were also increased by a factor of 10 for the brine, and for the condensate-rich injectate, to capture increased path lengths between injector and producer. Longer path lengths increase the potential for Li-bearing minerals controlled by kinetics to react and contribute to the depleted fluids as they migrate to the producer. All kinetic-rate parameters are as shown in Table 6.2.

If only Li-depleted brine is injected, the tendency for minerals to be out of thermodynamic equilibrium will be small, because Li is a trace component and will not significantly affect the mineral stability. However, condensate is likely undersaturated in most reservoir minerals, so there will be a much greater tendency to dissolve primary minerals (and potentially secondary minerals) releasing Li into solution. In the native-state model, most Li dissolved from primary minerals was incorporated in secondary Li-bearing minerals such as hectorite and cookeite and did not result in increased Li concentrations in the brine. Mineral equilibria may also be perturbed due to fluid mixing, changing P-T conditions, or reaction with differing mineral assemblages.

An arbitrary injection rate of 86.4 kg/day was used so that sufficiently long breakthrough times (i.e., midpoint in Li concentration) would occur at the observation point (about 68 years) and first arrivals of condensate after less than ten years (Figure 6.13). These timescales are roughly similar to observed injected condensate arrivals in productions wells in the SS-GF. Note that whereas these injection rates appear small, the system is 1-D, rather than 1-D radial, so the flow is confined to a constant area (100 m^2) and rock volume (1000 m^3 blocks) path, rather than radially increasing reservoir areas and volumes.

Concentrations of Li in fluids at the observation point (Figure 6.13) are nearly identical and drop to near zero (depleted fluid composition) regardless of injection fluid composition or increased reactive surface area. Injection fluids consisting predominantly of condensate drive the reservoir fluids to lower Li concentrations, because disequilibria just drive precipitation of more Li-rich minerals such as cookeite.

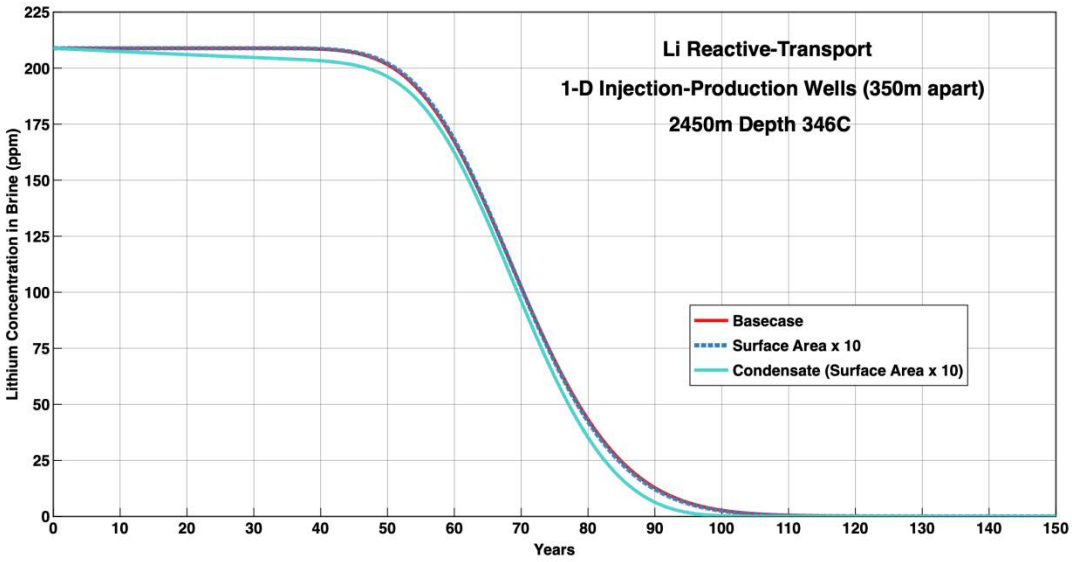

Figure 6.13. Li concentration over time at observation point 350 m from injection well.

A plot of the mineral evolution at the observation point (Figure 6.14) shows dissolution of Li-bearing albite and precipitation of cookeite and Li-bearing K-feldspar. Although cookeite shows relatively minor precipitation compared to Li-bearing K-feldspar, it has far higher Li concentrations; thus, Li is depleted in the fluid. Because cookeite is a Li-rich chlorite, and chlorite is stable over a wide range of temperatures and fluid compositions, it is not likely that any perturbations in reservoir conditions would lead to cookeite (or Li-bearing chlorite) breakdown and Li enrichment in the brine. Temperatures and pressures would have to increase such that chlorite is replaced by biotite, as is observed in the deepest sections of the accessible reservoir. However, like chlorite, biotite also can accept significant amounts of Li in its structure (Ellis et al., 2002), and therefore Li-enrichment in a brine by a prograde chlorite to biotite reaction, or a retrograde biotite-chlorite reaction, is also unlikely to increase Li concentrations significantly in the fluid (compared to the 200+ ppm observed). While Li enrichment in geothermal fluids is common (e.g., Yellowstone hydrothermal system; Cullen et al., 2021), the enrichments are typically a few tens of ppm, starting from fluids with a few ppm or less (see Figure 6.11).

Summary

Three-dimensional reactive-transport simulations over 4000 years using the SS-GF reservoir model, considering hypersaline brine convection in unaltered reservoir rocks, results in alteration to hectorite at lower temperatures and primarily cookeite (Li-chlorite) at temperatures over 300°C. The high initial Li concentration in the hypersaline brine leads to small increases/decreases in reservoir bulk rock Li concentrations, and little change in brine Li concentrations (except at the top of the reservoir, where more Li is removed from the brine).

In the surface evaporation model, reduced atmospheric relative humidity leads to hypersaline brine formation from Salton Sea water, with an increase in Li to 120 ppm after about 44X evaporative concentration. This forms the observed low-temperature phases of gypsum, barite, halite, glauberite, bloedite, carbonates, and the Li-rich clay hectorite, consistent with observed salt and clay mineral

assemblages. Preliminary models are consistent with high Li concentrations in SS-GF brines derived primarily from shallow evaporative concentration; however, the hydrologic conditions and Li concentrations of Lake Cahuilla waters are key uncertainties over the 400,000-plus year history of the system.

Under most conditions, Li-bearing minerals form through hydrothermal interactions with Li-bearing evaporitic brines. Reaction of Li-bearing minerals with Li-poor fluids generally results in dissolution of some Li-bearing minerals and co-precipitation of other more stable minerals without much change in the brine Li concentration.

The primary replenishment mechanism for Li is the upward flux of convecting Li-rich brine from below the producing reservoir, and unexploited brines in the reservoir. Assuming the calibrated upward basal fluxes in the reservoir model, and Li concentrations in the upwelling brine of about 200 ppm, Li enrichment of depleted brines at 2750 m depth is roughly 10 ppm per 100 years.

At the bottomhole depths of deep production wells (~2000-2700 m), with brine temperatures exceeding 300°C, reactions of relatively stable Li-bearing metamorphic minerals (primarily cookeite-chlorite, feldspars, and micas) are slow, and thus injection of Li-depleted brine or condensate is not enriched by mineral-water reactions over time periods of hundreds of years.

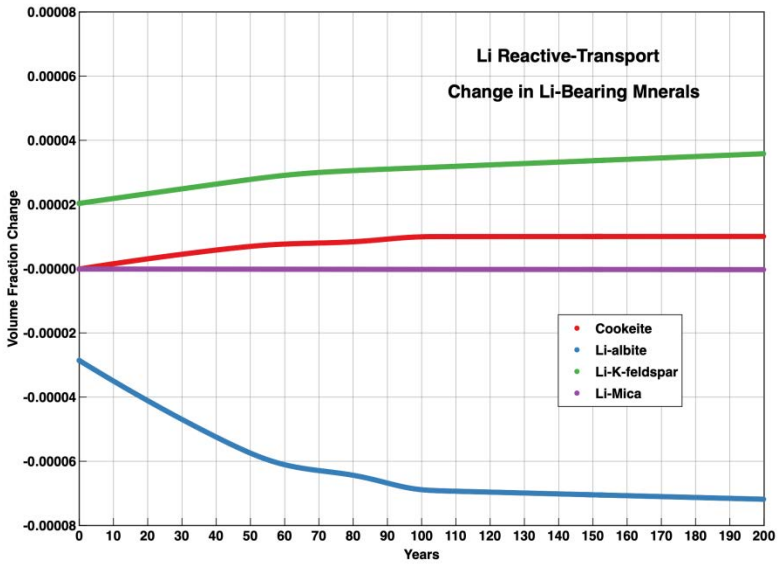

Figure 6.14. Change in Li-bearing mineral abundances over time at observation point 350 m from injection well. Note that while Li-bearing albite feldspar dissolves, cookeite and Li-bearing K-feldspar precipitates, resulting in no net gain of Li to the reservoir fluid.

SECTION THREE:
Environmental Considerations

Chapter 7: Evaluation of Potential Water Impacts Associated with Lithium Extraction and Potential Expansion of Geothermal Production

Key Takeaways

- Local surface water and groundwater resources exceed maximum thresholds for total dissolved solids and contaminant levels, and are not suitable for municipal or industrial use. Geothermal and lithium extraction processes would use water from the Colorado River.
- Water demand for lithium extraction is appreciable, representing 3.5-4X the freshwater requirement of geothermal energy production alone from a given volume of brine. However, this amount of water use is significantly less than that required for conventional approaches to lithium removal from brines, such as evaporation ponds.
- Regionally, the water demand for currently proposed geothermal production and lithium extraction facilities is modest, increasing demand for the region's historical Colorado River supply by ~3%. Due to the megadrought in the Colorado River basin, any increase in the region's water demand should be carefully evaluated.

Introduction

Planning for the electricity grid of the future must consider water resources, as they are a critical and often non-negligible input to both conventional and renewable energy generation, as well as their associated supply chains. For energy generation, water is used in varying amounts in almost all production and conversion processes, making the energy type and technology choice important factors for regional water use (Spang et al., 2014). In California, ~18% of total water withdrawals were used for thermoelectric power in 2015 (USGS, 2015; Dieter, 2018), considerably less than the national average of 45% (Maupin et al., 2014). "Water withdrawal" is defined as water diverted from a source for use, whereas "water consumption" is the portion of the withdrawal that is evaporated, transpired, incorporated into products/crops, or otherwise removed from the immediate water environment (Kenny et al., 2009). Traditional fossil-fuel based energy production requires large volumes of water to be withdrawn for cooling, but only a small portion of this is consumed due to evaporation and losses; most is returned to the local environment (Figure 7.1).

As we move away from conventional fossil-based energy, water needs will continue to be a concern. Renewable energy sources may have lower water withdrawal requirements overall, but in some cases have higher water consumption requirements. Significant amounts of energy storage will be required to optimize greater deployment of renewable energy generation at scale. The additional water needs of energy storage technologies are not captured in Figure 7.1.

Conventional methods of extracting and processing lithium from subterranean brines and hard rock ore deposits are water intensive. Currently, to extract lithium from brines, low-concentration brine must be pumped to the surface and stored in expansive evaporation ponds for a few months to years. Most of the water is lost to evaporation, concentrating lithium in the water that remains. Alternatively, lithium can be

extracted from pegmatite ore bodies and separated into valuable spodumene through crushing, milling, and flotation processes (Wietelmann and Steinbild, 2014). Extracting lithium from subterranean brines consumes large volumes of high-salinity brines, but consumes less freshwater per tonne than ore-based methods (Kelly et al., 2021).

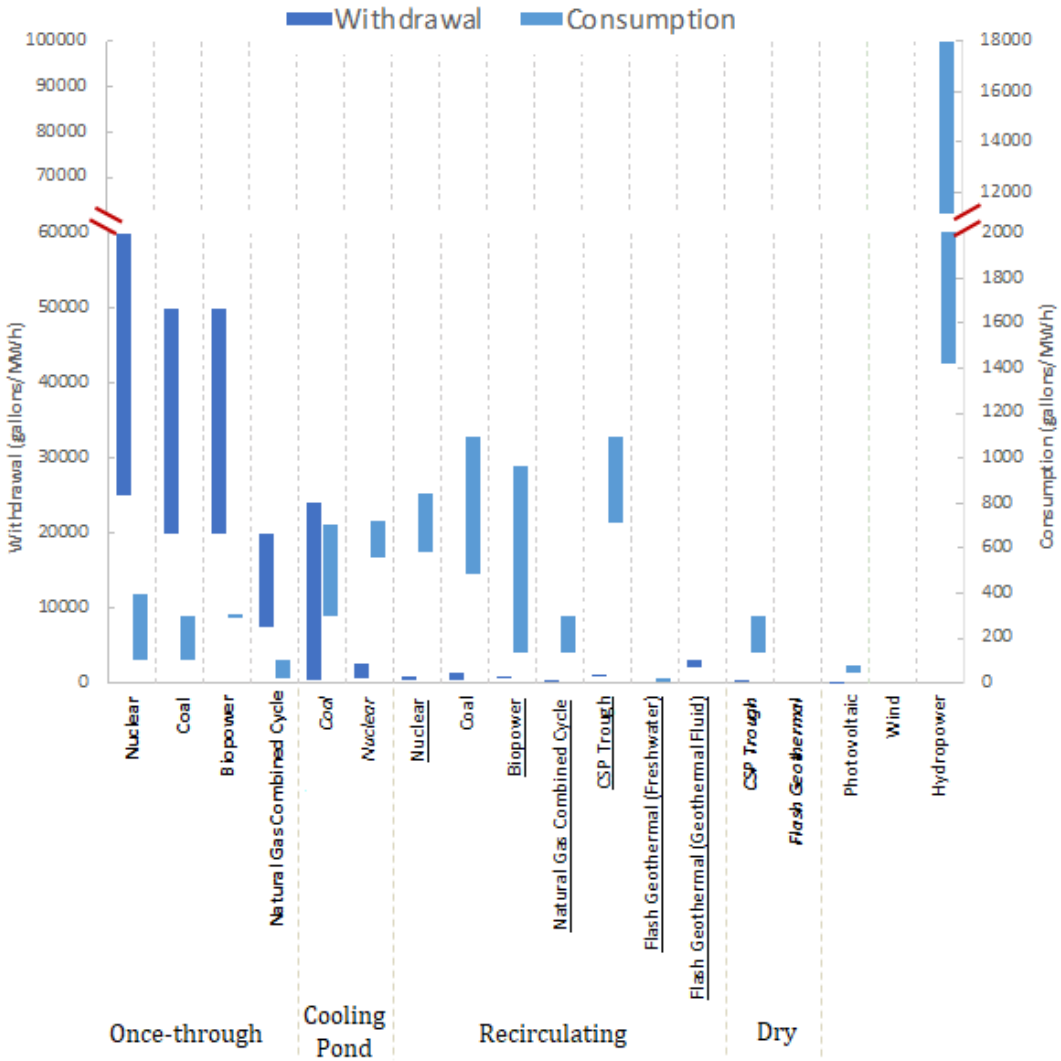

Figure 7.1. Water withdrawals and consumption rates for fossil-fuel and renewable power production depending on cooling type (bold = once-through; italics = cooling pond; underlined = recirculating; bold/italics = dry cooled) (MacKnick et al., 2011).

The U.S. may be able to produce significant quantities of lithium domestically with lower water consumption than conventional lithium extraction methods by extracting lithium from the geothermal brine that is already brought to the surface to produce renewable energy. This approach utilizes an existing waste stream from geothermal energy facilities (i.e., the separated brine), giving dual purpose to these renewable energy sources and minimizing the construction of additional wells or withdrawal of additional brine. Another possible synergy is to use the geothermal power to provide the energy needed to run the lithium extraction process. In the Salton Sea region, where significant reserves of geothermal

brines containing lithium exist, regional plans project that lithium extraction will be adopted at many if not all existing geothermal plants, and that additional facilities that optimize both geothermal energy production and lithium extraction will be built.

The Salton Sea region is a hot desert environment with limited local freshwater resources, and water availability is a high-priority issue for local communities. It is therefore critical to assess how growth in geothermal production and lithium extraction may impact water consumption. The sole source of freshwater in the region is the Colorado River, a watershed where a current megadrought has prompted a reexamination of water allocation in the region and necessitates evaluating the water source, the quality of the water, and the timing of the use. For processes that require high-quality water and exceed onsite water recycling capabilities, water will need to be diverted from other freshwater uses in the region.

To understand the potential impact of expanding geothermal and lithium production, this chapter focuses on three goals:

1. Understanding the current water availability, water quality, and water demands in the region, before any expansion of geothermal production or new lithium extraction facilities.
2. Quantifying water needs for expanding geothermal production and lithium extraction from geothermal brines in the region.
3. Evaluating the impact this additional demand would have on constrained water availability in the region.

To achieve the first goal, we reviewed public documents released by the regional water provider, the Imperial Irrigation District (IID); data collected by the State of California; and recent news on the status of negotiations on water use in the Colorado River Basin. We then summarized current uses, constraints, and pressures for local surface water, Colorado River water from IID, local groundwater, and the Salton Sea itself.

We pursued the second goal by using publicly available resources to develop both top-down (facility-based) and bottom-up (unit process-based) estimates of the water usage for the geothermal energy production process and additional lithium extraction in the area. We used the best available data to identify the water quality needed in each process step to contextualize onsite treatment requirements and new waste streams. Based on this, we estimated the annual water volume of freshwater needed from IID to support growth in these activities. (Note that data on the specific lithium extraction processes that will be used were limited, so projections are uncertain.)

For the third goal, the team reviewed and compiled publicly available resources on water quantity and quality in the region and current and anticipated negotiations over Colorado River water allocations. We also evaluated whether current allocations could support geothermal and lithium extraction activities, and discussed potential impacts from reallocation of existing water resources in this already water-scarce region.

Current Water Availability and Quality Concerns

The SS-GR is located in the Imperial Valley, which is part of the Colorado River watershed and is located in the southeastern corner of California (Figure 7.2). Four water resources in the region could be relevant to decisions about lithium production: local surface water, Colorado River water, groundwater, and the Salton Sea itself. Water availability and quality concerns for each of these resources are discussed below. Timing of use may become an issue if local water conveyance networks operate at maximum capacity during parts of the year (e.g., hot summer irrigation periods) but was not further evaluated in this report.

Local Surface Water

The region is arid, with average summer temperatures exceeding 100°F (37.8°C) and average annual precipitation of less than three inches. The New and Alamo Rivers flow into the Salton Sea and recharge it, but primarily function as agricultural drains. Because rainfall is limited in typical years and local channels are contaminated with agricultural runoff and sewage, local surface water resources available for use by the geothermal or lithium extraction industries are negligible. Local surface water is not included in long-term water resource planning for industry or municipal use in the region.

Colorado River Water

Surface water is conveyed from the Colorado River to the Imperial Valley by the IID through thousands of miles of canals. Irrigation typically consumes over 95% of IID's Colorado River supplies to the region; in 2023, over 97% of IID water was used for agriculture, whereas 1.5% was for municipal potable (drinking water) uses and nearly 1% was used for commercial and industrial purposes, including geothermal production. Industrial and municipal water from IID canals costs $85 and $20 per acre-foot (AF), respectively (IID, 2023), which is considerably less than water used in many other areas of California (AQUAOSO, 2021). An acre-foot is equivalent to water use by one to two average U.S. households for a year.

The legal right to this water source was established prior to and codified in the 1922 Colorado River Compact. The Compact specifies that 15 million acre-feet (MAF) be allocated for use by seven U.S. states: Arizona, California, Colorado, Nevada, New Mexico, Utah, and Wyoming. About one-third of the water (4.4 MAF) is allocated to California, and another 1.5 MAF is allocated to Mexico. IID has a senior water right to 2.6 MAF – over 700 billion gallons – of Colorado River water each year.

The allocations made in the 1922 Compact are now believed to have been based on a period of unusually high rainfall, making them overly optimistic about water availability in the basin. The Colorado River watershed has been experiencing a long-term megadrought in recent years, with river flows falling below 11 MAF annually. Withdrawals have decreased to 13 MAF, below legal allocations but still exceeding the flow currently available. Reservoirs along the Colorado River, particularly in the lower basin states of California, Arizona, and Nevada, have experienced depletion for years.

Use of Colorado River water is an active topic of negotiations (see Appendix Chapter 7 for more detail.) However, in late May 2023, the seven Colorado River basin states reached a voluntary agreement to

reduce water demand in the lower basin states. The lower basin states (California, Arizona, and Nevada) agreed to reduce water consumption by 14%, with each taking a proportional share of the shortage. Because California gets the largest allocation from the river, it will provide the largest volume of demand reductions under this plan. The 14% cuts are lower than the USBR originally requested, but the states argued that the exceptionally wet winter of 2023 should forestall the need for more substantial cuts. Because of this agreement, the USBR has temporarily withdrawn its Supplemental Environmental Impact Statement during its environmental review of the states' proposal.

If the voluntary agreement of the Colorado River basin states is approved by USBR, its effects will only be temporary, as the current drought contingency plan is set to expire in 2026. A new round of negotiations is set begin to establish longer-term water allocation agreements between the basin states. As a result, the implications for future water availability in the Imperial Valley are somewhat uncertain, though IID's senior water right remains.

Groundwater

Statewide, 40% of California's water supply comes from groundwater (SWRCB, 2020). In the Salton Sea region, however, groundwater is not an important source. Though a large groundwater basin stretching over 4800 km^2 (1,200,000 acres, or 1870 square miles) underlies the Imperial Valley region (California Department of Water Resources, 2004), poor groundwater quality prevents this basin from being a useful source of water for agricultural, municipal, or industrial purposes. Most groundwater wells in the region are less than 600 m (2,000 ft) deep, which is considered shallow well water. These wells are isolated from deeper wells, such as those used for geothermal brine extraction which can extend as deep as 6,000 m (20,000 ft) (Tompson et al., 2008). Further, the surface shallow aquifers and the Salton Sea are hydraulically separated from each other by deposits with low transmissivities (>1000 gallons per day per foot of depth). The primary source of recharge water for local aquifers is unlined agricultural canals (Morton Bay Geothermal LLC, 2023).

Using publicly available data from the California Water Board's Groundwater Ambient Monitoring and Assessment Program (GAMA), we collected groundwater monitoring data for wells in Imperial County for critical contaminants, including arsenic, perchlorate, hexavalent chromium, uranium, nitrate (as nitrogen), total dissolved solids (TDS), and lithium. Table 7.1 summarizes these contaminants and their federal and state maximum contaminant levels (MCL), maximum contaminant level goals (MCLG), and public health goals (PHG). Values are reported in milligrams per liter (mg/L). Water constituents' MCLGs represent the concentration at which the constituent causes no known adverse health effects. Federal allowable maximum contaminant levels (MCLs) for a constituent are established as close as possible to the MCLG while considering costs. A mg/L is sometimes reported as parts per million (ppm) and akin to dissolving a single grain of table salt in a liter of water. A detailed description of relevant federal and state water quality regulations is available in Appendix Chapter 7.

Table 7.1. Contaminant concentrations and limits in drinking water

Contaminant	Relevance	Federal MCL / MCLG (mg/L)[1]	California MCL[2] / PHG[3] (mg/L, unless noted)
Arsenic	Carcinogen; skin lesions	0.01 / 0	0.01 / 0.002
Perchlorate	Thyroid hormone disruptor	Being evaluated	0.006 / 0.001
Hexavalent Chromium	Carcinogen	None[4]	In progress / 0.00002
Uranium	Carcinogen		None / 0.43 pCi/L
Nitrate as nitrogen	Carcinogen; birth defects; thyroid disease	10 / 10	10 / 10
TDS	Affects aesthetics; may indicate high levels of other harmful contaminants	500[5] / None	500[5] / None

Acronyms: MCL = maximum contaminant limit; MCLG = maximum contaminant level goals; mg/L = milligram per liter; pCi/l = picocuries per liter (a measure of radioactivity); PHG = public health goal; TDS = total dissolved solids.

Notes and sources:

[1] (U.S. EPA, 2023a; b)

[2] (SWRCB, 2018a; b)

[3] (OEHHA, 2023)

[4] EPA regulates total chromium with an MCL and MCLG of 0.1 mg/L.

[5] The MCL for TDS is a secondary standard indicating that higher concentrations may affect aesthetics (e.g., taste and odor) but do not have health impacts. Other MCLs in the table are enforceable primary standards.

Water quality in Imperial Valley is highly variable. Regional analysis of water quality and quantity for well, geothermal, and irrigation water was conducted and summarized in 1970 (Werner and Olson, 1970). Most locations where water has been tested indicate that the water is undesirable for use without extensive treatment due to high TDS (489-7280 mg/L) and high levels of fluoride and boron (Werner and Olson, 1970; Loeltz et al., 1975). Concentrations of TDS, arsenic, and lithium are discussed below. Nitrate has been detected at moderate levels. Hexavalent chromium, perchlorate, and uranium have not been detected in the region of Imperial County near the Salton Sea. Appendix Chapter 7 presents additional information on the spatial distribution of perchlorate, hexavalent-chromium, uranium, and nitrate (as nitrogen).

TDS is regulated with a secondary MCL. Secondary MCLs reflect aesthetic requirements for water (e.g., taste, odor, appearance) rather than concerns about human health. Though the federal secondary MCL for TDS is 500 mg/L, anything above 100 mg/L is usually considered high TDS for drinking water. TDS requirements for agriculture vary depending on the crop being grown, the chemical species dissolved, and other factors. Figure 7.2 illustrates the locations and concentrations of wells that have been tested for TDS. In some cases, TDS varies over time. Figure 7.2 shows all measurements that have been taken; in some instances, multiple measurements have been taken at the same well. Because of the high concentration of TDS, it would require significant treatment using reverse osmosis (RO) or a similar technology to use this water for irrigation or municipal purposes. RO requires substantial energy to

operate and creates both a stream of clean water and a concentrated waste stream that must be disposed. The presence of other constituents in the water can sometimes complicate RO treatment.

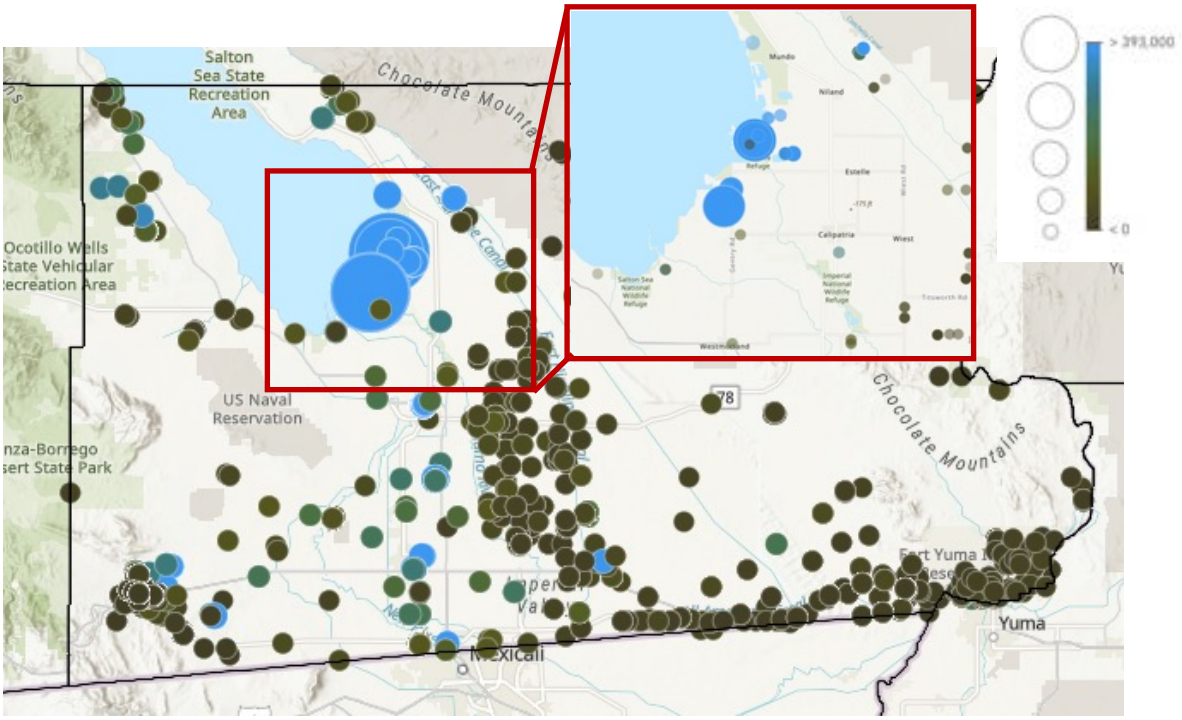

Figure 7.2. Spatial distribution of TDS measurements (mg/L) from wells in Imperial County. Color and size indicate the concentration.

Arsenic has been measured at high concentrations near the south shore of the Salton Sea (320 µg/L) (Figure 7.3), which far exceed the federal and state MCLs of 10 µg/L and the PHG of 2 µg/L. Arsenic is present in groundwater worldwide, often due to natural deposit in soils (Chakrabarti et al., 2019). It is of significant concern due to its toxicity and adverse health effects if consumed, even at low concentrations (NRC, 1999). There are many technologies to remove arsenic from drinking water based on principles of oxidation and filtration, biological oxidation, co-precipitation, adsorption, ion exchange, and membrane technologies (Jain and Singh, 2012).

Baseline concentrations of lithium in groundwater in the region were monitored to a limited extent between 1970 and 1989. More recent samples for lithium were not available in the GAMA dataset. The results from lithium sampling are shown in Figure 7.4 and Figure 7.5. Figure 7.4 shows the spatial distribution and concentrations of the samples. Figure 7.5 shows the limited trends we can see over time among samples collected within a 15-mile radius of the southern tip of the Salton Sea. Lines connect concentrations taken at the same well. Very few wells have been monitored for lithium concentrations over extended periods of time (i.e., between years) even though the concentration in the same well is highly variable within a year, as illustrated by the vertical lines connecting wells on the graphs in Figure 7.5. Within a single well in 1981, the lithium concentration varied between approximately 100-550 micrograms per liter (µg/L). Further, very few samples have been taken near the SS-GR after 1989. These limited samples indicate that lithium has been present in high concentrations in the area's groundwater for decades, and that the groundwater at these depths has substantially lower concentrations

of lithium than geothermal brines. Though there is a small risk that expanding geothermal energy in the region could add lithium to the groundwater due to well leaks or leaks in wellheads or pipelines (leading to infiltration of discharged water into shallow groundwater), this will not be a factor in decisions about whether groundwater can be used.

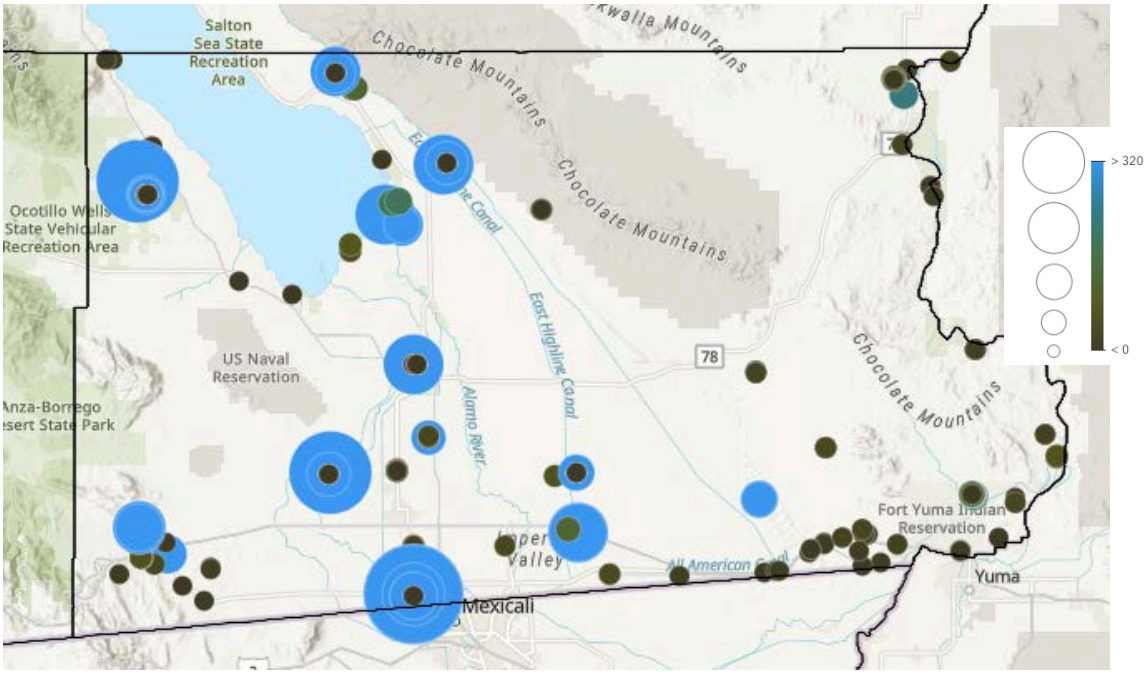

Figure 7.3. Arsenic concentrations (µg/l) in groundwater wells in Imperial County. Color and size indicate the concentration.

There is no current regulation for Li concentrations in drinking water at a state or federal level, although a national Health-Based Screening Level (HBSL) of 10 µg/L exists. HBSLs are non-enforceable water quality benchmarks developed by the USGS National Water-Quality Assessment Project (NAWQA) to set benchmarks for contaminants without MCLs (USGS, 2018; Dieter, 2015). Most of the well samples within a 15-mile radius of the southern border of the Salton Sea exceed the HBSL threshold of 10 µg/L for lithium (Figure 7.4), some by several orders of magnitude. Significant additional contamination caused by new lithium extraction from brines is possible via leaky wells but unlikely due to its economic value; even if it occurred, it is unlikely to significantly impact regional water quality. However, water quality can vary significantly between locations within a region. If lithium extraction expands, sites should be sampled to determine local baselines, and monitoring practices may be needed to verify that baseline concentrations of changes in lithium are not changing because of geothermal and lithium extraction practices. It may also make sense to begin considering enforceable standards for lithium and develop regulations around lithium in water sources for human protection.

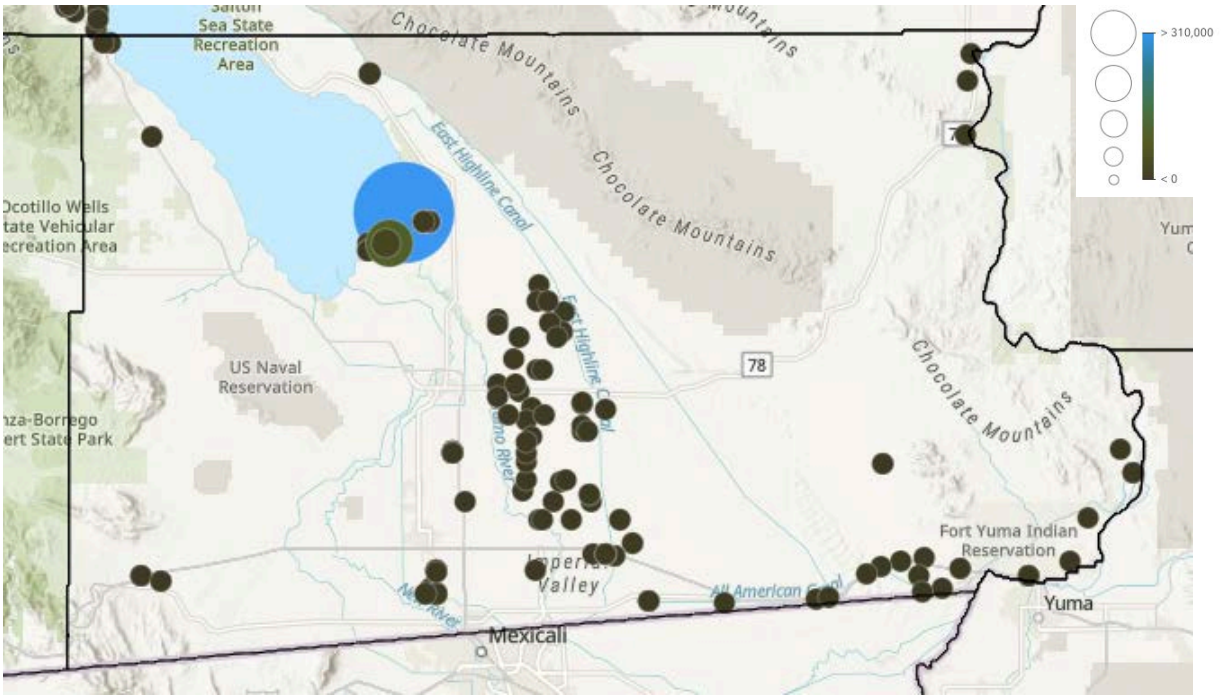

Figure 7.4. Spatial distribution of lithium concentrations in sampled groundwater in Imperial County. Color and size indicate the concentration.

In the future, we anticipate an increase in consistent groundwater monitoring, which may necessitate reconsideration of the conclusions of this report. The Salton Sea Monitoring Implementation Plan indicates that monitoring of groundwater in the region will include quarterly measurements of groundwater elevation, temperature, dissolved oxygen (DO), pH, salinity, and turbidity. Quarterly (and then semi-annually) TDS, total suspended solids (TSS), nutrients and contaminants (Se, Ar, Bo, etc.), and pesticides used in the area will be tested annually (Environmental Science Associates, 2022). Lithium was not explicitly mentioned as a targeted contaminant in this monitoring program.

Salton Sea

The Salton Sea has been alternately a large inland lake and a dry sink throughout California's geologic history. The current Salton Sea was created when levees built to transport water from the Colorado River failed in 1905. Vast quantities of water flooded the salt pan in the Colorado Desert and pooled at its lowest point, the Salton Sink, creating the sea. Since then, the Salton Sea has been sustained largely, though not exclusively, through agricultural runoff (Hanak et al., 2018).

In 2003, water transfers of 0.5 MAF from IID to cities in Southern California necessitated the implementation of new conservation measures on farms in IID's service area to reduce inflows into the Salton Sea. Mitigation water was transported to the Salton Sea to offset the loss of this inflow until the end of 2017 (Fogel et al., 2021). Since then, water levels in the Salton Sea have been falling and its areal extent has been shrinking. This has led to several environmental issues, including death of fish and birds in the area, increase in dust containing toxic constituents from the drying sea bed, and increasing salinity and concentration of toxic constituents in the remaining water of the Salton Sea (Fogel et al., 2021).

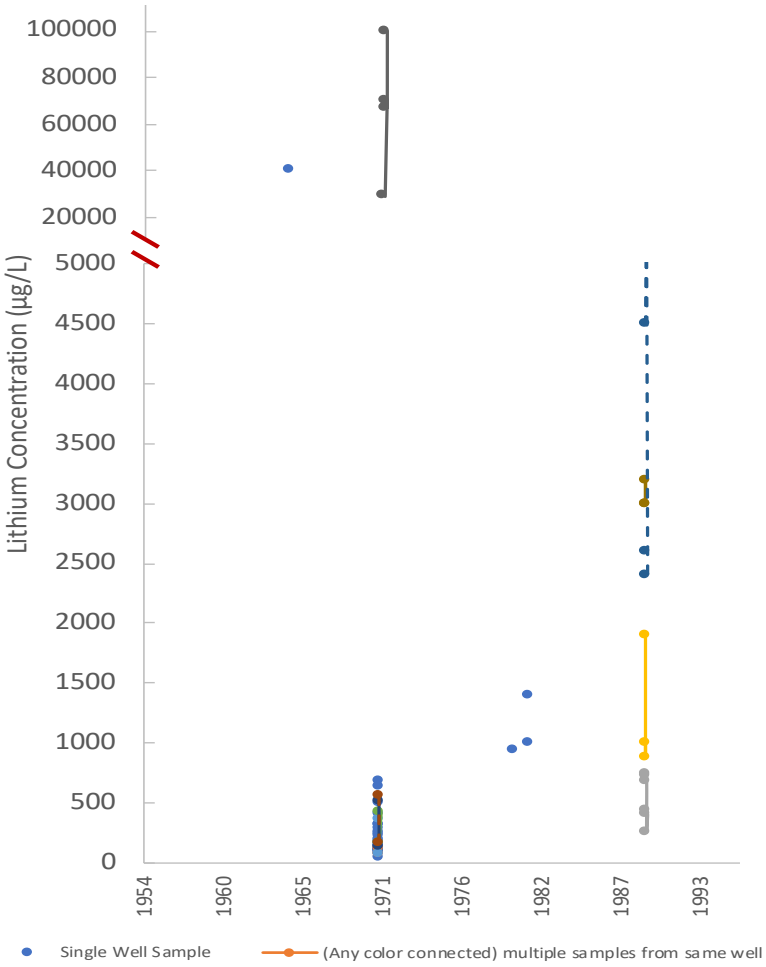

Figure 7.5. Lithium concentrations in groundwater wells south of the Salton Sea within a 15-mile radius. One well sample measured at 310,000 µg/L is not shown on the plot.

The Salton Sea is an important water resource in the region, in part because it serves as ecological habitat and, as it dries out, a source of air pollution (see Chapter 8). However, the Salton Sea is not a viable water source for municipal, industrial, or agricultural activities in the region, as the water is highly saline and contains other contaminants that preclude its use. Therefore, the expansion of geothermal and lithium production likely will not directly affect the Salton Sea.

Water Usage in the Geothermal and Lithium Extraction Process

There are over 90 geothermal power plants operating in the U.S., many of which have been operating for 30 years or more (Robins et al., 2021). There are several types of widely deployed geothermal plants: dry-steam, flash-steam, and binary cycle. Most geothermal plants in the SS-GF are flash-steam plants. A schematic of water flows in a flash-steam plant is presented in Figure 7.6, which also shows where water comes into and out of the system. Freshwater is needed to operate geothermal energy production facilities, in addition to the brines. Cooling towers use 70% of the freshwater as makeup water to offset water lost through evaporation, and most of the remainder is used to dilute brines (Energy Source, 2012; Morton Bay Geothermal LLC, 2023). Freshwater is also added to the brine before reinjection to prevent certain constituents from precipitating into solid form in the injection well and causing clogs. In the SS-GF,

freshwater is purchased from the IID and treated onsite, if needed, to achieve the water quality needed for each process.

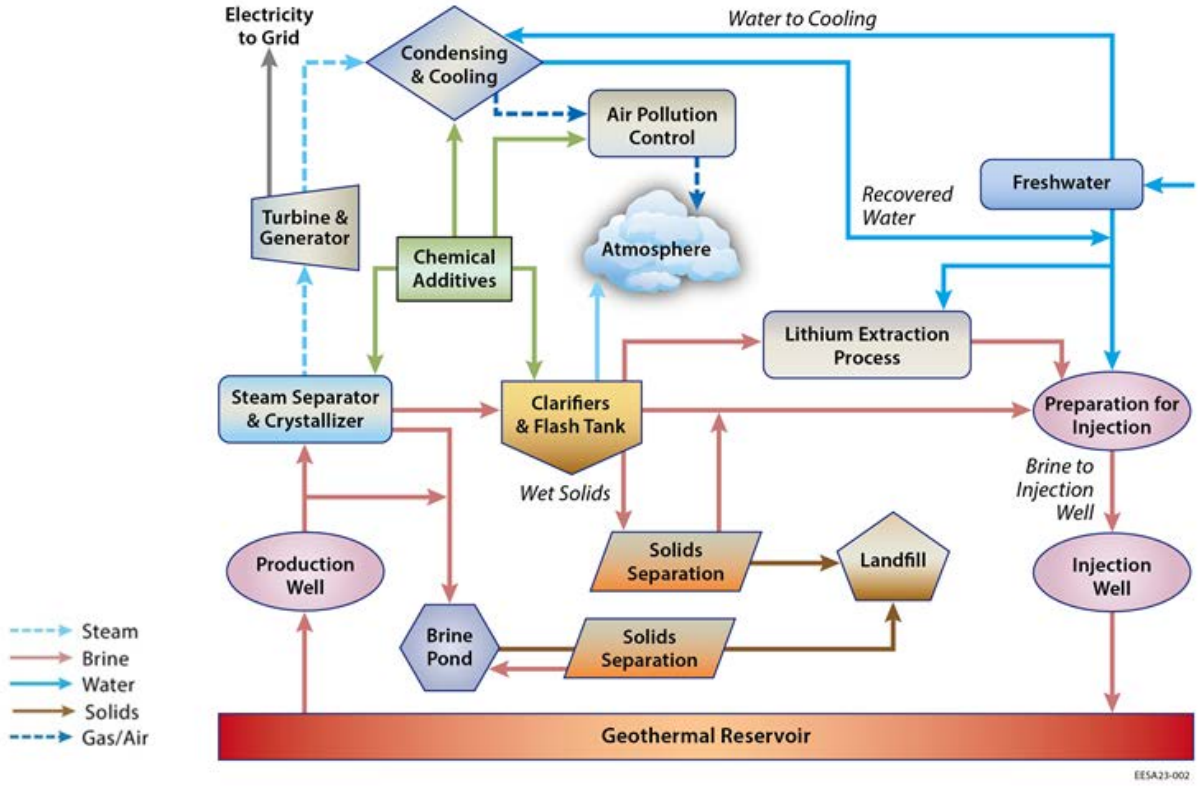

Figure 7.6. Simplified geothermal process schematic with representation of water flows in and out of the system.

In its most recent Integrated Regional Water Management Plan (IRWMP), the IID reported water use for all geothermal facilities in the county (GEI Consultants Inc., 2012). Based on historic and estimated water-demand data in this report, geothermal facilities in the SS-KGRA cumulatively purchase an average of 16 AF each year for every megawatt (MW) of net generation capacity. The water demand of individual facilities ranges widely, from 0.4 to 32 AF per MW annually.

According to the Environmental Impact Report (EIR) for the proposed Hudson Ranch Power II facility, which is designed for a capacity of 50 MW, the annual demand for cooling water is 2,800 AF per year. Steam condensate from the plant would be used to supply most of this water, but an additional 44 AF per year of makeup water would be needed from IID. Annually, an additional 1,100 AF would be needed for brine dilution water, 20 AF for freshwater pond evaporation, and 12 AF for miscellaneous uses (Energy Source, 2012). All of these demands would be met with water from IID. Overall, operation of this geothermal power plant would require the purchase of approximately 1200 AF per year from IID. This water demand corresponds to around 24 AF per MW per year.

Newly proposed geothermal facilities by BHER in the region have highly variable plans for meeting water needs. Morton Bay Geothermal (157 MW capacity) proposes use of 5560 AF per year (35 AF/MW), which is 50% of their water needs; the other 50% will be met by water recovered from the steam condenser (Morton Bay Geothermal LLC, 2023). Black Rock Geothermal (87 MW) proposes 1125 AF

per year (12.9 AF/MW), which is 20% of their water needs, and their remaining 80% will come from the steam condenser (Black Rock Geothermal LLC, 2023). Elmore North Geothermal (157 MW) plans to use 6480 AF per year of freshwater (44 AF/MW), meeting 50% of their demand and meeting the other 50% with the steam condenser (Elmore North Geothermal LLC, 2023). Additional water will be required at each of these facilities for startup, fire protection, and maintenance. Two of these new plants use more water per MW than the range reported in the 2012 IRWMP. It is possible that the water-use estimates for the new plants represent the high end of potential water use, and that actual water use in these facilities may be lower.

Comparison of Geothermal Water Consumption to Other Energy Sources

Figure 7.7 compares the estimated water consumption (gal/kWh) for energy production from geothermal plants in the SS-KGRA (GEI Consultants Inc., 2012; Black Rock Geothermal LLC, 2023; Elmore North Geothermal LLC, 2023; Morton Bay Geothermal LLC, 2023) to water usage for other geothermal energy (Clark et al., 2011) and other sources of electricity generation (Childress et al., 2021). Estimates for proposed plants are calculated using nameplate capacity, using water consumption data provided by the potential operator, and assuming the plants are operated continuously. Most electricity in California is generated by noncombustible renewables, natural gas, and nuclear sources. Note that while California uses no oil and virtually no coal to generate electricity (CEC, 2021), both technologies are represented in the figure for comparison.

The amount of water consumed for binary cycle geothermal plants is similar to that of other electricity sources such as nuclear, gas, or biomass. As mentioned, the SS-GF geothermal plants are primarily flash plants, which use more water than other sources shown in Figure 7.7. The higher water consumption from geothermal flash plants is a result of evaporation of high temperature steam being pulled from the wells, a unique feature of this type of plant. Water losses due to evaporation can vary between 14.5-33% of produced geothermal fluid at flash plants (Clark et al., 2011). Water usage for flash plants in Figure 7.7 is divided into operational freshwater (blue) and losses of geothermal brine due to evaporation, drift, and blowdown (yellow). The SS-GF water consumption is based on water that was purchased by each facility from IID in 2011 (GEI Consultants Inc., 2012) and the projected water use at new facilities (Black Rock Geothermal LLC, 2023; Elmore North Geothermal LLC, 2023; Morton Bay Geothermal LLC, 2023). Water purchases and water-use projections at SS-GF facilities exceed the estimates for water consumption at geothermal flash plants. This may be due to the arid region, unusual water-use patterns in the year for which data is reported, and/or uses of freshwater at these facilities that were not accounted for in other studies. Because water efficiency is a higher priority now than when the existing facilities were built, the reported values may overestimate the water that will be needed at future facilities. While uncertainty in these data remains, reported water purchases by existing geothermal facilities in the region provide reasonable approximations of the water needs of future facilities in the area.

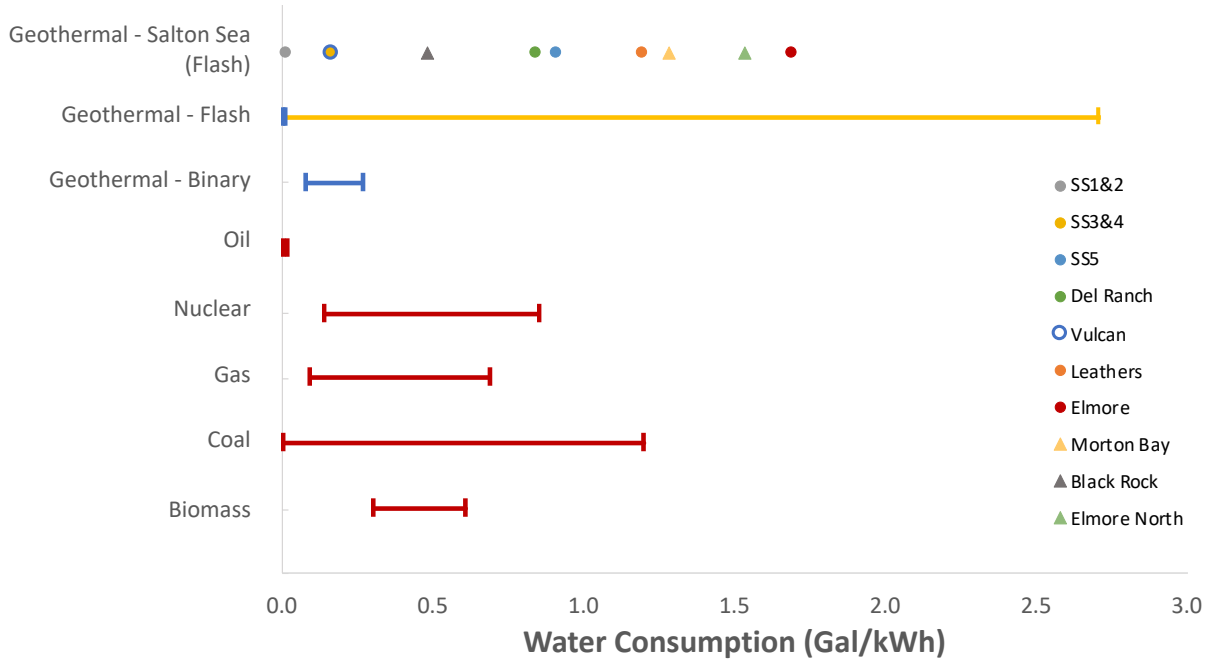

Figure 7.7. Water usage from different electricity sources adapted from Childress et al. (2021) to include general estimates for geothermal power plants (Clark et al., 2011) and geothermal plants in the SS-KGRA (Black Rock Geothermal LLC, 2023; Elmore North Geothermal LLC, 2023; GEI Consultants Inc., 2012; Morton Bay Geothermal LLC, 2023). Water usage for flash plants is divided into operational freshwater (blue) and losses of geothermal brine due to evaporation, drift, and blowdown (yellow).

Though it is outside the scope of this work, it is also important to acknowledge that there is water use associated with the construction and startup of new facilities for both geothermal production and lithium extraction. Geothermal plant construction requires water for drilling, constructing, and stimulating wells, constructing pipelines, and constructing plant infrastructure (Clark et al., 2011). Geothermal plant infrastructure construction for a 50 MW flash plant requires 688 m^3 (0.5 AF) of water (Clark et al., 2011). Stimulating wells requires 26,939 m^3 (21 AF) per well, and constructing pipelines requires 9.8-12.8 m^3 per 1000 meters of pipeline (Clark et al., 2011). If new facilities are located in areas of the Salton Sea region with no existing water services, new conveyance infrastructure may need to be established to obtain water from IID. Similarly, if sewer services are not present, a connection to a nearby sewer or a septic tank may need to be constructed.

EnergySource Minerals states in their EIR that construction will require around 190 m^3 (0.15 AF) of water per day for dust control. Construction is planned to occur five to six days a week for 24 months, equating to around 49,000-59,000 m^3 (40-48 AF) of water for the duration of construction. The report states potentially contradictory sources for this water. One statement indicates this water will come from onsite ponds or the Hudson Ranch facility, while another indicates it will be purchased from IID (Chambers Group Inc., 2021). It may be that the Hudson Ranch facility and/or onsite ponds use water purchased from IID.

Water Requirements for Lithium Extraction

Water requirements for obtaining lithium carbonate for use in batteries depend on the method used to concentrate and extract the lithium. Currently, lithium is commonly obtained either by (1) hard rock

mining or (2) brine evaporation. In hard rock mining, typically, spodumene ore is physically extracted, heated, pulverized, mixed with acid, re-heated, re-filtered, and concentrated to lithium carbonate, though the exact process varies depending on the characteristics of the deposit. It is an expensive and energy-intensive process. Lithium mining from spodumene occurs internationally but does not occur in the U.S. For evaporative processes, lithium-rich, highly saline brines are pumped from shallow wells (typically 1.5-60 m deep) and passed through a series of ponds for several months to a year or more, to concentrate the lithium as the brine evaporates. Once the brine has been concentrated, it typically goes through a filtration step (or similar process) to remove impurities, a precipitation step to isolate the lithium, and a carbonation step to produce lithium carbonate. Brine mining is a slow, land-intensive process. There is one operating mine in Nevada that extracts lithium from brines through evaporation.

In the Salton Sea region, lithium will be extracted using a more novel method known as direct lithium extraction (DLE). DLE is a class of extraction methods that directly removes lithium from solution through processes such as adsorption or ion exchange. Compared to ore mining and brine evaporation, DLE achieves extraction much more quickly and with higher recovery rates. A comparison of the documented water use for these lithium extraction methods is shown in Figure 7.8.

The values in Figure 7.8 were adapted from literature sources, including DLE marketing materials, and were not independently verified. Total water use for lithium brine evaporation ponds is based on operations in Chile (Vulcan Energy, 2021). Most of the water used for brine evaporation in Chile is considered fossil or relic water, defined as water that entered the basin more than 65 years ago (Moran et al., 2022). The estimates of freshwater use represent the median of observed freshwater for brine evaporation ponds in Chile (4%; visually approximated from a graph). One observation was considerably higher (14%), but all others were less than 8%. Lithium ore mining is based on mining operations in Australia and conversion in China (Vulcan Energy, 2021). The values for Vulcan DLE were reported in the company's own marketing materials.

Kelly et al. (2021) conducted a life-cycle assessment (LCA) for traditional lithium extraction and conversion processes using brine evaporation and ore-based methods. This LCA study quantified all freshwater used at lithium facilities themselves as well as water associated with the supply chain (e.g., producing electricity used at the facility; producing fuels used to transport materials). This study estimated that producing lithium carbonate from brine evaporation ponds requires 4,100-8,500 gallons (0.013-0.026 AF) of freshwater per tonne of lithium carbonate equivalent (LCE). (Note: Some data sources report lithium production as the mass of lithium metal, the mass of lithium hydroxide, or the mass of lithium carbonate. We converted these data to units of LCE to more consistently compare masses of lithium reported in different forms.) For lithium ore mining, freshwater use was estimated to be 20,000 gallons (0.061 AF) per tonne of LCE. These values are similar to the data reported in Figure 7.8, indicating that the supply chain does not appear to contribute significantly to water use for traditional lithium processes.

Data for the Energy Source Materials (ESM) Hudson Ranch facility and Berkshire Hathaway Energy Renewables (BHER) facilities were provided in the Report of the Blue Ribbon Commission on Lithium Extraction in California (Paz et al., 2022). The ESM data is based on the water allocation requested for its facility from IID and is inclusive of all water needs at the site. In a public meeting in May 2023, ESM indicated that they expect actual water use to be as much as one-third lower than the value shown. Since

this claim has not been documented to our knowledge, we have not updated the figure to reflect the lower estimate.

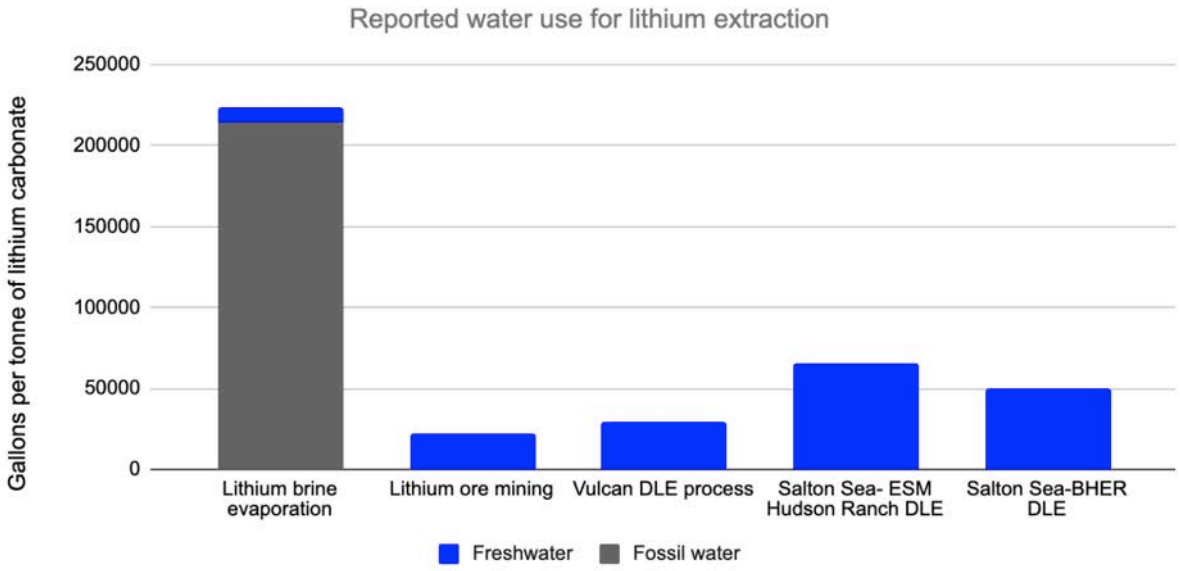

Figure 7.8. Water usage for different lithium extraction methods (Vulcan Energy, 2021; Moran et al., 2022; Paz et al., 2022). DLE is direct lithium extraction. ESM is Energy Source Materials. BHER is Berkshire Hathaway Energy Renewables.

Though we obtained facility-wide estimates of water use at lithium facilities near the Salton Sea, we were not able to obtain details about the specific DLE methods they plan to use, or more specific information about how water would be used for lithium extraction in the area. We understand that the proposed lithium extraction method in most area facilities involves or is similar to ion exchange. Figure 7.9 illustrates a proposed DLE process in Arkansas using ion exchange, as well as the water needed for multiple stages (Breuer et al., 2021). We expect water use in the area to be similar, but it could vary depending on the design of the process (e.g., whether acid or water is used to regenerate the ion exchange media). A recent review of the literature on environmental impacts of lithium production noted that very little quantitative information is available on freshwater needs for DLE, especially for pre- and post-processing steps (Vera et al., 2023). Without more information on the precise processes being used, we were unable to verify projections for water use at future facilities near the Salton Sea or identify opportunities to reduce water consumption through, for example, onsite water recycling.

Water Impacts of Geothermal Expansion and Addition of Lithium Extraction Processes in the Region

Figure 7.10 summarizes the regional water needs for expanding geothermal energy production in the region and the lithium production possible from the brines used at these plants. Water usage for geothermal plants was calculated based on an average water usage in AF/MW for the existing facilities in the SS-GF (GEI Consultants Inc., 2012). Lithium extraction was based on low, medium, and high estimates for LCE production (MT LCE per MWh) identified during our literature search. The low, medium, and high estimates represent proposed processes at Simbol/Hudson Ranch (Energy Source,

2012), Hell's Kitchen (County of Imperial, 2022), and ATLiS/Hudson Ranch I (Chambers Group Inc., 2021), respectively. Geothermal expansion scenarios include:

- Existing or allocated demand, which represents the 400 MW of existing geothermal in the region and 150,000 MT LCE for the medium LCE production case (130,000-150,000 MT LCE for low and high cases, respectively; medium and high case results round to the same value)
- Projected (3-4 year) geothermal capacity, representing an additional 520 MW of planned expansion (920 MW in total) and 340,000 (290,000-350,000) MT LCE
- Maximum possible capacity, representing an additional 2,030 MW capacity above the projected scenario to reach the region's estimated maximum geothermal capacity of 2,950 MW (Kaspereit et al., 2016) and 1,100,000 (950,000-1,100,000) MT LCE (medium and high case results round to the same value)
- Currently, we estimate about 6,500 AF of freshwater is used each year for the existing 400 MW of geothermal capacity, and 3,400 AF has been allocated by IID to ESM for its facility that will produce 17,000 tonnes of LCE. Assuming projected geothermal and lithium processes use water similarly to today – the averages of currently reported values are 16 AF per MW and 58,000 gallons per tonne of LCE – we estimate that the water needed for these processes will more than quadruple in coming years. Though this indicates significant growth, the water needs for geothermal and lithium production in the region are modest compared to total water use in the area. The increased demand for planned geothermal and lithium production will require an additional 3% and a total of 5.8% of IID's water right (2.6 MAF). The additional demand is similar to the volume of water needed to irrigate 14,000 acres in the region.

In a water-constrained region, however, any increase in planned water use should be carefully considered. The Imperial Valley's Integrated Regional Water Management Plan (IRWMP) projected region-wide water needs for renewable energy production, including geothermal energy, to be 144,000 AF per year (GEI Consultants Inc., 2012). This projection includes all of the Imperial Valley, not just the area around the SS-GR, and may be sufficient to accommodate the expected growth of geothermal but not that of lithium production. Further, this estimate does not account for the additional water required for lithium production, including large upfront water needs for new facility construction and for ongoing operations.

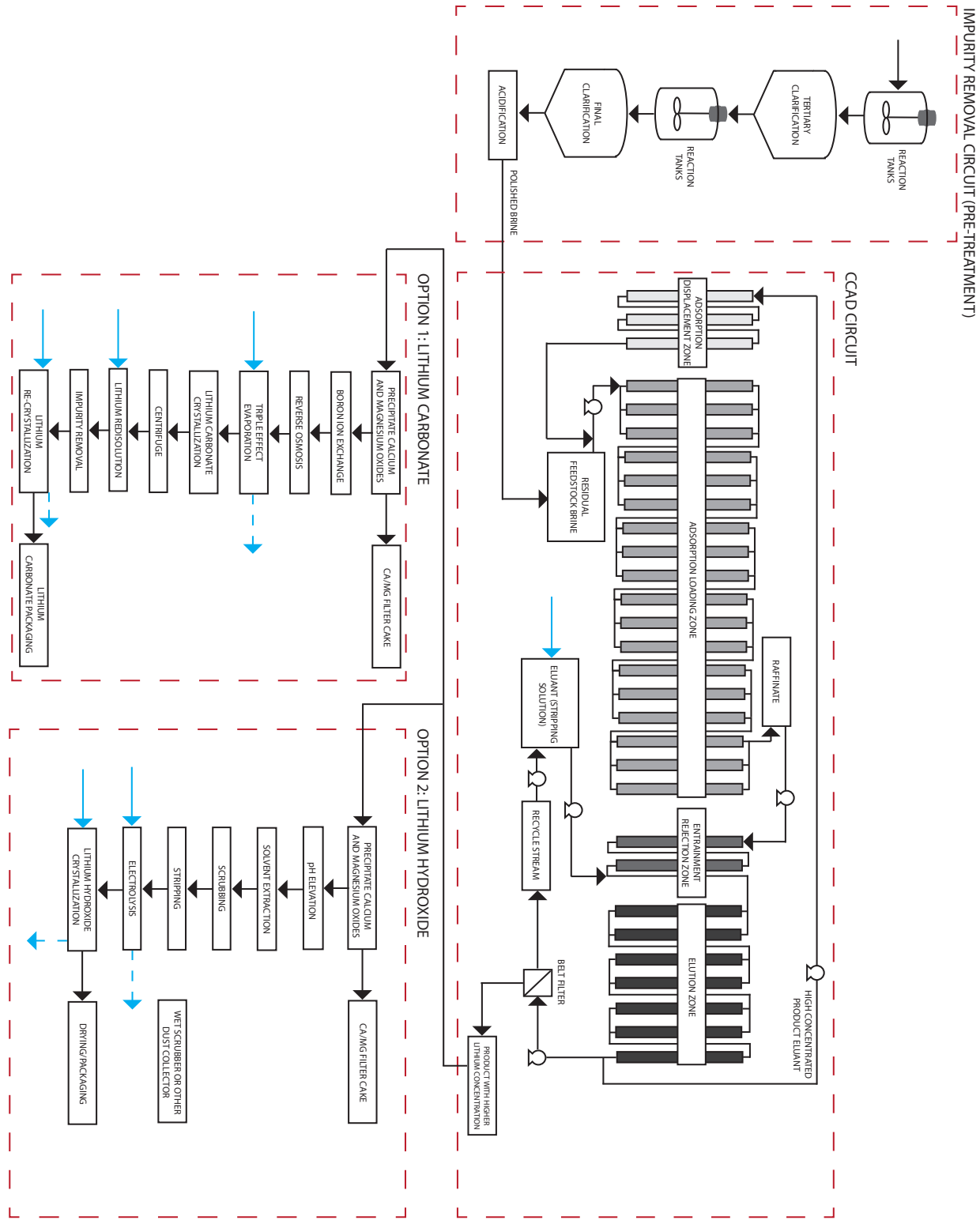

Figure 7.9. Proposed lithium extraction process and associated water usage based on an EnergySource lithium adsorption and recovery patent (Marston and Garska, 2022), Lithium extraction and processing from Smackover brines (Breuer et al., 2021), and extrapolation based on unit processes.

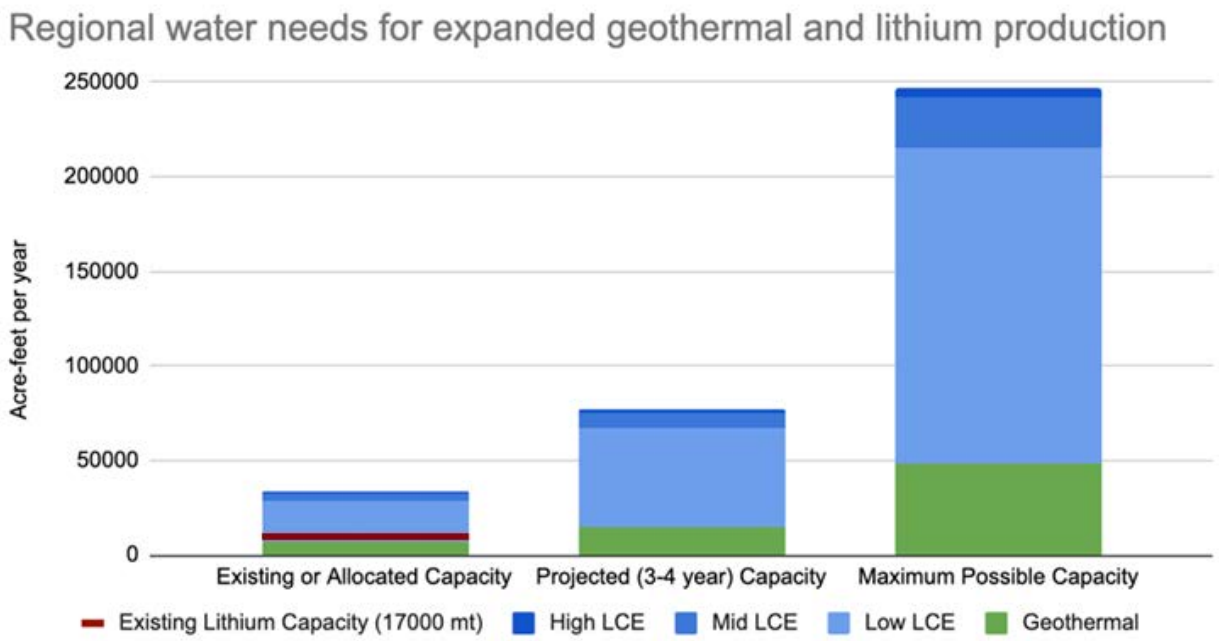

Figure 7.10. Current allocated and projected water needs for geothermal energy and lithium production in the region. The red bold line in the "Existing or Allocated" bar indicates allocations that have already been made for lithium capacity. Low, medium, and high water usage for LCE was determined from proposed processes at Simbol/Hudson Ranch (Energy Source, 2012), Hell's Kitchen (County of Imperial, 2022), and ATLiS/Hudson Ranch I (Chambers Group Inc., 2021), respectively.

Lithium production in the region is included in allocations for new nonagricultural water needs in IID's current water supply plan (GEI Consultants Inc., 2012). IID allocated up to 25,000 AF per year for future water needs for this category. Of this, IID has already allocated 4,600 AF to new projects, 75% of which will be used by ESM's lithium facility at Hudson Ranch. The remaining 20,400 AF could produce about 115,000 tonnes of LCE but is insufficient to meet regional goals for expanded lithium production.

In personal communication with IID, it indicated that the current water supply plan has not been updated to account for the potential water demands of lithium extraction because there is still adequate water available (Shields, 2022). IID indicated it would be able to expand this allocation if needed, and that the additional water would come from water conservation on agricultural lands.

Projecting future water availability in the region is complicated because of the extended drought in the Colorado River basin. Water availability in the Imperial Valley may be impacted by the recent agreement reducing California's allocations from the Colorado River by 14%; by a subsequent federal action if the proposed cuts are insufficient; and/or by a future drought contingency plan negotiated for the river, such as the one that must be adopted by 2026 (Flavelle, 2023). The magnitude of reductions required to maintain the Colorado River in the face of ongoing drought, if any, is unknown at this time. Any cuts that are imposed rather than resulting from a voluntary agreement may be contested in extended legal battles. However, given current trends of aridification in the Colorado River basin (Overpeck and Udall, 2020), even with IID's senior water right, it is likely there will be less water available in the Imperial Valley in coming decades compared to the past.

Figure 7.11 illustrates how water allocations could change compared to 2010 and to current (2022) uses, with the latter accounting for the voluntary 10% reduction announced in October 2022. We have estimated water allocations for 2050 based on the best available information. These projections account for anticipated growth in water demand for municipalities in the region (GEI Consultants Inc., 2012; City of Brawley, 2015; City of El Centro, 2020) and assume water is made available through conservation on agricultural lands. Six scenarios are considered:

- 2050 Proposed Supply **without** GT/Li expansion: Assumes future Colorado River allocations are consistent with the May 2023 voluntary agreement (i.e., a 14% reduction in water demand is made permanent with no additional cuts required) and no additional demand due to geothermal or lithium production.
- 2050 Proposed Supply **with planned** GT/Li expansion: Assumes future Colorado River allocations are consistent with the May 2023 voluntary agreement (i.e., a 14% reduction in water demand is made permanent with no additional cuts required) and additional demand due to geothermal or lithium production is consistent with projections included in the Blue Ribbon Commission Report (Paz et al., 2022).
- 2050 Proposed Supply **with potential** GT/Li expansion: Assumes future Colorado River allocations are consistent with the May 2023 voluntary agreement (i.e., a 14% reduction in water demand is made permanent with no additional cuts required) and additional demand due to geothermal or lithium production is sufficient to fully extract lithium resources available in the Salton Sea region, as reported in the Blue Ribbon Commission Report (Paz et al., 2022).
- 2050 Low Supply **without** GT/Li expansion: Assumes future Colorado River allocations are reduced significantly (i.e., a 40% reduction in water demand, the maximum we have seen suggested by USBR [Flavelle, 2023]) and no additional demand due to geothermal or lithium production.
- 2050 Low Supply **with planned** GT/Li expansion: Assumes future Colorado River allocations are reduced significantly (i.e., a 40% reduction in water demand) and additional demand due to geothermal or lithium production is consistent with projections included in the Blue Ribbon Commission Report (Paz et al., 2022).
- 2050 Low Supply **with potential** GT/Li expansion: Assumes future Colorado River allocations are reduced significantly (i.e., a 40% reduction in water demand) and additional demand due to geothermal or lithium production is sufficient to fully extract Li resources available in the Salton Sea region, as reported in the Blue Ribbon Commission Report (Paz et al., 2022).

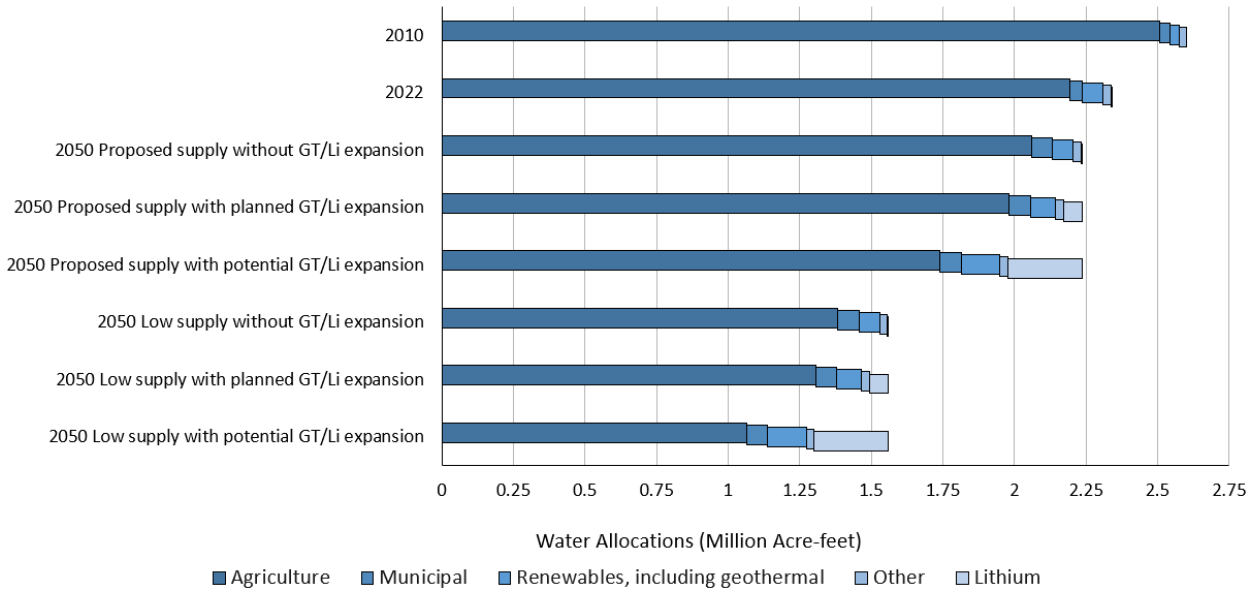

Figure 7.11. Estimate of IID water required from the expansion of geothermal energy production and addition of Li extraction processes from associated geothermal brines under assumptions of high and low water supply from the Colorado River compared to 2010 and 2022 allocations.

The water supply reductions shown in Figure 7.11 are significant and would have numerous impacts on the economy and communities in the region. Note that the biggest driver of water allocation changes between now and 2050 is likely to be negotiations around Colorado River water use, and not the expansion of geothermal and lithium production. The most aggressive water allocation restrictions evaluated would reduce the water available for agriculture in the region by almost 50% compared to IID's original water right. If these aggressive restrictions are implemented, the water consumption associated with the planned geothermal expansion and associated lithium extraction would only represent 10% of the region's water use, about twice what municipalities in the region consume. Nonetheless, in the timeframe when geothermal and lithium industries are expanding in the SS-KGRA, Imperial Valley stakeholders may experience significant changes to their communities and livelihoods as a result of reduced water availability in the region. Any increases in water demand may require careful communication with affected parties.

Changes in water availability may also impact the Salton Sea itself and, indirectly, the surrounding communities. Depending on how water withdrawal restrictions are implemented in the Colorado River basin and how many new geothermal and lithium extraction facilities are built, water available for agriculture in 2050 could be between 17-57% lower than it was in 2010. Such significant reductions in irrigation could have meaningful consequences for the health of the Salton Sea. The total water volume and areal extent of the Salton Sea may be further reduced, since agricultural irrigation runoff is the largest source of inflows (Hanak et al., 2018; Ajami, 2021). The shrinking of the Salton Sea that has led to the current environmental crisis is largely attributed to water conservation on agricultural land associated with the transfer of 0.5 MAF to Southern California cities. The future water projection assumes additional conservation of at least a similar magnitude, and possibly up to 1.5 MAF. Ongoing efforts to protect the Salton Sea should consider these potential changes to water runoff from irrigation.

Summary

Regionally, the water demand for currently proposed geothermal production and lithium extraction facilities is modest, accounting for ~3% of historical water supply. However, because a megadrought in the Colorado River basin is constraining water resources in the region, any increase in water demand should be carefully evaluated.

Our analysis projects water allocation scenarios for both geothermal expansion with lithium production and proposed reductions in Colorado River water allocated to IID. Expanding geothermal energy and lithium production in the region to currently proposed levels will only have a modest impact on overall water consumption in the Imperial Valley. Water demand for lithium extraction is appreciable, representing an additional 3.5-4X the freshwater requirements of geothermal energy production alone from a given volume of brine, based on published estimates for facilities planned in the Salton Sea region. However, this is significantly less than the water requirements of conventional approaches to lithium removal from brines, such as evaporation ponds. Based on communications with IID, we understand that water used for these purposes will be reallocated from agricultural uses (Shields, 2022).

The more influential factor on regional water allocation between now and 2050 is proposed cuts to IID's water allocation from the Colorado River. Cuts have been proposed as high as 40%, though only a 10% reduction has been agreed. The most aggressive water allocation restrictions evaluated would reduce water available in the region by almost 50% compared to IID's original water right. If these are implemented, the water consumption associated with planned geothermal expansion and associated lithium extraction would only represent 10% of the region's water use. However, the cumulative effect of regional water cuts and expansion of these industries would reduce the amount of water available to agriculture by almost 50% compared to 2010.

It is not anticipated that the addition of geothermal capacity or lithium production would impact the availability or quality of water used for human consumption. But changes in regional water allocation may impact the types of economic opportunities available in the region.

Additional water conservation on agricultural lands due to changes in water supply could exacerbate environmental issues in the Salton Sea itself. As mentioned, improvements in agricultural water conservation and irrigation practices have contributed substantially to a reduction in water levels in the Salton Sea, which has exposed playa, releasing particulate matter and harmful toxins concentrated in the Salton Sea into the air. The extent to which future water allocation scenarios may impact this dynamic was outside the scope of this report but, again, would be driven more by regional water allocations from the Colorado River than by expanded geothermal and lithium production.

Chapter 8: Evaluation of Potential Pollutant Emissions and Air Quality Impacts Associated with Lithium Extraction and Potential Expansion of Geothermal Production

Key Takeaways

- Current geothermal electricity production in the region produces very low emissions of carbon dioxide relative to electricity generation from fossil fuels.
- Current geothermal electricity produces 400X and 80X less PM_{10} and $PM_{2.5}$, respectively, than other regional sources, and 15X less hydrogen sulfide (H_2S) than naturally occurring emissions.
- Current geothermal electricity produces low levels of ammonia (<1% of areawide sources) and benzene.
- Geothermal energy expansion and the addition of lithium extraction will have a relatively small impact on overall regional emissions of all pollutants identified here, provided that appropriate mitigation measures are put in place.

Introduction

From an air quality perspective, geothermal energy production is generally considered clean. First and foremost, there is no need to combust fuel when withdrawing energy from a geothermal system. Fuel combustion is the primary cause of air pollution from electricity generation, so a system without fuel combustion is usually (though not always) clean.

A general description of geothermal energy operations is as follows. Underground fluid is naturally hot, and this heat is transported to the surface and used to produce electricity via generator turbines, and then the cooled fluid is returned to the aquifer for reheating and reuse. In this simple description (representing binary power generation, where the produced single-phase fluid heats a working fluid, and is completely returned to the reservoir without any surface discharge) there are essentially no sources of operational air pollution.

This description accurately reflects some configurations of geothermal electricity production. As discussed previously, geothermal energy operations in the SS-GF are flash plants, which involve different unit processes that lead to some limited emissions, as described in Chapter 7 and Appendix Chapter 7.

One among numerous motivations to pursue expanded geothermal energy generation, and to add lithium extraction to the process, is that the endeavor could yield exceptionally low air pollutant emissions compared to other types of electricity generation (e.g., from natural gas) and compared to other, mining-intensive approaches to lithium extraction.

With that in mind, this chapter has three goals:

1. Quantify actual emissions from existing geothermal energy operations in the Imperial Valley, with a focus on the SS-GF.
2. Estimate potential emissions from expanded geothermal energy operations.
3. Estimate potential emissions from future lithium extraction processes.

Regarding the first goal, this chapter does not include a new measurement campaign or air quality modeling component. Rather, the scope is limited to assembling and reviewing existing publicly available measurements and emissions inventories. We assess the strengths and weaknesses of existing emission inventories. Importantly, we compare emissions (or potential emissions) from geothermal operations to those from the region's other sectors to help contextualize the impact of geothermal operations on air quality in a manner that simply listing emission rates could not provide. Notably, this comparison will not provide an estimate of specific impacts from geothermal emissions on regional air quality and public health, which would require a more expansive study (e.g., air quality and population exposure modeling), which are outside the scope of this report. That said, the relative comparison to other emission sources provides important insight into potential impacts from geothermal lithium extraction.

Regarding the second and third goals, we note that our results contain substantial uncertainty, especially when describing potential emissions from lithium extraction processes (which are still being actively developed). Our approach for investigating potential emission impacts of these potential future activities is based on extrapolating current activities, or examining related active processes that share similar characteristics with lithium extraction processes. Importantly, this chapter assesses which aspects of both expanded energy generation and new lithium extraction processes are most uncertain and likely to be most influential on future emissions.

This analysis is informed by a variety of public data sources, including emissions inventories from the California Air Resources Board (CARB) and U.S. Environmental Protection Agency (U.S. EPA), as well as power generation data from the U.S. Energy Information Administration (U.S. EIA). In addition, there are several air monitoring networks operated by state agencies, local governments, and a local NGO (Comité Cívico del Valle). We describe these data sources in detail in Appendix Chapter 8.

Key Concepts: Geothermal Energy Production and Air Pollutant Emissions

As noted in other sections, the SS-GF geothermal power plants use a "flash" process, in which the hot fluid from underground flows to the surface, where it boils, with the separated steam phase flowing through a turbine to generate electricity. The fluid output from this whole process includes liquid brine as well as steam and "non-condensable" gases (CO_2, H_2S, etc.). The brine can be fully returned to the reservoir, but some of the steam and gases are released to the atmosphere. It is from this release of steam and gases that air pollution can be emitted (e.g., Kagel et al., 2005; Matek, 2013). Because emitted pollutants originate as elements or compounds that are naturally present within the subsurface fluid, geology plays an important role in the emissions that occur from flash geothermal energy systems. Due to subsurface variability, the magnitude of pollutant emissions will vary from site to site, and especially from region to region.

The four geothermal fields in the Imperial Valley have a mixture of plant types: Heber and Brawley have all binary plants, East Mesa has a combination of binary and flash plants, and the SS-GF has all flash

plants (Robertson-Tait et al., 2021; Robins et al., 2021). In this chapter we evaluate emissions of pollutants from Imperial Valley geothermal plants and compare them both to geothermal plants elsewhere and to other emissions sources in Imperial Valley.

Emissions also result from any industrial activity associated with energy production. In this chapter, we are interested in the potential emission impacts of the lithium recovery method, direct lithium extraction (DLE), that has been proposed for brines from the SS-GR.

Finally, control strategies are an important factor affecting overall emissions from geothermal operations. Air pollution emissions are regulated at the local, state, and federal levels, and as a result, all geothermal power plants in the Imperial Valley use various strategies and technologies to control emissions of specific pollutants. In this chapter, we review these control strategies and their impacts.

Overview of Air Pollution Concerns Within Imperial County

In Imperial County, there are two primary air pollution concerns: (1) particle pollution, including dust from playa and soot or other emissions from burning and combustion; and (2) ground-level ozone pollution.[1] Imperial County has developed specific plans to address both ground-level ozone and particle pollution (IC-APCD, 2017; IC-APCD, 2018).

Global warming can also damage air quality in Imperial County because increased temperatures can enhance the creation of ground-level ozone and lead to conditions that increase dust creation. The drop in the water level of the Salton Sea, and the exposure of more shoreline, is another climate-related process that has led to increased dust in the region (Bahreini et al., 2021). Therefore, carbon dioxide emissions and other heat-trapping pollutants are of concern, along with pollutants that directly lead to particle and ozone pollution.

There are also natural gas fluxes from springs, gas seeps, fumaroles, and mud volcanoes around the SS-GF (Muffler and White, 1968; Svensen et al., 2007; Mazzini et al., 2011; Tratt et al., 2016). These natural discharges contribute to overall emissions in the region.

More generally, many other pollutants are of concern from the perspective of human health (as well as other issues like crop damage, visibility, etc.). For example, the EPA categorizes and regulates six common air pollutants as "criteria" pollutants: particle pollution, ground-level ozone, carbon monoxide, sulfur oxides, nitrogen oxides, and lead. Many other chemicals and metals are classified as hazardous pollutants and regulated to various degrees.

---

[1] For example, the American Lung Association gives Imperial County failing grades for air pollution in the categories of ozone pollution and particulate pollution. See https://www.lung.org/research/sota/city-rankings/states/california/imperial.

Air Pollutants of Interest

This report focuses on a small subset of pollutants that are both relevant to air quality concerns in Imperial Valley and identified as possible components of emissions from geothermal power generation. Table 8.1 lists the pollutants we discuss, along with the primary reasons they are of concern. Note that inclusion simply indicates that we discuss the pollutant; it does not indicate the pollutant is emitted in meaningful quantities from geothermal power generation in Imperial Valley.

Table 8.1. List of air pollutants included in this study (note: inclusion only indicates evaluation, not emission from geothermal power generation in Imperial County)

Air Pollutant	Notes
Carbon Dioxide (CO_2)	Contributes to global warming
Hydrogen Sulfide (H_2S)	A direct human irritant, strong odor, and contributor to particle pollution (after atmospheric chemical transformation)
Ammonia (NH_3)	Can contribute to particle pollution (for example, through formation of ammonium nitrate)
Benzene	A carcinogen

Table 8.1 does not contain pollutants that exacerbate ground-level ozone, because their emissions from geothermal power plants are negligible. Common pollutants that increase ozone levels are nitrogen oxides and "volatile organic compounds" (e.g., evaporated gasoline, partially combusted gasoline, and some chemicals emitted by plants). Air pollution from geothermal energy generation derives specifically from elements or compounds that are originally dissolved within the geothermal brine, and then transfer into the air during the geothermal flashing process. Because the set of chemicals and elements found in geothermal brine does not include significant concentrations of nitrogen oxides or volatile organic compounds, we will not focus on ozone air quality in this report. Instead, this report will focus on potential exposure to individual pollutants (e.g., H_2S) and the potential for such emissions to lead to particulate matter formation (e.g., H_2S and NH_3 can be transformed into particulate matter in the atmosphere).

Particulate Matter

Particulate matter (PM) is a mixture of solid particles and liquid droplets suspended in the atmosphere. PM_{10} is comprised of particles with diameters less than 10 μm, and $PM_{2.5}$ indicates particles with diameters less than 2.5 μm. $PM_{2.5}$ is a subset of PM_{10}; thus, values for PM_{10} include $PM_{2.5}$. PM is released from a geothermal plant's cooling tower operations, as well as from loading and unloading dry materials onsite. (We assume brine ponds do not make a meaningful contribution to total emissions, but further analysis may be needed.) From the cooling tower, dissolved solids in the circulated cooling water are released as a result of "drift," in which small water droplets get picked up by the air stream leaving the cooling tower, estimated at 0.01 g/kWh (Chambers Group Inc., 2021). During unloading of dry reagents into storage tanks, 0.0001 g/kWh of PM_{10} are released (Chambers Group Inc., 2021). These emissions are minimized with fabric filter units (Chambers Group Inc., 2021).

Geothermal energy generation directly produces PM as well as H_2S and NH_3, both precursors to PM. In the atmosphere, H_2S can be chemically transformed to sulfur dioxide (SO_2) and then sulfuric acid (H_2SO_4) (Bottenheim and Strausz, 1980). Hydrogen sulfide is converted to sulfur dioxide in the atmosphere in a reaction catalyzed by hydroxyl radicals:

$$H_2S + HO\cdot \rightarrow HS\cdot + H_2O \quad \text{Eq. 1}$$

$$HS\cdot + O_2 \rightarrow HO\cdot + SO \quad \text{Eq. 2}$$

$$SO + O_2 \rightarrow SO_2 + O \quad \text{Eq. 3}$$

Sulfur dioxide is oxidized to sulfuric acid, which then reacts with ammonia to form ammonium sulfate, which contributes to $PM_{2.5}$ through the following pathway:

$$SO_2 + OH + M \rightarrow HOSO_2 + M \quad \text{Eq. 2}$$

$$HOSO_2 + O_2 \rightarrow HO_2 + SO_3 \quad \text{Eq. 5}$$

$$SO_3 + H_2O \rightarrow H_2SO_4 \quad \text{Eq. 6}$$

$$H_2SO_4 + NH_3 \rightarrow (NH_4)_2SO_4 \; or \; (NH_4)HSO_4 \quad \text{Eq. 7}$$

Exposure to PM, whether originating from dust or from emissions of H_2S or NH_3, is a health risk.

Non-condensable Gases

Non-condensable gases (NCGs) are gases that do not condense in the geothermal brine at the operating temperatures used at the plant. At flash geothermal plants, they are released from the cooling tower. The specific gases released depend on the compounds that naturally occur in the geothermal fluid, and therefore are specific to each geothermal plant. The main NCGs discussed herein are carbon dioxide, hydrogen sulfide, ammonia, and benzene (see Table 8.1). Reported NCG composition of brines from two wells in the Salton Sea Geothermal Field are provided in Table 8.2. Concentrations of NCGs can vary substantially, as can be seen in the H_2S and NH_3 concentrations from these two sites.

Hydrogen Sulfide

Hydrogen sulfide is a colorless toxic gas that has a strong odor of rotten eggs, and for this reason it is often referred to as "sewer gas" or "swamp gas." Exposure to H_2S gas at elevated concentrations can contribute to nausea and headache. Currently, the California Ambient Air Quality Standard (CAAQS) for H_2S is 0.03 ppm for one hour to prevent these responses to exposure (Collins and Lewis, 2000). Humans can detect the odor from H_2S at concentrations in the range of 0.0005-0.3 ppm (Chou et al., 2016) but average detection levels range from 0.03-0.05 ppm (CARB, 2023).

Table 8.2. Reported non-condensable gas composition of brine from geothermal well testing at the Salton Sea Geothermal Field (Chambers Group Inc., 2021; Elmore North Geothermal LLC, 2023)

Non-condensable Gases	ATLiS Nominal Concentrations (ppmw)	Elmore North Nominal Concentrations (ppmw)
Carbon Dioxide (CO_2)	1,532.00	1,120.00
Hydrogen Sulfide (H_2S)	13.00	99.40
Ammonia (NH_3)	47.00	1.01
Methane (CH_4)	1.90	27.90
Nitrogen (N_2)	4.70	52.00
Hydrogen (H_2)	0.13	29.80
Argon (Ar)	0.02	0.15
Benzene (C_6H_6)	0.04	0.33

Geothermal brines in many areas have significant hydrogen sulfide concentrations (Gill and Jacobs, 2018), which can range from several parts per billion (ppb) to a few hundred parts per million (ppm) (Arnórsson, 1995). Reported H_2S concentrations for two geothermal brine samples from the SS-GF range from 13-99.4 ppm (Table 8.2; Chambers Group Inc., 2021; Elmore North Geothermal LLC, 2023). H_2S is concentrated in the steam phase of a geothermal fluid, and a portion of the H_2S can be released from geothermal plant cooling towers (Gunnarsson et al., 2011). Geothermal plants use a variety of abatement technologies to remove H_2S from the steam condensate (Hoyer et al., 1991; Gallup, 1992; Gallup, 1996a, b; Rodríguez et al., 2014; Rodríguez et al., 2015). These methods convert 90-95% of the total H_2S into sulfate so that the dissolved sulfate is reinjected with the steam condensate back into the reservoir, but even after abatement small amounts of H_2S are released to the atmosphere.

Ammonia

Ammonia (NH_3) is a colorless gas with a pungent odor. In outdoor air, ambient concentrations range from 0.28-15 $\mu g/m^3$. Health effects of inhaling ammonia above this natural level are contained to the upper respiratory tract (U.S. EPA, 2016). Sources of atmospheric ammonia include agriculture, animal husbandry, industrial processes, vehicle emissions, and volatilization from soils and the ocean, along with fumarole and gas seeps (Behera et al., 2013; Tratt et al., 2016). It is also the most abundant alkaline gas in atmosphere, playing a key role in neutralizing the acidity of precipitation, cloud water, and airborne particulate matter (Shukla and Sharma, 2010; Xue et al., 2011; Behera et al., 2013).

Emissions from Geothermal Power Plant Operations

Figure 8.1 presents a schematic to help contextualize emissions from the flash geothermal process used in the SS-GF. The schematic highlights where air emissions occur and was created using environmental impact reports (Chambers Group Inc., 2021). Throughout these processes, hydrogen sulfide (H_2S), ammonia (NH_3), benzene, and emissions that contribute to atmospheric particulate matter (PM) are released. NO_x emissions from this process are considered negligible (Bayer et al., 2013).

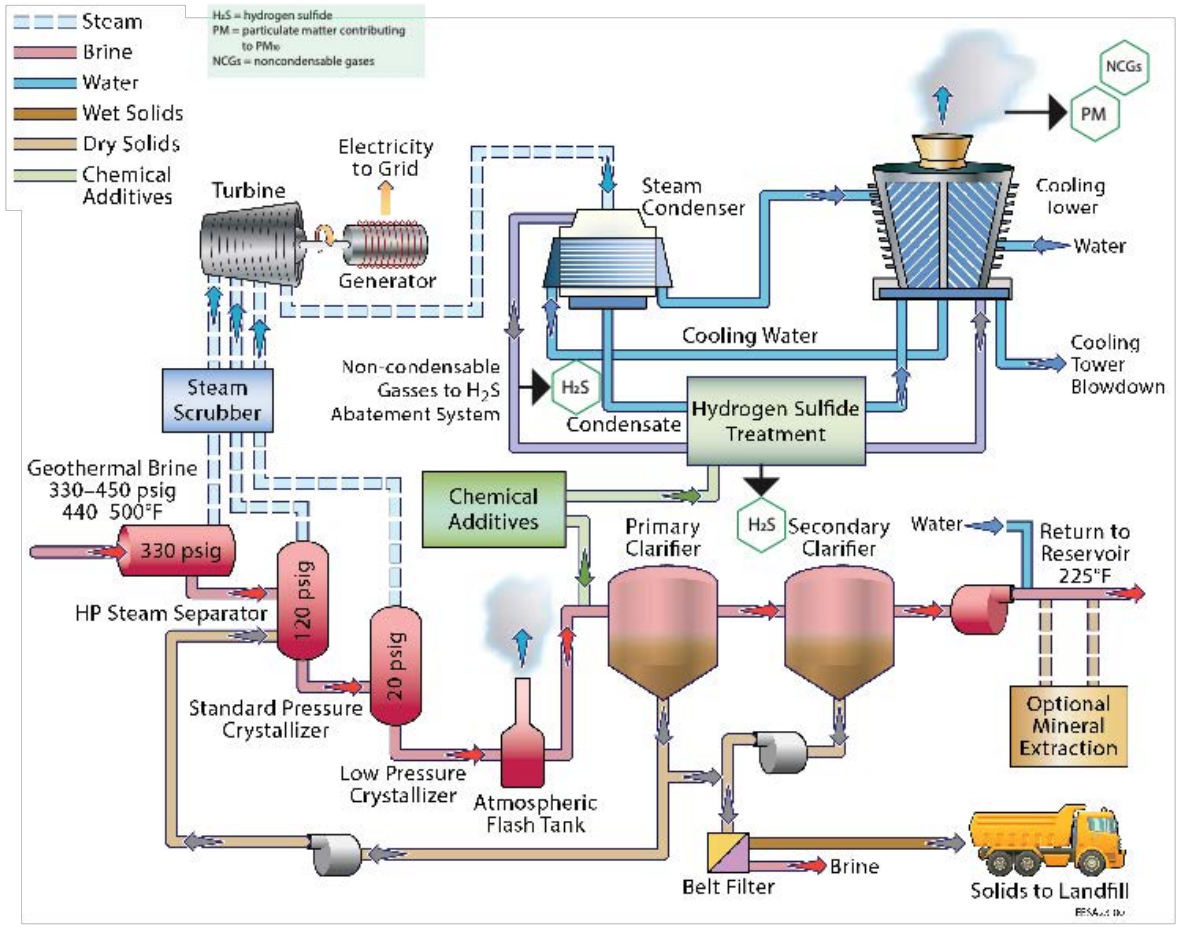

Figure 8.1. Detailed schematic of a geothermal flash plant like those found in the Imperial Valley, with associated air emissions indicated throughout the process.

Emissions from geothermal facilities are classified as point source emissions, which the EPA defines as emissions from a single, identifiable source (U.S. EPA, 2001). Once released from a point source, air pollutants disperse into the atmosphere based on local weather patterns. Understanding the potential impact of pollutant emissions is challenging because each region faces different weather patterns and emissions sources. An early study of emissions from geothermal power plant development in the Imperial Valley used atmospheric transport models to assess the dispersion and transport of gas concentrations away from these point sources to assess long-term air quality impacts within the region (Ermak et al., 1980).

Figure 8.2 illustrates how pollutants become diluted as they are dispersed horizontally and vertically in the atmosphere. It provides an illustration of a possible plume from a point source based on the National Oceanic Atmospheric Administration (NOAA) gaussian dispersion model[2] using default assumptions of

[2] https://www.ready.noaa.gov/READY_gaussian.php

wind direction, wind speed, atmospheric mixing depth, and atmospheric stability. In this simple example, by the time the pollutant is 2 km from the point source, it is on the order of 10 to 100 million times less concentrated than when it was released. For additional context, Figure 8.3 shows the Hudson Ranch Geothermal Plant with a 2 km radius. Notably, no residential areas exist within this radius, meaning that low levels of pollutant emissions could be substantially diluted prior to reaching populated locations. A real-world example of plume dilution can be observed in a 2016 study that investigated ammonia emissions and found that a distinct plume emanated from the Hudson Ranch Geothermal Plant in the SS-GF. Ammonia concentrations decreased substantially as the distance from the emissions source increased (Figure 8.4). Note that this figure includes vertically integrated concentrations, and thus only accounts for horizontal, not vertical, dispersion.

Quantification of Emissions from Existing Geothermal Energy in Imperial Valley

Carbon Dioxide Emissions

Electricity generation records for geothermal power plants in California were obtained from the U.S. Energy Information Administration (EIA). Electricity generation was reported based on groupings of individual geothermal plants, and therefore the plants reporting CO_2 to CARB were grouped into categories provided by EIA. Emissions factors were then calculated by dividing total emissions from the group of plants by the amount of energy generated by that group during 2020. Emissions factors for alternate energy sources were obtained from the World Bank Energy Sector Management Assistance Program (ESMAP, 2016); similar data can also be found in Kagel et al. (2005) and Matek (2013). The results from this analysis are presented in Figure 8.5.

Compared to other energy sources, geothermal plants in the SS-GF have substantially lower CO_2 emissions – approximately 6, 11, and 13 times lower than the lowest bounds of gas, oil, and coal operations, respectively. Additionally, SS-GF geothermal is also a lower emitter than other geothermal in California and is on the low end of emissions compared to global geothermal.

Toxins and Criteria Pollutants

For this analysis, data for toxic emissions from geothermal plants in California were obtained from CARB for 2020. Similar to the methods for CO_2 emission rate calculations, plants were grouped by EIA electricity reporting groups and normalized to the amount of electricity generated in the reporting group.

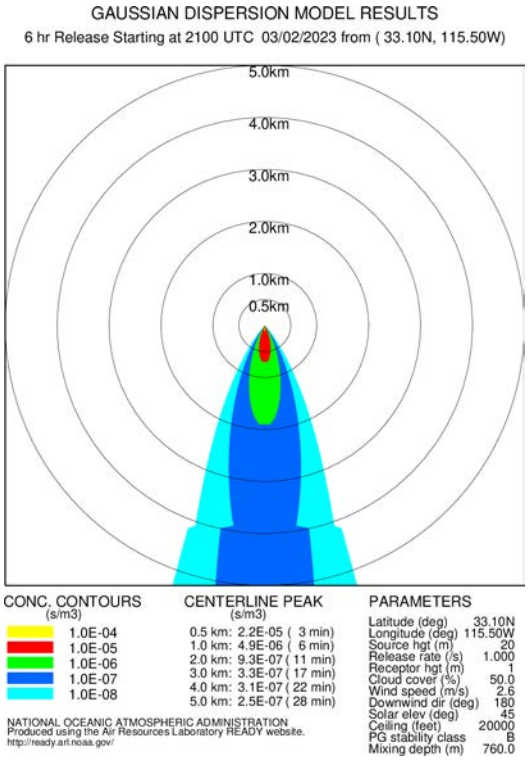

Figure 8.2. Illustration of point source emission dispersion under generalized atmospheric conditions in the Salton Sea region.

Figure 8.3. Map showing a 2 km radius from the Hudson Ranch Geothermal Plant near the Salton Sea.

Hydrogen Sulfide: There are two concerns about H_2S emissions: the direct effects of exposure to H_2S, and the potential for H_2S to become sulfate particulate matter (PM) after being emitted. For this reason, we compare H_2S to SO_2 emissions from other energy sources (since SO_2 also can become particulate matter after it is emitted). The H_2S emissions used herein are those reported to CARB after onsite abatement strategies were employed. All flash plants in the Imperial Valley employ a range of H_2S abatement technologies, including biochemical processes to convert dissolved sulfide to sulfate (BIOX process) and incineration (Hoyer et al., 1991; Gallup, 1992; Gallup, 1996a, b; Rodríguez et al., 2014; Rodríguez et al., 2015). These methods convert 90-95% of the total H_2S into sulfate, resulting in the dissolved sulfate being reinjected with brine back into the reservoir and greatly reducing potential H_2S emissions. CARB inventories suggest these emission rates are below those required for Best Available Control Technology (BACT) limits set by the EPA's Mercury and Air Toxics Standards (MATS) rule for coal power plants (U.S. EPA, 2015). A comparison of H_2S emissions from geothermal plants in the SS-KGRA to emissions reported for all other geothermal operations in California is presented in Figure 8.6. Geothermal emissions are compared to sulfur (SO_2) emissions on a mass/kWh basis from natural gas, coal, and oil used for generating electricity obtained from eGRID for 2020.

Compared to both coal and oil, emissions of sulfur compounds from geothermal energy production on a mass/kWh basis are substantially lower. While this is an interesting comparison at a national level, it is important to note that in 2021, coal and oil accounted for <0.2% and 0.0%, respectively, of California's electricity generation (CEC, 2021).

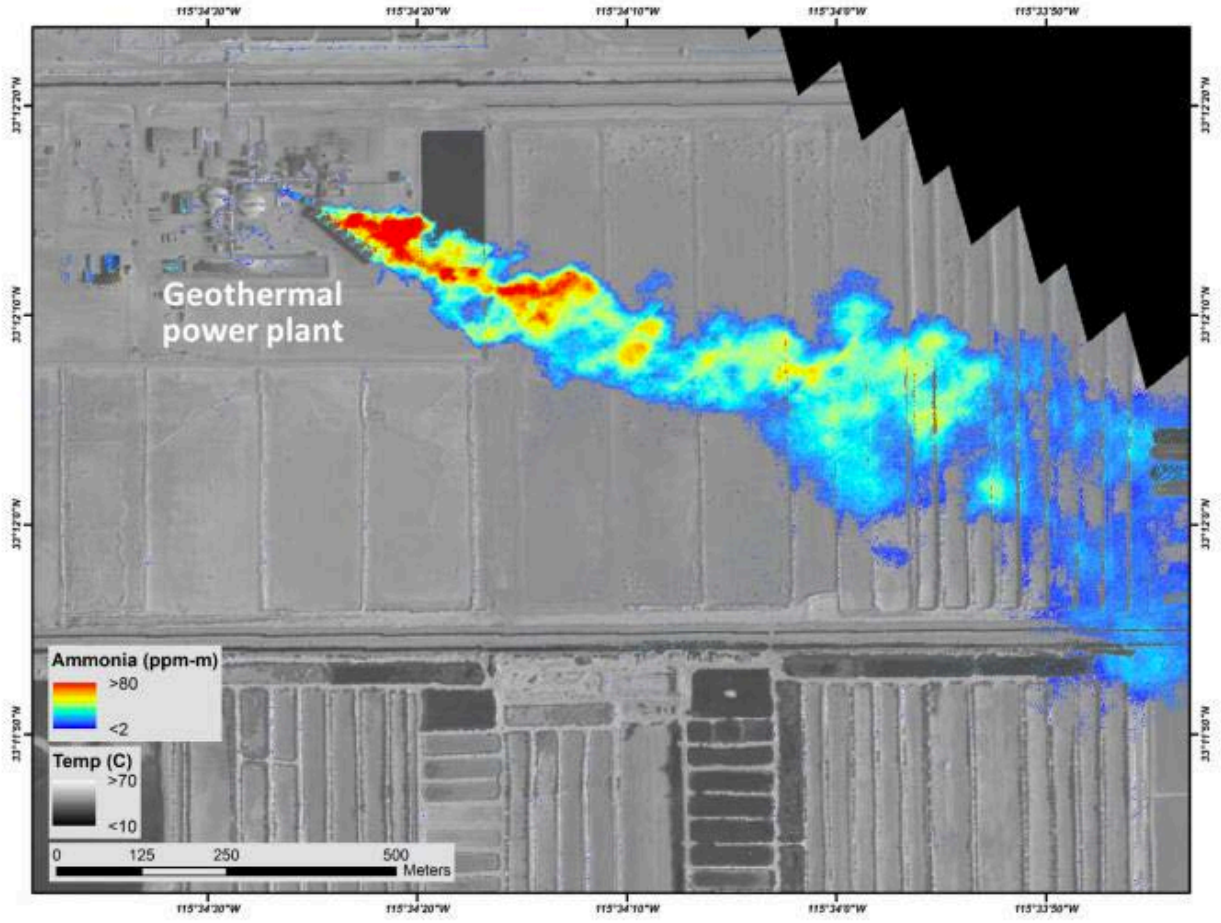

Figure 8.4. An ammonia plume emitted from the Hudson Ranch Geothermal Plant in the Salton Sea geothermal field, determined using airborne thermal-infrared hyperspectral imagery (Tratt et al., 2016).

Ammonia: Figure 8.7 compares ammonia emissions from geothermal plants in the SS-GF to a biomass plant and a natural gas plant in the Imperial Valley Air District (according to CARB toxins reporting), and to all other geothermal operations in California. Ammonia (NH_3) is a non-condensable gas, so emission rates are highly dependent on the concentration of NH_3 in the brine being extracted for geothermal energy production. In the SS-GF, most operations report zero NH_3 emissions. Sources have indicated ammonia is present in geothermal brines in the SS-GR (Bishop and Bricarello, 1978), and that ammonia is released during flash processes at these geothermal facilities (Tardiff, 1977; Gallup, 1998). For example, an ammonia plume can clearly be seen associated with the Hudson Ranch Geothermal Plant. Without measurements of NH_3 in the brine at each facility, it is difficult to assess whether a reporting level of zero is reflective of actual emissions. To account for the uncertainty associated with ammonia emissions, we include alternate ammonia emission rate estimates in our analytical sections that follow.

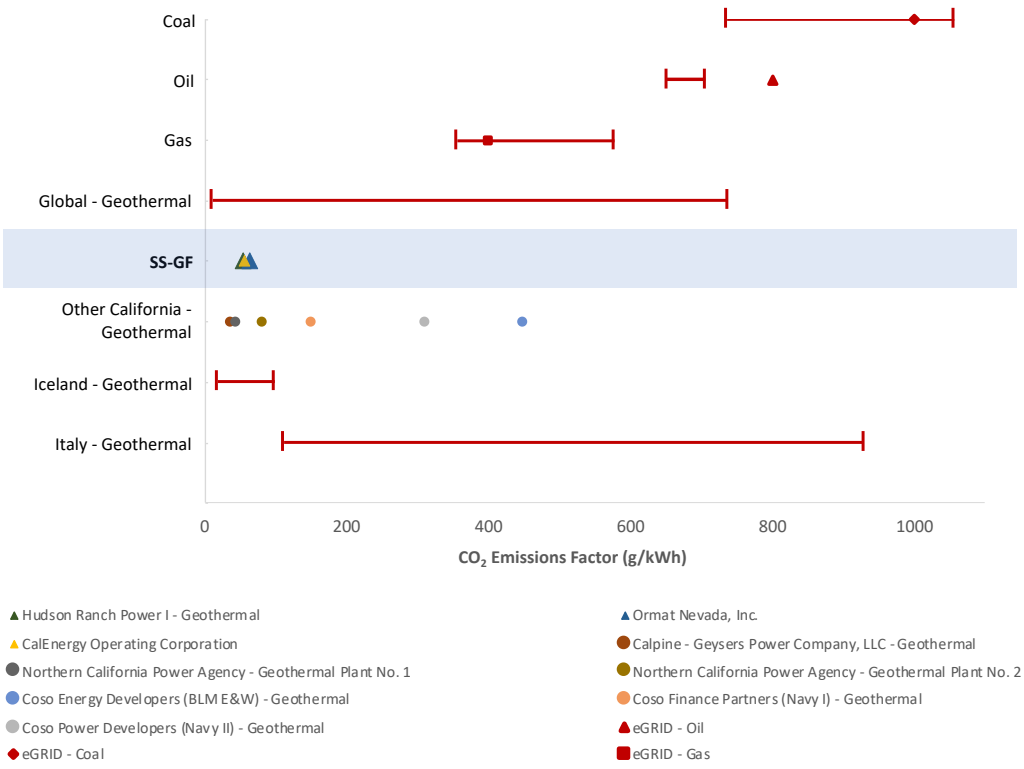

Figure 8.5. Comparison of CO_2 emissions factors from CARB database for existing geothermal operations in California to CO_2 emissions factors for other sources of energy obtained from the World Bank Energy Sector Management Assistance Program (ESMAP, 2016). ESMAP data are represented by the red brackets in the figure.

Proposed facilities such as the new Elmore North Geothermal Project have measured fluxes for ammonia and benzene at existing facilities operated by the same company, but only at specific locations within the system (Elmore North Geothermal LLC, 2023). They do not represent entire fluxes of NCGs from the facilities, and therefore have not been used to compare with the estimations in this work.

Particulate Matter (PM10): A comparison of PM_{10} and $PM_{2.5}$ emission rates from geothermal plants in the SS-GF to those of a biomass plant and a natural gas plant in the Imperial Valley Air District (according to CARB toxins reporting), as well as all other geothermal operations in California, is presented in Figure 8.8 and Figure 8.9. SS-GF geothermal plants have PM_{10} and $PM_{2.5}$ emission rates much lower than the biomass plant, but on par with or larger than the natural gas plant and other California geothermal plants.

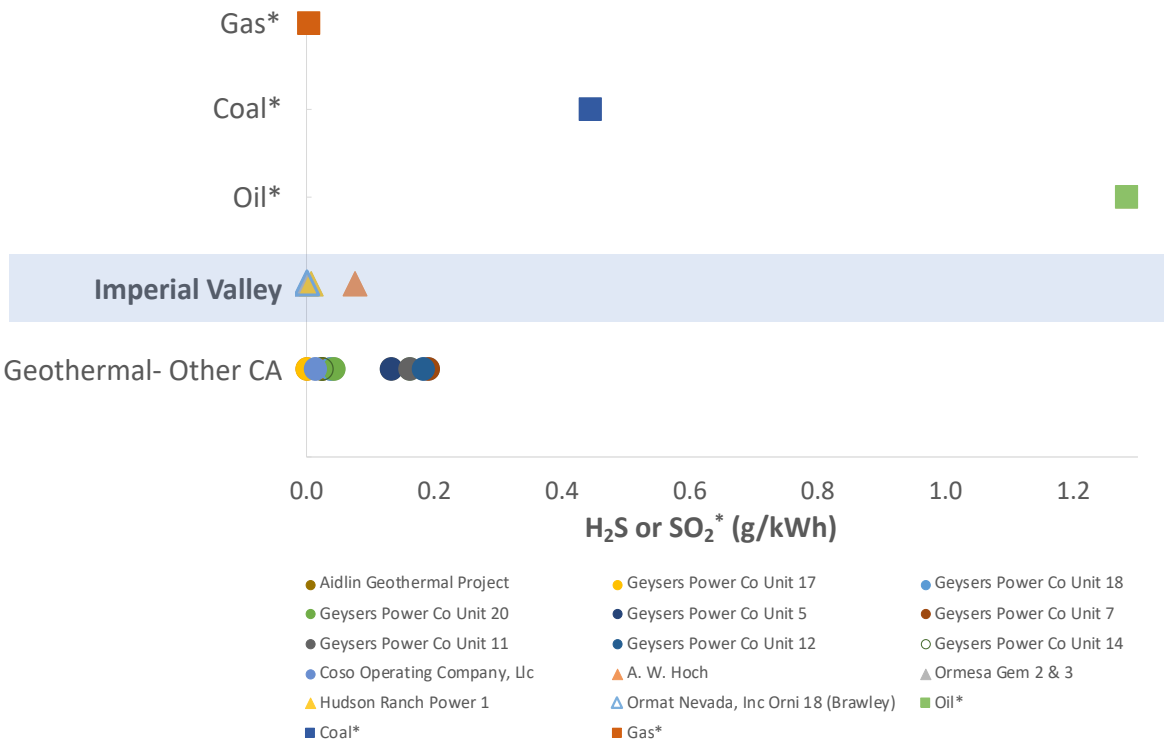

*Figure 8.6. Comparison of H_2S emissions from geothermal energy production in California and Imperial Valley to sulfur emissions from natural gas, coal, and oil as reported by eGRID. *Emissions for gas, coal, and oil are SO_2 emissions reported by eGRID divided by 2 to estimate mass/kWh of sulfur.*

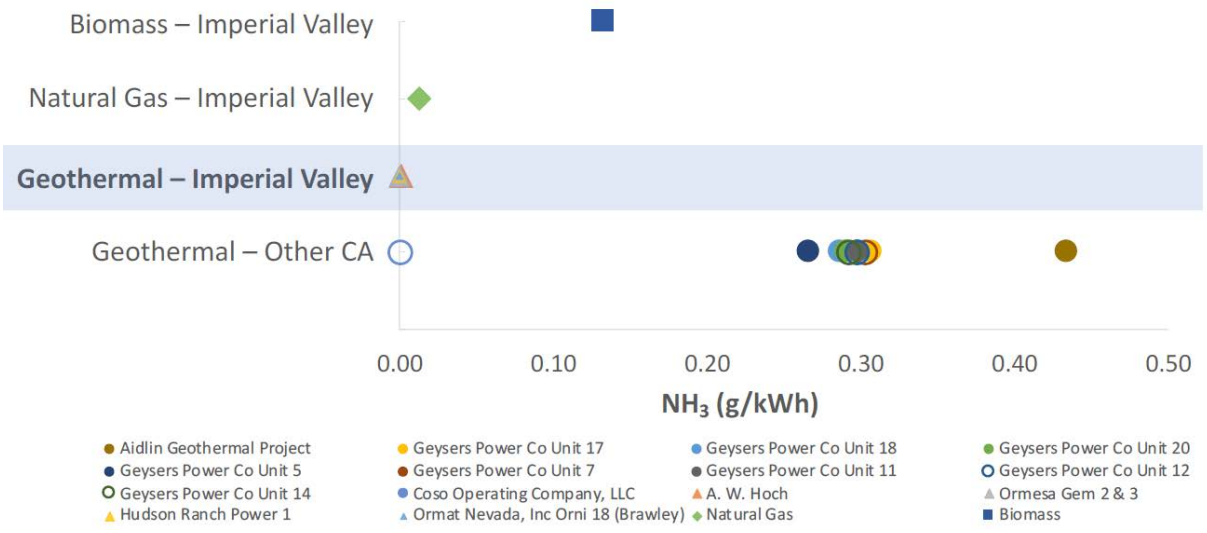

Figure 8.7. Comparison of ammonia (NH_3) emission rates from geothermal energy production in California and Imperial Valley to biomass and natural gas facilities reporting emissions in the Salton Sea Air Basin.

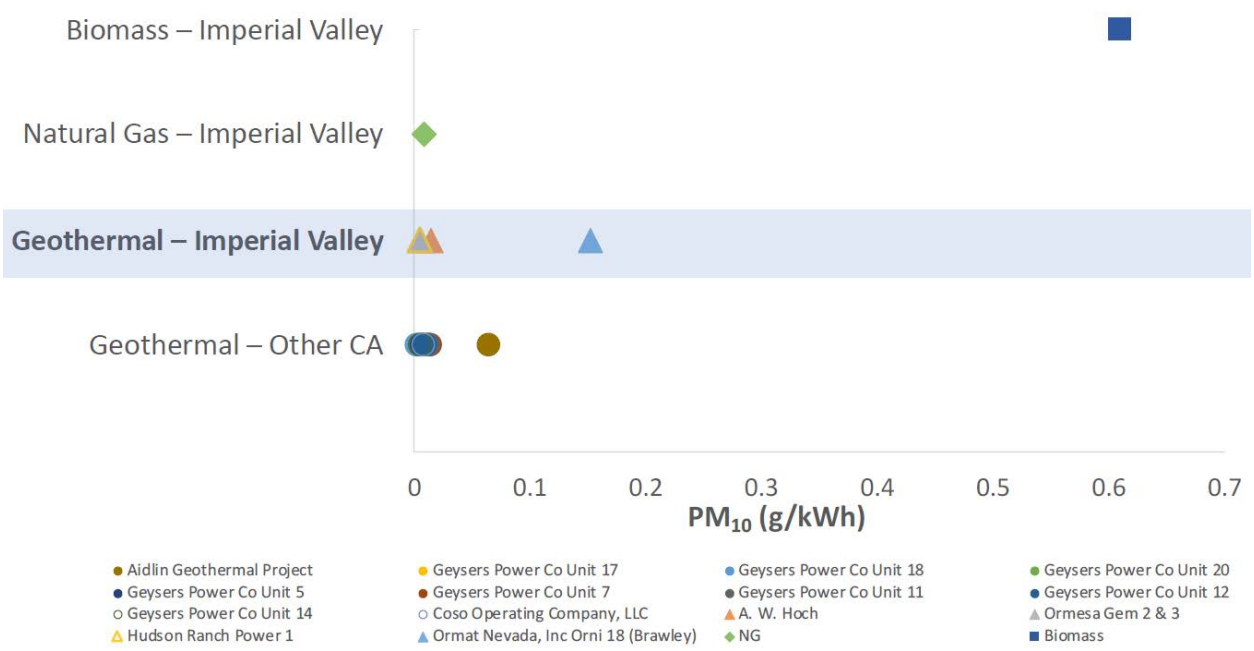

Figure 8.8. Comparison of PM_{10} emission rates from geothermal energy production in California and Imperial Valley to biomass and natural gas facilities reporting emissions in the Salton Sea Air Basin.

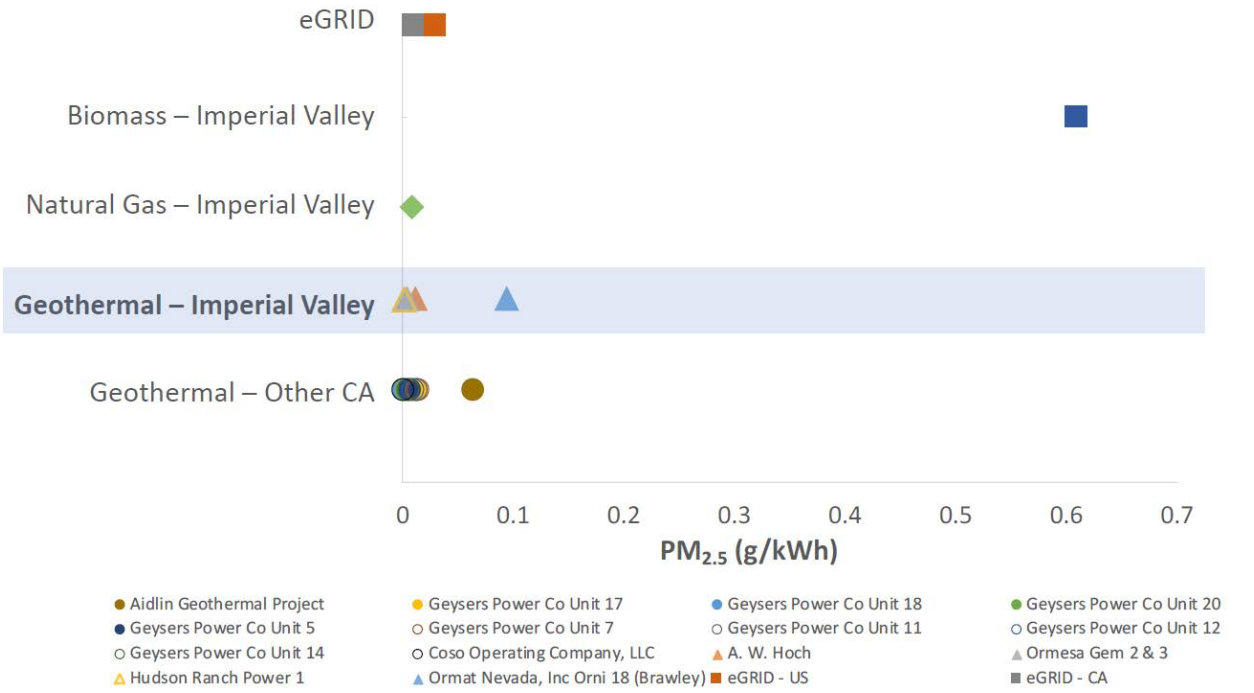

Figure 8.9. Comparison of $PM_{2.5}$ emission rates from geothermal energy production in California and Imperial Valley to biomass and natural gas facilities reporting emissions in the Salton Sea Air Basin.

Benzene: Benzene emission rates from geothermal plants in the SS-GF are compared to those of a biomass plant and a natural gas plant in the Imperial Valley Air District (according to CARB toxins reporting), as well as all other geothermal operations in California in Figure 8.10.

Rates of benzene emission from SS-KGRA geothermal plants range from 0 to 0.01 g benzene/kWh. This rate is higher than the natural gas plant but lower than the biomass facility in the area. Most other geothermal operations in California emit a lower amount of benzene than SS-GF plants, except for one outlier, Geysers Unit 17, which emits around 0.015 g benzene/kWh.

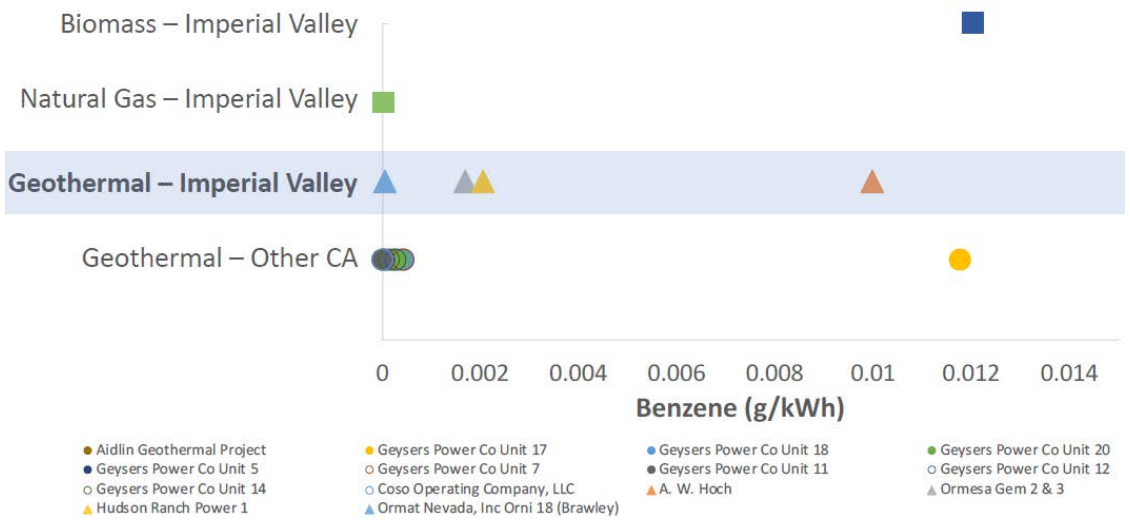

Figure 8.10. Comparison of benzene emission rates from geothermal energy production in California and Imperial Valley to biomass and natural gas facilities reporting emissions in the Salton Sea Air Basin.

Summary: Comparison of Geothermal Emissions to Emissions from Other Power Plants

Overall, SS-GF geothermal plants have low emission rates for CO_2, sulfur compounds, and PM relative to other types of power plants. Emission rates of NH_3 are also low compared to other power plants, but the total number of plants that reported emissions of ammonia was small, adding uncertainty to the assessment of ammonia emissions. To address this uncertainty, we have included alternate ammonia emission rate estimates in related analytical sections. Benzene is being emitted at rates that are within the same range as other power plants in the area, but it is important to note that power plants are not a large contributor to benzene emissions. Major sources of benzene emissions are burning coal and oil, motor vehicle exhaust, and evaporation from gas stations (U.S. EPA, 2012). Understanding emission rates is important for contextualizing geothermal with other energy sources. In the next section, we contextualize the impacts of total emissions from geothermal on local air quality.

Emission Rates in the Context of Air Quality Issues Within the Air Basin

In the comparisons of emissions below, emissions reported by geothermal facilities to the CARB toxins database are compared to categorized sources of area emissions from the Salton Sea Air Basin as reported to CARB (CARB, 2017). Stationary sources include fuel combustion, industrial processes, waste disposal, cleaning and surface coatings, and petroleum production. Areawide sources include solvent evaporation and miscellaneous processes (e.g., farming operations, paved/unpaved road dust, fugitive windblown dust, fires, cooking). Mobile sources include on-road motor vehicles and other mobile sources (e.g., aircraft, trains, recreational boats, farm equipment). Non-anthropogenic sources include biogenic sources,

geogenic sources, and wildfires (CARB, 2017). They are also compared to emissions from other industry and other power sources in Imperial County as reported by the National Emissions Inventory (NEI) (U.S. EPA, 2017).

Particulate Matter (PM_{10})

Figure 8.11 compares potential PM_{10} contributions from current geothermal plants to other regional emissions sources. The largest contributors to PM in the region are areawide sources, which are ~60X larger than the maximum potential contribution of current geothermal plants. Areawide sources include farming, construction, road dust, and fugitive wind-blown dust. For reference, in 2017-18, emissions from the playa itself were 1.23 metric tons/day, and emissions from the desert in the Imperial Irrigation District (IID) were 124 metric tons/day (Formation Environmental LLC., 2020). This indicates that geothermal emissions are small compared to both human-created and natural sources of PM in the area, equating to only about 0.5% of emissions from the desert alone.

To determine the estimate of PM_{10} emissions from geothermal production in the SS-GF, PM_{10} emissions reported to CARB in 2017 were scaled to the total current geothermal capacity. Additionally, an upper bound estimate for the contribution of H_2S and NH_3 to particulate matter was determined by assuming all H_2S and NH_3 were converted to particulate matter in the air basin. Scaling for PM_{10} was based on central estimates of emissions in the SS-GF. The contribution from H_2S was calculated by converting central emissions estimates for the SS-GF to SO_2-equivalent emissions and assuming a 1:1 ratio of SO_2 to PM_{10}. NH_3 emissions were scaled based on a remote sensing rate from the Heber facility (Tratt et al., 2016). Methods to describe the central estimates for PM_{10} and H_2S emissions, and the remote sensing rate for NH_3, can be found in "Toxins and Criteria Pollutants" above. These estimates are meant to be an upper bound of current geothermal contributions to PM_{10} emissions because these estimates assume all emissions of H_2S and NH_3 become particles prior to being removed from the atmosphere or transported out of region.

Hydrogen Sulfide

Geothermal emissions of H_2S are reported as ~40X lower than emissions directly from the Salton Sea, which is the largest contributor to sulfur emissions in the air basin. Geothermal is one of only a few "point source" contributors to H_2S in the SS-GF (Figure 8.12), but it is unlikely that the cause of any H_2S odor in the region would be a result of geothermal operations. As previously mentioned, H_2S from these facilities is being removed using abatement technologies and point source emissions will rapidly disperse in the atmosphere.

The more substantial source of H_2S odor in the region is the Salton Sea itself (Figure 8.12). In natural environments, hydrogen sulfide is produced through the anaerobic digestion of organic material by sulfate-reducing bacteria. Breakdown of organic matter in environments that lack oxygen is a significant source of H_2S. These environments include swamps, sulfur springs, volcanoes, and stagnant bodies of water. Yearly H_2S emissions from all land sources globally are estimated at 53-100 million metric tons of sulfur, with annual emissions from ocean sources estimated at 27-150 million metric tons (Hill, 1972; WHO, 2003).

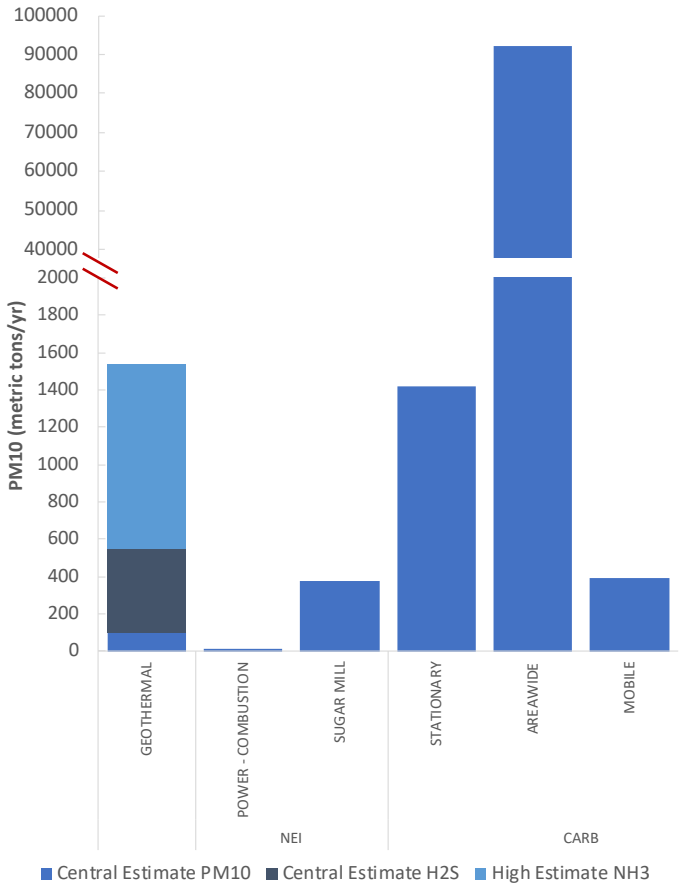

Figure 8.11. Total estimated annual PM_{10} emissions from currently operating geothermal plants compared to emissions reported for other power sources and a local sugar mill (CARB, 2017; U.S. EPA, 2017) in the Salton Sea Air Basin. Estimates of PM_{10} are calculated using central estimates of PM_{10} emission rates scaled to the current geothermal capacity, inclusive of the maximum possible contributions to PM_{10} from H_2S and ammonia, compared to Imperial County PM_{10} emissions reported from stationary, areawide, and mobile sources.

As a stagnant body of water, the Salton Sea releases H_2S. The release of H_2S into the environment from the Salton Sea itself is estimated to be around 3,400 short tons per year (Reese et al., 2008). Figure 8.13 compares geothermal emissions to other area sources of sulfur emissions reported to CARB in 2017, H_2S emissions reported to NEI in 2017, and emissions directly from the Salton Sea. These emissions have been converted to SO_2-equivalents for comparison across sources. Facilities reporting to CARB include A.W. Hoch, J.J. Elmore, J.M. Leathers, and Ormesa 2&3, accounting for 33% of net geothermal generation in the SS-GF. Facilities reporting to NEI include the same plants plus CalEnergy Region 1, collectively accounting for 72.4% of net geothermal generation in the SS-GF. Therefore, these reported emissions do not represent emissions from all geothermal facilities in the SS-GF.

Figure 8.12. Map from NEI of point source H_2S emitters in and around the Salton Sea and the SS-GF. Point sources are represented with red circles, and those circled in blue are geothermal plants in the SS-GF that report H_2S emissions.

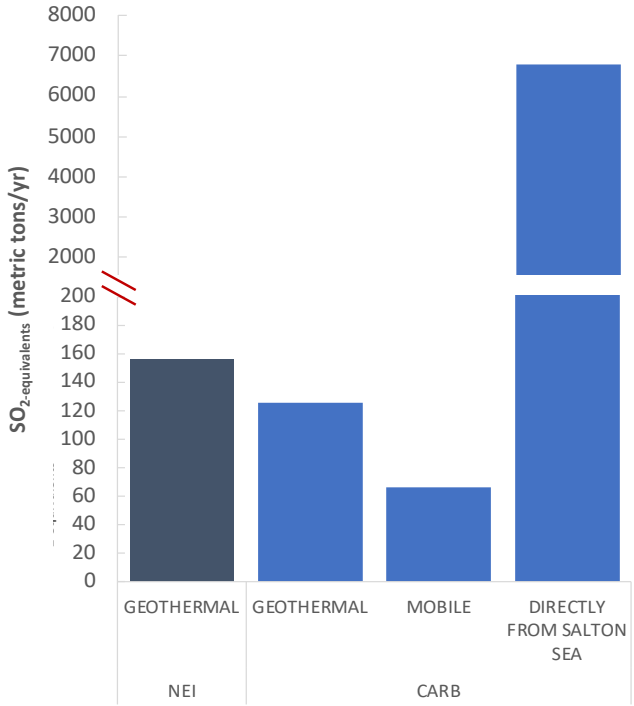

Figure 8.13. H_2S, SO_x, and SO_2 emissions reported to NEI and CARB in Imperial County in 2017, converted to SO_2-equivalents based on molecular weight (CARB, 2017; U.S. EPA, 2017). Reported emissions do not encompass all geothermal production in the region. Salton Sea emissions are directly from the sea itself.

Notably, the release of H_2S from the Salton Sea is cyclical: the flux from the water column to the atmosphere occurs from July through September, with a lower flux on the south side of the sea compared

to the rest of the shoreline. Fluxes from the sea have caused numerous public complaints from north of the sea about odor (Reese et al., 2008).

Ammonia

The amount of ammonia emitted by geothermal sources in the SS-KGRA and reported to the CARB toxins inventory in 2017 was low compared to areawide sources, and comparable to stationary and non-anthropogenic sources (Figure 8.14). Based on reporting to NEI in 2017, geothermal was the lowest point source emitter of ammonia in Imperial County, contributing only 18% of NH_3 point source emissions in the SS-KGRA – less than power combustion (22%) and a sugar mill (60%) (U.S. EPA, 2017). Note that only three geothermal facilities in the SS-KGRA (A. W. Hoch, J.M. Leathers, and J.J. Elmore) reported NH_3 emissions to CARB; in addition to these three, CalEnergy Region 1 also reported to NEI. Therefore, these reported emissions do not represent emissions from all geothermal facilities in the SS-GF. The facilities reporting to NEI account for 72.4% of the net MWh of geothermal energy produced in the SS-GF, and the facilities reporting to CARB account for 33%. NH_3 emissions reported to the CARB toxins inventory remained the same between 2017 and 2020.

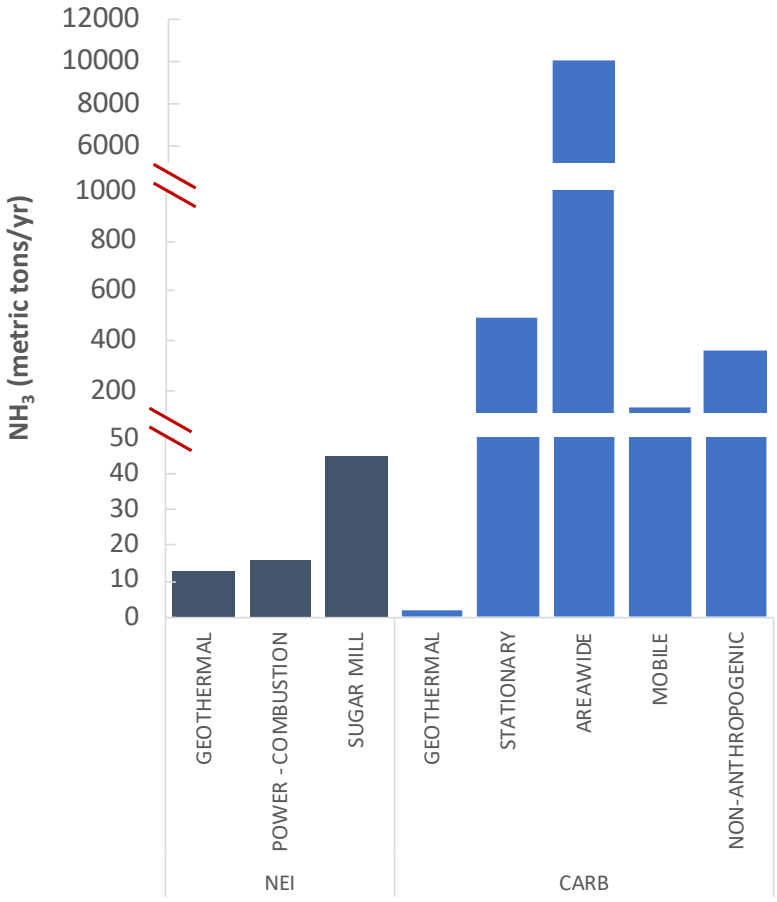

Figure 8.14. NH_3 emissions from sources in Imperial County that were reported to NEI and CARB in 2017 (CARB, 2017; U.S. EPA 2017). Reported emissions do not encompass all geothermal production in the region.

Based on these values, the rate at which these facilities are releasing ammonia is substantially lower than what is reported in the literature. Our calculated rate for emissions based on what is reported to CARB and the energy generation from each facility reported to NEI is 0.00005 g/kWh, 0.00188 g/kWh, 0.02981 g/kWh, and 0.00166 g/kWh for A. W. Hoch, J.M. Leathers, and J.J. Elmore, and CalEnergy Region 1, respectively. Based on a study evaluating NH_3 emissions from Hudson Ranch through remote sensing, the emission rate was estimated at ~0.3 g/kWh (Tratt et al., 2016), yet this facility did not report NH_3 emissions to CARB or NEI. Further, the general NH_3 emission rate for geothermal facilities in the literature is 0.06 g/kWh (Bayer et al., 2013). Based on this concern, we use the remote sensing rate, rather than the reported rate, for Hudson Ranch as a high estimate for total emissions of ammonia. This rate was used in Figure 8.14, Table 8.4, and Figure 8.18.

Potential Emissions from the Lithium Extraction Process

Here we begin to extrapolate these results to assess the impact that geothermal expansion and lithium production will have on air emissions in the Salton Sea Air Basin. These results should be considered simple first-order estimates that do not reflect any known impacts on air quality and contain substantial uncertainty. This section provides context for the possible impact of proposed expansion activities.

Some direct lithium extraction (DLE) processes require concentrated liquid hydrochloric acid (HCl) to remove lithium carbonate from the sorbent. Storage of HCl in onsite tanks will lead to HCl vapor emissions from evaporation. Scrubbers are used to control these emissions, but they can still reach 3.72 metric tons/yr for the production of 30,000 metric tons of lithium hydroxide monohydrate (Breuer et al., 2021). Onsite scrubbers are currently being used for acid storage at Salton Sea Region 1 facilities. Future lithium extraction systems have proposed a new process for sorbent stripping using water that is then recycled onsite, which can help reduce HCl use and associated emissions. More information is needed to understand the process that would be used for treating water for reuse to understand its impact on air emissions. A generalized lithium extraction process with expected air emission flows is presented in Figure 8.15.

Direct emissions occur during the drying, transfer, and packaging of the final lithium product, which release particulate matter that contributes to PM_{10}. During these processes, emissions can be minimized with wet scrubbers or other dust collection systems but are still expected to be 0.17 metric tons/yr based on 19,000 metric tons/yr of lithium hydroxide monohydrate (LiOH) (Chambers Group Inc., 2021). This equates to 8.11E-6 metric tons PM_{10} per metric ton of LiOH.

Additional emissions will occur from the transfer of the final product by truck. It is estimated that for a 19,000 metric tons/yr lithium hydroxide monohydrate facility, there would be one truck per day transporting the lithium product. Emissions from this single truck per day would be insignificant compared to annual average daily truck traffic (AADTT) for Imperial County on Route 86, a major highway that runs the length of the Salton Sea. For example, the average number of 4- and 5-axle trucks traveling this route, estimated at the Imperial/Riverside County line in 2016, was 2,459 trucks per day (State of California, 2020).

If energy from the geothermal facility is already allocated, the facility must buy energy from the grid to power its processes, thus contributing indirect emissions from the regional grid's electricity mix (which is already relatively clean and expected to become significantly more so over time).

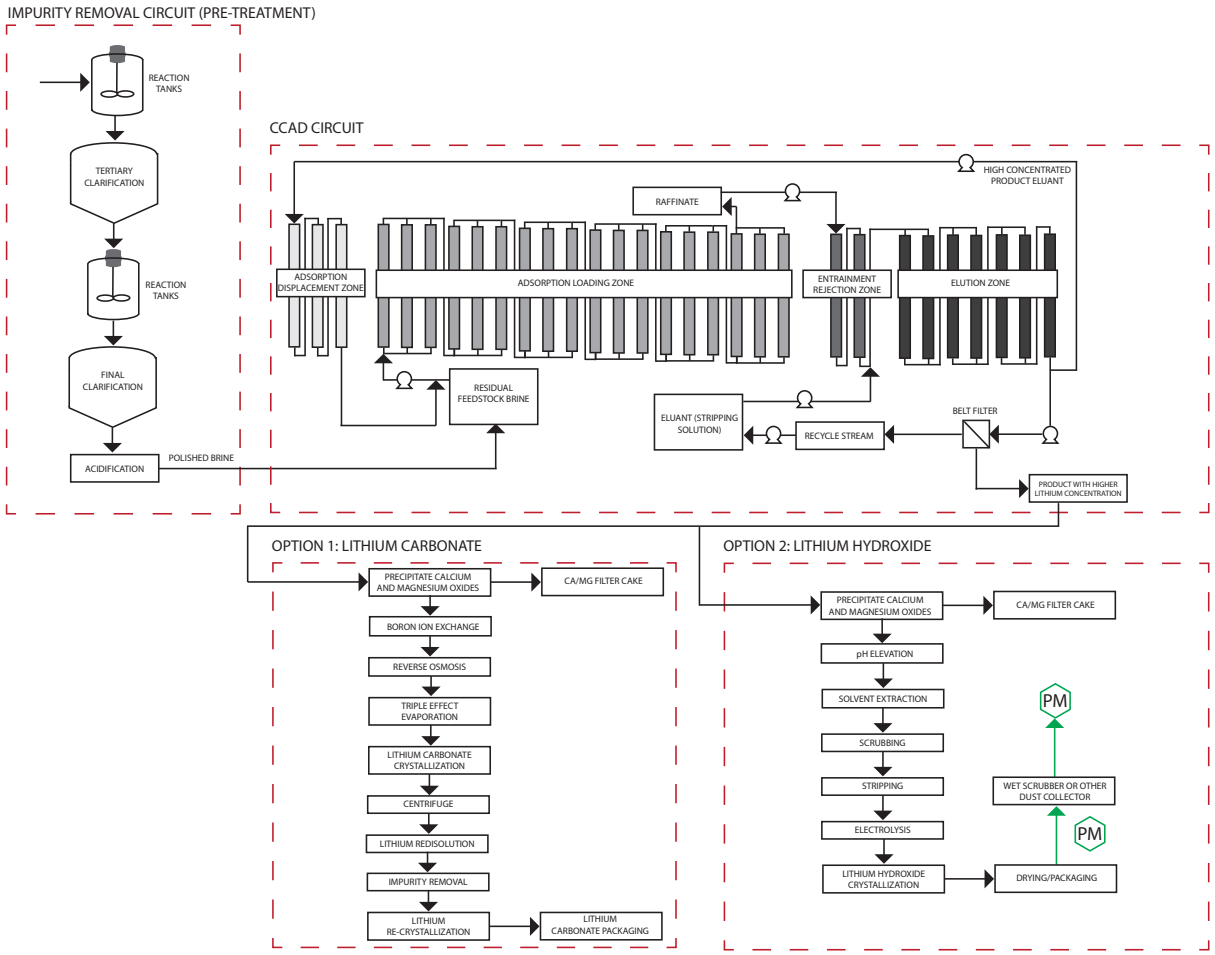

Figure 8.15. Detailed schematic of proposed lithium extraction process addition for geothermal flash plants in the Imperial Valley. The first process is to pre-treat the brine for impurity removal, followed by a circuit for sorbent-based selection of lithium. The concentrated lithium product is then processed to become lithium carbonate (Option 1) or lithium hydroxide (Option 2). Associated air emissions are indicated with arrows throughout the process.

Total Scope 1 and Scope 2 CO_2 emissions intensities from the production of lithium carbonate or lithium hydroxide from brine are compared to emissions from hardrock mining of the same compounds in Figure 8.16 (IEA, 2021). Scope 1 emissions are greenhouse gases (GHGs) that occur directly from sources owned by an organization, whereas Scope 2 emissions are associated with an organization's energy use (U.S. EPA, 2022). The analysis conducted by the International Energy Agency (IEA) to obtain these values was based on Roskill (2020), Vulcan Energy (2020), and S&P Global (2021). The values for lithium hydroxide from brine consider brine operations by evaporative mining in Chile, while hardrock considers lithium hydroxide mined in Australia and refined in China.

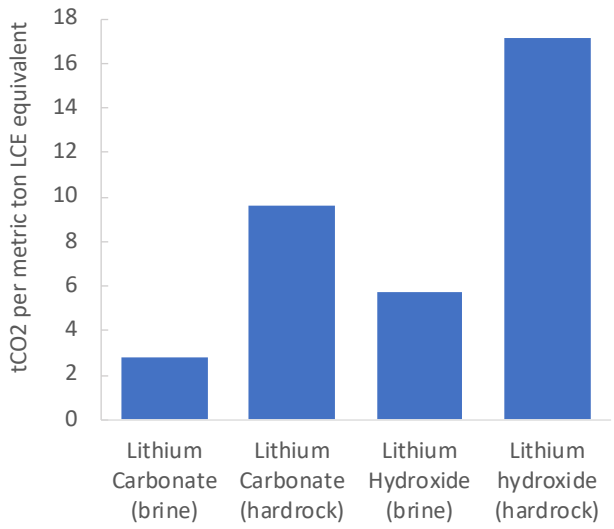

Figure 8.16. Comparison of CO_2 emissions from lithium production across forms of lithium and processing routes. Data extracted from (IEA, 2021).

Potential Emissions from Geothermal Expansion

Current Projections for Geothermal Expansion

To calculate the potential impact of geothermal expansion and lithium extraction on emissions, average emission rates for plants in the SS-GF as reported to CARB (excluding plants that reported zero emissions or did not report emissions) were used to estimate the air quality impact of additional geothermal energy production scenarios in the region. Expansion scenarios included the current level of geothermal production (400 MWe), projected geothermal expansion over the next 3-4 years (520 additional MWe), and the maximum geothermal capacity in the region (2,030 MWe beyond projected expansion levels) (Kaspereit et al., 2016).

Ermak et al. (1980) conducted a study of potential air quality impacts from geothermal expansion to maximum possible capacity in Imperial Valley, which they estimated at 3,000 MW. They concluded that ammonia and carbon dioxide were not expected to be generated at significant ground-level quantities, and that hydrogen sulfide was the pollutant of highest concern. They did not consider H_2S abatement in this study (Ermak et al., 1980).

Quantification of CO_2 Emissions

Based on CO_2 emissions rates from CARB, the low, central, and high estimates of emission rates in Imperial Valley were used to calculate CO_2 emissions from the geothermal expansion scenarios. These emission rates are summarized in Table 8.3.

Table 8.3. Carbon dioxide emission rates used for low, central, and high estimates

Category	Emission Rate (g/kWh)	Source Facility	Data Source
Low estimate	55.10	Hudson Ranch	CARB GHG Mandatory Reporting (2020); EIA Net MWh Generation (2020)
Central estimate	59.02	Average	
High estimate	64.53	Ormat Nevada (Brawley and GEM 2&3)	

The projected rate of lithium production in the SS-GF is 288 tons of lithium carbonate equivalent (LCE)/yr per MWe at 90% recovery efficiency (McKibben et al., 2023). Based on IEA calculations, CO_2 emissions from lithium carbonate production from brine occur at a rate of 2.8 tCO_2 per metric ton LCE. Therefore, the rate of CO_2 generation from LCE production from the SS-GR can be expected to be around 92 g/kWh. A comparison of projected emissions from both geothermal expansion scenarios and the supported LCE production is illustrated in Figure 8.17.

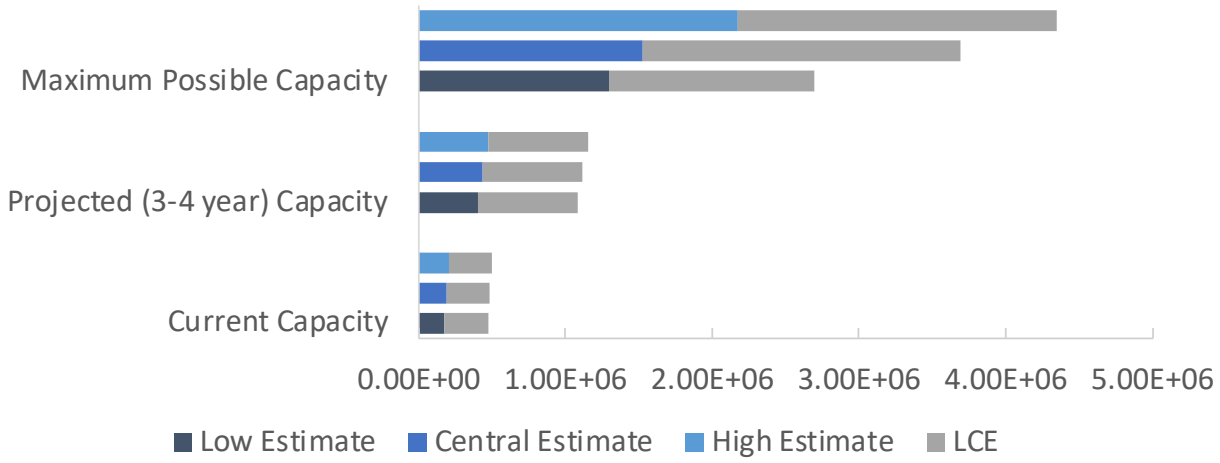

Figure 8.17. Estimated CO_2 emissions from geothermal expansion scenarios using low/medium/high emission rates from Table 8.3 and estimated emissions for the associated lithium production potential for each scenario.

This comparison indicates that lithium extraction will contribute to overall CO_2 emissions from geothermal energy in the region. The rate of emission, 92 g/kWh, is almost double the region's current average CO_2 emissions rate for geothermal energy (59 g/kWh). More importantly, however, is that SS-GR lithium extraction could displace other forms of lithium extraction that are much more carbon intensive, thereby lowering global emissions associated with lithium extraction.

Quantification of Toxin and Criteria Pollutant Emissions

Comparison of current, projected, and maximum possible emissions of PM_{10}, $PM_{2.5}$, benzene, H_2S, and NH_3 to the maximum contributor in each emissions category in the air basin are shown in Figure 8.18.

Low, central, and high estimates of emission rates were calculated based on the minimum, average, and maximum reported emission rates for each toxin or criteria pollutant to the CARB toxins database in 2020. Emissions reported as zero were excluded from the calculations of minimum and average emission rates. The emission rates used in calculations for Figure 8.18 are summarized in Table 8.4.

Figure 8.18 indicates that for PM_{10}, even at maximum geothermal capacity and assuming the high emission rate, geothermal emissions would only contribute around 6% compared to areawide sources. We also extrapolate the impact of DLE on direct PM_{10} emissions, which would be 1.88 metric tons PM_{10} per year. This contribution is also insignificant in the context of areawide PM_{10} sources, which are over 100,000 metric tons per year.

For H_2S, the current geothermal capacity using a central emission rate contributes only 7% of what the Salton Sea itself emits annually, around 3,400 metric tons/yr (Reese et al., 2008); further, these emissions would be spread more evenly across the year than H_2S emissions from the Salton Sea. Near-future projections for geothermal, again using a central emission rate, would increase this contribution to 15% of what the Salton Sea emits, while the maximum geothermal capacity would increase this contribution to 48%. Using the highest estimated emissions rate, expanding the region's geothermal capacity to the maximum possible would cause H_2S to exceed emissions from the Salton Sea on a yearly basis but the maximum capacity scenario is not expected to occur.

For NH_3, the current geothermal capacity using a central emission rate contributes less than 1% of what areawide sources emit annually. Considering a high emission rate, this increases to around 10%. Expanding the geothermal field to projected and maximum capacities would increase the high NH_3 emissions projections to 22% and 72% of areawide emissions, respectively.

Summary

Current geothermal electricity production in the SS-GF produces very low emissions of carbon dioxide relative to generation based on natural gas, coal, and oil. Current geothermal electricity production also produces relatively low emissions of particulate matter, hydrogen sulfide, ammonia, and benzene.

Emissions from current geothermal production are also generally very low compared to other sources in the region. For example, regional sources of particulate matter (such as from agriculture, road dust, and fires) produce ~400X more particulate matter in the air basin than does geothermal energy production (comparing PM_{10} totals specifically), and ~80X more $PM_{2.5}$. Naturally occurring emissions of hydrogen sulfide from the Salton Sea are estimated to be ~15X larger than those from current geothermal energy production. Additionally, reported emissions of ammonia are <1% of areawide sources (such as agriculture). One caveat related to ammonia is that there was a wider range of emission rate estimates in the literature than for the other pollutants. Finally, benzene emissions were small on an absolute basis, though there is not a major source of benzene emissions in the region with which to compare total emissions.

Table 8.4. Toxin and criteria pollutant emission rates used for low, central, and high estimates

Toxin or Criteria Pollutant	Category	Emission Rate (g/kWh)	Source Facility	Data Source
PM_{10}	Low estimate	0.0046	Hudson Ranch	CARB (2020); EIA Net MWh Generation (2020)
	Central estimate	0.0703	Average	
	High estimate	0.2505	Ormat (Brawley)	
$PM_{2.5}$	Low estimate	0.0030	Hudson Ranch	CARB (2020); EIA Net MWh Generation (2020)
	Central estimate	0.0457	Average	
	High estimate	0.1551	Ormat (Brawley)	
Benzene	Low estimate	4.771E-5	Ormat (Brawley)	CARB (2020); EIA Net MWh Generation (2020)
	Central estimate	0.0032	Average	
	High estimate	0.0106	Ormesa Gem 2 & 3	
H_2S	Low estimate	0.0004	Ormat (Brawley)	CARB (2020); EIA Net MWh Generation (2020)
	Central estimate	0.0702	Average	
	High estimate	0.3083	J.M. Leathers	
NH_3	Low estimate	5.484E-5	A.W. Hoch	CARB (2020); EIA Net MWh Generation (2020)
	Central estimate	0.0114	Average	EIA Net MWh Generation (2020)
	High estimate	0.3083	Hudson Ranch	Tratt et al. (2016); EIA Net MWh Generation (2020)

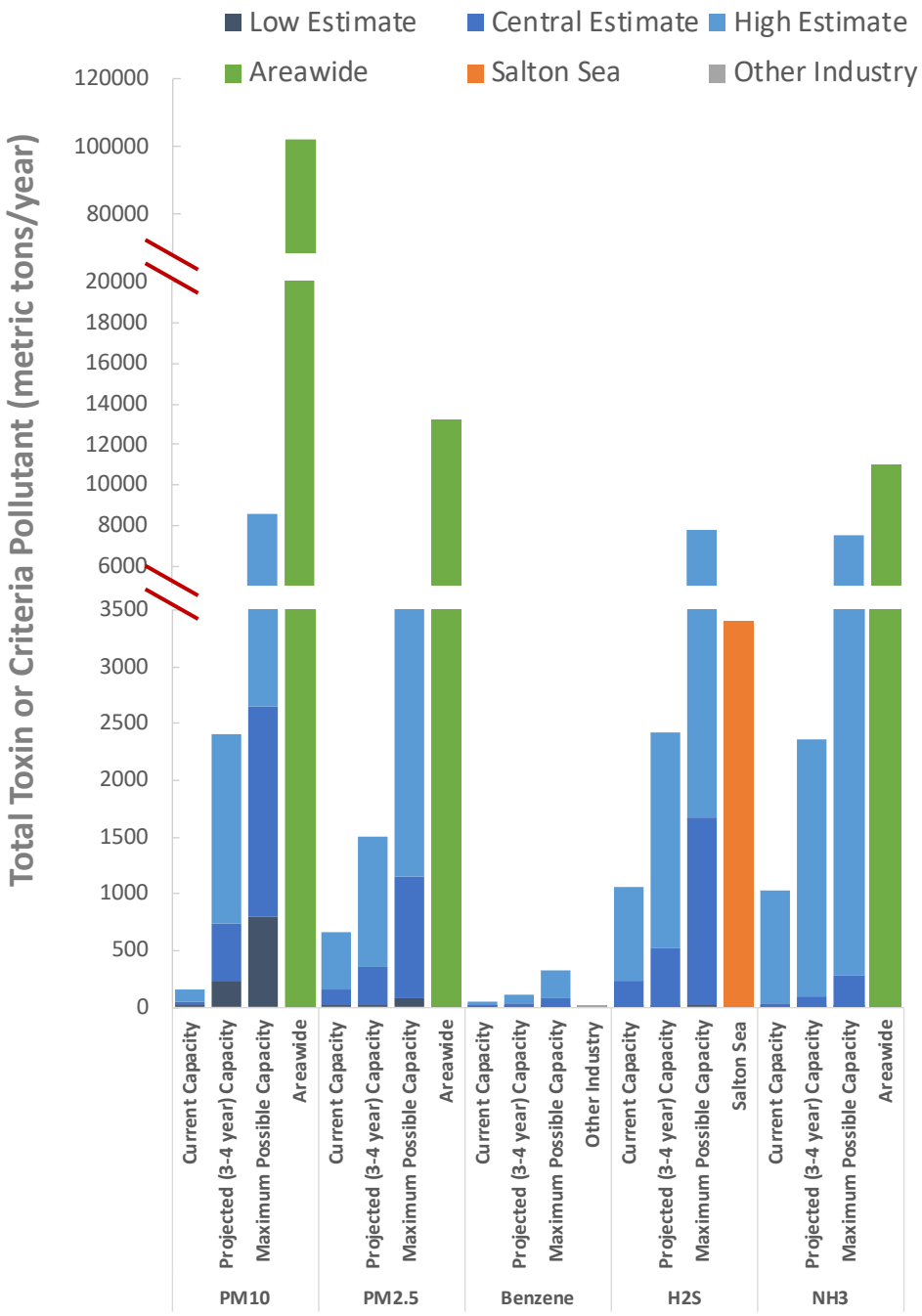

Figure 8.18. Estimated emissions (low/central/high) associated with geothermal expansion in the region and the potential lithium production this expansion could support, compared to the maximum of each of those emission sources in the Salton Sea Air Basin.

Expansion of geothermal electricity production from the SS-GR would support California and federal goals for clean energy expansion. State regulators, in working towards achieving 100% clean energy, plan

to double geothermal capacity.[3] Further, the California Public Utilities Commission (CPUC) announced in June 2021 a requirement for utilities to procure an additional 1 GW of geothermal energy by 2026. This requirement, together with the impetus for lithium production (and its associated revenue), has spurred the expansion of geothermal development in the region (CPUC, 2021). Expanding geothermal power generation over the next 3-4 years to support lithium production from the SS-GR would also support clean energy goals.

The impact of geothermal energy expansion and the addition of lithium extraction at these facilities will have relatively small impact on overall regional emissions of all pollutants identified here, provided that low or central emission rates are realized, and appropriate mitigation measures are put in place. In the case of PM_{10} and $PM_{2.5}$ emissions, even the high emission rate assumptions do not lead to a substantial change in total regional emissions across all sources. However, H_2S emissions from geothermal production could be comparable to H_2S emissions directly from the Salton Sea if it is emitted at the high estimate rate. Similarly, ammonia emissions from geothermal production remain small compared to other sources unless the high emission rate estimate is realized for most plants, in which case geothermal ammonia emissions could become comparable to other important regional sources. A conclusion from this study is that the emission rates of H_2S and ammonia from new geothermal production are key variables to assess within the context of expanding geothermal production and regional air quality.

In the case of expanded geothermal capacity and lithium extraction, key determinates of air quality impacts would be the emission rates of hydrogen sulfide and ammonia from new geothermal production. For hydrogen sulfide, future emission rates can be limited by the control technologies and strategies applied. For ammonia, uncertainty in current emission rates make bounding future emissions challenging; more measurements and data could resolve this uncertainty.

[3] https://www.latimes.com/environment/story/2020-01-22/california-needs-clean-energy-after-sundown-geothermal-could-be-the-answer

Chapter 9: Evaluation of Potential Chemical Use and Solid Waste

Key Takeaways

- Geothermal power plants in the Salton Sea Geothermal Field (SS-GF) currently produce approximately 80,000 metric tons of solid waste per annum, representing approximately 30 kg of solid waste per MWh of electrical production. These solid wastes are predominantly composed of iron-silicate filter cake, brine-pond solids, and solids generated during plant maintenance.
- Filter-cake solids are predominantly nonhazardous and are disposed of in regional Class II or Class III landfills. Brine-pond solids are predominantly hazardous wastes and are disposed of in Class II or Class I landfills, appropriate for industrial waste solids or hazardous waste solids, respectively.
- In the near term (2-5 years), the amount of solid wastes produced per year is expected to approximately double, as electrical production capacity doubles.
- Our analysis indicates that landfill capacity currently being expanded is adequate for management of expected new solid waste production from geothermal power plants in the near term. However, full utilization of the full electrical production capacity of the Salton Sea Geothermal Reservoir (SS-GR), which is a long-term goal, would undoubtedly require planning for additional landfill capacity.
- To produce lithium chloride from geothermal brine, the brine will be treated to remove silica and metals to produce "clean brine" prior to the direct lithium extraction (DLE) process step, creating a solid byproduct. More silica and metals will need to be removed to prepare the brine for lithium extraction will be more significant than what is currently needed to reinject the spent brine back into the formation.
- These results suggest that landfill capacity should be considered as part of development of both geothermal and lithium resources in the region. Efforts to divert waste solids from landfills to useful purpose should be encouraged to save landfill space.

Introduction

Geothermal brine in the SS-GR typically contains approximately 25% dissolved salts and minerals (Table 1.2). Dissolved salts and minerals can precipitate to become solids and are collectively referred to as total dissolved solids (TDS). Many of the dissolved solids in SS-GR geothermal brines are potentially valuable, such as lithium, manganese, zinc, and potassium. Other dissolved salts and minerals are potentially hazardous, such as arsenic and lead. Dissolved solids precipitate due to a broad variety of physical and chemical processes. Salts and minerals precipitate when they reach or exceed their saturation limits, which change as a function of the solution pH, temperature, and the presence of other dissolved chemicals or solid surfaces. For example, as the brine cools during power production, saturation limits decrease, and solids will precipitate out of solution.

Chemical precipitation can cause scaling, the deposition of mineral coatings on pipes and other surfaces. Mineral scale and processes associated with its control are the major sources of solid wastes at geothermal power plants. It is a common problem at power plants that is often associated with silica, iron, calcium, and barium, all of which are found in SS-GR geothermal brine (Table 1.2). As described in this chapter, all geothermal power plants in the SS-GF use a crystallizer-clarifier process that deliberately precipitates silica to avoid silica scaling in pipes, wells, and elsewhere in the plants. Chemicals are added to avoid the precipitation of barium and calcium scales. However, despite these controls, scaling and other mineral deposition does occur.

The other main use of chemicals is to abate emissions of hydrogen sulfide (H_2S) and other non-condensable gases (NCGs). As discussed in Chapter 8, these compounds occur naturally in SS-GR brine and must be mitigated so they are not released as harmful air pollutants. Finally, geothermal brine can also contain radioactive elements such as radium, cesium, potassium, thorium, and uranium, collectively referred to as naturally occurring radioactive material (NORM). Operators use chemical processes so that these elements stay in liquid form and can be reinjected back into the reservoir, rather than precipitating as solids.

This chapter provides an investigation and evaluation of chemical use during geothermal power production, as well as potential chemical use during geothermal lithium extraction and purification. The chapter includes an in-depth evaluation of the amounts and types of solid waste generated by geothermal power production, including hazardous wastes, based on publicly reported data. We then use a mass-balance approach to discuss potential solid waste production that could occur as a byproduct of lithium resource extraction in the region. The chapter focuses on analysis of environmental data collected by various state and federal agencies, mainly between 2014-2021; for data sources, see Appendix Chapter 9. The SS-GF power plants operate brine ponds for waste management that are Class II Surface Impoundments and require regulatory oversight. Some of the SS-GF power plants use common brine ponds as described in Table 9.3. Generation of solids wastes at the SS-GF and disposal in landfills results in additional regulatory oversight. The information contained in this chapter relies on data sets resulting from the regulatory requirements as described in Appendix Chapter 9.

Chemical Use at the Geothermal Power Plants

In the SS-GF power plants, chemicals are added to cooling water systems, brine processes, and steam condensate. The chemicals are added to reduce scaling, biological growth, and corrosivity, as well as to adjust fluid pH and limit emissions (primarily H_2S, although other air pollutants may be reduced as well).

Information about the chemicals used at existing facilities is publicly accessible through recent Waste Discharge Requirements (WDR) issued to the SS-GF power plants by the Regional Water Quality Control Board (RWQCB). These WDR are issued as the result of the brine ponds at the power plant facilities. The WDR contain tables of process chemicals used onsite (RWQCB, 2021, 2022, 2023a, 2023b). These tables include descriptions of the chemical purpose and product numbers, but do not include chemical descriptions or registry numbers. The most recent WDR for the BHER power plants, prepared for the Elmore Plant (Appendix Chapter 9, Table A9.1), has the most complete list of chemicals (RWQCB, 2023b; Table 2, p. 5-6). The WDR for the Salton Sea Unit 1-5 power plants (identified as Region 1 in the WDR) and for the Vulcan and Del Ranch power plants (identified as Region 2 in the

WDR) have similar lists, although those lists do not include ST-70 or the chemicals in the last five rows of Appendix Chapter 9, Table A9.1 (RWQCB, 2021, 2022). The WDR for the Leathers Power Plant has not been updated since 2015 and does not contain a similar list of chemicals (RWQCB, 2015). However, it is presumed that chemical dosing strategies at the Leathers Power Plant are similar to the strategies used at the other BHER power plants. The WDR for the Featherstone Power Plant is being updated; the tentative WDR contains a table with a list of chemicals used at the power plant, as shown in Appendix Chapter 9, Table A9.2 (RWQCB, 2023a; Table 2, p. 8-9).

These WDRs require RWQCB approval before new process chemicals are used. For example, the tentative WDR for the Featherstone Power Plant contains the following requirement: "At least 30 days prior to the use of a new chemical class for control of microbes, pH, scale, and corrosion of cooling tower water and/or geothermal brine, the Discharger shall notify the Regional Water Board's Executive Officer in writing. The use of a new class of chemicals may not be utilized until approved in writing by the Regional Water Board's Executive Officer" (RWQCB, 2023a; p. 34). The requests for use of new chemicals are typically contained in written correspondence to the RWQCB and are usually accompanied by Safety Data Sheets (SDS) for the chemical products proposed. Correspondence for chemical requests is posted on the California GeoTracker website (geotracker.waterboards.ca.gov).

Air Pollution Control Processes and Chemical Use

Most power plants, including geothermal, typically use some type of emissions control technology. In the SS-GF, air pollution control processes are used to reduce emissions of hydrogen sulfide (H_2S) and other air pollutants. Without sufficient abatement, the release of H_2S gas from geothermal brines would cause corrosion of plant infrastructure and result in sulfur emissions that are detrimental to air quality. (For more information about H_2S and other non-condensable gas emissions, see Chapter 8.) In California, atmospheric emissions of H_2S and other air pollutants from geothermal power plants are regulated by the California Air Resources Board (CARB) and the local air districts. This chapter discusses these air pollution prevention processes because of the chemical use involved and the solid waste produced.

There are many alternatives for H_2S abatement in industrial settings (Nagl, 1999; Pudi et al., 2022; Rodríguez et al., 2014). The most common approach is to oxidize H_2S to sulfate using oxygen, while under some conditions, such as oxygen limitation, H_2S can be partially oxidized to elemental sulfur. Oxidation of sulfide to sulfur and sulfate is mediated by bacteria that gain energy from the reaction; therefore, many H_2S control systems include significant biological activity and may need to use biocides to control excess bacterial growth. Some H_2S abatement systems, typically referred to as biofilters, are engineered to use bacteria that oxidize sulfide with oxygen (Iranpour et al., 2005; Rodríguez et al., 2014; Schiavon et al., 2016). Chemical oxidants other than air can also be used to convert sulfides to either sulfur or sulfate. For example, the conversion of H_2S to elemental sulfur can also be catalyzed by oxidation with ferric iron. Sodium hypochlorite and analogous bromine chemicals can be used to oxidize H_2S to sulfate. Hydrogen peroxide can be used to oxidize H_2S to elemental sulfur at neutral pH or sulfate at high pH conditions. Organic oxidizing acids, such as trichloroisocyanuric acid (TCCA) can also be used to oxidize H_2S to sulfate. Other chemicals that can be used for H_2S abatement include chlorine gas, permanganate, perborate, peroxysulfuric acid, transition metal oxides, and organic chemicals such as dibromopropionamide (DBNPA) and bromo-chlorohydantoin (BCH; see Appendix Chapter 9) (Gallup, 1992; Jacobs et al., 2017).

The most common H_2S abatement systems inject air as a source of oxygen and may or may not include other chemical oxidants alone or in combination. One commercial treatment marketed to the geothermal industry is a combination of multiple chemicals in combination with chemical stabilizers and air injection (Gill and Jacobs, 2018; Jacobs et al., 2017; Nalco-Ecolab, 2018). Some chemical treatments for H_2S abatement, such as sodium hypochlorite, have biocidal properties that also provide the benefit of limiting excess bacterial growth in treatment systems. The oxidation of H_2S to sulfate produces acid, so in most cases a base is added to control pH as part of H_2S abatement and to produce a chemically benign sulfate salt. The formation of sulfate, as opposed to elemental sulfur, as an end product of H_2S treatment is preferable, since sulfate is very water soluble, is not toxic or harmful, and is not volatile, so it does not cause air pollution. Production of elemental sulfur is typically less desirable because sulfur is a solid that can build up and plug H_2S abatement systems. Dissolved sulfate can be injected back into the subsurface formation with the injection fluid, whereas if elemental sulfur forms, the precipitants can cause scaling in the cooling towers, producing solids that must be sent to landfills and particulate matter that is detrimental to the reinjection of spent brine into the reservoir (Gallup, 1992; Gill and Jacobs, 2018; Jacobs et al., 2017; Rodríguez et al., 2014; Sanopoulos and Karabelas, 1997). However, sulfur is an acceptable end product because it is also nonvolatile and nontoxic, and can potentially be sold for fertilizer. For more details about H_2S abatement at geothermal power plants, see Appendix Chapter 9.

The 11 SS-GF geothermal power plants use varying methods for H_2S control (Figure 9.1, Table 9.1). The Region 1 power plants rely on oxidation of condensate in an oxidizer box, while non-condensable gases (NCGs) are treated in a regenerative thermal oxidizer (RTO) process. In the RTO process, NCGs are incinerated to produce oxidized gases such as carbon dioxide (CO_2) and sulfur dioxide (SO_2) (Rodríguez et al., 2014). At Region 1, the RTO process is used in combination with a gas scrubber (the "KinPactor" process) that treats gases and reduces dust prior to emission. At Region 2, condensate is also treated in an oxidizer box while the NCGs are treated in biofilters, a biological treatment system for sulfide removal from gases (Rodríguez et al., 2014). The Elmore and Leathers Power Plants use the oxidizer box for treatment of condensate, and NCGs are compressed and introduced into the cooling water by sparging. Sulfide abatement occurs in the oxidizer box and the cooling tower. A similar process is used at the Hudson Ranch Featherstone Power Plant (Nalco-Ecolab, 2018). In addition to the processes listed in Table 9.1, plants have drift eliminators (demisters) to minimize vapor droplets in the plant emissions. Also, Units 3 and 4 (Region 1) and Vulcan (Region 2) have scrubbers to minimize emissions from hydrochloric acid (HCl), which is used for cleaning and pH adjustment.

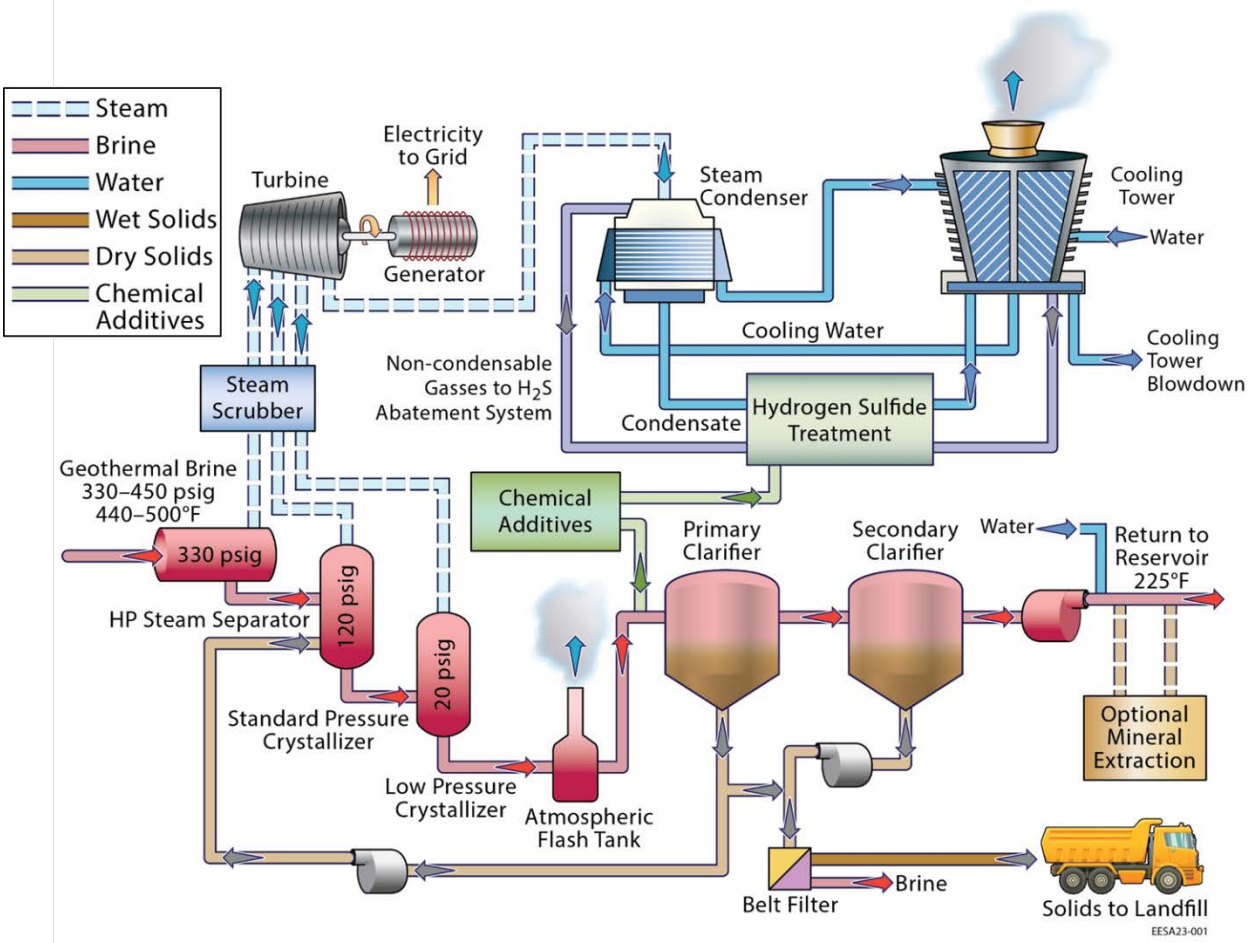

Figure 9.1. Schematic of a typical flash-steam geothermal power plant in the SS-GF.

The chemicals used at SS-GF power plants to control emissions vary with the type of abatement system used. One of the specialty products used for H_2S abatement is TowerBrom (Appendix Chapter 9). Monopotassium phosphate is used as a nutrient addition to the biofilters at both of the power plants in Region 2. Sodium hypochlorite, an oxidizing biocide, is used at all geothermal power plants that report data to the RWQCB. Propane is used at Region 1 to support the RTO process. In addition to the oxidizing biocides discussed above, other biocides are used at SS-GF geothermal power plants (Appendix Chapter 9: Table A9.1). Use of these chemicals is consistent with the recommendation to use a secondary nonoxidizing biocide to control biological growth in the cooling towers (Gallup, 1992).

Table 9.1. Hydrogen sulfide (H_2S) abatement processes used at SS-GF power plants

	H_2S Abatement Process			
Power Plant	Oxidizer box for chemical treatment of condensate before cooling tower	Sparger abatement for combined treatment of condensate & NCG[a] in the cooling tower	Regenerative thermal oxidizer (RTO) for thermal treatment of NCG before emission to atmosphere	Biofilter for biological treatment of NCG before emission to atmosphere
Region 1: Unit 1 and 2	X		X	
Region 1: Unit 3 and 4	X		X	
Region 2: Vulcan	X			X
Region 2: Del Ranch (Hoch)	X			X
Elmore	X	X		
Leathers	X	X		
Hudson Ranch/ Featherstone	X[b]	X		

[a] Non-condensable gases (NCGs).

[b] Reaction tank prior to cooling tower.

Table 9.2. Management of liquid and solid wastes at SS-GF power plants

Power Plant Management Designation	Power Plants included in Management Units	Brine Pond Size (million liters)	Waste Discharge Requirement (WDR) Number	EPA Handler ID	DTSC Name
Region 1	Units 1, 2, 3, 4, & 5	4.13	R7-2021-0008	CAD983663634, CAD983663600	Unit 1-2 or Unit
Region 2	Vulcan, Del Ranch, Turbo	9.34	R7-2022-0011	CAD983648429	Vulcan
Leathers	Leathers	6.17	R7-2015-0020	CAD983648403	Leathers
Elmore	Elmore	6.28	R7-2023-0011	CAD983648445	Elmore
Hudson Ranch 1	Featherstone	3.72	R7-2023-0012 (tentative)	CAR000221614	Hudson Ranch

Scale Control Processes and Chemical Use

"Scaling" refers to the buildup of mineral coatings on surfaces. Scaling is an issue in flash-steam geothermal power plants because the brines can contain high concentrations of dissolved salts that can form precipitants (i.e., become solids) when the fluid temperature and pressure decrease in the flash tanks (Gallup, 1998). Release of steam increases ion concentrations in the remaining brine, which can further promote scale formation. Other factors influencing scale formation are pH, redox conditions, contact time, ionic strength, fluid dynamics, and the presence of existing precipitants (Pardelli et al., 2021). Scaling can reduce fluid flow through pipes, reduce heat transfer, and have other negative consequences on process operations in power plants and other industries (Bishop and Bricarello, 1978; Brown, 2013;

Harrar et al., 1979a; Hoyer et al., 1991; Jamero et al., 2018; MidAmerican Energy Holding Co., 2003; Pambudi et al., 2015; von Hirtz, 2016). Scaling can also damage injection systems and reduce geothermal formation porosity where the fluid is injected.

Scale control processes are used in geothermal power plants to maintain efficient operations and allow reinjection of spent brine back into the geothermal formation. Scaling can be controlled by adjusting the temperature, pressure, pH, and redox conditions (Gallup, 1998). Additional methods for scale control include dilution of the brine with fresh water, controlled precipitation using cationic surfactants or metals, pond retention, addition of a reducing agent, crystallization followed by settling, and addition of inhibitor chemicals (Finster et al., 2015; Gallup, 2002; Gallup, 2011). Silica scale can also be managed by locating strainers near wellheads, steam wash systems, and turbine washing (Gallup, 2009).

Scale control in the SS-GF is unique because of the high salinity content of the brine, and silica scale formation is especially problematic. Metals precipitate with the silica, most notably oxidized iron. In SS-GR brines, other minerals co-precipitate with the iron silicate solids including $BaSO_4$ and CaF_2 (Harrar et al., 1979b). As barium precipitates, radium and other NORM present in the geothermal brine may also precipitate (Gallup and Featherstone, 1995; Zukin et al., 1987). Geothermal scale can also contain arsenic, lead, and zinc (Harrar et al., 1979b). Calcium carbonate can be problematic for other geothermal power plants but does not appear problematic for those in the SS-GF, likely because the low pH of the brine limits the carbonate concentration. More information about scale formation chemistry can be found in Appendix Chapter 9.

SS-GF power plants use crystallizer-clarifiers for scale control, although acidification was initially considered when operation of the power plants started. Both acidification and crystallizer-clarifier processes, as well as associated chemical applications, will be discussed below. The use of chemicals to inhibit scaling has also been investigated (see Appendix Chapter 9).

Crystallizer-Clarifiers for Scale Control

In SS-GF power plants, the crystallizer-clarifier process is used to control scaling (Figure 9.1). As discussed below, chemicals are used in association with the crystallizer-clarifier process, particularly NORM inhibitors, coagulants, and anti-foam agents (Appendix Chapter 9). The process depends on physical treatment: coagulation, settling, and separation of amorphous silicates as solid precipitates.

Crystallizer-clarifier technology was developed specifically to control silica in SS-GF power plants (Featherstone et al., 1979). The process consists of controlled precipitation followed by settling of solids; in SS-GF power plants, these solids mainly consist of iron silicate (Featherstone et al., 1995). Precipitation and settling occurs in two clarifiers that are operated in series and are referred to as the primary and secondary clarifiers, respectively. A portion of the solids from the first clarifier are recycled to the standard pressure flash tank (Figure 9.1) to provide nucleation sites for crystal growth (described as a "seed" for the crystallizer-clarifier process). Precipitation of iron silicate occurs in the flash vessels due to the reduced temperature and pressure that results when the steam is produced. Iron silica precipitation is observed to occur when the temperature drops below 200°C and when brine salinity increases (Gallup and Featherstone, 1995; Harrar et al., 1979b). The recycled iron silicate solids increase iron silica formation in the flash vessel and are an essential component of the crystallizer-clarifier process.

A disadvantage of using crystallizer-clarifier technology for silica control is NORM can precipitate with silica and iron, potentially resulting in solids with high radioactivity, so chemicals to prevent NORM deposition must be added. In addition to the use of a NORM control chemical, an antifoam chemical is also needed for the crystallization process because recycling of brine solids back to the standard pressure separator causes more foaming in the separator. Excess foam can result in carry-over of brine into the steam, which is undesirable in the turbine. Foaming can be controlled using polyglycol chemicals with a molecular weight of 1,000-2,500, as suggested by Gritters et al. (1988) with a dose of 0.2-1.5 ppm. The polyglycols recommended by Gritters et al. (1988) were combinations of polyethylene glycols and polypropylene glycols. The use of glycols as antifoam agents is consistent with the inventory of chemicals reported to the RWQCB (Appendix Chapter 9). Use of foam-controlling chemicals improves geothermal power production at SS-GF power plants because more brine can be cycled through the crystallizer flash tank (Featherstone et al., 1995).

The crystallizer-clarifier process has been used successfully in the SS-GF for approximately 30 years (Featherstone et al., 1995; Gallup, 2009; Hoyer et al., 1991; CEC, 2023a, 2023b, 2023c). However, removal of silica and other scaling minerals in the crystallizer-clarifiers is not complete, and dilution water may still be required for the injection water to limit mineral precipitation and scaling downstream of the power plant in the injection well and in the reservoir. Additionally, further treatment of the brine may be necessary for lithium recovery.

The crystallizer-clarifier process allows silica solid formation to occur in a controlled manner in the power plants. The resulting solid material (sludge) is a waste stream that must be dewatered and then disposed of offsite, typically in a landfill. Solids removed from the clarifiers are dewatered in a filter press to approximately 85% solids by weight (Featherstone et al., 1995). Because the solids are dewatered using a filter press system, the waste product is commonly referred to as "filter cake" (discussed below).

Acidification for Scale Control

Another method of scale mitigation is acidification, where the pH is lowered to prevent mineral precipitation (Baba et al., 2015; Gallup, 1996a, b; Gallup, 2009; Pambudi et al., 2015).

Acidification was initially intended for scale control in SS-GR brines. An early pilot study done on SS-GR brine showed that acidification from pH 6 to pH 4-5 significantly decreased scaling (Harrar et al., 1979b). The pilot study, performed by scientists from Lawrence Livermore National Laboratory at the Geothermal Loop Experimental Facility (GLEF) located in Niland, used brine from a single well: MagMaMax No. 1 (Harrar et al., 1979b; Morris and Stephens, 1981). Analyses of the scale suggested that acidification limited silica scaling while increasing the relative proportions of barium sulfate ($BaSO_4$) and fluorite (CaF_2) (Harrar et al., 1979b).

Acidification proved infeasible for SS-GR brines due to the high quantities of acids required and their cost, as well as the corrosion that resulted (Gallup, 1989; Gallup, 2009). Jost and Gallup (1985) developed an alternative strategy of keeping the brine temperature and pressure high (177-185°C and 5.5-7 bar) to reduce the pH reduction needed and acid required. A modification of this strategy was adopted to lower the pH by a modest amount (e.g., 0.5 units) and maintain a sufficiently high temperature to reduce scale

formation. To achieve this strategy, HCl was injected via in-line static mixers before the standard pressure separator. Featherstone et al. (1995) referenced a HCl dose of 100-120 ppm.

However, use of acidification has consequences at geothermal power plants. One negative consequence of acidification is that corrosion can occur due to the lower pH, and chemical costs are also a concern (Gallup, 2009). Acid addition requires steam from the separator to be scrubbed. Corrosion must be controlled using strategies such as lining the separators with alloys, lining the production and injection pipelines with cement, and using alloy tubulars in the pipelines (Featherstone et al., 1995). Geothermal power plants using pH modification are thought to use more brine and produce less flash-steam per unit of brine, resulting in larger volumes of spent brine but fewer waste solids (Featherstone et al., 1995).

Acidification has not been widely adopted by SS-GF power plants; rather, the crystallizer-clarifier process is used to control silica scaling. However, a modified version of acidification is still practiced at Region 1 (Salton Sea Units 1-5). Currently the pH reduction at Region 1 is minimal (~0.5 pH units), and its impact on silica control is thought to be modest. The purpose of acid addition at Region 1 is to reduce overall scaling and not specifically address silica control.

Chemical Control of NORM Scale

One area of power plant operations where chemical treatments have been highly successful is the application of chemicals to control deposition of NORM on pipes or in crystallizer-clarifier solids (i.e., filter cake). SS-GR brines contain radionuclides including radium-226 and radium-228, and these chemicals can co-precipitate with $BaSO_4$ when the brine temperature drops below 160°C (Gallup and Featherstone, 1995; Zukin et al., 1987).

To reduce NORM in the iron silica solids, scale-inhibiting chemicals are used to prevent precipitation of NORM. The scale-inhibiting chemicals are selected to minimize interference with iron silica precipitation. So-called "NORM inhibitors" were developed to prevent precipitation of barium and associated radioactive metals in the crystallizer-clarifier process (Gallup and Featherstone, 1995). In one study, the use of crystallizer-clarifiers with a NORM inhibitor resulted in the formation of 600 mg of iron silica sludge per kg of brine treated, and a sludge that contained approximately 65% iron silica, 3% CaF_2 and 31% $BaSO_4$ by weight (Gallup and Featherstone, 1995). Gallup and Featherstone (1995) found that NORM inhibitors were also effective for reducing $BaSO_4$ and CaF_2 precipitants.

In practice, Gallup and Featherstone (1995) found that the efficacy of the alkylaminophosphonate (see next paragraph) inhibitor was reduced following the removal of solids in the clarifiers, such that precipitation of NORM occurred downstream of the clarifiers (e.g., in the injection system). To reduce the occurrence of downstream precipitation, a dosing strategy was developed that consisted of adding the chemical in three locations: at the standard-pressure crystallizer, between the primary and secondary clarifiers, and downstream of the secondary clarifier (Gallup, 2009; Gallup and Featherstone, 1995).

The most common scale inhibitor used for NORM control in SS-GF power plants is an alkylaminophosphonate, an anionic polymeric organic compound (Appendix Chapter 9). This scale inhibitor causes NORM-containing solids to develop a negative surface charge, resulting in particles that disperse and stay suspended rather than flocculating and settling. The dispersed NORM-containing

particles can then be re-injected back into the formation so that they do not accumulate in filter-cake solids. Gallup and Featherstone (1995) found that using dispersant scale inhibitors for NORM control resulted in filter-cake solids that meet regulatory requirements for NORM (0.2 Bq/g or 5 pCi/g), allowing solids to be disposed of as nonhazardous waste.

At the BHER SS-GF power plants, the chemical product Nalco GEO901 is used for NORM control (Appendix Chapter 9). Nalco GEO901 contains a proprietary phosphate ester that is effective for inhibiting many types of divalent cation, scale-forming minerals including $CaCO_3$, $BaSO_4$, and CaF_2.

A disadvantage of using dispersant scale inhibitors for NORM control is that the surface charge of the iron silica solids is also altered, causing dispersion and poor settling of these solids as well. To resolve the issue of poorly settling solids, a cationic flocculant is used to improve settling of iron silicates in the secondary clarifier. Cationic flocculants function by neutralizing the negative surface charge of the solids and by encouraging aggregation or floc formation, especially by bridging together smaller particles to form larger particles. The flocculant chemical is added in between the two clarifiers (Featherstone et al., 1995; Gallup, 2009). Thus, the primary clarifier functions mainly as a reaction tank and the secondary clarifier is mainly used for settling; however, settled and thickened solids are removed from both clarifiers. The combination of the crystallizer-clarifier process with NORM control appears to be a good strategy for solids management in SS-GF power plants, because most filter cake can be disposed of in nonhazardous landfills (discussed below).

Our examination of the chemicals reported as being used for process control in geothermal power plants, and an examination of the literature, did not identify any persistent organic pollutants or acutely toxic chemicals. Nalco Chemical Co. (a subsidiary of Ecolab) and ChemTreat Inc. are the major suppliers of chemical products to geothermal power plants in the SS-GF. The chemicals being used appear consistent with their reported purposes and similar to chemicals used for water treatment and process control at other industrial facilities.

Management of Solid Wastes

Sources of Solid Wastes in Geothermal Power Plants

The main source of solid waste from SS-GF geothermal power plants is the filter cake resulting from the crystallizer-clarifier process described above. Filter cake is produced every day of plant operation and, since it is part of an engineered brine treatment process, the chemical and physical quality of the filter cake is reasonably consistent (see discussion of filter cake chemistry below). Solids from the clarifiers are sent to a filter press for dewatering, producing the filter cake, which is then put into metal boxes or dump trucks (loads) (Figure 9.1). Filter-cake loads are tested for hazardous materials, and filter-cake loads that are demonstrated to be nonhazardous are taken to regional landfills (see discussion below).

Other solids produced in geothermal power plants are more complex in their chemical composition and are managed separately from filter cake. The second most important source of solid wastes is the brine ponds (Figure 9.2). Most brine used for geothermal power production is reinjected back into the reservoir formation; however, during maintenance and start-up procedures, brine from the production well can be diverted into permitted Class II holding ponds, called brine ponds (e.g., California RWQCB Colorado

River Basin Region, 2015b, 2023b, 2023c). Geothermal brine put into brine ponds cools and evaporates, eventually forming precipitated solids of formerly dissolved constituents (Table 1.2). The function of the brine pond is to allow solids to separate from liquid brine, which is reinjected back into the formation. Settled solids accumulate in the brine pond until there is a sufficiently large volume to be collected, further dried in a shaker separator, and then shipped to an appropriate landfill for disposal.

In addition to brine from the production well during start-up operations, brine ponds receive other wastes from geothermal power plants. Maintenance activities that include physical and chemical cleaning of pipes and other equipment to remove scale produces a solid or semi-solid waste. The pipe scale solids and other waste materials are produced intermittently, during cleaning operations and plant shutdowns, and are stored in brine ponds before being shipped offsite for disposal. Other materials in addition to brine that may be discharged into brine ponds include scale cleaned from pipes and other equipment, hydro-blasting and other cleaning wastewater, cooling tower blow-down, biofilter effluent, and sump effluent (California RWQCB Colorado River Basin Region, 2015b, 2023b, 2023c).

Due to the chemical composition of the brine placed in the pond (Table 1.2), the pond solids that form in the pond may contain regulated or hazardous chemicals. Scale that is removed from pipes and other equipment can contain toxic or hazardous elements, including arsenic and lead. The type of landfill to which the brine-pond solids are shipped is dependent on the results of tests conducted on the solid waste (as discussed below), but brine pond solids are typically hazardous waste.

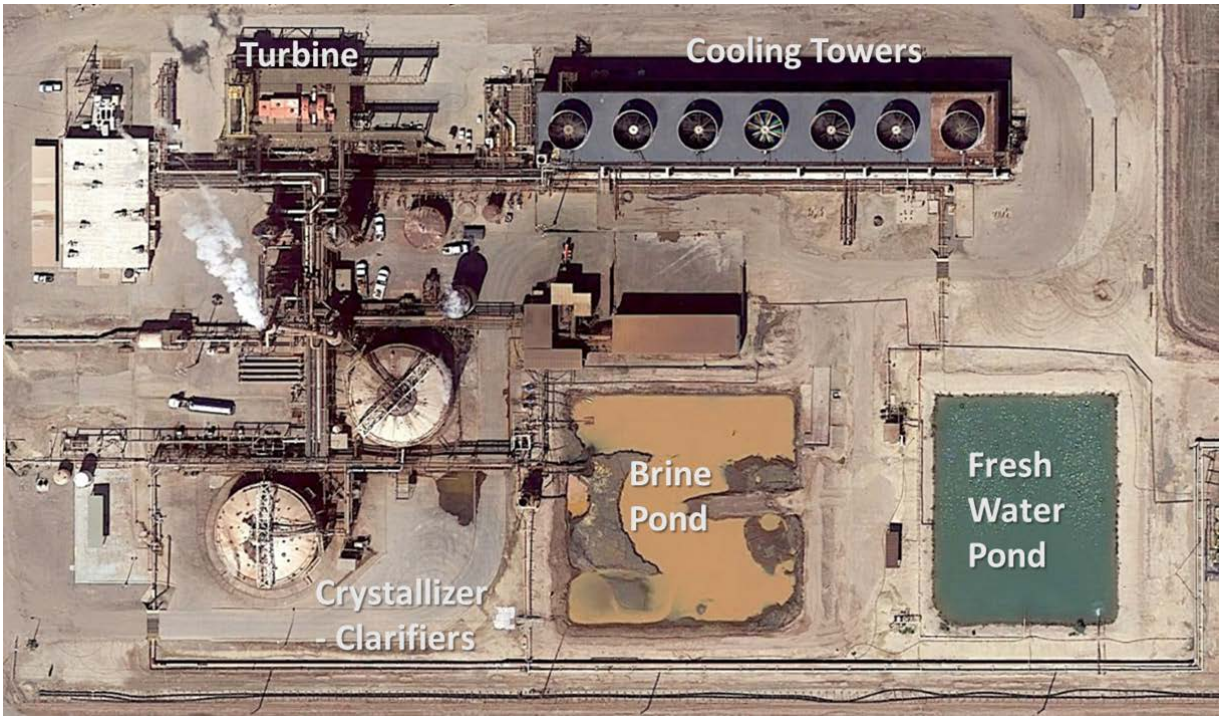

Figure 9.2. Aerial image of the Elmore Geothermal Power Plant showing features typical of geothermal power plants in the region. Features relevant to the environmental analysis include the brine pond for brine solids management, the water pond for freshwater storage, the crystallizer-clarifiers where iron-silicate solids are produced, and cooling towers where most atmospheric emissions occur.

Classification of Geothermal Power Plant Solid Wastes: Filter Cake and Hazardous Wastes

Management of geothermal power plant solid wastes is subject to federal, state, and local regulations. Under federal regulations, solid wastes produced during the exploration, development, and production of geothermal energy are "special wastes" exempted from Subtitle C of the Resource Conservation and Recovery Act (RCRA), the federal regulations governing hazardous waste management (U.S. EPA, 2023b). However, landfills that receive geothermal power plant solid wastes for disposal are regulated under RCRA Subtitle D (solid waste) and Subtitle C (hazardous waste) or under the Toxic Substances Control Act (TSCA) (U.S. EPA, 2023a). RCRA specifically identifies eight so-called "heavy metals" that are of concern in landfills: arsenic, barium, cadmium, chromium, lead, mercury selenium, and silver (U.S. EPA, 2023b).

In California, solid wastes from geothermal facilities are regulated under the Water Code and the Health and Safety Code (California DTSC, 2022, 2023a). Solid wastes that are exempt from RCRA (i.e., special wastes) are classified as "designated wastes" in California if they contain potential pollutants, such as lead or arsenic. Arsenic and lead are found in SS-GF geothermal brine (Table 1.2), and consequently designated wastes from geothermal facilities must be tested to determine if they meet California's definition of hazardous wastes (California DTSC, 2022). In addition, solid waste management facilities are regulated by the counties in which they reside. In Imperial County, the Imperial County Public Health Department regulates solid waste landfills.

Under both federal and state regulations, even non-RCRA or nonhazardous wastes that contain potentially hazardous substances are subject to testing before they are sent to landfills to insure proper disposal (California DTSC, 2022, 2023a; U.S. EPA, 2023a, 2023b). The purpose of the testing is to determine if a solid waste contains regulated pollutants, and if those pollutants could be released into the environment under conditions typical of landfills and result in contamination of water (California DTSC, 2022; Clarke, 2022). Both state and federal regulations include batch tests protocols for solid wastes that were developed to simulate the leaching process of waste materials in landfills or other disposal scenarios (California DTSC, 2022). These tests are used to evaluate potential risks to humans and groundwater and determine how solid wastes are managed.

To determine if a waste is hazardous, solid wastes are characterized for dangerous properties such as ignitability, corrosivity, reactivity, or toxicity (California DTSC, 2022; U.S. EPA, 2023b). When hazardous waste is disposed of in a landfill, some toxic constituents in the waste could leach into soil and groundwater. To limit the risks of leaching, the EPA requires generators to show the amount of hazardous chemicals that may leach is below threshold values. Under federal rules, the potential to leach toxic materials under landfill conditions is evaluated using the Toxicity Characteristic Leaching Procedure (TCLP) (U.S. EPA, 2023b).

In the TCLP, solid waste is extracted with an acetic acid solution under test conditions intended to mimic what would happen over time in a landfill. The TCLP determines if a solid waste has met requirements for the land disposal restriction, which regulates how solid wastes are disposed of in landfills; wastes with specific hazardous substances above allowable values in the leachate are considered hazardous. TCLP threshold limit values for inorganic compounds are shown in Appendix Chapter 9, Table A9.3. Under

federal standards, solid wastes that do not pass the TCLP test are "characteristic wastes" that must be disposed of in Class I (hazardous waste) landfills. Industrial wastes that pass the TCLP are not hazardous wastes and can be disposed of in Class II (industrial waste) landfills. Both Class I and Class II landfills have liners and leachate control systems to protect groundwater from contamination; however, Class I landfills have redundant systems and often have associated facilities for the treatment of hazardous waste (U.S. EPA, 2023a).

California regulations differ from federal regulations and are generally considered more stringent (Barclays Official California Code of Regulations, 2015; California DTSC, 2022). Under California regulations, special wastes that are exempt from RCRA can still be classified as "designated wastes" and strictly regulated as hazardous wastes if they meet certain criteria. Even if wastes are not hazardous wastes under RCRA (e.g., geothermal industry wastes), individuals generating solid waste must determine if it meets California hazardous waste criteria. Brine pond and filter cake solids from geothermal power plants are inorganic wastes and are not hazardous wastes based on physical properties such as ignitability, corrosivity, or reactivity. However, geothermal power plant solid wastes do contain regulated inorganic toxic elements and are therefore "designated wastes" subject to California regulations (California DTSC, 2022).

To determine if designated wastes are considered hazardous waste under California rules, both the total amount of regulated chemical present and the leachable amount of substance is considered (as opposed to federal rules, which only consider the leachability of the waste). Solid wastes are digested, extracted, or otherwise analyzed to determine the total amount of regulated compound present. For inorganic analytes, the whole sample is digested, and the total amount of regulated substances present in the solid waste is determined. When any target analyte exceeds the Total Threshold Limit Concentration (TTLC) standard or limit (Appendix Chapter 9, Table A9.4), the waste is classified as hazardous waste, even if the regulated component of the waste is in an inert form.

In California, the leachable amount of substance in solid waste is determined by the Waste Extraction Test (WET). The WET uses a citric acid solution and other conditions, such as a longer extraction time, that are considered more aggressive than the federal TCLP test. Like the federal TCLP test, the WET is intended to simulate a landfill environment and to determine how much of a regulated compound will leach into the environment. The extract from the WET is analyzed to determine if any of the regulated substances are found in the simulated leachate (citric acid solution) at concentrations that exceed the Soluble Threshold Limit Concentration (STLC) (see Appendix Chapter 9, Table A9.4). If any analyte in the test leachate exceeds the STLC standard, the waste is classified as a hazardous waste, even if it passes the TTLC standard (or the TCLP).

In summary, geothermal power plant solid wastes, including filter cake and brine pond solids, are subject to federal, state, and local regulations. Solid waste is evaluated to determine if it is appropriate for a Class II landfill or is a hazardous waste that must be sent to a Class I landfill. A simplified decision tree for geothermal solid wastes is presented in Figure 9.3. As shown in Figure 9.3, wastes that do not pass the TTLC or STLC standards can still be sent to a Class II landfill in other states, such as Arizona, that adhere to federal standards.

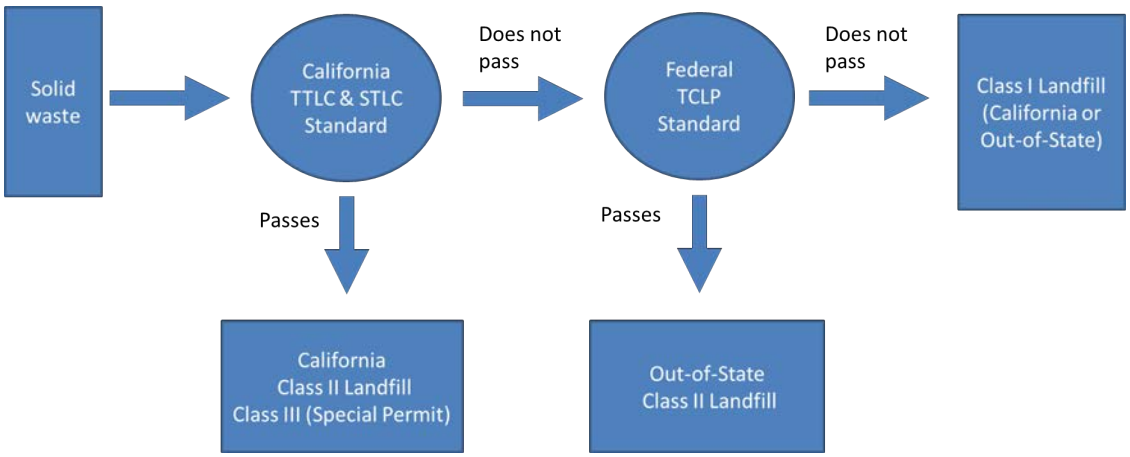

Figure 9.3. Simplified decision tree for disposal of geothermal power plant solid wastes.

Brine pond solids contain potential pollutants at higher concentrations and are more frequently classified as hazardous wastes based on the STLC standard and, less frequently, can also exceed TTLC and TCLP standards. When geothermal power plant solid wastes exceed state criteria, the solids are manifested as hazardous wastes and are reported to the Department of Toxic Substances Control (DTSC) hazardous waste tracking system (California DTSC, 2023c). Combining the DTSC manifest data with reports submitted to the RWQCB from the Desert Valley Monofill and the Salton City Landfill, we can analyze and understand geothermal power plant solid waste management.

Amount of Solid Wastes Produced by SS-GF Geothermal Power Plants

Based on information from 2014-2022 collected by various agencies, approximately 80,000 metric tons of solid waste are produced each year by geothermal power plants in the SS-GF (Table 9.3, 9.6; Appendix Chapter 9). Approximately 54%, or 45,000 metric tons of solid waste per year, were sent to regional landfills over the period 2014-2022. The remainder is shipped out of state or sent to hazardous waste landfills in California. Waste disposal practices of individual geothermal power plant operational units are shown in Appendix Chapter 9, Figure A9.1 and Table A9.5.

Table 9.3. Types and amounts of solid wastes produced from geothermal power plants in the SS-GF. Filter cake waste disposal is reported to the RWQCB and Imperial County. Other solid wastes are reported to DTSC. Waste codes and waste descriptions are State of California hazardous waste codes as reported to DTSC as part of the manifest waste program.

Waste Description	California Hazardous Waste Code	No. Years Waste was Produced (2014-2021)	Metric Tons per Year
Filter cake sent to Desert Valley Monofill[a]	Non-hazardous	8	39,000
Filter cake sent to Salton City Landfill	Non-hazardous	2021-2022[b]	5,900
Other inorganic solid waste	181	8	35,000
Other organic solids	352	8	1,500
Unspecified sludge waste	491	5	1,200
Alkaline solution (pH >=12.5) with metals	121	4	140
Oil-water separation sludge	222	8	70
Unspecified aqueous solution (2 < pH < 12.5)	135	5	29
Waste oil and mixed oil	221	5	17
Asbestos-containing waste	151	2	12
Liquids, pH<=2, with metals	792	8	6.6
Off-spec, aged, or surplus organics	331	8	1.8
Laboratory waste chemicals	551	5	1.6
Hydrocarbon solvents	213	8	1.3
Aqueous solution (2 < pH < 12.5) with organic residues < 10%	134	2	0.8
Liquid with halogenated organic compounds >= 1000 mg/L	741	4	0.3
Off-spec, aged, or surplus inorganics	141	3	0.2

[a] Desert Valley Monofill is used by geothermal power plants owned by BHER.

[b] Featherstone Power Plant started using Salton City Landfill in late 2020. Value is average of data from 2021 and 2022.

Between 2014-2021, an average of approximately 38,000 tons per year of hazardous waste (or "manifested waste") was generated from geothermal facilities in the SS-GF (California DTSC, 2023c). Wastes that were generated frequently or routinely are shown in Table 9.3. Table 9.3 shows the average annual hazardous waste production by geothermal power plants in the SS-GF by name and California waste code for the years 2014-2021, as reported in the DTSC manifest tracking system (California DTSC, 2023c). Wastes that were only generated in one year (out of eight years), including drilling mud, oil and solvent wastes, empty drums, and aqueous solutions of high and low pH, are not included in Table 9.3. Most of the wastes in Table 9.3 are wastes considered typical for industrial operations involving resource extraction. However, the iron-silicate filter-cake solids and brine-pond solids are specific to geothermal power plants.

Filter cake that is nonhazardous by both federal and state standards is sent to regional landfills. BHER sends filter cake to the Desert Valley Monofill, a Class II landfill (Appendix Chapter 9, Table A9.5) (BRG Consulting Inc., 2021; California RWQCB Colorado River Basin Region, 2016a, 2016b; Desert Valley Company, 2022a). Filter cake shipments to Desert Valley Monofill by BHER geothermal power plants are reported to various state agencies. Filter cake shipments to Desert Valley Monofill by BHER geothermal power plants are shown in Appendix Chapter 9, Table A9.6.

Using a 12-month moving average to address short-term variability in power and solids production, the filter-cake solids production relative to power production was plotted for the four BHER facilities (Figure 9.4). While the relative solids production is variable, a typical range appears to be between 15-30 tons of filter cake per GWh. The Region 1 facility, which has the highest capacity compared to other facilities, appears to have more stable filter-cake solids production at lower levels than the other facilities. Solids production from the Elmore Power Plant, which is smaller than the Region 1 facility, is most variable (Figure 9.4).

Table 9.4 shows the destination of wastes generated by geothermal power plants in the SS-GF that are tracked by the DTSC manifest system (California DTSC, 2023c). By common practice, only wastes that fail both the California and federal standards are sent to the Buttonwillow Clean Harbor facility. In 2021, 33,965 metric tons of solid waste was manifested from the SS-GF power plants and 32.1% of this manifested waste was sent to the Buttonwillow Clean Harbors Class I hazardous waste landfill (Table 9.4), representing almost 11,000 metric tons of hazardous waste in one year. A few shipments of hazardous wastes are sent to various oil recovery facilities. Approximately 97% of geothermal power plants' manifested wastes were sent to landfills (Table 9.4).

Filter Cake Characteristics

Filter cake is well characterized chemically. As an example, the safety data sheet for BHER filter cake is summarized in Table 9.5 and can be read in its entirety in Appendix Chapter 9. As discussed above, filter cake is analyzed regularly as part of landfill disposal regulations. Specific, analytical results for filter cake as reported by the Desert Valley Monofill are summarized in Appendix Chapter 9, Tables A9.7 and A9.8. Analytical data representing average filter cake composition for 10 of the 11 geothermal power plants in the SS-GF were obtained from annual reports submitted by the Desert Valley Company to Imperial County Planning and Development Services (Desert Valley Company, 2018a, 2019a, 2020a, 2021a, 2022a). Such reporting is required due to the facility's Conditional Use Permit. The annual reports were distributed to the RWQCB and subsequently posted on the GeoTracker website. Data were reported for the BHER facilities that send filter-cake solids to the Desert Valley Monofill (i.e., Region 1, Region 2, Elmore, and Leathers Power Plants). Similar analytical data were not found for the Featherstone Power Plant.

We compared analytical results from the STLC and TTLC tests for filter cake from the different facilities (Figure 9.5; Appendix Chapter 9, Figures A9.2-A9.5). Arsenic, barium, lead, and zinc were consistently measured in filter cake samples. Arsenic and lead results are particularly important, since they are judged to be the most problematic components for management of solid wastes from geothermal power plants (see analysis below). Since Region 1 is operated using a modified acidification process with the crystallizer-clarification process, it was of interest to compare solid wastes from this operational unit with filter-cake solids produced by geothermal power plants using just the crystallization-clarification process alone. Results from the TTLC tests indicate that Region 1 filter-cake solids have lower total arsenic content than filter-cake solids from the other facilities; however, the quantity of soluble arsenic measured by the SCLC tends to be higher (Appendix Chapter 9, Figure A9.2). Region 1 filter-cake solids also tend to have higher total and soluble barium content relative to the filter cake from the other facilities; however, Region 2 also had some samples with high barium content, notably the sample from 2018 (Appendix Chapter 9, Figure A9.3). Region 1 filter-cake solids were low in lead and zinc compared to filter cake from the other facilities

(Appendix Chapter 9, Figures A9.14 and 9.15). The lower lead and zinc content observed in Region 1 filter cake could be attributed to the acidification process used at Region 1, which may reduce lead and zinc solid formation.

Figure 9.4. Twelve-month moving average of filter cake solid waste tonnage per GWh produced and disposed of at the Desert Valley Monofill from the BHER SS-GF geothermal power plants.

Table 9.4. Destinations of manifested waste from SS-GF power plants between 2019-2021. The first year TSDF destination was available in the DTSC Hazardous Waste Tracking System was 2019.

Treatment storage or disposal facility (TSDF)	TSDF Name	State	Percent[a] 2019-2021	Percent 2019	Percent 2020	Percent 2021
AZR000002428	Copper Mountain Landfill	AZ	73.9	75.0	78.8	65.8
CAD980675276	Buttonwillow Landfill (Clean Harbors)	CA	22.6	17.9	19.1	32.1
CAT000646117	Kettleman Hill Facility[b]	CA	2.6	6.2	1.5	0.3
CAT080013352	Demenno-Kerdoon	CA	0.6	0.4	0.4	1.2
AZR000510065	US Fuel Oil LLC	AZ	0.2	0.3	0.1	0.2
CAT000613976	Safety-Kleen Systems Inc.	CA	0.1	<0.1	<0.1	0.1
CAT080025711	Adv. Environ. Inc. (World Oil)	CA	<0.1	<0.1	<0.1	0.1
None	Not specified	NA	<0.1	<0.1	<0.1	<0.1
AZR000031823	Environmental Management Systems	AZ	<0.1	<0.1	<0.1	<0.1
CAD982444481	Haz Mat TSDF Inc.	CA	<0.1	<0.1	<0.1	<0.1
Sum sent to landfills	Copper Mt. and Buttonwillow Landfills		96.5	92.9	97.9	97.9

[a] Based on number of manifests for each destination.

[b] Chemical Waste Management, Inc. has landfill, treatment, and oil recycling facilities.

Table 9.5. Chemical composition of filter cake as described in the BHER safety data sheet (SDS). Filter cake produced as part of the geothermal power plant process in the SS-GF is consistent enough to allow standard characterization and publication of an SDS. See Appendix Chapter 9 for complete filter cake SDS.

Chemical Name	Identifiers	Composition	LD50/LC50
Silica, amorphous	CAS:7631-86-9	50%	NDA
Iron	CAS:7439-89-6	15%	Ingestion/Oral-Rat LD50 • 30 g/kg
Barium	CAS:7440-39-3	4%	NDA
Calcium	CAS:7440-70-2	3%	NDA
Strontium	CAS:7440-24-6	6000ppm	NDA
Sodium chloride	CAS:7647-14-5	6000ppm	Ingestion/Oral-Rat LD50 • 3000 mg/kg
Manganese	CAS:7439-96-5	3500ppm	Ingestion/Oral-Rat LD50 • 9 g/kg
Potassium chloride	CAS:7447-40-7	1300ppm	Ingestion/Oral-Rat LD50 • 2600 mg/kg
Arsenic	CAS:7440-38-2	300ppm	Ingestion/Oral-Rat LD50 • 763 mg/kg
Copper	CAS:7440-50-8	250ppm	NDA

Lead	CAS:7439-92-1	30ppm	NDA
Beryllium	CAS:7440-41-7	10ppm	NDA
Antimony	CAS:7440-36-0	10ppm	Ingestion/Oral-Rat LD50 • 100 mg/kg
Cobalt	CAS:7440-48-4	4ppm	Ingestion/Oral-Rat LD50 • 6171 mg/kg
Nickel	CAS:7440-02-0	1.5ppm	NDA
Chromium	CAS:7440-47-3	1ppm	NDA
Silver	CAS:7440-22-4	0.4ppm	NDA
Cadmium	CAS:7440-43-9	0.2ppm	Ingestion/Oral-Rat LD50 • 2330 mg/kg

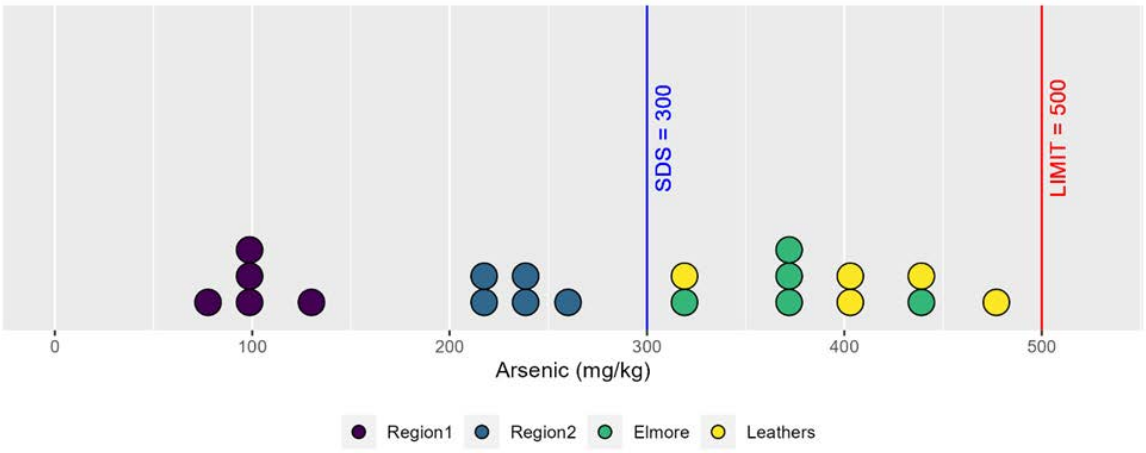

Figure 9.5. Arsenic levels in filter cake. Dot plot for total threshold limit concentration (TTLC) test results for arsenic in filter-cake solids. Each dot represents a result. Annual filter-cake analyses were completed and reported by the Desert Valley Company to Imperial County Planning and Development Services (2017-2021). The value for arsenic shown on the safety data sheet (SDS) for filter cake is indicated as the limit for nonhazardous solid waste.

The pH of annual samples indicates that the filter-cake solids are acidic, with pH values reported in the 4.09 to 6.10 range (Appendix Chapter 9, Table A9.9). For Region 1, where modified acidification is practiced, the pH of the filter cake is slightly lower. Results of volatile organic compound (VOC) analyses for the filter cake indicate that VOCs are typically not present in measurable amounts (Appendix Chapter 9, Table A9.10). However, acetone was observed in some samples, but was not observed regularly or frequently. Acetone is a volatile compound, which suggests that it does not originate in the geothermal brine, and the presence of acetone could indicate microbial activity, since acetone is a fermentation byproduct. This would be consistent with the low pH of the filter cake. Where acetone is originating in the filter cake is not known, but it could be a product from the breakdown of polymers and other organic chemical additives used during the crystallization-clarification process.

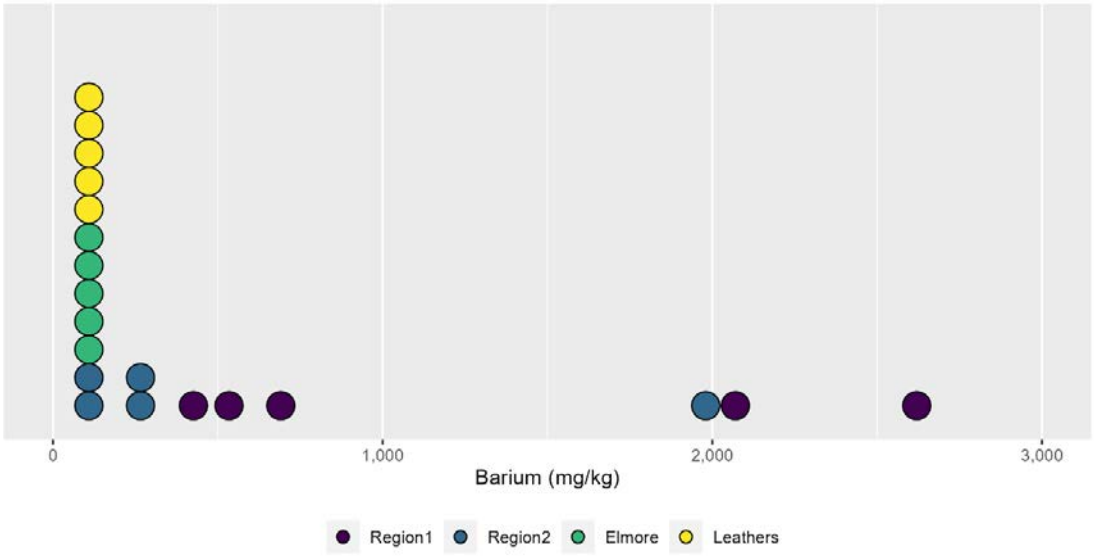

Figure 9.6. Barium in filter cake. Dot plot for total threshold limit concentration (TTLC) test results for barium in filter-cake solids. Each dot represents a result. Annual filter-cake analyses were completed and reported by the Desert Valley Company to Imperial County Planning and Development Services (2017-2021). There is no value for barium on the safety data sheet (SDS) for filter cake. The limit for nonhazardous solid waste is 10,000 mg/kg and is not shown.

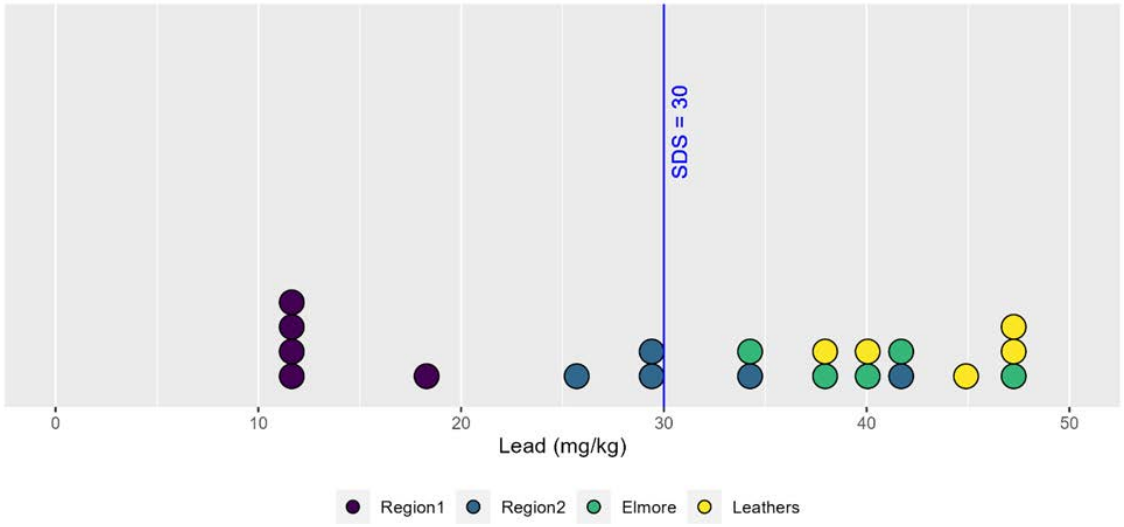

Figure 9.7. Lead in filter cake. Dot plot for total threshold limit concentration (TTLC) test results for lead in filter-cake solids. Each dot represents a result. Annual filter-cake analyses were completed and reported by the Desert Valley Company to Imperial County Planning and Development Services (2017-2021). The value for lead shown on the safety data sheet (SDS) for filter cake is indicated. The limit for nonhazardous solid waste is 1,000 mg/kg and is not shown.

Results from the TTLC test were compared with data found in the BHER Safety Data Sheet (SDS) (Table 9.5) for filter-cake solids, and to the TTLC threshold limit (Figures 9.5-9.8). Ten metals were included in the SDS description: antimony, arsenic, beryllium, cadmium, chromium, cobalt, copper, lead, nickel, and silver (Table 9.5). Results of this analysis for arsenic, barium, lead, and zinc are also shown in Figures 9.5-9.8. All metals observed in the filter cake were below hazardous limits, as is required for disposal at the Desert Valley Monofill. Observed values did not always match the metal

content stated in the SDS but are still well below any TTLC thresholds. For most metals, the metal content stated in the SDS was in the range of the observed values. It can be concluded that the SDS for the filter cake is representative of the filter cake disposed of at the landfill.

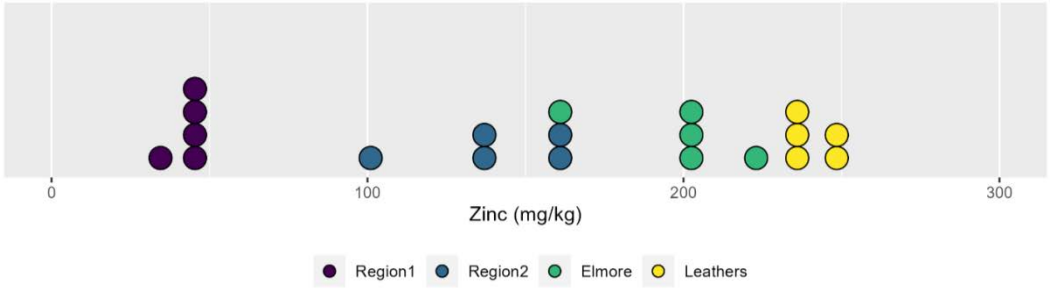

Figure 9.8. Zinc in filter cake. Dot plot for total threshold limit concentration (TTLC) test results for zinc in filter-cake solids. Each dot represents a result. Annual filter-cake analyses were completed and reported by the Desert Valley Company to Imperial County Planning and Development Services (2017–2021). There is no value for zinc shown on the safety data sheet (SDS) for filter cake. The limit for nonhazardous solid waste is 5,000 mg/kg and is not shown.

As discussed above, chemicals are used to control NORM in geothermal power plants and to prevent the accumulation of NORM in filter cake. As part of regulatory requirements, filter-cake solids are tested for radioactivity. As is required for disposal in a Class II landfill, filter-cake materials sent to the Desert Valley Monofill were low in radioactivity and did not exceed radiation requirements for land disposal (e.g., U.S. EPA, 2000) (Appendix Chapter 9, Table A9.10). Filter cake from the Featherstone Power Plant has also been evaluated for NORM as part of acquiring a permit for the disposal of filter cake at the Salton City Landfill, and its filter cake was found to be below background levels observed at the landfill (Burrtec Waste Industries Inc., 2020). It can be concluded that geothermal power plants in the SS-GF that control NORM chemically will produce filter cake that is low in NORM. In addition, as part of solid waste disposal permitting, filter cake is routinely tested for radioactivity, both at the point of origin and at the landfill, to ensure that no radioactive materials are accidently disposed of in an inappropriate landfill (e.g., Burrtec Waste Industries Inc., 2020; Desert Valley Company, 2022a).

Hazardous Waste Characteristics

The vast majority of the solid wastes generated by geothermal power plants in the SS-GF that are manifested in the DTSC Hazardous Waste Tracking System are classified as Code 181, Other Inorganic Solid Waste (Table 9.3). Examination of individual manifests from 2021 and spot-checking manifests from other years show that Code 181 wastes are predominantly brine-pond solids and shipments of filter cake that did not pass the STLC standards for arsenic or, less frequently, lead. Approximately 37% of Code 181 wastes from BHER facilities were sent to Buttonwillow Clean Harbors, a Class I RCRA hazardous waste facility, and the remainder were sent to the Copper Mountain Class II Landfill in Arizona (Appendix Chapter 9, Table A9.11). In the case of Featherstone Power Plant, approximately 5% of Code 181 wastes were sent to Buttonwillow Clean Harbors and 95% were sent to the Copper Mountain Landfill in Arizona (Appendix Chapter 9, Table A9.11). As discussed above, it appears that Featherstone was sending all of its filter cake to the Copper Mountain Landfill until late 2020, when it received permission to dispose of nonhazardous filter cake in the Salton City Landfill.

The second most common wastes were classified as Code 352, Other Organic Solid Wastes. Wastes in this category were more diverse. Code 352 wastes from BHER facilities between 2014-2021 were exclusively petroleum-contaminated solids, which may include oil filters, oil-contaminated soils, oily rags, and similar items. These were sent to Buttonwillow Clean Harbors, which has oil recycling and recovery facilities (Appendix Chapter 9, Table A9.11). Code 352 wastes from Featherstone Power Plant included petroleum-contaminated solids, but many shipments were described as cooling tower packaging and brine-pond solids. Petroleum-contaminated solids from Featherstone were sent to US Fuel Oil LLC in Arizona (Appendix Chapter 9, Table A9.11). The remainder of Code 352 wastes, including cooling tower wastes, were sent to the Copper Mountain Landfill in Arizona.

Code 491 wastes, Unspecified Sludge Wastes (Table 9.3), were generated by BHER facilities in 2014, 2015, 2018, 2019, and 2020, but not in 2016, 2027, or 2021. Code 491 wastes were further described in manifests as liquid geothermal scales containing arsenic and liquid environmentally hazardous substances (identification no. UN 3082). The liquid nature of the geothermal scale waste, and the fact that the waste is not generated every year, suggests that this waste is associated with geothermal power plant maintenance, which occurs every few years and includes descaling of pipes and other equipment by power washing and other methods. Code 491 wastes were sent to the Chemical Waste Management Kettleman Hills Facility. The Kettleman Hills Facility receives and manages solid, semi-solid, and liquid wastes (California DTSC, 2023d). The Featherstone Power Plant did not report any Code 491 wastes between 2014-2021.

Potential Solid Waste Impacts of Expanded Geothermal Power Production

Geothermal Energy Production and Solid Waste Generation

It is expected that there will be an increase in geothermal energy production in the SS-GF as California implements its climate plan and cuts net production of greenhouse gases (CDC, 2023; Kaspereit et al., 2016; Paz et al., 2022). Currently, BHER is planning to construct three new geothermal power plants with a combined nameplate capacity of 401 MW and combined expected net output of 357 MW (CEC, 2023a, 2023b, 2023c). CTR is applying to build a 50 MW geothermal power plant and has ambitions to build an additional 130 MW of capacity (Controlled Thermal Resources, 2023; County of Imperial Planning and Development Services Department, 2022; Hell's Kitchen Power Co., 2021). EnergySource once proposed building an additional 50 MW geothermal power plant, but this is not currently an active project (EnergySource, 2012).

Current SS-GF power plants have varying capacities, power generation, and solid waste production rates. If we compare annual net electricity production with annual average total solids production, we can calculate the average solid waste production per MWh of electricity produced (Table 9.6). The amount of solid waste generated relative to the energy produced varies somewhat among SS-GF power plant operating units (Table 9.6). Region 2, Elmore, and Leathers Power Plants have nearly the same amount of solids generation relative to energy production, an average of 0.031 metric tons per MWh. These plants have similar processes and are operated by the same company (BHER). Region 1 produces less solid waste, about 0.016 metric tons per MWh, possibly as a result of the acidizing process reducing metals precipitation. The Featherstone Power Plant also produces less solids (0.024 metric tons per MWh) than the BHER plants. It is not clear why Featherstone produces less solid waste relative to its energy

production, but the plant is newer and operated by a different company. Although there is some variability for scenario analysis, we are using a median solids production of 0.030 metric tons per MWh as representative of future solids production (Table 9.6).

The construction of new geothermal power plants, and the generation of new geothermal power in the region, will also result in new solid waste production. Three projects have recently submitted applications for certification to the California Energy Commission (CEC). The application for certification contains similar information as an Environmental Impact Report (EIR), including estimates of annual solid waste production. Information reported to the CEC concerning solid waste production is summarized in Table 9.7. These plants estimate they could produce up to nearly 90,000 metric tons of solid waste per year, of which over 37% will be hazardous waste by California standards, requiring a Class I landfill or recycling facility or out-of-state Class II landfill. Based on the nameplate capacity of the proposed power plants and assuming an efficiency of 86%, BHER has estimated a solids production rate of 0.034 metric tons solid waste per MWh. This estimate is about a 13% higher production rate than our 0.030 metric tons per MWh calculated from previous operations (above), suggesting that BHER is assuming a higher operational efficiency than 86% or making a responsibly conservative estimate.

Scenario Estimation of Future Solid Waste Production Impacts

It is of interest to estimate the potential impacts of increased solid waste production from expanded geothermal energy development on landfill capacity. Current net geothermal production is approximately 400 MWe, and it has been projected that in the near future (3-5 years) there will be construction and operation of up to an additional 520 MWe of geothermal capacity. In the long term, scientific studies estimate that the maximum geothermal capacity in the region could be as high as 2,950 MWe (Kaspereit et al., 2016). Since the amount of geothermal power that will ultimately be produced is not known, we created two potential expansion scenarios: a "proposed" scenario indicating a 520 MWe expansion in the near term, and a "maximum" scenario indicating a 2,950 MWe expansion in the long term, as shown in Table 9.8. The proposed near-term increase, from 400 to 920 MWe, represents a 2.3X increase relative to current production. The maximum long-term increase, from 400 to 2,950 MWe, represents a 7.4X increase relative to current production.

In Table 9.8, multipliers of 2.3 and 7.4 were used to estimate projected solid waste generation under the proposed and maximum expansion scenarios. Under the proposed (near-term) scenario, the expected filter-cake solid waste that will require disposal at regional landfills is ~113,000 metric tons per year, and ~71,000 metric tons will need to be sent to Class I hazardous waste landfills, or Class II industrial waste landfills out of state. Under the maximum (long-term) scenario, total solids production is projected to be ~590,000 metric tons per year. In the near term, regional landfill disposal capacity appears adequate for disposal of nonhazardous filter cake based on on-going and planned expansion of existing facilities.

Table 9.6. Annual solid waste and power production at SS-GF power plants, 2015-2021 (DTSC, 2023a-d; SWRCB, 2023; U.S. EIA, 2023). Solid wastes consisted of waste disposed of in the Desert Valley Monofill, Salton City Landfill, and various Class I and II landfills.

Facility	Annual Average Filter Cake Production (metric tons)	Annual Average Manifest Waste Production (metric tons)	Annual Average Total Solids Production (metric tons)	Annual Average Gross Generation (MWh)	Annual Average Solids Waste Production Per Gross Generation (metric tons/MWh)
Region 1	14,923	6,662	21,585	1,326,627	0.016
Region 2	12,127	10,693	22,820	753,709	0.030
Elmore	6,883	5,307	12,190	373,518	0.033
Leathers	7,089	4,986	12,075	378,152	0.032
Featherstone	8,015[b]	3,117[b]	11,132	456,856	0.024

[a] Data from 2014 was not used because only data from July to December were available for the Monofill.

[b] Estimated using the 2022 ratio of filter cake (72%) to manifest waste (28%) for the Featherstone plant and applying this to the average total solids for 2015-2021.The Featherstone plant started using the Salton City Landfill in late 2020 after gaining approval and has increasingly diverted filter cake to that landfill. The values in this table and in Table 9.9 reflect use of the Salton City Landfill by the Featherstone plant.

The Desert Valley Monofill recently applied to increase its capacity by opening another disposal area, Cell 4 (BRG Consulting Inc., 2021). Currently, the facility is permitted to accept up to 680 metric tons per day of solid waste, representing approximately 924 cubic yards of filter cake at a density of 1.18 metric tons (1.32 short tons) per cubic yard (BRG Consulting Inc., 2021). At current rates of filter-cake production, Cell 3, the current disposal cell, is projected to reach capacity in 2025. The proposal for Cell 4 will increase the Monofill's disposal capacity by 2.6 million cubic yards, equivalent to approximately 3.1 million metric tons of filter-cake solids (BRG Consulting Inc., 2021; p. 3-2). The Desert Valley Monofill expects that opening Cell 4 will extend its operational life until approximately 2080, that is 55 years beyond its current remaining capacity. This life expectancy was calculated using a daily average of 227 metric tons per day, or ~82,000 metric tons per year (BRG Consulting Inc., 2021; p. 4-7).

BHER, which uses the Desert Valley Monofill, has published plans to build three new power plants with an expected net output of 367 MW (CEC, 2023a, 2023b, 2023c). Considering that the median solids production from geothermal power plants is 0.030 metric tons per gross MWh (Table 9.6), the new geothermal plants can be expected to produce about 3,214,920 MWh per year that will result in total solids production of 96,500 metric tons per year. This value compares well with BHER's combined estimate of 89,730 metric tons per year (Table 9.7). Based on records at BHER's existing geothermal power plants (Appendix Chapter 9, Table A9.12), about 63% of the total solids, or 61,000 metric tons, will be filter cake that can be sent to the Desert Valley Monofill, in addition to the ~45,000 metric tons of filter cake that is currently disposed of at the Monofill. These calculations support the conclusion that sufficient Monofill capacity exists for currently planned expansions of geothermal power production in the region.

Table 9.7. Solid waste production estimates as described in environmental impact reports submitted to California Energy Commission. Information shown for wastes produced in quantities over one metric ton only.

Waste	Classification	Disposal	Elmore North Estimated Quantity (metric tons/year)	Morton Bay Estimated Quantity (metric tons/year)	Black Rock Estimated Quantity (metric tons/year)	Total Estimated Waste (metric tons/year)
Geothermal filter cake	Nonhazardous	DVC Monofill	21,773	21,773	12,701	56,246
Brine pond solids	Hazardous	TSDF	6,804	6,804	6,350	19,958
Geothermal Scale	Hazardous	TSDF	3,175	3,175	2,722	9,072
Geothermal filter cake	Hazardous	TSDF	1,179	1,179	726	3,084
Cooling tower debris and sludge	Hazardous	TSDF	272	272	181	726
Commercial Trash	Nonhazardous	Local landfill	109	109	68	286
Petroleum contaminated solids (>51%)	Hazardous	TSDF	50	50	45	145
Oil, water, sludge	Hazardous	TSDF	50	50	45	145
Used Oil	Hazardous	Oil recycler	23	23	18	64
Laboratory analysis waste	Hazardous	TSDF	1	1	1	4
Total			33,436	33,436	22,858	89,730

Table 9.8. Anticipated solid waste generation under projected and maximum capacity scenarios

Scenario	Power Production (MWe)	Regional Landfill[a,b] (metric tons/year)	Manifested (metric tons/year)[b]	Total Solid Waste (metric tons/year)
Current	400	49,036	30,766	79,802
Near-term	920	112,783	70,761	183,544
Long-term	2,950	362,866	227,668	590,534

[a]Solid waste to regional landfills includes filter cake disposed of in the Desert Valley Monofill and at the Salton City Landfill.

[b] Solid waste values are averages and are described in more detail in Table 9.7. These values are based on continued use of the Salton City Landfill by Featherstone.

It is difficult to estimate the remaining service life of the Salton City Landfill, in part because the landfill accepts several types of waste from multiple producers and is developing separate facilities for some waste streams (e.g., green waste and municipal biosolids). However, it is expected that companies other than BHER will build new geothermal power plants and therefore increase the use of the Salton City Landfill. Using an optimistic outlook for power production, ~19,000 metric tons of filter cake per year could be produced. The Salton City Landfill was estimated to have a remaining capacity of 488,000 cubic meters (639,014 cubic yards) in August 2021 (CalRecycle, 2023). Using a density factor of 1.18 metric tons per cubic yard as described above (BRG Consulting Inc., 2021), this volume is equivalent to ~754,000 metric tons of filter cake. Given that the planned capacity of the Salton City Landfill is approximately 50 million

cubic meters (65.1 million cubic yards), and that the facility is being periodically expanded (only one of six expansion phases is complete and in-use), it seems reasonable to expect there will be sufficient capacity for future filter-cake waste. Geothermal filter cake would represent approximately 10% of the total solid waste received at the landfill. It is also possible that filter cake could be disposed of in other Class III landfills in Imperial County (Appendix Chapter 9, Table A9.13).

Landfill capacity for hazardous or otherwise restricted wastes can be evaluated in a similar fashion. According to a 2022 air permit application document (SCS Engineers, 2022), the design capacity of the Copper Mountain Class II Landfill in Wellton, Arizona is estimated to be 54.5 million cubic meters; based on current compaction rates, this translates to about 56 million metric tons of waste. At year-end 2020, 4,853,023 Mg of waste was in place at the landfill, which is not expected to reach capacity until the year 2285 (SCS Engineers, 2022). Although future use of the Copper Mountain Landfill is not certain, it appears that the landfill has capacity to accept geothermal power plant solid wastes under the near-term scenario (Table 9.8).

While the remaining capacity of the Clean Harbors Buttonwillow Class I Landfill is not posted in the Solid Waste Information System (SWIS) database, its maximum permit capacity is listed as 13,250,000 cubic yards, and its maximum throughput is 9,500 metric tons per day. Although its future use is not certain, it appears that the landfill has capacity to accept geothermal power plant solid wastes. Other hazardous landfills may also be used, especially for recycling and specialty purposes (e.g., Kettleman Hills Facility), but the quantities of solid waste disposed of at these landfills is small and should not significantly impact landfill capacity.

Under the long-term scenario, over 590,000 metric tons of solid waste could be produced by geothermal power plants in the SS-GF (Table 9.8), over 200,000 metric tons of which could be hazardous waste. At that rate of production, current local landfill capacity would be inadequate, and it is likely that hazardous waste landfill capacity would become less readily available, as competition for landfill space would increase. However, given the current rate of geothermal energy development, it will be a number of years before full exploitation of the SS-GR resource could be achieved. Landfill capacity will need to be developed in parallel with expansion of geothermal energy production. This will be particularly critical as the lithium extraction and battery material production industry grows. Diversion of filter cake and other geothermal power plant solid wastes from landfills to useful purpose, as has been proposed in the past, could be a viable alternative to landfill disposal and should be investigated.

Potential Solid Waste Impacts of Future Lithium Resource Extraction

As of 2023, no company or facility is commercially extracting and producing lithium from geothermal brine in the SS-GR. However, three companies are investigating or engineering processes for the extraction of lithium: EnergySource, CTR, and BHER. All of these companies are including direct lithium extraction (DLE) technologies as part of their geothermal lithium resource extraction process (Paz et al., 2022; Stringfellow and Dobson, 2021). Since the companies are developing proprietary processes, there is a dearth of public information about the specific extraction and purification process that will be used, and how much solid wastes and other byproducts will be produced. However, we can use publicly available information to create a generalized process for lithium extraction from geothermal brine (Figure 9.9).

The initial steps of the extraction process produce solid materials during the removal of silica and metals in order to make "clean brine" for the DLE step (Figure 9.9). The DLE step produces a lithium chloride solution that also contains other ions including sodium, calcium, and magnesium. Since the DLE process is proprietary, the exact composition of the lithium chloride concentrate is not known. However, the typical processes used for purification of lithium chloride and conversion to lithium carbonate are well known and involve the removal of calcium and magnesium as solid waste products (Figure 9.9). Other forms of lithium products have been proposed for manufacture, particularly lithium hydroxide; lithium carbonate is also a common intermediate for its production, which also requires calcium and manganese removal (Chambers Group Inc., 2021; Featherstone et al., 2020b; Hell's Kitchen Power Co., 2021; Paz et al., 2022; Warren, 2021). As this study's focus is resource extraction, solid waste production by the lithium battery manufacturing process was not evaluated.

EnergySource Minerals is developing a full-scale lithium extraction facility adjacent to the Featherstone Power Plant and has published a draft EIR (Chambers Group Inc., 2021). According to the EIR, the EnergySource ATLiS project will process 27,000 liters per minute (7,000 gallons per minute) of geothermal brine and create "19,000 metric tons of lithium product, 10,000 to 20,000 metric tons of zinc product(s), and up to 60,000 metric tons of manganese product(s)" (Chambers Group Inc., 2021). Presuming the product is lithium carbonate, this would be equivalent to about 3,500 metric tons of lithium metal (or about 3,100 metric tons lithium metal, if the product is lithium hydroxide monohydrate). The lithium extraction facility is also projected to produce about 136,200 metric tons per year of iron-silica filter cake, of which 10% is estimated to require management as hazardous waste (Chambers Group Inc., 2021). These numbers suggest that the ATLiS project will produce between 41-66 metric tons of solids per metric ton of lithium metal extracted, of which an estimated 60% (25-38 metric tons per metric ton lithium) will require land disposal, with the balance being sold as products. The ATLiS project intends to use Salton City Landfill for disposal of nonhazardous filter cake and Arizona facilities (presumably Copper Mountain Landfill) for disposal of hazardous wastes (Chambers Group Inc., 2021). However, it should be considered that a market must be created for the metal products, or they will also require disposal in landfills.

Similar information allowing estimation of solid materials and solid waste production was not found for other proposed SS-GR geothermal brine extraction projects (BHER Minerals, 2020; CEC, 2019; County of Imperial Planning and Development Services Department, 2020; Hell's Kitchen Power Co., 2021; Paz et al., 2022). However, presentations by BHER to state agencies showed ratios of metal production to lithium production that are similar to that expected by the ATLiS project. BHER expects production of about 90,000 metric tons of LCE to also include production of 32,000 metric tons of zinc and almost 98,000 metric tons of manganese (Besseling, 2018). This suggests approximately 1.9 tons of zinc and 5.8 tons of manganese per ton of lithium metal, which is similar to what ATLiS is predicting (1.7 tons of zinc and 6.7 tons of manganese per ton of lithium metal), assuming that the ATLiS metal products are about 40% elemental metal.

Mass-Balance Estimation of Future Lithium Extraction Solid Waste Production

Agreement in solids production among geothermal power plants and apparent agreement between expected future solids production from various lithium extraction and purification ventures suggests that a

mass-balance approach could be useful for providing an independent evaluation of both past and future solids production in the region.

A mass balance was calculated on one of the geothermal power plants for the purpose of determining if the solids data reported by industry to the DTSC, CalRecycle, and the RWQCB could be independently verified. Data for production well flow and chemistry and injection well flow and chemistry were used to calculate the mass loss of solids from the Elmore Power Plant (Table 9.9). The stand-alone Elmore plant provides detailed reporting for brine flows and solid waste production. A comparison of the calculated solids production based on the detailed mass balance (averaging 1,371 metric tons per month), and the reported production of solid wastes reported to the DTSC manifest system and the RWQCB (reported as an average of 1,137 metric tons per month) agree very closely (Table 9.9). In addition, the TDS of the brine, combined with the production and injection flow data, was used to calculate a mass balance based on TDS (Table 9.9). The mass-balance calculation based on TDS of an average of 1,108 metric tons per month also agrees with the reported solid waste disposal values (Table 9.9).

The results of this mass-balance analysis suggest that reporting required by California State Agencies is comprehensive, and that both hazardous and nonhazardous solid waste production is being reported accurately by industry. The ability to use TDS measurements to conduct a reasonable mass balance is also significant. Getting detailed chemical analysis on geothermal production and injection wells is difficult; however, TDS is routinely measured along with flow and reported to CalGEM, the state agency regulating geothermal brine production. This analysis suggests that TDS can be used for predicting future solids production associated with lithium extraction and purification from geothermal brines.

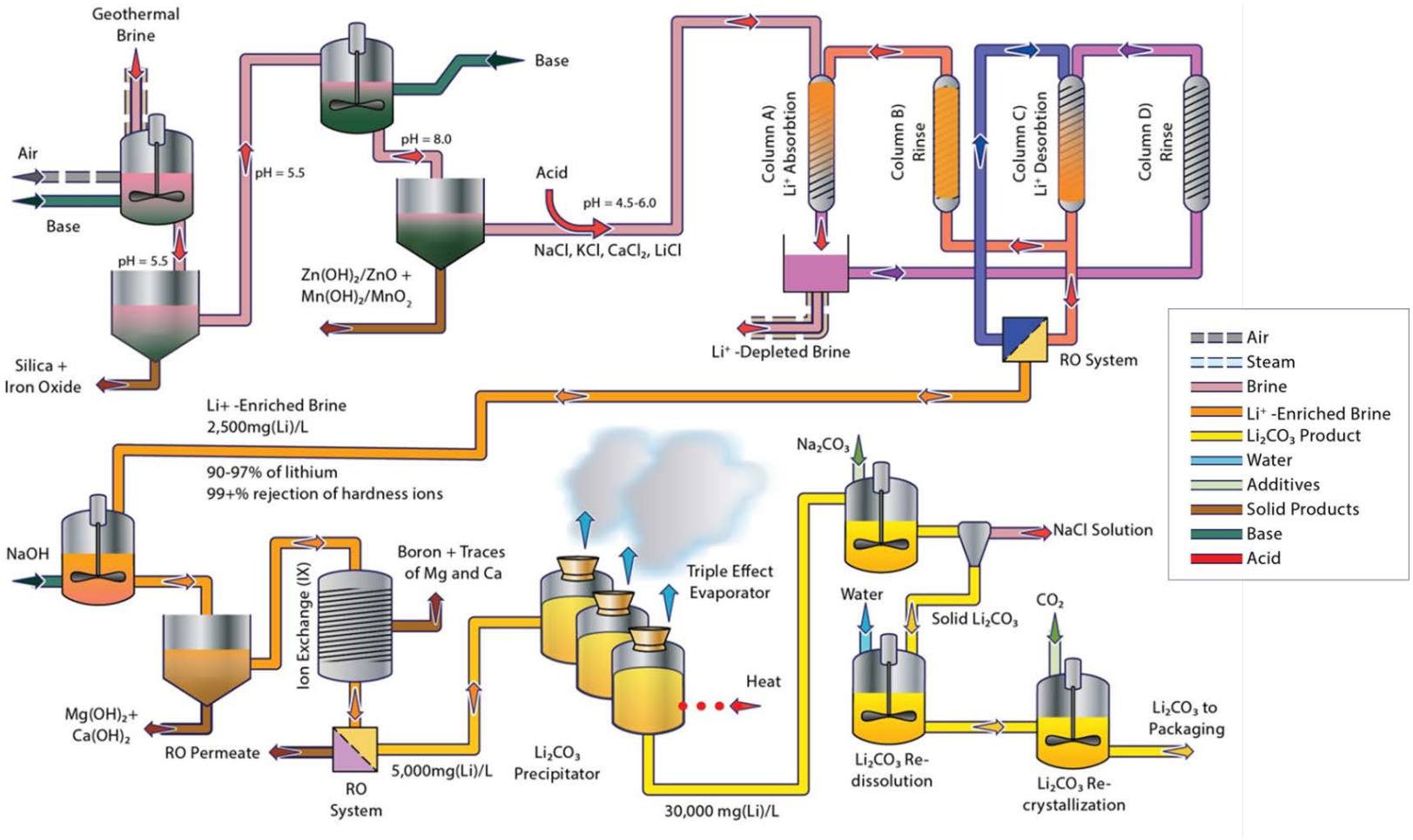

Figure 9.9. Conceptual process for the extraction and refining of lithium from geothermal brines from the SS-GR.

Table 9.9. Mass balance on the Elmore Power Plant and comparison of calculated solid waste production versus reported solid waste production

Analyte	Inflow (metric tons per month)	Outflow (metric tons per month)	In-Out (metric tons per month)[a]	% Removed[a]	Filter Cake Components	Solid Components
Chlorides (Cl-)	201,375	201,935	-559	-0.3		
Sodium (Na)	70,204	69,477	727	1.0		727
Iron (Fe)	1,936	2,038	-101	-5.2		0
Silica (SiO2)	570	180	390	68.4	390	390
Zinc (Zn)	545	508	38	6.9		38
Barium (Ba)	252	187	65	25.9	65	65
Lead (Pb)	125	128	-3	-2.6		
HCO3	98	25	73	74.2	73	73
Copper (Cu)	71	3	68	95.7	68	68
Fluoride (F)	26	16	10	38.9	10	10
Flow, mean 2015-2021	1,244,037	1,081,273	162,764	13.1		
Total Dissolved Solids (TDS)	341,687	340,579	1,108	0.3		
Calculated solids removed					**606**	**1,371**
Reported solids disposed					**649**	**1,137**
Calculated solids from TDS						**1,108**

[a] Negative values indicate more mass is measured as being injected than being produced.

According to the analysis in Table 9.9, less than 1% of the TDS is being removed in the power plant crystallizer-clarifier process, including about 70% of the silica (SiO_2). This is consistent with values reported in publications and other sources (Featherstone et al., 1995; Gallup, 2009; Hoyer et al., 1991). The crystallizer-clarifier is optimized for operation of the power plant, and it is expected that the brine from the power plant will need to be further treated to produce a "clean" brine suitable for the DLE technology step. Based on published requirements for mineral content of brines suitable for DLE sorbents, it is likely that over 90% of the silica, iron, manganese, and zinc in the geothermal brine will need to be removed prior to DLE (e.g., Bhave et al., 2019; Burba et al., 2014; Chambers Group Inc., 2021; Featherstone et al., 2019; Hell's Kitchen Power Co., 2021; Materials Research LLC, 2020; Stringfellow and Dobson, 2021).

Based on the known brine chemistry of the SS-GR (e.g., Table 1.2), a mass-balance approach suggests that for every metric ton of lithium extracted, approximately 1.2 million metric tons of TDS will be co-processed, and that up to about 1,700 metric tons of silica and about 15,000 metric tons of iron, manganese, zinc, and lead could be precipitated to form solids. Some of the solids will be wastes that will need to be either disposed of in a landfill or re-dissolved and injected back into the reservoir (Besseling, 2018; Paz et al., 2022). However, the precipitated solids could also potentially be valuable mineral products and sold (e.g., Maimoni, 1982; Schultze and Bauer, 1982a, b; Sizemore, 2023; U.S. Department of the Interior, 2018).

Based on the process hypothesized in Figure 9.9 and the brine chemistry in Table 1.2, a mass balance suggests that producing 3,500 metric tons of lithium would require the removal of about 8,000 metric tons of zinc and 20,800 metric tons of manganese, assuming a 100% removal efficiency. Considering that metal compounds are typically precipitated as oxides and hydroxides, which are about 65% percent metals, the total mass for zinc and manganese solids could be 12,300 and 32,000, respectively. We do not know the exact chemistry of the brine used at each facility, the exact process being used, or the metal product being produced by the ATLiS project. Despite that limitation, these numbers agree within reason with the projection that ATLiS will produce "10,000 to 20,000 metric tons of zinc product(s), and up to 60,000 metric tons of manganese" (Chambers Group Inc., 2021; Paz et al., 2022). By the mass-balance calculation, the ratios of metal produced to lithium produced are approximately 2.3 and 6.0 for zinc and manganese, respectively. This estimate is between 2% and 27% of the estimated ratios calculated from industry disclosures (see above), suggesting the mass-balance approach is helpful for estimating potential future solids and solids waste production from prospective lithium extraction and purification processes.

Using this same approach, the mass balance would predict about 36,000 metric tons of iron-hydroxide and 6,000 metric tons of amorphous silicate, which is unlikely to be of significant value and would presumably be landfilled (42,000 metric tons total). The ATLiS project projects that it will produce 136,200 metric tons of solid wastes for landfill. The source of the difference between the mass-balance calculation and the ATLiS projection could be that ATLiS is including in its total filter cake from the Featherstone Power Plant (about 8,000 metric tons per year; see Table 9.6). Additional solid wastes may also come from the purification of lithium chloride before the production of lithium carbonate, which includes a process step to remove calcium and manganese as hydroxides (Figure 9.9). The exact process will determine how much calcium is residual in the lithium chloride and how much calcium hydroxide solid is produced, but calcium levels in the brine are very high. There is approximately 127X as much calcium as lithium in the geothermal brine, on a mass basis (Table 1.2). Calcium removed as calcium hydroxide could easily account for the balance of solids predicted by EnergySource minerals in their EIR (Chambers Group Inc., 2021), and it is likely that the ATLiS projection includes the production of calcium and magnesium hydroxide solids during the lithium purification process (Figure 9.9).

Although lithium extraction and purification processes are still in development, and full utilization of the resource is many years in the future, it is prudent to consider how this industry could impact local and regional landfill capacity. BHER is operating a pilot project and estimates that a full-scale facility could produce 90,000 metric tons of LCE, based on the flow of their existing geothermal power plant operations, with a potential capacity of over 300,000 metric tons LCE, based on lease holdings (Besseling, 2018). CTR expects to produce 25,000 metric tons per year of lithium hydroxide monohydrate (21,900 metric tons LCE) during initial operations, and plans for an eventual capacity of 300,000 metric tons per year of lithium products (Controlled Thermal Resources, 2023; Hell's Kitchen Power Co., 2021). If these processes produce equivalent amounts of solid wastes as projected by ATLiS (seven tons landfill waste per ton LCE), full-scale production could produce well over 700,000 tons of solids for landfill per year. This is about 14X the amount of filter cake currently produced per year (Table 9.6).

These results suggest that landfill capacity should be considered as part of development of lithium resources in the region. Efforts to monetize solids produced as part of the lithium extraction and purification process should be encouraged. Most companies intend to sell the metal hydroxide products

(Figure 9.9), but the market may become less attractive as more of this product is produced. If high-value metal containing solids can be generated, it could significantly offset needs for landfill space, particularly Class II and I landfill space. Additionally, diversion from landfills of lower-value products, such as iron-silicate filter cake, should be encouraged.

It should also be noted that it has been proposed that solid wastes from the lithium extraction and purification process could be re-dissolved in the thermally spent or lithium-depleted geothermal brine and reinjected into the formation. However, this technology has not been proven, and potential costs and negative consequences on the reservoir need to be considered for this to be a viable alternative to land disposal.

Summary

Geothermal power plants use chemical additives throughout. The chemicals are added to reduce scaling (mineral buildup on pipes and other surfaces), biological growth, and corrosivity, as well as to adjust fluid pH and limit air pollution emissions. The SS-GF power plants are required to disclose the chemicals they use to the Regional Water Quality Control Board (RWQCB) and gain approval before new process chemicals are used. Our examination of the chemicals reported as being used in geothermal power plants and an examination of the literature did not identify any persistent organic pollutants or acutely toxic chemicals as being used for process control in geothermal power plants. Most of the chemicals used fall into common categories of chemicals used in industrial processes and water treatment facilities. Many of the chemicals used (e.g., barium inhibitors) are reinjected into the reservoir with the spent brine. The chemicals being used in geothermal power plants appear consistent with their reported purposes.

Geothermal power plants in the SS-GF currently produce approximately 80,000 metric tons of solid waste per annum, representing approximately 30 kg of solid waste per MWh of electrical production. These solid wastes are predominantly composed of iron-silicate filter cake, brine-pond solids, and solids generated during plant maintenance. Filter-cake solids are predominantly nonhazardous and disposed of in regional Class II or Class III landfills. Brine-pond solids are predominantly hazardous wastes and are disposed of in Class II or Class I landfills, appropriate for industrial waste solids or hazardous waste solids, respectively. Approximately one-fifth to one-third of geothermal power plant solid wastes contain sufficient levels of hazardous materials to require management as hazardous wastes under California regulations.

It is expected that geothermal solid waste production will increase proportionally to geothermal power production due to construction of new power plants in the region. In the near term (2-5 years) the amount of solid wastes produced per year is expected to approximately double, as electrical production capacity doubles. Our analysis indicates that current landfill capacity is adequate for management of expected new solid waste production from geothermal power plants in this timeframe. However, full utilization of the full electrical production capacity of the SS-GR, a long-term goal, would undoubtedly require planning for additional landfill capacity.

As of yet, there is no commercial geothermal lithium extraction and purification industry in the SS-GF. The exact process that will be used is not certain; however, general process steps are known. All of the lithium extraction and purification processes being developed so far include the application of DLE

technology. To produce lithium chloride from geothermal brine, the brine will be treated to remove silica and metals to produce "clean brine" prior to the DLE process step, creating a solid byproduct. The removal of silica and metals to prepare the brine for lithium extraction will be more significant than what is currently needed to reinject the spent brine back into the formation. In addition, the processing of lithium chloride to lithium carbonate and other final products will also produce solid byproducts. The amount of solid waste that will be produced during the process for lithium extraction and purification is dependent on the exact process applied and whether the solids produced during pretreatment can be monetized; some solids produced during pretreatment contain manganese and other potentially valuable metals. However, the extraction and purification of lithium will produce iron-silicate solids and possibly solids containing calcium and other elements (e.g., magnesium) that are unlikely to have value, and must be landfilled.

One company in the region estimates it will produce over seven tons of solid waste per ton of LCE produced (of which ~10% or more will be hazardous), whereas another company expects to sell all of its solid products and therefore produce no solid wastes. Based on our independent calculations, we expect that solid waste production may be less than seven tons per ton LCE, but it is unlikely that all solid materials produced during the lithium chloride production process will be marketable and that no solid wastes will be produced.

These results suggest that landfill capacity should be considered as part of development of both geothermal and lithium resources from the SS-GR. Efforts to divert waste solids from landfills to useful purpose should be encouraged to save landfill space. Many companies expect to monetize solids produced as part of the lithium extraction and purification process, but current processes are not necessarily optimized for production of high-value byproducts. Efforts to increase product value and utilization of byproducts could help offset future pressure on regional landfill capacity.

Chapter 10: Induced Seismicity in the Salton Sea Geothermal Field

Key Takeaways

- The level of seismic hazard in the Salton Sea Geothermal Field (SS-GF) since the onset of geothermal power production, in 1982, has not exceeded that in the broader tectonic host region, the Brawley Seismic Zone (BSZ), in a statistically significant way.
- The SS-GF was "seismically quiescent" (i.e., exhibited low seismicity) relative to the BSZ in the decade before commercial energy production began (1972-1982).
- While seismic hazard has increased in the SS-GF since commercial energy production began, it has not exceeded the level in the broader BSZ.
- Seismic hazard in the entire BSZ, including the SS-GF, decreased in the post-production period (1982-2022) compared to the pre-production period (1972-1982).

Introduction

The movement of fluids in the earth's subsurface due to extraction or injection for producing geothermal power or lithium can cause changes in pressure and stresses in the subsurface, which in turn can trigger seismic activity. The Salton Sea area, like many regions in California, has a significant level of natural background seismicity: the Brawley Fault runs through the SS-GF, and the area exists within the broader Brawley Seismic Zone (BSZ). This chapter uses historical seismic activity data to analyze seismicity in and around the SS-GF and explore any relationships to geothermal power production activities. This historical analysis can inform an appropriate level of concern associated with increasing development in the region.

Earthquake Data Used in the Analysis

The earthquake catalog from the Southern California Earthquake Data Center (Hutton et al., 2010) documents seismic history in Southern California, beginning in 1932 and extending to the present. Hauksson et al. (2012) published a waveform-relocated catalog with high-precision hypocenter coordinates and have updated it regularly since 1981. We combine data from both catalogs, retaining one set of coordinates for each unique event and preferring coordinates from the Hauksson catalog when available (Figure 10.1). The focus region of this study clearly shows the spatial correlation between the location of production and injection wells and seismicity (Figure 10.2). Noticeably, earthquakes in the SS-GF are shallower than the events in the greater Brawley Fault Zone. The magnitude history of the hybrid catalog (Figure 10.3) indicates that the catalog's completeness within the SS-GF increased significantly circa 1972, so we consider post-1972 event history only. In the beginning of the 1980s, sensor density increased by around 10X (Figure 10.1). We find that the minimum event magnitude for which the catalog contains 95% complete records in every five years during the analyzed period is M2.34 (Figure 10.4a). Thus, we restrict our analysis to M>2.34 earthquakes. Note that local CalEnergy seismic network data were available for much smaller earthquakes between 2008-2014. Such local networks help in understanding the evolution of seismicity, but because we are interested in the seismicity trend for the entire SS-GF from 1972-2022, we select a consistent magnitude threshold (M>2.34) throughout.

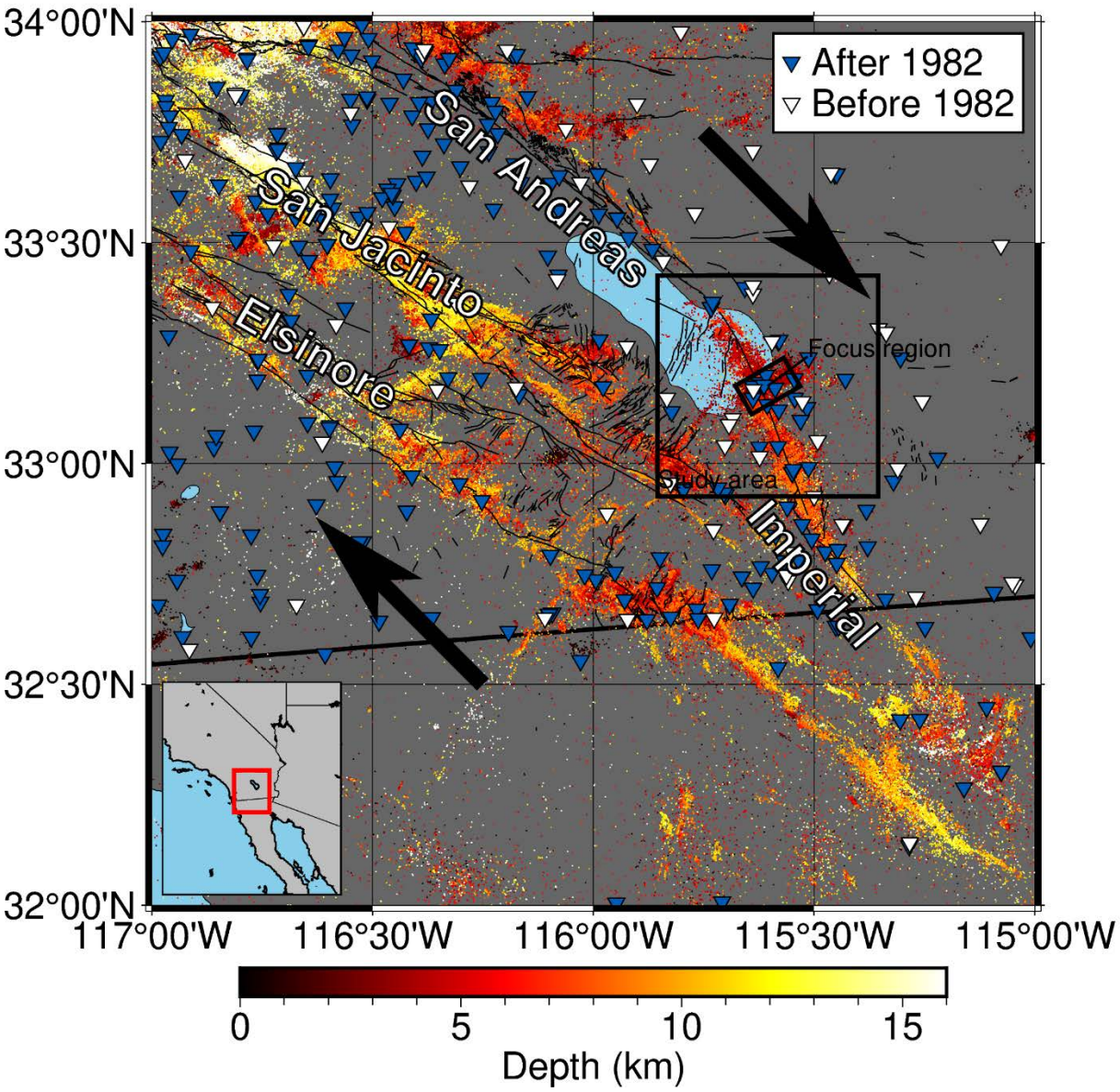

Figure 10.1. Regional context of our Study Area and Focus Region. Dots represent locations of earthquakes in the Augmented Hauksson et al. (2012) catalog between 1972 and 2022, color-coded by hypocenter depth. Large black arrows show nominal relative motions of the Pacific (NW direction) and North American (SE direction) tectonic plates. Triangles show locations of seismometers, color-coded by year deployed.

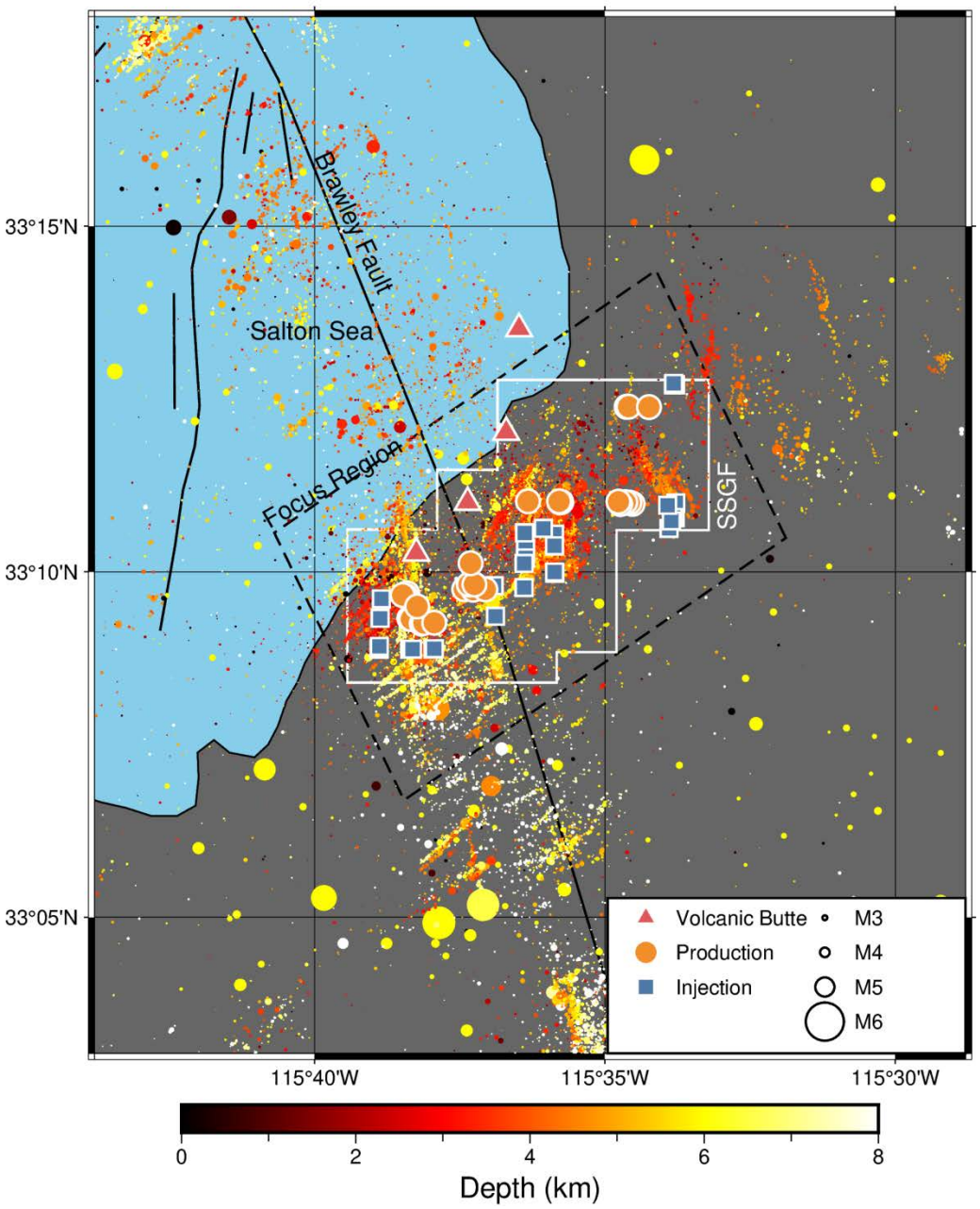

Figure 10.2. Local overview of our Study Area (mapped area) and Focus Region (dashed rectangle). White-edged orange circles and blue squares represent locations of all active production or injection wells, respectively, in our Study Area. Other circles represent seismicity between 1972 and 2022 from the Augmented Hauksson et al. (2012) catalog, color-coded by depth and scaled according to magnitude. Red triangles represent locations of volcanic rhyolite domes. The polygon delineated by the solid white line represents the Salton Sea Geothermal Field. Solid black lines represent known Quaternary fault traces.

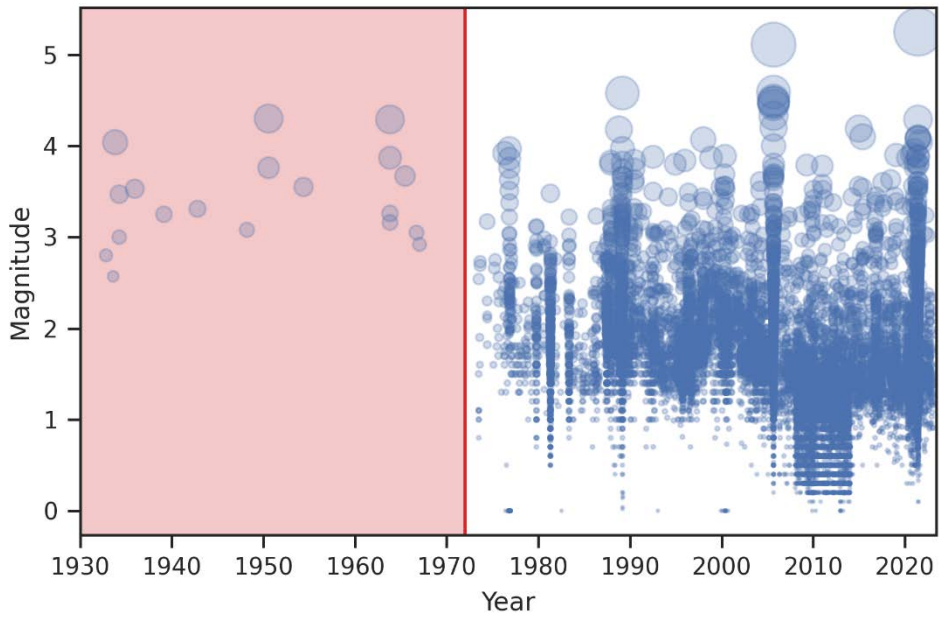

Figure 10.3. Observed event magnitudes (translucent blue circles) versus time. The shaded red region represents a period (pre-1972) during which the catalog is relatively incomplete in the Study Area. We focus on seismicity after 1972.

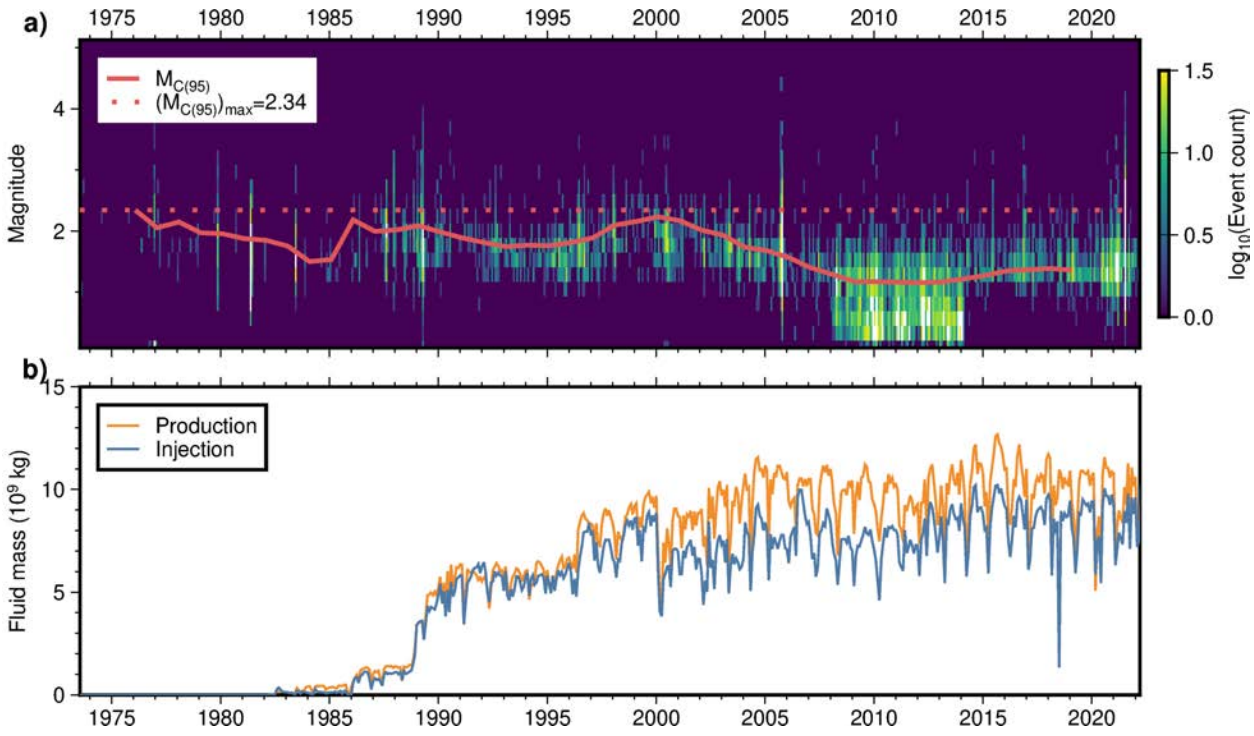

Figure 10.4. (a) shows the frequency-magnitude distribution as a function of time (background color), magnitude of 95% completeness ($M_{C(95)}$) computed using a five-year rolling window (solid red curve), and minimum value of $M_{C(95)}$ (dotted red line). (b) shows production and injection histories.

Approach for Quantitively Evaluating Historical Trends and Correlations

The California Department of Conservation (CDC) mandates that geothermal plant operators report the gross masses of fluids produced and injected in geothermal operations each month. The CDC makes these monthly values publicly available on a per well basis. We download these data via the GeoSteam application. Figure 10.4b shows the net masses of fluids produced and injected across the entire SS-GF. In addition to the clustering of shallow earthquakes near geothermal wells (Figure 10.2), the number of background earthquakes (i.e., excluding foreshocks and aftershocks) observed within the SS-GF was greater in the first ten years of geothermal energy production (1982-1992) than in the ten years prior (1972-1982) (Figure 10.5). In seeking to model the relationship between geothermal plant operations and earthquake occurrences in the SS-GF, Brodsky and Lajoie (2013) proposed the following simple linear-regression model for retrospectively modeling ("hindcasting") background seismicity rates as a function of injection and production rates:

$$\hat{\mu}(t) = \begin{cases} \beta_0 P(t) + \gamma_0 I(t) & t_0 \le t < t_1 \\ \beta_1 P(t) + \gamma_1 I(t) & t_1 \le t < t_2 \\ \vdots & \vdots \\ \beta_n P(t) + \gamma_n I(t) & t_n \le t < t_{n+1}, \end{cases} \qquad \text{Eq. 1}$$

in which $\hat{\mu}$ is the background seismicity rate (earthquakes per unit time, excluding foreshocks and aftershocks); t is time; β_I and γ_1 are coefficients determined using ordinary least-squares regression on six years of data; P and I are production and injection rates, respectively; and $t_k = t_0 + k\Delta t$ for integer k and Δt equal to six months. Such a model comprises four regression coefficients per year, thus requiring 160 parameters to model the entire 40-year history of the geothermal field we analyze. Brodsky and Lajoie (2013) concluded their model provided meaningful insights into the causal relationship between well operations and the earthquake occurrence rate.

In this chapter, we simplify the model of Brodsky and Lajoie (2013) by reducing the number of free parameters used to hindcast seismicity rates. We conclude that seismicity rates can indeed be hindcast as a function of production and injection at geothermal wells; however, the fidelity of our simplified hindcasting model varies significantly throughout the analyzed period (Figure 10.8). We correlate these variations with changes in well operations.

Mainshock-aftershock sequences alter the occurrence rate of earthquakes orders-of-magnitude more than do any external physical controls (e.g., geothermal plant operations). The background seismicity rate, however, is insensitive to intense aftershock sequences and reveals subtler variations, such as those potentially caused by geothermal plant operations. The background seismicity rate is thus often preferred when investigating the relationships between physical controls and earthquake occurrences (Brodsky and Lajoie, 2013; Trugman et al., 2016; Martínez-Garzón et al., 2018).

We estimate the background seismicity rate using two independent methods (Figure 10.6). The first approach follows that of Brodsky and Lajoie (2013) based on the Epidemic Type Aftershock Sequence (ETAS) model (Ogata, 1988). The second approach uses de-clustered catalogs obtained via the Nearest-Neighbor Distance (NND) algorithm of Zaliapin and Ben-Zion (2020). In the following analysis, we consider only the trend of the seismicity-rate histories, which we obtain by decomposing each history into

(1) seasonal, (2) trend, and (3) residual components with the Seasonal-Trend decomposition using the LOESS (STL) algorithm (Cleveland et al., 1990). The seismicity-rate histories from these independent methods agree well (coefficient of determination R^2=0.92).

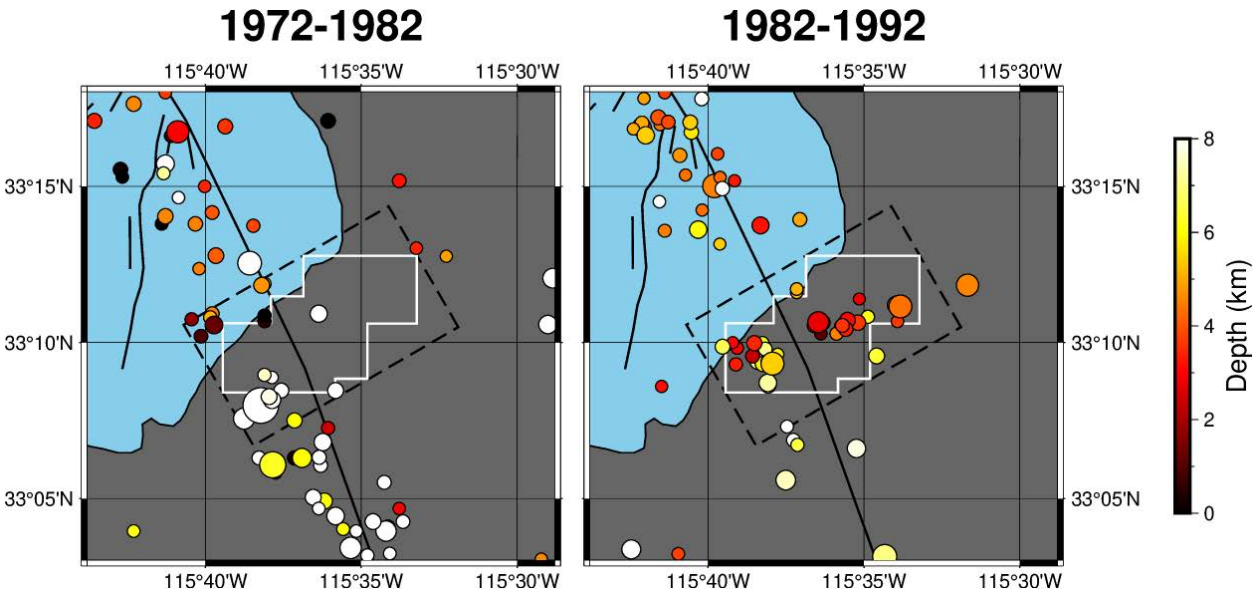

Figure 10.5. Background seismicity in our Study Area during a) the ten years preceding geothermal energy production (1972-1982) and b) the ten years following (1982-1992).

We assume a model of the form:

$$\hat{\mu}(t) = \begin{cases} \alpha_0 + \beta_0 P(t) + \gamma_0 I(t) & t_0 \le t < t_1 \\ \alpha_1 + \beta_1 P(t) + \gamma_0 I(t) & t_1 \le t < t_2 \\ \vdots & \vdots \\ \alpha_n + \beta_n P(t) + \gamma_n I(t) & t_n \le t < t_{n+1}, \end{cases} \quad \text{Eq. 2}$$

in which we have added a constant term α_i to the model expressed by Equation (1) and allow t_k to take on arbitrary values. A cumulative sum of residuals (CUSUM) test (Brown et al., 1975) indicates that a statistically significant change (at the 95% confidence level) in regression coefficients occurs in 1996. This change point coincides with the beginning of a period (1996-2005) during which the average temperature of fluid being injected into the subsurface fluctuated significantly around the relatively stable temperature during the preceding period (Figure 10.7). Furthermore, the apparatus used to monitor fluid production and injection rates changed circa 2005-2006 (Emily Brodsky; personal communication). We thus divide the 40-year history of geothermal energy operations into (1) "early" (1982-1996), (2) "intermediate" (1996-2006), (3) and "late" (2006-present) time periods, and build a hindcasting model of the form:

$$\hat{\mu}(t) = \begin{cases} \alpha_0 + \beta_0 P(t) + \gamma_0 I(t) & 1982 \le t < 1996 \\ \alpha_1 + \beta_1 P(t) + \gamma_1 I(t) & 1996 \le t < 2006 \\ \alpha_2 + \beta_2 P(t) + \gamma_2 I(t) & 2006 \le t \end{cases} \quad \text{Eq. 3}$$

We determine two separate hindcasting models by fitting Equation (3) via OLS regression to seismicity rate histories obtained by each of the two methods described above (i.e., the ETAS and NND methods).

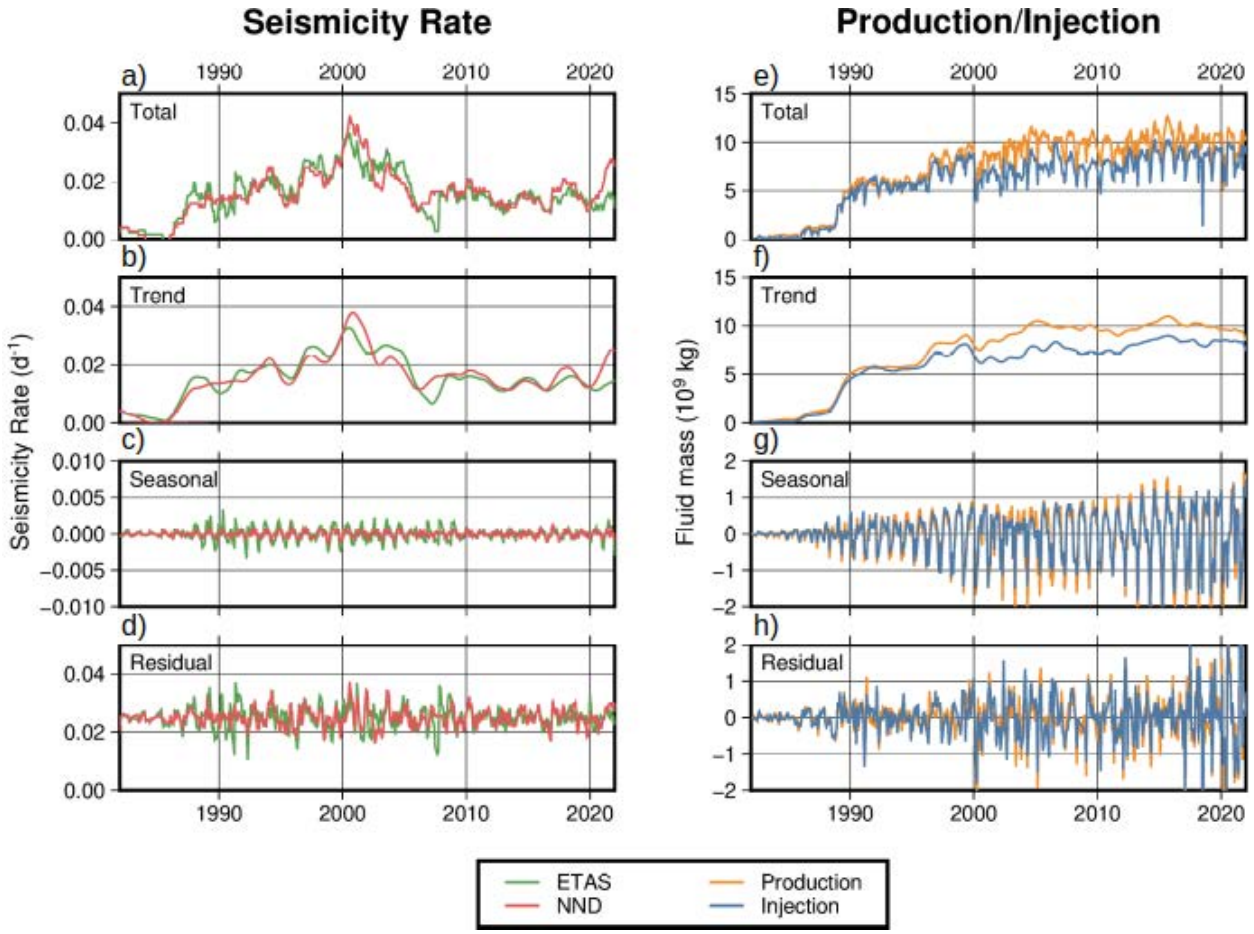

Figure 10.6 shows observed a) seismicity rate and e) production/injection histories; b) and f) show the secular trend of the observed histories; c) and g) show the seasonal component of the observed histories; d) and h) show the residual component of the observed histories.

Although the model proposed by Brodsky and Lajoie (2013) expresses a simple linear relationship between plant operations and background seismicity, it has many free parameters: one for every three data points. Such a piecewise model can fit the data arbitrarily well by fitting a sufficiently large number of pieces to sufficiently small subsets of data. Speaking philosophically, the interpretability of a physical model is inversely proportional to the number of free parameters it comprises. We have shown that many of these parameters can be effectively eliminated, particularly during the first 14 years of energy production. Whereas the Brodsky and Lajoie (2013) model comprises 56 free parameters during this period, ours maintains much of the explanatory power using only three. By fixing our model discontinuities to coincide with known changes in plant operations, we have made it easier to interpret.

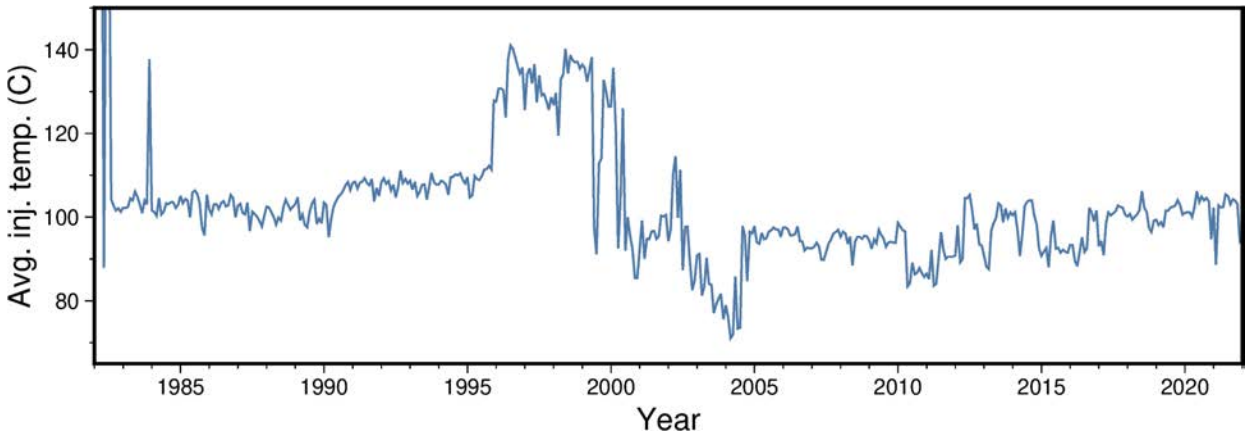

Figure 10.7. Average temperature of injected fluid.

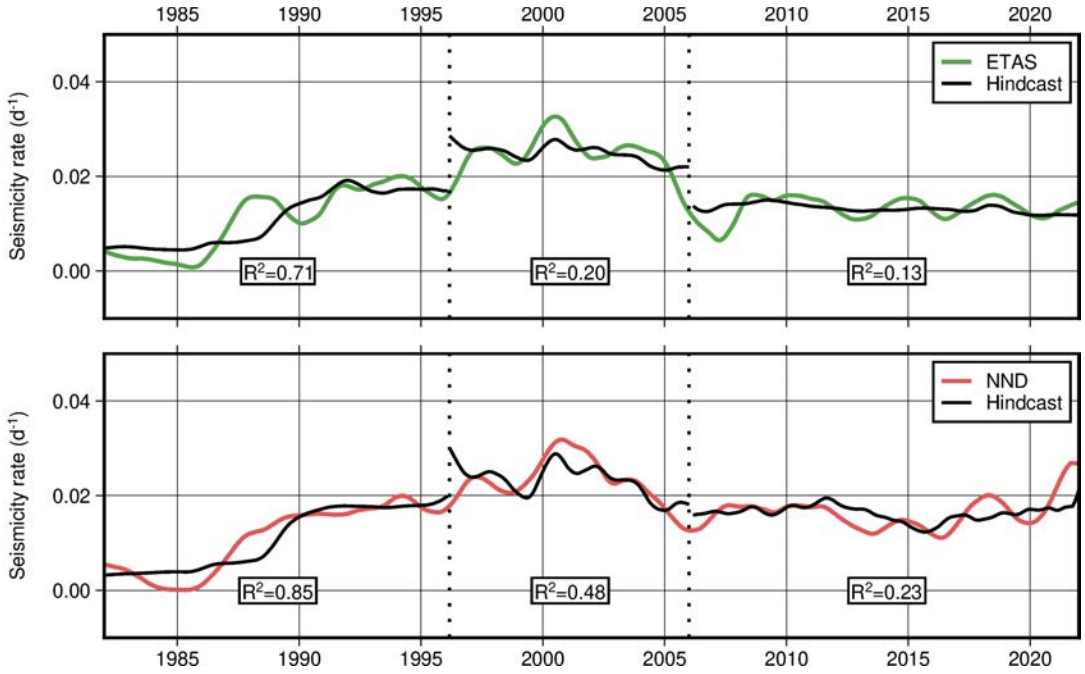

Figure 10.8. Background seismicity rate estimated from the Augmented Hauksson et al. (2012) catalog using a) the ETAS model and b) the NND de-clustered catalog. Solid black curves show the piecewise-linear hindcast model. Dotted black lines represent discontinuities in the hindcast models. R^2 values quantify the correlation between the observed seismicity rate and hindcast model for each time period.

Correlations Between Energy Production and Seismicity in Different Time Periods

- During the first 14 years of geothermal energy production (1982-1996), background seismicity rates appear to be directly proportional to production and injection rates. In other words, the hindcasting fidelity between 1982-1996 can be described as moderate to strong (R^2 values of 0.71 and 0.85 for ETAS and NND results, respectively).

- During the next 10 years (1996-2006), the correlation can be described as weak to moderate (R^2 values of 0.20 and 0.48 for ETAS and NND results, respectively). This period coincides with significant fluctuations in the average temperature of injected fluids.
- After 2006, the correlation between energy production and seismicity is weak. Models based on injection and production histories during this period provide marginally more explanatory power than simply assuming a constant background seismicity rate. The background seismicity rate remains elevated during this period, despite the lack of a simple relationship to geothermal plant activity. These results motivate the development of more sophisticated models.

We interpret our model results as follows: Prior to geothermal plant operations, we consider the reservoir and surrounding crust as existing in a steady state within the ambient tectonic stress regime, with a pre-existing network of faults related to basin extension randomly distributed throughout. Pre-production movement of secondary faults is minimal, as most tectonic stress is accommodated by movement on the Brawley Fault and aseismic creep (Lohman and McGuire, 2007). As geothermal plant activity increased, pore-pressure perturbations propagated away from the injection well flow intervals (i.e., permeable zones in the injection wells between the casing shoe and the bottom of the well), causing many pre-existing faults to become critically stressed and move. A roughly proportional increase in the background seismicity rate accompanied fluid production and injection, and the number of nearly critical pre-existing faults thus decreased over time. The seismogenic response of the crust to well activity was strongest early in the history of plant operations. By the early 1990s, plant operations and the background seismicity rate both stabilized. Movement was induced on pre-existing faults at a relatively steady rate as fluids moved through the subsurface at a relatively steady rate.

The average temperature of injected brine increased from 105°C (standard deviation 4.4°C) between 1985-1996 to 132.8°C (standard deviation 5.1°C) between 1996-1999 (Figure 10.7). The average temperature then fluctuated between 1999-2005 before stabilizing at 96.5°C (standard deviation 5.2°C) after 2005. Pore-pressure perturbations between 1996-2005 were thus influenced by both fluid transfer rates and fluctuating fluid temperatures. Interpreting induced movement as a simple function of a homogeneous diffusion process is insufficient during this period, and the relationship of proportionality between background seismicity rate and fluid transfer rates weakens.

Injection temperatures stabilized after 2005, and although plant activity remained high, the number of nearly critical pre-existing faults was substantially lower than earlier in production history. Heterogeneity of Earth structure and the induced stress field have predominantly controlled the rate of induced earthquakes during this period, and the rate of fluid transfer offers marginally more insight into the rate of induced earthquakes than simply assuming a constant rate.

Importance of the Brawley Fault

In this report, we model the geomechanical response of the crust to production and injection at geothermal wells, averaged over the entire SS-GF; no spatial dependence is incorporated into our model. The termination of seismic lineations at the Brawley Fault, however, suggests that it constitutes a significant structural barrier. Furthermore, low-permeability fault gouge is likely associated with the Brawley Fault (Morrow et al., 1984; Ikari et al., 2009). Both features suggest that the Brawley Fault may act as a hydraulic barrier inhibiting fluid flow between the eastern and western portions of the field.

Seismicity in the BSZ is generally characterized by "ladder-like" structures (Hauksson et al., 2022), in which the "rungs" of the ladder comprise lineations oriented orthogonally to the Brawley Fault (i.e., with roughly NE/SW trend). Many of these lineations in the SS-GF do not extend across the Brawley Fault, which suggests that the Brawley Fault may act as a structural barrier imposing first-order constraints on crustal hydraulics and response to the transfer of geothermal brine. We investigate the potential hydraulic impacts of the Brawley Fault by dividing our focus region into two sub-regions – one to the W of the Brawley Fault and one to the E (Figure 10.9) – and analyzing them independently.

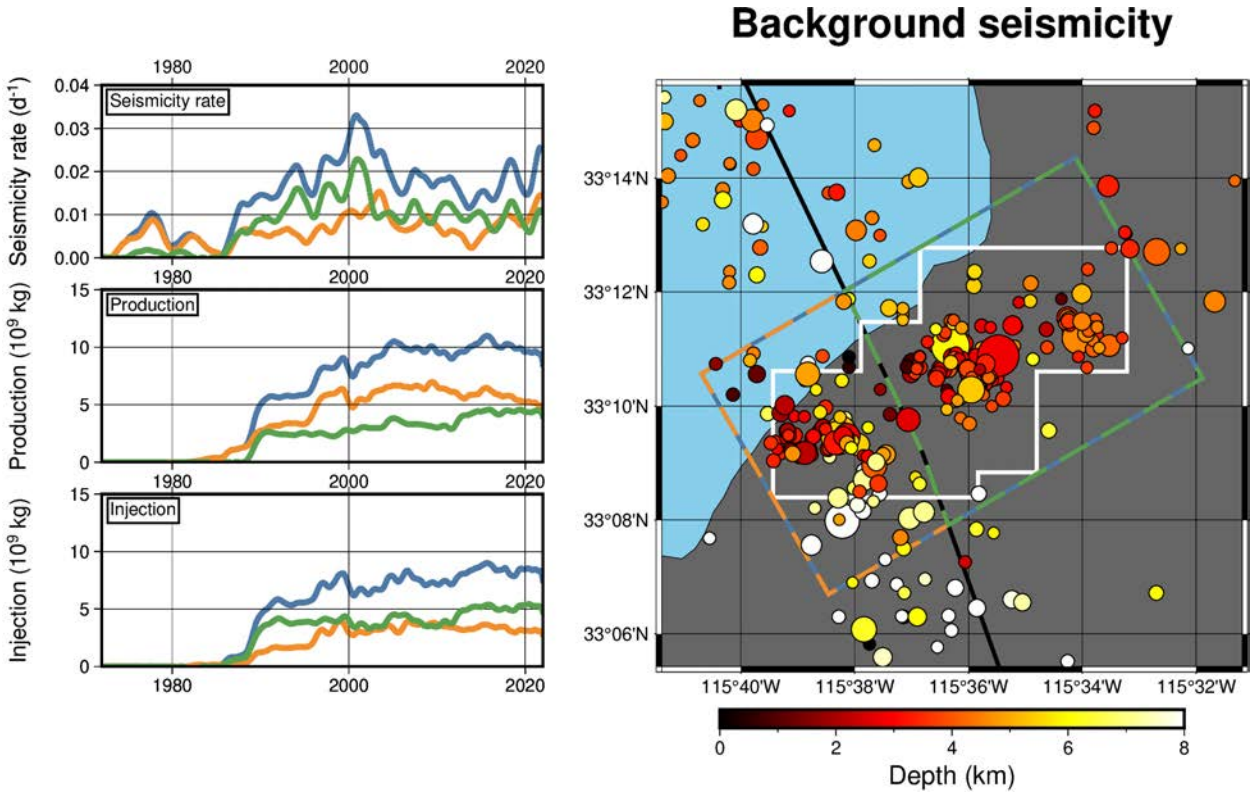

Figure 10.9. Shows the a) seismicity rate, b) production, and c) injection histories for three regions. Blue curves represent observations for the entire Focus Region shown in the map. Orange curves represent observations for the region W of the Brawley Fault (dashed orange-blue rectangle). Green curves represent observations for the region E of the Brawley Fault (dashed green-blue rectangle).

Before commercial geothermal plant operations, background seismicity to the W of the fault significantly exceeded that to the E; after operations began, the converse is true (Figures 10.5 and 10.9). This suggests that most natural tectonic seismicity in the SS-GF occurs to the W of the Brawley Fault. Seismicity rates to the W of the fault increase moderately during the period of geothermal operations, whereas those to the E of the fault increase significantly.

Furthermore, production rates exceed injection rates to the W of the fault, implying net production occurs to the W of the fault (Figures 10.9b and 10.9c). To the E of the fault, injection rates exceed production rates, implying net injection occurs to the E of the fault. Thus, we expect average pore pressure to increase to the E of the fault and decrease to the W of the fault. The significant increase in seismicity rates associated with net injection to the E of the fault, and the accompanying increase in average pore

pressure, agree with our first-order expectations based on Mohr-Coulomb failure theory. Our results support the conclusion that, to the E of the fault, increased average pore pressure resulting from net fluid injection unclamps preexisting faults, which subsequently move under the ambient tectonic stress field. The physical processes driving seismicity to the W of the fault, on the other hand, may be related to subtler effects of subsidence and poroelastic compaction, and likely retain a significant tectonic component.

We determine hindcasting models for each of these sub-regions using the NND method (Figure 10.10). As in the earlier analysis of the entire focus region, the hindcast fidelity is generally moderate to strong between 1982-1996, weak to moderate between 1996-2006, and weak after 2006. The fidelity of the model for the region E of the fault is significantly greater than that for the region to the W for both time periods prior to 2006. This supports the notion that seismicity to the E of the fault has a stronger, explicit dependence on geothermal operations. The fidelity of the hindcast model is weak for both sub-regions after 2006, likely indicating the increasingly complex relationship between expanding geothermal operations and background seismicity.

Probabilistic Seismic Hazard Analysis Across Different Time Periods

We compare probabilistic seismic hazard forecasts for four different combinations of regions and time periods: (1) inside the SS-GF before and after production onset; (2) inside vs. outside the SS-GF in the pre-production period; (3) inside vs. outside the SS-GF in the post-production period; and (4) inside the entire BSZ before and after production onset.

Seismicity Inside the SS-GF Before and After Production Onset

First, we consider the impact of energy production on seismic hazard within the SS-GF (Figures 10.11-13). Figure 10.11 shows seismicity within the SS-GF before and after the onset of production. There is significantly more seismicity in the post-production period, particularly in the eastern portion of the field. Note, however, that the pre-production period spans only 10 years (1972-1982), whereas post-production spans 40 years (1982-2022).

We estimate the probability of a range of magnitude events occurring within a 50-year period (Figure 10.12) based on the statistical relationship derived in Appendix Chapter 10 and the rates of the earthquake frequency-magnitude distribution and time between events before and after the onset of commercial energy production shown in Figure 10.11. Figure 10.12 shows that the seismic hazard within the SS-GF significantly increased during the post-production period. Prior to the onset of production, there was a 2% chance of a M5.2 earthquake occurring within a 50-year period inside the SS-GF; after the onset of production, this magnitude threshold increased to M7.0.

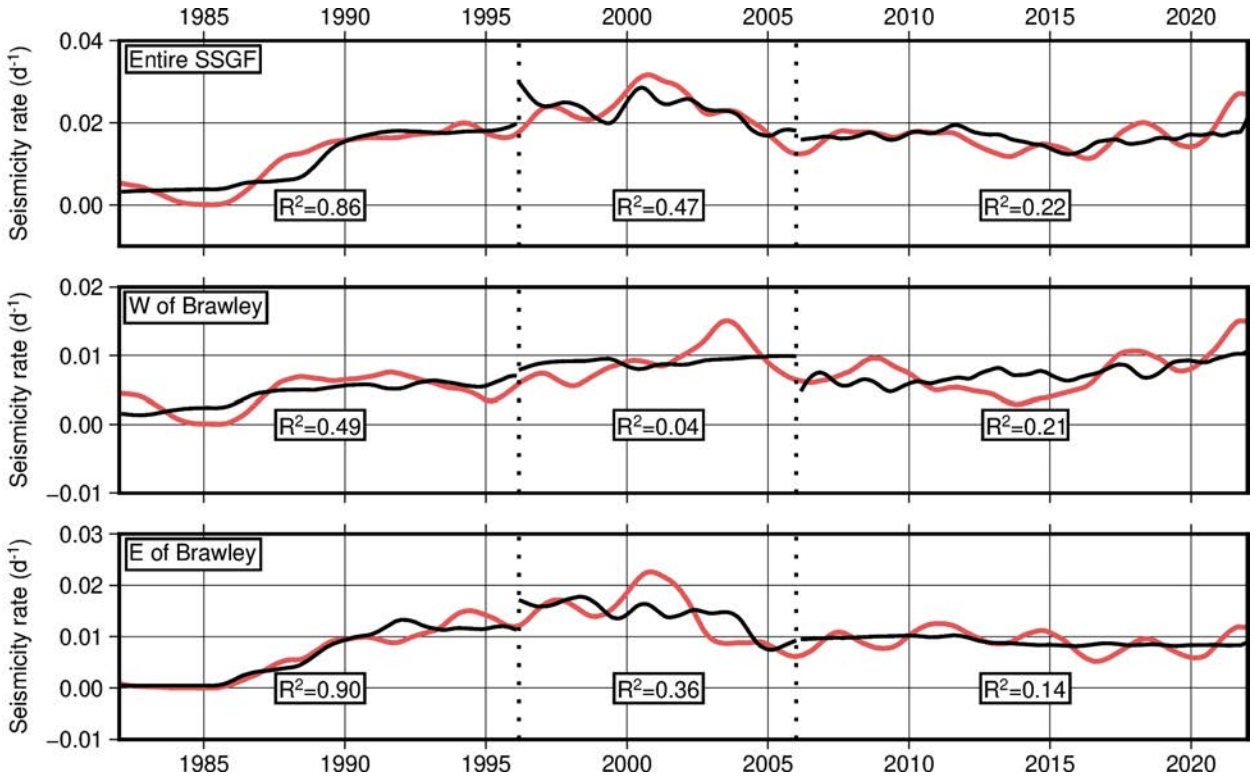

Figure 10.2. Background seismicity rate for a) the entire Focus Region, b) the region W of the Brawley Fault, and c) the region E of the Brawley Fault. Estimated from the Augmented Hauksson et al. (2012) catalog using the NND de-clustered catalog. Solid black curves show the piecewise-linear hindcast model. Dotted black lines represent discontinuities in the hindcast model. R^2 values quantify the correlation between the observed seismicity rate and hindcast model for each time period.

Figure 10.13 illustrates the causes of this increased seismic hazard. First, we see that the average number of events per year in the post-production period is greater than in the pre-production period. Note that this is technically different than the λ parameter in Equation (15) (Appendix Chapter 10), which represents the rate of background events (excluding foreshocks and aftershocks) but is similar in principle. Second, we see that the slope of the exponential distribution that models the frequency-magnitude distributions differs in a statistically significant way. To confirm this, we conduct a Welch's t-test to test the following null hypothesis H_0: "The mean magnitude of events in the pre-production period is less than or equal to the mean magnitude of events in the post-production period." Because the maximum likelihood estimation (MLE) for the slope of an exponential distribution is equal to the mean value of the variable being modeled, this test is equivalent to testing for a statistically significant difference in the slope of the two distributions. We reject the null hypothesis at the $\alpha = 0.05$ significance level (95% confidence). There is sufficient evidence to conclude that the b-value (the slope of the earthquake frequency-magnitude distribution and which indicates the probability of the smaller number of larger magnitude earthquakes.; Gutenberg and Richter, 1944) in the post-production period is less than in the pre-production period.

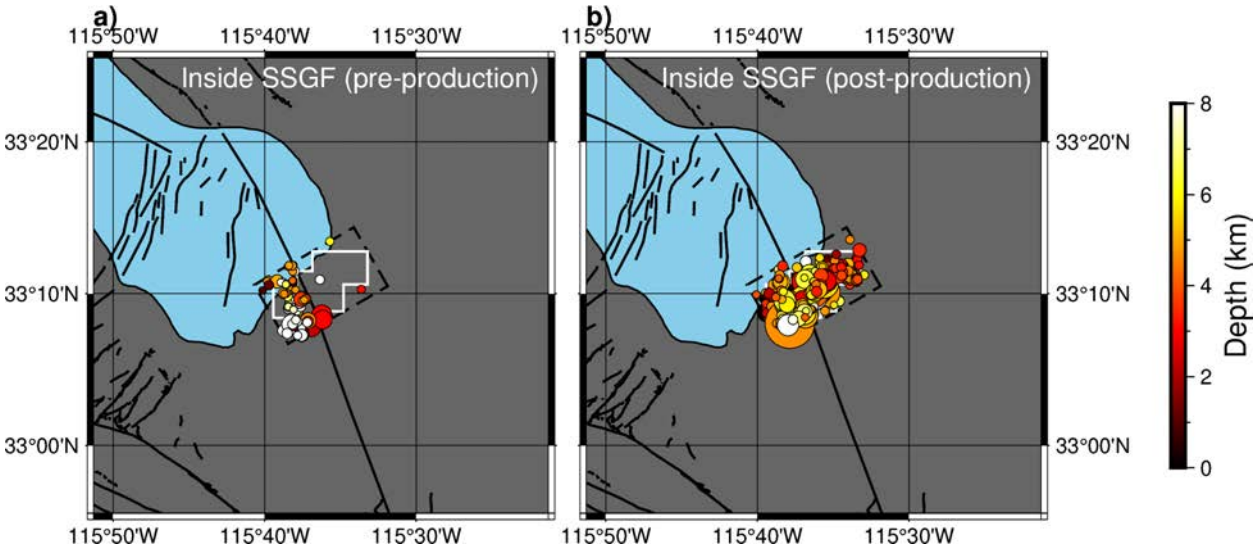

Figure 10.3. Seismicity inside the SS-GF (a) prior to and (b) following the onset of commercial energy production.

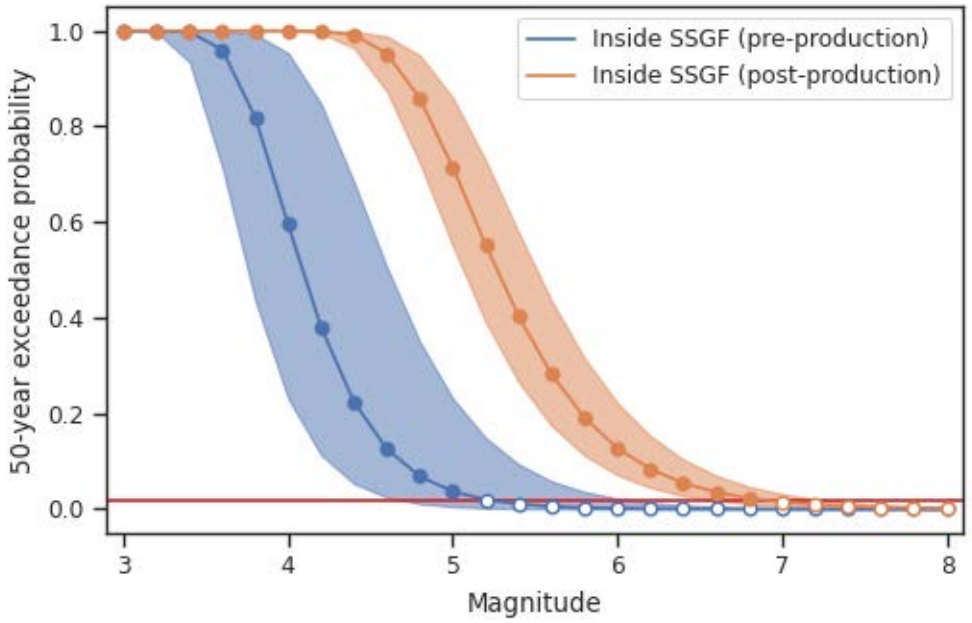

Figure 10.4. Probability of one or more events of a given magnitude occurring within a 50-year period inside the SS-GF during the pre-production (blue circles and curve) and post-production (orange circles and curve) periods. Shaded regions represent 95% confidence intervals. Horizontal red line represents 2% chance of occurrence.

The increased seismic hazard in the post-production period is thus a result of the increased seismicity rate and the relative proportion of large magnitude events in the post-production period. Taken in isolation, the results of this section are misleading as they suggest that energy production in the SS-GF has increased seismic hazard there in a potentially unnatural way. To appropriately contextualize these results, it is

important to compare seismic hazard within the SS-GF with that outside the SS-GF, which is done in the following sections.

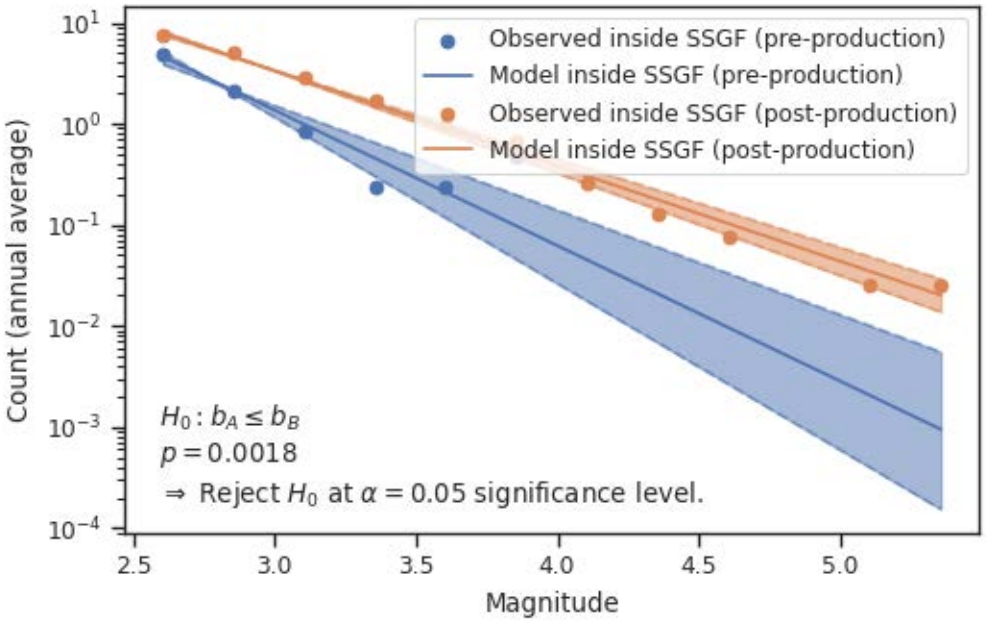

Figure 10.5. Observed frequency-magnitude distribution for seismicity within the SS-GF during the pre-production (blue circles) and post-production (orange circles) periods, respectively. Solid lines represent the best-fitting (in the maximum likelihood sense) exponential distributions for the observations. Dashed lines and shaded regions represent 95% confidence intervals.

Seismicity Inside Versus Outside the SS-GF in the Pre-production Period

In this subsection, we compare seismic hazard within the SS-GF with that outside the SS-GF in the pre-production period (Figure 10.14).

Repeating the analysis above for the two data sets shown in Figure 10.14, we observe similar features. Most notably, the seismic hazard within the SS-GF is significantly lower than outside the SS-GF (i.e., in the broader BSZ) during the pre-production period (Figure 10.15).

Figure 10.16 shows that the low seismic hazard in the SS-GF relative to the broader BSZ in the pre-production period is the result of the lower seismicity rate and the increased *b*-value.

Seismicity Inside Versus Outside the SS-GF in the Post-production Period

Next, we compare the seismic hazard within the SS-GF with that outside the SS-GF during the post-production period (Figure 10.17).

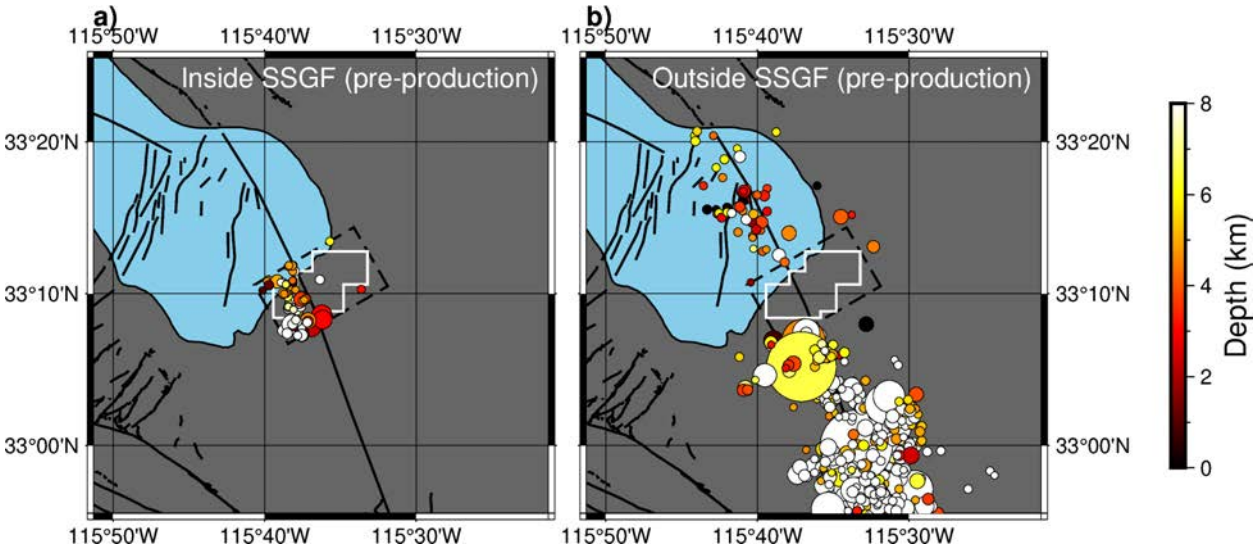

Figure 10.6. Seismicity for (a) inside and (b) outside the SS-GF during the pre-production period.

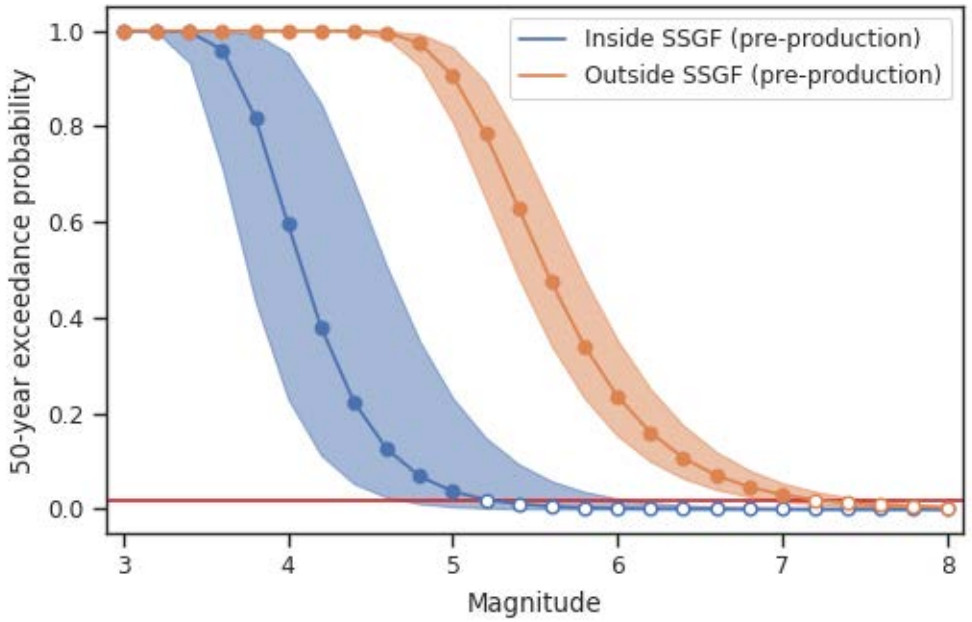

Figure 10.7. Probability of one or more events of a given magnitude occurring within a 50-year period for inside (blue circles, curve and shaded region) and outside (orange circles, curve, and shaded region) the SS-GF during the pre-production period.

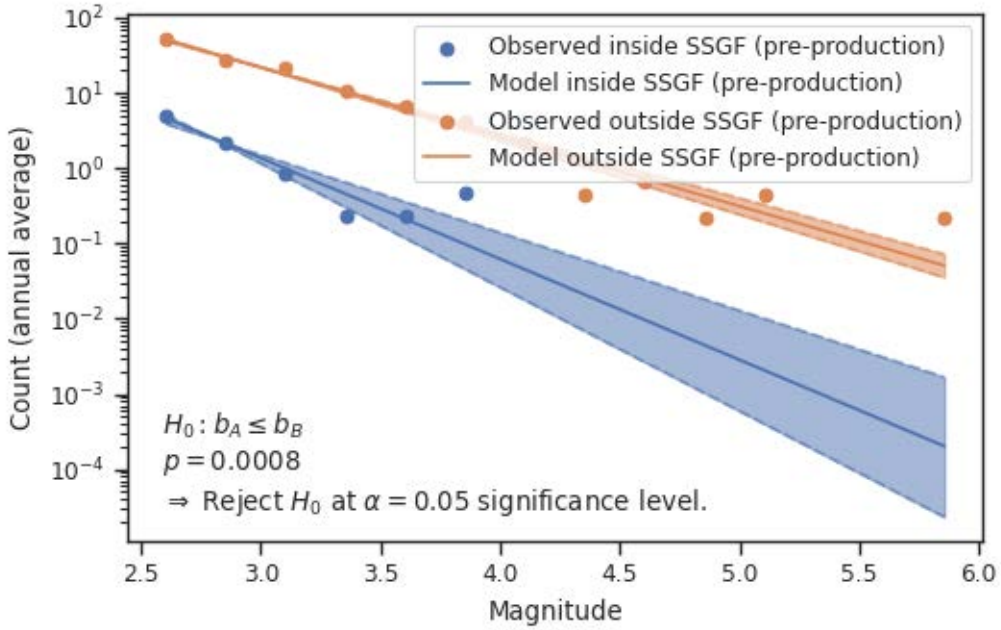

Figure 10.8. Observed frequency-magnitude distribution for inside (blue circles, curve and shaded region) and outside (orange circles, curve, and shaded region) the SS-GF during the pre-production period.

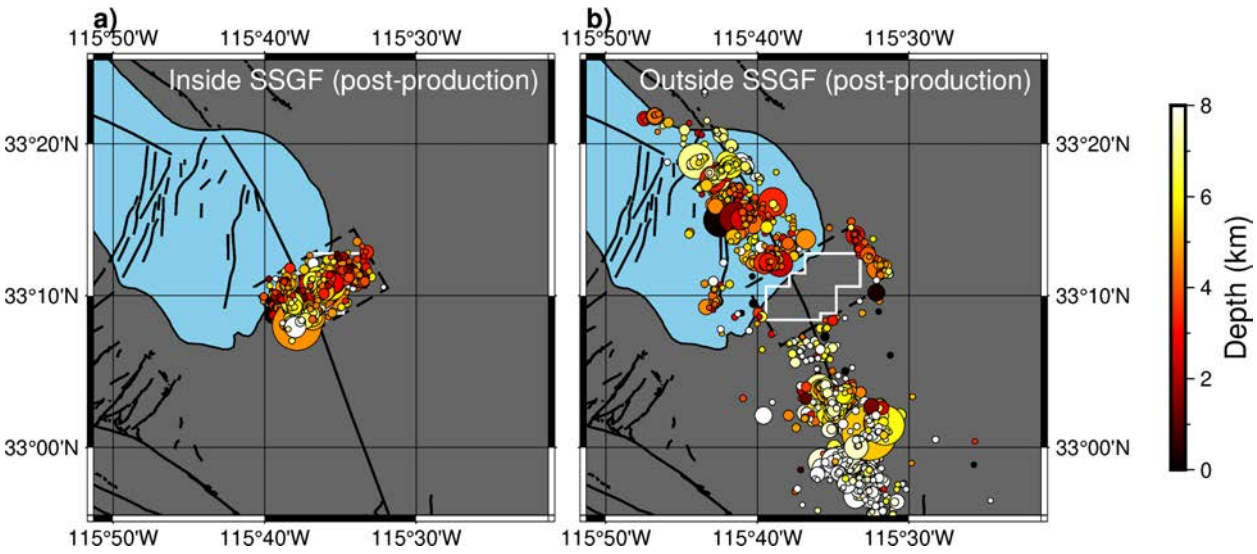

Figure 10.17. Seismicity for (a) inside and (b) outside the SS-GF during the post-production period.

The seismic hazard inside the SS-GF is slightly increased above that outside the SS-GF (Figure 10.18). This slight increase is due almost entirely to the slightly greater seismicity rate inside the SS-GF. We fail to reject the null hypothesis that the *b*-values (which indicates the probability of the smaller number of larger magnitude earthquakes) for the two data sets are different which means that they are not different in a statistically significant way at the 95% confidence level.

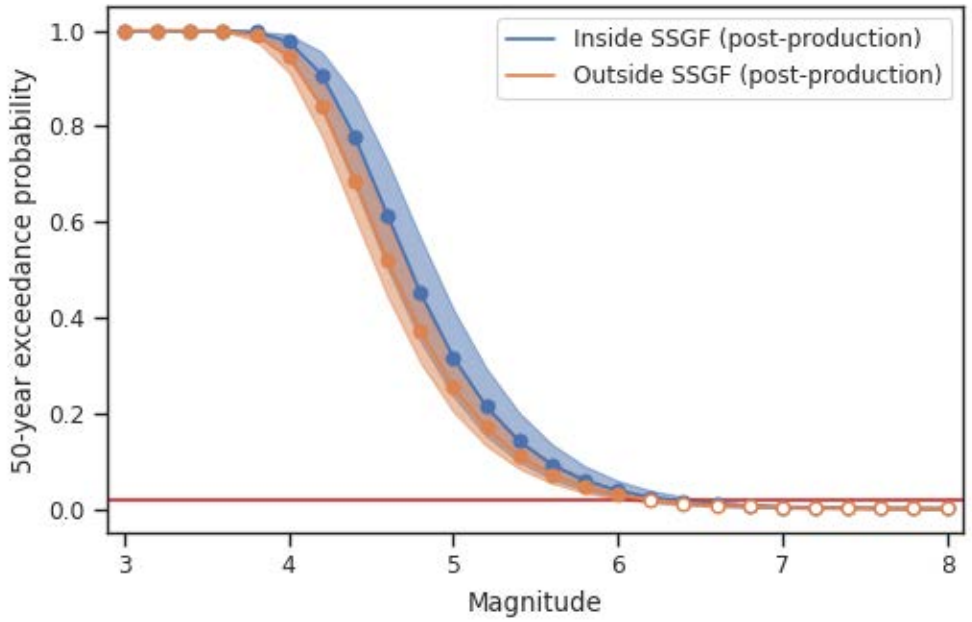

Figure 10.9. Probability of one or more events of a given magnitude occurring within a 50-year period for inside (blue circles, curve and shaded region) and outside (orange circles, curve, and shaded region) the SS-GF during the post-production period.

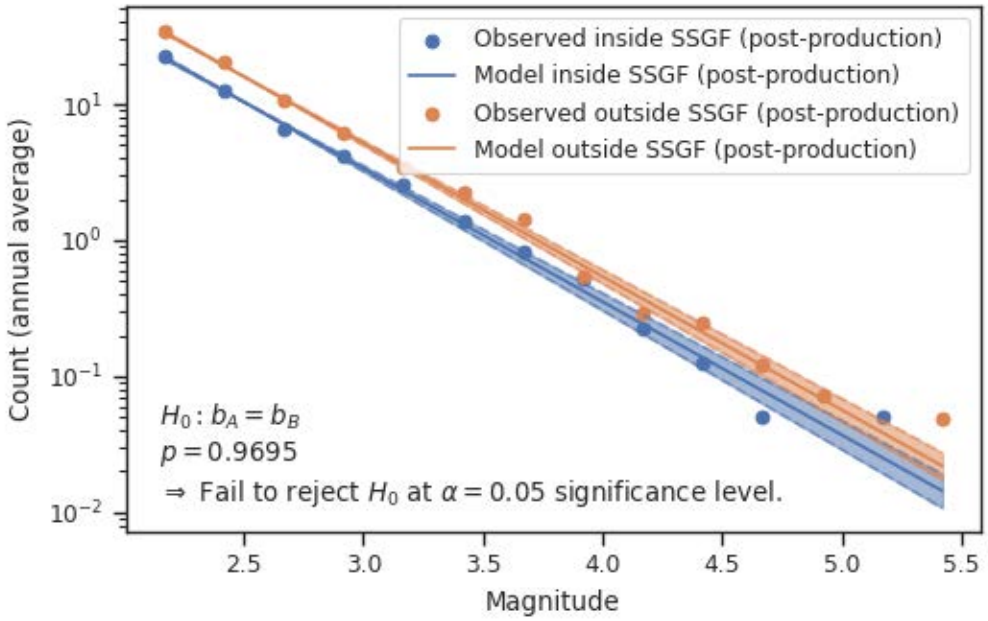

Figure 10.19. Observed frequency-magnitude distribution for inside (blue circles, curve and shaded region) and outside (orange circles, curve, and shaded region) the SS-GF during the post-production period.

Seismicity in the Entire BSZ Before and After Production Onset

Finally, we investigate the impact of energy production within the SS-GF on the seismic hazard of the entire BSZ by comparing hazard in the BSZ in the pre-production period with the post-production period (Figure 10.20).

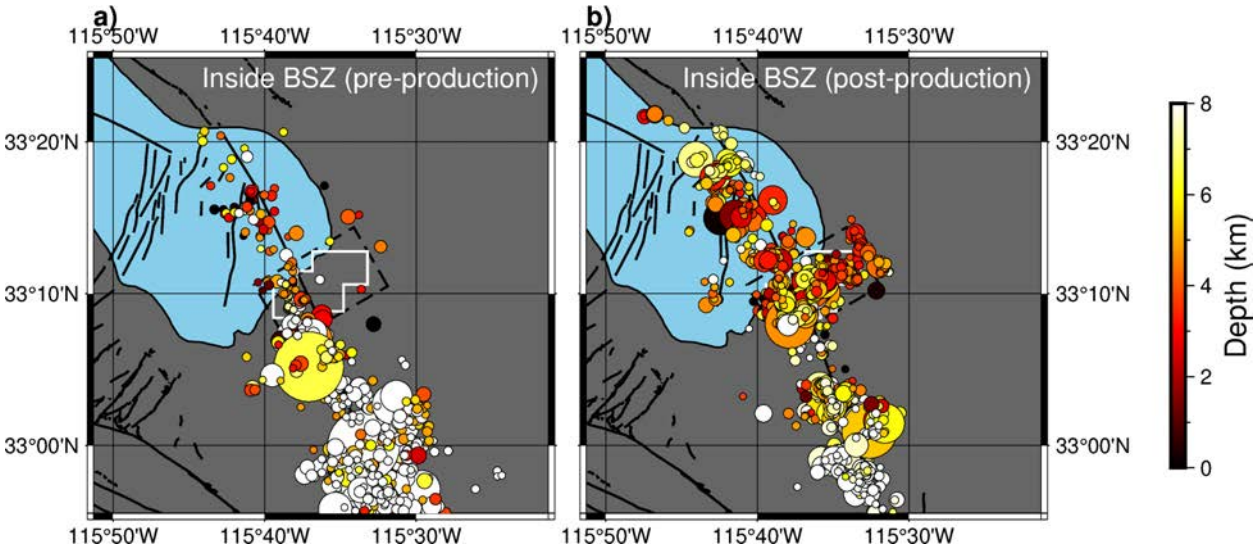

Figure 10.10. Seismicity for the entire BSZ during the (a) pre-production and (b) post-production periods.

Interestingly, we observe that the seismic hazard slightly decreases in the post-production period (Figure 10.21). This is due to the overall decrease in seismicity rate and increase in *b*-value during the post-production period (Figure 10.22).

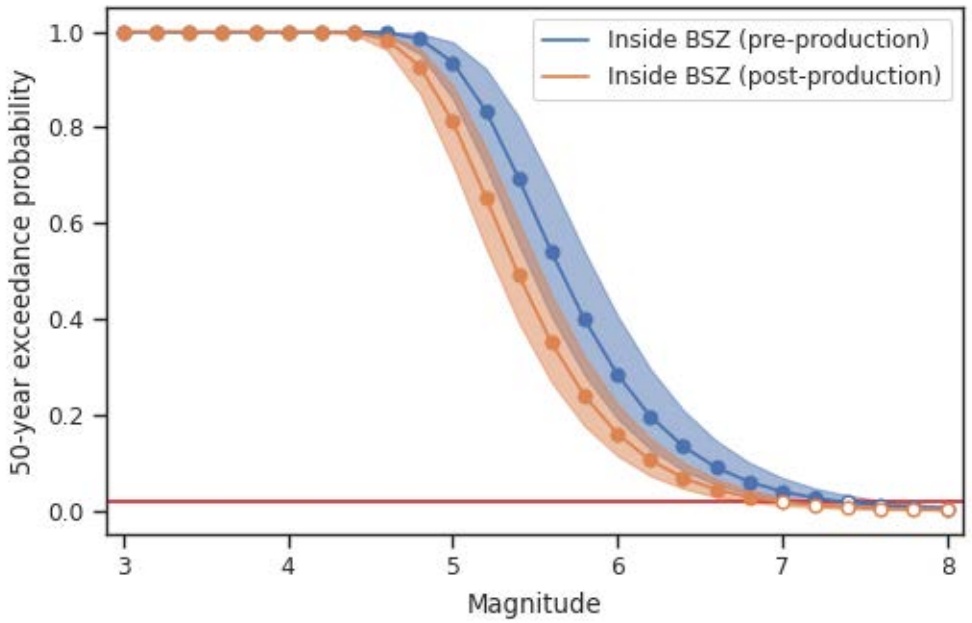

Figure 10.11. Probability of one or more events of a given magnitude occurring within a 50-year period for the entire BSZ during the pre-production (blue circles, curve and shaded region) and post-production (orange circles, curve, and shaded region) periods.

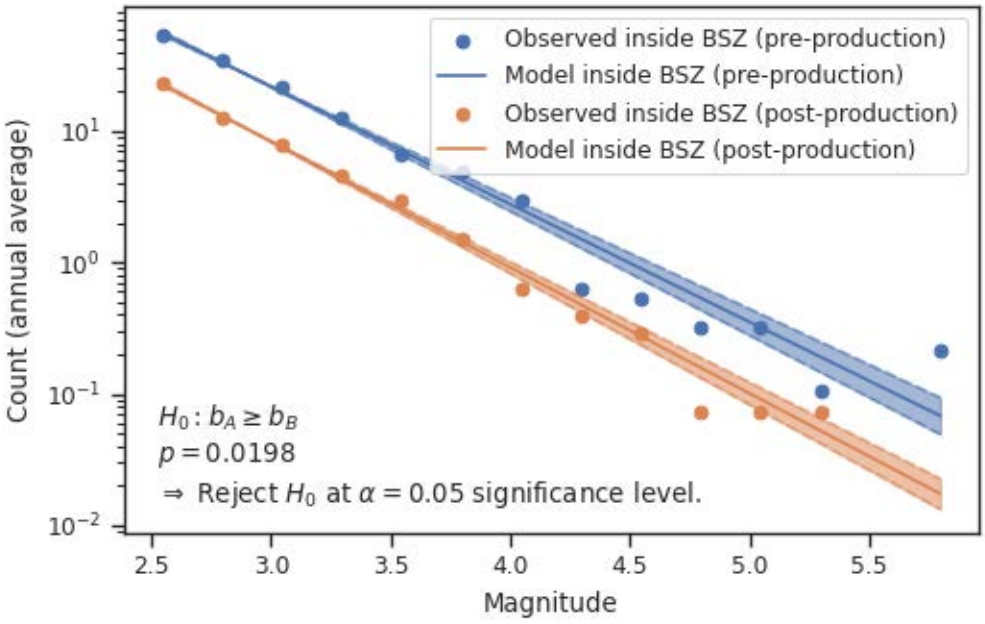

Figure 10.12. Observed frequency-magnitude distribution for the entire BSZ during the pre-production (blue circles, curve and shaded region) and post-production (orange circles, curve, and shaded region) periods.

Summary and Recommendations

We analyze the relationship between geothermal energy production and seismicity in the SS-GF between 1972 and 2022. The seismicity ratio increased in this period. A simple linear relationship of proportionality between energy production and seismicity exists for the first 14 years of production (until 1996), but not thereafter. The increase in seismic activity associated with energy production is greatest to the east of the Brawley fault, where the amount of injection exceeds the amount of production. Interestingly, the SS-GF appears seismically quiescent (i.e., exhibits relatively low seismicity) relative to the surrounding region prior to energy production. Energy production in the SS-GF correlates with an increase of seismic hazards within the field – not beyond that of the broader tectonic regime, but rather from a quiescent state to a state statistically the same as the broader regional tectonic conditions. The detailed subsurface response to the expected increase in injection and production is still unclear, and further study is needed to forecast the seismicity ratio and magnitude.

SECTION FOUR:
Community Outreach

Chapter 11: Community Engagement

Key Takeaways

- To make the information from this report more accessible to community members, we developed a Frequently Asked Questions (FAQ) document and held in-person Q&A sessions with community members in Niland and students at Imperial Valley College.
- To address community concerns, we recommend transparent monitoring of the air emissions and water consumption from geothermal and lithium extraction facilities, continued attention to the impact on local seismicity, and further research to help identify strategies to minimize waste streams.
- Future research teams could incorporate more community participation by establishing a community advisory board to maintain ongoing dialogue, hiring local project interns and team members, and/or formally partnering with a community organization with shared decision-making power and clearly defined roles and responsibilities for each party established before the project starts.
- Communities near the Salton Sea Geothermal Field (SS-GF) are engaged and highly motivated to participate when opportunities are accessible to them. Several community engagement initiatives related to Lithium Valley development, led by community-based organizations, the local government, and the companies themselves, are ongoing.

Introduction

"Lithium Valley" represents an effort to develop a supply chain that will benefit the local community and minimize environmental impacts. Researchers at academic institutions and National Laboratories can play an important role by providing transparent, third-party information that not only addresses environmental concerns, but also empowers local stakeholders to participate in decision-making processes. Doing so requires that researchers incorporate more community engagement (CE) than is typical for most technical projects so they can address issues that are a high priority for local communities, share information effectively, and learn from local stakeholders who have expertise and knowledge about the area. This chapter introduces our efforts to incorporate CE in our assessment of geothermal lithium resources in the Salton Sea region.

The overarching objectives of our CE efforts were threefold:

1. To make sure that information generated by the research team addresses questions that are relevant to frontline communities and is accessibly communicated.
2. To gather input from local stakeholders about how to improve and incorporate community engagement in future research efforts.
3. To contextualize lithium and geothermal energy production within the broader history and socioenvironmental conditions of the region.

In what follows, we provide more background on community-engaged research methods and describe how we sought to make our research more accessible by creating a Frequently Asked Questions document and hosting in-person outreach events. We summarize community feedback about these events and identify community-informed areas for future study. Finally, we discuss our lessons learned from this process, and provide recommendations about incorporating CE in future research efforts. This study was informed by visits to the Salton Sea region, conversations with environmental justice organizers, observation of public meetings, and review of relevant literature about the Salton Sea and community-engaged research.

Background on Community-engaged Research

Community engagement (CE) in research is not new; it has been practiced in the field of public health for decades, ever since practitioners recognized a critical need for more equitable partnerships between researchers and communities (Key et al., 2019). However, incorporating CE is not typical for technical reports in disciplines like geology or energy. In these fields, "outreach" is generally limited to presentations at academic conferences or institutional press releases that simplify the results of a study after research has concluded. Nonetheless, such a departure is necessary to respond to recommendations from environmental justice scholarship, which calls for context-specific climate solutions that integrate the perspectives of grassroots and community advocates (Elmallah et al., 2022). It is also consistent with recommendations from the field of science communication, where practitioners have called for models of communicating that are tailored to specific audiences and encourage two-way dialogue (Bielak et al., 2008).

Community-engaged research is most well-developed in the field of public health. Community-based participatory research (CBPR) is generally considered the "gold standard" or best practice for CE (Hacker, 2013). In CBPR, community organizations are equal partners throughout the research process, helping to determine research questions and objectives, collect and analyze data, and disseminate findings. CBPR is action-oriented, seeking to generate information that will be directly used to improve community health and well-being. CBPR requires a high degree of trust and transparency, which in turn requires time and resources. However, it is also associated with higher quality research outcomes. When practiced well, CBPR can enable a richer understanding of the phenomenon being studied as researchers learn from the community's insight and experience, improve data collection and analysis, and make the research more relevant and accessible to community stakeholders (Viswanathan et al., 2004).

However, CBPR is not the only way to incorporate CE in research. Practitioners have proposed a continuum of CE in research (Figure 11.1) spanning from "no community involvement" to "community-led" (Key et al., 2019). Scientific research has historically fallen on the left-hand end of the spectrum, where the community is not included in any aspects of the research and the researcher works independently of the community.

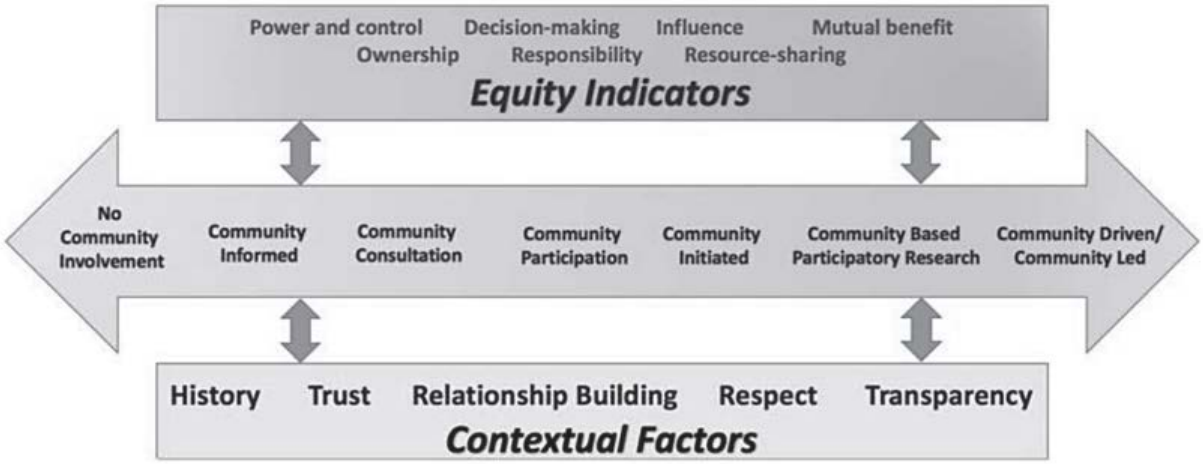

Figure 11.1. Continuum of Community Engagement in Research, taken from Key et al. (2019).

The work described in this chapter most closely matches the description of community consultation, where "the community provides input and feedback to researchers to inform the research," and the researcher "consults with the community and includes the community in the research (front end or back end)." CBPR was not possible in this project, primarily because the goals and scope of the research had already been determined before community engagement was added to the project.

Frequently Asked Questions

The topics investigated by this project are important to community stakeholders and have been brought up repeatedly in various public forums. However, if the information is only shared as a technical report, it is likely to be inaccessible to most people. To make it easier for stakeholders to find answers to their questions, we have developed a Frequently Asked Questions (FAQ) resource as well as a photo and video StoryMap as a companion document to the report (*What are ArcGIS StoryMaps?*, 2019). The California Energy Commission (CEC) also created a Lithium Valley Fact Sheet (CEC, 2022), but that document mainly focuses on the role of lithium in the clean energy transition and the benefits of direct lithium extraction (DLE), whereas our scope includes the process, resource potential, and environmental impact associated with introducing lithium extraction to the Salton Sea region.

The FAQ is an extension of previous efforts to understand local questions and priorities through analysis of Lithium Valley Commission (LVC) meeting transcripts, observation of community town hall meetings, and consultation with community-based organizations (CBOs). That analysis and results are described in greater detail in Slattery et al. (2023), which identified the following topics as high-priority research areas:

- Water, including the source of process water, quantity of water consumed, and impact to water quality and availability for surrounding communities
- Local air emissions and impact on air quality for surrounding communities, particularly given existing public health challenges
- Byproducts and waste management
- Evaluating local employment and benefit to local communities

- Evaluating decision-making processes and barriers to participation
- Induced seismicity and potential impact on active faults.

We built upon the analysis referenced above by reviewing public comments submitted to the LVC docket, soliciting additional input from representatives of CBOs, and adding questions gathered by the research team during presentations and site visits. In total, we recorded 112 questions, which we synthesized and organized into a final FAQ list (Table 11.1). During this process, we also gathered comments about communication and outreach that informed our strategy and recommendations.

As mentioned in the Introduction to this chapter, several important questions were outside the scope of this study. This was either because they were outside our team's area of expertise, further analysis is required to build on this study, or the industry is not advanced enough for the information to be available. A section of the FAQ is dedicated to topics that fall outside the scope of this project, explaining why they are not addressed and/or pointing to other resources.

Some of stakeholders' most critical questions relate to public health. Will lithium extraction or geothermal power expansion impact public health? How will public health be monitored and protected? Can revenue from lithium extraction be used to address public health crises? While our study compiled important data about emissions and waste streams that can inform future study about public health impacts, further research involving public health experts would be necessary to definitively answer those and similar questions. Another area that falls outside our scope relates to the benefits and socioeconomic impacts of a new industry. For instance, stakeholders often ask how the community will benefit, how tax revenue will be invested, what infrastructure will be provided, and how members of the public can participate in shaping the outcome of the development. These questions are essential to consider from an environmental justice perspective and are better directed towards local government and advocacy organizations.

The full FAQ document is currently under review to gain feedback from DOE and industry and community stakeholders. Once completed, it will also be translated into Spanish and distributed to local organizations, government agencies, and residents who have indicated interest in receiving newly available information from the research team. Many of our local contacts were established through the community workshop described in the next section.

Outreach Events

As a first step towards connecting the research team with local communities near the Salton Sea Geothermal Field (SS-GF), we conducted an outreach visit in May 2023, shortly before this report's scheduled completion. Members of the research team toured the Hudson Ranch Power Plant, held a community workshop in Niland, and spoke with students at Imperial Valley College (IVC). These events and the feedback we received are described in detail below.

Table 11.1. FAQ list

Category	Question
Background	● What is lithium? ● Where are lithium deposits located, and why are they there? ● What is geothermal energy?
About Direct Lithium Extraction	● How is lithium extracted from the brine? ● Can other minerals be extracted from the brine? ● How much lithium can sustainably be extracted from the geothermal field? ● How long will the resource last? Does the lithium recharge over time? ● What happens after the lithium is extracted? ● I have heard people talk about Lithium Valley becoming a "Battery Supply Hub." What does that mean?
Water Use	● Where will geothermal/lithium facilities get water from? ● Will the facilities take water from communities around the lake or impact their water quality? How will community water be protected? ● How much water does geothermal and lithium production consume? ● How does that compare to other ways of producing lithium? ● Why do they need to consume water? Where in the process is water consumed? ● Will the companies recycle water? ● Is the supply of water enough to meet demand for the industry? ● Will DLE use water from the Salton Sea or affect Salton Sea water levels?
Environmental Impacts	● What are the air emissions from geothermal and lithium extraction? What is in the vapor that we see near the power plants today? ● What are the byproducts? ● How will waste be managed? ● Will lithium extraction impact soil and water quality? ● What are the impacts of extracting and reinjecting brine? ● Will geothermal or lithium extraction affect the San Andreas Fault? ● What chemicals are used? ● Are facilities safe for workers? ● How do you study environmental impacts if it's a new process? ● Are there long-term concerns about geothermal DLE? ● What measures are in place to protect the environment and local communities?
Outside scope	● Public health ● Workforce development ● How revenue will be invested ● Infrastructure ● Salton Sea restoration ● Who pays for impacts and/or mitigation? ● Public participation in Lithium Valley Commission and Imperial County planning processes

Outreach Event 1: Community Workshop

The Community Workshop was held at Grace Smith Elementary School in Niland, California on May 15, 2023. Prior to the event, we solicited feedback about timing, location, and outreach from a Calipatria City Council member and an environmental justice practitioner at a local CBO. We also attempted to

incorporate feedback that members of the public and CBOs had shared about the Lithium Valley Commission's outreach efforts. The goals of this workshop were to:

1. Share information about geothermal energy and direct lithium extraction (DLE) with people who live in nearby communities.
2. Provide a comfortable space for people to ask questions.
3. Allow researchers to better understand the area they are studying and see facilities for themselves.
4. Receive feedback from community members about our research and outreach efforts.

Workshop Format and Logistics: We selected Niland as the location because it is the closest community to the geothermal facilities. The event was held at Grace Smith Elementary School, which has been selected for events hosted by the California Energy Commission and Comité Cívico del Valle, an important local CBO. It was scheduled from 6:00-8:00 pm, which a local EJ practitioner suggested as the optimal time slot for hosting public meetings since many people cannot attend meetings during the day. Because the event was held during dinnertime, we provided food from a local restaurant ("El Jumping Bean" in Brawley, California). Serving food was also intended to create a more comfortable atmosphere.

Figure 11.2. Research team members (P. Dobson, M. Slattery) speak with residents at the May 15 workshop in Niland, CA.

To publicize the event, we created two flyers, one in English and one in Spanish, which we distributed via email to representatives from CBOs, local government, and lithium and geothermal companies (Appendix Chapter 11). Flyers included a registration link which asked for contact information, how people learned about the event, what they hoped to learn from the workshop, whether they would require translation, and whether they had any dietary restrictions. The flyer for Spanish-speaking community members linked to an equivalent form in Spanish.

The event format consisted of a brief introduction and overview of lithium and geothermal power, followed by small group discussions to give people time to generate questions. At this time, some members of the research team went around to tables to introduce themselves, engage with participants, and note questions and comments. After 15 minutes, the facilitator brought everyone back into one conversation and called on different tables to ask questions. The team had prepared slides with anticipated FAQ responses and used these when appropriate.

During the last 15 minutes, we asked participants to share feedback they had about the event. Finally, we distributed a survey to gauge meeting effectiveness and gather additional feedback. Copies of outreach flyers, printed meeting materials, and surveys are available in Appendix Chapter 11.

We also had pictures and samples of the geothermal brine, spodumene ore, and lithium chloride solution that we passed around (Figure 11.2). This was an effective tool to demystify lithium and illustrate the process in a way that was easier for people to imagine. The samples were mainly provided by EnergySource Minerals, highlighting the importance of industry collaboration.

The purpose of structuring the workshop in this way was to foster two-way dialogue and create an opportunity for attendees to network with each other. We also prepared to address a variety of questions and let the participants dictate what we focused on, rather than delivering one long presentation that risked overwhelming participants with too much information at once. This was based on feedback that had been shared about other lithium-related presentations that were too dense and did not allow enough time for community participation. There were pros and cons to our approach; overall, the meeting was engaging and conversational, but it also may have made the delivery of information less cohesive. The formats of the workshop and survey were informed by science communication articles about different types of information-sharing activities and methods of evaluating effectiveness (Illingworth, 2017; Spicer, 2017).

Workshop Registration and Attendance: Seventeen people registered for the workshop in advance, and 48 attended. As such, the turnout was substantially larger than expected, which demonstrates that residents have great interest in this topic and want to be involved, and that online registration numbers should not be taken as the only indicator for logistics and planning purposes. Participants started arriving about 20 minutes before the event was scheduled to start, and none left before the event concluded.

The majority of attendees were residents of Imperial County, as well as representatives from CBOs, geothermal and lithium companies, and local governments. The organizations and communities represented include the following:

- NorthEnd Alliance 111
- Bombay Beach Community Service District
- Imperial Valley Equity and Justice Coalition
- Calipatria Chamber of Commerce
- Comité Cívico del Valle
- Alianza Coachella Valley
- California Farmworker Foundation
- Fountain of Youth RV Park
- Los Amigos de la Comunidad
- Calipatria Chamber of Commerce
- County of Imperial
- BHE Renewables
- EnergySource Minerals
- Controlled Thermal Resources

According to the survey, attendees learned about the workshop through social media, posted flyers, word of mouth, as well as through community organizations and emails from organizers. We communicated with the Mayor of Calipatria, Maria Nava-Froelich, during the organizing process, and she posted the flyer to Facebook; the NorthEnd Alliance 111 also printed flyers and distributed them in Niland and Calipatria. Without their efforts, we likely would have had a very low turnout. This again demonstrates

the community's level of engagement with the topic and the importance of local partnerships. Several community advocates and organizations expressed interest in collaborating to host additional workshops in other nearby communities, and future outreach efforts should build on these relationships to coordinate in the future.

We had planned to provide simultaneous interpretation in Spanish during the event; but ended up canceling the service because of the relatively low number of people who registered in advance, none of whom required Spanish translation. Three members of the research team speak Spanish, and one is a native speaker; as such, we reasoned that translation could be provided to a small number of people if needed. All printed materials were still provided in English and Spanish. In the end, no one at the event required Spanish translation. Given the large number of attendees who did not register in advance, it may be advisable to include interpretation in future events regardless of registration data and incorporate it into workshop design so that language is not a barrier to participation.

Workshop Survey Results – Community Perspectives on Geothermal and Lithium: In the surveys, we asked participants whether they thought expanded geothermal production and lithium extraction would have a positive impact on the local community (Figure 11.3), and what they considered to be the most important potential benefits of geothermal lithium extraction (Figure 11.4). The list of potential benefits was based on topics that had been mentioned during public forums, expert presentations, and literature review about the social impacts of mining for other commodities (Mancini and Sala, 2018). We also asked participants to rate their level of concern about the environmental impact of geothermal energy production and lithium extraction (Figure 11.5).

The majority of respondents either agreed or strongly agreed that lithium and expanded geothermal energy production would have a positive impact on the local community, with slightly higher scores for geothermal compared to lithium extraction (Figure 11.3). On a scale of 1-5 (1= strongly disagree, 5= strongly agree), the mean scores for geothermal were a 3.9 and 4.0 (pre/post), and 3.7 and 4.0 for lithium extraction. It should be noted that fewer people filled out a post-meeting survey (n= 25 vs. n=29). The highest-ranked benefit was creating jobs in the region (n=17), followed by providing a more environmentally friendly source of lithium (n=14) (Figure 11.4). Four respondents chose "other," adding "investment in infrastructure" as a text entry.

At the same time, more than half of the group indicated they are at least somewhat concerned about the environmental impacts of geothermal and lithium extraction (Figure 11.5). The average score was a 3.2 and 3.3 for geothermal (1= not at all concerned, 5= extremely concerned), and a 3.3 for lithium extraction in both pre- and post-workshop surveys. Compared to the responses about potential benefits, there was a smaller change in pre- and post-workshop responses. However, this question had a lower response rate overall (n=26 pre-survey, n=23 post-survey).

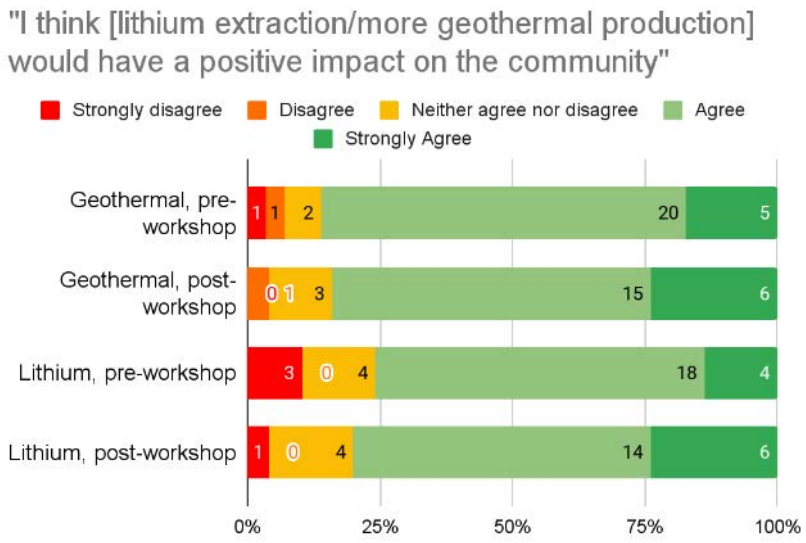

Figure 11.3. Respondents were asked to rate to what extent they agreed with statements that lithium extraction and more geothermal energy production would have a positive impact on the community.

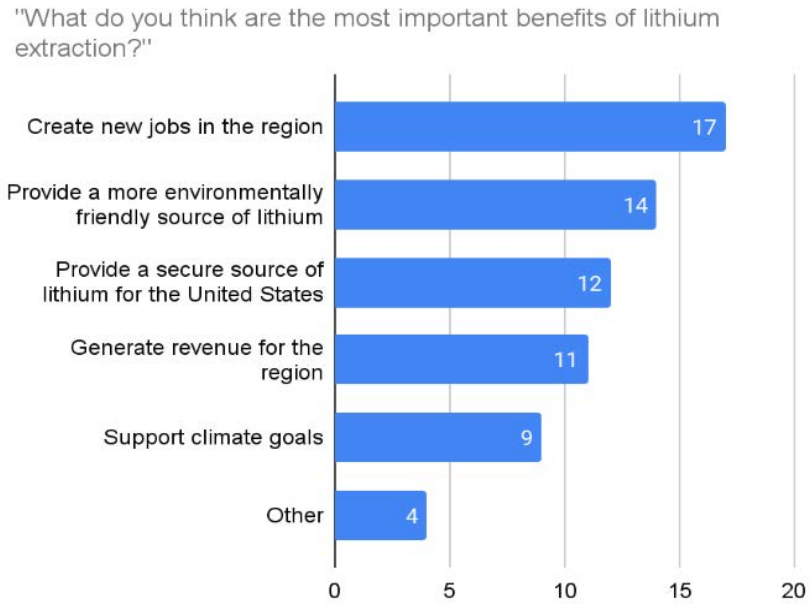

Figure 11.4. How participants prioritized potential benefits of lithium extraction. All four respondents who selected "other" further specified "investment in infrastructure" as a text entry.

These results suggest that just because people think a new or expanded industry would be a positive development, it does not mean they are not concerned about the environmental impact (and vice versa). This is just one subset of the community and further outreach efforts are needed, both to share information more broadly and better understand diverse community perspectives. However, these results are consistent with the sentiments and questions asked by IVC students, who expressed both interest in potential opportunities and concern about safety and the environment, as discussed later in this chapter.

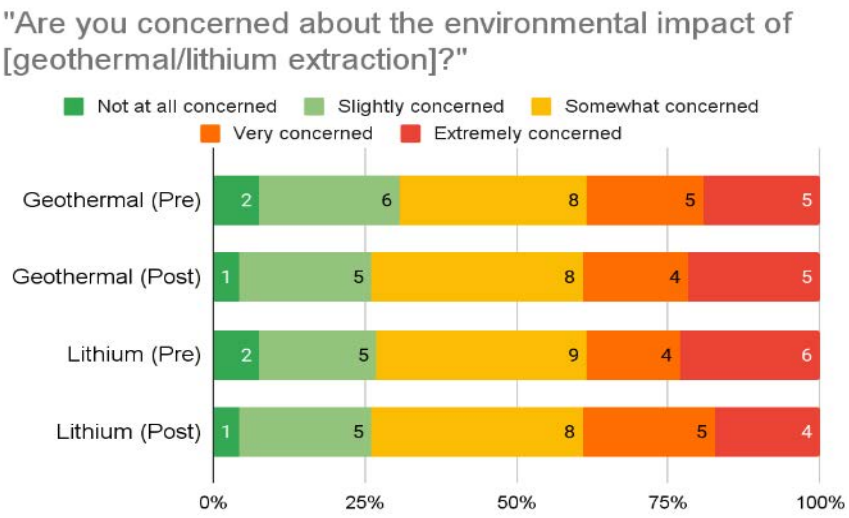

Figure 11.5. Survey results indicating respondents' level of concern about the environmental impacts of geothermal and lithium production pre- and post-workshop.

The questions we received during the workshop were generally consistent with the FAQ list. The questions within our team's scope included how much water would be used, what the air emissions are, what waste is generated by the process, and whether geothermal or lithium production would impact seismicity in the area. We were also asked how we had engaged with the community to inform our results. The sustainability of resource extraction is a high-priority topic, both in terms of what it means for the community to be investing in a finite industry, as well as from a broader societal perspective. For several groups at the workshop, one of the most important questions was how long the resource would last, and what would happen once it had been exhausted. People also asked about recycling, with questions ranging from whether electric vehicle (EV) batteries are recyclable, to why recycling infrastructure isn't being developed near the Salton Sea to source lithium more sustainably.

"How will the community benefit?" is a very common question that is consistently brought up at lithium-related community meetings, including our workshop. People also asked specific questions about how revenue will be invested, what jobs will be available, and what training will be provided to local residents. One survey respondent said they wished we talked more about community benefits agreements. During the workshop, we clarified that these questions did not fall inside our area of expertise, and instead pointed to efforts by the county and Comité Cívico del Valle regarding the lithium excise tax and the certificate programs being developed at IVC. The county supervisor, Ryan Kelley, attended the event and was able to speak to the county's efforts directly. For future outreach efforts, it would be valuable to collaborate with local government and organizations who can speak to a wide variety of issues.

Workshop Survey Results – Community Workshop Feedback: Overall, the workshop was received positively. On a scale of 1-10, survey participants (n=24) rated the overall effectiveness of the workshop at an 8 on average, and everyone who responded to the survey said they would attend similar events in the future. On average, respondents also indicated that they thought the content of the workshop was interesting and easy to understand (Figure 11.6).

To help gauge the effectiveness of the presentation and Q&A session, we asked respondents to rate their understanding of geothermal energy and lithium extraction on a scale of 1-5 before and after the workshop (1= I have never heard of it, 5= I am an expert). While it is a small sample size (n=24), the results indicate an overall improvement in perceived understanding, from 3.0 to 3.7 on average for geothermal, and 2.6 to 3.4 for lithium extraction (Figure 11.7).

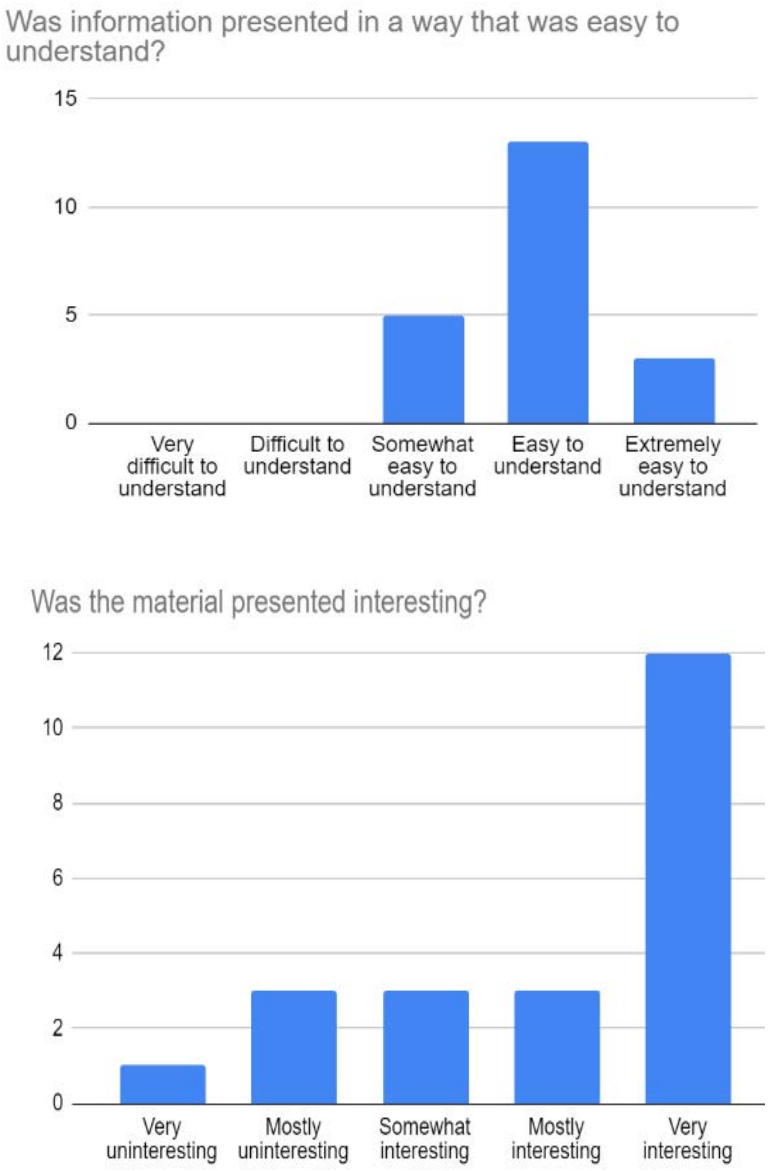

Figure 11.6. Participant feedback about the content of the community workshop.

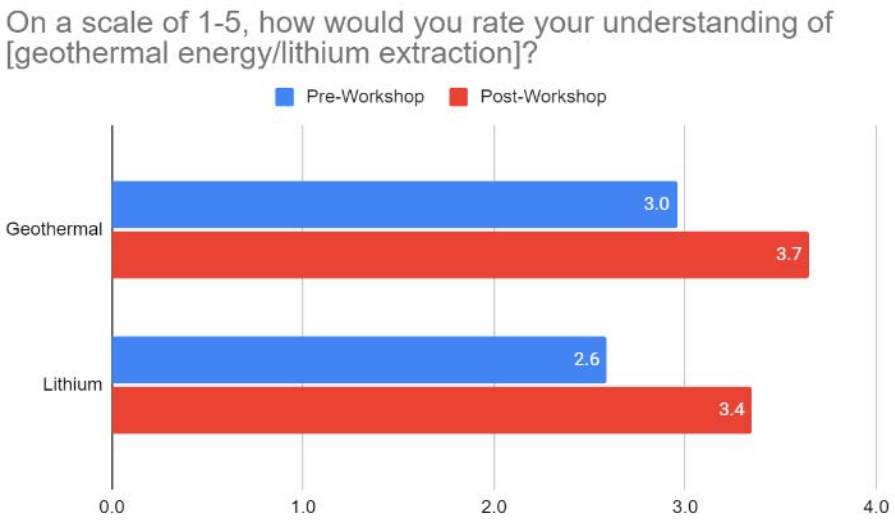

Figure 11.7. Participants' self-assessed level of understanding about geothermal energy and lithium extraction.

Finally, we asked if there were topics people wished we had discussed more or less, if they had questions that had not been addressed, and for general feedback for the research team. No one indicated wishing we had talked less about anything; however, there were a variety of suggestions about how the event could be improved, and areas where people still wanted to learn more (Table 11.2). The most common areas that people wanted to learn more about were (1) details about how the geothermal and DLE process works, and (2) more information about the resource. There were also requests for additional information about environmental impacts and community benefit. In terms of feedback about the workshop, attendees suggested that we should host more workshops in the surrounding communities and online for people who had not been able to attend. For future workshops, participants suggested that we coordinate with Imperial County and companies to provide more information about jobs, and that we explain the research project in more detail. There were also basic suggestions for improvement regarding accessibility; for instance, passing around the microphone and securing a larger projector screen.

Table 11.2: Summary of event feedback and topics where participants had remaining questions or wanted further discussion.

Requests for information	Feedback
• More about environmental impacts • More about how the process works • More about the resource: what is the status, when will production start, how much lithium is there, how long will the resource last • More about jobs and community benefits • More data on water waste	• Host additional workshops in other communities and online • Coordinate with Imperial County • Familiarize ourselves with the history of Imperial County • Pass around microphone • Have companies discuss jobs • Spend more time explaining the project and our background

We received critical feedback as well, as the workshop was perceived by at least one CBO representative as an instance of outsiders "parachuting in." We consulted with staff from this organization to seek input

about the event prior to organizing, but it is true that we hosted the event without partnering with a local organization. Our intention was to avoid placing an administrative burden on local organizations, as we considered it our responsibility to make the research more accessible. However, this approach had several disadvantages and should be avoided in the future – particularly because the last thing we want is to conduct our work in a way that could be perceived as erasing CBOs from the conversation. In addition, there are several tasks related to outreach, workshop design, and logistics that would be performed better with a local collaborator, which in turn would facilitate a more successful event.

We also received criticism that it had taken too long for us to host an event of this type. This may indicate a downside of the listening-based approach described earlier (Slattery et al., 2023). Our intention in attending and observing other groups' meetings was to hear local perspectives without placing additional burden on local stakeholders or organizations. However, this was largely an effort by one member of our team and does not seem to have built the community's sense of institutional trust or familiarity. This may also indicate a disadvantage of dedicating one person to community engagement rather than integrating it more fully into the project and involving more team members throughout.

Inevitably, getting the timing right for Q&A or workshop-based events is a difficult balance to strike, since there are limitations on how much information is available or ready to be shared. Ongoing communication and engagement are vital so that research teams can build trust and familiarity, receive ongoing feedback, and share information as it becomes available.

Outreach Event 2: Imperial Valley College Campus Visit

Imperial Valley College (IVC) is a two-year college located in El Centro that serves approximately 11,000 students per year, the majority of whom come from local high schools (Office of Institutional Effectiveness, 2021). In April 2023, the school was awarded the Aspen Prize, which recognizes the nation's best community colleges (Larkin, 2023).

IVC is developing programs to prepare students for careers in the geothermal and lithium industry, with a plant operator certification program starting in fall 2023 (*Plant Operator FAQ - Academics*, n.d.). They are also working on laboratory technician and instrumentation technician certification programs. These efforts are being led by IVC's workforce development and continuing education department, which identified the job skills needed and developed curricula in partnership with industry. IVC already offers welding, HVAC, and maintenance technician courses and estimates that 80% of new hires in the lithium and geothermal industries would come out of these existing programs.

We arranged a campus tour and presentation at IVC to learn about their lithium workforce development initiatives, and to share information with students who might work in the lithium industry in the future and are therefore important stakeholders in its development. We coordinated with an administrator in the workforce development program, who suggested we speak with students in relevant programs during their regularly scheduled class time. To make the information more widely accessible, we had two presentations, one at 9:00 am and another at 6:00 pm for students enrolled in night school.

The IVC presentations followed a typical lecture format but incorporated live polling with Slido software to gather questions and feedback. The content of the presentations included overviews of lithium and

geothermal energy, including how they are produced and their roles in the clean energy transition; background and status of development at the Salton Sea Geothermal Field; information about IVC's upcoming plant operator program (delivered by Efrain Silva, IVC's dean of workforce development) as well as the Department of Energy's Community College Internship program; and preliminary results from the environmental impact assessment.

Feedback from IVC Presentations: The students who attended the presentations were largely from surrounding towns in Imperial County (e.g., El Centro, Brawley, Imperial, Calexico, Holtville, Westmorland, and Heber), with several from cities in Mexico. The programs represented included welding, building construction, HVAC, and automotive technology (Figure 11.8).

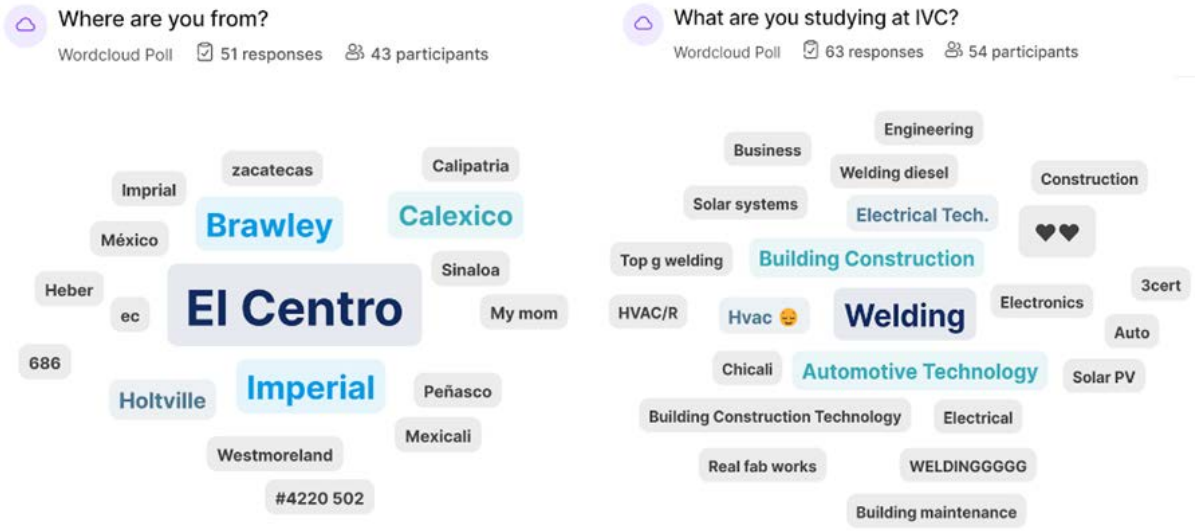

Figure 11.8. Word cloud results from live polling about student backgrounds during the IVC presentations.

Students asked questions about a wide variety of topics, many of which demonstrated a high level of interest and understanding of the material. Students were also able to upvote each other's questions, which both enabled us to prioritize our responses and provided insight about students' priorities. The most common topics were jobs and safety and the environment. Job-related questions (n=11) included what degree was needed to work in the industry, what software was used at plants, whether jobs had benefits, and expected salary levels. There were eight questions relating to safety and environmental impact, including how the industry would affect air quality, whether lithium was explosive, effects on tectonic plates, and if there were safety hazards for workers. The environment- and safety-related questions received a total of 20 upvotes, while job-related questions got 14.

Students also asked multiple questions about the extraction method and market for lithium – for example, which method was most cost-effective, the relative economics of recycling used batteries vs. mining, the value of lithium, and whether lithium extraction would attract other battery-related industries to the area. Additionally, students in both sections asked why there was suddenly so much interest in geothermal and lithium, and why the resources hadn't been developed before. Finally, students asked whether lithium would impact agriculture and how agriculture would be protected from pollution, and one student commented that water should be prioritized for agriculture and not a new industry.

The responses to a poll asking for feedback about the presentation were overall positive. Most thanked the team for visiting the group and sharing new information. However, some questions and comments were more critical or indicated some level of distrust, particularly during the evening session. Students asked where the research team was from and why we were talking to them. They also expressed frustration that presentations seemed to focus on the positive aspects of lithium while downplaying potential negative impacts. It will be important for future research teams to spend more time explaining the background and purpose of their visit, and to acknowledge and mitigate their own biases so they can present information in a neutral way.

Several instructors attended the presentation and expressed interest in setting up a partnership through the Department of Energy's Community College Internship program, which places students in a National Laboratory for a semester. This could be a valuable opportunity to involve local students directly in research and empower them to make an impact as the industry develops. The participating Laboratories could also benefit from the perspectives and lived experience of local students, and from the instructors' practical insights and experience working in power plants and other related industries.

Community-informed Research Areas

Our geothermal and lithium research provides important information that addresses many, but not all, of the community's high-priority questions. Our study provides more accurate information about how much lithium is recoverable and how long the resource might last. We also examine water consumption in the context of agriculture and Colorado River water supply, potential air emissions from expanded geothermal and DLE, and expected waste streams. Remaining questions that we were not able to address should be included in future efforts.

The impact of geothermal and DLE on public health is one of, if not the most important question for many community members. Imperial County will include a Health Impact Assessment as part of its Programmatic Environmental Impact Review; however, it is still valuable to have additional peer-reviewed research on the topic. Our study analyzes air emissions from geothermal facilities and provides a preliminary assessment of potential DLE emissions, which could be built upon to model potential air quality and associated health impacts. Ongoing monitoring is recommended, following the example of community-based participatory research studies that have been conducted in Imperial County and the Eastern Coachella Valley with local organizations (e.g., Cheney et al., 2023; Johnston et al., 2019; Madrigal et al., 2020).

The waste stream generated by DLE will require attention moving forward. While it is a high priority for community advocates, waste streams are rarely included in research about the environmental impact of lithium (Slattery et al., 2023; Williams et al., 2022). Future research can build on this project's analysis by identifying ways to minimize waste streams from DLE; for example, by investigating methods to extract and use constituent materials, or avoiding the precipitation of harmful compounds during the pretreatment process.

Recycling is an area of community interest that was not part of this project, but it would be valuable to consider the role recycling could play in a potential battery supply hub. As the lithium content of recoverable brine decreases over time, more end-of-life batteries will become available for material

recovery. Recycling these batteries could complement and perhaps ultimately replace raw material extraction as a source of lithium, making the industry more sustainable in the longer term. Co-locating recycling infrastructure with cathode and cell production also enables more efficient recycling of production scrap.

A fundamental limitation of our study was that since DLE is still under development, we can only estimate its potential impacts. Transparently monitoring and reporting facility performance in terms of air emissions and water consumption is recommended to validate the sustainability of the process as it develops. At present, some information is reported and available from State of California agency websites, but it is incomplete and difficult to access; users generally need to know what they are looking for and be able to navigate state agency websites and interpret spreadsheet data.

One option that was suggested by a CBO representative was to create a dashboard where people could easily access information about the status of development, opportunities to participate, and monitor the impacts. As an example, Figure 11.9 shows a screenshot from SQM's online environmental monitor, where people can easily access data about the brine and water use of its lithium operations in Chile. Impact on seismicity is also a high-priority environmental issue where further research and transparent monitoring is recommended. Here, the Geysers Geothermal Development operated by Calpine provides an example: the company has established a Seismic Monitoring Advisory Committee that meets twice a year to provide information and updates to the public (Calpine, n.d.).

Lessons Learned and Recommendations

Including community engagement is a departure from the norm for this type of project, and inevitably there were challenges and learning opportunities throughout the process that will be valuable for future teams. As a starting point, we recommend dedicating more resources to community engagement (CE) in future research efforts and agreeing on the goals and scope of CE as a team before the project starts. To facilitate more community participation and ongoing dialogue, we recommend establishing a community advisory board and recruiting local team members, for example through an internship program.

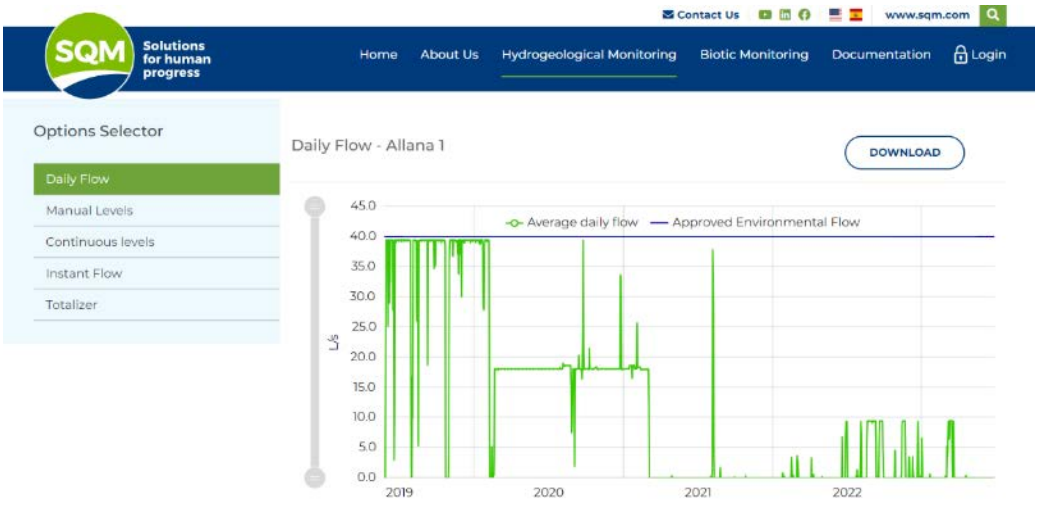

Figure 11.9. Screenshot of SQM's environmental dashboard, which provides data about water flow from a selection of wells. Users can also access information about brine composition and extraction rates, and meteorological data including wind speed, precipitation, and temperature (SQM monitor en línea, n.d.).

Lessons Learned

1. **Dedicating time to listening and visiting the area as often as possible is essential.** The researcher responsible for community engagement attended local public meetings and traveled to the area for more than a year before this research project started. Having a baseline understanding of community questions, observing outreach efforts from other institutions, and forming personal connections was key to organizing effective outreach events. Our workshop achieved high attendance, received mostly positive feedback, and fostered numerous connections with organizations and individuals who could be valuable partners moving forward – none of which would have been possible without the researcher's prior efforts.

2. **Including community engagement requires a variety of skill sets that are different from traditional quantitative research.** Based on our experience, this includes:

    - A research team "bridge" who understands both the technical material and community perspectives to develop FAQs and presentations and to identify ways to incorporate feedback into the research
    - Experience in social science and/or community-based participatory research to design surveys and other qualitative research methods
    - Graphic design to develop effective flyers, infographics, and other communication materials
    - Facilitation
    - Event planning (logistics and communication)

    These do not all necessarily need to be separate people (although that might be a best-case scenario). However, in this effort they were all essentially fulfilled by one person, with some additional support on the day leading up to the workshop. This is not sustainable or effective. It would also be preferable to have at least one team member who is based in the community and

can help identify potential partners, give feedback on the accessibility of presentations and printed material, involve more community members, and coordinate logistics for local events.

3. **CE requires defining CE-related roles and responsibilities within the research team in addition to researchers' technical scope of work,** or at minimum, establishing each team member's level of commitment to community engagement. Otherwise, it is not clear how much community input can influence the research, and input is difficult to integrate.
4. **Direct lithium extraction is a complex and novel technology.** Some information is proprietary, and the fact that the technology has not been commercially deployed means that many impacts can only be estimated. On top of that, direct lithium extraction (DLE) involves concepts from geology, chemical engineering, and thermodynamics that are challenging to understand, even for people with some technical background. Considerable effort is required to explain the process and potential impacts in a clear and straightforward manner, while also conveying appropriate uncertainty where necessary. This points to the need for ongoing CE to facilitate dialogue and information-sharing as more information becomes available.

Recommendations

The following recommendations are listed in order of where they fall on the community engagement continuum − i.e., earlier recommendations would improve the effectiveness of the community consultation model described in this report, while later recommendations would move the research towards a more participatory approach. Incorporating these practices will require a high degree of inter-team coordination, with additional resources dedicated to CE to make sure it is done effectively.

1. **Identify the goals and scope of community engagement for the project with the entire research team, not as an isolated effort.**

2. **Budget additional time and funding to develop documents that communicate research findings to specific audiences, in addition to the technical report.** This includes time for members of the research team and community engagement lead to develop the content of outreach documents and get feedback from local partners, as well as a communications specialist to assist with the content and graphic design.

3. **Budget additional time and funding for events and document translation.** All informational materials should be available in both English and Spanish, and this should be included in project budget and design. Translating documents requires additional upfront effort to coordinate with the translator, ensure materials are ready on time, and minimize the use of jargon prior to translation (Harvard Catalyst, n.d.). Providing simultaneous interpretation is the preferred way to ensure events are accessible to multilingual audiences and increases the budget needed for outreach events.

4. **Host outreach events in partnership with local government, CBOs, and industry.** Holding in-person workshops with opportunities for two-way dialogue is an effective way to share information with local communities. Hosting them in partnership with other institutions will facilitate more successful events that can speak to a broader variety of issues. Better partnership

will also help avoid duplicating efforts, as there are already multiple initiatives aimed at enabling community participation in Lithium Valley development.

5. **Establish a community advisory board.** Community advisory boards are a common mechanism to maintain ongoing dialogue and formally bridge the gap between researchers and communities (Collins et al., 2018). To create a community advisory board (CAB), researchers first identify a selection criteria and recruitment strategy. Once CAB members are selected, the operating mechanisms are agreed collectively (Newman et al., 2011). There should also be a plan for evaluating CAB effectiveness and soliciting members' experience, either through surveys or qualitative methods such as interviews (Schulz et al., 2003). Alternatively, the research team could seek to participate in a community working group that is already established.

6. **Include participating community members when sharing or discussing research findings.** For example, by inviting people to speak on panels related to lithium research and offering co-authorship where appropriate.

7. **Hire local project interns to support CE efforts and/or contribute to technical research areas.** For example, an internship program could be created in partnership with IVC or San Diego State University – Brawley. A student intern could assist in local outreach and organization efforts, particularly if they are studying a field related to communications. Students studying chemistry or geology could also contribute to the technical research. This would facilitate a valuable learning opportunity for both the student and the research team, who could learn from the student's perspective. There should be a clear plan to support the intern's integration into the project team to ensure they are meaningfully involved.

8. **Partner with local organizations to co-create research,** with a scope of work and funding for both parties determined collectively during the grant proposal stage.

It is important to honestly assess whether a research team has the capacity to successfully follow more participatory approaches. For example, sharing decision-making power with a local organization would be a significant departure from standard practice for many researchers. The urgency of the topic and the short turnaround time for funding opportunities are also likely to make community-based participatory research (CBPR) more challenging without a preexisting relationship. Furthermore, research on CBPR outcomes suggests that practicing CBPR effectively is only possible when researchers understand their own positionality and address the power relations that exist between the research team and the community (Muhammad et al., 2015). Reflecting on positionality is not common practice in engineering and earth sciences. It may be more effective to focus on improving the community consultation practices in the short term, while working to develop the internal capacity to conduct more participatory research in the future.

Conclusions

The regional context shapes local stakeholders' perspectives about any new industry, including lithium. Industry proponents often point to the high unemployment rates in the region to underscore the immense promise of what Lithium Valley could mean to surrounding communities, and this is indeed a vital part of the story. However, other important considerations exist beyond the promise of jobs. First, for any

proposed development, it is essential to address the implications for public health and plans to restore the Salton Sea ecosystem. For example, as described elsewhere in this report, geothermal lithium resources exist under the Salton Sea that would become available if the sea evaporates further (McKibben et al., 2020). It is important to be aware of the public health impacts implied by this scenario, and not consider the resource potential in a vacuum. On the other hand, revenue from a lithium economy could support environmental restoration efforts and improve public health.

Second, it is important to contextualize a potential lithium economy as it relates to the role of agriculture in the region. During public meetings and researchers' site visits, multiple stakeholders expressed a desire to see the Lithium Valley vision become a reality because it would provide career pathways outside agriculture, particularly for young people in the area. At the same time, others expressed concern that a new industry could displace agriculture, which has historically been a reliable source of employment and is foundational to the county's history and identity.

Third, communities around the Salton Sea have seen researchers visit for decades but have yet to see a meaningful improvement in their quality of life. From their perspective, California has allocated millions of dollars to address local issues, and all funding seems to have disappeared into research. Many people are thus skeptical of researchers and government representatives from outside the area, including the team for this project. Developing the trust and relationships necessary for deeper CE and community partnership therefore requires time and resources that extend well beyond a yearlong pilot study.

The goals of incorporating community engagement into this project were to understand diverse community perspectives about a potential lithium industry, make information accessible to frontline communities, and contextualize our research within the complex historical and socioenvironmental factors that have shaped the Salton Sea region. To make the information more accessible, we developed a Frequently Asked Questions (FAQ) document and held in-person Q&A sessions with community members in Niland and students at Imperial Valley College. Holding in-person events yielded valuable insight for our team and created connections with local organizers, instructors, and government representatives. The community workshop was mainly received positively by community members, who indicated that the content of the workshop was interesting and easy to understand, and that they would attend similar events in the future. However, there are opportunities for improvement regarding accessibility and building deeper and more equitable local partnerships.

The community members and students we interacted with demonstrated a nuanced perspective about geothermal and lithium, which simultaneously acknowledges the potential benefits while holding concern about the environmental impacts. Key question areas that were within the project's scope included how much lithium was in the reservoir, how long the resource would last, how geothermal and lithium production would impact air quality and public health, how much water the process would consume, and how waste would be managed. However, due to the novelty of the technology, some answers are unavailable or cannot be provided with certainty. To address community concerns, we recommend transparent monitoring of the air emissions and water consumption from geothermal and lithium extraction facilities, and continued attention to the impact on local seismicity.

One of the key takeaways from this report is that the communities near the SS-GF are engaged and highly motivated to participate when opportunities are accessible to them. There are also multiple initiatives that are working on community engagement as it relates to the Lithium Valley development, which are led by community-based organizations, the local government, and the companies themselves. Research teams should seek to complement, rather than duplicate, these efforts by partnering with participating organizations.

By practicing community-engaged research, scientists can generate information in a way that not only addresses environmental concerns but also empowers local stakeholders to participate as industry develops. Future research teams can incorporate community engagement more effectively by budgeting additional time and resources to organize events and develop audience-friendly outreach materials, and by integrating community engagement more into the overall project management strategy. To increase community participation in the research, we recommend establishing a community advisory board, hiring local student interns, and collaborating with local organizations. These efforts will require more resources – above all, time – but they are expected to strengthen the quality and impact of the research.

APPENDICES

Appendix Chapter 2

Descriptive Data for Production Wells Used in Chapter 2

Well Name	API	Year Drilled	Latitude	Longitude	Elevation GL (ft)	Well depth (ft)	TVD (ft)	Casing shoe depth (ft)	KB reference (ft)	Casing shoe depth below ground level (ft)	Casing shoe depth below ground level (m)	Well depth (corrected for KB)	TVD corrected for KB (ft)	TVD corrected for KB (m)	Difference between casing shoe and TVD (ft)	Difference between casing shoe and TVD (m)	Midpoint production depths (m)		
CalEnergy Wells																			
Vonderahe 1	02590633	1986	33.155418	-115.639475	-227	5524		2033	31	2002	610	5493	5493	1674	3491	1064	1142		
Vonderahe 2	02591252	1996	33.154353	-115.635322	-216	5047	4837	2388	26.5	2361.5	720	5020.5	4810.5	1466	2449	746	1093		
Vonderahe 3	02591239	1996	33.161446	-115.640074	-222	7100	6953	3120	26.5	3093.5	943	7073.5	6926.5	2111	3833	1168	1527		
Vonderahe 4	02591267	2001	33.154386	-115.632329	-223	6785		2685	31	2654	809	6754	6754	2059	4100	1250	1434		
Vonderahe 5	02591513	2017	33.161086	-115.641416	-201.5	7000		3200	30	3170	966	6970	6970	2124	3800	1158	1545		
Vonderahe 6	02591518	2019	33.158333	-115.637222	-228	8000	7674	2788	27	2761	842	7973	7647	2331	4886	1489	1586		
Sinclair 10	02590871	1988	33.155293	-115.638924	-230.6	6011	5740	1934	28.3	1905.7	581	5982.7	5711.7	1741	3806	1160	1161		
Sinclair 11	02591251	1995	33.154191	-115.635948	-227	6050	6036	2174	26.5	2147.5	655	6023.5	6009.5	1832	3862	1177	1243		
IID 16	02591240	1995	33.160837	-115.640518	-221	5770	5754	2388	26.5	2361.5	720	5743.5	5727.5	1746	3366	1026	1233		
M 6B	02591193	1991	33.162499	-115.623731	-225	3971		2227	27.5	2199.5	670	3943.5	3943.5	1202	1744	532	936		
M 10	02590619	1985	33.163279	-115.621363	-222	6016	5560	2139	27	2112	644	5989	5533	1686	3421	1043	1165		
Del Ranch 10	02591258	1997	33.16234	-115.621132	-221	6850	6729	2446	24	2422	738	6826	6705	2044	4283	1305	1391		
Del Ranch 11	02591261	1998	33.163648	-115.622385	-224	6104	5722	2248	27	2221	677	6077	5695	1736	3474	1059	1206		
Del Ranch 12	02591264	1999	33.16245	-115.61767	-225	6465	6170	2530	33	2497	761	6432	6137	1871	3640	1109	1316		
Del Ranch 14	02591451	2008	33.163619	-115.620818	-213	5500	5343	2704	30	2674	815	5470	5313	1619	2639	804	1217		
Del Ranch 15	02591522	2020	33.16876	-115.621924	-228.5	5500	5259	2500	31	2469	753	5469	5228	1593	2759	841	1173		
Elmore 12	02590705	1988	33.183691	-115.605432	-225	6717	6698	2698	27.5	2670.5	814	6689.5	6670.5	2033	4000	1219	1424		
Elmore 14	02590681	1988	33.183479	-115.596353	-225	3296		2965	26	2939	896	3270	3270	997	331	101	946		
Elmore 15	02591205	1992	33.183507	-115.595913	-226	2942		2448	26	2422	738	2916	2916	889	494	151	814		
Elmore 16	02591254	2001	33.183674	-115.596525	-221	9132		3479	31.5	3447.5	1051	9100.5	9100.5	2774	5653	1723	1912		
River Ranch 8	02590863	1988	33.183154	-115.578475	-225	8701		4012	27.5	3984.5	1214	8673.5	8673.5	2644	4689	1429	1929		
River Ranch 9	02591097	1989	33.183456	-115.577528	-225	8500	8076	4465	27.5	4437.5	1353	8472.5	8048.5	2453	3611	1101	1903		
River Ranch 11	02590890	1989	33.183389	-115.576353	-225	5500		4565	27.5	4537.5	1383	5472.5	5472.5	1668	935	285	1526		
River Ranch 12	02590876	1989	33.183075	-115.575409	-223	6118	6109	3997	27.5	3969.5	1210	6090.5	6081.5	1854	2112	644	1532		
River Ranch 14	02591194	1991	33.183051	-115.578962	-225	4822	4669	3898	25.5	3872.5	1180	4796.5	4643.5	1415	771	235	1298		
River Ranch 18	02591257	1997	33.183591	-115.579469	-222	7300	6712	4048	31	4017	1224	7269	6681	2036	2664	812	1630		
Hudson Ranch Wells																			
Hudson Ranch 13-1	02591444	2008	33.20648	-115.57713	-222	8600	8442.5	4100	28	4072	1241	8572	8414.5	2565	4342.5	1324	1903		
Hudson Ranch 13-2	02591492	2011	33.2064	-115.5707	-225	6895	6834	3800	30	3770	1149	6865	6804	2074	3034	925	1611		
Hudson Ranch 13-3	02591448	2008	33.2065	-115.576583	-222	7500	7352.6	3203	30	3173	967	7470	7322.6	2232	4149.6	1265	1600		
								Average values			908			1878		971	1393		
								well depth used as a proxy for TVD where TVD isn't reported					removing 4 wells with < 300 m production zone					1095	

Descriptive Data for Injection Wells Used in Chapter 2

Well Name	API	Year Drilled	Latitude	Longitude	Elevation GL	Well depth (ft)	TVD (ft)	Casing shoe depth (ft)	KB reference (ft)	Monthly injection data	Well injection test data	Notes
CalEnergy Wells												
IID 4	02591170	1989	33.160165	-115.647477	-233	5500	5392.4	1811	31	Yes		2018 report gives location as Lat. 33.160229, Long. -115.647989
IID 5	02590193	1979	33.155488	-115.64784	-228	3254	3254	1884	18	Yes	No	2012 CalEnergy summary report gives surface location as Lat. 33.155283, Long. -115.647499
IID 17	02591256	1998	33.148686	-115.648082	-228.6	6344	6044.12	3608	27	yes	yes	2016 report gives location as lat. 33.148820161, long. -115.6525981
Elmore 101	02591253	1996	33.148468	-115.648096	-230.6	6498	6233.19	3594	31	yes	no	2020 report gives location as lat. 33.148428, long. -115.648082
Sinclair 15	02590196	1978	33.148037	-115.648135	-230	6128		3017	19	yes	no	casing may extend to 3282 ft.- no directional survey information
Sinclair 21	02590846	1988	33.148007	-115.639379	-219.16	7100	6829.29	3120	27	yes		2018 report gives location as lat. 33.148026, long. -115.639355
Sinclair 22	02590848	1988	33.148022	-115.63915	-223.8	6769	6521	3820	28.3	yes		Directional survey gives TD of 6757, TVD of 6510.65
Sinclair 23	02598059	1988	33.148046	-115.63891								idle since 2012
Sinclair 24	02591236	1994	33.148017	-115.63857	-230.9	7200	6934	3924	24	yes	no	2018 report gives location as lat. 33.148028, long. -115.638545
Sinclair 26	02591247	1995	33.148085	-115.632642	-222.5	6015	6006	3600	27.9	yes	yes	2018 report gives location as lat. 33.14814001, long. -115.6326559
Sinclair 27	02591248	1995	33.148141	-115.632317	-222	6300	6120.74	3202	27.5	yes	yes	2017 report gives location as lat. 33.148113, long. -115.632406
M 16	02590604	1984	33.16337	-115.615138								idle since 2017
M 17	02591268	2002	33.16299	-115.615429								idle since 2012
IW 1	02590623	1985	33.172729	-115.606515								idle since 2010
IW 4	02590626	1985	33.176286	-115.609676								idle since 2014
IW 8	02591227	1993	33.17609	-115.6064								idle since 2012
Del Ranch Inj 1	02590677	1988	33.172509	-115.606159								idle since 2012
Del Ranch Inj 2	02590678	1988	33.172337	-115.606069	-229.3	7230	6779	2832	22	Yes		2017 report gives location as Lat. 33.172297, Long. -115.605245; 2020 report has Lat. 33.17099581, Long. -115.6063432 (perhaps TD loc?)
Del Ranch Inj 3	02590679	1988	33.172115	-115.606095	-220	7500	7184.17	2604	22	Yes	yes	TD coordinates reported as 33.170484036, -115.601924356
Del Ranch Inj 8	02591485	2009	33.170028	-115.60611	-223	6200	6073	3216	30	Yes	no	Has three sonic logs
Del Ranch Inj 9	02591514	2017	33.168707	-115.606557	-218.6	6000	5943	2463	31	yes	no	
J.J. Elmore IW 3	02590708	1988	33.170591	-115.597822								idle since 2013
J.J. Elmore IW 4	02590709	1988	33.175772	-115.597833	-221.78	6500	6340.73	2063	27.49	Yes	yes	2018 report gives location as Lat. 33.175866, Long. -115.597728
J.J. Elmore IW 5	02590710	1988	33.172959	-115.597824	-225	6100	6095	2106	30	Yes	yes	2017 report gives location as lat. 33.172481, long. -115.597674
J.J. Elmore IW 6	02590711	1988	33.177194	-115.600987	-229.9	3809	3089	2517	22	Yes		2012 report gives location as lat. 33.177132, long. -115.601083
Smith IW 1	02591259	1997	33.166372	-115.597735	-222.7	8300	7582.79	4113	29	Yes	no	2019 report gives location as lat. 33.166167, long. -115.597633
Smith IW 2	02591263	1998	33.166618	-115.597797	-223.8	7832	7741.78	3844	31.8	Yes	no	2020 report gives location as lat. 33.172496, long. -115.605102
River Ranch 2	02591269	2003	33.183222	-115.563588								idle since 2014
River Ranch 3	02590665	1987	33.18333	-115.562989	-214.7	9600	9499.45	5434	22	Yes	Yes	complete directional surveys (use RD3 info)
River Ranch 4	02590885	1988	33.177194	-115.565489								Idle since 2018
River Ranch 5	02590886	1989	33.177173	-115.56496	-217.1	7082	7069.88	4610	27.5	Yes	yes	
River Ranch 6	02590889	1989	33.179788	-115.56314	-225	7846	7806	3701	27.5	yes		
River Ranch 13	02591191	1990	33.179784	-115.563791	-219.7	7073	6988	5300	24.3	yes		2019 report gives 33.17978822, -115.5637864
River Ranch 16	02591096	1989	33.177112	-115.562962								Idle since 2011
River Ranch 19	02591515	2017	33.17899	-115.56425	-216.1	7000	6845.32	4280	31	yes	no	
River Ranch 20	02591523	2020	33.18273	-115.565355	-216.25	6000	5950.5	4147	31	yes	no	
MagmaMax 18	02591510	2014	33.155989	-115.614749								Idle since 2018
MagmaMax 19	02591516	2018	33.162902	-115.606536	-219.5	8000	7490.18	2718	33.5	yes	no	2018 report gives location as lat. 33.161086, long. -115.641418
Hudson Ranch Wells												
IW-1	02591493	2011	33.2118	-115.5631	-216	8668	8461.8	4274	31	yes		
IW-2	02591494	2011	33.211806	-115.563361	-216	8396	8395	4395	22	yes		2016 report gives long. as -115.563417 (same lat.); well survey gives well TMD as 8356, TVD as 8351
IW-3	02591495	2011	33.2118	-115.5637	-216	8325	7964.2	4473	31	yes		
IW-4	02591496	2011	33.2065	-115.5769	-222	2740	2703	1800	30	yes		2011 report gives lat. as 33.206472, long. -115.576889
IW-5	02591519	2019	33.212125	-115.563631	-215	4092	4092	2700	21.5	yes		2019 report gives lat. 33.21207, long. -115.563325

Rock Property Data for Figures Shown in Chapter 2

Well Name	Rock type	Depth (ft)	Depth (m)	Porosity	Permeability (md)	Grain density (g/cc)	Bulk density (g/cc)	Sonic velocity (km/s)	Reference	Comments	Depth range	Average depth (m)	Average porosity
State 2-14	Sandstone	1553	473.4	0.33	726	2.67	1.79	2.5	McDowell (1987)				
State 2-14	Mudstone	1566	477.3	0.25			2.02	3.15	McDowell (1987)				
State 2-14	Siltstone	1985	605.0	0.24		2.72	2.06	3.18	McDowell (1987)				
State 2-14	Siltstone	1995	608.1	0.22		2.73	2.12	3.04	McDowell (1987)		450-650 m	550	0.25
State 2-14	Mudstone	2011	613.0	0.19			2.2		McDowell (1987)				
Sinclair #4	Mudstone	2405	733.0	0.162	0.4	2.66	2.23		Somerton et al. (1974)				
State 2-14	Sandstone	2451	747.1	0.15		2.67	2.26	2.98	McDowell (1987)				
State 2-14	Siltstone	2456	748.6	0.2		2.7	2.16		McDowell (1987)				
State 2-14	Siltstone	2457	748.9	0.18		2.7	2.23	2.76	McDowell (1987)				
State 2-14	Mudstone	2458	749.2	0.16			2.27		McDowell (1987)				
State 2-14	Mudstone	2476	754.7	0.21		2.81	2.28	3.33	McDowell (1987)				
Woolsey #1	black shale	2568	782.7	0.199		2.874			Tewhey (1977)				
Woolsey #1	black shale	2568	782.7	0.23		2.874			Tewhey (1977)				
Woolsey #1	black shale	2568	782.7	0.221		2.874			Tewhey (1977)				
Woolsey #1	gray shale	2568	782.7	0.185		2.717			Tewhey (1977)				
Woolsey #1	gray shale	2568	782.7	0.171		2.717			Tewhey (1977)				
Woolsey #1	gray shale	2568	782.7	0.202		2.717			Tewhey (1977)				
Woolsey #1	Sandstone	2570	783.3	0.21		2.66			Tewhey (1977)				
Woolsey #1	Sandstone	2570	783.3	0.203		2.66			Tewhey (1977)				
Woolsey #1	Sandstone	2570	783.3	0.217		2.66			Tewhey (1977)				
Woolsey #1	gray shale	2589	789.1	0.202		2.755			Tewhey (1977)				
Woolsey #1	gray shale	2589	789.1	0.184		2.755			Tewhey (1977)				
Woolsey #1	gray shale	2589	789.1	0.201		2.755			Tewhey (1977)		650-850 m	750	0.19
State 2-14	Mudstone	2977	907.4	0.16			2.27		McDowell (1987)				
State 2-14	Mudstone	2993	912.3	0.16		2.82	2.38		McDowell (1987)				
State 2-14	Siltstone	3003	915.3	0.11			2.41		McDowell (1987)				
State 2-14	Siltstone	3025	922.0	0.24			2.06		McDowell (1987)				
State 2-14	Sandstone	3085	940.3	0.23	1.05	2.73	2.11	2.61	McDowell (1987)				
State 2-14	Sandstone	3085	940.3	0.18	29.8	2.67	2.18	3.25	McDowell (1987)				
State 2-14	Mudstone	3107	947.0	0.16	0.121		2.29	4.25	McDowell (1987)				
State 2-14	Siltstone	3119	950.7	0.25	1.97		2.04	3.15	McDowell (1987)				
State 2-14	Sandstone	3127	953.1	0.19		2.69	2.18		McDowell (1987)				
State 2-14	Sandstone	3135	955.5	0.23	32	2.68	2.08	2.47	McDowell (1987)				
State 2-14	Sandstone	3143	958.0	0.09	0.243	2.69	2.44		McDowell (1987)				
State 2-14	Sandstone	3146	958.9	0.28	263	2.67	1.92	2.25	McDowell (1987)				
State 2-14	Sandstone	3153	961.0	0.24	14.4	2.67	2.02	2.3	McDowell (1987)				
State 2-14	Mudstone	3157	962.3	0.07			2.54		McDowell (1987)				
Sinclair #4	Sandstone	3324.3	1013.2	0.186	0.8	2.69	2.19		Somerton et al. (1974)	depth range from 3320-3328.5			
Woolsey #1	green-gray shale	3418	1041.8	0.161		2.679			Tewhey (1977)				
Woolsey #1	green-gray shale	3418	1041.8	0.149		2.679			Tewhey (1977)				
Woolsey #1	green-gray shale	3418	1041.8	0.159		2.679			Tewhey (1977)				
Woolsey #1	green-gray shale	3419	1042.1	0.175		2.684			Tewhey (1977)				
Woolsey #1	green-gray shale	3419	1042.1	0.167		2.684			Tewhey (1977)				
Woolsey #1	green-gray shale	3419	1042.1	0.173		2.684			Tewhey (1977)		850-1050 m	950	0.18
State 2-14	Mudstone	3475	1059.2	0.12		2.72	2.38	3.8	McDowell (1987)				
State 2-14	Siltstone	3484	1061.9	0.13		2.7	2.35	3.59	McDowell (1987)				
State 2-14	Mudstone	3492	1064.4	0.12		2.73	2.4		McDowell (1987)				
State 2-14	Siltstone	3493	1064.7	0.1	0.042	2.7	2.42	3.83	McDowell (1987)				
State 2-14	Siltstone	3791	1155.5	0.11		2.79	2.49	3.74	McDowell (1987)				
State 2-14	Mudstone	3797	1157.3	0.06		2.73	2.56		McDowell (1987)				
State 2-14	Siltstone	3797	1157.3	0.07	0.042	2.69	2.5	4.08	McDowell (1987)				
State 2-14	Sandstone	3807	1160.4	0.18	3.52	2.66	2.19	2.59	McDowell (1987)				
State 2-14	Mudstone	3812	1161.9	0.11		2.79	2.48		McDowell (1987)				
State 2-14	Siltstone	3814	1162.5	0.1	0.017	2.73	2.46		McDowell (1987)				
State 2-14	Mudstone	3817	1163.4	0.07		2.72	2.53		McDowell (1987)				
State 2-14	Sandstone	3820	1164.3	0.16	2.94	2.66	2.25	2.72	McDowell (1987)				
State 2-14	Mudstone	3826	1166.2	0.06		2.78	2.61		McDowell (1987)				
State 2-14	Siltstone	3832	1168.0	0.12		2.75	2.43	3.21	McDowell (1987)				
State 2-14	Siltstone	3841	1170.7	0.11		2.73	2.43	3.81	McDowell (1987)				
State 2-14	Siltstone	4009	1221.9	0.13		2.93	2.54		McDowell (1987)				
State 2-14	Mudstone	4017	1224.4	0.05		2.77	2.61		McDowell (1987)				
State 2-14	Siltstone	4019	1225.0	0.1	0.022	2.8	2.53	4.09	McDowell (1987)				
State 2-14	Mudstone	4022	1225.9	0.06		2.81	2.63		McDowell (1987)				
State 2-14	Mudstone	4029	1228.0	0.04	0.006	2.74	2.63	4.99	McDowell (1987)				
State 2-14	Mudstone	4038	1230.8	0.06			2.56		McDowell (1987)				
State 2-14	Mudstone	4049	1234.1	0.05		2.73	2.59		McDowell (1987)				
State 2-14	Mudstone	4054	1235.7	0.06		2.74	2.57		McDowell (1987)				
State 2-14	Mudstone	4064	1238.7	0.04	0.006	2.73	2.62	4.99	McDowell (1987)		1050-1250	1150	0.09
State 2-14	Siltstone	4243	1293.3	0.13	0.191	2.69	2.34	4.16	McDowell (1987)				
State 2-14	Mudstone	4258	1297.8	0.05			2.59		McDowell (1987)				
State 2-14	Mudstone	4265	1300.0	0.04		2.73	2.61		McDowell (1987)				
State 2-14	Siltstone	4279	1304.2	0.1	1.53	2.69	2.41	3.86	McDowell (1987)				
State 2-14	Sandstone	4282	1305.1	0.15	7.93	2.71	2.3	3.39	McDowell (1987)				
State 2-14	Mudstone	4291	1307.9	0.08		2.68	2.53		McDowell (1987)				
State 2-14	Sandstone	4294	1308.8	0.1	1.07	2.68	2.41	3.47	McDowell (1987)				
State 2-14	Sandstone	4302	1311.2	0.13	0.868	2.69	2.34	3.16	McDowell (1987)				
State 2-14	Mudstone	4305	1312.2	0.11		2.75	2.45		McDowell (1987)				
State 2-14	Mudstone	4307	1312.8	0.04	0	2.72	2.61		McDowell (1987)				
State 2-14	Mudstone	4317	1315.8	0.06		2.71	2.55		McDowell (1987)				
State 2-14	Mudstone	4318	1316.1	0.06		2.77	2.6		McDowell (1987)				
State 2-14	Mudstone	4324	1318.0	0.03		2.71	2.62		McDowell (1987)				
State 2-14	Siltstone	4324	1318.0	0.11	0.106	2.71	2.43	3.8	McDowell (1987)				
State 2-14	Mudstone	4331	1320.1	0.06		2.74	2.59		McDowell (1987)				
State 2-14	Mudstone	4336	1321.6	0.02		2.76	2.71		McDowell (1987)				
State 2-14	Mudstone	4337	1321.9	0.04		2.82	2.71		McDowell (1987)				
Sinclair #4	Siltstone	4430.5	1350.4	0.109	0.4	2.62	2.32		Somerton et al. (1974)				
State of California #1	Siltstone	4525	1379.2	0.099		2.71			Tewhey (1977)				
State of California #1	Siltstone	4592	1399.6	0.075		2.75			Tewhey (1977)				
State 2-14	Siltstone	4644	1415.5	0.17	0.224	2.8	2.34	4.13	McDowell (1987)				
State 2-14	Sandstone	4658	1419.8	0.06		2.88	2.7		McDowell (1987)				
State 2-14	Siltstone	4660	1420.4	0.14		2.87	2.48		McDowell (1987)				
State 2-14	Sandstone	4679	1426.2	0.11		2.84	2.52		McDowell (1987)				
State 2-14	Siltstone	4682	1427.1	0.2	1.39	2.68	2.14		McDowell (1987)		1250-1450	1350	0.09
State of California #1	Siltstone	4842	1475.8	0.065		2.76			Tewhey (1977)				
State of California #1	Siltstone	4847	1477.4	0.054		2.69			Tewhey (1977)				
State of California #1	Siltstone	4847	1477.4	0.062		2.67			Tewhey (1977)				
State of California #1	Siltstone	4848	1477.7	0.074		2.69			Tewhey (1977)				
IID #2	Sandstone	5073.5	1546.4	0.163	10	2.66	2.23		Somerton et al. (1974)	data also available for bulk compressibility, Biot constant,			
State 2-14	Mudstone	5190	1581.9	0.02		2.7	2.64		McDowell (1987)		1450-1650	1550	0.07
State 2-14	Mudstone	5574	1699.0	0.11		2.76	2.45		McDowell (1987)				
State 2-14	Mudstone	6029	1837.6	0.04		2.69	2.59		McDowell (1987)				
State 2-14	Sandstone	6029	1837.6	0.04		2.73	2.63		McDowell (1987)				
State 2-14	Mudstone	6033	1838.9	0.04	0.011	2.69	2.57	4.96	McDowell (1987)				
State 2-14	Siltstone	6034	1839.2	0.07	0.046	2.68	2.5	4.44	McDowell (1987)				
State 2-14	Mudstone	6038	1840.4	0.07		2.72	2.54		McDowell (1987)		1650-1850	1750	0.06
State 2-14	Siltstone	6510	1984.2	0.06	0.007	2.67	2.51		McDowell (1987)				
State 2-14	Siltstone	6511	1984.6	0.18	3.84	2.82	2.66	5.09	McDowell (1987)				
State 2-14	Mudstone	6513	1985.2	0.03		2.65	2.57		McDowell (1987)		1850-2050	1950	0.09
State 2-14	Siltstone	6760	2060.4	0.08	0.025	2.77	2.55	4.47	McDowell (1987)				
State 2-14	Mudstone	6881	2097.3	0.01		3.24	2.69		McDowell (1987)	grain density value looks off			
State 2-14	Mudstone	7100	2164.1	0		2.7	2.72		McDowell (1987)				
State 2-14	Mudstone	7106	2165.9	0		2.7	2.73		McDowell (1987)				
State 2-14	Siltstone	7301	2225.3	0.23		3.09	2.38		McDowell (1987)				
State 2-14	Mudstone	7302	2225.6	0.11		2.83	2.52		McDowell (1987)				
State 2-14	Mudstone	7304	2226.3	0.06		2.71	2.55		McDowell (1987)		2050-2250	2150	0.07
State 2-14	Mudstone	7547	2300.3	0.02		2.7	2.66		McDowell (1987)				
State 2-14	Siltstone	7550	2301.2	0.2		3.14	2.51		McDowell (1987)				
State 2-14	Mudstone	7553	2302.2	0			2.72		McDowell (1987)				
State 2-14	Mudstone	7709	2349.7	0			2.73		McDowell (1987)				
State 2-14	Mudstone	7712	2350.6	0			2.73		McDowell (1987)		2250-2450	2350	0.04
State 2-14	Mudstone	8138	2480.5	0		2.7	2.71		McDowell (1987)				
State 2-14	Siltstone	8146	2482.9	0.21		2.85	2.61		McDowell (1987)				
State 2-14	Mudstone	8157	2486.3	0		2.68	2.71		McDowell (1987)				
State 2-14	Mudstone	8395	2558.8	0.04	0		2.62		McDowell (1987)				
State 2-14	Mudstone	8397	2559.4	0.02			2.68		McDowell (1987)				
State 2-14	Sandstone	8591	2618.5	0.14	5.6	2.69	2.31		McDowell (1987)				
State 2-14	Sandstone	8591	2618.5	0.14		2.69	2.35		McDowell (1987)		2450-2650	2550	0.08
State 2-14	Mudstone	8800	2682.2	0.01		2.7	2.68		McDowell (1987)				
State 2-14	Siltstone	8803	2683.2	0.04	0.005	2.71	2.61		McDowell (1987)				
State 2-14	Mudstone	9008	2745.6	0			2.7		McDowell (1987)				
State 2-14	Sandstone	9095	2772.2	0.02					McDowell (1987)				
State 2-14	Sandstone	9095	2772.2	0.01					McDowell (1987)				
State 2-14	Mudstone	9250	2819.4	0.02			2.67		McDowell (1987)				
State 2-14	Mudstone	9251	2819.7	0		2.7	2.7		McDowell (1987)		2650-2850	2750	0.01
State 2-14	Mudstone	9462	2884.0	0.01			2.69		McDowell (1987)				
State 2-14	Siltstone	9462	2884.0	0			2.73		McDowell (1987)				
State 2-14	Siltstone	9474	2887.7	0.1	0.026	3.09	2.78		McDowell (1987)				
State 2-14	Siltstone	9474	2887.7	0.08		2.96	2.73		McDowell (1987)				
State 2-14	Sandstone	9694	2954.7	0.06		2.78	2.62		McDowell (1987)				
State 2-14	Siltstone	9697	2955.6	0.01		2.74	2.71		McDowell (1987)				
State 2-14	Sandstone	9908	3020.0	0.09		3.12	2.84		McDowell (1987)		2850-3050	2950	0.05
											Total average (141)		**0.112**

Brine Composition for Chapter 2 Analysis

Well ID	Date sampled	Prod. Depth (m)	T	pH	Reported units	Na	Ca	K	Fe	Mn	SiO2	Al	Rb	Zn	Ag	As	Sr	B	Ba	Li	Mg	Pb	Cu	Cd	Cs	NH4	Cl	F	Br	I	SO4	TDS (%)	Li/6.941	Cl/35.453	References	Comments
SSSDP State 2-14	Dec-85	1850-1890	305	5.4	ppm	53000	27400	16700	1560	1450	>461	2	170	518			411	257	203	194	33	100	5.9	2.2	20	333	151000	15	99	20	65	25.6	27.949863	4259.16	Williams&McKibben, 1989; McKibben&I	flash corrected brine analyses
SSSDP State 2-14	Mar-86	2500-3220	330	5.1	ppm	54800	28500	17700	1710	1500	>588			507			421	271	<353	209	49	102	6.8	2.3	NA	330	157500		111		53	26.5	30.110935	4442.5013	Williams&McKibben, 1989; McKibben&I	flash corrected brine analyses - may be contaminated by drilling fluids
SSSDP State 2-14	Jun-88	1830-2200	320	5.3	ppm	53700	26300	17100	1620	1470	>840			510			410	380	218	215	43	107	5.8	2.2	23	356	152000		111	123	25.6	30.975364	4287.3664	Williams&McKibben, 1989; McKibben&I	flash corrected brine analyses - may be contaminated by drilling fluids
SSSDP State 2-14	Dec-85	1829-1898	287		ppm	52843	27048	16736	1548	1397	>380			514			409	257	202	193	37	98				325	153410				25.5	27.805792	4327.1373	Michels, 1986	flash corrected and averaged brine analyses
SSSDP State 2-14	Dec-85	1829-1898	297		ppm	52661	26515	16502	1522	1385	>387			506			405	253	194	190	36	95				336	153668				25.4	27.373577	4334.4146	Michels, 1986	flash corrected and averaged brine analyses
11b		660-1070	300	5.2	ppm	46200	22800	12500	582	801	>336			321			376	204	183	157	19	69	NA		1	NA	339	128000		95	100	21.4	22.619219	3610.4138	Williams&McKibben, 1989; McKibben&I	flash corrected brine analyses
10		700-1070	295	5.3	ppm	41400	20900	11800	969	855	>404			323			345	197	156	152	33	67	2	1.4	NA	341	116000		78	53	20	21.898862	3271.9375	Williams&McKibben, 1989; McKibben&I	flash corrected brine analyses
unnamed SS well				5.3	ppm	52700	26500	16500	1550	1390	475	3		506	2	5		268	194	230	36	91					174900				29.5	33.136436	4933.292	Duyvesteyn, 1992	
Magmamax 1	Jul-79	855			mg/L	43000	22300	7550	220	420				105			460		130	170	150	50	2.5			335	115200				21.5	24.492148	3249.3724	Featherstone&Powell, 1981	
Magmamax 1	8/10/76	855	215	5.2	ppm	42000	20000	8600	256	690	432	1	64	361			388		118	141	80	78	1			45	121000				20.8	20.314076	3412.9693	Maimoni, 1982	
Magmamax 1		732				49000	21000	8300	150		>71		5.3	293	0.39		368		33	143	100	29	0.49		16	504	102000	4.6	109		50	18.2	20.602219	2877.0485	Berthold et al., 1975	flashed sample - abundant silica loss due to precipitation
Magmamax 1	Aug. 1976			5.2	ppm	46900	17400	9310	451								783			149							114000					18.9	21.466647	3215.5248	Needham et al., 1980	average brine - flow rate of 9.3 L/s
Magmamax 1	Oct-Nov 1976			5.1	ppm	47900	22116	8870	265	617					0.6		725			170	95	51	0.5				95780					17.7	24.492148	2701.6049	Needham et al., 1980	average brine - flow rate of 32 L/s
Sinclair well?		1524	300		ppm	51000	40000	25000	3200	2000	>100	450	169	970	1	15	750	520	200	300	730	104	10		20	482	185000	18	146	22	56	31.9	43.221458	5218.1762	White, 1965; Werner, 1970	sample analyzed by USGS in 1963 - many values seem highly suspect relative to newer analyses
Hudson Ranch well					ppm	56275	29778	18006	1411	1700	437			487		12	316	563	167	228	43	108	0.9				165442	7.2				27.9	32.848293	4666.5162	CA regional water quality control board	average produced brine composition (production wells 13-1, 13-2, & 13-3)
IID-1	1962				ppm	54000	40000	23800	3000	1000				500	2		2000	500	200	321		100	20				184000					33.2	46.246938	5189.9698	White et al., 1963	
IID-1	4/21/66	1595	340	5.2	ppm	50400	28000	17500	2090	1560	400	4.2	137	790	0.8	12	609	390	235	215	54	84	8		16	409	155000	15	120	18	5.4	25.8	30.975364	4371.9854	Skinner et al., 1967; Werner&Olson, 197	corrected for steam loss, Muffler&White list flow from 3500-5000 ft, temperature of ~300C
IID-1	1963					51000	40000	24000	3200	2000	>110	450	168	970	1	15	740	520	200	300	35	104	10		22	482	185000	18	146	22	56	31.9	43.221458	5218.1762	Werner&Olson, 1970; Palmer, 1975; Hol	not corrected for steam loss, average analysis
IID-2	1967	1776	332		ppm	53000	27800	16500	2000	1370	400			500	2		440	390	250	210	10	80	3		20		155000					25.9	30.255006	4371.9854	Skinner et al., 1967; Palmer, 1975; Helg	average analysis, corrected for steam loss (Helgeson Ca value listed as 28,800 ppm - producing depth listed as 1113 m
IID-3	1965	518	188	7.5	ppm	10600	1130	1250	<1	6	120	2				<1	85	100	3	40	74					321	19700	1	15	5	621	3.56	5.7628584	555.66525	Palmer, 1975; Hoffman, 1975; Muffler&	average analysis, corrected for steam loss; Muffler&White list flow from ~1575 ft
		1155-1579;																																	
Sinclair #3	Apr-62	1619-2093	252	5.3	ppm	36340	14550	7820		410						10	360	210	540	49	780	80				340	93650	2			58	18.37	7.0595015	2641.5254	Palmer, 1975; Hoffman, 1975	average analysis, not known if corrected for steam loss; ; discrepancies in Li between two sources
Sinclair #3	Apr-63		252	4.3	ppm	50600	23000	13200		1000						10	510		570	80	1940	200	1			570	141500	5				27.61	11.525717	3991.1996	Palmer, 1975; Hoffman, 1975	average analysis, not known if corrected for steam loss; discrepancies in Li between two sources
Sinclair #3	May-63			5.62	ppm	47000	23000	13000	1200	1300	1200			360			420	310	300	210	130	82	10				132240					22	30.255006	3730.0087	Analytical report for Helgeson (DOGGR | data base, 1963)
Sinclair #4		1615	260	5.3	ppm	58443	26992	14918	1148	1025	90					10	434	332		287	736						154590	14	25	13	19	26.7	41.348509	4360.4208	Palmer, 1975; Hoffman, 1975	average analysis, corrected for steam loss
Sinclair #4		1646				71000	35000	18000	870	1470	>44		17	492	0.77		570	344	118	238	152	141	0.69		32	611	186000	5.8	162		42	31.5	34.289007	5246.3825	Berthold et al., 1975	flashed sample - abundant silica loss due to precipitation
Sinclair #4						70000	35000	19000	1200	2000	>40	0.6	25	500	0.5	3	600	400	200	250	150	100	0.5	0.9		650	190000	10	200	0.5	0.04	32.0	36.017865	5359.208	Christopher et al., 1975	typical composition - post-flashed brine
Sinclair #4		1307-1542	260	5	ppm	78000	37735	20690	1300	1700	625			600	1		455		1100	400	2225	60	3				210700				75	38.75	57.628584	5943.0796	Palmer, 1975; Hoffman, 1975	average analysis, not known if corrected for steam loss; discrepancies in Li between two sources
Fee 5	8/15/84	~2500	~300		ppm	43500	27700	16200	1890	1430	354			551			426	319	270	228	96	63	3.9	2.2			139000		94		35	23.8	32.848293	3920.6837	Zukin et al., 1987	flash corrected brine analyses
Fee 6	3/1/85	~2500	~300		ppm	48100	28700	14500	1920	1650	243	1.8		558			489	274	300	216	81	111	2.3	2.2			127000		90		74	23	31.119435	3582.2074	Zukin et al., 1987	flash corrected brine analyses
Shell #1 State	1964	1394-1448	320		ppm	47800	21200	14000	1200	950			65	500	<1			290	190	180	27	80	2		17		127000					21.95	25.932863	3582.2074	Helgeson, 1968; Palmer, 1975; hoffman	averaged flash corrected brine analyses: Palmer lists T of 305C
Sportsman #1	8/31/61	1213-1439	310	4.82-6.1	ppm	70000	34470	24000	4200									149		150	18						201757				34	33.5	21.610719	5690.8301	Werner&Olson, 1970; Palmer, 1975; Hol	not corrected for steam loss, average analysis
Wooley #1	2/1/72				ppm	49257	8550	2881	84	121	240									65	651						59015					12.07	9.3646449	1664.5982	Hoffman, 1975	Si was converted to silica
Wooley #1	Mar-72				ppm	28195	7284	3055	141	150	302									63	113						49342					8.848	9.0765019	21.610719	Hoffman, 1975	Si was converted to silica
Wooley #1	Mar-72	569-724	238	6.25	ppm	49729	12658	6510	244	488	388									90	136						83183					15.1	12.966431	2346.2895	Palmer, 1975; Hoffman, 1975	personal communication from 1972, not known if corrected for steam loss, Si was converted to silica
Magmamax 1	1/20/78			6	ppm	44000	16000	8000	134	453	443	<10		44	201		7	392	405		110	78	37	0.7	1.2	10							15.847861	0	Harrar et al., 1979	flashed sample
Magmamax 1	1/31/78			6.12	ppm	51000	20000	9000	200	596	469	<10		52	252		11	341	440	300	124	72	61	0.9	1.3	11							17.864861	0	Harrar et al., 1979	flashed sample
Magmamax 1	1/31/78			4.14	ppm	57000	23000	10000	233	680	548	<10		58	289		13	418	512		142	84	61	0.8	1.5	11							20.458147	0	Harrar et al., 1979	flashed sample

Appendix Chapter 4

Description and Preparation of Rock and Brine Samples Studied

Samples in this study include igneous and sedimentary surface rocks, geothermal brines collected from 22 commercial wells in the SS-GF, as well as previously analyzed commercial drill cuttings (Schmitt and Hulen, 2008), newly analyzed commercial drill cuttings, and State 2-14 drill core specimens (e.g., McKibben et al., 1988a; McKibben et al., 1988b; Elders and Sass, 1988; Herzig et al., 1988; Herzig and Elders, 1988). Surface igneous samples were collected from Obsidian Butte and Rock Hill (Robinson et al., 1976; Herzig and Jacobs, 1994). Unmetamorphosed sedimentary and evaporitic samples were collected from surface exposures of the Durmid Hills (Babcock, 1974).

Surface rhyolitic samples collected for analysis in this study include spherulitic obsidian from Obsidian Butte (Figure A4.1). The spherulites in these samples are centered around fine-grained, subhedral-to-anhedral phenocrysts of plagioclase and are composed of radiating, acicular crystals of feldspar and quartz. Sparse (<1% of the thin section area), fine-grained, subhedral clinopyroxene phenocrysts can be found at the center of some spherulites, adjacent to the larger fine-grained plagioclase phenocrysts. Medium grey, vesicular, aphanitic-to-glassy rhyolite was collected from Rock Hill (Figure A4.2a). Within this sample are sparse (<1% of the thin section area) amounts of fine-grained euhedral-subhedral, plagioclase, clinopyroxene, and Fe-Ti oxide crystals. Also collected from Rock Hill are dark grey, vesicular, glassy rhyolite (Figure A4.2b). Sparse (<1% of the thin section area) amounts of fine grained subhedral and rounded plagioclase, clinopyroxene, and Fe-Ti oxide crystals are present within the rhyolite. Vesicles within this sample are elongated in one direction.

Four outcrop samples were collected from the Durmid Hills. One sample is a light grey mudstone (Figure A4.3) with minor amounts of fine-to-medium-grained pyrite crystals. Also collected is a grey-translucent gypsum (Figure A4.4a and A4.4b) with light grey, interbedded mudstone. The gypsum beds range from very fine-grained layers a few millimeters in thickness to coarser grained, acicular blocks of about 1 cm in thickness. Additionally, white, cryptocrystalline gypsum (Figure A4.5) was collected. A light to medium grey, calcite-cemented, fine-grained sandstone (Figure A4.6) was also collected.

Subsurface samples from the State 2-14 drill core have previously been described in the literature (e.g., McKibben et al., 1988b; Charles et al., 1988; Cho et al., 1988; Elders and Sass, 1988; Herzig et al., 1988; Herzig and Elders, 1988). This study adds to those descriptions using microanalytical analyses (see Scanning Electron Microscope, below). The specific State 2-14 drill core samples analyzed (Figure A4.7 through A4.15) include samples from ~1866 m depth (flow zone ejecta; Charles et al., 1988), ~2358 m depth, ~2485 m depth, ~2745 m depth, ~2819 m depth, and ~2882 m depth. The sample from ~1866 m depth is a monomineralic, interlocking, very fine grained, granular, subhedral epidote (Figure A4.7). The sample from ~2358 m depth is an interbedded grey-green mudstone and white, coarse- to fine-grained anhydrite with medium to fine-grained pyrite intermittently present near the mudstone-anhydrite interfaces (Figure A4.8). The sample from ~2485 m depth is an interbedded medium-grey mudstone and light grey to light green epidotized mudstone (Figure A4.9; Cho et al., 1988). The sample from ~2745 m depth is a medium grey, interbedded mudstone and white, very coarse-grained to fine-grained, angular anhydrite (Figure A4.10). The sample from ~2819 m depth is a dark green epidotized mudstone with light

green veins and spots of larger fine-grained minerals of epidote, quartz, and anhydrite (Figure A4.11). The sample from ~2882 m depth is a brecciated diabase and mudstone (Figure A4.12; Herzig and Elders, 1988).

Three additional drill core samples (two samples were from State 2-14) were analyzed for Li isotopes (and one for whole rock Li concentration) during this study. These samples are from depths of ~1039 m (massive anhydrite with < ~10% grey-green mudstone interlayered within the anhydrite collected from Magma-max-11; Figure A4.13; McKibben et al., 1988a), ~1294 m (epidotized metasedimentary mudstone; Figure A4.14), and ~1427 m (metasedimentary mudstone with hematite veins; Figure A4.15).

Samples were sawn with a diamond-coated blade and washed in de-ionized water before being sent for commercial polished thin section preparation by Burnham Petrographics, LLC. Drill cuttings were mixed with Petropoxy 154 and mounted within 0.7 cm round brass spacers cut to be 0.6 cm in length. Brass spacer mounted samples were polished using progressively finer grain sized polish paper down to 0.25 µm, until the samples were exposed on one side with areas of optically smooth surface. These exposed samples along with previously analyzed State 2-14 samples and newly created thin sections of State 2-14 and surface samples were then carbon coated in preparation for Scanning Electron Microscope (SEM) analysis.

Scanning Electron Microscope

Carbon-coated samples were analyzed at the Brounce Geochemical Laboratory at the University of California, Riverside on a JEOL JCM-7000 NeoScope Benchtop scanning electron microscope, equipped with a mapping stage using an accelerating voltage of 15 kV in high vacuum mode. Elemental and back-scattered electron maps of the samples in this study were analyzed to identify major mineral phases in conjunction with visible light petrographic observations. Selected regions of interest were analyzed *in situ* for major and trace-element concentrations via laser ablation induced coupled plasma mass spectrometry (LA-ICP-MS). A subset of samples from Obsidian Butte and 7738 m depth were analyzed by two interns, Hoover and Wenzel, working on this project (see Broader Impacts: *Mineralogic Investigation Interns*, Appendix Chapter 4).

Laser Ablation Inductively Coupled Mass Spectrometry

Trace-element abundances for the samples in this study were analyzed at the Lyons ICP-MS Facility at the University of California, Riverside via LA-ICP-MS using an Agilent Technologies 7900 single quadrupole mass spectrometer that is coupled to a short pulse width coherent 193 nm ArF excimer laser. Samples in this study were analyzed for 60 major, minor, and trace elements, of which ^{7}Li, ^{23}Na, ^{26}Mg, ^{27}Al, ^{29}Si, ^{39}K, ^{44}Ca, ^{55}Mn, and ^{56}Fe are presented in this study. Spot sizes analyzed ranged from 25-30 µm in diameter. A repeat rate of 5 Hz and energy on sample surface of 0.040 – 0.052 mJ was used. USGS glass standards BIR-1 g, BCR-2 g, and BHVO-2 g; Max Planck Institute glass standards KL2-G, ML3B-G, StHls-G, GOR-128-G, GOR-132-G, ATHO-G, and T1-G; and National Institute of Science and Technology Standard Reference Material glasses 610 and 612 were used to create linear calibration curves ($R2 > 0.999$) for each analytical session (Pearce et al., 1997; Jochum et al., 2000; Kelley et al., 2003). Counting statistics were examined carefully for each element. Those elements that did not return strong signals for the entire length of the ablation period were discarded. Samples with two distinct, strong

signals during the ablation period had both signals analyzed, and sample names were amended to include the interval period in their name (e.g., sample 9005m_Aa_10-14 and 9005m_Aa_18-21 are from one analysis period). For minerals where sulfur and/or carbon was a major elemental constituent (i.e., pyrite, anhydrite, gypsum, and calcite), analyses were normalized to either ^{44}Ca (for anhydrite, gypsum, and calcite) or ^{56}Fe (for pyrite) using an assumed calculated CaO or FeO stochiometric concentration (41.3 wt% CaO for anhydrite, 32.6 wt% CaO for gypsum, 56.0 wt% CaO for calcite, and 59.9 wt% FeO for pyrite). Since this method calculates the values of Si, Ca, and Fe using identical standard measurements (e.g., KL2-G SiO_2 = 50.3 wt% for both ^{28}Si and ^{29}Si), ^{29}Si, and ^{56}Fe were chosen to calculate elemental abundances. Samples with major element totals less than 95% were discarded from analysis. A subset of samples from Obsidian Butte and 7738 m depth were analyzed by two interns, Hoover and Wenzel, working on this project (see Broader Impacts: *Mineralogic Investigation Interns*, below).

Lithium Isotopes

Lithium isotopic compositions of brines and selected rock powders were analyzed at the Geochemistry Center at Yale University via a Thermo Finnigan Neptune Plus ICP-MS using the methods of Kalderon-Asael et al. (2021). For the brines, an aliquot of 1 mL of each sample was dried at 93°C into a pre-acid-cleaned Teflon beaker. The aliquots were subsequently digested with aqua regia (200 microliters of distilled HNO_3 and 600 microliters of distilled HCl), capped and left on a hotplate at 130°C for 48 hours, and dried again. At a second digestion step, 1 mL of distilled HNO_3 and three drops of H_2O_2 were added to each sample, capped and left on a hotplate at 130°C for 48 hours, and dried again. The samples were then redissolved in 10 mL of 6N HCl. Splits were taken for lithium column procedure. The rock samples were digested using the total digest protocol. At the end, the samples were redissolved in 5 mL of 6N HCl. The few evaporitic samples were dissolved in MQ H_2O. Splits were taken for the lithium column procedure.

Whole Rock Lithium Analysis

Whole rock powders were dissolved using Environmental Protection Agency Method 3051A: Microwave Assisted Acid Digestion of Sediments, Sludges, Soils, and Oils using a temperature of 220°C for ~15 minutes. Lithium concentrations of selected rock powders were analyzed at Berkeley Lab via an Agilent 8900 triple quadrupole ICP-MS (Agilent 8900 QQQ ICP-MS) that has been used to measure the concentrations of 36 elements simultaneously for environmental samples, of which Li (measured using standard no-gas mode) is reported here. The instrument settings and analytical methods are similar to those reported by Belkouteb et al. (Belkouteb et al. 2023) and Agilent application notes (Agilent 4th Edition). All samples were prepared/diluted with 2% (v/v) ultrapure nitric acid in Milli-Q water (18.2 mΩ·cm) and analyzed under a rigorous quality assurance and quality control (QA/QC) process.

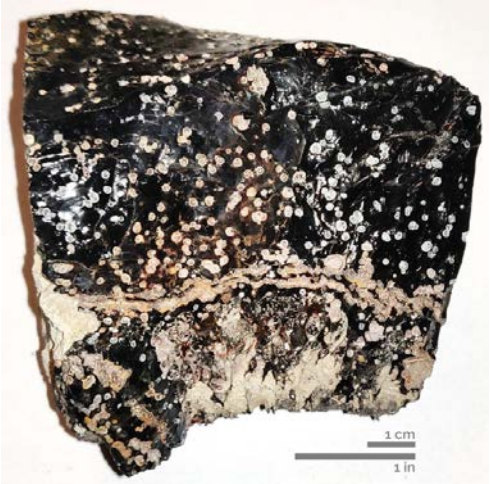

Figure A4.1. Spherulitic Obsidian from Obsidian Butte.

Figure A4.2a. Glassy rhyolite from Rock Hill.

Figure A4.2b. Glassy rhyolite from Rock Hill.

Figure A4.3. Mudstone from the Durmid Hills.

Figure A4.4a. Interbedded gypsum and mudstone from the Durmid Hills.

Figure A4.4b. Interbedded gypsum and mudstone from the Durmid Hills.

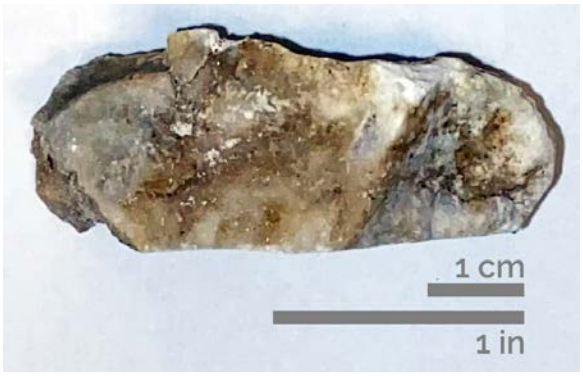

Figure A4.5. Cryptocrystalline gypsum from the Durmid Hills.

Figure A4.6. Sandstone from the Durmid Hills.

Figure A4.7. Monomineralic epidote from 1866 m (6122 ft) depth in the State 2-14 drill core.

Figure A4.8. Interbedded mudstone and anhydrite from 2357.8 m (7735.5 ft) depth in the State 2-14 drill core.

Figure A4.9. Epidotized mudstone from 2485 m (8153 ft) depth in the State 2-14 drill core.

Figure A4.10. Interbedded mudstone and anhydrite from 2744.6 m (9004.6 ft) depth in the State 2-14 drill core.

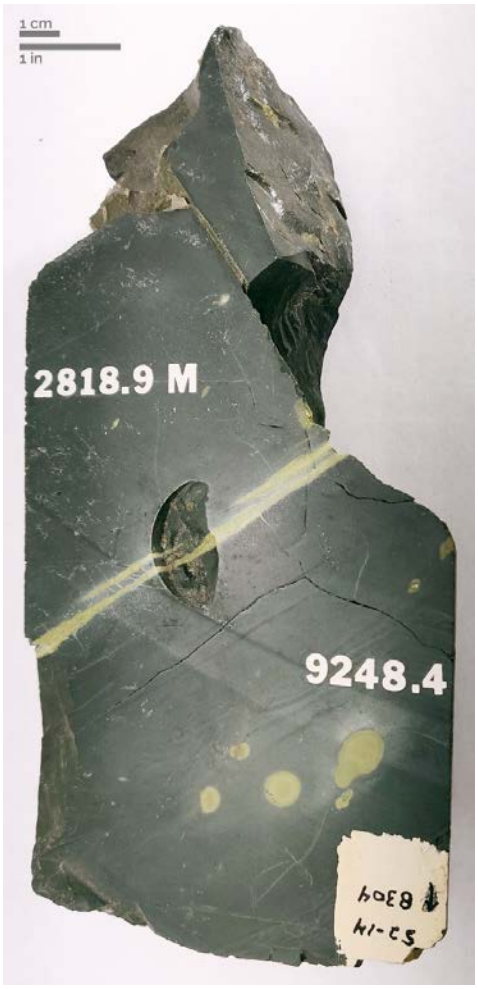

Figure A4.11. Epidotized mudstone from 2818.9 m (9248.4 ft) depth in the State 2-14 drill core.

Figure A4.12. Brecciated diabase and mudstone from 2881.99 m (9455 ft) depth in the State 2-14 drill core.

Figure A4.13. Interbedded anhydrite and mudstone from the Magmamax 2 drill core.

Figure A4.14. Epidotized metasedimentary mudstone from 1293.5 m (4243.7 ft) depth in the State 2-14 drill core.

Figure A4.15. Metasedimentary mudstone with hematite veins from 1426.8 m (4681 ft) depth in the State 2-14 drill core.

Broader Impacts

Museum Curation Interns. Andrea Valdes and Jesus Uribe worked as museum curation interns. Both interns worked on curating specimens collected in the 1980s from cores in the Salton Sea area for the purpose of scientific research. Curation involved labeling specimens with unique specimen numbers (Figure A4.16), adding specimen data (specimen number, specimen description, locality, storage location, etc.) into the museum database (Figure A4.17), and researching locality data to ensure its completeness and accuracy. The museum database these specimens have been added to is available upon request to any qualified researchers, with plans to make all non-sensitive data freely available online in the future.

Figure A4.16. A selection of specimens curated over the course of this project.

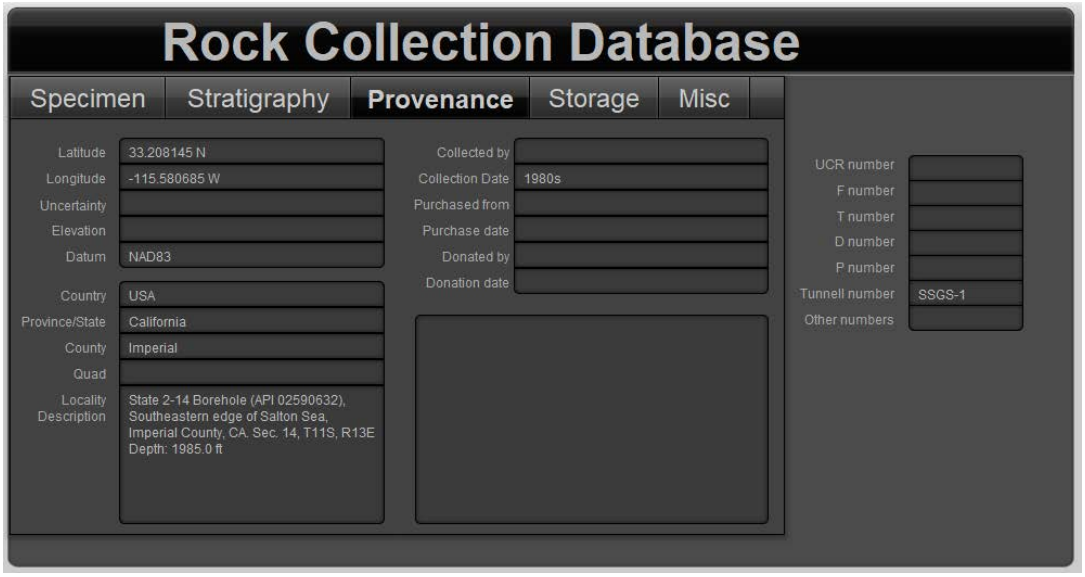

Figure A4.17. Photograph of a State 2-14 sample which was taken by an intern who worked on this study.

The work completed by the interns ensures that any future scientists who wish to revisit these specimens for any future studies will be able to easily locate and access them, with confidence that the information associated with them is accurate. Uribe additionally volunteered to work with other members of the Lithium Valley Quantification project on community outreach.

Mineralogic Investigation Interns. Hannah Rose Hoover and Brianna Wenzel worked as mineralogic investigation interns starting in the summer of 2022. Javier Calzada, Grace Huseman, and Alejandro Ramirez joined the intern team in the fall of 2022 to expand upon the research-related activities that the interns were undertaking. All interns investigated Li contents in rock samples from the Salton Sea Geothermal Field using a variety of methods. All students worked on sample preparation and documentation. This work involved photo-documenting samples (Figure A4.18), recording laboratory notes as they worked on the samples (Figure A4.19), picking and sorting samples under a microscope, and powdering rock samples for whole rock analyses using an alumina crucible. Through these tools, the interns investigated Li content variations of textural and mineralogic differences within their thin sections. Calzada investigated mineral abundances in the thin sections using MATLAB and the SEM backscatter electron maps that were made over the course of this study to extrapolate possible whole rock Li concentrations of the host rocks by pairing the relative abundance of Li-bearing minerals in the rocks with known Li-concentrations for those minerals from the same rocks that were measured in this study via LA-ICP-MS. When examining the sample from ~2358 m depth in the State 2-14 well, the intern found an average chlorite abundance of ~30% for the regions analyzed. Pairing this with the average observed concentration for Li at this depth being ~410 ppm, the whole rock estimate for the sample from ~2358 m is 125 ppm Li. This value is higher than the average measured whole rock Li concentration in this rock sample, ~82 ppm. Given that the backscatter maps made of this sample for this study were biased in favor of sampling the mudstone heavy regions rather than the anhydrite heavy regions (where the Li concentration is nearly 0 ppm), it is expected that the estimated whole rock Li concentration would be higher than the measured value.

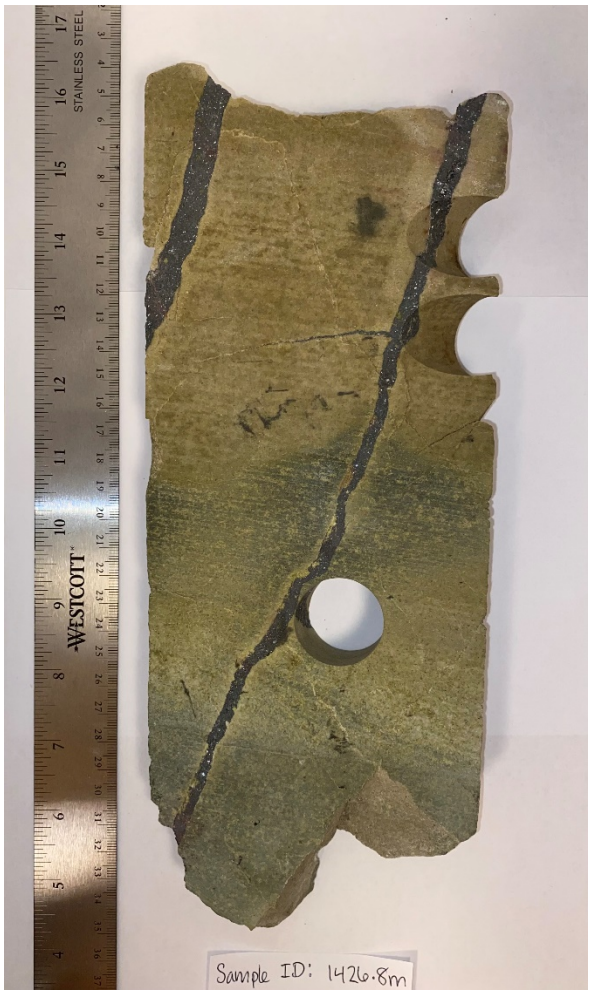

Figure A4.18. Example of a database entry for a State 2-14 specimen.

About the Interns. This work supported researchers at the University of California Riverside, a federally designated HSI- and AANAPISI-serving institution that has been ranked No. 1 nationally in social mobility by US News and World Report for four consecutive years for the success with which Pell grant recipients are graduated on 4-year time scales. This specific research was accomplished with the help of five undergraduate students from a variety of backgrounds and identities, including students who are the first generation to attend college, nontraditional (i.e., undergraduates who are older and thus more likely to have increased responsibilities beyond the classroom than the typical undergraduate student), Latina, Chicano, Mexican American, LGBTQ+, second-generation immigrants, and from lower socio-economic backgrounds. Several interns have reported that the skills acquired through the course of this internship have been useful in other research projects they have worked on or plan to work on. Another intern reported that working on this project helped ground the theory that they were learning. The interns were actively mentored by two Ph.D. holders and one Ph.D. candidate, one of whom is a woman and two of whom are nonbinary. Following their research experiences, four of the interns graduated from their undergraduate programs. Two of the interns are continuing to graduate school, and the remaining two interns are either in the process of applying or are considering applying to graduate school in disciplines that are in or adjacent to the earth and environmental sciences.

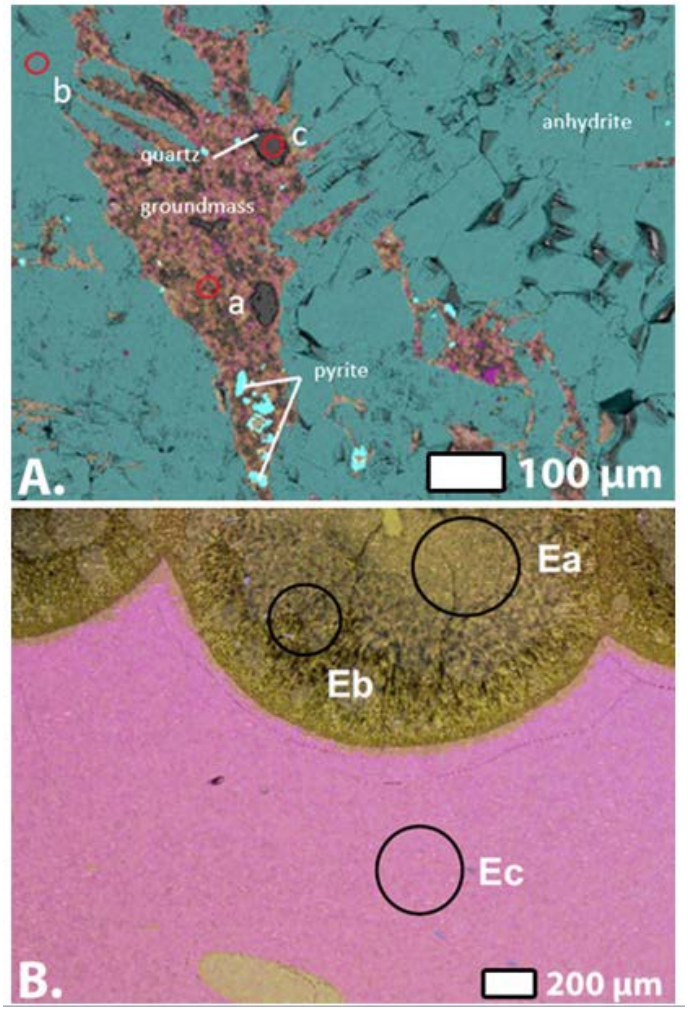

Figure A4.19. Maps of those regions, and then specific spots to analyze further via LA-ICP-MS. A. Backscatter Electron map of metasedimentary anhydrite and mudstone from ~2358 m depth. Regions relatively high in Mg concentrations are yellow. Regions relatively high in Al concentrations are pink. Regions relatively high in S concentrations are blue. Minerals identified by the intern are labeled on the map. Spots analyzed via LA-ICP-MS are circled in red and annotated with lowercase letters. B. Backscatter Electron map of spherulitic obsidian from Obsidian Butte, a surface sample. Regions relatively high in Na concentrations are yellow. Regions relatively high in K concentrations are pink. Regions relatively high in Ca concentrations are blue. Spots analyzed via LA-ICP-MS are circled in black and annotated with both uppercase and lowercase letters.

Appendix Chapter 7

Recent Colorado River Negotiations

In June 2022, the U.S. Bureau of Reclamation (USBR), the watermaster for the Colorado River, raised concerns about water levels in Lake Mead and Lake Powell, which were falling and could impede the functioning of their dams. Specifically, USBR wanted to ensure reservoir water levels would not fall below elevations where hydropower could no longer be produced (the "minimum power pool" elevation) or, worse, the water level at which water could no longer flow downstream of the dam (the "dead pool" elevation; USBR, 2023). In May 2023, Lake Mead's reservoir elevation was about 1050 feet above sea level, and it was operating at ~27% capacity; the minimum power pool elevation for Lake Mead is 950 feet (7% capacity), and the dead pool elevation is 895 feet (0% capacity).

To prevent a loss of hydropower production, the USBR asked states in the Colorado River basin to revise their most recent drought contingency plans from 2019 with voluntary agreements to significantly reduce water withdrawals by 2-4 MAF per year, or up to one-third of current allocations (13 MAF) (USBR, 2023). The deadline for the agreement was January 31, 2023 (Partlow, 2023). After that, the USBR could impose new water use requirements at a federal level (Shields, 2022).

In October 2022, the State of California, including Imperial Irrigation District (IID), voluntarily reduced its water consumption by about 10% (400,000 AF per year), of which 250,000 AF per year would come from IID (Becker, 2022). On January 31, 2023, the deadline for voluntary agreement, six of the basin's seven states proposed a plan to reduce water use by 20%, with the largest cuts coming from Arizona and California (Partlow, 2023). This plan, which California did not endorse, asked California to cut its water use by 1 million AF per year. California said it would offer an alternative plan. In April 2023, the USBR released a draft Supplemental Environmental Impact Statement (SEIS) analyzing potential near-term reservoir operation decisions along the Colorado River. It concluded that, unless the lower basin states reduced their water demand, Lake Powell and Lake Mead could reach minimum power pool elevation and could no longer produce hydropower by 2026 (USBR, 2023).

Water Quality Data and Regulations

Data for this study was collected from the Groundwater Ambient Monitoring and Assessment Program (GAMA) of the California Water Board, which compiles groundwater testing data for almost 300,000 wells in California collected by multiple agencies. These data are publicly accessible through the **GeoTracker GAMA interactive map** (SWRCB 2020).

Water constituents' maximum contaminant level goals (MCLGs) represent the concentration at which the constituent causes no known adverse health effects. Federal allowable maximum contaminant levels (MCLs) for a constituent are established as close as possible to the MCLG while considering costs. The Safe Drinking Water Act (SDWA) establishes the federal MCLs, and the EPA sets and enforces them. States are allowed to set regulations that are more strict than federal regulations. Every five years, the EPA releases a contaminant candidate list (CCL), a list of contaminants that are likely present in public water supplies but are not currently regulated by the EPA. Once the list is released, the EPA must carefully evaluate available data for at least five contaminants from this list to decide if they will be

regulated under the SDWA. For example, in Table 8.1, perchlorate is indicated as being on CCL. It is currently being evaluated to determine if the EPA will regulate this contaminant in drinking water at a federal level. California has already set regulations for perchlorate.

The public health goals (PHGs) are set by the California Office of Environmental Health and Hazard Assessment (OEHHA) and indicate the contaminant level that could be associated with adverse health effects. PHGs indicate the concentration of a contaminant that poses no significant health risk if consumed in drinking water over a lifetime, based on the current state of knowledge, for contaminants with MCLs or MCLs that will be adopted (OEHHA, 2023). State MCLs are set by the State Water Resources Control Board (SWRCB) and are adopted as regulations. These are set as close to the PHGs as possible while being technically and economically feasible.

Total dissolved solids (TDS) are regulated by a secondary MCL, a standard set to address aesthetic concerns about drinking water (e.g., taste, odor). Contaminants regulated by secondary MCLs are not harmful to health, and therefore they only need to be tested on a voluntary basis (U.S. EPA, 2023). Secondary MCLs have no associated PHGs or MCLGs. The recommended secondary MCL in California for TDS is 500 mg/L, the upper level is 1,000 mg/L, and the MCL for short term exposure is 1,500 mg/L (SWRCB, 2018a; b).

Geothermal Flash Process Description

In flash-steam geothermal plants, water is extracted from production wells. In the SS-GF, these wells are between approximately 600-2500 meters (2000-8000 ft) deep. Natural pressure pushes the fluid to the surface. The water begins at a temperature of 225-260°C (440-500°F) and a pressure of 2.4-3.2 megapascals (MPa; 330-450 pounds per square inch gauge [PSIG]). As the fluid approaches the surface and pressure decreases, it is vaporized, or "flashed." The vapor drives a turbine that powers a generator to produce electricity. Any fluid that was not vaporized initially may be transferred to a series of separators or crystallizers operating at successively lower pressures to be "flashed." Each flash generates vapor used to produce electricity in a turbine. After the turbine, the spent geothermal vapor is condensed back to a liquid and cooled for reinjection. Non-condensable gases that were mixed with the steam are treated to remove hydrogen sulfide (see Chapters 8 and 9) and released into the atmosphere.

Any remaining unflashed geothermal fluid is moved to a final flash tank operating at atmospheric pressure. This fluid contains concentrated constituents from the brine. A portion of the remaining fluid is treated and recirculated back into the crystallizers as dilution water. The remaining fluid is treated through clarifiers that allow suspended solids (mostly iron silicate) in the liquid to settle out before the brine is reinjected into the injection well. The number of clarifiers needed depends on the quality and quantity of fluid being treated and what the remaining liquid will be used for (e.g., reinjection or Li extraction).

Hexavalent-chromium

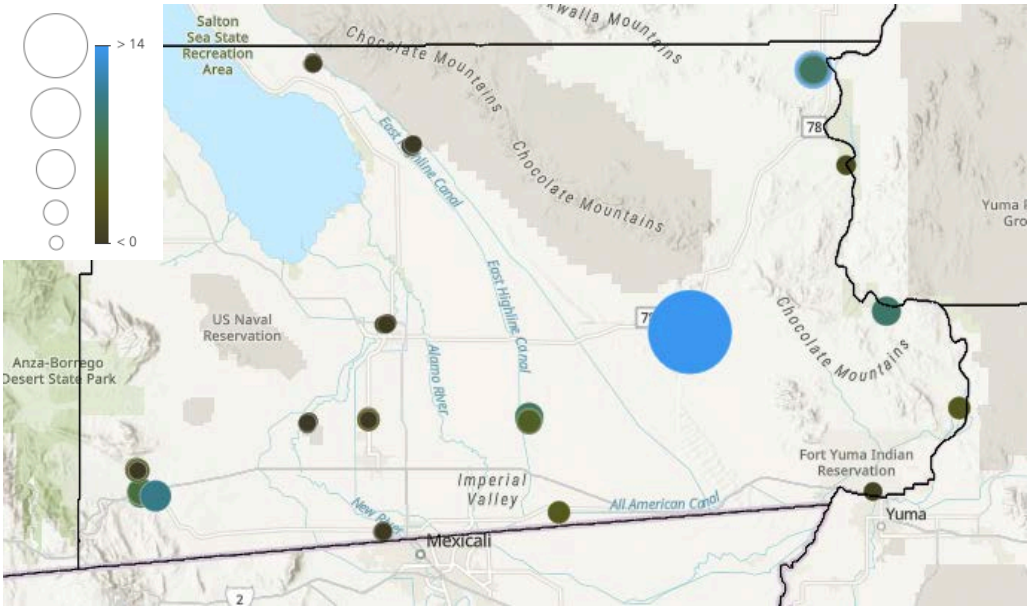

Figure A7.1. Hexavalent-chromium concentrations in groundwater wells in Imperial County. Color and size indicate the concentration.

NO_3-N

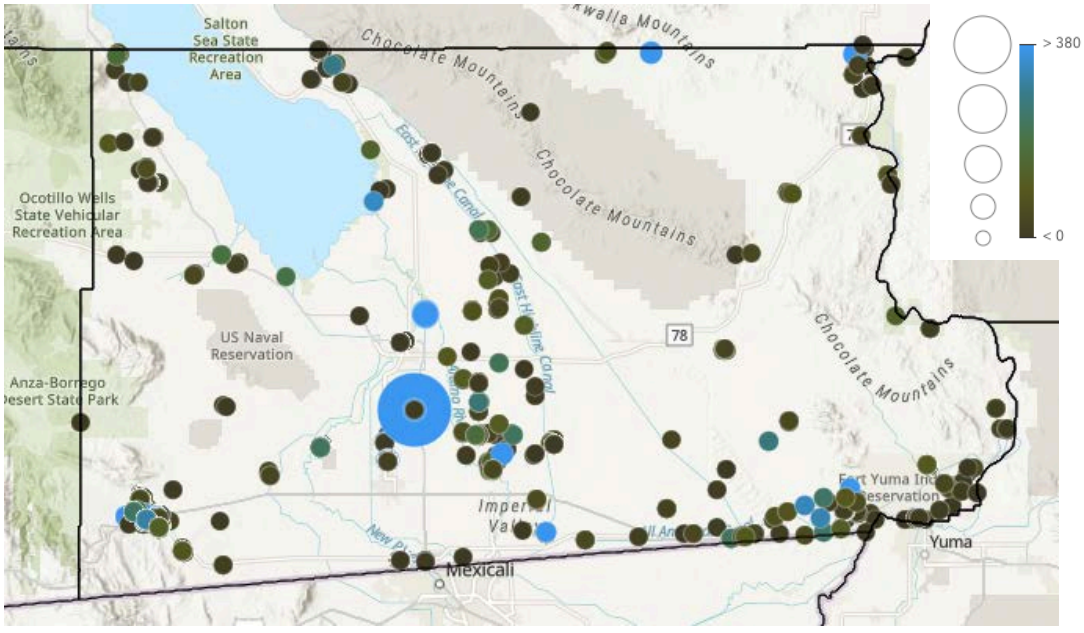

Figure A7.2. NO_3-N concentrations in groundwater wells in Imperial County. Color and size indicate the concentration.

Perchlorate

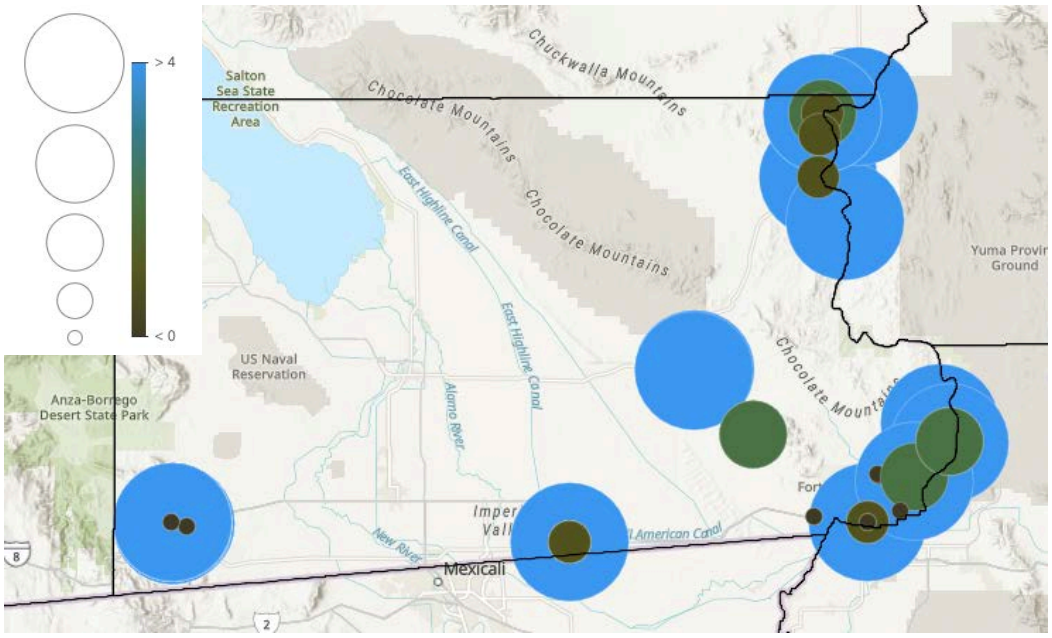

Figure A7.3. Perchlorate concentrations in groundwater wells in Imperial County. Color and size indicate the concentration.

Uranium

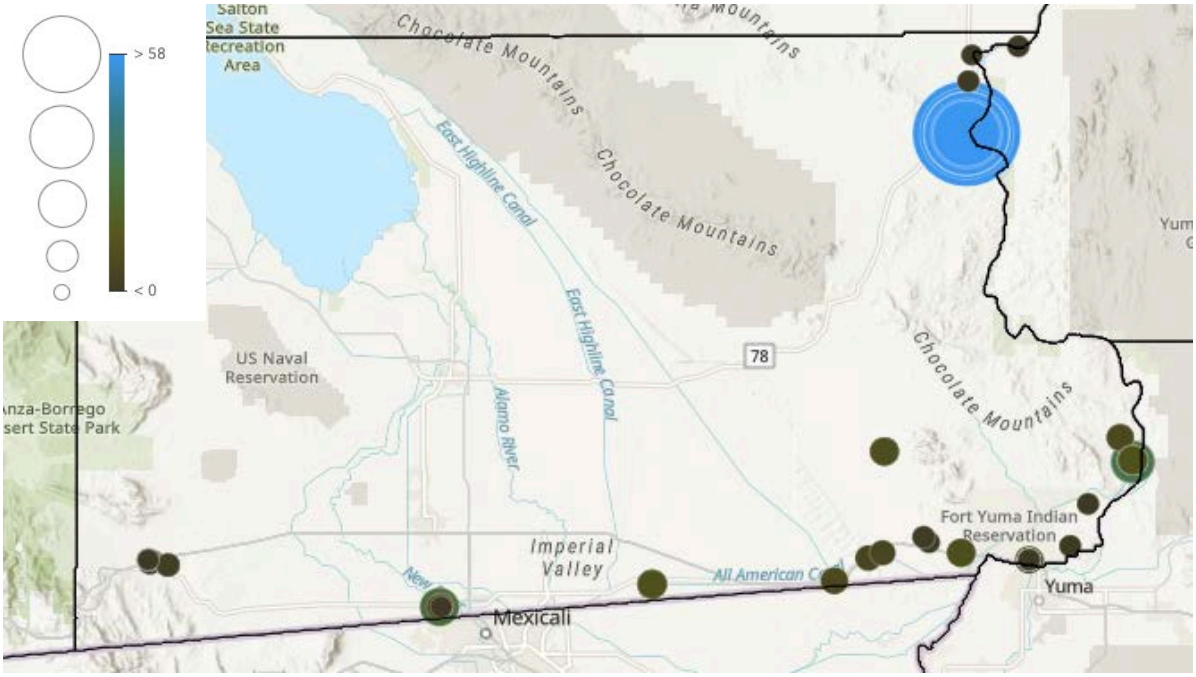

Figure A7.4. Uranium concentrations in groundwater wells in Imperial County. Color and size indicate the concentration.

Appendix Chapter 8

Sources for Evaluating Emissions

To understand the context of geothermal emissions in relation to other sources, we need to determine both the rate of pollutant emission and how much energy production is associated with that rate. Doing so is non-trivial, due to variations in reporting methods. Each reporting agency has its own evaluation and reporting methods, as well as facility groupings/naming conventions. It is also difficult to determine whether nonreporting for certain emissions reflects emission levels below reporting limits or non-compliance with reporting requirements. Therefore, in an effort to clearly define these discrepancies as well as the limitations of our results, we provide a summary of the data sources used to account for both energy production and emissions from geothermal energy in the SS-KGRA.

U.S. Energy Information Administration (EIA)

The U.S. Energy Information Administration (EIA) reports net generation for energy sources at the facility level each year. Figure A8.1. shows the many types of power plants, in addition to geothermal, in California. According to the California Energy Commission (CEC), geothermal energy accounted for 5.7% of energy production in California in 2021 (CEC, 2021). We compare emissions from geothermal electricity production to emissions from other types of electricity generation, including biomass and natural gas (important in California), coal (important outside of California), and oil (minimally used for electricity in the U.S.).

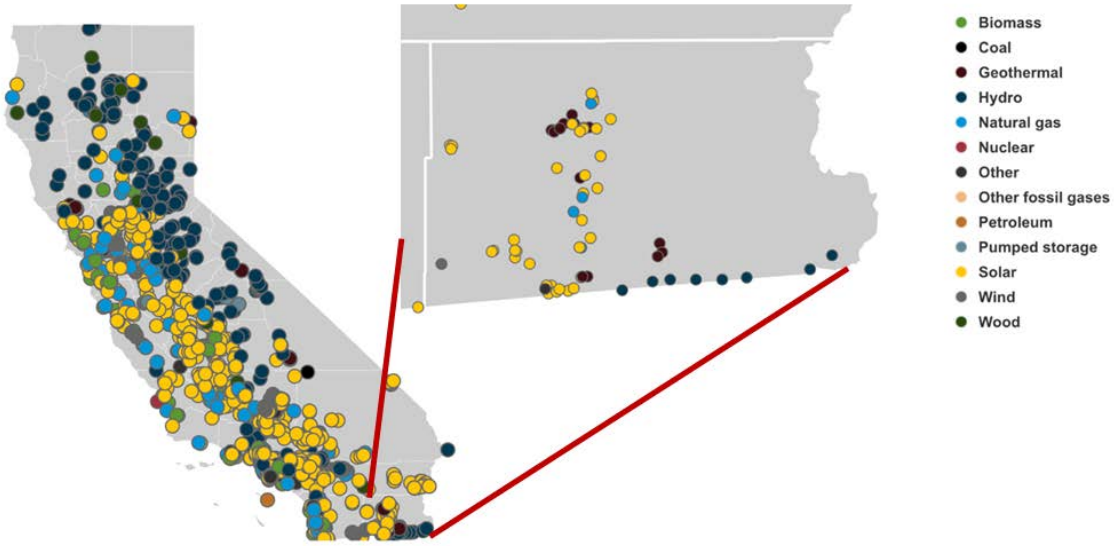

Figure A8.1. Map of energy production facilities in Imperial County, California. The figure has been adapted from the EIA interactive mapping tool.

EIA provides data on annual generation and fuel consumption for power plants. This information is collected through Form EIA-923, which is mandatory for regulated and unregulated power plants to complete under the Federal Energy Administration Act of 1974 (Public Law 93-275). These data are used

to determine net generation from each geothermal facility in California for the years associated with emissions reporting.

California Air Resources Board (CARB)

Carbon dioxide emissions: Carbon dioxide emissions for geothermal energy plants were obtained from the California Air Resources Board (CARB) for 2014-2020, and results from 2020 are used in this report. When reporting these values to CARB, individual facilities must provide specific descriptions of the methods used to monitor or calculate these emissions. The chosen method of monitoring or calculating must be kept consistent between reporting years. Emissions are calculated based on Tiers that describe the level of direct measurement versus modeling assumptions (higher Tiers depend more on direct measurements). To generate estimates of emissions, Tier 1 uses emission factors and default heat values, Tier 2 uses emission factors and a fuel's measured heat value, Tier 3 utilizes a fuel's measured carbon content, and Tier 4 uses quality assured data from a continuous emission monitoring system (CARB, 2019).

Toxins and Criteria Pollutants: CARB has also developed an emissions inventory requiring statewide annual reporting of air pollutant and toxic emissions as part of the "Regulation for the Reporting of Criteria Air Pollutants and Toxic Air Contaminants (CTR)." The amendment took effect on January 1, 2020, and the first round of reporting was required on May 1, 2020. Actual emissions refer to emissions measured, observed, or estimated to have been released.[4] For each pollutant, facilities are required to report actual emissions, and if estimated, the emissions factor, source of emissions factor, and emissions calculation method. The method of measuring or calculating each pollutant is not reported in the public CARB database. Toxins emissions for geothermal energy plants in the SS-KGRA as well as biomass and natural gas facilities in the same region were obtained for 2014-2020, and results from 2017 are used in this report to allow for comparison to other sources of toxin reporting (see NEI description below).

National Emissions Inventory (NEI)

The National Emissions Inventory (NEI) provides an estimate of air emissions from point, nonpoint, on-road, nonroad, and "event" sources. To develop this estimate, the U.S. EPA collects data from State, Local, and Tribal air agencies, and supplements these data with additional U.S. EPA data. The inventory is built through the Emissions Inventory System (EIS) (U.S. EPA, 2015a; b). The 2017 reporting year was used to verify toxins reporting from CARB in the same year; the reporting to these inventories matched. Further, these data were used to contextualize geothermal emissions with emissions from other sectors in California. In 2017, 75% of geothermal facilities in the SS-KGRA (on an energy generation weighted basis) reported PM_{10} and $PM_{2.5}$ emissions to NEI. Similarly, 86% and 84% of facilities (also on an energy generation weighted basis) reported benzene and H_2S emissions, respectively.

[4] https://ww2.arb.ca.gov/sites/default/files/barcu/regact/2018/ctr2018/ctrfro.pdf

Emissions and Generation Resource Integrated Database (eGRID)

The U.S. EPA provides a comprehensive data set for environmental characteristics of electric power generation in the United States through the Emissions and Generation Resources Integrated Database (eGRID). Emissions data is based on plant-specific data reported to the U.S. government, and for facilities with no measurement capability, emissions are calculated. Additionally, all geothermal emissions in the database are estimated. Data is published annually (U.S. EPA, 2020).

Summary of Naming Conventions kWh basis in upcoming sections.

Table A8.1 provides a summary of the naming conventions for facilities through each reporting agency (energy production and emissions) in the SS-KGRA. This table defines how plants were grouped when emissions were evaluated on a g/kWh basis in upcoming sections.

Table A8.1. Summary of naming conventions for reporting agencies for geothermal facilities in Imperial Valley for 2017

EIA		CARB Toxins		CARB		California Geothermal Energy Statistics and Data			NEI - EPA	
eiaID	eiaName	FAC ID	Name	ARBID	Facility Name	ID	Plant Name - CA Energy Commission	ALIAS	EIS ID	FACILITY
10632	Del Ranch Company	50	A. W. Hoch	100716	CalEnergy Operating Corporation - Region 2 – Geothermal	T0012	AW HOCH	DEL RANCH LTD. (NILAND #2)	180011	A. W. HOCH
50210	Vulcan-BN Geothermal Power Company	44				T0053	VULCAN	BN GEOTHERMAL - VULCAN, (NILAND #1)		
10634	Elmore Company	49	J.J. Elmore	100692	CalEnergy Operating Corporation - J J Elmore - Geothermal	T0015	JJ ELMORE	ELMORE LTD. (NILAND #3)	179911	J.J. ELMORE
54996	Salton Sea Power Gen Co - Unit 4		CalEnergy Operating Company Region 1	100712	CalEnergy Operating Corporation - Region 1 - Geothermal	T0016	SALTON SEA 4		179711	CALENERGY OPERATING COMPANY REGION 1
55983	Salton Sea Power LLC - Unit 5					T0017	SALTON SEA 5	SALTON SEA POWER LLC (CALENERGY)		
10878	Salton Sea Power Gen Co - Unit 1					T0047	SALTON SEA 1	SALTON SEA POWER GENERATION L.P. #1		
10879	Salton Sea Power Gen Co - Unit 2					T0048	SALTON SEA 2	SALTON SEA POWER GENERATION L.P. #2		

EIA		CARB Toxins		CARB		California Geothermal Energy Statistics and Data			NEI - EPA	
eiaID	eiaName	FAC ID	Name	ARBID	Facility Name	ID	Plant Name - CA Energy Commission	ALIAS	EIS ID	FACILITY
10759	Salton Sea Power Gen Co - Unit 3	72	Salton Sea Power Gen/unit 3			T0049	SALTON SEA 3	SALTON SEA POWER GENERATION L.P. #3		
10631	CE Leathers	51	J.M. Leathers	100703	CalEnergy Operating Corporation - J M Leathers - Geothermal	T0034	JM LEATHERS	LEATHERS,L.P.(NILAND #4), LEATHERS L.P.	180111	J.M. LEATHERS
55984	CE Turbo LLC					T0073	CE TURBO LLC			
57475	John L. Featherstone Plant		Hudson Ranch Power 1	104346	Hudson Ranch Power I - Geothermal					
54689	Heber Geothermal	43	Ormat Nevada, Inc (Heber)			T0033	HEBER GEOTHERMAL CO.	HEBER FIELD COMPANY		
54038	Geo East Mesa II	53	Ormesa Gem 2 & 3	100695	Ormat Nevada, Inc./ GEM 2 & 3 - Geothermal	T0021	GEM II	GEM RESOURCES II, LLC	5812911	ORMESA GEM 2 AND 3
10763	Geo East Mesa III			100695	Ormat Nevada, Inc./ GEM 2 & 3 - Geothermal	T0022	GEM III	GEM RESOURCES III, LLC		

EIA		CARB Toxins		CARB		California Geothermal Energy Statistics and Data			NEI - EPA	
eiaID	**eiaName**	**FAC ID**	**Name**	**ARBID**	**Facility Name**	**ID**	**Plant Name - CA Energy Commission**	**ALIAS**	**EIS ID**	**FACILITY**
56832	North Brawley Geothermal Plant		Ormat Nevada, Inc Orni 18 (Brawley)	104495	Ormat Nevada, Inc. / ORNI 18 North Brawley - Geothermal					

Availability of Overall Air Quality Sensors

In the region, there are multiple sources of air quality sensors that measure ambient air quality. Both CARB and Imperial County have air quality sensors. Note: these sensors do not measure emissions from geothermal facilities, but simply measure air quality at their location.

CARB Monitoring Network

Locations of the CARB sensors around the Salton Sea are illustrated in Figure A8.2. Commonly reported pollutants relevant to this report are PM_{10} and $PM_{2.5}$. Data from these monitors can be publicly accessed by selecting a monitoring site through the CARB website (CARB, 2023a; b; c). CARB has developed standard operating procedures for each of the measurements they conduct at these sites, including methods and specific instrumentation (CARB, 2023a; b; c).

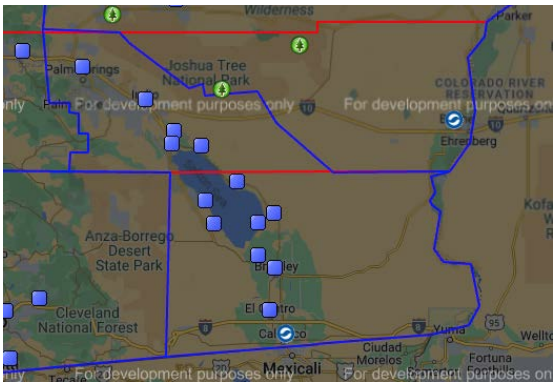

Figure A8.2. CARB air quality monitoring.

Imperial County Monitoring Network

Imperial County air quality monitoring stations are illustrated in Figure A8.3. These sites also report PM_{10} measurements in the area as well as the potential health implications of the current air quality level. Emissions from this network can be publicly accessed (CARB, Imperial County Air Pollution Control District et al., 2023). This information can also be accessed by requesting air quality forecast emails or through a smart phone application.

Figure A8.3. Imperial County air quality monitoring stations.

Local and NGO Monitoring Efforts

The California Environmental Health Tracking Program, Comité Cívico del Valle (a local community organization), and the University of Washington partnered to develop a real-time, community-level air quality monitoring network through a National Institute of Environmental Health Sciences (NIEHS) grant from the National Institutes of Health (NIH). Through this effort, Comité Cívico del Valle has installed 40+ air quality monitors to measure PM_{10}; locations of these monitors are illustrated in Figure A8.4. The associated data can be publicly accessed (Imperial County Department of Toxic Substance and Comité Cívico del Valle, 2023). Gray monitors are offline, and the colored stations indicate community air quality levels and associated recommendations for the safety of outdoor activity. Monitors measure PM_{10} and $PM_{2.5}$.

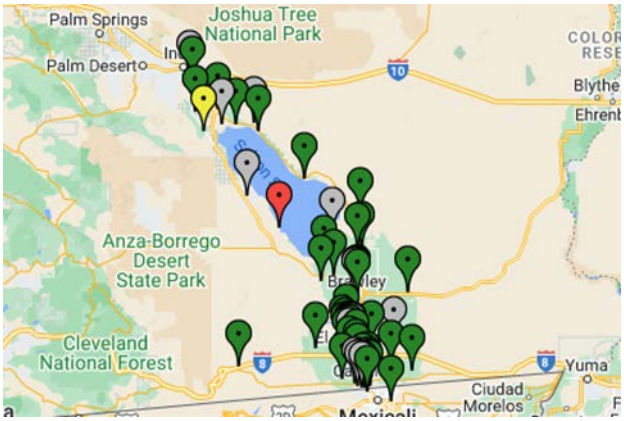

Figure A8.4. Network of IVAN monitoring stations.

Table A8.2. Summary of naming conventions and plant IDs for geothermal plants in California for each of the air emissions reporting agencies used in this report

EIA				CARB Toxins		CARB		California Geothermal Energy Statistics and Data			NEI - EPA	
eiaID	eiaName	eiaOperator	Operator ID	FAC ID	Name	ARBID	Facility Name	ID	Plant Name - CA Energy Commission	ALIAS	EIS ID	FACILITY
10632	Del Ranch Company	CalEnergy Operating Corporation		50	A. W. Hoch	100716	CalEnergy Operating Corporation - Region 2 - Geothermal	T0012	AW HOCH	DEL RANCH LTD. (NILAND #2)	180011	A. W. HOCH
10634	Elmore Company	CalEnergy Operating Corporation		49	J.j. Elmore	100692	CalEnergy Operating Corporation - J J Elmore - Geothermal	T0015	JJ ELMORE	ELMORE LTD. (NILAND #3)	179911	J.J. ELMORE
54996	Salton Sea Power Gen Co - Unit 4	CalEnergy Operating Corporation						T0016	SALTON SEA 4			
55983	Salton Sea Power LLC - Unit 5	CalEnergy Operating Corporation			Calenergy Operating Company Region 1			T0017	SALTON SEA 5	SALTON SEA POWER LLC (CALENERGY)		
10878	Salton Sea Power Gen Co - Unit 1	CalEnergy Operating Corporation				100712	CalEnergy Operating Corporation - Region 1 - Geothermal	T0047	SALTON SEA 1	SALTON SEA POWER GENERATION L.P. #1	179711	CALENERGY OPERATING COMPANY REG
10879	Salton Sea Power Gen Co - Unit 2	CalEnergy Operating Corporation						T0048	SALTON SEA 2	SALTON SEA POWER GENERATION L.P. #2		
10759	Salton Sea Power Gen Co - Unit 3	CalEnergy Operating Corporation		72	Salton Sea Power Gen/unit 3			T0049	SALTON SEA 3	SALTON SEA POWER GENERATION L.P. #3		
10631	CE Leathers	CalEnergy Operating Corporation		51	J.m. Leathers	100703	CalEnergy Operating Corporation - J M Leathers - Geothermal	T0034	JM LEATHERS	LEATHERS,L.P.(NILAND #4), LEATHERS L.P.	180111	J.M. LEATHERS
50210	Vulcan-BN Geothermal Power Company	CalEnergy Operating Corporation		44		100716	CalEnergy Operating Corporation - Region 2 - Geothermal	T0053	VULCAN	BN GEOTHERMAL - VULCAN, (NILAND #1)		
55984	CE Turbo LLC	CalEnergy Operating Corporation						T0073	CE TURBO LLC			
57475	John L. Featherstone Plant	Hudson Ranch Power I LLC			Hudson Ranch Power 1	104346	Hudson Ranch Power I - Geothermal					
54689	Heber Geothermal	ORCAL Geothermal, Inc	49748	43	Ormat Nevada, Inc (Heber)			T0033	HEBER GEOTHERMAL CO.	HEBER FIELD COMPANY		
54038	Geo East Mesa II	Ormat Nevada Inc	34691	53	Ormesa Gem 2 & 3	100695	Ormat Nevada, Inc./ GEM 2 & 3 - Geothermal	T0021	GEM II	GEM RESOURCES II, LLC	5812911	ORMESA GEM 2 AND 3
10763	Geo East Mesa III	Ormat Nevada Inc	34691			100695	Ormat Nevada, Inc./ GEM 2 & 3 - Geothermal	T0022	GEM III	GEM RESOURCES III, LLC		
56832	North Brawley Geothermal Plant	Ormat Nevada Inc	34691		Ormat Nevada, Inc Orni 18 (Brawley)	104495	Ormat Nevada, Inc. / ORNI 18 North Brawley - Geothermal					
52158	Aidlin Geothermal Power Plant	Geysers Power Co LLC	7160	10006024	Aidlin Geothermal Project	101527	Calpine - Geysers Power Company, LLC - Geothermal	T0023	AIDLIN I	GEOTHERMAL ENERGY PARTNERS 1	6577311	AIDLIN GEOTHERMAL PROJECT
								T0027	QUICK SILVER 16	CALPINE GEOTHERMAL UNIT 16, UNIT 16		
				10006014	GEYSERS POWER CO UNIT 17	101527	Calpine - Geysers Power Company, LLC - Geothermal	T0028	LAKEVIEW 17	CALPINE GEOTHERMAL UNIT 17, UNIT 17	1302811	GEYSERS POWER CO UNIT 17
				10006015	GEYSERS POWER CO UNIT 18	101527	Calpine - Geysers Power Company, LLC - Geothermal	T0029	SOCRATES 18	CALPINE GEOTHERMAL UNIT 18	1302911	GEYSERS POWER CO UNIT 18
				10006016	GEYSERS POWER CO UNIT 20	101527	Calpine - Geysers Power Company, LLC - Geothermal	T0030	GRANT 20	CALPINE GEOTHERMAL UNIT 20, UNIT 20	1303011	GEYSERS POWER CO UNIT 20
				10006004	GEYSERS POWER CO UNIT 5	101527	Calpine - Geysers Power Company, LLC - Geothermal	T0055	MCCABE 5 & 6	CALPINE GEOTHERMAL UNIT 5 & 6, UNIT 5 & 6	2008911	GEYSERS POWER CO UNIT 5
				10006005	GEYSERS POWER CO UNIT 6	101527	Calpine - Geysers Power Company, LLC - Geothermal				1302111	GEYSERS POWER CO UNIT 6
286	Geysers Unit 5-20	Geysers Power Co LLC	7160	10006006	GEYSERS POWER CO UNIT 7	101527	Calpine - Geysers Power Company, LLC - Geothermal	T0056	RIDGE LINE 7 & 8	PG&E #7-#8, GEYSERS #7-#8, UNIT 7 & 8	1302211	GEYSERS POWER CO UNIT 7
				10006007	GEYSERS POWER CO UNIT 8	101527	Calpine - Geysers Power Company, LLC - Geothermal				3945711	GEYSERS POWER CO UNIT 8
				10006010	GEYSERS POWER CO UNIT 11	101527	Calpine - Geysers Power Company, LLC - Geothermal	T0058	EAGLE ROCK 11	CALPINE GEOTHERMAL UNIT 11, UNIT 11	1302511	GEYSERS POWER CO UNIT 11
				10006011	GEYSERS POWER CO UNIT 12	101527	Calpine - Geysers Power Company, LLC - Geothermal	T0059	COBB CREEK 12	CALPINE GEOTHERMAL UNIT 12, UNIT 12	1302611	GEYSERS POWER CO UNIT 12
				10006012	GEYSERS POWER CO UNIT 14	101527	Calpine - Geysers Power Company, LLC - Geothermal	T0061	SULPHUR SPRINGS 14	CALPINE GEOTHERMAL UNIT 14, UNIT 14	1302711	GEYSERS POWER CO UNIT 14
				230	Calpine Unit 13: Power/steam F	101527	Calpine - Geysers Power Company, LLC - Geothermal	T0060	BIG GEYSER 13 & 16	CALPINE GEOTHERMAL UNIT 13, 16	4197311	CALPINE UNIT 13: POWER/STEAM F
				240	Calpine Unit 16: Power/steam F	101527	Calpine - Geysers Power Company, LLC - Geothermal				4197411	CALPINE UNIT 16: POWER/STEAM F
510	Sonoma California Geothermal	Geysers Power Co LLC	7160			101527	Calpine - Geysers Power Company, LLC - Geothermal	T0046	SONOMA 3	SONOMA	6577211	SONOMA POWER PLANT
				290	Calpine - Calistoga Geothermal	101527	Calpine - Geysers Power Company, LLC - Geothermal	T0050	CALISTOGA 19	CALISTOGA GEOTHERMAL PARTNERS, L.P., CALISTOGA	50511	CALPINE - CALISTOGA GEOTHERMAL
50066	Calistoga Power Plant	Geysers Power Co LLC	7160	30	Calpine - Bear Canyon Creek	101527	Calpine - Geysers Power Company, LLC - Geothermal	T0005	BEAR CANYON 2	CALPINE GEYSERS CO.	50611	CALPINE - BEAR CANYON CREEK
				50	Calpine - West Ford Flat	101527	Calpine - Geysers Power Company, LLC - Geothermal	T0007	WEST FORD FLAT 4	WEST FORD FLAT/CALPINE GEYSERS CO, LP	50811	CALPINE - WEST FORD FLAT
											14368411	CALPINE - SIVERADO STEAM FIELD
											14338711	CALPINE 11/17 - NORTH STEAM F
											14369111	CALPINE UNIT 18 - SOUTH FIELD
10480	Mammoth Pacific I	Ormat Nevada Inc	34691	1316	Mammoth-pacific			T0035	MAMMOTH-PACIFIC I			
10481	Mammoth Pacific II	Ormat Nevada Inc	34691					T0036	MAMMOTH-PACIFIC II	MAMMOTH-PACIFIC LP II		
10479	Ples I	Ormat Nevada Inc	34691					T0038	PLES1			
54724	Ormesa II	Ormat Nevada Inc	34691	62	Ormesa 2			T0043	ORMESA GEOTHERMAL II			
50766	Ormesa I	Ormat Nevada Inc	34691	65	Ormesa 1			T0062	ORMESA GEOTHERMAL I			
7368	Geothermal 1	Northern California Power Agny	40613	10006017	Ncpa 1	101529	Northern California Power Agency - Geothermal Plant No. 1	T0039	GEOTHERMAL 1	NCPA 1, GEOTHERMAL PLANT 1	1303111	NCPA PLANTS 1 AND 2
7369	Geothermal 2	Northern California Power Agny	40613	10006020	Ncpa 2	101530	Northern California Power Agency - Geothermal Plant No. 2	T0040	GEOTHERMAL 2	NCPA 2, GEOTHERMAL PLANT 2		
				10006017	Ncpa Plants 1 And 2			T0039				
10873	Coso Finance Partners	Coso Operating Co LLC	4397	3050309	Coso Operating Company, Llc	100690	Coso Energy Developers (BLM E&W) - Geothermal	T0009	COSO ENERGY DEVELOPERS UNIT 7-9	COSO BLM EAST 7-8 AND WEST 9		
10874	Coso Power Developers	Coso Operating Co LLC	4397			101670	Coso Finance Partners (Navy I) - Geothermal	T0010	COSO FINANCE PARTNERS UNIT 1- 3	COSO NAVY 1		
10875	Coso Energy Developers	Coso Operating Co LLC	4397			101669	Coso Power Developers (Navy II) - Geothermal	T0011	COSO ENERGY DEVELOPERS UNIT 4-6	COSO NAVY 2		
54111	Second Imperial Geothermal	ORCAL Geothermal, Inc	49748					T0051	SECOND IMPERIAL GEOTHERMAL	SECOND IMPERIAL GEOTHERMAL CO SIGC PLANT		
10763	Ormesa III	Ormat Nevada Inc	34691									
902	Bottle Rock Power	Bottle Rock Power LLC	56589									
50964	Amedee Geothermal Venture I	Amedee Gethrm Venture I LP	472					T0001	AMEDEE GEOTHERMAL VENTURE I			
								T0063	ORMESA IE			
50762	Ormesa IH	Ormat Nevada Inc	34691					T0066	ORMESA IH			

Appendix Chapter 9

Regulatory Data Obtained from Agencies Operating in the SS-KGRA

Numerous county, state, and federal agencies oversee geothermal energy production and mineral extraction in the SS-KGRA. As part of this regulatory activity, many agencies collect data on various aspects and activities concerning geothermal energy and power production, including troves of information related to energy production, potential environmental impacts, and related issues. In addition, detailed information concerning routine and nonroutine activities are documented as part of extensive reporting requirements for numerous environmental and other operating permits. A major part of this study was the integration of publicly available information into a coherent and complete picture of the current environmental impacts of geothermal energy production in the SS-KGRA, and then using that information to make projections concerning potential future impacts from expanded geothermal energy production and the expected development of a *de novo* lithium mineral extraction industry. The following are descriptions of the agencies involved in the regulatory oversight of environmental and related issues for the SS-KGRA geothermal power plants (GTPPs). This regulatory oversight includes data collection that were used in this study. Note that only regulatory oversight related to geothermal brine, chemical use, and solid waste management are covered here. Data collected to evaluate air quality and water use are covered in other sections.

California Geologic Energy Management Division

In California, the Geologic Energy Management Division (CalGEM) regulates the geothermal industry. As part of this oversight, CalGEM collects data on geothermal brine extraction, including information on geothermal wells and the quantities and properties of brine produced from wells. Additionally, data are collected on the quantities of spent brine injected back into the geothermal reservoir. Data maintained by CalGEM is made publicly available through the GeoSteam database and can be accessed through their website (CalGEM, 2023a). Data on geothermal brine production – that was provided by CalGEM – was used in this study. The locations of the production and injection wells were obtained through CalGEM using their WellFinder website (CalGEM, 2023b). These locations were subsequently confirmed using Google Earth Pro.

California Energy Commission

The California Energy Commission (CEC) provides oversight on energy facilities and transmission systems in California. Data on power plants, including geothermal power plants, is provided on the CEC website. Additionally, energy production data are available through the U.S. Energy Information Administration (EIA). Energy data are made publicly available on their website (U.S. EIA, 2023). Data from EIA on gross and net power production at the SS-KGRA GTPPs were used in this study. Data on power plant capacity was obtained from the CEC.

California Department of Resources Recycling and Recovery

The California Department of Resources Recycling and Recovery (CalRecycle) provides oversight on waste management in California. Data on solid waste management facilities is collected by CalRecycle and made available in their Solid Waste Information System (SWIS) database that can be accessed

through their website (CalRecycle, 2023). The SWIS contains information such as facility locations, capacity, and classification. Documentation on the facilities is also available through SWIS (e.g., permit documents and regulatory correspondence). In this study, information on waste management facilities was obtained using SWIS to better understand how the SS-KGRA GTPPs are currently using waste management facilities and how they might access waste management options under expanded capacity and with the addition of lithium extraction processes. Although Imperial County is the local enforcement agency for waste management in Imperial County, all of the information and data that we needed for this study were obtained from CalRecycle and the Water Board (discussed below).

California Department of Toxic Substances Control (DTSC)

The SS-KGRA power plants produce solid wastes as part of normal operations. Solid wastes and other wastes that have dangerous properties such as ignitability, corrosivity, reactivity, or toxicity are managed separately from nonhazardous solid wastes (California DTSC, 2022). In California, solid wastes that have characteristics of hazardous wastes according to state criteria are managed as hazardous wastes, even if they are not hazardous wastes by federal standards. As per state requirements, GTPP solid wastes that are deemed hazardous are tracked using a manifest system that requires "cradle to grave" tracking of these wastes, even if they are being disposed out-of-state as nonhazardous wastes. Records of these "manifest wastes" are publicly available in the DTSC Hazardous Waste Tracking System (HWTS) (California DTSC, 2023c). Using the HWTS data, we can evaluate how much hazardous waste is generated and how this waste is managed.

The HWTS requires a manifest be entered for each shipment of hazardous materials. The manifest includes complete information on wastes generated, transported, or disposed of. The manifest contains information about the quantity and types of waste transferred, as well as the ID numbers for both the generator and the transporter. The manifest also contains information about the receiver of the hazardous waste. The receivers are referred to as a treatment, storage, and disposal facility (TSDF). Data from the manifests is maintained by DTSC and made publicly available on the HWTS website (California DTSC, 2023b). Waste manifest information reported to the DTSC and posted in the HWTS was used in this study to evaluate quantities and types of wastes transported from SS-KGRA power plants.

To locate the generator IDs for geothermal power plants located in the Salton Sea KGRA, searches were completed of the HWTS database. The following search terms were used: "Salton Sea," "Energysource," "Calenergy Operating Corp Admin," "Calenergy Operating Company," "Elmore" AND "County = Imperial," "Hudson Ranch," "Leathers," "Vulcan," and "Featherstone." The search results were evaluated to determine if the resulting generator IDs were from Salton Sea geothermal power plants.

California State Water Resources Control Board

Regulation of Geothermal Power Plants

SS-KGRA GTPPs have lined ponds on-site that provide temporary storage of liquid and solid wastes. These "brine ponds" are classified by the State Water Resources Control Board (SWRCB) as Class II surface impoundments that require compliance with site-specific Waste Discharge Requirements (WDR) and a corresponding Monitoring and Reporting Program (MRP). The Colorado River Basin RWQCB

has jurisdiction in Imperial County, where the SS-KGRA power plants are located. Accordingly, the WDR and MRP for the SS-KGRA GTPPs are issued by the Colorado River Basin RWQCB, and all reporting is to the same RWQCB. Reporting and correspondence regarding the WDR and MRP are maintained and made publicly available on the SWRCB GeoTracker website (California SWRCB, 2023). GeoTracker contains the WDR as well as periodically submitted monitoring reports (annual reports, quarterly reports, etc.). GeoTracker also contains correspondence regarding chemical use, permit renewal, inspections, accidental spills, financial assurances, and proposed modifications to the facilities.

Brine ponds at the GTPPs have various configurations and sizes. The Salton Sea Units 1-5 power plants, comprising Region 1, share a single pond (California RWQCB Colorado River Basin Region, 2021b). The Vulcan and Del Ranch power plants along with the CE Turbo power plant, comprising Region 2, share two ponds (California RWQCB Colorado River Basin Region, 2022b). The Leathers, Elmore, and Featherstone power plants each have their own brine pond (California RWQCB Colorado River Basin Region, 2013c, 2015b, 2023b, 2023c). The WDRs are issued according to the pond locations. For example, the Salton Sea Units 1-5 share a single pond, and therefore, share a WDR and MRP with its corresponding monitoring and reporting requirements.

The WDRs and MRPs are intended to be updated approximately every five years. The process of updating the WDR for the Featherstone geothermal power plant is in progress (California RWQCB Colorado River Basin Region, 2023b). The WDR for the Leathers geothermal power plant will likely be updated soon, as it was last updated in 2015. The WDRs and MRPs are similar for all SS-KGRA power plants, although each document contains site-specific background information.

The brine ponds are permitted to receive a variety of wastes, as described in the WDR. For example, the Region 1 WDR contains the following language about which wastes are allowed in the brine pond (California RWQCB Colorado River Basin Region, 2021b). The orders for the other geothermal facilities contain similar language on allowable wastes.

"All of the following wastewater streams are directed to the Brine Pond and/or to the injection wells for direct injection into the geothermal reservoir:

- Cooling tower blowdown
- Geothermal drilling wastes
- Geothermal waste:
    - Geothermal brine (liquids)
    - Geothermal brine precipitates (solids)
- Portable shower effluent
- Spills and water from hydroblasting
- Wastewater generated from plant cleanups and washdowns from the plant conveyance system
- Vehicle wash station effluent
- Process filtrate from the Brine Pond filter press, geotextile solids-dewatering bags (used to dewater geothermal solids before final disposal), or other mechanical separator BMPs that the Discharger is granted approval to use by the Executive Officer
- Lime sump effluent

- Effluent from emission abatement equipment" (California RWQCB Colorado River Basin Region, 2021b; p. 9)

While liquid from the brine pond may be directed to the injection wells for injection into the geothermal reservoir, solids from the brine pond are periodically removed from the pond and disposed of off-site.

The WDR for the GTPP contains restrictions on activities that could impact operation of the brine pond (e.g., discharge of wastes to groundwater is prohibited). The WDR also contains specifications for operating the brine pond (e.g., a leachate collection and removal system [LCRS] and a leak detection system [LDS] are both required). The LCRS is designed to collect and remove leachate that develops between the first and second liner of the brine pond. The LDS is designed to detect any leakage from the second liner.

The MRPs specify monitoring related to operation of the brine ponds (California RWQCB Colorado River Basin Region, 2013a, 2015a, 2021a, 2022a, 2023a, 2023b). Routine monitoring is done to assess potential impacts to groundwater. This monitoring consists of groundwater monitoring done using monitoring wells, vadose zone monitoring, surface water monitoring, observed surface water monitoring, seep monitoring, and inspection and maintenance of the LCRS and LDS. Reporting also includes the monthly tonnage of solids removed from the brine ponds and disposed of off-site; these data are contained in semi-annual reports. The more recent MRPs (e.g., California RWQCB Colorado River Basin Region, 2021a) require reporting on monthly volumes of wastewater discharged to the brine pond, as well as average daily volumes of wastewater removed from the brine pond and a metals analysis on brine-pond solids (that includes arsenic, barium, cadmium, lead, and zinc). These more recent MRPs also require analyses of the brine-pond wastewater for pH, TDS, specific conductance, metals, other ions (e.g., calcium), carbonate, and alkalinity. The new WDR for the Featherstone plant requires monitoring of the mud sump that is covered by the WDR (California RWQCB Colorado River Basin Region, 2023b). Since older WDRs and MRPs were in place during the period where most of the data were collected for this study (e.g., 2014-2021), analytical data on the brine pond liquids and solids are not available. We were able to extract data on the monthly tonnage of brine pond solids removed and disposed of off-site for the 2014-2021 period. The tonnage data from the semi-annual reports and the brine pond solids analytical data, where available, were used in this study. Routine monitoring done to assess potential impacts on groundwater is overseen by the RWQCB. Analysis of results from routine monitoring of groundwater, surface water, the vadose zone, and the LCRS and LDS were not included in this report.

The SS-KGRA power plants are required to disclose the chemicals they use to the RWQCB and also gain approval from the RWQCB before new process chemicals are used (e.g., California RWQCB Colorado River Basin Region, 2021b, 2022b, 2023c). For example, the tentative WDR for the Featherstone geothermal power plant contains the following requirement: "At least 30 days prior to the use of a new chemical class for control of microbes, pH, scale, and corrosion of cooling tower water and/or geothermal brine, the Discharger shall notify the Regional Water Board's Executive Officer in writing. The use of a new class of chemicals may not be utilized until approved in writing by the Regional Water Board's Executive Officer" (California RWQCB Colorado River Basin Region, 2023b; p. 34). The requests for use of new chemicals are typically contained in written correspondence to the RWQCB and are usually accompanied by Safety Data Sheets (SDS) for the chemical products proposed. Correspondence for

chemical requests is publicly available on the GeoTracker website. Information on chemical requests and approval was used in this report.

Regulation of the Desert Valley Monofill

The Desert Valley Monofill is located in Brawley and is permitted as a Class II solid waste management facility (BRG Consulting Inc., 2021; California RWQCB Colorado River Basin Region, 2016a, 2016b). The Desert Valley Monofill is run by a subsidiary company of BHER, Desert Valley Company, and only GTPP operated by the BHER subsidiary CalEnergy (i.e., Region 1, Region 2, Elmore, and Leathers) dispose of their filter cake at the Desert Valley Monofill. The Featherstone power plant does not use the Desert Valley Monofill. Although the Monofill primarily accepts filter-cake solids, the facility is allowed to accept "geothermal drilling mud, sump material, filter cake, plastic liners, and soils contaminated with geothermal materials" (California RWQCB Colorado River Basin Region, 2016b; p. 2).

The Monofill has been in operation since 1991 (BRG Consulting Inc., 2021; California RWQCB Colorado River Basin Region, 2016a, 2016b). Construction of Cells 1 and 2 occurred in 1990 and 1999, respectively (California RWQCB Colorado River Basin Region, 2016b). Cells 1 and 2 were closed in 2008 after reaching their capacity. Construction of Cell 3 was completed in 2005 (California RWQCB Colorado River Basin Region, 2016b). Cell 3 is still active and receives filter cake, although it is expected to reach its capacity in 2025 (BRG Consulting Inc., 2021). The capacity of Cell 3 is approximately 1.3 million cubic yards (cy) and there was an estimated 590,546 cy remaining capacity as of 2020 (BRG Consulting Inc., 2021). The current limit for waste received is 750 tons per day (680 metric tons), and this limit has been in place since 2003 (CalRecycle, 2023).

A fourth cell at the Monofill, Cell 4, has been proposed to increase the Monofill's capacity. A CEQA process was initiated for the expansion that yielded a Notice of Determination (NOD) based on expected significant environmental impacts. An Environmental Impact Report (EIR) was prepared and distributed (BRG Consulting Inc., 2021). The EIR describes anticipated impacts, such as continuing truck traffic, and proposed mitigation measures.

Since the monofill is a Class II solid waste management facility, it can accept industrial wastes, but not hazardous wastes. There are various regulatory requirements and agencies involved in permitting and oversight of the monofill (BRG Consulting Inc., 2021). Relevant regulatory agencies include the California Department of Resources Recycling and Recovery (CalRecycle) and RWQCB (Colorado River Basin). The Monofill holds a Conditional Use Permit that was issued by Imperial County and as a result, various departments within the County are involved in oversight of the Monofill: Planning and Development Services, Air Pollution Control District, Environmental Health Services, and Public Works.

To demonstrate compliance with the Conditional Use Permit, the Desert Valley Company submits annual reports to Imperial County Planning and Development Services. These reports contain information about insurance policies, designated truck routes, and annual waste analyses for filter cake from the Region 1, Region 2, Elmore, and Leathers GTPP (Desert Valley Company, 2018a, 2019a, 2020a, 2021a, 2022a). The analytical data are collected on annual composite filter cake samples from each facility. The analytical data for the filter cake were used in this study.

As a result of the Class II solid waste management facility status, the Colorado River Basin RWQCB has issued WDR with the associated MRP for the Monofill (California RWQCB Colorado River Basin Region, 2016a, 2016b). Reporting done to show compliance with the WDR is sent to the RWQCB. Documentation and regulatory correspondence regarding this compliance are posted on the SWRCB's GeoTracker website (California State Water Resources Control Board, 2023). The annual reports to Imperial County to show compliance with the Conditional Use Permit are also posted on GeoTracker. Quarterly reports to the RWQCB contain summaries of monthly tonnage of filter cake and associated waste received at the Monofill from Region 1, Region 2, Elmore, and Leathers (Desert Valley Company, 2014, 2015a, 2015b, 2015c, 2015d, 2016a, 2016b, 2016c, 2016d, 2017a, 2017b, 2017c, 2017d, 2018b, 2018c, 2018d, 2018e, 2019b, 2019c, 2019d, 2019e, 2020b, 2020c, 2020d, 2020e, 2021b, 2021c, 2021d, 2021e, 2022b). The tonnage data from the quarterly reports and the filter-cake analytical data from the annual reports were used in this study.

The WDR and its associated MRP requires monitoring that includes monitoring of groundwater, surface water, and the vadose zone, as well as inspection and maintenance of the LCRS and LDS. The results of routine monitoring are reported to the RWQCB in quarterly and annual reports. Groundwater sampling is done on-site for turbidity, pH, conductivity, and temperature. Water levels are also reported. Groundwater samples are collected and analyzed for the following parameters quarterly: TDS, chloride, sulfate, arsenic, barium, cadmium, lead, sodium, zinc, gross alpha radiation, gross beta radiation, and gamma radiation. A trend analysis is completed using the groundwater data. The groundwater flow rate is calculated based on estimated hydraulic conductivity and porosity. The groundwater direction is estimated using an online U.S. EPA tool for site assessment. Monitoring of the following additional constituents of concern is required every five years: fluoride, nitrate, gross alpha particles, gross beta particles, cesium-137, cobalt-60, radium-226, potassium-40, thorium-228, thorium-232. Routine monitoring is overseen by the RWQCB, and results from groundwater monitoring, vadose zone monitoring, LCRS inspection, and LDS inspection are publicly available.

Regulation of the Salton City Landfill

The Salton City Landfill is permitted as a Class III municipal solid waste management facility. The landfill is owned by Imperial County and operated by a private company, Burrtec Waste Industries, Inc. Class III landfills are allowed to receive household and most other municipal wastes. In addition, the Salton City Landfill also has state and county permission to accept specific types of industrial wastes, including specific geothermal solid wastes. Since it is a landfill, various regulatory requirements apply, and there are various regulatory agencies involved, including the California Department of Resources Recycling and Recovery (CalRecycle) and RWQCB (Colorado River Basin). Imperial County is the Local Enforcement Agency (LEA) and is designated to provide regulatory oversight.

The ultimate planned capacity of the Salton City Landfill is approximately 50 million cubic meters (65.1 million cubic yards) where expansion is planned to occur in eight steps: Phase 1A and 1B, Phase 2A and 2B, and Phases 3 through 6 (Burrtec Waste Industries Inc., 2022). Phase 1 is complete and has an estimated closure date of 2028 (Burrtec Waste Industries Inc., 2022). The permitted capacity of Phase 1 is 1.7 million cubic meters (2,237,400 cubic yards) with 488,000 cubic meters (639,014 cubic yards) of that capacity remaining (CalRecycle, 2023). Construction of Phase 2A is complete and provides an additional

1.68 million cubic meters (2.2 million cubic yards) capacity that is projected to last 53 months (Geo-Logic Associates, 2021).

A Joint Technical Document (JTD) prepared for the Salton City Landfill as part of the landfill expansion planning describes operation of the facility, including descriptions of waste streams and testing procedures (Burrtec Waste Industries Inc., 2020, 2022). The JTD is periodically updated to reflect changes in operation, such as new waste streams. The JTD was updated in August 2020 to identify geothermal filter cake from the Featherstone geothermal power plant as one of its waste streams. The geothermal filter cake is described as "inert geothermal waste" with supporting documentation (Burrtec Waste Industries Inc., 2020). The JTD specifically excludes filter cake from any other geothermal source, drilling mud or cuttings from exploration activities, or waste originating from any geothermal well rejuvenation work (Burrtec Waste Industries Inc., 2020).

As described in the amended JTD, inclusion of geothermal filter cake as a waste stream at the Salton City Landfill is based on a review by the California Department of Public Health Radiologic Health Branch (CDPH-RHB). The CDPH-RHB concluded that filter cake waste was exempt from their regulations under normal operation of the geothermal power plant, because the radioactive constituents were typically below background concentrations found at the landfill, and because the radioactive constituents occur naturally (i.e., were not additives; Burrtec Waste Industries Inc., 2020). Radiation requirements are discussed on page 47 of the amended JTD, where it states: "Radiation levels are below the established protective health-base level for Radium of 5 pCi/g above background per USEPA the top 15 centimeters of soil at superfund cleanup projects" (Burrtec Waste Industries Inc., 2020).

The JTD states that the filter-cake waste produced during pipe-cleaning operations should not be sent to the landfill. Pipe-cleaning operations result in the release of accumulated scale within the power plant, and scales can contain higher content of radioactive constituents, such as radium (see discussion of scale below). In a review of the data for the Featherstone filter cake, CDPH-RHB found that only three out of 161 samples exceeded background radium levels at the Salton City Landfill. Two of the exceedances occurred during pipe cleaning operations. The resulting agreement between operators of the Featherstone power plant and CDPH-RHB was that the filter cake waste would not be sent to Salton City Landfill during pipe-cleaning events (Burrtec Waste Industries Inc., 2020).

The Salton City Landfill does not accept filter cake from any GTPP other than the Featherstone GTPP, referred to as Hudson Ranch Power I in the JTD. As stated on page 46 in the JTD: "Filter cake originating from a geothermal power operation other than the Hudson Ranch Power 1 operation will require a separate review and approval by Imperial County EHS and RWQCB" (Burrtec Waste Industries Inc., 2020). To our knowledge, no additional review of geothermal filter-cake waste from other sources has been requested.

Testing protocols for filter-cake waste are described in the amended JTD (Burrtec Waste Industries Inc., 2020). Each trailer load is tested for solids contents, pH, metals, and radioactivity. Incoming loads are scanned with a radiation detector. The expected solids content is 70%, while the minimum allowable solids content is 50%. Trailers are not delivered to Salton City until the test results are available and the acceptability of the waste can be evaluated. Third-party testing is done on every 10th trailer.

The JTD also contains information on the expected contribution of waste from the Featherstone geothermal power plant. As stated on page 49, "SCLF has a daily capacity of up to 124 cubic yards (approximately 9 truckloads of 14 cy per load) of Filter Cake. SCLF anticipates receiving up to 4 truckloads per day, Monday thru Saturday" (Burrtec Waste Industries Inc., 2020).

Monthly and quarterly tonnages reports for the Salton City Landfill were obtained from the GeoTracker website (California State Water Resources Control Board, 2023). The monthly reports contain daily sums of incoming waste by waste classification. The quarterly reports contain total tons received by the facility and this data is aggregated for the entire facility. These data were used in this study.

Chemicals Used in the SS-KGRA GTPP

In the SS-KGRA power plants, chemicals are added to cooling water systems, brine processes, and steam condensate. The chemicals are added to reduce scaling, biological growth, and corrosivity, as well as adjust fluid pH and limit emissions (primarily H_2S, although other air pollutants may be reduced as well).

The newer Waste Discharge Requirements (WDR) issued to the SS-KGRA power plants contain tables of process chemicals used on-site (RWQCB, 2021, 2022, 2023a, 2023b). These tables include descriptions of the chemical purpose and product numbers, but do not include chemical descriptions or registry numbers. The most recent WDR for the CalEnergy power plants, prepared for the Elmore plant (Table A9.1), has the most complete list of chemicals (RWQCB, 2023b; Table 2, p. 5-6). The WDR for Regions 1 and 2 have similar lists although those lists do not include ST-70 or the chemicals in the last five rows of Table A9.1 (RWQCB, 2021, 2022). The WDR for the Leathers power plant has not been updated since 2015 and the WDR does not contain a similar list of chemicals (RWQCB, 2015). However, it is presumed that chemical dosing strategies at the Leathers power plant are similar to the strategies used at the other CalEnergy power plants. The WDR for the Featherstone power plant is in the process of being updated. The tentative WDR contains a table with a list of chemicals used at the power plant, as shown in Table A9.2 (RWQCB, 2023a; Table 2, p. 8-9).

The WDR issued to the SS-KGRA power plants require RWQCB approval before new process chemicals are used. For example, the tentative WDR for the Featherstone geothermal power plant contains the following requirement: "At least 30 days prior to the use of a new chemical class for control of microbes, pH, scale, and corrosion of cooling tower water and/or geothermal brine, the Discharger shall notify the Regional Water Board's Executive Officer in writing. The use of a new class of chemicals may not be utilized until approved in writing by the Regional Water Board's Executive Officer (RWQCB, 2023a; p. 34)." The requests for use of new chemicals are typically contained in written correspondence to the RWQCB and are usually accompanied by Safety Data Sheets (SDS) for the chemical products proposed. Correspondence for chemical requests is posted on the GeoTracker website.

As part of this project, we aggregated the chemical request information and SDS to identify descriptions of the chemicals used on-site. We also referenced other sources where the chemical request could not be located on the GeoTracker website. The following are descriptions of the chemicals used at the SS-KGRA power plants.

Dispersants

The following are listed as dispersants used at the SS-KGRA power plants operated by CalEnergy: ChemTreat CL5428 and Nalco 3DT121, 3DT133, 3DT191, and 3DT102. Nalco 3DT121 is also listed as a dispersant used at the Featherstone power plant. The chemical products Nalco 3DT121 and 3DT133 are polyphosphate-based dispersants used to control scaling and protect against corrosion (Lue, 2016). No CASRN was given for these chemical products. Dispersants Nalco 3DT121 and 3DT191 were discontinued in 2017 (Lue, 2016).

Biodetergent/Surfactant

ChemTreat CL456, CL452, and CL453, as well as Nalco 73551 and 73550, are listed as being used as biodetergents at the CalEnergy power plants while only Nalco 73551 and 73550 are listed in the Featherstone WDR. ChemTreat CL453 is a proprietary blend of aliphatic amide hydrolysates (Lue, 2020; Rasmussen, 2020). The biodetergent CL452 contains a polyglucoside surfactant (68515-73-1) and a lauryl glucoside surfactant (110615-47-9) (Lue, 2019a).

Corrosion Inhibitor – Phosphate Based

Corrosion inhibitors listed as being used by CalEnergy included ChemTreat CT775, CT709, CT788, CL5788, CT790, and CL1495, as well as Nalco 3DT487, 3DT184, and 3DT195. The only corrosion inhibitor listed by Featherstone was EC1304A. The corrosion inhibitor products CT775 and 3DT487 both contain phosphoric acid (7664-38-2) (Lue, 2016, 2019a). The products CT788 and CT790 also contain phosphoric acid but also contain zinc sulfate (7733−02−0) and phosphoric acid, zinc salt (2:1) (13598−37−3), respectively (Lue, 2020). The corrosion inhibitor CL1495 contains potassium phosphate, tribasic (7778−53−2) and tetrapotassium pyrophosphate (7320−34−5 5) (Lue, 2020). Another corrosion inhibitor, FlexPro Plus CL 5788, contains 2-butenedioic acid (Z)-, homopolymer and 2-butenedioic acid (26099-09-2), and an unspecified proprietary chemical (Lue, 2020). While an SDS for EC1304A could not be located on the GeoTracker website, an SDS was located online that stated the following active ingredients: thioglycolic acid (68-11-1), proprietary imidazoline salts, and a proprietary quaternary ammonium compound.[5]

Non-Oxidizing Biocides

Non-oxidizing biocides listed as being used by CalEnergy included ChemTreat CL216, CL2250, CL2150, CL2115, and CL2065, as well as Nalco 7614, 7330, 7320, 7338, and ST-70. Of these, only ST-70 is listed in the Featherstone WDR. Note that ST-70 is an oxidizing biocide and is described in the next section. The non-oxidizing biocide ChemTreat CL2150 (also referred to as CL2250) contains 5-chloro-2-methyl-4-isothiazolin-3-one (26172-55-4) and 2-methyl-4-isothiazolin-3-one (2682-20-4) (Lue, 2020). The non-oxidizing biocide ChemTreat CL2115 contains glutaraldehyde (111-30-8), alkyl dimethyl benzyl ammonium chloride (68424-85-1), and ethanol (64-17-5) (Lue, 2020). ChemTreat CL2065 is another

[5] https://downloads.regulations.gov/EPA-R09-OW-2020-0359-0006/attachment_12.pdf.

non-oxidizing biocide used that contains tributyltetradecyl phosphonium chloride (81741-28-8) (Lue, 2019c).

Chlorine and Bromine Oxidizing Biocides

Sodium hypochlorite (12.5%) is listed that is an oxidizing biocide. Nalco Stabrex ST-70 is another oxidizing biocide used at power plants operated by CalEnergy and Featherstone; ST-70 contains sodium hypochlorite (7681-52-9), sodium bromide (7647-15-6), and sodium hydroxide (1310-73-2) (Lue, 2015).

Anti-Foam

The anti-foam products ChemTreat CL241 and Nalco 7471 are listed as being used by CalEnergy. Nalco 7471 is also listed for the Featherstone power plant, and this product contains a proprietary polyglycol ester chemical.

TowerBrom Tablets

TowerBrom tablets are used (TowerBrom 991 or C2187T) to reduce H_2S emissions in the cooling towers. The C2187T product contains trichloroisocyanuric acid (87-90-1), sodium bromide (7647-15-6), and boric acid (10043-35-3) (Lue, 2019a).

TowerBrom Granular

Granular TowerBrom 960 is also used (C2184G) to reduce H_2S emissions in the cooling towers. The C2184G product contains dichloroisocyanuric acid, sodium salt (2893-78-9), sodium bromide (7647-15-6), and sodium chloride (7647-14-5) (Lue, 2019a).

Table A9.1. List of process chemicals used at the Elmore geothermal power plant as identified in the most recent Waste Discharge Requirements (WDR) for the CalEnergy SS-KGRA power plants (RWQCB, 2023b; Table 2, p. 5-6). These chemicals have been approved by the Colorado River Basin RWQCB. The WDR for Regions 1 and 2 have similar lists although those lists do not include ST-70 or the chemicals in the last five rows of this table (RWQCB, 2021, 2022).

ChemTreat Product Names	**Purpose**	**Nalco Equivalents**
CL5428	Dispersants	3DT121, 3DT133, 3DT191, 3DT102
CL456, CL452, CL453	Biodetergent/Surfactant	73551, 73550
CT775, CT709, CT788, CL5788, CT790, CL1495	Corrosion Inhibitor - phosphate based	3DT487, 3DT184, 3DT195
CL216, CL2250, CL2150, CL2115, CL2065	Non-Oxidizing Biocides	7614, 7330, 7320, 7338, ST-70
12.5% Sodium Hypochlorite (Bleach)	Bleach Oxidizing Biocide	-
CL41, CL4520	Chlorine / bromine oxidizing biocides used in conjunction with an oxidant such as bleach (NaOCl)	1318
CL241	Anti-Foam	7471
C2187T	TowerBrom tablets	TowerBrom 991
C2184G	TowerBrom granular	TowerBrom 960
GS5810	Tower Cleaning	-
CL4822, P8000L	Prevent Iron Deposition	-
-	Flocculant	N9907
-	Anti Foam	N7471
-	NORMS Inhibitor	GE0901
-	Oxygen Scavenger	1720
-	Scale Inhibitor	GE0912, GE0906

Table A9.2. List of process chemicals used at the Featherstone geothermal power plant as identified in the most recent Waste Discharge Requirements (RWQCB, 2023a; Table 2, p. 8-9). These chemicals are approved for use by the Colorado River Basin RWQCB.

Purpose	Chemical Product Names (Nalco)
Cooling Tower Dispersant	3D TRASAR 3DT121
Bio-detergent	73550, 73551
Towerbrom Tablets Oxidizing Biocide / H2S Abatement	TB960
Towerbrom granular Oxidizing Biocide / H2S Abatement	TB991
Stabilized Bromine Utility Water Treatment	ST70
Antifoam	7471
Scale Inhibitor NORMS	GEO901
Flocculant	9907, 8170
Silica Scale Inhibitor	GEO982
Calcium Sulfate Scale Inhibitor	GEO 906
Steam Corrosion Inhibitor	EC1304A
Anti-Scalant used for Injection Well Scaling	GEO 991
Hydrochloric Acid	HCL
Phosphoric Acie	H3PO4
Caustic	NaOH
Hydrogen Peroxide 35%	H2O2

Tower Cleaning

The tower cleaning product listed in the CalEnergy WDR, GS5810, contains a non-specified chemical that is reported to be non-hazardous or present in a low concentration (Lue, 2019a).

Prevent Iron Deposition

The product ChemTreat P8000L (also referred to as CL4822) is used to prevent iron deposition; it contains sodium dimethyldithiocarbamate (128-04-1) (Lue, 2020).

Flocculant

A cationic flocculant, Nalco 9907, is used by both CalEnergy and Featherstone; no CASRN was provided for this product. The Featherstone power plant also lists Nalco 8170 as a flocculant that is used.

NORMS Inhibitor

The NORM inhibitor, GE0901, is used by both CalEnergy and Featherstone. GEO901 contains a proprietary phosphate ester chemical.

Oxygen Scavenger

An oxygen scavenger product is used at the CalEnergy power plants, Nalco 1720, that contains sodium bisulfite (7631-90-5) and potassium bisulfite (7773-03-7) according to an SDS found online (https://public.deq.virginia.gov/WPS/BRRO/VA0003026%20GP%20Big%20Island/2020%20Permit%20Reissuance%20Application/MSDS/NALCO%201720.pdf). Oxygen scavengers are useful for inhibiting scale formation.

Scale Inhibitor

Scale inhibitors used include Nalco GEO906 that contains formaldehyde (50-00-0) (Lue, 2018), and Nalco GEO912 that contains a non-specified chemical that is reported to be nonhazardous or present in a low concentration (Lue, 2019b). GEO982 is also listed as a silica scale inhibitor that is used. An SDS was submitted for GEO982 although the SDS does not list the ingredients (Lue, 2018).

Hydrogen Sulfide Control Chemistry

There are many alternatives for H_2S abatement in industrial settings (Nagl, 1999; Pudi et al., 2022; Rodríguez et al., 2014). The most common approach is to oxidize H_2S to sulfate using oxygen according to Equation 1:

$$H_2S + 2O_2 \rightarrow H_2SO_4 \qquad \text{Eq. 1}$$

Under some conditions, such as oxygen limitation, H_2S can be partially oxidized to elemental sulfur (Equation 2).

$$H_2S + 0.5O_2 \rightarrow S^0 + H_2O \qquad \text{Eq. 2}$$

Oxidation of sulfide to sulfur and sulfate (Eqs. 1 and 2) is mediated by bacteria that gain energy from the reaction; therefore, many H_2S control systems include significant biological activity and may need to use biocides to control excess bacterial growth. Some H_2S abatement systems, typically referred to as biofilters, are engineered to use bacteria that oxidize sulfide with oxygen (Eq. 1) (Iranpour et al., 2005; Rodríguez et al., 2014; Schiavon et al., 2016).

Chemical oxidants other than air can also be used to convert sulfides to either sulfur or sulfate. For example, the conversion of H_2S to elemental sulfur can also be catalyzed by oxidation with ferric iron (Eq. 3).

$$2\ Fe^{+3} + H_2S \rightarrow 2\ Fe^{+2} + S^0 + 2\ H^+ \qquad \text{Eq. 3}$$

Sodium hypochlorite (Eq. 4) and analogous bromine chemicals can be used to oxidize H_2S to sulfate.

$$4\ NaOCl + H_2S \rightarrow H_2SO_4 + 4\ NaCl \qquad \text{Eq. 4}$$

Hydrogen peroxide can be used to oxidize H_2S to elemental sulfur at neutral pH (Eq. 5) or sulfate at high pH conditions.

$$H_2O_2 + H_2S \rightarrow S^0 + 2\ H_2O \qquad \text{Eq. 5}$$

Organic oxidizing acids, such as trichloroisocyanuric acid (TCCA) (Eq. 6, Figure 10.7) can also be used to oxidize H_2S to sulfate.

$$4\ C_3N_3O_3Cl_3 + 3\ H_2S \rightarrow 4\ C_3H_3N_3O_3 + 3\ H_2SO_4 + 12\ HCl \qquad \text{Eq. 6}$$

Other chemicals that can be used for H_2S abatement include chlorine gas, permanganate, perborate, peroxysulfuric acid, transition metal oxides, and organic chemicals such as dibromopropionamide (DBNPA) and bromo-chlorohydantoin (BCH, Figure 10.8) (Gallup, 1992; Jacobs et al., 2017).

The most common sulfide control systems inject air as a source of oxygen, and may or may not include other chemical oxidants alone or in combination. One commercial treatment marketed to the geothermal industry is a combination of multiple chemicals in combination with chemical stabilizers and air injection (Gill and Jacobs, 2018; Jacobs et al., 2017; Nalco-Ecolab, 2018).

Some chemical treatments for H_2S abatement, such as sodium hypochlorite, have biocidal properties that also provide the benefit of limiting excess bacterial growth in treatment systems. The oxidation of H_2S to sulfate produces acid, Eqs. 1, 4 and 6., so in most cases a base is added to control pH as part of H_2S control systems and to produce a chemical benign sulfate salt (equation not shown).

Sulfate vs. Elemental Sulfur as an End Product

The formation of sulfate is beneficial, since sulfate is very water soluble, is not toxic or harmful, and is not volatile, so it does not cause air pollution. Production of elemental sulfur (S^0) is typically less desirable because sulfur is a solid that can build up and plug sulfide removal systems. In addition to causing scale, elemental sulfur formation produces solid waste. However, sulfur is an acceptable end-product because it is also nonvolatile and nontoxic, and can potentially be sold for fertilizer.

In the SS-KGRA, it is preferable that sulfide be oxidized to sulfate and not partially oxidized to elemental sulfur. Dissolved sulfate can be injected back into the formation with the injection fluid, whereas if elemental sulfur forms, the precipitants can cause scaling in the cooling towers, production of solids that must be sent to landfills, and particulate matter that is detrimental to reinjection of spent brine into the reservoir (Gallup, 1992; Gill and Jacobs, 2018; Jacobs et al., 2017; Rodríguez et al., 2014; Sanopoulos and Karabelas, 1997).

Hydrogen Sulfide Control in Geothermal Power Plants

H_2S abatement at geothermal power plants presents unique challenges (Nagl, 1999; Rodríguez et al., 2014; Sanopoulos and Karabelas, 1997). In geothermal power plants, H_2S abatement can be done in the steam flow prior to the turbine or after the turbine (Sanopoulos and Karabelas, 1997). Treatment of the steam protects the turbine from corrosion, but has negative impacts on steam flow and energy content,

which makes this alternative unattractive (Nagl, 1999). Technology options for H_2S abatement in the geothermal power industry are also limited by other factors, such as the type of condenser installed (either direct or surface condensers), the amount of ammonia in the NCG, and the pH of the condensate (Rodríguez et al., 2014). For example, chemical oxidation of NCG is less efficient at facilities with high ammonia concentrations (Rodríguez et al., 2014). The geothermal power plants in the SS-KGRA have surface condensers and high ammonia concentrations in the condensate and cooling water (Gallup, 1992).

At geothermal power plants, H_2S abatement is typically done after the turbine, in association with the condenser and cooling tower processes, which typically requires both treatment of H_2S in the NCG stream and dissolved sulfide in the condensate stream (Gallup, 1992; Gill and Jacobs, 2018; Nagl, 1999; Rodríguez et al., 2014). Generally, about half the sulfide is found in the condensate, and the rest is in the NCG stream (Ecolab USA Inc., 2018). One study examining plants in the SS-KGRA found that 40% of H_2S partitioned to the NCG while 60% partitioned to the condensate (Gallup, 1992). Since condensate is used for make-up water for the cooling tower, the condensate must also be treated to avoid volatilization of H_2S in the cooling towers and subsequent "secondary" emissions (Gill and Jacobs, 2018).

The gas and liquid streams from the condenser can be treated independently or in combination (Gallup, 1992; Gallup, 1996a, b; Gill and Jacobs, 2018; Nagl, 1999; Rodríguez et al., 2014; Sanopoulos and Karabelas, 1997). Several air pollution treatment technologies are applicable to the treatment of the NCG stream, including air oxidation (Eqs. 1 and 2) in biofilter or wet-air oxidizers, absorption in packed-bed filters, or thermal oxidation. In thermal oxidation, H_2S is combusted to sulfur dioxide (Eq. 7) or elemental sulfur (Eq. 8) in thermal oxidizers or other combustion-based air pollution control systems.

$$H_2S + 1\frac{1}{2}\ O_2 \rightarrow SO_2 + H_2O \qquad \text{Eq. 7}$$

$$3\ H_2S + 1\frac{1}{2}\ O_2 \rightarrow 3\ H_2O + 3\ S^0 \qquad \text{Eq. 8}$$

Together, these thermal reactions (Eqs. 7 and 8) are referred to as the "Claus process." These reactions occur at high temperatures (> 850°C) and conversion to sulfur (Eq. 8) also requires a catalyst.

Treatments for the liquid condensate stream include aeration, chemical oxidation, and catalytic oxidation with iron additives (Eqs. 1-6) in tanks, trickling filters, or bio-towers (Nagl, 1999; Rodríguez et al., 2014). Where aeration is practiced, the operational target for dissolved oxygen is to have aqueous concentrations above 5 ppm (Jacobs et al., 2017).

Treatment of combined liquid and gaseous streams typically involves compressing the NCG and bubbling the gases through fine-bubble diffusers submerged in the condensate stream. The diffusion of NCG and addition of reactants such as oxygen or chemical oxidizers may occur in specially designed "oxidizer boxes" or in the bottom of the cooling tower (Gallup, 1992; Gill and Jacobs, 2018; Nagl, 1999; Nalco-Ecolab, 2018; Rodríguez et al., 2014). In combined systems, sulfide abatement primarily occurs in solution and abatement reactions (e.g., Eqs. 1, 2, and 4) that occur either in the oxidation box or in the cooling tower, depending on the configuration of where and how the gas and oxidizing chemicals are injected into the liquid stream.

BIOX and TowerBrom Processes

Two processes for the simultaneous treatment of sulfide in both the NCG and the condensate have been developed specifically for geothermal power plants in the SS-KGRA. The BIOX process was developed by Unocal for use in power plants now operated BHER (Gallup, 1992; D. L. Gallup, 1996a, b; Rodríguez et al., 2014). The TowerBrom process was developed by Nalco-Ecolab for use in the Hudson Ranch Featherstone power plant operated by EnergySource (Gill and Jacobs, 2018; Jacobs et al., 2017; Nalco-Ecolab, 2018).

In the BIOX process, the NCG stream is compressed and sparged into the condensate before or at the oxidation box and the cooling tower. The oxidation box is a mixing chamber used for the addition of an oxidizing chemical and the partial oxidation of sulfide, prior to atmospheric exposure (and potential H_2S volatilization) in the cooling tower. Trichloroisocyanuric acid (TCCA) oxidation of sulfide (Eq. 6) is a key component of the BIOX system (Gallup, 1992; D. L. Gallup, 1996a, b; Nardini et al., 1995). The BIOX process can also use bromo-chlorohydantoin (BCH, Figure 10.8) as an oxidant, alone or in combination with TCCA and other chlorine or bromine-based oxidizers (e.g., Eq. 3) (Gallup, 1992). BIOX oxidants are added in granular and tablet forms to the oxidizer box or directly to the cooling tower. Tablets provide a slower release of the chemicals. The chemicals are added at doses lower than the stoichiometric ratios (Gallup, 1992; Gallup, 1996a, b; Nardini et al., 1995), suggesting that oxidation by bacteria or other chemical oxidants (e.g., dissolved oxygen) is also occurring.

In pilot studies, Gallup (1992) found that chlorine gas, sodium and calcium hypochlorite, and chlorine dioxide were less effective for H_2S abatement than BIOX chemicals. The high ammonia concentrations in the condensate and cooling water make breakpoint chlorination prohibitively expensive at the Salton Sea plants (Gallup, 1992). When used in combination with other, typically non-oxidizing biocides, the BIOX process also controls NO_2 emissions and arsenic in the "cooling tower drift," as well as controls biological growth in the cooling towers (Gallup, 1992). Arsenic in geothermal steam is typically in the reduced form; BIOX results in the oxidation of arsenic and its precipitation into geothermal scale as it forms solids with iron and calcium (Gallup, 1992). The BIOX process works best at near-neutral pH, so the use of acids, bases, or buffers may be necessary.

Gallup (1992) reported two scenarios for BIOX at SS-KGRA geothermal power plants. In the first example, H_2S abatement is only considered in the condensate. In this example, the cooling tower receives 3.6 kg/hr H_2S in the condensate and 5-10 kg of TCCA tablets are added. Without abatement, the H_2S emissions would have been 0.7 ppm, but with the addition of the tablets, the measured H_2S was less than 0.05 ppm. They observed 11 kg/hr sulfate generation and almost 100% removal of H_2S from the emissions.

In the second example reported by Gallup (1992), H_2S abatement was done on both the condensate and NCG in combination. Here, total H_2S introduced to the cooling tower in the NCG and in the condensate was 9.1 kg/hr (the gas contributed 5.5 kg/hr H_2S to the cooling tower). Without abatement, H_2S emissions would have been 1.7 ppm, but the addition of 10 kg/hr of the TCCA tablets resulted in sulfate production of 25 kg/hr and cooling tower H_2S of 0.15 ppm, representing approximately 93% removal of H_2S.

The TowerBrom process was developed for use at the Featherstone (aka Hudson Ranch I) geothermal power plant in the SS-KGRA (Nalco-Ecolab, 2018). Chemicals used to oxidize H_2S in the condensate include a mixture of TCCA, chlorine, bromine, and hydrogen peroxide (Jacobs et al., 2017).

Balancing the chemistry described by Gill and Jacobs (2018), the chemical reaction for TowerBrom sulfide oxidation can be described by Eq. 9:

$$H_2S + O_2 + H_2O_2 + HOBr \rightarrow Br^- + H_2SO_4 + H_2O + H^+ \qquad \text{Eq. 9}$$

Gill and Jacobs (2018) report that TCCA is only used as a "stabilizer catalyst" that increases the efficacy of the chlorine and bromine reactions. However, if TCCA is also actively oxidizing H_2S, then the reaction shown in Eq. 6 would also occur in the TowerBrom process. In this process, hypobromous acid (HOBr) is formed by reacting hypochlorous acid (HOCl) and sodium bromide (NaBr), hydrogen peroxide is added as a solution, and oxygen is supplied from air-sparging or atmospheric contact in the cooling tower (Gill and Jacobs, 2018; Nalco-Ecolab, 2018).

In this process, the condensate is treated first separately, then in combination with the NCG stream in the cooling tower (Nalco-Ecolab, 2018). The process uses a "reaction tank" rather than a specifically designed oxidation box more typically used to treat condensate streams in the SS-KGRA (Hoyer et al., 1991; Nalco-Ecolab, 2018). Prior to the reaction tank, the TowerBrom chemicals are added to the condensate stream, and, in the reaction tank, air is sparged to saturate the condensate to approximately 5 mg/L oxygen (Nalco-Ecolab, 2018). The treated condensate is sent to the cooling towers where sulfide oxidation is completed.

The NCG stream is treated in the cooling tower by micro-sparging the gas stream into the recirculating cooling water, which includes treated condensate water (Nalco-Ecolab, 2018). Additional TowerBrom chemicals are added directly to the recirculating cooling tower water, to supplement the residual chemicals in the treated condensate. The cooling tower is in full contact with atmospheric oxygen, which promotes sulfide oxidation (Eqs. 1 and 2). Balancing the ratio of the three oxidants (air, hydrogen peroxide, and hypobromous acid) and the amount of TCCA used is important for cost-effective treatment (Gill and Jacobs, 2018).

Table A9.3. Toxicity Characteristic Leaching Procedure (TCLP) standards for inorganic substances. TCLP tests are part of Federal regulations governing hazardous wastes (40 CFR 261.24).

Substance	U.S. EPA Hazardous Waste Number	TCLP Regulatory Level
Arsenic	D004	5.0 mg/l
Barium	D005	100.0 mg/l
Cadmium	D006	1.0 mg/l
Chromium	D007	5.0 mg/l
Lead	D008	5.0 mg/l
Mercury	D009	0.2 mg/l
Selenium	D010	1.0 mg/l
Silver	D011	5.0 mg/l

Table A9.4. List of inorganic persistent and bio-accumulative toxic substances regulated by California in solid wastes (22 CCR 66261.24). Solid wastes with concentrations less that the Total Threshold Limit Concentration (TTLC) values and pass the Waste Extraction Test (WET) with Soluble Threshold Limit Concentration (STLC) less than the values shown are not hazardous wastes and can be disposed of in Class 2 landfills.

Substance	STLC (mg/l)	TTLC (Wet-Weight mg/kg)
Antimony and/or antimony compounds	15	500
Arsenic and/or arsenic compounds	5.0	500
Asbestos		10,000
Barium and/or barium compounds (excluding barite)	100	10,000
Beryllium and/or beryllium compounds	0.75	75
Cadmium and/or cadmium compounds	1.0	100
Chromium (VI) compounds	5	500
Chromium and/or chromium (III) compounds	5d	2,500
Cobalt and/or cobalt compounds	80	8,000
Copper and/or copper compounds	25	2,500
Fluoride salts	180	18,000
Lead and/or lead compounds	5.0	1,000
Mercury and/or mercury compounds	0.2	20
Molybdenum and/or molybdenum compounds	350	3,500
Nickel and/or nickel compounds	20	2,000
Selenium and/or selenium compounds	1.0	100
Silver and/or silver compounds	5	500
Thallium and/or thallium compounds	7.0	700
Vanadium and/or vanadium compounds	24	2,400
Zinc and/or zinc compounds	240	5,000

Table A9.5. Summary statistics for annual solid waste generated at the SS-KGRA power plant and disposed of in the Desert Valley Monofill, or manifested and disposed of out-of-state or in designated landfills, 2015-2021 (DTSC, 2023a-d; SWRCB, 2023).

Facility	Type	Percent Average of Total	Annual Solid Waste (metric tons)			
			Average	Standard Deviation	Minimum	Maximum
Region 1	Monofill	69%	14,923	3,374	8,150	18,233
	Manifested	31%	6,662	4,265	2,253	14,278
	Total		21,585	4,447	16,544	28,384
Region 2	Monofill	53%	12,127	2,068	8,299	15,036
	Manifested	47%	10,693	9,218	3,799	31,096
	Total		22,819	10,082	12,098	44,021
Elmore	Monofill	56%	6,883	2,593	2,171	9,795
	Manifested	44%	5,307	1,390	3,256	7,325
	Total		12,190	2,461	8,797	16,144
Leathers	Monofill	59%	7,089	563	5,949	7,696
	Manifested	41%	4,986	2,832	2,286	10,884
	Total		12,075	3,116	8,235	18,232
Featherstone	Total		11,131	1,696	8,070	12,803

Table A9.6. Annual waste metric tons of solid waste disposed of at the Desert Valley Monofill from the BHER CalEnergy SS-KGRA geothermal power plants.

Year	Region 1 (metric tons)	Region 2 (metric tons)	Elmore (metric tons)	Leathers (metric tons)	Total (metric tons)
2015	18,233	12,925	9,795	7,493	48,446
2016	14,290	8,299	6,538	5,949	35,076
2017	16,680	12,277	7,760	7,025	43,742
2018	15,421	15,036	8,098	7,051	45,606
2019	17,583	12,714	5,000	7,061	42,359
2020	14,105	12,637	2,171	7,348	36,262
2021	8,150	10,994	8,819	7,696	35,659

Table A9.7. Summary statistics for total threshold limit concentration (TTLC) testing done as part of annual filter cake analyses for 2017-2021, as reported by the Desert Valley Company to Imperial County, for all facilities (Region 1, Region 2, Elmore, and Leathers). Limits are as described in 22 CCR § 66261.24. Units are mg/kg.

Metal	Mean	Standard Deviation	Minimum	Maximum	Below Detection Limit (%)	Limit
Antimony	128	92.2	29.7	293	0	500
Arsenic	280	130	77.6	477	0	500
Barium	496	773	72.7	2,620	0	10,000
Beryllium	20.6	15.2	2.75	46.6	0	75
Cadmium	6.06	3.68	1.11	12.9	0	100
Chromium	1.62	0.539	0.913	2.47	50	500
Cobalt	2.72	1.68	1.02	5.76	30	8,000
Copper	124	177	28.1	679	0	2,500
Lead	32.2	12.9	11.3	47.6	0	1,000
Mercury	0.509	NA	0.509	0.509	95	20
Molybdenum	NA	NA	NA	NA	100	3,500
Nickel	0.859	0.289	0.53	1.07	85	2,000
Selenium	NA	NA	NA	NA	100	100
Silver	26.9	20.7	8.19	77.3	0	500
Thallium	NA	NA	NA	NA	100	700
Vanadium	6.08	3.24	1.56	9.95	5	2,400
Zinc	155	77.9	34.5	252	0	5,000

NA = not available because most or all observation are below the detection limits.

Table A9.8. Summary statistics for soluble threshold limit concentration (STLC) testing done as part of annual filter cake analyses for 2017-2021, as reported by the Desert Valley Company to Imperial County, for all facilities (Region 1, Region 2, Elmore, and Leathers). Limits are as described in 22 CCR § 66261.24. Units are mg/L.

Metal	Mean	Standard Deviation	Minimum	Maximum	Below Detection Limit (%)	Limit
Antimony	0.776	0.376	0.413	2	0	15
Arsenic	0.885	0.502	0.242	2.1	0	5
Barium	10.9	6.68	4.63	26.7	0	100
Beryllium	0.0759	0.0412	0.0106	0.169	15	0.75
Cadmium	0.0724	0.0103	0.0583	0.0978	30	1
Chromium	NA	NA	NA	NA	100	5
Cobalt	NA	NA	NA	NA	100	80
Copper	3.40	4.57	0.463	16.2	0	25
Lead	1.75	0.888	0.248	3.02	0	5
Mercury	NA	NA	NA	NA	100	0.2
Molybdenum	NA	NA	NA	NA	100	350
Nickel	NA	NA	NA	NA	100	20
Selenium	NA	NA	NA	NA	100	1
Silver	0.251	0.163	0.0611	0.506	35	5
Thallium	NA	NA	NA	NA	100	7
Vanadium	NA	NA	NA	NA	100	24
Zinc	10.4	6.19	1.07	20.2	0	250

Table A9.9. Results for pH testing done as part of annual filter cake analyses, as reported by the Desert Valley Company to the RWQCB.

Year	Region 1	Region 2	Elmore	Leathers
2017	4.70	6.10	4.90	5.10
2018	4.09	5.67	5.10	5.20
2019	4.48	5.74	4.96	4.83
2020	4.61	5.86	5.18	4.89
2021	5.26	6.05	5.76	4.68

Table A9.10. Measurement of naturally occurring radioactive materials (NORM) in filter cake received by the Desert Valley Monofill (2017-2020).

Constituent	Units	Elmore Maximum Minimum	Leathers Maximum Minimum	Region 1 Maximum Minimum	Region 2 Maximum Minimum
Co^{60}	pCi/g	0.07 -0.0101	0.085 0.0225	0.3 -0.0832	0.143 -0.118
Cs^{137}	pCi/g	0.077 0.00171	0.092 -0.00523	0.41 -0.0237	0.174 -0.0329
Gross Alpha	pCi/g	9.39 5.85	8.01 4.21	22 2.96	20.2 3.03
Gross Beta	pCi/g	13.7 7.41	10 7.4	20.5 4.36	16.8 2.06
K^{40}	pCi/g	10.2 6.96	10.3 7.91	4.03 1.69	8.37 5.47
Ra^{226}	pCi/g	0.628 0.27	0.718 0.413	14.9 2.11	11.5 1.26
Th^{228}	pCi/g	0.587 -0.0398	0.504 0.315[a]	12.16 2.14	9.57 1.11
Th^{234}	pCi/g	3.48 0.907	2.73 0.972	5.54 1.38	4.29 0.713

[a]*Reported as less than this value.*

Table A9.11. Results for volatile organic compound (VOC) testing done as part of annual filter cake analyses, as reported by the Desert Valley Company to the RWQCB.

Year	Constituent	Units	Region 1	Region 2	Elmore	Leathers
2017	VOC Analytes	ug/kg	ND	ND	ND	ND
2018	VOC Analytes	ug/kg	ND	ND	ND	ND
2018	Acetone	ug/kg	26	19	25	25
2019	VOC Analytes	ug/kg	ND	ND	ND	ND
2019	Acetone	ug/kg	ND	ND	33	11
2020	VOC Analytes	ug/kg	ND	ND	ND	ND
2021	VOC Analytes	ug/kg	ND	ND	ND	ND
2021	Acetone	ug/kg	ND	ND	ND	53

ND = not detected.

Table A9.12. Destination of Code 181 and Code 352 wastes from BHER and EnergySource geothermal power plants (2021 only).

Company	Waste Code	Treatment Storage Disposal Facility (TSDF) Name	N Manifests	% of Manifests
BHER	352	Buttonwillow Clean Harbor	25	96.2
BHER	352	HazMat TSDF Filter Recycling Services	1	3.8
EnergySource	352	Copper Mountain AZ	55	93.2
EnergySource	352	US Fuel Oil LLC	4	6.8
BHER	181	Buttonwillow Clean Harbor	681	37.0
BHER	181	Copper Mountain AZ	1160	63.0
EnergySource	181	Buttonwillow Clean Harbor	20	5.1
EnergySource	181	Copper Mountain AZ	372	94.9

Table A9.13. Summary statistics for annual solid waste generated at the SS-KGRA power plant and disposed of in the Desert Valley Monofill, or manifested and disposed of out-of-state or in designated landfills, 2015-2021 (DTSC, 2023a-d; SWRCB, 2023).

Facility	Type	Percent Average of Total	Annual Solid Waste (metric tons)			
			Average	Standard Deviation	Minimum	Maximum
Region 1	Monofill	69%	14,923	3,374	8,150	18,233
	Manifested	31%	6,662	4,265	2,253	14,278
	Total		21,585	4,447	16,544	28,384
Region 2	Monofill	53%	12,127	2,068	8,299	15,036
	Manifested	47%	10,693	9,218	3,799	31,096
	Total		22,819	10,082	12,098	44,021
Elmore	Monofill	56%	6,883	2,593	2,171	9,795
	Manifested	44%	5,307	1,390	3,256	7,325
	Total		12,190	2,461	8,797	16,144
Leathers	Monofill	59%	7,089	563	5,949	7,696
	Manifested	41%	4,986	2,832	2,286	10,884
	Total		12,075	3,116	8,235	18,232
Featherstone	Total		11,131	1,696	8,070	12,803

Table A9.14. Permitted and active land disposal sites listed in Imperial County in the CalRecycle Solid Waste Information System (SWIS)[a].

Name and address	Operator and SWIS Number	Landfill Type	Remaining Capacity (cy)	Remaining Capacity Date	Max Permit Capacity (cy)	Max Permit Throughput (tons/day)
Monofill Facility 3301 West Highway 86, Brawley, CA 92227	Desert Valley Co. 13-AA-0022	Class II (Industrial)	789,644	3/1/2015	1,729,800	750
Salton City Solid Waste Site 935 W. Hwy 86, Salton City, CA 92275	Burrtec Waste Industries, Inc. 13-AA-0011	Class III (Municipal)	1,264,170	9/30/2018	65,100,000	6,000
Imperial Landfill 104 E Robinson Rd, Imperial, CA 92251	Imperial Landfill, Inc. 13-AA-0019	Class III (Municipal)	12,384,000	3/31/2019	19,514,700	1,700
Calexico Solid Waste Site New River & Hwy 98, Calexico, CA 92231	County of Imperial Public Works 13-AA-0004	Class III (Municipal)	1,561,235	8/1/2019	3,437,800	150
Niland Solid Waste Site 8450 Cuff Road; 3 Miles NE of Niland, Niland, CA 92257	County of Imperial Public Works 13-AA-0009	Class III (Municipal)	211,439	6/30/2020	318,673	55

[a]Not included are transfer stations, recycling facilities, composting facilities, and facilities exclusively handling construction/ demolition solid waste and inert debris.

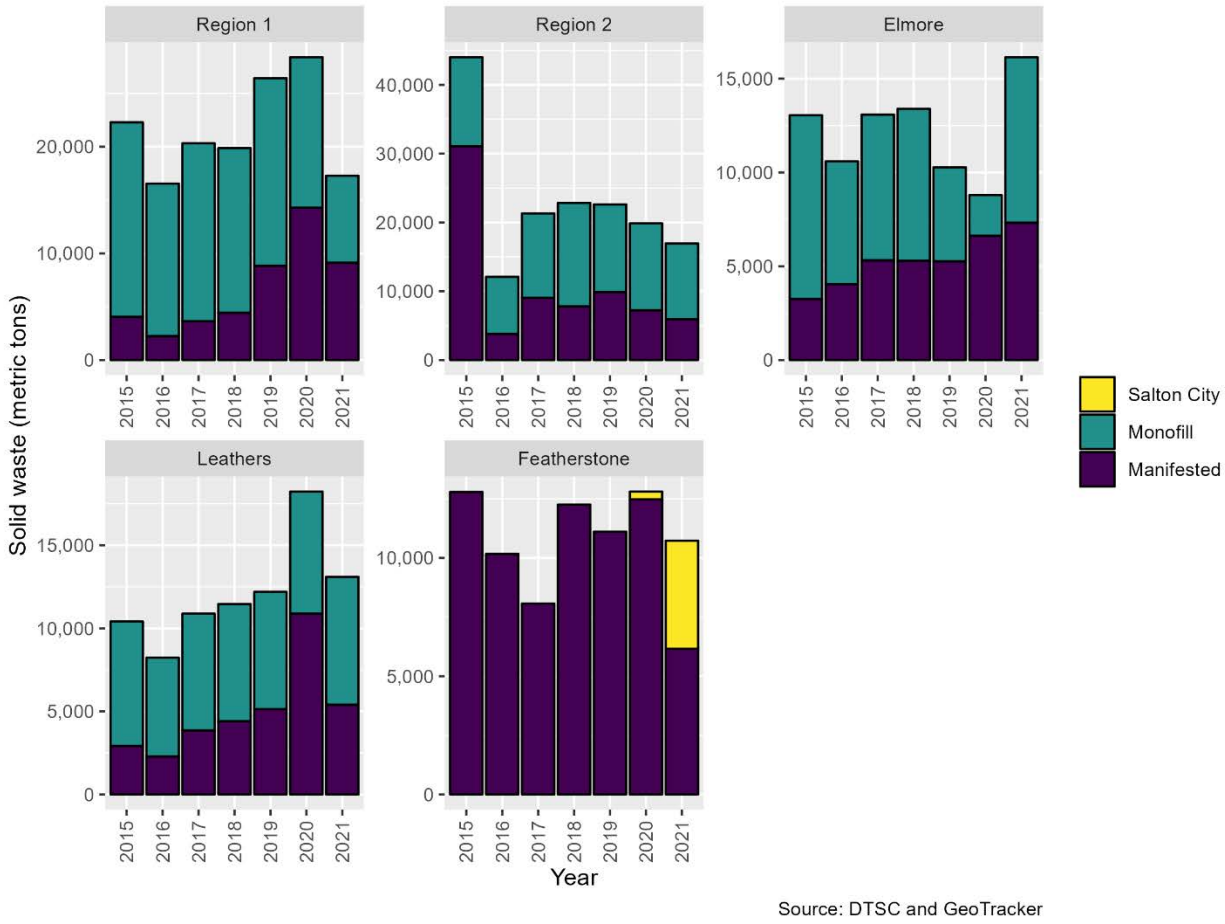

Figure A9.1. Solid waste production and disposal by geothermal power plant management area. Colors indicate waste management practices.

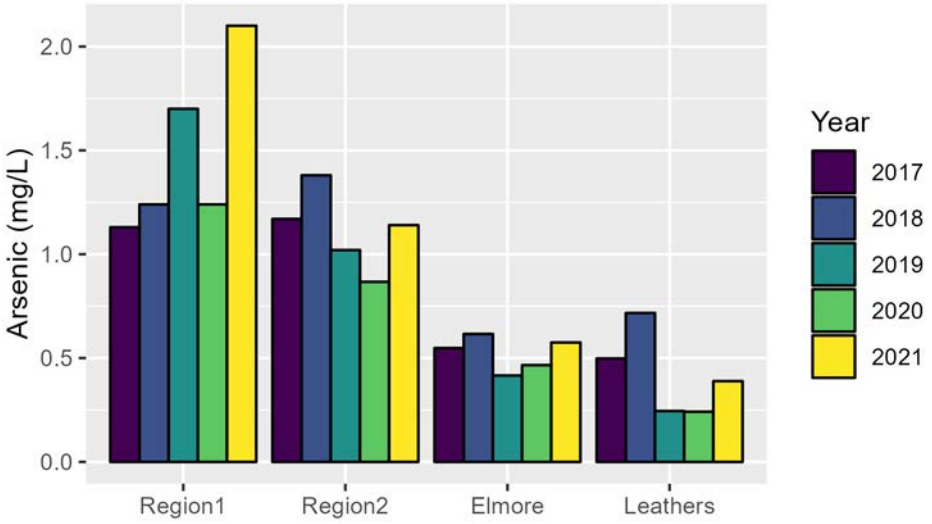

a)

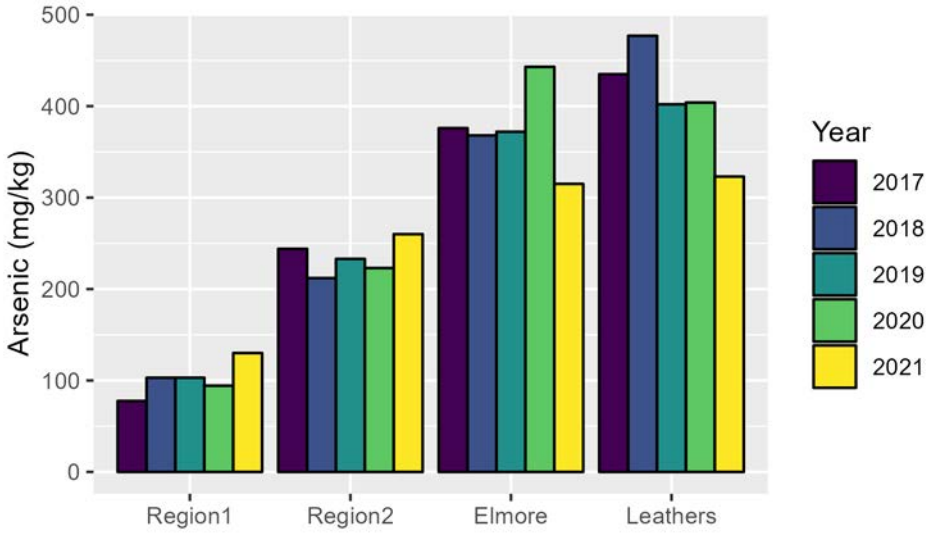

b)

Figure A9.2. Arsenic results for a) soluble threshold limit concentration (STLC) and b) total threshold limit concentration (TTLC) testing for filter cake solids. Annual filter cake analyses were completed and reported by the Desert Valley Company to the Imperial County Planning and Development Services.

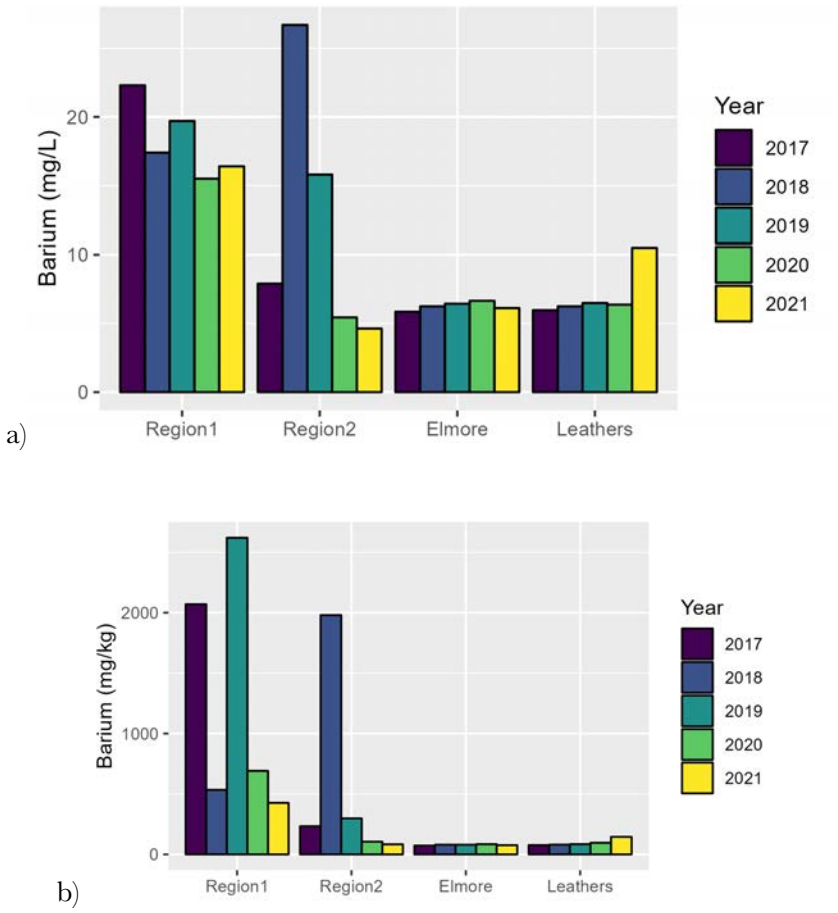

Figure A9.3. Barium results for a) soluble threshold limit concentration (STLC) and b) total threshold limit concentration (TTLC) testing for filter cake solids. Annual filter cake analyses were completed and reported by the Desert Valley Company to the Imperial County Planning and Development Services.

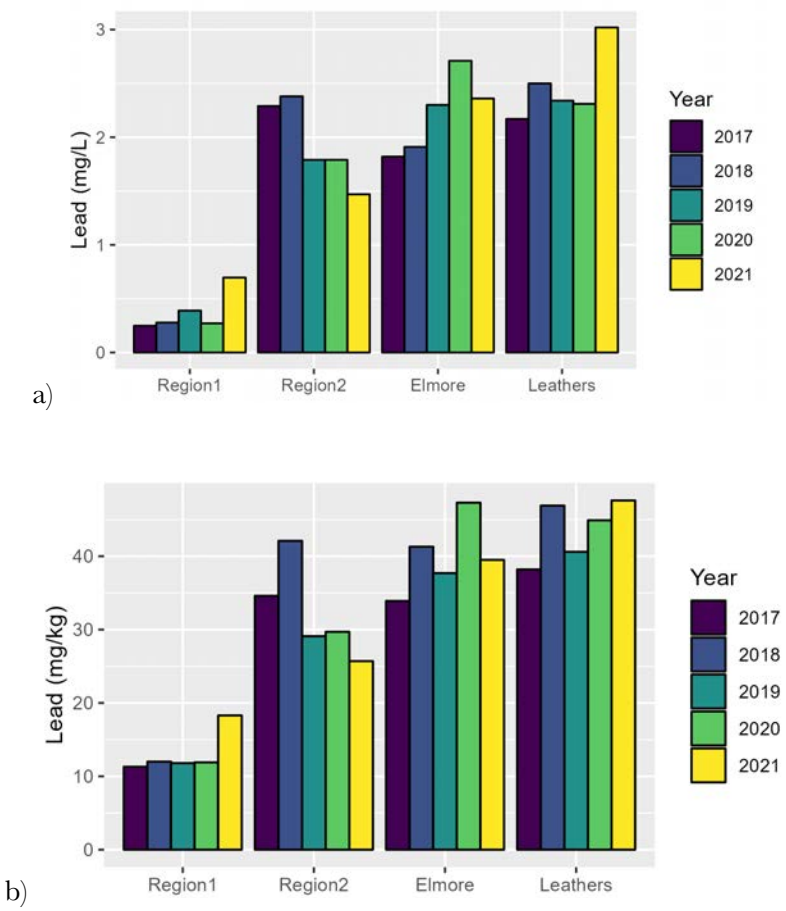

Figure A9.4. Lead results for a) soluble threshold limit concentration (STLC) and b) total threshold limit concentration (TTLC) testing for filter cake solids. Annual filter-cake analyses were completed and reported by the Desert Valley Company to the Imperial County Planning and Development Services.

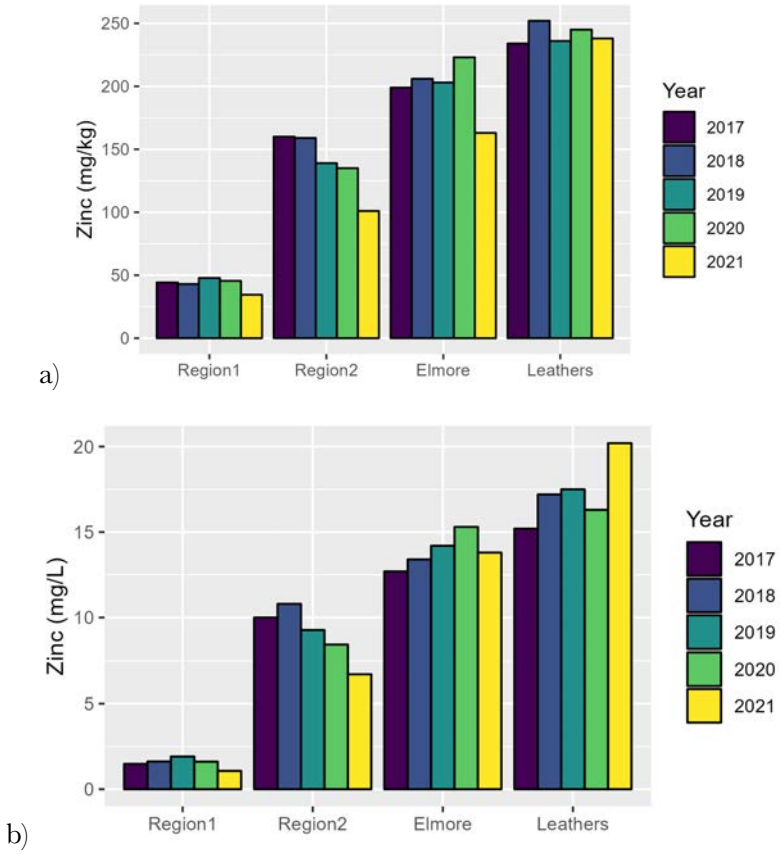

Figure A9.5. Zinc results for a) soluble threshold limit concentration (STLC) and b) total threshold limit concentration (TTLC) testing for filter cake solids. Annual filter cake analyses were completed and reported by the Desert Valley Company to the Imperial County Planning and Development Services.

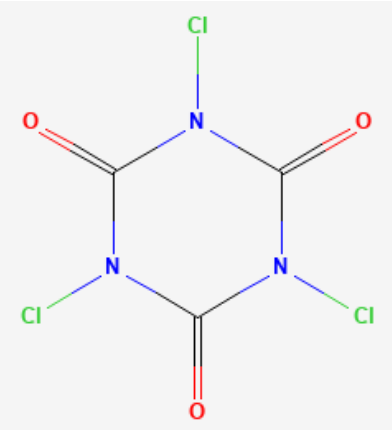

Figure A9.6. The structure of trichloroisocyanuric acid (image from PubChem).

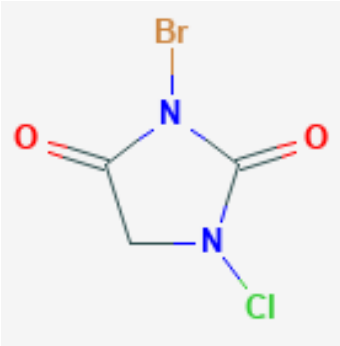

Figure A9.7. The structure of bromo-chlorohydantoin (image from PubChem).

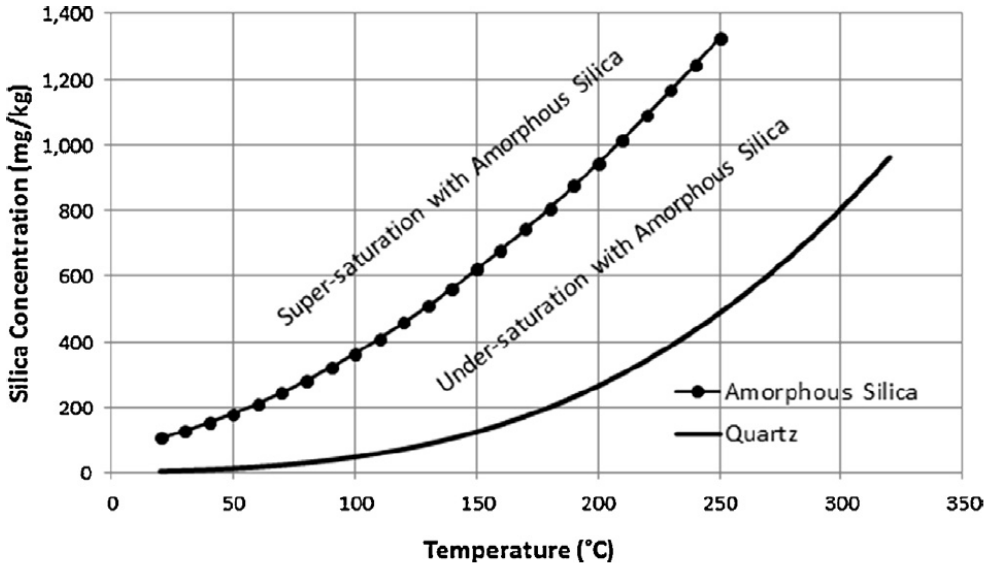

Figure A9.8. Solubility of quartz (crystalline SiO_2) and amorphous silica (amorphous SiO_2) as a function of temperature. Silica will precipitate and form scale as steam is extracted from brine and temperatures decrease in geothermal power plants. The crystallizer-clarifier process is designed to precipitate scale under controlled conditions and prevent to formation of scale on pipes and other surfaces in geothermal power plants (Zarrouka & Purnanto, 2015).

Waste Disposal Details

Since 2020, EnergySource (now Cyrq) has sent nonhazardous filter cake from the Featherstone geothermal power plants to the Salton City Landfill, a Class III municipal landfill, under a special permit (Burrtec Waste Industries Inc., 2020, 2022). Prior to 2019, filter cake from the Featherstone geothermal power plants was sent to the Copper Mountain Landfill, a Class II landfill in Arizona (Table 10.5). Between 2014 and 2019, Featherstone geothermal power plants produced an average of approximately 11,000 metric tons of solid waste per year, according to DTSC records. According to documents submitted to state and county agencies, a significant percentage of this solid waste was filter cake and not hazardous waste (Chambers Group Inc., 2021; EnergySource, 2012). In 2021, 4,569 metric tons of filter-cake waste was sent to the Salton City landfill, and 5,880 metric tons of solid waste was sent to the Copper Mountain Landfill. In 2022, the Salton City Landfill received 7,205 metric tons of filter cake, and the solid waste sent to Copper Mountain was 3,124 metric tons.

Filter Cake Safety Data Sheet (BHER)

Safety Data Sheet

Section 1: Identification

Product identifier

Product Name • Geothermal Filter Cake

Synonyms • Filter Cake

Product Description • Fine solids that have been removed from spent brine by a filter press, centrifuge or other separation processes.

Relevant identified uses of the substance or mixture and uses advised against

Recommended use • Material is considered as waste and is a by-product of the process

Details of the supplier of the safety data sheet

Manufacturer • CalEnergy Operating Corp
7030 Gentry Road
Calipatria, CA 92233
United States
www.calenergy.com

Telephone (Technical) • 760-348-4275 - EHS Telephone No.

Emergency telephone number

Manufacturer • 760-348-4271

Section 2: Hazard Identification

United States (US)
According to OSHA 29 CFR 1910.1200 HCS

Classification of the substance or mixture

OSHA HCS 2012 • Specific Target Organ Toxicity Repeated Exposure 1 - H372

Label elements

OSHA HCS 2012

DANGER

Hazard statements • Causes damage to organs - Lungs through prolonged or repeated exposure - H372

Precautionary statements

Prevention • Do not breathe dust. - P260
Wash thoroughly after handling. - P264
Do not eat, drink or smoke when using this product. - P270

Response • Get medical advice/attention if you feel unwell. - P314

Storage/Disposal • Dispose of content and/or container in accordance with local, regional, national, and/or international regulations. - P501

Other hazards

OSHA HCS 2012 • Under United States Regulations (29 CFR 1910.1200 - Hazard Communication Standard), this product is considered hazardous.

Other information

• This product contains trace quantities of naturally occurring radioactive material (NORM)

Section 3 - Composition/Information on Ingredients

Substances

• Material does not meet the criteria of a substance.

Mixtures

Composition				
Chemical Name	**Identifiers**	**%**	**LD50/LC50**	**Comments**
Silica, amorphous	CAS:7631-86-9	50%	NDA	NDA
Iron	CAS:7439-89-6	15%	Ingestion/Oral-Rat LD50 • 30 g/kg	NDA
Barium	CAS:7440-39-3	4%	NDA	NDA
Calcium	CAS:7440-70-2	3%	NDA	NDA
Strontium	CAS:7440-24-6	6000ppm	NDA	NDA
Sodium chloride	CAS:7647-14-5	6000ppm	Ingestion/Oral-Rat LD50 • 3000 mg/kg	NDA
Manganese	CAS:7439-96-5	3500ppm	Ingestion/Oral-Rat LD50 • 9 g/kg	NDA
Potassium chloride	CAS:7447-40-7	1300ppm	Ingestion/Oral-Rat LD50 • 2600 mg/kg	NDA
Arsenic	CAS:7440-38-2	300ppm	Ingestion/Oral-Rat LD50 • 763 mg/kg	NDA
Copper	CAS:7440-50-8	250ppm	NDA	NDA
Lead	CAS:7439-92-1	30ppm	NDA	NDA
Beryllium	CAS:7440-41-7	10ppm	NDA	NDA
Antimony	CAS:7440-36-0	10ppm	Ingestion/Oral-Rat LD50 • 100 mg/kg	NDA
Cobalt	CAS:7440-48-4	4ppm	Ingestion/Oral-Rat LD50 • 6171 mg/kg	NDA
Nickel	CAS:7440-02-0	1.5ppm	NDA	NDA
Chromium	CAS:7440-47-3	1ppm	NDA	NDA
Silver	CAS:7440-22-4	0.4ppm	NDA	NDA
Cadmium	CAS:7440-43-9	0.2ppm	Ingestion/Oral-Rat LD50 • 2330 mg/kg	NDA

Section 4: First-Aid Measures

Description of first aid measures

Inhalation • Move victim to fresh air. Give artificial respiration if victim is not breathing. Administer oxygen if breathing is difficult. Get medical attention.

Skin • In case of contact with substance, immediately flush skin with running water for at least 20 minutes.

Eye • In case of contact with substance, immediately flush eyes with running water for at least 20 minutes.

Ingestion • Rinse mouth. Do not give anything by mouth to an unconscious person. Get medical attention.

* View the full document (pdf) here: https://drive.google.com/file/d/1Y2_61vVLYkDwFRC0zYLNPC6kaZLtJrO-/view?usp=sharing

Most important symptoms and effects, both acute and delayed

- Refer to Section 11 - Toxicological Information.

Indication of any immediate medical attention and special treatment needed

Notes to Physician

- All treatments should be based on observed signs and symptoms of distress in the patient. Consideration should be given to the possibility that overexposure to materials other than this product may have occurred.

Section 5: Fire-Fighting Measures

Extinguishing media

Suitable Extinguishing Media

- LARGE FIRE: Water spray, fog or regular foam.
  SMALL FIRES: Dry chemical, CO_2, water spray or regular foam.

Unsuitable Extinguishing Media

- No data available.

Special hazards arising from the substance or mixture

Unusual Fire and Explosion Hazards

- No hazard due to fire or explosion expected.

Hazardous Combustion Products

- No data available.

Advice for firefighters

- Wear positive pressure self-contained breathing apparatus (SCBA).
  Structural firefighters' protective clothing will only provide limited protection.

Section 6 - Accidental Release Measures

Personal precautions, protective equipment and emergency procedures

Personal Precautions

- Ventilate enclosed areas. Do not walk through spilled material. Do not touch damaged containers or spilled material unless wearing appropriate protective clothing. Wear appropriate personal protective equipment, avoid direct contact. Do not breathe dust.

Emergency Procedures

- As an immediate precautionary measure, isolate spill or leak area for at least 25 meters (75 feet) in all directions. If tank, rail car or tank truck is involved in a fire, ISOLATE for 800 meters (1/2 mile) in all directions; also, consider initial evacuation for 800 meters (1/2 mile) in all directions. Keep unauthorized personnel away.

Environmental precautions

- Avoid run off to waterways and sewers.

Methods and material for containment and cleaning up

Containment/Clean-up Measures

- Avoid generating dust.
  SMALL DRY SPILLS: With clean shovel place material into clean, dry container and cover loosely; move containers from spill area.
  LARGE SPILLS: Cover powder spill with plastic sheet or tarp to minimize spreading.

Section 7 - Handling and Storage

Precautions for safe handling

Handling

- Use only with adequate ventilation. Minimize dust generation and accumulation. Wear appropriate personal protective equipment, avoid direct contact. Do not breathe dust. Avoid contact with skin, eyes or clothing. Wash thoroughly with soap and water after handling and before eating, drinking, or using tobacco. Wash contaminated clothing before reuse.

Conditions for safe storage, including any incompatibilities

Storage

- Store in a well-ventilated place. Keep container tightly closed.

Section 8 - Exposure Controls/Personal Protection

Control parameters

Exposure Limits/Guidelines

	Result	ACGIH	NIOSH	OSHA
Cadmium (7440-43-9)	Ceilings	Not established	Not established	0.3 mg/m3 Ceiling (applies to any operations or sectors for which the Cadmium standard is stayed or otherwise not in effect, fume); 0.6 mg/m3 Ceiling (applies to any operations or sectors for which the Cadmium standard is stayed or otherwise not in effect, dust)
	TWAs	0.01 mg/m3 TWA; 0.002 mg/m3 TWA (respirable fraction)	Not established	0.1 mg/m3 TWA (fume, applies to any operations or sectors for which the Cadmium standard is stayed or otherwise not in effect); 0.2 mg/m3 TWA (dust, applies to any operations or sectors for which the Cadmium standard is stayed or otherwise not in effect); 5 µg/m3 TWA
Silver (7440-22-4)	TWAs	0.1 mg/m3 TWA (dust and fume)	0.01 mg/m3 TWA (dust)	0.01 mg/m3 TWA
Chromium (7440-47-3)	TWAs	0.5 mg/m3 TWA	0.5 mg/m3 TWA	1 mg/m3 TWA
Nickel (7440-02-0)	TWAs	1.5 mg/m3 TWA (inhalable fraction)	0.015 mg/m3 TWA	1 mg/m3 TWA
Cobalt (7440-48-4)	TWAs	0.02 mg/m3 TWA	0.05 mg/m3 TWA (dust and fume)	0.1 mg/m3 TWA (dust and fume)
Barium (7440-39-3)	TWAs	0.5 mg/m3 TWA	Not established	Not established
Beryllium as Beryllium compounds	Ceilings	Not established	0.0005 mg/m3 Ceiling	5 µg/m3 Ceiling
	TWAs	0.00005 mg/m3 TWA (inhalable fraction)	Not established	2 µg/m3 TWA
Antimony as Antimony compounds	TWAs	0.5 mg/m3 TWA	0.5 mg/m3 TWA	0.5 mg/m3 TWA
Lead as Lead, inorganic compounds	TWAs	0.05 mg/m3 TWA	0.050 mg/m3 TWA	50 µg/m3 TWA
Silica, amorphous (7631-86-9)	TWAs	Not established	6 mg/m3 TWA	Not established
Copper (7440-50-8)	TWAs	0.2 mg/m3 TWA (fume)	1 mg/m3 TWA (dust and mist); 0.1 mg/m3 TWA (fume)	0.1 mg/m3 TWA (fume); 1 mg/m3 TWA (dust and mist)
Arsenic (7440-38-2)	TWAs	0.01 mg/m3 TWA	Not established	Not established
	Ceilings	Not established	0.002 mg/m3 Ceiling (15 min)	Not established
Manganese as Manganese compounds	Ceilings	Not established	Not established	5 mg/m3 Ceiling (fume)
	TWAs	0.02 mg/m3 TWA (respirable fraction); 0.1 mg/m3 TWA (inhalable fraction)	1 mg/m3 TWA (fume)	Not established

* View the full document (pdf) here: https://drive.google.com/file/d/1Y2_61vVLYkDwFRC0zYLNPC6kaZLtJrO-/view?usp=sharing

	STELs	Not established	3 mg/m3 STEL	Not established

Exposure controls

Engineering Measures/Controls
- Good general ventilation should be used. Ventilation rates should be matched to conditions. If applicable, use process enclosures, local exhaust ventilation, or other engineering controls to maintain airborne levels below recommended exposure limits. If exposure limits have not been established, maintain airborne levels to an acceptable level.

Personal Protective Equipment

Respiratory
- In case of insufficient ventilation, wear suitable respiratory equipment. For limited exposure use an N95 dust mask. For prolonged exposure use an air-purifying respirator with high efficiency particulate air (HEPA) filters.

Eye/Face
- Wear safety goggles.

Skin/Body
- Wear appropriate gloves. Wear long sleeves and/or protective coveralls.

Environmental Exposure Controls
- Controls should be engineered to prevent release to the environment, including procedures to prevent spills, atmospheric release and release to waterways. Follow best practice for site management and disposal of waste.

Key to abbreviations

ACGIH = American Conference of Governmental Industrial Hygiene
NIOSH = National Institute of Occupational Safety and Health
OSHA = Occupational Safety and Health Administration
STEL = Short Term Exposure Limits are based on 15-minute exposures
TWA = Time-Weighted Averages are based on 8h/day, 40h/week exposures

Section 9 - Physical and Chemical Properties

Information on Physical and Chemical Properties

Material Description			
Physical Form	Solid	Appearance/Description	A very fine powder-type material, color can range from light green to light rust-like to black with no odor.
Color	Light green to light rust-like to black.	Odor	Odorless
Particulate Size	< 10 µ	Odor Threshold	No data available
General Properties			
Boiling Point	No data available	Melting Point	No data available
Decomposition Temperature	No data available	pH	Not relevant
Specific Gravity/Relative Density	No data available	Water Solubility	Negligible < 0.1 %
Viscosity	No data available		
Volatility			
Vapor Pressure	No data available	Vapor Density	No data available
Evaporation Rate	No data available		
Flammability			
Flash Point	Not relevant	UEL	Not relevant
LEL	Not relevant	Autoignition	No data available
Flammability (solid, gas)	No data available		
Environmental			
Octanol/Water Partition coefficient	No data available		

Section 10: Stability and Reactivity

Reactivity

- No dangerous reaction known under conditions of normal use.

Chemical stability
- Stable under normal temperatures and pressures.

Possibility of hazardous reactions
- Hazardous polymerization not indicated.

Conditions to avoid
- No data available.

Incompatible materials
- None have been noticed.

Hazardous decomposition products
- At very high temperatures the materials may emit sulfur oxide gases and metal fumes.

Section 11 - Toxicological Information

Information on toxicological effects

Component Name	CAS	Data
Silica, amorphous (50%)	7631-86-9	**Acute Toxicity:** ihl-rat LCLo:2190 mg/m3/4H; **Irritation:** eye-rbt 25 mg/24H MLD
Iron (15%)	7439-89-6	**Multi-dose Toxicity:** ihl-rat TCLo:250 mg/m3/6H/4W-I
Barium (4%)	7440-39-3	**Multi-dose Toxicity:** orl-rat TDLo:26622 mg/kg/69W-C
Sodium chloride (6000ppm)	7647-14-5	**Acute Toxicity:** orl-rat LD50:3000 mg/kg; **Irritation:** eye-rbt 10 mg MOD; skn-rbt 500 mg/24H MLD
Manganese (3500ppm)	7439-96-5	**Acute Toxicity:** orl-rat LD50:9 gm/kg; **Irritation:** eye-rbt 500 mg/24H MLD; skn-rbt 500 mg/24H MLD; **Reproductive:** orl-rat TDLo:90 mg/kg (18D post)
Potassium chloride (1300ppm)	7447-40-7	**Acute Toxicity:** orl-rat LD50:2600 mg/kg; **Irritation:** eye-rbt 500 mg/24H MLD

GHS Properties	Classification
Acute toxicity	**OSHA HCS 2012 -** Data lacking
Aspiration Hazard	**OSHA HCS 2012 -** Data lacking
Carcinogenicity	**OSHA HCS 2012 -** Data lacking
Germ Cell Mutagenicity	**OSHA HCS 2012 -** Data lacking
Skin corrosion/irritation	**OSHA HCS 2012 -** Data lacking
Skin sensitization	**OSHA HCS 2012 -** Data lacking
STOT-RE	**OSHA HCS 2012 -** Specific Target Organ Toxicity Repeated Exposure 1
STOT-SE	**OSHA HCS 2012 -** Data lacking
Toxicity for Reproduction	**OSHA HCS 2012 -** Data lacking
Respiratory sensitization	**OSHA HCS 2012 -** Data lacking
Serious eye damage/irritation	**OSHA HCS 2012 -** Data lacking

Potential Health Effects

Inhalation

Acute (Immediate)
- Exposure to dust may cause irritation. Processes such as cutting, grinding, crushing.

* View the full document (pdf) here: https://drive.google.com/file/d/1Y2_61vVLYkDwFRC0zYLNPC6kaZLtJrO-/view?usp=sharing

or impact may result in generation of excessive amounts of airborne dusts in the workplace. Nuisance dust may affect the lungs but reactions are typically reversible.

Chronic (Delayed)
- Repeated and prolonged exposure to dust may cause lung effects including pneumoconiosis.

Skin

Acute (Immediate)
- Exposure to dust may cause mechanical irritation.

Chronic (Delayed)
- No data available.

Eye

Acute (Immediate)
- Exposure to dust may cause mechanical irritation. Excessive concentrations of nuisance dust in the workplace may reduce visibility and may cause unpleasant deposits in eyes.

Chronic (Delayed)
- No data available.

Ingestion

Acute (Immediate)
- Excessive concentrations of nuisance dust in the workplace may cause mechanical irritation to mucous membranes.

Chronic (Delayed)
- No data available.

Carcinogenic Effects
- This material does contain components that may cause cancer, however, based on regulatory criteria this material is not classified as a carcinogen.

Carcinogenic Effects

	CAS	OSHA	IARC	NTP
Lead 210	14255-04-0	Not Listed	Group 1-Carcinogenic	Not Listed
Radium 226	13982-63-3	Not Listed	Group 1-Carcinogenic	Not Listed
Radium 228	15262-20-1	Not Listed	Group 1-Carcinogenic	Not Listed
Cadmium	7440-43-9	Specifically Regulated Carcinogen	Group 1-Carcinogenic	Known Human Carcinogen
Nickel	7440-02-0	Not Listed	Group 2B-Possible Carcinogen	Reasonably Anticipated to be Human Carcinogen
Nickel as Nickel Compounds	NDA	Not Listed	Group 1-Carcinogenic	Known Human Carcinogen
Beryllium	7440-41-7	Not Listed	Group 1-Carcinogenic	Known Human Carcinogen
Beryllium as Beryllium Compounds	NDA	Not Listed	Group 1-Carcinogenic	Known Human Carcinogen
Lead	7439-92-1	Not Listed	Group 2A-Probable Carcinogen	Reasonably Anticipated to be Human Carcinogen
Arsenic	7440-38-2	Not Listed	Group 1-Carcinogenic	Known Human Carcinogen
Cobalt	7440-48-4	Not Listed	Group 2B-Possible Carcinogen	Not Listed

Key to abbreviations

LD = Lethal Dose TC = Toxic Concentration
MLD = Mild TD = Toxic Dose
MOD = Moderate

Section 12 - Ecological Information

Toxicity
- No data available at this time.

Persistence and degradability
- No data available at this time.

Bioaccumulative potential
- No data available at this time.

Mobility in Soil
- No data available at this time.

Other adverse effects
- No data available at this time.

Section 13 - Disposal Considerations

Waste treatment methods

Product waste
- Dispose of content and/or container in accordance with local, regional, national, and/or international regulations.

Packaging waste
- Dispose of content and/or container in accordance with local, regional, national, and/or international regulations.

Section 14 - Transport Information

	UN number	UN proper shipping name	Transport hazard class(es)	Packing group	Environmental hazards
DOT	UN3077	Environmentally Hazardous Substance, Solid, N.O.S., (Geothermal Scale)	9	III	NDA

Special precautions for user
- 10x Particulate Respirators and safety glasses with side protectors required when handling. Dispose in Class III Non Hazardous Landfill. 24 hour emergency phone, 1-800-424-9300.

Transport in bulk according to Annex II of MARPOL 73/78 and the IBC Code
- Transported in end-dumps, wetted, and covered.

Section 15 - Regulatory Information

Safety, health and environmental regulations/legislation specific for the substance or mixture

SARA Hazard Classifications
- Chronic

Inventory

Component	CAS	TSCA
Antimony	7440-36-0	Yes
Arsenic	7440-38-2	Yes
Barium	7440-39-3	Yes
Beryllium	7440-41-7	Yes
Cadmium	7440-43-9	Yes
Calcium	7440-70-2	Yes
Chromium	7440-47-3	Yes
Cobalt	7440-48-4	Yes
Copper	7440-50-8	Yes
Iron	7439-89-6	Yes
Lead	7439-92-1	Yes

* View the full document (pdf) here: https://drive.google.com/file/d/1Y2_61vVLYkDwFRC0zYLNPC6kaZLtJrO-/view?usp=sharing

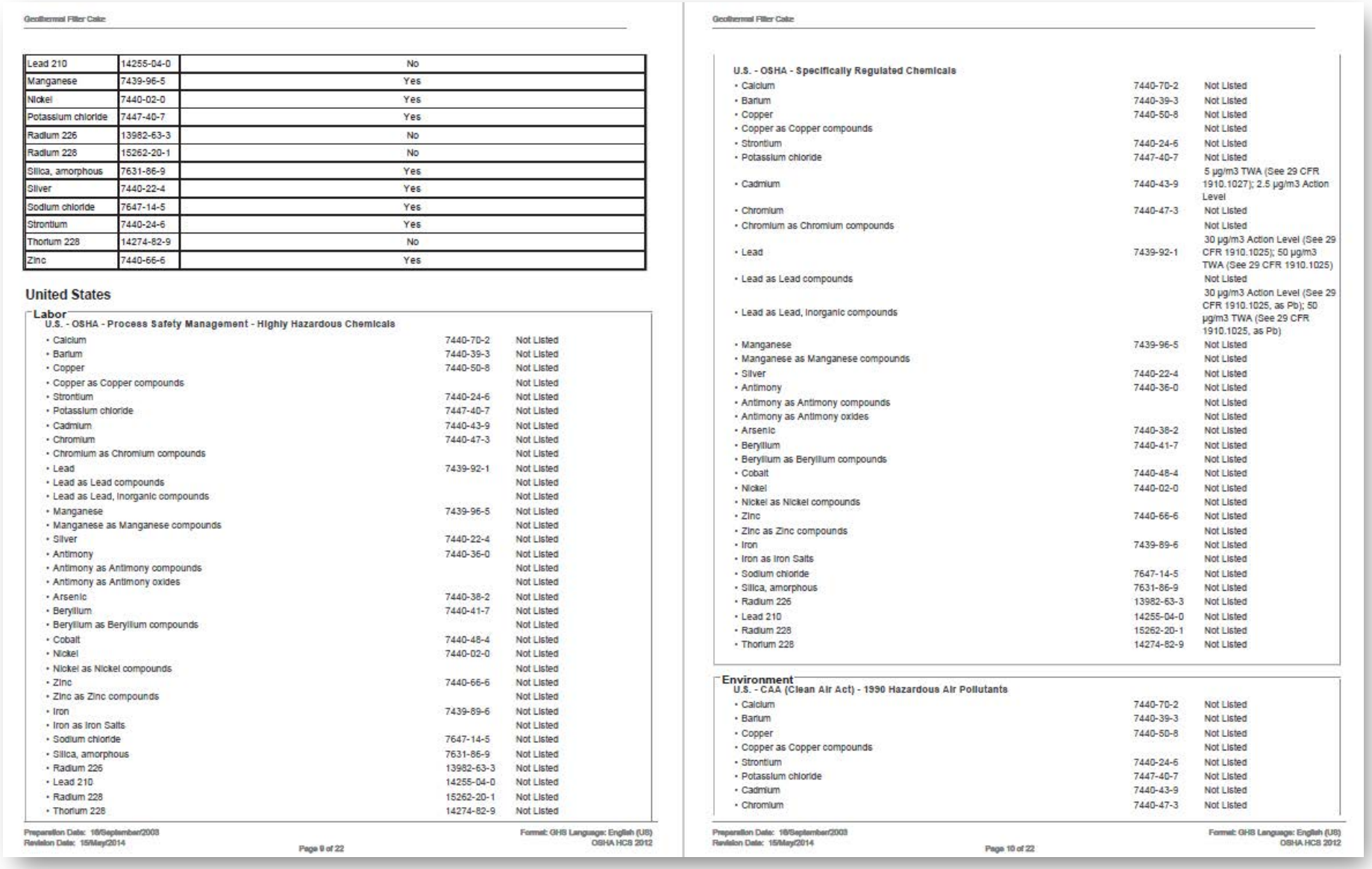

Geothermal Filter Cake

Lead 210	14255-04-0	No
Manganese	7439-96-5	Yes
Nickel	7440-02-0	Yes
Potassium chloride	7447-40-7	Yes
Radium 226	13982-63-3	No
Radium 228	15262-20-1	No
Silica, amorphous	7631-86-9	Yes
Silver	7440-22-4	Yes
Sodium chloride	7647-14-5	Yes
Strontium	7440-24-6	Yes
Thorium 228	14274-82-9	No
Zinc	7440-66-6	Yes

United States

Labor

U.S. - OSHA - Process Safety Management - Highly Hazardous Chemicals

• Calcium	7440-70-2	Not Listed
• Barium	7440-39-3	Not Listed
• Copper	7440-50-8	Not Listed
• Copper as Copper compounds		Not Listed
• Strontium	7440-24-6	Not Listed
• Potassium chloride	7447-40-7	Not Listed
• Cadmium	7440-43-9	Not Listed
• Chromium	7440-47-3	Not Listed
• Chromium as Chromium compounds		Not Listed
• Lead	7439-92-1	Not Listed
• Lead as Lead compounds		Not Listed
• Lead as Lead, Inorganic compounds		Not Listed
• Manganese	7439-96-5	Not Listed
• Manganese as Manganese compounds		Not Listed
• Silver	7440-22-4	Not Listed
• Antimony	7440-36-0	Not Listed
• Antimony as Antimony compounds		Not Listed
• Antimony as Antimony oxides		Not Listed
• Arsenic	7440-38-2	Not Listed
• Beryllium	7440-41-7	Not Listed
• Beryllium as Beryllium compounds		Not Listed
• Cobalt	7440-48-4	Not Listed
• Nickel	7440-02-0	Not Listed
• Nickel as Nickel compounds		Not Listed
• Zinc	7440-66-6	Not Listed
• Zinc as Zinc compounds		Not Listed
• Iron	7439-89-6	Not Listed
• Iron as Iron Salts		Not Listed
• Sodium chloride	7647-14-5	Not Listed
• Silica, amorphous	7631-86-9	Not Listed
• Radium 226	13982-63-3	Not Listed
• Lead 210	14255-04-0	Not Listed
• Radium 228	15262-20-1	Not Listed
• Thorium 228	14274-82-9	Not Listed

Preparation Date: 16/September/2003
Revision Date: 15/May/2014

Page 9 of 22

Format: GHS Language: English (US)
OSHA HCS 2012

Geothermal Filter Cake

U.S. - OSHA - Specifically Regulated Chemicals

• Calcium	7440-70-2	Not Listed
• Barium	7440-39-3	Not Listed
• Copper	7440-50-8	Not Listed
• Copper as Copper compounds		Not Listed
• Strontium	7440-24-6	Not Listed
• Potassium chloride	7447-40-7	Not Listed
• Cadmium	7440-43-9	5 µg/m3 TWA (See 29 CFR 1910.1027); 2.5 µg/m3 Action Level
• Chromium	7440-47-3	Not Listed
• Chromium as Chromium compounds		Not Listed
• Lead	7439-92-1	30 µg/m3 Action Level (See 29 CFR 1910.1025); 50 µg/m3 TWA (See 29 CFR 1910.1025)
• Lead as Lead compounds		Not Listed
• Lead as Lead, Inorganic compounds		30 µg/m3 Action Level (See 29 CFR 1910.1025, as Pb); 50 µg/m3 TWA (See 29 CFR 1910.1025, as Pb)
• Manganese	7439-96-5	Not Listed
• Manganese as Manganese compounds		Not Listed
• Silver	7440-22-4	Not Listed
• Antimony	7440-36-0	Not Listed
• Antimony as Antimony compounds		Not Listed
• Antimony as Antimony oxides		Not Listed
• Arsenic	7440-38-2	Not Listed
• Beryllium	7440-41-7	Not Listed
• Beryllium as Beryllium compounds		Not Listed
• Cobalt	7440-48-4	Not Listed
• Nickel	7440-02-0	Not Listed
• Nickel as Nickel compounds		Not Listed
• Zinc	7440-66-6	Not Listed
• Zinc as Zinc compounds		Not Listed
• Iron	7439-89-6	Not Listed
• Iron as Iron Salts		Not Listed
• Sodium chloride	7647-14-5	Not Listed
• Silica, amorphous	7631-86-9	Not Listed
• Radium 226	13982-63-3	Not Listed
• Lead 210	14255-04-0	Not Listed
• Radium 228	15262-20-1	Not Listed
• Thorium 228	14274-82-9	Not Listed

Environment

U.S. - CAA (Clean Air Act) - 1990 Hazardous Air Pollutants

• Calcium	7440-70-2	Not Listed
• Barium	7440-39-3	Not Listed
• Copper	7440-50-8	Not Listed
• Copper as Copper compounds		Not Listed
• Strontium	7440-24-6	Not Listed
• Potassium chloride	7447-40-7	Not Listed
• Cadmium	7440-43-9	Not Listed
• Chromium	7440-47-3	Not Listed

Preparation Date: 16/September/2003
Revision Date: 15/May/2014

Page 10 of 22

Format: GHS Language: English (US)
OSHA HCS 2012

* View the full document (pdf) here: https://drive.google.com/file/d/1Y2_61vVLYkDwFRC0zYLNPC6kaZLtJrO-/view?usp=sharing

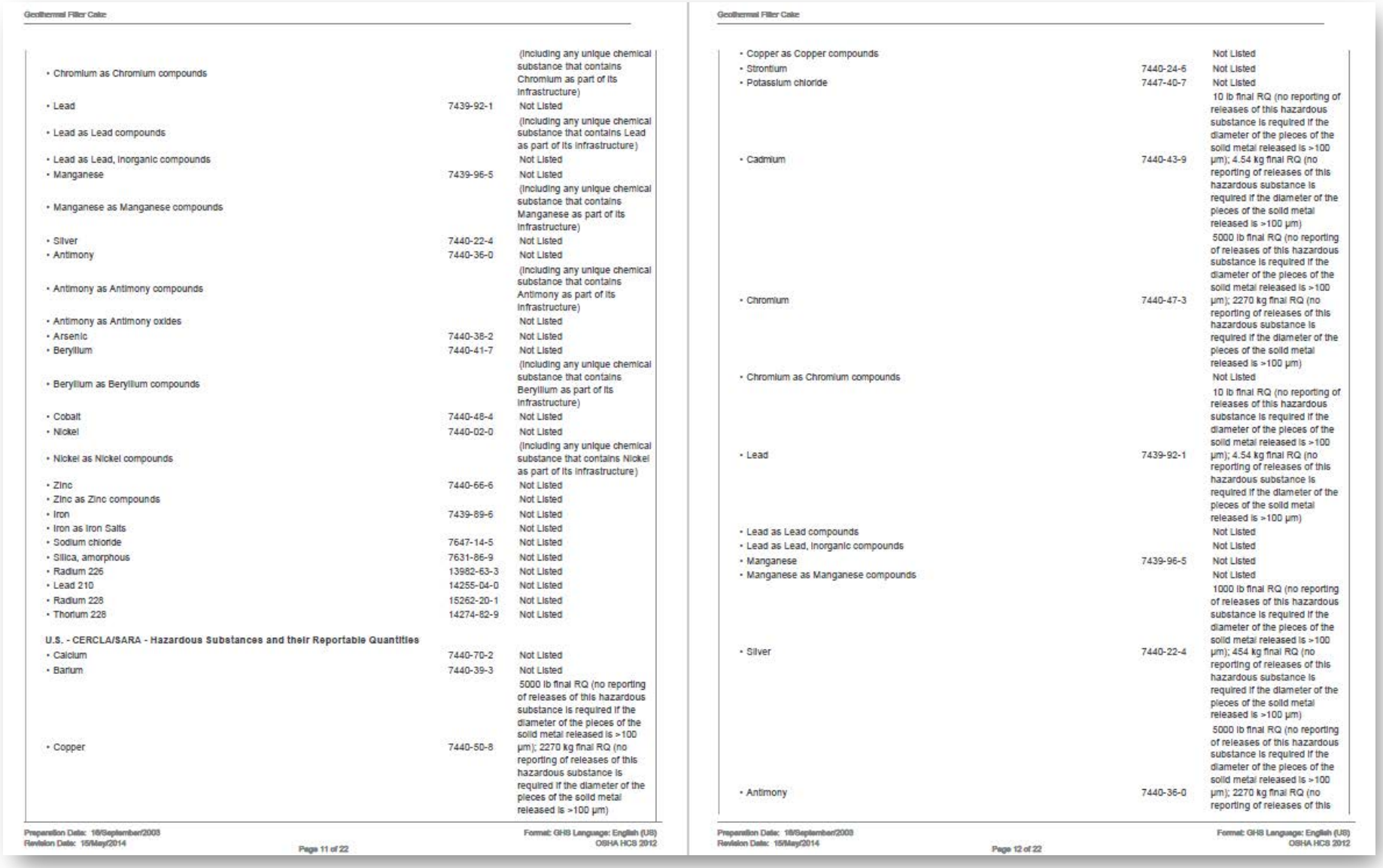

Geothermal Filter Cake

• Chromium as Chromium compounds		(including any unique chemical substance that contains Chromium as part of its infrastructure)
• Lead	7439-92-1	Not Listed
• Lead as Lead compounds		(including any unique chemical substance that contains Lead as part of its infrastructure)
• Lead as Lead, inorganic compounds		Not Listed
• Manganese	7439-96-5	Not Listed
• Manganese as Manganese compounds		(including any unique chemical substance that contains Manganese as part of its infrastructure)
• Silver	7440-22-4	Not Listed
• Antimony	7440-36-0	Not Listed
• Antimony as Antimony compounds		(including any unique chemical substance that contains Antimony as part of its infrastructure)
• Antimony as Antimony oxides		Not Listed
• Arsenic	7440-38-2	Not Listed
• Beryllium	7440-41-7	Not Listed
• Beryllium as Beryllium compounds		(including any unique chemical substance that contains Beryllium as part of its infrastructure)
• Cobalt	7440-48-4	Not Listed
• Nickel	7440-02-0	Not Listed
• Nickel as Nickel compounds		(including any unique chemical substance that contains Nickel as part of its infrastructure)
• Zinc	7440-66-6	Not Listed
• Zinc as Zinc compounds		Not Listed
• Iron	7439-89-6	Not Listed
• Iron as Iron Salts		Not Listed
• Sodium chloride	7647-14-5	Not Listed
• Silica, amorphous	7631-86-9	Not Listed
• Radium 226	13982-63-3	Not Listed
• Lead 210	14255-04-0	Not Listed
• Radium 228	15262-20-1	Not Listed
• Thorium 228	14274-82-9	Not Listed
U.S. - CERCLA/SARA - Hazardous Substances and their Reportable Quantities		
• Calcium	7440-70-2	Not Listed
• Barium	7440-39-3	Not Listed
• Copper	7440-50-8	5000 lb final RQ (no reporting of releases of this hazardous substance is required if the diameter of the pieces of the solid metal released is >100 µm); 2270 kg final RQ (no reporting of releases of this hazardous substance is required if the diameter of the pieces of the solid metal released is >100 µm)

Preparation Date: 18/September/2008
Revision Date: 15/May/2014
Page 11 of 22
Format: GHS Language: English (US)
OSHA HCS 2012

Geothermal Filter Cake

• Copper as Copper compounds		Not Listed
• Strontium	7440-24-6	Not Listed
• Potassium chloride	7447-40-7	Not Listed
• Cadmium	7440-43-9	10 lb final RQ (no reporting of releases of this hazardous substance is required if the diameter of the pieces of the solid metal released is >100 µm); 4.54 kg final RQ (no reporting of releases of this hazardous substance is required if the diameter of the pieces of the solid metal released is >100 µm)
• Chromium	7440-47-3	5000 lb final RQ (no reporting of releases of this hazardous substance is required if the diameter of the pieces of the solid metal released is >100 µm); 2270 kg final RQ (no reporting of releases of this hazardous substance is required if the diameter of the pieces of the solid metal released is >100 µm)
• Chromium as Chromium compounds		Not Listed
• Lead	7439-92-1	10 lb final RQ (no reporting of releases of this hazardous substance is required if the diameter of the pieces of the solid metal released is >100 µm); 4.54 kg final RQ (no reporting of releases of this hazardous substance is required if the diameter of the pieces of the solid metal released is >100 µm)
• Lead as Lead compounds		Not Listed
• Lead as Lead, inorganic compounds		Not Listed
• Manganese	7439-96-5	Not Listed
• Manganese as Manganese compounds		Not Listed
• Silver	7440-22-4	1000 lb final RQ (no reporting of releases of this hazardous substance is required if the diameter of the pieces of the solid metal released is >100 µm); 454 kg final RQ (no reporting of releases of this hazardous substance is required if the diameter of the pieces of the solid metal released is >100 µm)
• Antimony	7440-36-0	5000 lb final RQ (no reporting of releases of this hazardous substance is required if the diameter of the pieces of the solid metal released is >100 µm); 2270 kg final RQ (no reporting of releases of this

Preparation Date: 18/September/2008
Revision Date: 15/May/2014
Page 12 of 22
Format: GHS Language: English (US)
OSHA HCS 2012

* View the full document (pdf) here: https://drive.google.com/file/d/1Y2_61vVLYkDwFRC0zYLNPC6kaZLtJrO-/view?usp=sharing

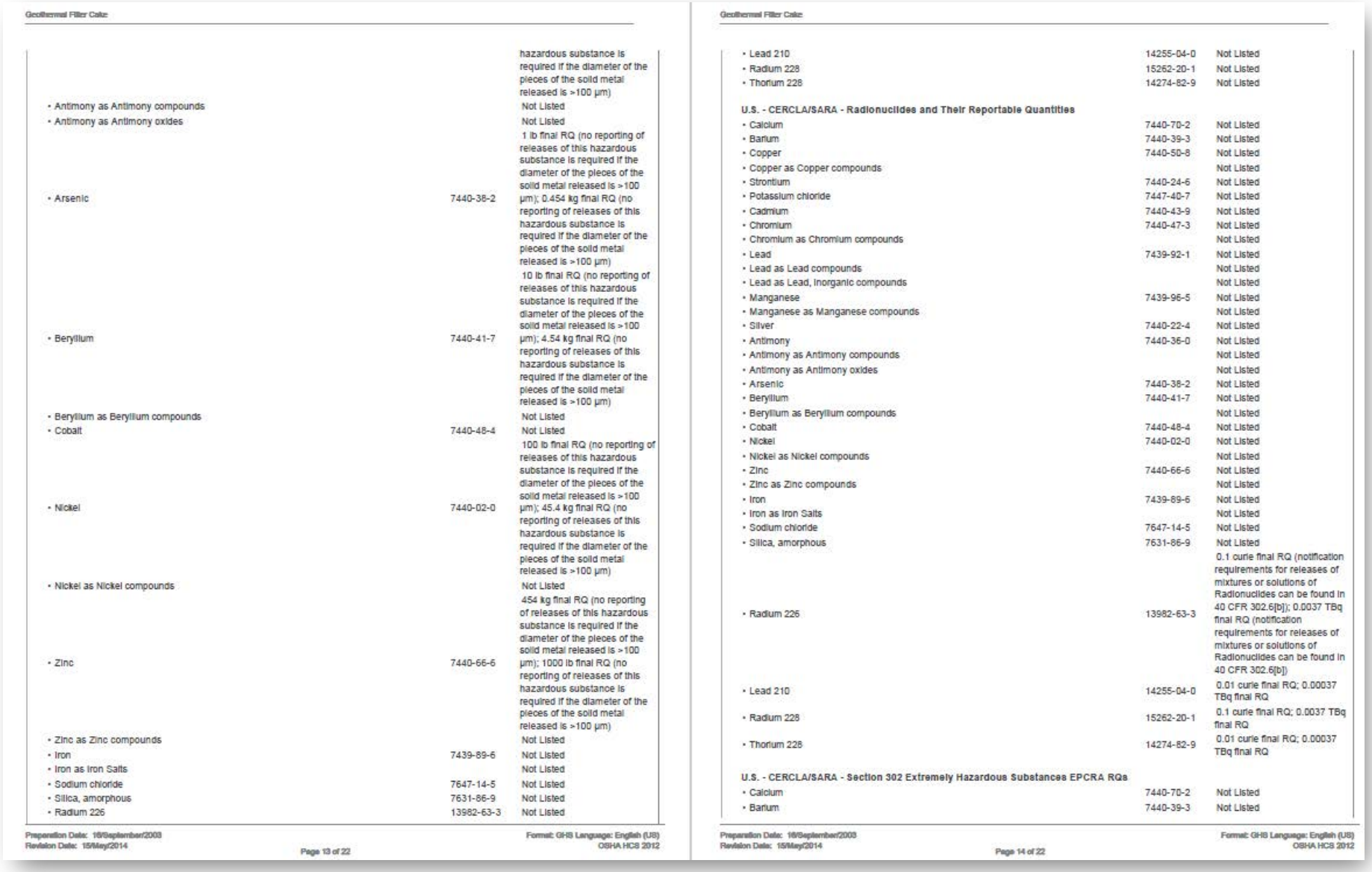

		hazardous substance is required if the diameter of the pieces of the solid metal released is >100 µm)
• Antimony as Antimony compounds		Not Listed
• Antimony as Antimony oxides		Not Listed
• Arsenic	7440-38-2	1 lb final RQ (no reporting of releases of this hazardous substance is required if the diameter of the pieces of the solid metal released is >100 µm); 0.454 kg final RQ (no reporting of releases of this hazardous substance is required if the diameter of the pieces of the solid metal released is >100 µm)
• Beryllium	7440-41-7	10 lb final RQ (no reporting of releases of this hazardous substance is required if the diameter of the pieces of the solid metal released is >100 µm); 4.54 kg final RQ (no reporting of releases of this hazardous substance is required if the diameter of the pieces of the solid metal released is >100 µm)
• Beryllium as Beryllium compounds		Not Listed
• Cobalt	7440-48-4	Not Listed
• Nickel	7440-02-0	100 lb final RQ (no reporting of releases of this hazardous substance is required if the diameter of the pieces of the solid metal released is >100 µm); 45.4 kg final RQ (no reporting of releases of this hazardous substance is required if the diameter of the pieces of the solid metal released is >100 µm)
• Nickel as Nickel compounds		Not Listed
• Zinc	7440-66-6	454 kg final RQ (no reporting of releases of this hazardous substance is required if the diameter of the pieces of the solid metal released is >100 µm); 1000 lb final RQ (no reporting of releases of this hazardous substance is required if the diameter of the pieces of the solid metal released is >100 µm)
• Zinc as Zinc compounds		Not Listed
• Iron	7439-89-6	Not Listed
• Iron as Iron Salts		Not Listed
• Sodium chloride	7647-14-5	Not Listed
• Silica, amorphous	7631-86-9	Not Listed
• Radium 226	13982-63-3	Not Listed

• Lead 210	14255-04-0	Not Listed
• Radium 228	15262-20-1	Not Listed
• Thorium 228	14274-82-9	Not Listed
U.S. - CERCLA/SARA - Radionuclides and Their Reportable Quantities		
• Calcium	7440-70-2	Not Listed
• Barium	7440-39-3	Not Listed
• Copper	7440-50-8	Not Listed
• Copper as Copper compounds		Not Listed
• Strontium	7440-24-6	Not Listed
• Potassium chloride	7447-40-7	Not Listed
• Cadmium	7440-43-9	Not Listed
• Chromium	7440-47-3	Not Listed
• Chromium as Chromium compounds		Not Listed
• Lead	7439-92-1	Not Listed
• Lead as Lead compounds		Not Listed
• Lead as Lead, Inorganic compounds		Not Listed
• Manganese	7439-96-5	Not Listed
• Manganese as Manganese compounds		Not Listed
• Silver	7440-22-4	Not Listed
• Antimony	7440-36-0	Not Listed
• Antimony as Antimony compounds		Not Listed
• Antimony as Antimony oxides		Not Listed
• Arsenic	7440-38-2	Not Listed
• Beryllium	7440-41-7	Not Listed
• Beryllium as Beryllium compounds		Not Listed
• Cobalt	7440-48-4	Not Listed
• Nickel	7440-02-0	Not Listed
• Nickel as Nickel compounds		Not Listed
• Zinc	7440-66-6	Not Listed
• Zinc as Zinc compounds		Not Listed
• Iron	7439-89-6	Not Listed
• Iron as Iron Salts		Not Listed
• Sodium chloride	7647-14-5	Not Listed
• Silica, amorphous	7631-86-9	Not Listed
• Radium 226	13982-63-3	0.1 curie final RQ (notification requirements for releases of mixtures or solutions of Radionuclides can be found in 40 CFR 302.6[b]); 0.0037 TBq final RQ (notification requirements for releases of mixtures or solutions of Radionuclides can be found in 40 CFR 302.6[b])
• Lead 210	14255-04-0	0.01 curie final RQ; 0.00037 TBq final RQ
• Radium 228	15262-20-1	0.1 curie final RQ; 0.0037 TBq final RQ
• Thorium 228	14274-82-9	0.01 curie final RQ; 0.00037 TBq final RQ
U.S. - CERCLA/SARA - Section 302 Extremely Hazardous Substances EPCRA RQs		
• Calcium	7440-70-2	Not Listed
• Barium	7440-39-3	Not Listed

* View the full document (pdf) here: https://drive.google.com/file/d/1Y2_61vVLYkDwFRC0zYLNPC6kaZLtJrO-/view?usp=sharing

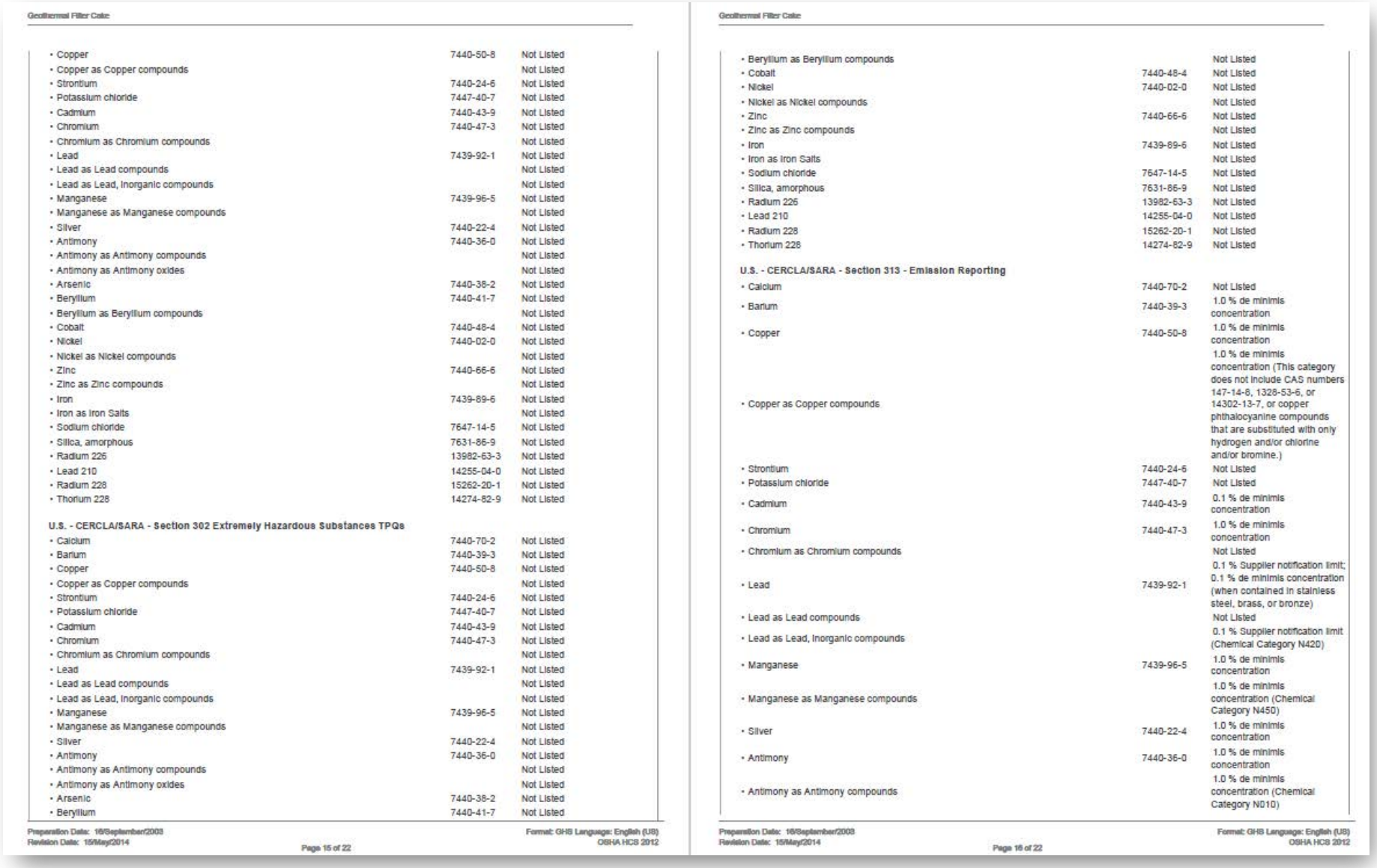

Geothermal Filter Cake

• Copper	7440-50-8	Not Listed
• Copper as Copper compounds		Not Listed
• Strontium	7440-24-6	Not Listed
• Potassium chloride	7447-40-7	Not Listed
• Cadmium	7440-43-9	Not Listed
• Chromium	7440-47-3	Not Listed
• Chromium as Chromium compounds		Not Listed
• Lead	7439-92-1	Not Listed
• Lead as Lead compounds		Not Listed
• Lead as Lead, Inorganic compounds		Not Listed
• Manganese	7439-96-5	Not Listed
• Manganese as Manganese compounds		Not Listed
• Silver	7440-22-4	Not Listed
• Antimony	7440-36-0	Not Listed
• Antimony as Antimony compounds		Not Listed
• Antimony as Antimony oxides		Not Listed
• Arsenic	7440-38-2	Not Listed
• Beryllium	7440-41-7	Not Listed
• Beryllium as Beryllium compounds		Not Listed
• Cobalt	7440-48-4	Not Listed
• Nickel	7440-02-0	Not Listed
• Nickel as Nickel compounds		Not Listed
• Zinc	7440-66-6	Not Listed
• Zinc as Zinc compounds		Not Listed
• Iron	7439-89-6	Not Listed
• Iron as Iron Salts		Not Listed
• Sodium chloride	7647-14-5	Not Listed
• Silica, amorphous	7631-86-9	Not Listed
• Radium 226	13982-63-3	Not Listed
• Lead 210	14255-04-0	Not Listed
• Radium 228	15262-20-1	Not Listed
• Thorium 228	14274-82-9	Not Listed

U.S. - CERCLA/SARA - Section 302 Extremely Hazardous Substances TPQs

• Calcium	7440-70-2	Not Listed
• Barium	7440-39-3	Not Listed
• Copper	7440-50-8	Not Listed
• Copper as Copper compounds		Not Listed
• Strontium	7440-24-6	Not Listed
• Potassium chloride	7447-40-7	Not Listed
• Cadmium	7440-43-9	Not Listed
• Chromium	7440-47-3	Not Listed
• Chromium as Chromium compounds		Not Listed
• Lead	7439-92-1	Not Listed
• Lead as Lead compounds		Not Listed
• Lead as Lead, Inorganic compounds		Not Listed
• Manganese	7439-96-5	Not Listed
• Manganese as Manganese compounds		Not Listed
• Silver	7440-22-4	Not Listed
• Antimony	7440-36-0	Not Listed
• Antimony as Antimony compounds		Not Listed
• Antimony as Antimony oxides		Not Listed
• Arsenic	7440-38-2	Not Listed
• Beryllium	7440-41-7	Not Listed

Preparation Date: 16/September/2003
Revision Date: 16/May/2014
Page 15 of 22
Format: GHS Language: English (US)
OSHA HCS 2012

Geothermal Filter Cake

• Beryllium as Beryllium compounds		Not Listed
• Cobalt	7440-48-4	Not Listed
• Nickel	7440-02-0	Not Listed
• Nickel as Nickel compounds		Not Listed
• Zinc	7440-66-6	Not Listed
• Zinc as Zinc compounds		Not Listed
• Iron	7439-89-6	Not Listed
• Iron as Iron Salts		Not Listed
• Sodium chloride	7647-14-5	Not Listed
• Silica, amorphous	7631-86-9	Not Listed
• Radium 226	13982-63-3	Not Listed
• Lead 210	14255-04-0	Not Listed
• Radium 228	15262-20-1	Not Listed
• Thorium 228	14274-82-9	Not Listed

U.S. - CERCLA/SARA - Section 313 - Emission Reporting

• Calcium	7440-70-2	Not Listed
• Barium	7440-39-3	1.0 % de minimis concentration
• Copper	7440-50-8	1.0 % de minimis concentration
• Copper as Copper compounds		1.0 % de minimis concentration (This category does not include CAS numbers 147-14-8, 1328-53-6, or 14302-13-7, or copper phthalocyanine compounds that are substituted with only hydrogen and/or chlorine and/or bromine.)
• Strontium	7440-24-6	Not Listed
• Potassium chloride	7447-40-7	Not Listed
• Cadmium	7440-43-9	0.1 % de minimis concentration
• Chromium	7440-47-3	1.0 % de minimis concentration
• Chromium as Chromium compounds		Not Listed
• Lead	7439-92-1	0.1 % Supplier notification limit; 0.1 % de minimis concentration (when contained in stainless steel, brass, or bronze)
• Lead as Lead compounds		Not Listed
• Lead as Lead, Inorganic compounds		0.1 % Supplier notification limit (Chemical Category N420)
• Manganese	7439-96-5	1.0 % de minimis concentration
• Manganese as Manganese compounds		1.0 % de minimis concentration (Chemical Category N450)
• Silver	7440-22-4	1.0 % de minimis concentration
• Antimony	7440-36-0	1.0 % de minimis concentration
• Antimony as Antimony compounds		1.0 % de minimis concentration (Chemical Category N010)

Preparation Date: 16/September/2003
Revision Date: 16/May/2014
Page 16 of 22
Format: GHS Language: English (US)
OSHA HCS 2012

* View the full document (pdf) here: https://drive.google.com/file/d/1Y2_61vVLYkDwFRC0zYLNPC6kaZLtJrO-/view?usp=sharing

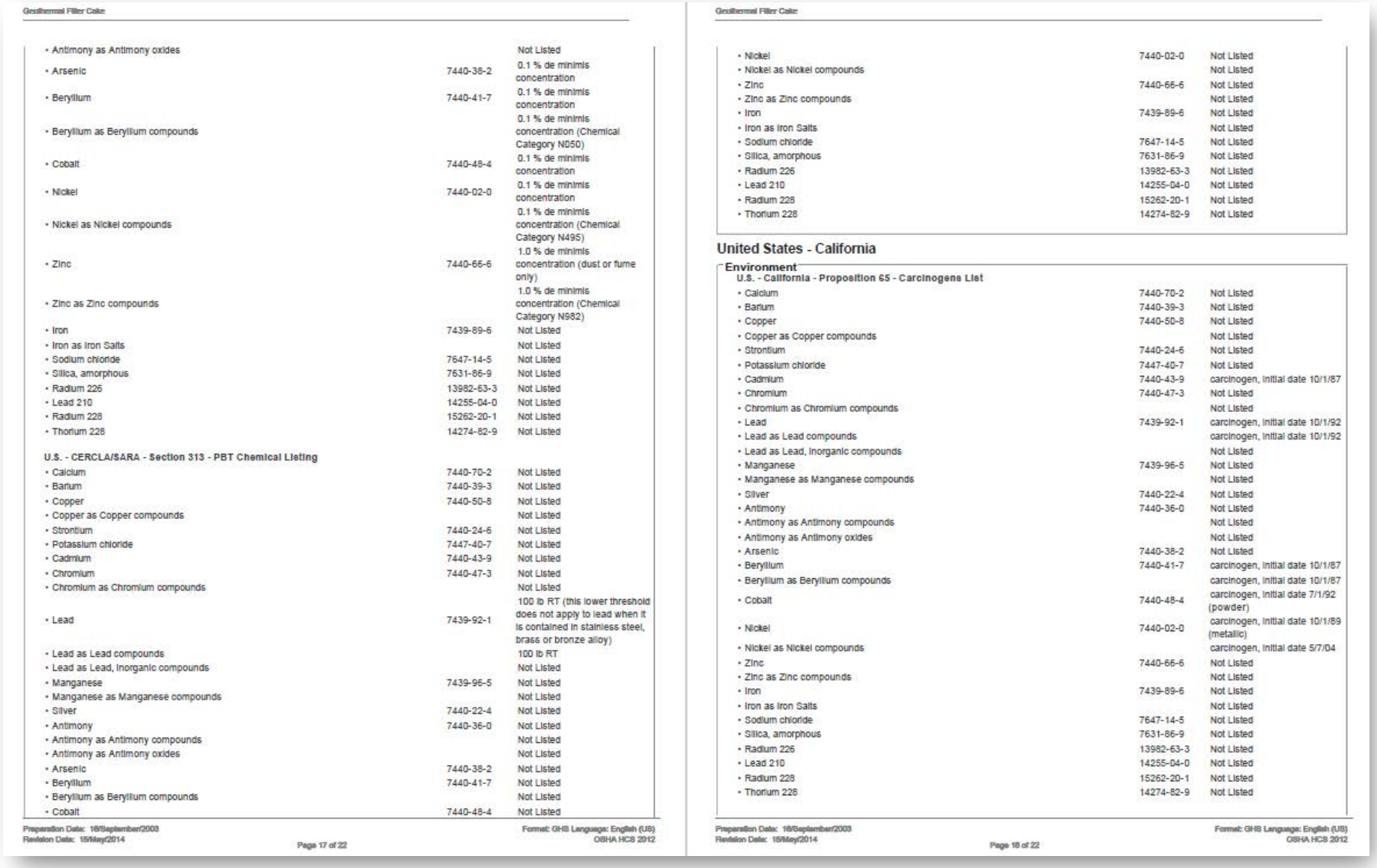

Geothermal Filter Cake:

• Antimony as Antimony oxides		Not Listed
• Arsenic	7440-38-2	0.1 % de minimis concentration
• Beryllium	7440-41-7	0.1 % de minimis concentration
• Beryllium as Beryllium compounds		0.1 % de minimis concentration (Chemical Category N050)
• Cobalt	7440-48-4	0.1 % de minimis concentration
• Nickel	7440-02-0	0.1 % de minimis concentration
• Nickel as Nickel compounds		0.1 % de minimis concentration (Chemical Category N495)
• Zinc	7440-66-6	1.0 % de minimis concentration (dust or fume only)
• Zinc as Zinc compounds		1.0 % de minimis concentration (Chemical Category N982)
• Iron	7439-89-6	Not Listed
• Iron as Iron Salts		Not Listed
• Sodium chloride	7647-14-5	Not Listed
• Silica, amorphous	7631-86-9	Not Listed
• Radium 226	13982-63-3	Not Listed
• Lead 210	14255-04-0	Not Listed
• Radium 228	15262-20-1	Not Listed
• Thorium 228	14274-82-9	Not Listed

U.S. - CERCLA/SARA - Section 313 - PBT Chemical Listing

• Calcium	7440-70-2	Not Listed
• Barium	7440-39-3	Not Listed
• Copper	7440-50-8	Not Listed
• Copper as Copper compounds		Not Listed
• Strontium	7440-24-6	Not Listed
• Potassium chloride	7447-40-7	Not Listed
• Cadmium	7440-43-9	Not Listed
• Chromium	7440-47-3	Not Listed
• Chromium as Chromium compounds		Not Listed
• Lead	7439-92-1	100 lb RT (this lower threshold does not apply to lead when it is contained in stainless steel, brass or bronze alloy)
• Lead as Lead compounds		100 lb RT
• Lead as Lead, Inorganic compounds		Not Listed
• Manganese	7439-96-5	Not Listed
• Manganese as Manganese compounds		Not Listed
• Silver	7440-22-4	Not Listed
• Antimony	7440-36-0	Not Listed
• Antimony as Antimony compounds		Not Listed
• Antimony as Antimony oxides		Not Listed
• Arsenic	7440-38-2	Not Listed
• Beryllium	7440-41-7	Not Listed
• Beryllium as Beryllium compounds		Not Listed
• Cobalt	7440-48-4	Not Listed

Preparation Date: 18/September/2003
Revision Date: 15/May/2014
Page 17 of 22
Format: GHS Language: English (US)
OSHA HCS 2012

Geothermal Filter Cake:

• Nickel	7440-02-0	Not Listed
• Nickel as Nickel compounds		Not Listed
• Zinc	7440-66-6	Not Listed
• Zinc as Zinc compounds		Not Listed
• Iron	7439-89-6	Not Listed
• Iron as Iron Salts		Not Listed
• Sodium chloride	7647-14-5	Not Listed
• Silica, amorphous	7631-86-9	Not Listed
• Radium 226	13982-63-3	Not Listed
• Lead 210	14255-04-0	Not Listed
• Radium 228	15262-20-1	Not Listed
• Thorium 228	14274-82-9	Not Listed

United States - California

Environment

U.S. - California - Proposition 65 - Carcinogens List

• Calcium	7440-70-2	Not Listed
• Barium	7440-39-3	Not Listed
• Copper	7440-50-8	Not Listed
• Copper as Copper compounds		Not Listed
• Strontium	7440-24-6	Not Listed
• Potassium chloride	7447-40-7	Not Listed
• Cadmium	7440-43-9	carcinogen, initial date 10/1/87
• Chromium	7440-47-3	Not Listed
• Chromium as Chromium compounds		Not Listed
• Lead	7439-92-1	carcinogen, initial date 10/1/92
• Lead as Lead compounds		carcinogen, initial date 10/1/92
• Lead as Lead, Inorganic compounds		Not Listed
• Manganese	7439-96-5	Not Listed
• Manganese as Manganese compounds		Not Listed
• Silver	7440-22-4	Not Listed
• Antimony	7440-36-0	Not Listed
• Antimony as Antimony compounds		Not Listed
• Antimony as Antimony oxides		Not Listed
• Arsenic	7440-38-2	Not Listed
• Beryllium	7440-41-7	carcinogen, initial date 10/1/87
• Beryllium as Beryllium compounds		carcinogen, initial date 10/1/87
• Cobalt	7440-48-4	carcinogen, initial date 7/1/92 (powder)
• Nickel	7440-02-0	carcinogen, initial date 10/1/89 (metallic)
• Nickel as Nickel compounds		carcinogen, initial date 5/7/04
• Zinc	7440-66-6	Not Listed
• Zinc as Zinc compounds		Not Listed
• Iron	7439-89-6	Not Listed
• Iron as Iron Salts		Not Listed
• Sodium chloride	7647-14-5	Not Listed
• Silica, amorphous	7631-86-9	Not Listed
• Radium 226	13982-63-3	Not Listed
• Lead 210	14255-04-0	Not Listed
• Radium 228	15262-20-1	Not Listed
• Thorium 228	14274-82-9	Not Listed

Preparation Date: 18/September/2003
Revision Date: 15/May/2014
Page 18 of 22
Format: GHS Language: English (US)
OSHA HCS 2012

* View the full document (pdf) here: https://drive.google.com/file/d/1Y2_61vVLYkDwFRC0zYLNPC6kaZLtJrO-/view?usp=sharing

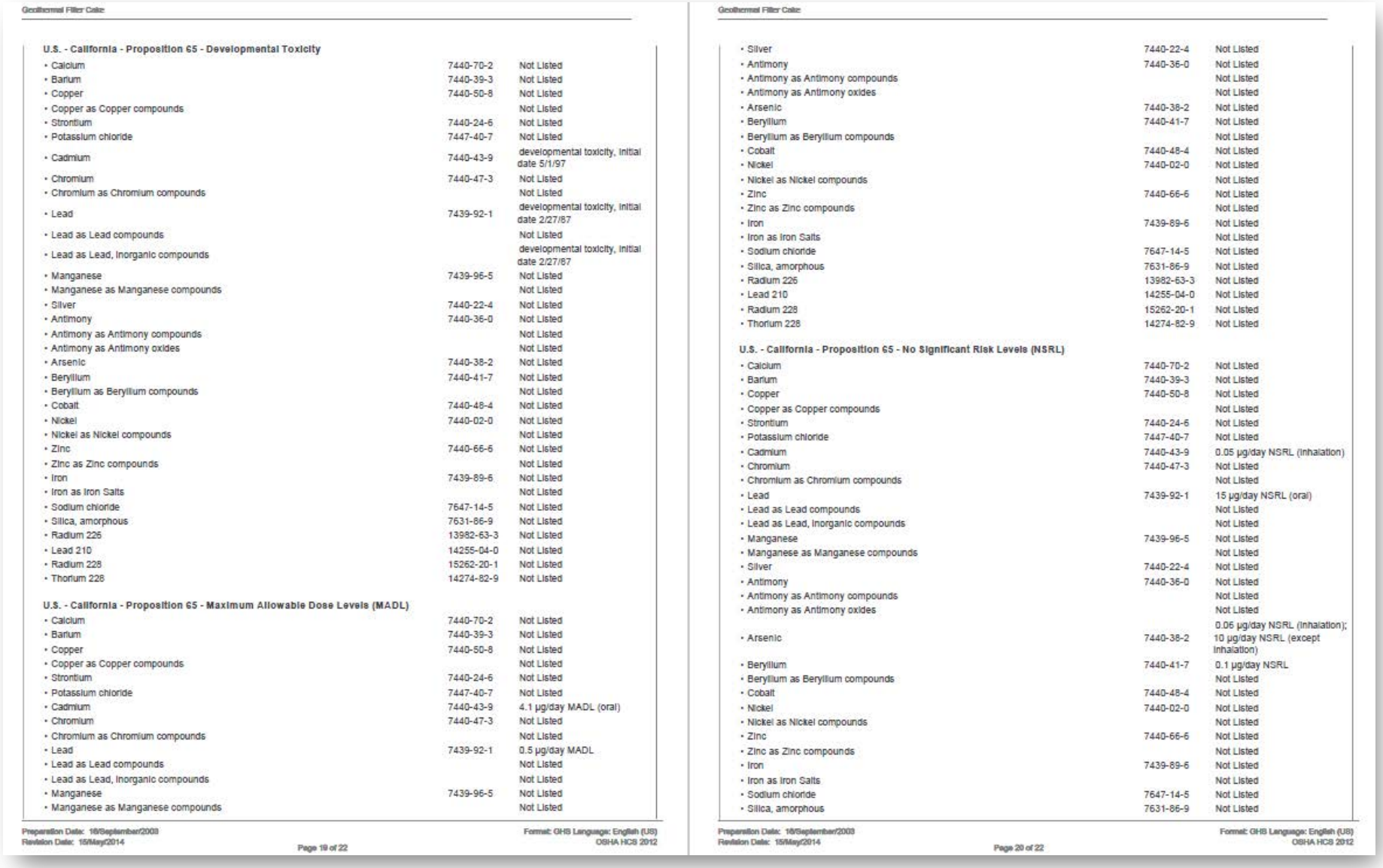

U.S. - California - Proposition 65 - Developmental Toxicity

• Calcium	7440-70-2	Not Listed
• Barium	7440-39-3	Not Listed
• Copper	7440-50-8	Not Listed
• Copper as Copper compounds		Not Listed
• Strontium	7440-24-6	Not Listed
• Potassium chloride	7447-40-7	Not Listed
• Cadmium	7440-43-9	developmental toxicity, initial date 5/1/97
• Chromium	7440-47-3	Not Listed
• Chromium as Chromium compounds		Not Listed
• Lead	7439-92-1	developmental toxicity, initial date 2/27/87
• Lead as Lead compounds		Not Listed
• Lead as Lead, Inorganic compounds		developmental toxicity, initial date 2/27/87
• Manganese	7439-96-5	Not Listed
• Manganese as Manganese compounds		Not Listed
• Silver	7440-22-4	Not Listed
• Antimony	7440-36-0	Not Listed
• Antimony as Antimony compounds		Not Listed
• Antimony as Antimony oxides		Not Listed
• Arsenic	7440-38-2	Not Listed
• Beryllium	7440-41-7	Not Listed
• Beryllium as Beryllium compounds		Not Listed
• Cobalt	7440-48-4	Not Listed
• Nickel	7440-02-0	Not Listed
• Nickel as Nickel compounds		Not Listed
• Zinc	7440-66-6	Not Listed
• Zinc as Zinc compounds		Not Listed
• Iron	7439-89-6	Not Listed
• Iron as Iron Salts		Not Listed
• Sodium chloride	7647-14-5	Not Listed
• Silica, amorphous	7631-86-9	Not Listed
• Radium 226	13982-63-3	Not Listed
• Lead 210	14255-04-0	Not Listed
• Radium 228	15262-20-1	Not Listed
• Thorium 228	14274-82-9	Not Listed

U.S. - California - Proposition 65 - Maximum Allowable Dose Levels (MADL)

• Calcium	7440-70-2	Not Listed
• Barium	7440-39-3	Not Listed
• Copper	7440-50-8	Not Listed
• Copper as Copper compounds		Not Listed
• Strontium	7440-24-6	Not Listed
• Potassium chloride	7447-40-7	Not Listed
• Cadmium	7440-43-9	4.1 µg/day MADL (oral)
• Chromium	7440-47-3	Not Listed
• Chromium as Chromium compounds		Not Listed
• Lead	7439-92-1	0.5 µg/day MADL
• Lead as Lead compounds		Not Listed
• Lead as Lead, Inorganic compounds		Not Listed
• Manganese	7439-96-5	Not Listed
• Manganese as Manganese compounds		Not Listed

• Silver	7440-22-4	Not Listed
• Antimony	7440-36-0	Not Listed
• Antimony as Antimony compounds		Not Listed
• Antimony as Antimony oxides		Not Listed
• Arsenic	7440-38-2	Not Listed
• Beryllium	7440-41-7	Not Listed
• Beryllium as Beryllium compounds		Not Listed
• Cobalt	7440-48-4	Not Listed
• Nickel	7440-02-0	Not Listed
• Nickel as Nickel compounds		Not Listed
• Zinc	7440-66-6	Not Listed
• Zinc as Zinc compounds		Not Listed
• Iron	7439-89-6	Not Listed
• Iron as Iron Salts		Not Listed
• Sodium chloride	7647-14-5	Not Listed
• Silica, amorphous	7631-86-9	Not Listed
• Radium 226	13982-63-3	Not Listed
• Lead 210	14255-04-0	Not Listed
• Radium 228	15262-20-1	Not Listed
• Thorium 228	14274-82-9	Not Listed

U.S. - California - Proposition 65 - No Significant Risk Levels (NSRL)

• Calcium	7440-70-2	Not Listed
• Barium	7440-39-3	Not Listed
• Copper	7440-50-8	Not Listed
• Copper as Copper compounds		Not Listed
• Strontium	7440-24-6	Not Listed
• Potassium chloride	7447-40-7	Not Listed
• Cadmium	7440-43-9	0.05 µg/day NSRL (inhalation)
• Chromium	7440-47-3	Not Listed
• Chromium as Chromium compounds		Not Listed
• Lead	7439-92-1	15 µg/day NSRL (oral)
• Lead as Lead compounds		Not Listed
• Lead as Lead, Inorganic compounds		Not Listed
• Manganese	7439-96-5	Not Listed
• Manganese as Manganese compounds		Not Listed
• Silver	7440-22-4	Not Listed
• Antimony	7440-36-0	Not Listed
• Antimony as Antimony compounds		Not Listed
• Antimony as Antimony oxides		Not Listed
• Arsenic	7440-38-2	0.06 µg/day NSRL (inhalation); 10 µg/day NSRL (except inhalation)
• Beryllium	7440-41-7	0.1 µg/day NSRL
• Beryllium as Beryllium compounds		Not Listed
• Cobalt	7440-48-4	Not Listed
• Nickel	7440-02-0	Not Listed
• Nickel as Nickel compounds		Not Listed
• Zinc	7440-66-6	Not Listed
• Zinc as Zinc compounds		Not Listed
• Iron	7439-89-6	Not Listed
• Iron as Iron Salts		Not Listed
• Sodium chloride	7647-14-5	Not Listed
• Silica, amorphous	7631-86-9	Not Listed

* View the full document (pdf) here: https://drive.google.com/file/d/1Y2_61vVLYkDwFRC0zYLNPC6kaZLtJrO-/view?usp=sharing

• Radium 226	13982-63-3	Not Listed
• Lead 210	14255-04-0	Not Listed
• Radium 228	15262-20-1	Not Listed
• Thorium 228	14274-82-9	Not Listed

U.S. - California - Proposition 65 - Reproductive Toxicity - Female

• Calcium	7440-70-2	Not Listed
• Barium	7440-39-3	Not Listed
• Copper	7440-50-8	Not Listed
• Copper as Copper compounds		Not Listed
• Strontium	7440-24-6	Not Listed
• Potassium chloride	7447-40-7	Not Listed
• Cadmium	7440-43-9	Not Listed
• Chromium	7440-47-3	Not Listed
• Chromium as Chromium compounds		Not Listed
• Lead	7439-92-1	female reproductive toxicity, initial date 2/27/87
• Lead as Lead compounds		Not Listed
• Lead as Lead, Inorganic compounds		Not Listed
• Manganese	7439-96-5	Not Listed
• Manganese as Manganese compounds		Not Listed
• Silver	7440-22-4	Not Listed
• Antimony	7440-36-0	Not Listed
• Antimony as Antimony compounds		Not Listed
• Antimony as Antimony oxides		Not Listed
• Arsenic	7440-38-2	Not Listed
• Beryllium	7440-41-7	Not Listed
• Beryllium as Beryllium compounds		Not Listed
• Cobalt	7440-48-4	Not Listed
• Nickel	7440-02-0	Not Listed
• Nickel as Nickel compounds		Not Listed
• Zinc	7440-66-6	Not Listed
• Zinc as Zinc compounds		Not Listed
• Iron	7439-89-6	Not Listed
• Iron as Iron Salts		Not Listed
• Sodium chloride	7647-14-5	Not Listed
• Silica, amorphous	7631-86-9	Not Listed
• Radium 226	13982-63-3	Not Listed
• Lead 210	14255-04-0	Not Listed
• Radium 228	15262-20-1	Not Listed
• Thorium 228	14274-82-9	Not Listed

U.S. - California - Proposition 65 - Reproductive Toxicity - Male

• Calcium	7440-70-2	Not Listed
• Barium	7440-39-3	Not Listed
• Copper	7440-50-8	Not Listed
• Copper as Copper compounds		Not Listed
• Strontium	7440-24-6	Not Listed
• Potassium chloride	7447-40-7	Not Listed
• Cadmium	7440-43-9	male reproductive toxicity, initial date 5/1/97
• Chromium	7440-47-3	Not Listed
• Chromium as Chromium compounds		Not Listed

• Lead	7439-92-1	male reproductive toxicity, initial date 2/27/87
• Lead as Lead compounds		Not Listed
• Lead as Lead, Inorganic compounds		Not Listed
• Manganese	7439-96-5	Not Listed
• Manganese as Manganese compounds		Not Listed
• Silver	7440-22-4	Not Listed
• Antimony	7440-36-0	Not Listed
• Antimony as Antimony compounds		Not Listed
• Antimony as Antimony oxides		Not Listed
• Arsenic	7440-38-2	Not Listed
• Beryllium	7440-41-7	Not Listed
• Beryllium as Beryllium compounds		Not Listed
• Cobalt	7440-48-4	Not Listed
• Nickel	7440-02-0	Not Listed
• Nickel as Nickel compounds		Not Listed
• Zinc	7440-66-6	Not Listed
• Zinc as Zinc compounds		Not Listed
• Iron	7439-89-6	Not Listed
• Iron as Iron Salts		Not Listed
• Sodium chloride	7647-14-5	Not Listed
• Silica, amorphous	7631-86-9	Not Listed
• Radium 226	13982-63-3	Not Listed
• Lead 210	14255-04-0	Not Listed
• Radium 228	15262-20-1	Not Listed
• Thorium 228	14274-82-9	Not Listed

Other Information

- WARNING: This product contains a chemical known to the State of California to cause cancer, birth defects, or other reproductive harm.

Section 16 - Other Information

Last Revision Date
- 15/May/2014

Preparation Date
- 16/September/2003

Disclaimer/Statement of Liability
- This material is transported in accordance with DOT regulations and disposed at a Class II landfill.

Key to abbreviations
NDA = No Data Available

* View the full document (pdf) here: https://drive.google.com/file/d/1Y2_61vVLYkDwFRC0zYLNPC6kaZLtJrO-/view?usp=sharing

Appendix Chapter 10

Maximum Possible Magnitude Forecasting

We implement three different models (McGarr, 2014; van der Elst et al., 2016; Galis et al., 2017) to forecast the maximum potential magnitude as a function of time. Of these three, the model by van der Elst et al. (2016) most accurately forecasts the magnitude of future events. The model of van der Elst et al. (2016) considers only the statistics of past events (i.e., omits any explicit dependence on production/injection volumes). The model by McGarr (2014) performs second best; however, it slightly underestimates the magnitude of future events.

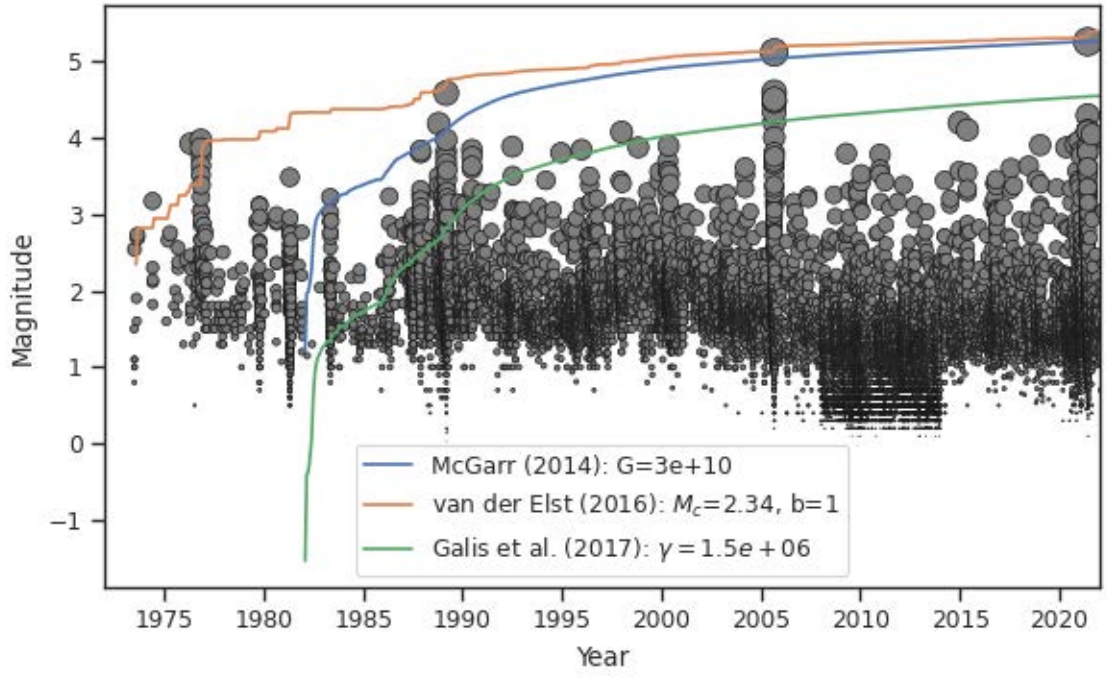

Figure A10.1. Observed event magnitudes (grey circles) versus time and three different predictions for the maximum potential magnitude versus time (orange, blue, and green curves).

Despite its strong performance, the van der Elst et al. (2016) model depends on ongoing observations of seismicity, which renders it ineffective for forecasting seismicity associated with various resource development scenarios. On the other hand, because the McGarr (2014) model explicitly depends on injection volumes, it is more useful in this regard. One major limitation of the McGarr (2014) model, however, is that it does not account for the effect of production.

Data Visualization

To visualize seismicity and investigate spatiotemporal patterns related to energy production activity, we developed 3-D visualization software using the open-source PyVista API (Figures A10.2-A10.5). This software enables visualization of earthquake space-time-magnitude parameters in relation to surface topography and production/injection well trajectories. Further development can enable animation to

explore and illustrate spatiotemporal patterns with greater clarity. The interactive display currently helps illuminate clustering behavior of seismicity that is otherwise difficult to discern in 2-D projections.

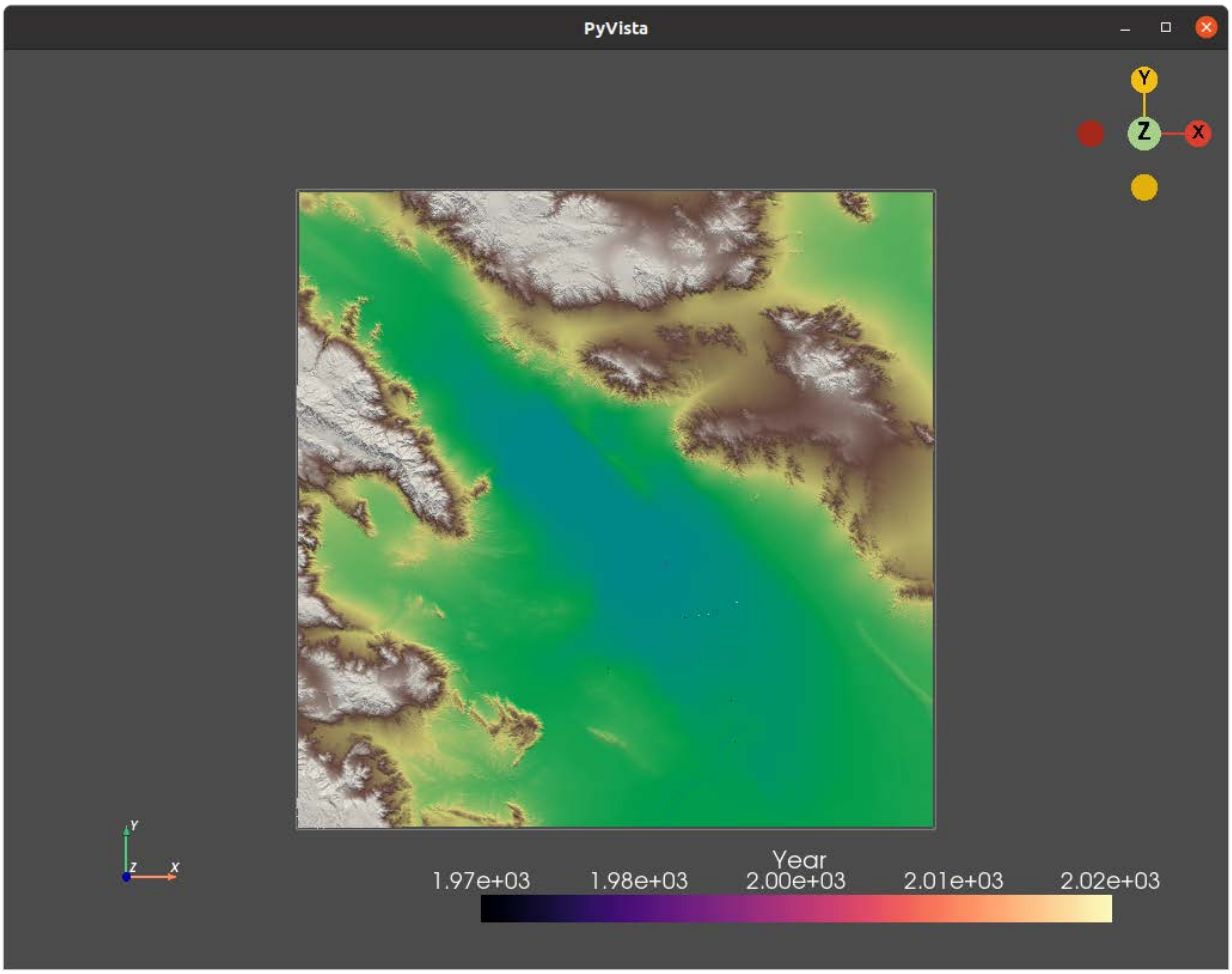

Figure A10.2. Map view of 3-D visualization showing topography.

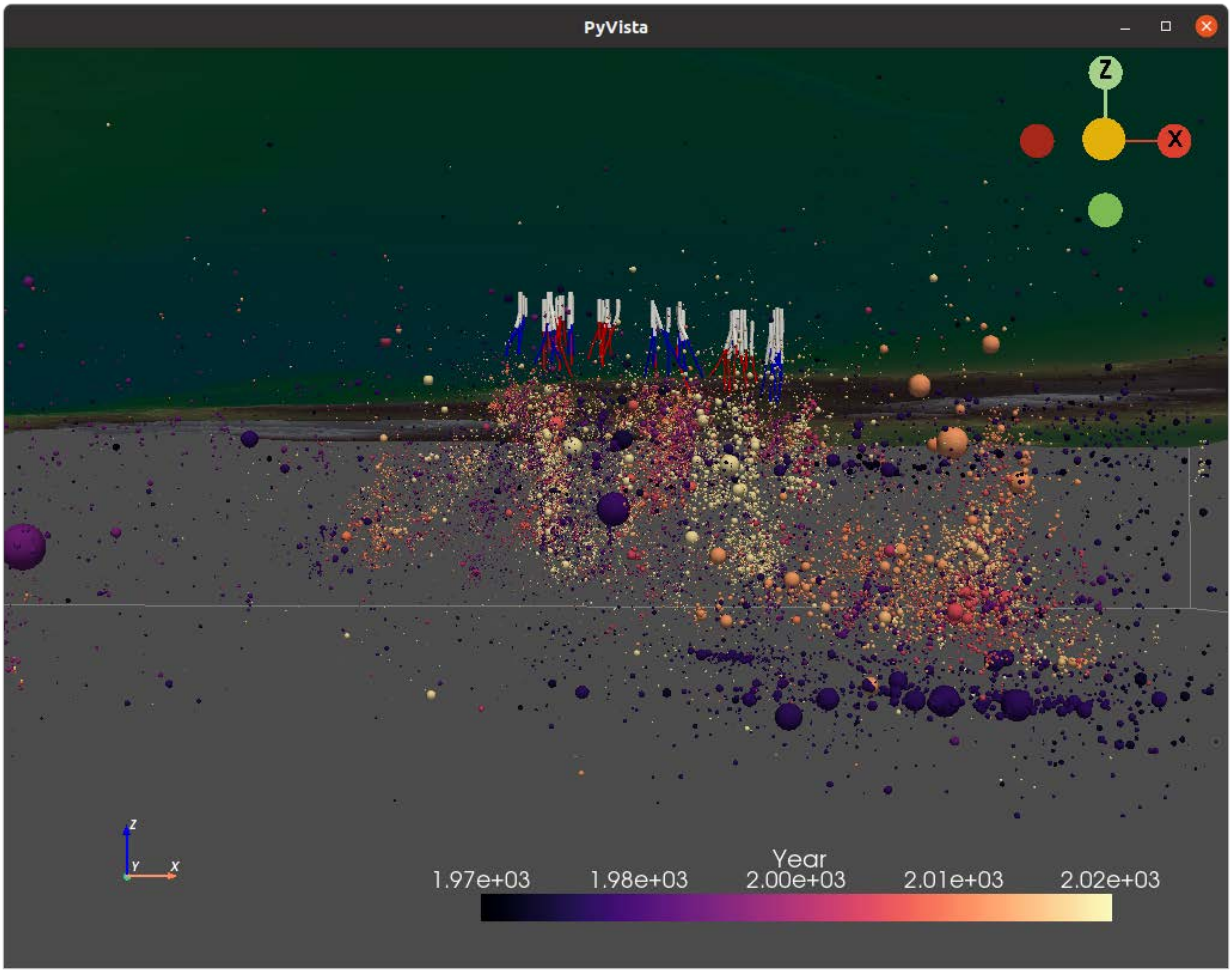

Figure A10.3. North-facing view of seismicity (colored spheres) and topography in 3-D. Earthquake hypocenters are color-coded by the time of occurrence according to the color bar at the bottom of the figure. The size of each sphere is proportional to the magnitude of the earthquake it represents.

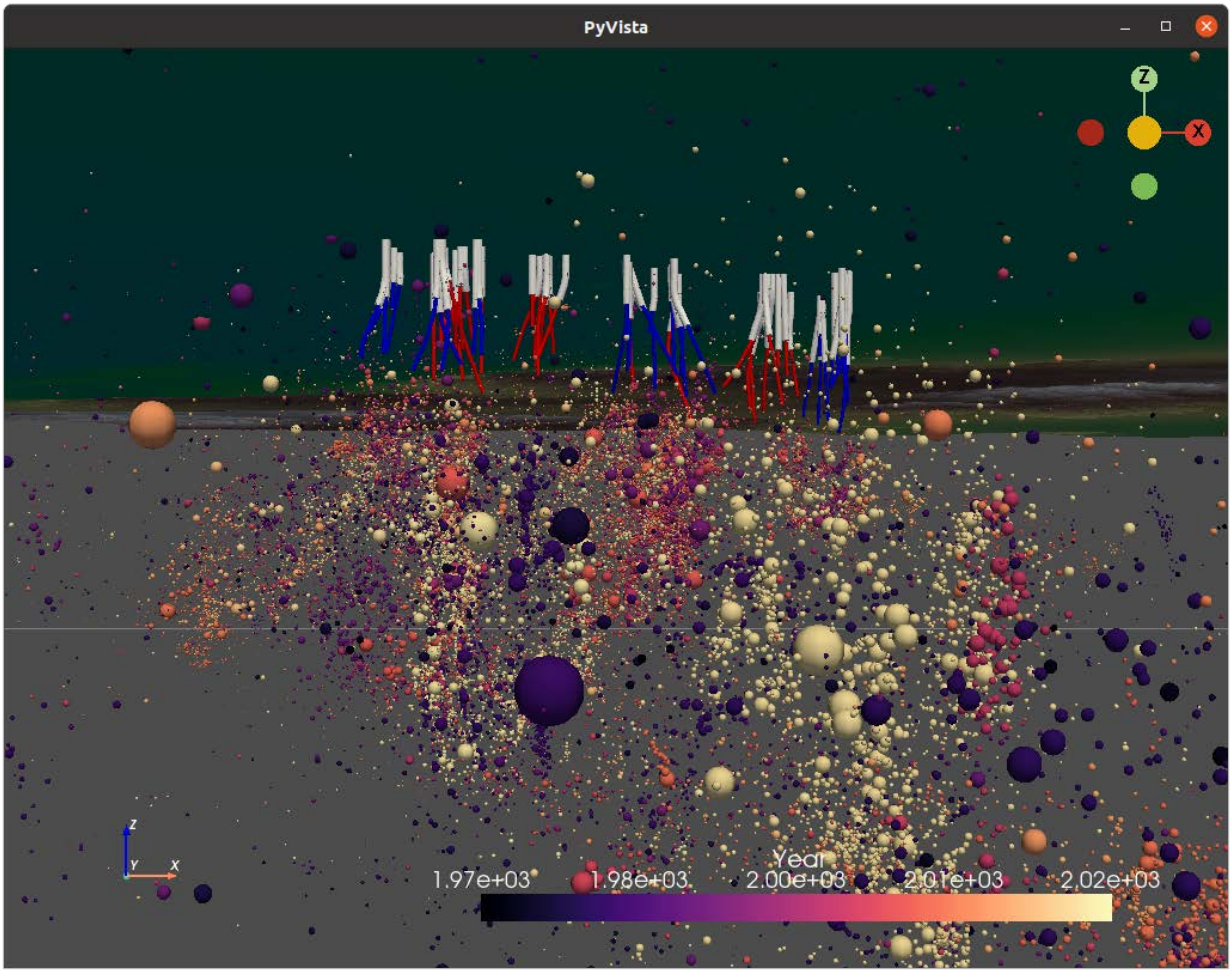

Figure A10.4. Oblique view of seismicity. Open sections of production and injection well trajectories are shown in red and blue, respectively. White sections represent cased well sections.

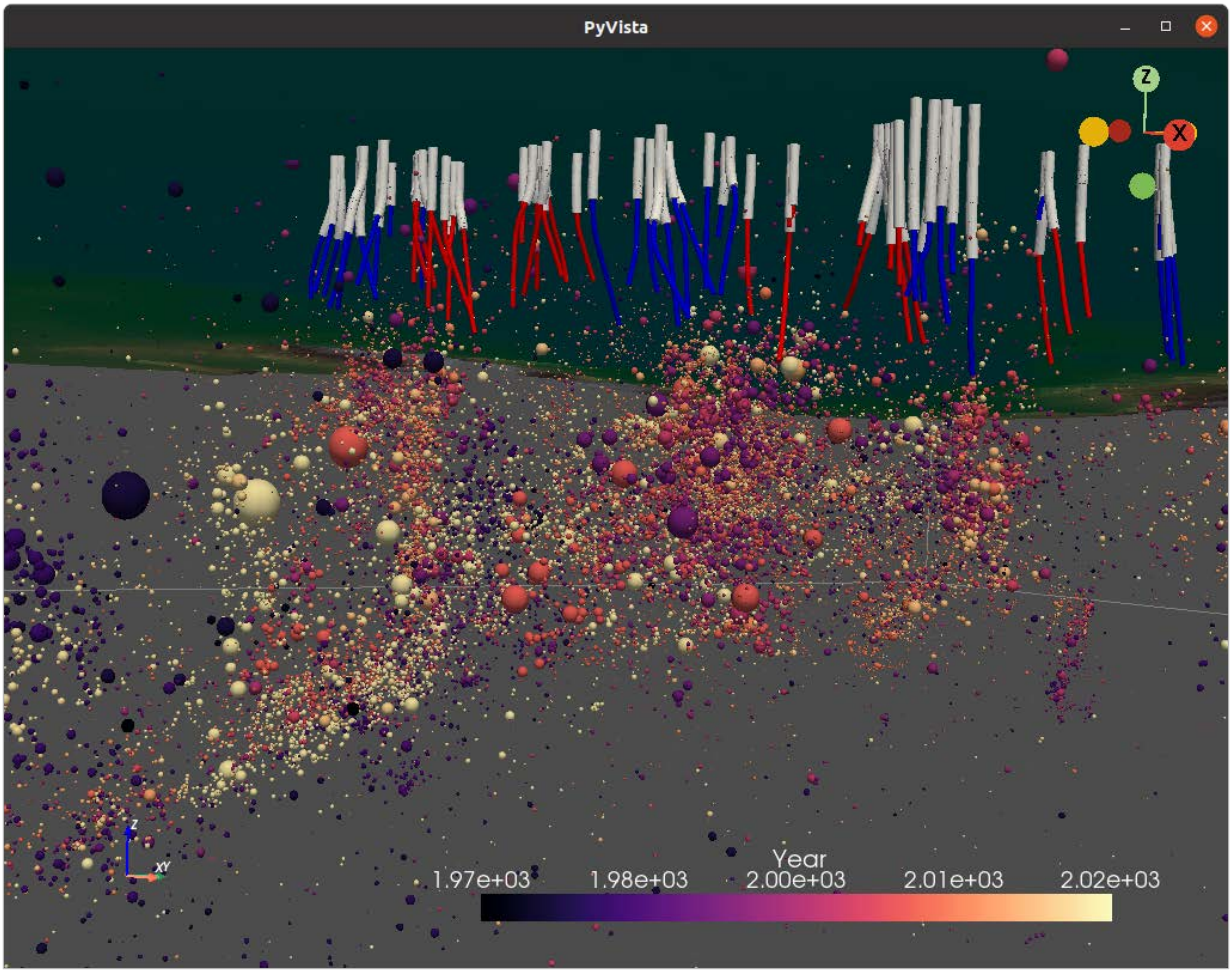

Figure A10.5. Oblique view of seismicity and well trajectories as in Figure A10.4.

Methods

Estimating Magnitude of Catalog Completeness M_C

The frequency-magnitude distribution of an incomplete catalog can be modeled using an exponentially modified Gaussian probability density function (note: see Chapter 10 for Eq. 1 through Eq. 3) (White et al. 2019):

$$f(m;\ \mu,\sigma,\beta) = \beta \exp\left(\frac{\beta}{2}(2\mu + \beta\sigma^2)\right) \exp(-\beta m)\ \Phi\left(\frac{m-(\mu+\beta\sigma^2)}{\sigma}\right) \qquad \text{Eq. 4}$$

in which $\beta \exp(-\beta m)$ is an exponential distribution with decay rate β, which represents classical Gutenberg-Richter statistics for a complete catalog; $\Phi\left(\frac{m-(\mu+\beta\sigma^2)}{\sigma}\right)$ is a Gaussian CDF with mean $(\mu + \beta\sigma^2)$ and standard deviation σ, which represents a "thinning operator"; and $\exp\left(\frac{\beta}{2}(2\mu + \beta\sigma^2)\right)$ is a normalization constant. The thinning operator represents the proportion of earthquakes of a given magnitude that are registered in an incomplete catalog. We define the level of catalog completeness $M_C =$

$M_{C(95)}$ such that $\Phi\left(M_{C(95)}\right) = 0.95$. This implies that 95% of events that occur with $M = M_{C(95)}$ are registered in the catalog. We compute $M_{C(95)}$ using a five-year rolling window and take the maximum resulting value of the level of completeness for our analysis M_C.

Estimating Background Seismicity Rate with the ETAS Model

Let

$$\mathcal{H}_{1,2} \stackrel{\text{def}}{=} \{(t_i, M_i) | \tau_1 \leq t_i < \tau_2\} \qquad \text{Eq. 5}$$

be the history of earthquake occurrences between times τ_1 and τ_2 in which (t_i, M_i) represents the time and magnitude, respectively, of the i^{th} earthquake. Then the ETAS model for the occurrence of earthquakes with magnitude greater than some threshold M_C is given by an inhomogeneous point process with "conditional intensity factor" $\lambda_\theta\left(t | \mathcal{H}_{1,2}\right)$ at time t given history $\mathcal{H}_{1,2}$:

$$\lambda_\theta\left(t | \mathcal{H}_{1,2}\right) \stackrel{\text{def}}{=} \mu + \sum_{i | t_i < t} \frac{K}{(t - t_i + c)^p} 10^{\alpha(M_i - M_C)} \qquad \text{Eq. 6}$$

for $\tau_1 \leq t < \tau_2$, in which $\theta \stackrel{\text{def}}{=} \langle \mu, K, c, \alpha, p \rangle$ is the vector of free parameters μ, K, c, α, and p. μ, our parameter of interest, represents the background seismicity rate, K represents the productivity of aftershock sequences, c and p represent the temporal decay of aftershock sequences, and α represents Gutenberg-Richter statistics.

In this work, we follow Brodsky and Lajoie (2013) by fixing $\alpha = 1$, $c = 0.006\ d$, and $M_C = 2.34$ (Brodsky and Lajoie (2013) used $M_C = 1.75$), and inverting for the three remaining parameters μ, K, and p using the maximum-likelihood method in two-year rolling windows.

Estimating Background Seismicity Rate with Declustered Catalogs

We compute the normalized nearest-neighbor proximity α_i for each event (indexed by i) in the catalog following Zaliapin and Ben-Zion (2020). We then decluster the catalog by stochastically discarding events with probability $P_i = \min(\alpha_i A_0, 1)$ in which we set the inverse threshold $A_0 = 10$. We then estimate the background seismicity rate by computing the average number of events per unit time in a two-year sliding window. Because the declustering procedure is stochastic, we report the background seismicity rate averaged over 128 declustered catalogs in Figure 10.8.

Decomposing Signals into Seasonal, Trend, and Residual Components

The production and injection histories show strong seasonal dependence as energy demands cycle annually. Because our background seismicity rates are computed in a two-year rolling window, we want to remove high-frequency fluctuations that are significantly shorter than this length of time. We decompose production, injection, and background seismicity rate histories into secular trend, seasonal, and residual components using Seasonal-Trend LOESS (Cleveland et al., 1990) (Figure 10.6).

Probabilistic Earthquake Forecasting

Consider only background events with magnitude greater than some threshold M_C. Assume inter-event times are exponentially distributed (i.e., background seismicity is a homogeneous Poisson point process) with rate parameter λ. Let N be a random variable representing the number of such background events to occur in a fixed time interval. Then the probability mass function for N is

$$P(N = n) = \frac{\lambda^n e^{-\lambda}}{n!} \quad \text{Eq. 7}$$

Next, assume background event magnitudes are exponentially distributed, independent random variables above the cutoff magnitude, and let M_i represent the magnitude of the i^{th} event. The probability density function for M_i is

$$P(M_i = m) = \beta \exp\big(-\beta(m - M_C)\big) \quad \text{Eq. 8}$$

Consider each earthquake occurrence as a Bernoulli trial for which success is defined as occurring when the event magnitude M_i is greater than or equal to some threshold magnitude M^* (i.e., $M_i \geq M^*$). Then the probability of success p is

$$p = P(M_i \geq M^*) \quad \text{Eq. 9}$$

$$= \int_{M^*}^{\infty} \beta e^{-\beta(m - M_C)} dm \quad \text{Eq. 10}$$

$$= e^{-\beta(M^* - M_C)} \ (10) \quad \text{Eq. 11}$$

The probability $P(N_{M \geq M^*} = k)$ of exactly k events with $M \geq M^*$ occurring in a fixed time interval is

$$P(N_{M \geq M^*} = k) = \sum_{n=k}^{\infty} [P(N = n) \cdot P(N_{M \geq M^*} = k | N = n)] \quad \text{Eq. 12}$$

$$= \sum_{n=k}^{\infty} \Big[P(N = n) \binom{n}{k} p^k (1 - p)^{n-k} \Big] \quad \text{Eq. 13}$$

$$= \sum_{n=k}^{\infty} \left[\frac{\lambda^n e^{-\lambda}}{n!} \frac{n!}{k!(n-k)!} \left(e^{-\beta(M^* - M_C)}\right)^k \left(1 - e^{-\beta(M^* - M_C)}\right)^{n-k} \right] \quad \text{Eq. 14}$$

Thus,

$$P(N_{M \geq M^*} \geq j) = \sum_{k=j}^{\infty} \sum_{n=k}^{\infty} \left[\frac{\lambda^n e^{-\lambda}}{n!} \frac{n!}{k!(n-k)!} \left(e^{-\beta(M^* - M_C)}\right)^k \left(1 - e^{-\beta(M^* - M_C)}\right)^{n-k} \right] Eq. 15$$

Appendix Chapter 11

Community Workshop Flyers

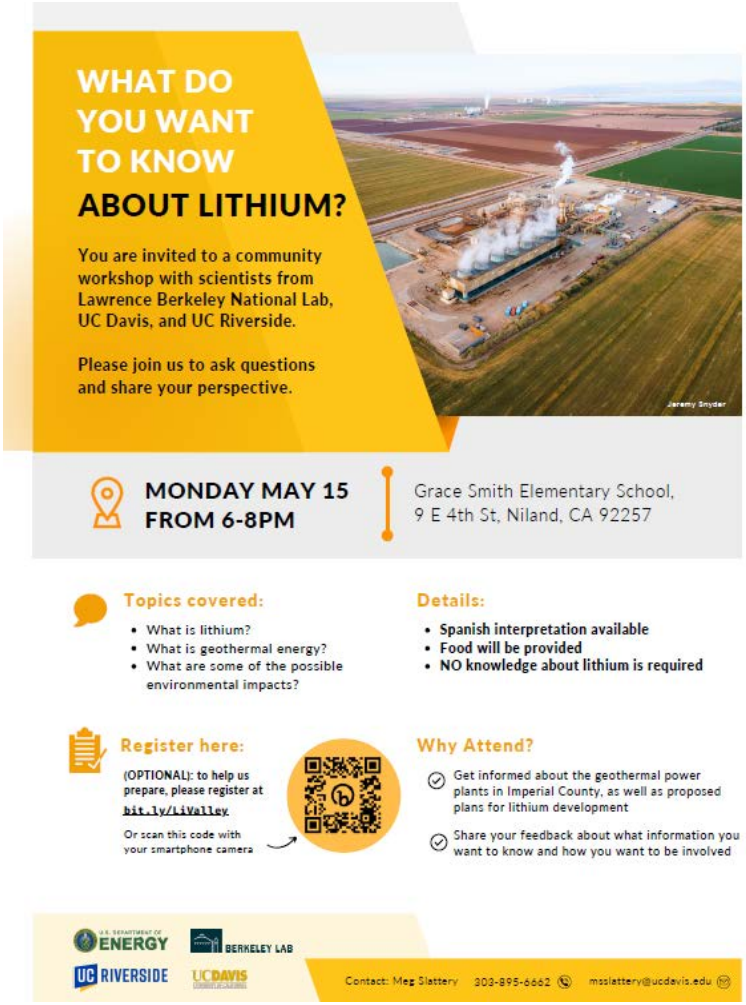

Appendix 11 (continued): Community Workshop Agenda

THE GOALS OF THIS WORKSHOP ARE TO:

- Share information about geothermal energy and lithium
- Provide a comfortable space for people to ask questions
- Get community input to improve our research and outreach efforts

MONDAY MAY 15 FROM 6-8PM

Grace Smith Elementary School, 9 E 4th St, Niland, CA 92257

AGENDA:

6:00-6:15: Arrival, pre-workshop survey (optional)
6:15-6:30: Introductions
6:30-6:50: Overview of lithium and geothermal
6:50-7:00: Breakout groups to brainstorm questions
7:00-7:30: Question and answer session
7:30-7:45: Debrief
7:45-8:00: Post-workshop survey (optional)

SURVEY:

If you are over 18 and live in Imperial or Eastern Coachella Valley, you are eligible to participate in a research survey to help us improve our communication and community engagement practices

If you would prefer to fill out the survey online, please visit:

Contact: Meg Slattery 303-895-6662 msslattery@ucdavis.edu

U.S. DEPARTMENT OF ENERGY · BERKELEY LAB · UC RIVERSIDE · UC DAVIS

LOS OBJETIVOS DE ESTE TALLER SON:

- Compartir información sobre energía geotérmica y litio
- Proporcionar un espacio cómodo para hacer preguntas.
- Obtener retroalimentación para mejorar nuestros esfuerzos de investigación y comunicacion.

LUNES 15 DE MAYO DESDE 6-8PM

Grace Smith Elementary School, 9 E 4th St, Niland, CA 92257

HORARIO:

6:00-6:15: Llegada, encuesta previa al taller (opcional)
6:15-6:30: Presentaciones
6:30-6:50: Visión general de litio y geotermia
6:50-7:00: Grupos de trabajo para hacer preguntas
7:00-7:30: Sesión de preguntas y respuestas
7:30-7:45: Recapitulación
7:45-8:00: Encuesta posterior al taller (opcional)

ENCUESTA:

Si tiene más de 18 años y vive en Imperial o en el este del Valle de Coachella, es elegible para participar en una encuesta de investigación para ayudarnos a mejorar nuestras prácticas de comunicación y participación comunitaria.

Si prefiere completar la encuesta en línea, visite:

Contact: Meg Slattery 303-895-6662 msslattery@ucdavis.edu

U.S. DEPARTMENT OF ENERGY · BERKELEY LAB · UC RIVERSIDE · UC DAVIS

Appendix 11 (continued): Community Workshop 1-pager

3 2 1
Li
LITHIUM
6.941

WHAT IS LITHIUM?

- A light, silvery metal found in certain types of rock ("pegmatite"), claystones, and brines.
- Lithium is light and stores electrical energy efficiently, which is why it works so well in batteries.
- To meet demand for clean energy technologies, global lithium demand is forecasted to increase by as much as 500% by 2030

WHAT IS GEOTHERMAL ENERGY?

- Geothermal power plants use heat from underground to create steam.
- The steam is used to generate electricity, similar to a conventional power plant.
- The geothermal plants in the Salton Sea region use hot, high-pressure brine from an underground reservoir that is 2,500-8,000 feet below the Earth's surface

WHAT IS BRINE?

- "Brine" is a word for a liquid with a high concentration of dissolved salts.
- The brines in the Salton Sea Geothermal Field contain lithium along with other minerals, including calcium, potassium, iron, zinc, and manganese.

WHAT'S HAPPENING NOW AT THE SALTON SEA?

- Geothermal power plants have been operating since 1982. There are currently 11 active power plants.
- Three companies are developing direct lithium extraction (DLE) technology to recover lithium before the brine is reinjected underground.
- DLE is in the pilot and demonstration phase

LEARN MORE ABOUT:

Lithium and geothermal energy here:
https://www.energy.gov/eere/geothermal/lithium

Berkeley Lab here:
https://www.lbl.gov/about/

UC Riverside Salton Sea Task Force:
https://www.saltonseataskforce.ucr.edu/

UC Davis Material Circularity group here:
https://ie.ucdavis.edu/research/material-circularity/

Contact: Meg Slattery 303-895-6662 msslattery@ucdavis.edu

U.S. DEPARTMENT OF ENERGY · BERKELEY LAB · UC RIVERSIDE · UCDAVIS UNIVERSITY OF CALIFORNIA

3 2
Li
LITIO
6.941

¿QUÉ ES EL LITIO?

- Es un metal ligero y plateado que se encuentra en ciertos tipos de rocas ("pegmatita"), arcillas y salmueras.
- El litio es liviano y almacena energía eléctrica de manera eficiente, por lo que funciona muy bien en las baterías.
- Para satisfacer la demanda de tecnologías de energía limpia, se prevé que la demanda mundial de litio aumente hasta en un 500 % para 2030

¿QUÉ ES LA ENERGÍA GEOTÉRMICA?

- Las plantas de energía geotérmica usan calor desde el subsuelo para crear vapor.
- El vapor se utiliza para generar electricidad, similar a una planta de energía convencional.
- Las plantas geotérmicas en la región de Salton Sea usan salmuera caliente a alta presión de un depósito subterráneo que es2,500-8,000 pies debajo de la superficie de la Tierra

¿QUÉ ES SALMUERA?

- "Salmuera" es una palabra para un líquido con una alta concentración de sales disueltas.
- Las salmueras en el campo geotérmico de Salton Sea contienen litio junto con otros minerales, incluidos calcio, potasio, hierro, zinc y manganeso.

¿QUÉ ESTÁ PASANDO AHORA EN SALTON SEA?

- Las plantas de energía geotérmica han estado operando desde 1982. Actualmente hay 11 plantas de energía activas.
- Tres empresas están desarrollando tecnología de extracción directa de litio (DLE) para recuperar litio antes de que la salmuera se reinyecte bajo tierra.
- DLE se encuentra en fase piloto y de demostración

CONOCE MÁS ACERCA DE:

Litio y energía geotérmica:
https://www.energy.gov/eere/geothermal/lithium

Berkeley Lab:
https://www.lbl.gov/about/

UC Riverside Salton Sea Task Force:
https://www.saltonseataskforce.ucr.edu/

UC Davis Material Circularity:
https://ie.ucdavis.edu/research/material-circularity/

Contact: Meg Slattery 303-895-6662 msslattery@ucdavis.edu

U.S. DEPARTMENT OF ENERGY · BERKELEY LAB · UC RIVERSIDE · UCDAVIS UNIVERSITY OF CALIFORNIA

Appendix 11 (continued): Pre- and Post-Workshop Surveys: Niland Community Workshop Survey

MAY 2023

Welcome! We invite you to participate in a survey about lithium extraction from geothermal brines in the Salton Sea region. This survey was created by researchers from the Material Circularity Research Group at the University of California, Davis and the Lithium Resource Research and Innovation Center (LiRRIC) at Lawrence Berkeley National Laboratory.

For more information **about LiRRIC, please visit**:

You are invited to participate in a research study. If you agree to participate in this research, you will be asked to complete a pre- and post-meeting survey. Your responses will be used to help our team improve the way we communicate information and identify high-priority topics for future research. The questions are about your perception of lithium and geothermal, and any feedback you have about this workshop. The surveys are expected to take ten minutes each.

Taking part in research is completely voluntary. You are free to decline to take part and you can stop at any time. When you participate you will be asked to provide contact information in case you would like to receive future updates from the research team. We will also ask if you are willing to be contacted for a follow-up interview to give us more in-depth feedback. Providing your contact information is voluntary. Your survey responses will not be shared or linked to your name.

You will receive a $20 gift card upon completion of the survey.

We appreciate your time and thank you for helping us improve our community engagement practices.

If you have any questions or concerns, please contact **Meg Slattery**:

Email: msslattery@lbl.gov Phone: 303-895-6662

Any questions you have about your rights as a research subject can be directed to:

The Berkeley Lab Human Subjects Committee at 510-486-6005

Pre-workshop Survey
Survey number: _____

1. **Marking the consent button below indicates that you are 18 or older and consent to participate in the survey.**
   - Yes, I consent to participate in the survey
   - No, I do not wish to participate in the survey

2. **What is your name? (Optional)**

   ---

3. **Where do you live?**
   - Imperial County
   - Torres Martinez Desert Cahuilla Indian Reservation
   - Riverside County
   - In California, but outside Imperial or Riverside
   - Outside California

4. **Which of the following best describes you or your organization? *Check all that apply*.**
   - Community member
   - Community-based organization
   - Indigenous community member
   - Indigenous tribal council member
   - Geothermal, lithium, or EV industry
   - Labor union
   - Government
   - Utility
   - Environmental organization
   - Research Institution
   - Not listed: _____

5. **Please specify your community or affiliation:**

   ---

6. What is lithium used for?

- Solar panels
- Electric vehicles
- Fertilizer
- I don't know

7. How many geothermal power plants are currently operating near the Salton Sea?

- 11
- 18
- 0
- I don't know

8. Please rate your level of understanding about <u>geothermal energy</u> on a scale of 1-5:

1	2	3	4	5
☐	☐	☐	☐	☐

1 = I have never heard of it
2 = I have heard of it but don't understand it
3 = I understand it somewhat
4 = I mostly understand it
5 = I am an expert

9. Please rate your level of understanding about <u>lithium extraction</u> on a scale of 1-5:

1	2	3	4	5
☐	☐	☐	☐	☐

10. Please rate your agreement with the following statements

10a. I think lithium extraction would have a positive impact on the local community

- Strongly disagree
- Disagree
- Neither agree nor disagree
- Agree
- Strongly agree

10b. I think more geothermal energy would have a positive impact on the community

- Strongly disagree
- Disagree
- Neither agree nor disagree
- Agree
- Strongly agree

11. Are you concerned about the environmental impact of geothermal energy production?

- Not at all
- Slightly concerned
- Somewhat concerned
- Very concerned
- Extremely concerned

12. Are you concerned about the environmental impact of lithium extraction?

- Not at all
- Slightly concerned
- Somewhat concerned
- Very concerned
- Extremely concerned

13. What do you think are the most important benefits of lithium extraction? Choose up to two.

- Support climate goals
- Provide a secure source of lithium for the United States
- Provide a more environmentally friendly source of lithium
- Create new jobs in the region
- Generate revenue for the region
- None of the above
- Other: _____

Post-meeting survey
Survey #: _____

1. **What is lithium used for?**
   - Solar
   - panels
   - Electric vehicles
   - Fertilizer
   - I don't know

2. **How many geothermal power plants are currently operating near the Salton Sea?**
   - 11
   - 18
   - 0
   - I don't know

3. **Please rate your level of understanding about <u>geothermal energy</u> on a scale of 1-5:**

1	2	3	4	5
☐	☐	☐	☐	☐

1 = I have never heard of it
2 = I have heard of it but don't understand it
3 = I understand it somewhat
4 = I mostly understand it
5 = I am an expert

4. **Please rate your level of understanding about <u>lithium extraction</u> on a scale of 1-5:**

1	2	3	4	5
☐	☐	☐	☐	☐

5. **Please rate your agreement with the following statements**

5a. I think <u>lithium extraction would have a positive impact</u> on the local community
   - Strongly disagree
   - Disagree
   - Neither agree nor disagree
   - Agree
   - Strongly agree

5b. I think more <u>geothermal energy would have a positive impact</u> on the community
   - Strongly disagree
   - Disagree
   - Neither agree nor disagree
   - Agree
   - Strongly agree

6. **Are you concerned about the environmental impact of geothermal energy production?**
   - Not at all
   - Slightly concerned

- Somewhat concerned
- Very concerned
- Extremely concerned

7. Are you concerned about the environmental impact of lithium extraction?

- Not at all
- Slightly concerned
- Somewhat concerned
- Very concerned
- Extremely concerned

8. What do you think are the most important benefits of lithium extraction? Choose up to two.

- Support climate goals
- Provide a secure source of lithium for the United States
- Provide a more environmentally friendly source of lithium
- Create new jobs in the region
- Generate revenue for the region
- None of the above
- Other: _____

9. Overall, how would you rate the effectiveness of this workshop? (1= terrible, 10= excellent)

1	2	3	4	5	6	7	8	9	10
☐	☐	☐	☐	☐	☐	☐	☐	☐	☐

10. Would you attend more events like this in the future?

- Yes
- No
- Not sure

11. Was the content of this workshop interesting?

- Very uninteresting
- Mostly uninteresting
- Somewhat interesting
- Mostly interesting
- Very interesting

12. Was information presented in a way that was easy to understand?

- Very difficult to understand
- Somewhat difficult to understand
- Somewhat easy to understand
- Easy to understand
- Extremely easy to understand

13. Was the meeting scheduled at a time that was convenient for you?

- Yes
- No

If not, what would have been a better time?_____

14. What is your main takeaway from this workshop?

15. Is there anything you wish we'd talked about more?

16. Is there anything you wish we'd talked about less?

17. How did you hear about this event?

18. Do you have any additional questions or feedback for the research team?

Survey number: _____

Gift card preference:

- Walmart
- Amazon
- Visa ($15)

How would you like to receive your gift card?

- In-person (Walmart only)
- Email

- Mail:

Would you be willing to provide a follow-up interview to elaborate on any of your responses?

- Yes (please provide your email if you haven't already) _____
- No

References

Executive Summary

Office of Governor Gavin Newsom. (2023). *Governor Newsom Visits Lithium Valley to Highlight Momentum on Becoming Global Source for Battery Production* https://www.gov.ca.gov/2023/03/20/governor-newsom-visits-lithium-valley-to-highlight-momentum-on-becoming-global-source-for-battery-production/

The White House. (2022). *FACT SHEET: Biden-Harris Administration Driving U.S. Battery Manufacturing and Good-Paying Jobs*. https://www.whitehouse.gov/briefing-room/statements-releases/2022/10/19/fact-sheet-biden-harris-administration-driving-u-s-battery-manufacturing-and-good-paying-jobs/

Chapter 1

About Us. (2021, January 7). Alianza Coachella Valley; Alianza Coachella Valley. https://www.alianzacv.org/about/

Berkshire Hathaway Inc. (2005). *2004 Annual Report*. SEC.Gov. https://www.sec.gov/Archives/edgar/data/1067983/000119312505046527/dex991.htm

Besseling, E. (2018) Lithium recovery from geothermal brine – CEC Workshop and Discussion. BHE Renewables. CEC Docket#17-GDRA-01, TN#225903, Nov. 15, 2018.

BHER (Berkshire Hathaway Energy Renewables), (2023). *Application for Certification for the Elmore North Geothermal Project*. California Energy Comission. https://www.energy.ca.gov/powerplant/steam-turbine/elmore-north-geothermal-project-engp

Biello, D. (2011, September 29). Geothermal Power Plants Could Help Produce Lithium for Electric Cars. *Scientific American*. https://www.scientificamerican.com/article/geothermal-power-plants-could-help-produce-lithium-for-electric-cars/

Blake, R. L. (1974). Extracting minerals from geothermal brines: A literature study (Information Circular 8638).

CalEnviroScreen 4.0. (2021, September 20). Office of Environmental Health and Hazard Assessment (OEHHA). https://oehha.ca.gov/calenviroscreen/report/calenviroscreen-40

California Department of Public Health. (n.d.). *CHIS Data-Current Asthma Prevalence by County*. California Health and Human Services Open Data Portal. Retrieved June 28, 2023, from https://data.chhs.ca.gov/dataset/asthma-prevalence/resource/a440b99b-ccc6-473c-bea1-2baf36b05dbe

Calpine. (n.d.). *Seismic Monitoring Advisory Committee(SMAC)*. The Geysers. Retrieved June 28, 2023, from https://geysers.com/smac

CDC (California Department of Conservation), (2023). *Geothermal Resources*. California Department of Conservation. https://www.conservation.ca.gov/calgem/geothermal

CEC (California Energy Commission), (n.d.). *Lithium Valley Commission Meetings, Notices, and Documents*. Retrieved September 17, 2021, from https://www.energy.ca.gov/data-reports/california-power-generation-and-power-sources/geothermal-energy/lithium-valley/lithium

CEC (California Energy Commission), (2023a). *Black Rock Geothermal Project (BRGP)*. https://www.energy.ca.gov/powerplant/steam-turbine/black-rock-geothermal-project-brgp

CEC (California Energy Commission), (2023b). *Elmore North Geothermal Project (ENGP)*. Retrieved June from https://www.energy.ca.gov/powerplant/steam-turbine/elmore-north-geothermal-project-engp

CEC (California Energy Commission), (2023c). *Morton Bay Geothermal Project (MBGP)*. https://www.energy.ca.gov/powerplant/steam-turbine/morton-bay-geothermal-project-mbgp

Cheney, A. M., Ortiz, G., Trinidad, A., Rodriguez, S., Moran, A., Gonzalez, A., Chavez, J., & Pozar, M. (2023). Latinx and Indigenous Mexican Caregivers' Perspectives of the Salton Sea Environment on Children's Asthma, Respiratory Health, and Co-Presenting Health Conditions. *International Journal of Environmental Research and Public Health*, *20*(11). https://doi.org/10.3390/ijerph20116023

Clutter, T. J. (2000, June). Mining Economic Benefits from Geothermal Brine: CalEnergy Mineral Recovery Project Creates Jobs and Increases Revenues from Geothermal Power Operations in California's Imperial Valley. *GHC Bulletin*. https://oregontechsfcdn.azureedge.net/oregontech/docs/default-source/geoheat-center-documents/quarterly-bulletin/vol-21/art14d90ee4362a663989f6fff0000ea57bb.pdf?sfvrsn=d0368d60_4

Collins, S. E., Clifasefi, S. L., Stanton, J., The Leap Advisory Board, Straits, K. J. E., Gil-Kashiwabara, E., Rodriguez Espinosa, P., Nicasio, A. V., Andrasik, M. P., Hawes, S. M., Miller, K. A., Nelson, L. A., Orfaly, V. E., Duran, B. M., & Wallerstein, N. (2018). Community-based participatory research (CBPR): Towards equitable involvement of community in psychology research. *The American Psychologist*, *73*(7), 884–898.

Comité Cívico del Valle. (n.d.). *Lithium Valley Charger Equity Initiative*. Ccvhealth.Org. Retrieved June 29, 2023, from https://ccvhealth.org/programs-single.php?program=18

Council on Environmental Quality. (n.d.). *Climate and Economic Justice Screening Tool*. Geoplatform.Gov. Retrieved June 23, 2023, from https://screeningtool.geoplatform.gov/en/methodology

Elmallah, S., Reames, T. G., & Spurlock, C. A. (2022). Frontlining energy justice: Visioning principles for energy transitions from community-based organizations in the United States. *Energy Research & Social Science*, *94*, 102855.

Gagne, D., Haase, S., Oakleaf, B., Hurlbut, D., Akar, S., Wall, A., Turchi, C., Pienkos, P., Melius, J., & Melaina, M. (2015). The Potential for Renewable Energy Development to Benefit Restoration of the Salton Sea. Analysis of Technical and Market Potential. NREL/TP-7A40-64969. National Renewable Energy Lab (NREL), Golden, CO.

Garcia, Eduardo. 2020. *State Energy Resources Conservation and Development Commission: Blue Ribbon Commission on Lithium Extraction in California: Report.* https://leginfo.legislature.ca.gov/faces/billNavClient.xhtml?bill_id=201920200AB1657.

Gates, T., & Crawford, K. (2010). Ethnographic Assessment of the Importance of Obsidian Butte to the Native American Community, Imperial County, California (NSR Project #29411). California Energy Commission.

Georgetown Climate Center. (n.d.). *Equitable Adaptation Legal & Policy Toolkit*. Georgetown Climate Center. Retrieved June 27, 2023, from https://www.georgetownclimate.org/adaptation/toolkits/equitable-adaptation-toolkit/introduction.html

Grant, C. (2019, July 22). New committee provides voice for north end communities. *The Desert Review*. https://www.thedesertreview.com/news/new-committee-provides-voice-for-north-end-communities/article_9bea88da-ac88-11e9-a987-17d07351b550.html

Green Car Congress. (2013, October 11). *Simbol produces first lithium carbonate from geothermal brine*. Green Car Congress. https://www.greencarcongress.com/2013/10/20131011-simbol.html

Hacker, K. (2013). *Community-Based Participatory Research*. SAGE Publications.

Harvard Catalyst. (n.d.). *Translation Guidelines for Equity in Research*. Harvard Catalyst Community Engagement Program. Retrieved June 28, 2023, from https://catalyst.harvard.edu/community-engagement/translation-guidelines-for-equity-in-research/

Heffron, R. J. (2020). The role of justice in developing critical minerals. *Extractive Industries and Society*, *7*(3), 855–863.

Home. (n.d.). Lithium Valley Community Coalition. Retrieved June 19, 2023, from https://www.lithiumvalleycommunitycoalition.org/

House, W. (2021). Building resilient supply chains, revitalizing American manufacturing, and fostering broad-based growth. 100-Day Reviews under Executive Order 14017. 250 p. *A Report by The White House*.

Illingworth, S. (2017). Delivering effective science communication: advice from a professional science communicator. *Seminars in Cell & Developmental Biology*, *70*, 10–16.

Inflation Reduction Act of 2022, 5376, House of Representatives, 117th Congress (2022). http://www.congress.gov/

IVEJC (IV Equity and Justice Coalition). n.d. "Home." IV Equity and Justice Coalition. Accessed June 21, 2023. http://ivequityjustice.org/.

Johnston, J. E., Razafy, M., Lugo, H., Olmedo, L., & Farzan, S. F. (2019). The disappearing Salton Sea: A critical reflection on the emerging environmental threat of disappearing saline lakes and potential impacts on children's health. *The Science of the Total Environment*, *663*, 804–817.

Jones, A., Orr, D., & Cooper, D. (2019). *Status of Birds at the Salton Sea*. National Audobon Society. https://ca.audubon.org/sites/default/files/salton_sea_bird_status_042419_final.pdf

Key, K. D., Furr-Holden, D., Lewis, E. Y., Cunningham, R., Zimmerman, M. A., Johnson-Lawrence, V., & Selig, S. (2019). The Continuum of Community Engagement in Research: A Roadmap for Understanding and Assessing Progress. *Progress in Community Health Partnerships: Research, Education, and Action*, *13*(4), 427–434.

Langholz, J., & DePaolis, F. (2021). *Economic Contribution of Imperial County Ag*. Imperial County Office of the Agricultural Commissioner. https://agcom.imperialcounty.org/wp-content/uploads/2021/08/2021-Economic-Contribution-of-Imperial-County-Ag.pdf

Larkin, A. (2023, April 20). *2023 Aspen Prize for Community College Excellence Awarded to Amarillo College & Imperial Valley College*. The Aspen Institute. https://www.aspeninstitute.org/news/2023-aspen-prize-amarillo-college-imperial-valley-college/

Leadership Counsel. 2016. "Home." Leadership Counsel for Justice and Accountability. February 20, 2016. https://leadershipcounsel.org/.

Lithium Valley. (2022, February 2). Lithium Valley; Imperial County. https://lithiumvalley.imperialcounty.org/

Los Amigos de la Comunidad. n.d. "About Us." Los Amigos de La Comunidad, Inc. Accessed June 21, 2023. https://losamigosdelacomunidad.com/.

Madrigal, D., Claustro, M., Wong, M., Bejarano, E., Olmedo, L., & English, P. (2020). Developing Youth Environmental Health Literacy and Civic Leadership through Community Air Monitoring in Imperial County, California. *International Journal of Environmental Research and Public Health*, *17*(5). https://doi.org/10.3390/ijerph17051537

Maimoni, A., 1982, Minerals recovery from Salton Sea geothermal brines: a literature review and proposed cementation process: Geothermics, v. 11, no. 4, p. 239–258.

Maizlish, N., English, D., Chan, J., Dervin, K., & English, P. (2017). *Climate Change and Health Profile Report: Imperial County*. Office of Health Equity, California Department of Public Health. https://scag.ca.gov/sites/main/files/file-attachments/chpr025imperial_county2-23-17.pdf?1604524054

Mancini, L., & Sala, S. (2018). Social impact assessment in the mining sector: Review and comparison of indicators frameworks. *Resources Policy*, *57*, 98–111.

McCauley, D., & Heffron, R. (2018). Just transition: Integrating climate, energy and environmental justice. *Energy Policy*, *119*, 1–7.

McKibben, M. A., Elders, W. A., & Raju, A. S. K. (2020). Lithium and other geothermal mineral and energy resources beneath the Salton Sea. *Crisis at the Salton Sea: Research Gaps and Opportunities, Salton Sea Task Force, The EDGE Institute, UC Riverside*, 107–122.

Mendoza, A., Pardo, E. I., & Gutierrez, A. A. (2010). Chemical characterization and preliminary source contribution of fine particulate matter in the Mexicali/Imperial Valley border area. *Journal of the Air & Waste Management Association*, *60*(3), 258–270.

Morales, J. (2022, March 28). NorthEnd Allliance 111 Aims to Serve. *Calexico Chronico*.

Morales, J. (2023, April 19). County Awards $720k for Lithium Valley Outreach Efforts. *Holtville Tribune*. https://holtvilletribune.com/2023/04/19/county-awards-720k-for-lithium-valley-outreach-efforts/

Morton, P. K. (1977). *Geology and Mineral Resources of Imperial, California*. California Division of Mines and Geology. https://nrm.dfg.ca.gov/FileHandler.ashx?DocumentID=8417

Moss, W. E., Whitescarver, D., & Yamasaki, R. N. (1982). The Salton Sea 10 MWe power plant, Unit 1. *Geothermal Resources Council, TRANSACTIONS*, *6*.

Muhammad, M., Wallerstein, N., Sussman, A. L., Avila, M., Belone, L., & Duran, B. (2015). Reflections on Researcher Identity and Power: The Impact of Positionality on Community Based Participatory Research (CBPR) Processes and Outcomes. *Critical Sociology*, *41*(7–8), 1045–1063.

Nava-Froelich, M. (2023, March 7). *Disadvantaged Communities in Imperial Valley: Neglect is Not an Option*. Desert Report. https://desertreport.org/disadvantaged-communities-in-imperial-valley/

Newell, P., & Mulvaney, D. (2013). The political economy of the "just transition." *The Geographical Journal*, *179*(2), 132–140.

Newman, S. D., Andrews, J. O., Magwood, G. S., Jenkins, C., Cox, M. J., & Williamson, D. C. (2011). Community advisory boards in community-based participatory research: a synthesis of best processes. *Preventing Chronic Disease*, *8*(3), A70.

Northey, H., & Cama, T. (2023). 'Silicon Valley of lithium': Nevada mine breaks ground. *Greenwire*. https://www.eenews.net/articles/silicon-valley-of-lithium-nevada-mine-breaks-ground/#:~:text=Nevada%20is%20currently%20home%20to,began%20operating%20in%20the%201960s.

Office of Governor Gavin Newsom. (2023). *Governor Newsom Visits Lithium Valley to Highlight Momentum on Becoming Global Source for Battery Production* https://www.gov.ca.gov/2023/03/20/governor-newsom-visits-lithium-valley-to-highlight-momentum-on-becoming-global-source-for-battery-production/

Office of Institutional Effectiveness. (2021). *Imperial Valley College 2020 Fact Book*. Imperial Valley College. https://legacy.imperial.edu/docs/research-planning/fact-books/11033-2020-ivc-fact-book/file

Paz, S., Kelley, R.-C., Castaneda, S., Colwell, R., Dolega, R., Flores, M., Hanks, J., Lopez, A., Olmedo, L., Reynolds, A., Ruiz, F., Scott, M., Soto, T., & Weisgall, J. (2022). *Report of the Blue Ribbon Commission on Lithium Extraction in California* (CEC-300-2022-009-F). California Energy Commission.

Plant Operator FAQ - Academics. (n.d.). Imperial Valley College. Retrieved June 19, 2023, from https://www.imperial.edu/academics/plant-operator-faq/

Rick Engineering Company. (2023). *Community Engagement Phase 1 Summary*. County of Imperial. https://lithiumvalley.imperialcounty.org/wp-content/uploads/2023/05/Final_LVEngagementPhase1Summary.pdf

Richter, A. (2021a, 19 Mar). *Another major geothermal acquisition by Macquarie in the U.S.* Think Geothermal. Retrieved June from https://www.thinkgeoenergy.com/another-major-geothermal-acquisition-by-macquarie-in-the-u-s/

Richter, A. (2021b, June 21). Newly released procurement order for California, creates 1,000 MW opportunity for geothermal providing required baseload power to the state. Think Geothermal. https://www.thinkgeoenergy.com/new-california-procurement-order-opportunity-for-geothermal/

Riofrancos, T. (2022). The Security–Sustainability Nexus: Lithium Onshoring in the Global North. *Global Environmental Politics*. https://doi.org/10.1016/j.oneear.2020.10.012

Roth, S. (2015, April 10). Simbol faces lawsuit over alleged financial wrongdoing. *The Desert Sun*. https://www.desertsun.com/story/news/environment/2015/04/10/simbol-materials-faces-lawsuit/25594883/

Salton Sea Authority. (n.d.). *F.A.Q.* The Salton Sea Authority. Retrieved June 28, 2023, from https://saltonsea.com/about/faq/

Schulz, A. J., Israel, B. A., & Lantz, P. (2003). Instrument for evaluating dimensions of group dynamics within community-based participatory research partnerships. *Evaluation and Program Planning*, *26*(3), 249–262.

Senate Budget and Fiscal Review Committee. 2022. *SB-125 Public Resources: Geothermal Resources: Lithium.* https://leginfo.legislature.ca.gov/faces/billNavClient.xhtml?bill_id=202120220SB125.

Shackley, M. S. (2019). Natural and Cultural History of the Obsidian Butte Source, Imperial County, California. *California Archaeology*, *11*(1), 21–43.

Simbol Materials. (2011, September 28). *Simbol Materials Advances U.S. EV Battery Material Production, Introduces World's Highest Purity Lithium*. PR Newswire. https://www.prnewswire.com/news-releases/simbol-materials-advances-us-ev-battery-material-production-introduces-worlds-highest-purity-lithium-130682848.html

Sizemore, T. (2023). Personal communication May 16th. In.

Skinner, B.J., White, D.E., Rose, H.J., and Mays, R.E., 1967, Sulfides associated with the Salton Sea geothermal brine: Economic Geology, v. 62, no. 3, p. 316–330.

Slattery, M., Kendall, A., Helal, N., & Whittaker, M. L. (2023). What do frontline communities want to know about lithium extraction? Identifying research areas to support environmental justice in Lithium Valley, California. *Energy Research & Social Science*, *99*, 103043.

Stringfellow, W. T., & Dobson, P. F. (2021). Technology for the Recovery of Lithium from Geothermal Brines. *Energies*, *14*, 6805. https://doi.org/https://doi.org/10.3390/en14206805

The White House. (2022). *FACT SHEET: Biden-Harris Administration Driving U.S. Battery Manufacturing and Good-Paying Jobs*. https://www.whitehouse.gov/briefing-room/statements-releases/2022/10/19/fact-sheet-biden-harris-administration-driving-u-s-battery-manufacturing-and-good-paying-jobs/

Thorman, T., Hsieh, V., & Bohn, S. (2019, January 14). *2020 Census: Counting Imperial County*. Public Policy Institute of California. https://www.ppic.org/blog/2020-census-counting-imperial-county/

Thrash, M. E., & Hanlon, J. W. (2019). Southern California water politics at the Salton Sea: When "increased efficiency" is not enough. *Case Studies in the Environment*, *3*(1), 1–6.

UNDP Climate Promise (United Nations Development Programme), (2022, November 3). *What is just transition? And why is it important?* UNDP Climate Promise. https://climatepromise.undp.org/news-and-stories/what-just-transition-and-why-it-important

U.S. DOE (Department of Energy). (2022). *Creating a Community and Stakeholder Engagement Plan*. U.S. Department of Energy. https://www.energy.gov/sites/default/files/2022-08/Creating%20a%20Community%20and%20Stakeholder%20Engagement%20Plan_8.2.22.pdf

U.S. DOE (Department of Energy), (2023). *Electricity Generation*. Geothermal Technologies Office. https://www.energy.gov/eere/geothermal/electricity-generation

U.S. DOE (Department of Energy), (2019). *GeoVision: Harnessing the Heat Beneath Our Feet (DOE/EE–1306)* (DOE/EE–1306 • MAY 2019). G. T. Office.

U.S. Census Bureau. (n.d.). *QuickFacts: Imperial County, California* [Data set]. Retrieved October 26, 2021, from https://www.census.gov/quickfacts/imperialcountycalifornia

Walker, B. W. (1961). Fish Bulletin No. 113. The Ecology of the Salton Sea, California, in Relation to the Sportfishery. https://escholarship.org/uc/item/1r11f7hq

Williams, A.E., and McKibben, M.A. (1989) A brine interface in the Salton Sea geothermal system, California: Fluid geochemical and isotopic characteristics. Geochimica et Cosmochimica Acta 53, 1905–1920

World Resources Institute. (n.d.). *About Just Transitions*. World Resources Institute. Retrieved August 8, 2023, from https://www.wri.org/just-transitions/about

Zukin, J.G., Hammond, D.E., Ku, T.-L., and Elders, W.A. (1987) Uranium-thorium radionuclides in brines and reservoir rocks from two deep geothermal boreholes in the Salton Sea geothermal field, southeastern California. Geochimica et Cosmochimica Acta 51, 271

Chapter 2

Antunez, E.U., Bodvarsson, G.S., and Walters, M.A. (1994) Numerical simulation study of the Northwest Geysers geothermal field, a case study of the Coldwater Creek steamfield. Geothermics, v. 23(2), 127-141.

Besseling, E. (2018) Lithium recovery from geothermal brine – CEC Workshop and Discussion. BHE Renewables. CEC Docket#17-GDRA-01, TN#225903, Nov. 15, 2018.

Featherstone, J.L., and Powell, D.R. (1981) Stabilization of highly saline geothermal brines. Journal of Petroleum Technology, April 1981, 727–734.

Helgeson, H.C. (1968) Geologic and thermodynamic characteristics of the Salton Sea geothermal system. American Journal of Science 266, 129–166.

Hoffman, M.R. (1975) Brine Chemistry – Scaling and Corrosion. Geothermal research study in the Salton Sea region of California. Environmental Quality Laboratory, California Institute of Technology, EQL Memorandum No. 14.

Hulen, J., Kaspereit, D., Norton, D.L., Osborn, W., and Pulka, F.S. (2002) Refined conceptual modeling and a new resource estimate for the Salton Sea geothermal field, Imperial Valley, California. Geothermal Resources Council Transactions 26, 29–36.

Hulen, J.B., Nielson, D.L., and Martin, W. (1992) Early calcite dissolution as a major control on porosity development in The Geysers steam field, California: Additional evidence from core from Unocal well NEGU-17. GRC Transactions, v. 16, 167-174.

Hulen, J.B., Walters, M.A., and Nielson, D.L. (1991) Comparison of reservoir and caprock core from the Northwest Geysers steam field - Implications for the development of reservoir porosity. GRC Transactions, v. 15, 11-18.

Humphreys, J., Brounce, M., McKibben, M., Dobson, P.F., Planavsky, N.J., and Kalderon-Asael, B. (2023) Distribution and isotopic composition of Li in the Salton Sea geothermal field. Geothermal Rising Conference (in prep.).

Kaspereit, D., Mann, M., Sanyal, S., Rickard, B., Osborn, W., and Hulen, J. (2016) Updated conceptual model and reserve estimate for the Salton Sea geothermal field, Imperial Valley, California. Geothermal Resources Council Transactions 40, 57–66.

Klein, C.W., Lovekin, J.W., and Sanyal, S.K. (2004) New geothermal site identification and Qualification. Consultant Report prepared for the California Energy Commission by GeothermEx, P500-04-051, April, 2004.

Maimoni, A. (1982) Minerals recovery from Salton Sea geothermal brines: A literature review and proposed cementation process. Geothermics 11, 239–258.

McDowell, S.D. (1987) Geothermal alteration of sediments in the Salton Sea Scientific Drill Hole: Petrophysical properties and mass changes during alteration. Final research report for U.S. DOE Grant DE-FG02-85ER13409.

McKibben, M.A., and Hardie, L.A. (1997) Ore-forming brines in active continental rifts. In: Geochemistry of Hydrothermal Ore Deposits, H.L. Barnes, ed., Third Ed., John Wiley & Sons, 877–935.

McKibben, M.A., Elders, W.A., and Raju, A.S.K. (2021) Lithium and other geothermal mineral and energy resources beneath the Salton Sea, in Crisis at the Salton Sea: The Vital Role of Science (M. L. Fogel, Ed.), Salton Sea Task Force, The EDGE Institute, U.C. Riverside, 15 pp.

Michels, D.E. (1986) SSSDP fluid compositions at first flow test of State 2-14. Geothermal Resources Council Transactions 10, 461–465.

Muffler, L.J.P., and White, D.E. (1969) Active metamorphism of Upper Cenozoic sediments in the Salton Sea geothermal field and the Salton Trough, southeastern California. Geological Society of America Bulletin 80, 157–182.

Newmark, R.L., Kasameyer, P.W., Younker, L.W., and Lysne, P. (1988) Shallow drilling in the Salton Sea region – The thermal anomaly. Journal of Geophysical Research 93, 13,005–13,024.

Norton, D.L., and Hulen, J.B. (2006) Magma-hydrothermal activity in the Salton Sea geothermal field, Imperial County, California. Geothermal Resources Council Transactions 30, 991–998.

Palmer, T.D. (1975) Characteristics of geothermal wells located in the Salton Sea geothermal field, Imperial County, California. Lawrence Livermore National Laboratory Report UCRL-51976, 54 p.

Skinner, B.J., White, D.E., Rose, H.J., and Mays, R.E. (1967) Sulfides associated with the Salton Sea geothermal brine. Economic Geology 62, 316–330.

Somerton, W.H. (1973) Deformation of water bearing formations at elevated temperatures – Annual Report – July 1, 9172 – June 30, 1973. (OWRR A-042-CAL)

Somerton, W.H., El-Shaarani, A.H., and Mobarak, S.M. (1974) High temperature behavior of rocks associated with geothermal type reservoirs. Paper presented at the SPE California Regional Meeting, San Francisco, California, April 1974. https://doi.org/10.2118/4897-MS

Tewhey, J.D. (1977) Geologic characteristics of a portion of the Salton Sea geothermal field. Lawrence Livermore National Laboratory Report UCRL-52267.

Weber, K., and Bakker, M. (1981) Fracture and vuggy porosity. 56th Fall SPE Meeting, San Antonio, Texas, SPE paper #10332

Werner, S.L., and Olson, L.J. (1970) Geothermal wastes and the water resources of the Salton Sea area. California Department of Water Resources Bulletin 143-7, 123 p.

Williams, A.E. (1997) Fluid density distribution in a high temperature, stratified thermohaline system: implications for saline hydrothermal circulation; Earth and Planetary Science Letters 146, 12, 1- 136.

Williams, A.E., and McKibben, M.A. (1989) A brine interface in the Salton Sea geothermal system, California: Fluid geochemical and isotopic characteristics. Geochimica et Cosmochimica Acta 53, 1905–1920.

Younker, L., and Kasameyer, P.W. (1978) A revised estimate of recoverable thermal energy in the Salton Sea geothermal resource area. Lawrence Livermore National Laboratory Report UCRL-52450.

Younker, L., Kasameyer, P.W., and Tewhey, J.D. (1982) Geological, geophysical, and thermal characteristics of the Salton Sea geothermal field, California. Journal of Volcanology and Geothermal Research 12, 221–258.

Zukin, J.G., Hammond, D.E., Ku, T.-L., and Elders, W.A. (1987) Uranium-thorium radionuclides in brines and reservoir rocks from two deep geothermal boreholes in the Salton Sea geothermal field, southeastern California. Geochimica et Cosmochimica Acta 51, 271

Chapter 3

Atwater, T., 1970, Implications of Plate Tectonics for the Cenozoic Tectonic Evolution of Western North America: Geological Society of America Bulletin, v. 81, no. 12, p. 3513–3536.

Brothers, D.S., Driscoll, N.W., Kent, G.M., Baskin, R.L., Harding, A.J., and Kell, A.M., 2022, Seismostratigraphic analysis of Lake Cahuilla sedimentation cycles and fault displacement history beneath the Salton Sea, California, USA: Geosphere, v. 18, no. 4, p. 1354–1376.

Cho, M., Liou, J.G., and Bird, D.K., 1988, Prograde Phase Relations in the State 2-14 Well Metasandstones, Salton Sea Geothermal Field, California: Journal of Geophysical Research: Solid Earth, v. 93, no. B11, p. 13081–13103.

Coplen, T., 1976, Cooperative geochemical resource assessment of the Mesa Geothermal system: Final Report Univ. California Riverside, IGPP-UCR-76-1, 97 p.

Dorsey, R. "Stratigraphy, Tectonics, and Basin Evolution in the Anza-Borrego Desert Region." In G. T. Jefferson and L. Lindsay, *Fossil Treasures of the Anza-Borrego Desert*, Sunbelt Publication, (2006) 89-104.

Elders, W.A., Rex, R.W., Robinson, P.T., Biehler, S., and Meidav, T., 1972, Crustal Spreading in Southern California: The Imperial Valley and the Gulf of California formed by the rifting apart of a continental plate.: Science, v. 178, no. 4056, p. 15–24.

Elders, W.A., and Sass, J.H., 1988, The Salton Sea Scientific Drilling Project: Journal of Geophysical Research: Solid Earth, v. 93, no. B11, p. 12953–12968.

Han, L., Hole, J.A., Stock, J.M., Fuis, G.S., Williams, C.F., Delph, J.R., Davenport, K.K., and Livers, A.J., 2016, Seismic imaging of the metamorphism of young sediment into new crystalline crust in the actively rifting Imperial Valley, California: Geochemistry, Geophysics, Geosystems, v. 17, no. 11, p. 4566–4584.

Helgeson, H.C., 1968, Geologic and thermodynamic characteristics of the Salton Sea geothermal system: American Journal of Science, v. 266, p. 129–166.

Hulen, J., Kaspereit, D., Norton, D.L., Osborn, W., Pulka, F.S. "Refined Conceptual Modeling and a New Resource Estimate for the Salton Sea Geothermal Field, Imperial Valley, California." *Geothermal Resources Council Transactions,* 26, (2002), 29-36.

Lachenbruch, A.H., Sass, J.H., and Galanis, S.P. Jr. "Heat flow in southernmost California and the origin of the Salton Trough." *Journal of Geophysical Research*, 90 (B8), (1985), 6709-6736.

Lonsdale, P., 1989, Geology and tectonic history of the Gulf of California, in Winterer, E.L., Hussong, D.M., and Decker, R.W. eds., The Eastern Pacific Ocean and Hawaii: The Geology of North America, v. N, Geological Society of America, p. 499–521.

MacDougal, D.T., 1914, The Salton Sea: A Study of the Geography, the Geology, the Floristics, and the Ecology of a Desert Basin: Carnegie Institution of Washington.

Maimoni, A., 1982, Minerals recovery from Salton Sea geothermal brines: a literature review and proposed cementation process: Geothermics, v. 11, no. 4, p. 239–258.

Mammerickx, J., and Klitgord, K.D., 1982, Northern East Pacific Rise: Evolution from 25 m.y. B.P. to the present: Journal of Geophysical Research: Solid Earth, v. 87, no. B8, p. 6751–6759.

McDowell, S.D., and Elders, W.A., 1980, Authigenic layer silicate minerals in borehole Elmore 1, Salton Sea Geothermal Field, California, USA: Contributions to Mineralogy and Petrology, v. 74, no. 3, p. 293–310.

McKibben, M., and Hardie, L., 1997, Ore-forming brines in active continental rifts: Geochemistry of hydrothermal ore deposits, v. 3, p. 877–935.

McKibben, M.A., Williams, A.E., and Okubo, S., 1988, Metamorphosed Plio-Pleistocene evaporites and the origins of hypersaline brines in the Salton Sea geothermal system, California: Fluid inclusion evidence: Geochimica et Cosmochimica Acta, v. 52, no. 5, p. 1047–1056.

McKibben, M.A. "The Salton Trough Rift." *SBCMA Special Publication*, 9, (1991), 76-80.

Muffler, L.P., and White, D.E., 1969, Active metamorphism of upper Cenozoic sediments in the Salton Sea geothermal field and the Salton Trough, southeastern California: Geological Society of America Bulletin, v. 80, no. 2, p. 157–181.

Philibosian, B., Fumal, T., and Weldon, R., 2011, San Andreas Fault Earthquake Chronology and Lake Cahuilla History at Coachella, California: Bulletin of the Seismological Society of America, v. 101, no. 1, p. 13–38.

Rex, R., 1983, The origin of the brines of the Imperial Valley, California: Trans. Geotherm. Resour. Counc, v. 7, p. 321–324.

Robinson, P.T., Elders, W.A., and Muffler, L.J.P., 1976, Quaternary volcanism in the Salton Sea geothermal field, Imperial Valley, California: Geological Society of America Bulletin, v. 87, no. 3, p. 347.

Rockwell, T.K., Meltzner, A.J., Haaker, E.C., and Madugo, D., 2022, The late Holocene history of Lake Cahuilla: Two thousand years of repeated fillings within the Salton Trough, Imperial Valley, California: Quaternary Science Reviews, v. 282, p. 107456.

Sanjuan, B., Millot, R., Ásmundsson, R., Brach, M., and Giroud, N., 2014, Use of two new Na/Li geothermometric relationships for geothermal fluids in volcanic environments: Chemical Geology, v. 389, p. 60–81.

Sanjuan, B., Gourcerol, B., Millot, R., Rettenmaier, D., Jeandel, E., and Rombaut, A., 2022, Lithium-rich geothermal brines in Europe: An up-date about geochemical characteristics and implications for potential Li resources: Geothermics, v. 101, p. 102385.

Sass, J.H., Galanis, S.P., Jr., Lachenbruch, A.H., Marshall, B.V., and Munroe, R.J. "Temperature, Thermal Conductivity, Heat Flow, and Radiogenic Heat Production from Unconsolidated Sediments of the Imperial Valley, California." *USGS Open File Report*, 84-490, (1984).

Sass, J.H., Priest, S.S., Duda, L.E., Carson, C.C., Hendricks, J.D., and Robison, L.C., 1988, Thermal Regime of the State 2-14 Well, Salton Sea Scientific Drilling Project: Journal of Geophysical Research: Solid Earth, v. 93, no. B11, p. 12995–13004.

Schmitt, A.K., and Hulen, J.B., 2008, Buried rhyolites within the active, high-temperature Salton Sea geothermal system: Journal of Volcanology and Geothermal Research, v. 178, no. 4, p. 708–718.

Schmitt, A.K., Perrine, A.R., Rhodes, E.J., and Fischer, C., 2019, Age of Obsidian Butte in Imperial County, California, Through Infrared Stimulated Luminescence Dating of Potassium Feldspar from Tuffaceous Sediment: California Archaeology, v. 11, no. 1, p. 5–20.

Skinner, B.J., White, D.E., Rose, H.J., and Mays, R.E., 1967, Sulfides associated with the Salton Sea geothermal brine: Economic Geology, v. 62, no. 3, p. 316–330.

Stock, J., and Hodges, K., 1989, Pre-Pliocene extension around the Gulf of California and the transfer of Baja California to the Pacific plate: Tectonics, v. 8, no. 1, p. 99–115.

Tompson, A.F.B., 2016, Born from a flood: The Salton Sea and its story of survival: Journal of Earth Science, v. 27, no. 1, p. 89–97.

Van De Kamp, P.C., 1973, Holocene Continental Sedimentation in the Salton Basin, California: A Reconnaissance: Geological Society of America Bulletin, v. 84, no. 3, p. 827.

Waters, M.R., 1983, Late Holocene Lacustrine Chronology and Archaeology of Ancient Lake Cahuilla, California: Quaternary Research, v. 19, no. 03, p. 373–387.

Wilke, P.J., 1976, Late Prehistoric Human Ecology at Lake Cahuilla, Coachella Valley, California: University of California, Riverside.

Williams, A.E., and McKibben, M.A., 1989, A brine interface in the Salton Sea Geothermal System, California: Fluid geochemical and isotopic characteristics: Geochimica et Cosmochimica Acta, v. 53, no. 8, p. 1905–1920.

Williams, A.E., 1997, Fluid density distribution in a high temperature, stratified thermohaline system: implications for saline hydrothermal circulationEarth and Planetary Science Letters 146, 12, 1- 136.

Winker, C.D., and Kidwell, S.M., 1986, Paleocurrent evidence for lateral displacement of the Pliocene Colorado River delta by the San Andreas fault system, southeastern California: Geology, v. 14, no. 9, p. 788–791.

Wright, H.M., Vazquez, J.A., Champion, D.E., Calvert, A.T., Mangan, M.T., Stelten, M., Cooper, K.M., Herzig, C., and Schriener, A., 2015, Episodic Holocene eruption of the Salton Buttes rhyolites, California, from paleomagnetic, U-Th, and Ar/Ar dating: Salton Buttes rhyolites: Geochemistry, Geophysics, Geosystems, v. 16, no. 4, p. 1198–1210.

Chapter 4

Agilent, Ed. (4th Edition). Handbook of ICP-QQQ Applications using the Agilent 8800 and 8900.

Araoka, D., Kawahata, H., Takagi, T., Watanabe, Y., Nishimura, K., and Nishio, Y., 2014, Lithium and strontium isotopic systematics in playas in Nevada, USA: constraints on the origin of lithium: Mineralium Deposita, v. 49, no. 3, p. 371–379.

Babcock, E.A., 1974, Geology of the Northeast Margin of the Salton Trough, Salton Sea, California: Geological Society of America Bulletin, v. 85, no. 3, p. 321–332.

Belkouteb, N., Schroeder, H., Arndt, J., Wiederhold, J.G., Ternes, T.A., and Duester, L., 2023, Quantification of 68 elements in river water monitoring samples in single-run measurements: Chemosphere, v. 320, p. 138053.

Chan, L.-H., Alt, J.C., and Teagle, D.A.H., 2002, Lithium and lithium isotope profiles through the upper oceanic crust: a study of seawater-basalt exchange at ODP Sites 504B and 896A: Earth and Planetary Science Letters, v. 201, no. 1, 187–201.

Chan, L.-H., Gieskes, J.M., Chen-Feng, Y., and Edmond, J.M., 1994, Lithium isotope geochemistry of sediments and hydrothermal fluids of the Guaymas Basin, Gulf of California: Geochimica et Cosmochimica Acta, v. 58, no. 20, p. 4443–4454.

Charles, R.W., Janecky, D.R., Goff, F., and McKibben, M.A., 1988, Chemographic and Thermodynamic Analysis of the Paragenesis of the Major Phases in the Vicinity of the 6120-Foot (1866 m) Flow Zone, California State Well 2-14: Journal of Geophysical Research: Solid Earth, v. 93, no. B11, p. 13145–13157.

Cho, M., Liou, J.G., and Bird, D.K., 1988, Prograde Phase Relations in the State 2-14 Well Metasandstones, Salton Sea Geothermal Field, California: Journal of Geophysical Research: Solid Earth, v. 93, no. B11, p. 13081–13103.

Coffey, D.M., Munk, L.A., Ibarra, D.E., Butler, K.L., Boutt, D.F., and Jenckes, J., 2021, Lithium Storage and Release From Lacustrine Sediments: Implications for Lithium Enrichment and Sustainability in Continental Brines: Geochemistry, Geophysics, Geosystems, v. 22, no. 12.

Coplen, T.B., 2002, Compilation of Minimum and Maximum Isotope Ratios of Selected Elements in Naturally Occurring Terrestrial Materials and Reagents: U.S. Geological Survey Water- Resources Investigations Report 01-4222.

Dellinger, M., Gaillardet, J., Bouchez, J., Calmels, D., Louvat, P., Dosseto, A., Gorge, C., Alanoca, L., and Maurice, L., 2015, Riverine Li isotope fractionation in the Amazon River basin controlled by the weathering regimes: Geochimica et Cosmochimica Acta, v. 164, p. 71–93.

Desaulty, A.-M., Monfort Climent, D., Lefebvre, G., Cristiano-Tassi, A., Peralta, D., Perret, S., Urban, A., and Guerrot, C., 2022, Tracing the origin of lithium in Li-ion batteries using lithium isotopes: Nature Communications, v. 13, no. 1, p. 4172.

Dyar, M., Guidotti, C., Harper, G., McKibben, M., and Saccocia, P., 1992, Controls on ferric iron in chlorite: Geological Society of America, Abstracts with Programs, v. 24, A130.

Elders, W.A., and Sass, J.H., 1988, The Salton Sea Scientific Drilling Project: Journal of Geophysical Research: Solid Earth, v. 93, no. B11, p. 12953–12968.

Elliott, T., Thomas, A., Jeffcoate, A., and Niu, Y., 2006, Lithium isotope evidence for subduction-enriched mantle in the source of mid-ocean-ridge basalts: Nature, v. 443, no. 7111, p. 565–568.

Ellis, B.S., Szymanowski, D., Harris, C., Tollan, P.M.E., Neukampf, J., Guillong, M., Cortes-Calderon, E.A., and Bachmann, O., 2022, Evaluating the Potential of Rhyolitic Glass as a Lithium Source for Brine Deposits: Economic Geology, v. 117, no. 1, p. 91–105.

Fan, J.-J., Tang, G.-J., Wei, G.-J., Wang, H., Xu, Y.-G., Wang, Q., Zhou, J.-S., Zhang, Z.-Y., Huang, T.-Y., and Wang, Z.-L., 2020, Lithium isotope fractionation during fluid exsolution: Implications for Li mineralization of the Bailongshan pegmatites in the West Kunlun, NW Tibet: Lithos, v. 352–353, p. 105236.

Garcia, M.G., Borda, L.G., Godfrey, L.V., López Steinmetz, R.L., and Losada-Calderon, A., 2020, Characterization of lithium cycling in the Salar De Olaroz, Central Andes, using a geochemical and isotopic approach: Chemical Geology, v. 531, p. 119340.

Godfrey, L., and Álvarez-Amado, F., 2020, Volcanic and Saline Lithium Inputs to the Salar de Atacama: Minerals, v. 10, no. 2, p. 201.

Godfrey, L.V., Chan, L.-H., Alonso, R.N., Lowenstein, T.K., McDonough, W.F., Houston, J., Li, J., Bobst, A., and Jordan, T.E., 2013, The role of climate in the accumulation of lithium-rich brine in the Central Andes: Applied Geochemistry, v. 38, p. 92–102.

He, M.-Y., Luo, C.-G., Yang, H.-J., Kong, F.-C., Li, Y.-L., Deng, L., Zhang, X.-Y., and Yang, K.-Y., 2020, Sources and a proposal for comprehensive exploitation of lithium brine deposits in the Qaidam Basin on the northern Tibetan Plateau, China: Evidence from Li isotopes: Ore Geology Reviews, v. 117, p. 103277.

Helgeson, H.C., 1968, Geologic and thermodynamic characteristics of the Salton Sea geothermal system: American Journal of Science, v. 266, p. 129–166.

Herzig, C.T., and Elders, W.A., 1988, Nature and Significance of Igneous Rocks Cored in the State 2-14 Research Borehole: Salton Sea Scientific Drilling Project, California: Journal of Geophysical Research: Solid Earth, v. 93, no. B11, p. 13069–13080.

Herzig, C.T., and Jacobs, D.C., 1994, Cenozoic volcanism and two-stage extension in the Salton trough, southern California and northern Baja California: Geology, v. 22, no. 11, p. 991.

Herzig, C.T., Mehegan, J.M., and Stelting, C.E., 1988, Lithostratigraphy of the State 2-14 Borehole: Salton Sea Scientific Drilling Project: Journal of Geophysical Research: Solid Earth, v. 93, no. B11, p. 12969–12980.

Huh, Y., Chan, L.-H., Zhang, L., and Edmond, J.M., 1998, Lithium and its isotopes in major world rivers: implications for weathering and the oceanic budget: Geochimica et Cosmochimica Acta, v. 62, no. 12, p. 2039–2051.

Huh, Y., Chan, L.-H., and Edmond, J.M., 2001, Lithium isotopes as a probe of weathering processes: Orinoco River: Earth and Planetary Science Letters, v. 194, nos. 1–2, p. 189–199.

Humphreys, J, Brounce, M., McKibben, M. A., Dobson, P., Planavsky, N., & Kalderon-Asael, B., 2023, SS-GF Mineral Major Elements and Li Concentration. United States. https://gdr.openei.org/submissions/1515

Jochum, K.P., Dingwell, D.B., Rocholl, A., Stoll, B., Hofmann, A.W., Becker, S., Besmehn, A., Bessette, D., Dietze, H.-J., Dulski, P., Erzinger, J., Hellebrand, E., Hoppe, P., Horn, I., et al., 2000, The Preparation and Preliminary Characterisation of Eight Geological MPI-DING Reference Glasses for In-Situ Microanalysis: Geostandards and Geoanalytical Research, v. 24, no. 1, p. 87–133.

Kalderon-Asael, B., Katchinoff, J. A., Planavsky, N. J., Hood, A. V. S., Dellinger, M., Bellefroid, E. J., ... & Pogge von Strandmann, P. A. (2021). A lithium-isotope perspective on the evolution of carbon and silicon cycles. *Nature*, *595*(7867), 394-398.

Kelley, K.A., Plank, T., Ludden, J., and Staudigel, H., 2003, Composition of altered oceanic crust at ODP Sites 801 and 1149: Geochemistry, Geophysics, Geosystems, v. 4, no. 6, 8910.

Kısakűrek, B., James, R.H., and Harris, N.B.W., 2005, Li and δ7Li in Himalayan rivers: Proxies for silicate weathering? Earth and Planetary Science Letters, v. 237, nos. 3–4, p. 387–401.

Lemarchand, E., Chabaux, F., Vigier, N., Millot, R., and Pierret, M.-C., 2010, Lithium isotope systematics in a forested granitic catchment (Strengbach, Vosges Mountains, France): Geochimica et Cosmochimica Acta, v. 74, no. 16, p. 4612–4628.

Liu, X.-M., Wanner, C., Rudnick, R.L., and McDonough, W.F., 2015, Processes controlling δ7Li in rivers illuminated by study of streams and groundwaters draining basalts: Earth and Planetary Science Letters, v. 409, p. 212–224.

Lonsdale, P., 1989, Geology and tectonic history of the Gulf of California, in Winterer, E.L., Hussong, D.M., and Decker, R.W. eds., The Eastern Pacific Ocean and Hawaii: The Geology of North America, v. N, Geological Society of America, p. 499–521.

Lynton, S.J., Walker, R.J., and Candela, P.A., 2005, Lithium isotopes in the system Qz-Ms-fluid:An experimental study: Geochimica et Cosmochimica Acta, v. 69, no. 13, p. 3337–3347.

Magenheim, A.J., Spivack, A.J., Alt, J.C., Bayhurst, G., Chan, L.-H., Zuleger, E., and Gieskes, J.M., 1995, 13. Borehole fluid chemistry in hole 504B, LEG 137: formation water or in-situ reaction? Proceedings of the Ocean Drilling Program, Ocean Drilling Program.

Magna, T., Novák, M., Cempírek, J., Janoušek, V., Ullmann, C.V., and Wiechert, U., 2016, Crystallographic control on lithium isotope fractionation in Archean to Cenozoic lithium-cesium-tantalum pegmatites: Geology, v. 44, no. 8, p. 655–658.

Marschall, H.R., and Tang, M., 2020, High-temperature processes: Is it time for lithium isotopes?: Elements, v. 16, p. 247–252.

McDowell, S.D., and Elders, W.A., 1980, Authigenic layer silicate minerals in borehole Elmore 1, Salton Sea Geothermal Field, California, USA: Contributions to Mineralogy and Petrology, v. 74, no. 3, p. 293–310.

McKibben, M.A., and Elders, W.A., 1985, Fe-Zn-Cu-Pb mineralization in the Salton Sea geothermal system, Imperial Valley, California: Economic Geology, v. 80, no. 3, p. 539–559.

McKibben, M.A., Williams, A.E., and Okubo, S., 1988a, Metamorphosed Plio-Pleistocene evaporites and the origins of hypersaline brines in the Salton Sea geothermal system, California: Fluid inclusion evidence: Geochimica et Cosmochimica Acta, v. 52, no. 5, p. 1047–1056.

McKibben, M.A., Andes, J.P., and Williams, A.E., 1988b, Active ore formation at a brine interface in metamorphosed deltaic lacustrine sediments; the Salton Sea geothermal system, California: Economic Geology, v. 83, no. 3, p. 511–523.

Millot, R., Guerrot, C., and Vigier, N., 2004, Accurate and High-Precision Measurement of Lithium Isotopes in Two Reference Materials by MC-ICP-MS: Geostandards and Geoanalytical Research, v. 28, no. 1, p. 153–159.

Millot, R., Scaillet, B., and Sanjuan, B., 2010, Lithium isotopes in island arc geothermal systems: Guadeloupe, Martinique (French West Indies) and experimental approach: Geochimica et Cosmochimica Acta, v. 74, no. 6, p. 1852–1871.

Moriguti, T., and Nakamura, E., 1998, Across-arc variation of Li isotopes in lavas and implications for crust/mantle recycling at subduction zones: Earth and Planetary Science Letters, v. 163, nos. 1–4, p. 167–174.

Muffler, L.P., and White, D.E., 1969, Active metamorphism of upper Cenozoic sediments in the Salton Sea geothermal field and the Salton Trough, southeastern California: Geological Society of America Bulletin, v. 80, no. 2, p. 157–181.

Munk, L., Jochens, H., Jennings, M., Bradley, D., Hynek, S., and Godfrey, L., 2011, Geochemistry of lithium-rich brines in Clayton Valley, Nevada, USA: Biennial Meeting of SGA, Antofagasta, Chile.

Munk, L.A., Boutt, D.F., Hynek, S.A., and Moran, B.J., 2018, Hydrogeochemical fluxes and processes contributing to the formation of lithium-enriched brines in a hyper-arid continental basin: Chemical Geology, v. 493, p. 37–57.

Nishio, Y., Nakai, S., Ishii, T., and Sano, Y., 2007, Isotope systematics of Li, Sr, Nd, and volatiles in Indian Ocean MORBs of the Rodrigues Triple Junction: Constraints on the origin of the DUPAL anomaly: Geochimica et Cosmochimica Acta, v. 71, no. 3, p. 745–759.

Pearce, N.J.G., Perkins, W.T., Westgate, J.A., Gorton, M.P., Jackson, S.E., Neal, C.R., and Chenery, S.P., 1997, A Compilation of New and Published Major and Trace Element Data for NIST SRM 610 and NIST SRM 612 Glass Reference Materials: Geostandards and Geoanalytical Research, v. 21, no. 1, p. 115–144.

Penniston-Dorland, S., Liu, X.-M., and Rudnick, R.L., 2017, Lithium Isotope Geochemistry: Reviews in Mineralogy and Geochemistry, v. 82, no. 1, p. 165–217.

Philibosian, B., Fumal, T., and Weldon, R., 2011, San Andreas Fault Earthquake Chronology and Lake Cahuilla History at Coachella, California: Bulletin of the Seismological Society of America, v. 101, no. 1, p. 13–38.

Plank, T., 2014, The Chemical Composition of Subducting Sediments, in Treatise on Geochemistry: Elsevier, p. 607–629.

Pogge Von Strandmann, P.A.E., and Henderson, G.M., 2015, The Li isotope response to mountain uplift: Geology, v. 43, no. 1, p. 67–70.

Pogge Von Strandmann, P.A.E., Burton, K.W., James, R.H., Van Calsteren, P., Gíslason, S.R., and Mokadem, F., 2006, Riverine behaviour of uranium and lithium isotopes in an actively glaciated basaltic terrain: Earth and Planetary Science Letters, v. 251, nos. 1–2, p. 134–147.

Pogge Von Strandmann, P.A.E., Burton, K.W., James, R.H., Van Calsteren, P., and Gislason, S.R., 2010, Assessing the role of climate on uranium and lithium isotope behaviour in rivers draining a basaltic terrain: Chemical Geology, v. 270, nos. 1–4, p. 227–239.

Pogge Von Strandmann, P.A.E., Kasemann, S.A., and Wimpenny, J.B., 2020, Lithium and lithium isotopes in Earth's surface cycles: Elements, v. 16, no. 4, p. 253–258.

Robinson, P.T., Elders, W.A., and Muffler, L.J.P., 1976, Quaternary volcanism in the Salton Sea geothermal field, Imperial Valley, California: Geological Society of America Bulletin, v. 87, no. 3, p. 347.

Rockwell, T.K., Meltzner, A.J., Haaker, E.C., and Madugo, D., 2022, The late Holocene history of Lake Cahuilla: Two thousand years of repeated fillings within the Salton Trough, Imperial Valley, California: Quaternary Science Reviews, v. 282, p. 107456.

Sanjuan, B., Millot, R., Innocent, Ch., Dezayes, Ch., Scheiber, J., and Brach, M., 2016, Major geochemical characteristics of geothermal brines from the Upper Rhine Graben granitic basement with constraints on temperature and circulation: Chemical Geology, v. 428, p. 27–47.

Sanjuan, B., Gourcerol, B., Millot, R., Rettenmaier, D., Jeandel, E., and Rombaut, A., 2022, Lithium-rich geothermal brines in Europe: An up-date about geochemical characteristics and implications for potential Li resources: Geothermics, v. 101, p. 102385.

Sass, J.H., Priest, S.S., Duda, L.E., Carson, C.C., Hendricks, J.D., and Robison, L.C., 1988, Thermal Regime of the State 2-14 Well, Salton Sea Scientific Drilling Project: Journal of Geophysical Research: Solid Earth, v. 93, no. B11, p. 12995–13004.

Sauzéat, L., Rudnick, R.L., Chauvel, C., Garçon, M., and Tang, M., 2015, New perspectives on the Li isotopic composition of the upper continental crust and its weathering signature: Earth and Planetary Science Letters, v. 428, p. 181–192.

Schauble, E.A., 2004, Applying stable isotope fractionation theory to new systems. Reviews in Mineralogy and Geochemistry, v. 55, p. 65−111

Schmitt, A.K., and Hulen, J.B., 2008, Buried rhyolites within the active, high-temperature Salton Sea geothermal system: Journal of Volcanology and Geothermal Research, v. 178, no. 4, p. 708–718.

Sturz, A., 1989, Low-temperature hydrothermal alteration in near-surface sediments, Salton Sea Geothermal Area: Journal of Geophysical Research: Solid Earth, v. 94, no. B4, p. 4015–4024.

Teng, F.-Z., McDonough, W.F., Rudnick, R.L., Dalpé, C., Tomascak, P.B., Chappell, B.W., and Gao, S., 2004, Lithium isotopic composition and concentration of the upper continental crust: Geochimica et Cosmochimica Acta, v. 68, no. 20, p. 4167–4178.

Tomascak, P.B., Hemming, N.G., and Hemming, S.R., 2003, The lithium isotopic composition of waters of the Mono Basin, California: Geochimica et Cosmochimica Acta, v. 67, no. 4, p. 601–611.

Tomascak, P.B., Langmuir, C.H., Le Roux, P.J., and Shirey, S.B., 2008, Lithium isotopes in global mid-ocean ridge basalts: Geochimica et Cosmochimica Acta, v. 72, no. 6, p. 1626–1637.

Tompson, A.F.B., 2016, Born from a flood: The Salton Sea and its story of survival: Journal of Earth Science, v. 27, no. 1, p. 89–97.

Van De Kamp, P.C., 1973, Holocene Continental Sedimentation in the Salton Basin, California: A Reconnaissance: Geological Society of America Bulletin, v. 84, no. 3, p. 827.

Vigier, N., Gislason, S.R., Burton, K.W., Millot, R., and Mokadem, F., 2009, The relationship between riverine lithium isotope composition and silicate weathering rates in Iceland: Earth and Planetary Science Letters, v. 287, nos. 3–4, p. 434–441.

Waters, M.R., 1983, Late Holocene Lacustrine Chronology and Archaeology of Ancient Lake Cahuilla, California: Quaternary Research, v. 19, no. 03, p. 373–387.

Wilke, P.J., 1976, Late Prehistoric Human Ecology at Lake Cahuilla, Coachella Valley, California: University of California, Riverside.

Williams, A.E., and McKibben, M.A., 1989, A brine interface in the Salton Sea Geothermal System, California: Fluid geochemical and isotopic characteristics: Geochimica et Cosmochimica Acta, v. 53, no. 8, p. 1905–1920.

Winker, C.D., and Kidwell, S.M., 1986, Paleocurrent evidence for lateral displacement of the Pliocene Colorado River delta by the San Andreas fault system, southeastern California: Geology, v. 14, no. 9, p. 788–791.

Wunder, B., Meixner, A., Romer, R.L., Feenstra, A., Schettler, G., and Heinrich, W., 2007, Lithium isotope fractionation between Li-bearing staurolite, Li-mica and aqueous fluids: An experimental study: Chemical Geology, v. 238, nos. 3–4, p. 277–290.

Chapter 5

Araya and O'Sullivan. "A 3D Conceptual and Natural-State Model of the Salton Sea Geothermal Field." *GRC Transactions*, 46, (2022). 2123-2155.

CDC (California Department of Conservation). "Geological Map of California [Data File]." (2015). https://maps.conservation.ca.gov/cgs/#datalist

Croucher, A., O'Sullivan, M., O'Sullivan, J., Yeh, A., and Burnell, J. "Waiwera: A parallel open-source geothermal flow simulator." *Computers and Geosciences*, 141, (2020).

de Beer, A., Gravatt, M., Renaud, T., Nicholson, R., Maclaren, O. J., Dekkers, K., O'Sullivan, M., O'Sullivan, J., "Geologically Consistent Prior Parameter Distributions for Uncertainty Quantification of Geothermal Reservoirs." *48th Stanford Workshop on Geothermal Reservoir Engineering*, California, (2023).

Dekkers, K., Gravatt, M., Maclaren, O. J., Nicholson, R., Nugraha, R., O'Sullivan, M., O'Sullivan, J., "Resource Assessment: Estimating the Potential of a Geothermal Reservoir." *47th Stanford Workshop on Geothermal Reservoir Engineering*, California, (2022).

Dorsey, R. "Stratigraphy, Tectonics, and Basin Evolution in the Anza-Borrego Desert Region." In G. T. Jefferson and L. Lindsay, *Fossil Treasures of the Anza-Borrego Desert*, Sunbelt Publication, (2006) 89-104.

Dorsey, R.J., Housen, B.A., Janecke, S.U., Fanning, C.M., and Spears, A.L.F. "Stratigraphic Record of Basin Development Within the San Andreas Fault System: Late Cenozoic Fish Creek-Vallecito Basin, Southern California." *Geol. Soc. Am. Bul.*, 123, (2011), 771-793.

Helgeson, H.C. "Geologic and Thermodynamic Characteristics of the Salton Sea Geothermal System." *American Journal of Science*, 266, (1968), 129-166.

Hulen, J., Norton, D., Kaspereit, D., Murray, L., Van de Putte, T., and Wright, M. "Geology and a Working Conceptual Model of the Obsidian Butte (Unit 6) Sector of the Salton Sea Geothermal Field, California." *GRC Transactions*, 27, (2003), 227-240.

Kaspereit, D., Mann, M., Sanyal S., Rickard, B., Osborn, W., and Hulen, J. "Updated Conceptual Model and Reserve Estimate for the Salton Sea Geothermal Field, Imperial Valley, California." *GRC Transactions*, 40, (2016), 57-66.

Kirby, S.M., Janecke, S.U., Dorsey, R.J., Housen, B.A, Langenheim, V.E., McDougall, K.A., and Steely, A.N. "Pleistocene Brawley and Ocotillo Formations: Evidence for Initial Strike-Slip Deformation Along the San Felipe and San Jacinto Fault Zones, Southern California." *Journal of Geology*, 115, (2007).

Lynch, D.K., and Hudnut, K.W. "The Wister Mud Pot Lineament: Southeastward Extension or Abandoned Strand of the San Andreas Fault?" *Bulletin of Seismological Society of America*, 98, (2008), 1720-1729.

Marshall, S., Plesch, A., Shaw, J., and Nicholson, C. "SCEC Community Fault Model v. 5.3.2." (2022). https://www.scec.org/research/cfm-viewer/

Mazzini, A., Svensen, H., Etiope, G., Onderrdonk, N., and Banks, D. "Fluid origin, gas fluxes and plumbing system in the sediment-hosted Salton Sea geothermal system (California, USA)." *Journal of Volcanology and Geothermal Research*, 205, (2011), 67-83.

McGuire, J.J., Lohman, R.B., Catchings, R.D., Rymer, M.J., and Goldman, M.R. "Relationships Among Seismic Velocity, Metamorphism, and Seismic and Aseismic Fault Slip in the Salton Sea Geothermal Field region." *Journal of Geophysical Research*, 120, (2015), 2600-2615.

Nichols, E. "Geothermal Exploration Under the Salton Sea Using Marine Magnetotellurics." California Energy Commission, PIER Renewable Energy Technologies Program, CEC-500-2009-005, (2009).

Norton and Hulen. "Magma-Hydrothermal Activity in the Salton Sea Geothermal Field Imperial County, California." *GRC Transactions*, 30, (2006). 991-998.

O'Sullivan, M., Pruess, K., and Lippmann, M. "Geothermal Reservoir Simulation: The state-of Practice and Emerging trends." *Proceedings World Geothermal Congress*, (2000).

O'Sullivan, M., and O'Sullivan, J. "Reservoir Modelling and Simulation for Geothermal Resource Characterization and Evaluation." *Geothermal Power Generation*, (2016), 165-199.

O'Sullivan, J., Popineau, J., Gravatt, M., Renaud, T., Riffault, J., Croucher, A., Yeh, A. & O'Sullivan M. "An integrated, mesh-independent geothermal modelling framework." *Environmental Modelling and Software*, 163, (2023), 105666.

Omagbon, J., Doherty, J., Yeh, A., Colina, R., O'Sullivan, J., McDowell, J., ... O'Sullivan, M. (2021). Case studies of predictive uncertainty quantification for geothermal models. *Geothermics*, *97*, 102263. doi:10.1016/j.geothermics.2021.102263

Palmer, T.D. "Characteristics of Geothermal Wells Located in the Salton Sea Geothermal Field, Imperial County, California." *Lawrence Livermore Laboratory,* UCRL-51976, (1975).

Popineau, J., O'Sullivan, J., O'Sullivan, M., Archer, R., and Williams, B. "An integrated Leapfrog /TOUGH2 Workflow for a Geothermal Production Modelling." *7th African Rift Geothermal Conference*, (2018).

Rao, A.P. "The hydraulic connectivity, perennial warming and relationship to seismicity of the Davis-Schrimpf seep field, Salton Trough, California from new and recent temperature time-series." *M.S. thesis, California State University, Long Beach*, (2016), 107 p.

Sass, J.H., Priest, S.S., Duda, L.E., Carson, C.C., Hendricks, J.D., and Robison, L.C. "Thermal Regime of the State 2-14 well, Salton Sea Scientific Drilling Project." *Journal of Geophysical Research*, 93 (B11), (1988), 12,995-13,004.

Svensen, H., Karlsen, D.A., Sturz, A., Backer-Owe, K., Banks, D.A., and Planke, S. "Processes Controlling Water and Hydrocarbon Composition in Seeps from the Salton Sea Geothermal System, California, USA." *Geology*, 35, (2007), 85-88.

Wagoner, J.L. "Stratigraphy and Sedimentology of the Pleistocene Brawley and Borrego Formations, San Felipe Hills, Imperial County, California." Lawrence Livermore Laboratory, UCRL-84041, (1980).

Younker, L.W., Kasameyer, P.W., and Tewhey, J.D. "Geological, Geophysical, and Thermal Characteristics of the Salton Sea Geothermal Field, California." *Journal of Volcanology and Geothermal Research*, 12, (1981), 221-258.

Chapter 6

Alai, M., M. Sutton, and S. Carroll, 2005, Evaporative evolution of a Na–Cl–NO3–K–Ca–SO4– Mg–Si brine at 95 °C: Experiments and modeling relevant to Yucca Mountain, Nevada, *Geochemical Transactions*, 6 (2) 31-45.

Araoka, D., H. Kawahata, T. Takagi, Y. Watanabe, K. Nishimura, Y. Nishio, 2014. Lithium and strontium isotopic systematics in playas in Nevada, USA: Constraints on the origin of lithium. Miner. Depos. 49, 371–379. https://doi.org/10.1007/s00126-013-0495-y

Araya and O'Sullivan. "A 3D Conceptual and Natural-State Model of the Salton Sea Geothermal Field." *GRC Transactions*, 46, (2022). 2123-2155.

Boschetti, T., 2022a. A revision of lithium minerals thermodynamics: Possible implications for fluids geochemistry and geothermometry. Geothermics 98. https://doi.org/10.1016/j.geothermics.2021.102286

Boschetti, T., 2022b. Comments on "Lithium-rich geothermal brines in Europe: An up-date about geochemical characteristics and implications for potential Li resources" by Sanjuan et al. (2022). Geothermics 105, 102518. https://doi.org/10.1016/j.geothermics.2022.102518

Brothers, D.S., Driscoll, N.W., Kent, G.M., Harding, A.J., Babcock, J.M., Baskin, R.L., 2009. Tectonic evolution of the Salton Sea inferred from seismic reflection data. Nat. Geosci. 2, 581–584. https://doi.org/10.1038/ngeo590

Cullen, J.T., Hurwitz, S., Barnes, J.D., Lassiter, J.C., Penniston-Dorland, S., Meixner, A., Wilckens, F., Kasemann, S.A., McCleskey, R.B., 2021. The Systematics of Chlorine, Lithium, and Boron and δ37Cl, δ7Li, and δ11B in the Hydrothermal System of the Yellowstone Plateau Volcanic Field. Geochemistry, Geophys. Geosystems 22, 1–24. https://doi.org/10.1029/2020GC009589

DePaolo, D.J., Sonnenthal, E.L., Pester, N.J., 2022. Thermo-Hydro-Chemical Simulation of Mid-Ocean Ridge Hydrothermal Systems: Static 2D Models and Effects of Paleo-Seawater Chemistry. GEOCHEMISTRY Geophys. GEOSYSTEMS 23. https://doi.org/10.1029/2022GC010524

Ellis, B.S., Neukampf, J., Bachmann, O., Harris, C., Forni, F., Magna, T., Laurent, O., Ulmer, P., 2022. Biotite as a recorder of an exsolved Li-rich volatile phase in upper-crustal silicic magma reservoirs. Geology 50, 481–485. https://doi.org/10.1130/G49484.1

Harvie, C. E., Moller, N., and J. H. Weare, 1984. The Prediction of Mineral Solubilities in Natural Waters: The Na-K-Mg-Ca-H-Cl-SO_4-OH-HCO_3-CO_3-H_2O System to High Ionic Strengths at 25°C, *Geochimica et Cosmochimica Acta*, 48, (4), 723-751.

Helgeson, H.C., 1968. Geologic and thermodynamic characteristics of the Salton Sea geothermal system. Amer. Jour. Sci. https://doi.org/10.2475/ajs.266.3.129

Holdren, G.C., Montaño, A., 2002. Chemical and physical characteristics of the Salton Sea, California. Hydrobiologia 473, 1–21. https://doi.org/10.1023/A:1016582128235

Humphreys, J, Brounce, M., McKibben, M. A., Dobson, P., Planavsky, N., & Kalderon-Asael, B., 2023, SS-GF Mineral Major Elements and Li Concentration. United States. https://gdr.openei.org/submissions/1515

Lassin, A., Christomir, C., Andre, L., Mohamed, A., 2015. A thermodynamic model of aqueous electrolyte solution behavior and solid-liquid equilibrium in the Li-H-Na-K-Cl-OH-H2O system to very high concentrations (40 molal) and from 0 to 250 °C. Am. J. Sci. 315, 204–256. https://doi.org/10.2475/03.2015.02

Lichtner, P. C., 1996. Continuum formulation of multicomponent-multiphase reactive transport, in Lichtner, P. C., Steefel, C. I., and Oelkers, E. H. (eds.), *Reactive transport in porous media*, Reviews in Mineralogy, Mineral Society of America, v. 34, p. 1-79.

Magnusdottir, L., Finsterle, S., 2015. An iTOUGH2 equation-of-state module for modeling supercritical conditions in geothermal reservoirs. Geothermics 57, 8–17. https://doi.org/10.1016/j.geothermics.2015.05.003

McKibben, M., and Hardie, L., 1997, Ore-forming brines in active continental rifts: Geochemistry of hydrothermal ore deposits, v. 3, p. 877–935.

McKibben, M.A., Williams, A.E., Okubo, S., 1988. Metamorphosed Plio-Pleistocene evaporites and the origins of hypersaline brines in the Salton Sea geothermal system, California: Fluid inclusion evidence. Geochim. Cosmochim. Acta 52, 1047–1056. https://doi.org/10.1016/0016-7037(88)90259-1

Narasimhan, T. N., P.A. Witherspoon, 1976. An integrated finite difference method for analyzing fluid flow in porous media, *Water Resour. Res.*, v. 12, p. 57–64.

Palandri, J. Y. Kharaka, 2004. A compilation of rate parameters of water–mineral interaction kinetics for Application to geochemical modeling. In *U.S. Geological Survey open file report 2004-1068*.

Pitzer, K. S. 1973, Thermodynamics of electrolytes, I. Theoretical basis and general equations, *J. Phys. Chem.*, 77, 268– 277.

Pitzer, K. S., and G. Mayorga, 1973, Thermodynamics of electrolytes. II. Activity and osmotic coefficients for strong electrolytes with one or both ions univalent, *J. Phys. Chem.*, 77, 2300-2307.

Pitzer, K.S., 1991, Ion Interaction Approach: Theory and Data Correlation, Chapter 3 of Activity Coefficients in Electrolyte Solutions, 2nd Edition, Pitzer, K.S., ed. Boca Raton, Florida: CRC Press, TIC: 251799.

Pruess, K., Oldenburg, C., and Moridis, G., TOUGH2 user's guide, Version 2.0, Lawrence Berkeley Laboratory Report LBL-43134, Berkeley, California, 1999.

Rard J. A., and A. M. Wijesinghe, 2003, Conversion of parameters between different variants of Pitzer's ion-interaction model, both with and without ionic strength dependent higher-order terms, *J. Chem. Thermodynamics*, 35, 439-473.

Schmitt, A.K., and Hulen, J.B., 2008, Buried rhyolites within the active, high-temperature Salton Sea geothermal system: Journal of Volcanology and Geothermal Research, v. 178, no. 4, p. 708–718.

Sonnenthal, E., N. Spycher, T. Xu, and L. Zheng, 2021. TOUGHREACT V4.12-OMP and TReactMech V1.0 Geochemical and Reactive-Transport User Guide. LBNL Report 2001410. https://tough.lbl.gov/software/toughreact.

Sonnenthal, E., A. Ito, N. Spycher, M. Yui, J. Apps, Y. Sugita, M. Conrad, and S. Kawakami, 2005. Approaches to modeling coupled thermal, hydrological, and chemical processes in the Drift Scale Heater Test at Yucca Mountain, *International Journal of Rock Mechanics and Mining Sciences*, v. 42, p. 698-719.

Sonnenthal, E., N. Spycher, T. Xu, and L. Zheng, 2021. TOUGHREACT V4.12-OMP and TReactMech V1.0 Geochemical and Reactive-Transport User Guide. LBNL Report 2001410. https://tough.lbl.gov/software/toughreact.

Spycher, N., G. Zhang, E. Sonnenthal, 2021. TOUGHREACT-Brine: Supplement to TOUGHREACT-V4.0-OMP User's Guide for Modeling Concentrated Solutions and Osmosis Using the Pitzer Ion-Interaction Model. LBNL-2001-387.

Steefel, C. I., and A.C. Lasaga, 1994. A coupled model for transport of multiple chemical species and kinetic precipitation/dissolution reactions with applications to reactive flow in single phase hydrothermal system, *Am. J. Sci.*, v. 294, p. 529-592.

Sturz, A., 1989, Low-temperature hydrothermal alteration in near-surface sediments, Salton Sea Geothermal Area: Journal of Geophysical Research: Solid Earth, v. 94, no. B4, p. 4015–4024.

Tomascak, P.B., Hemming, N.G., Hemming, S.R., 2003. The lithium isotopic composition of waters of the Mono Basin, California. Geochim. Cosmochim. Acta 67, 601–611. https://doi.org/10.1016/s0016-7037(02)01132-8

Walter, A. L., Frind, E. O., Blowes, D. W., Ptacek, C. J., and Molson, J. W., 1994. Modeling of multicomponent reactive transport in groundwater: 1, Model development and evaluation, *Water Resour. Res.*, v. 30, p. 3137-3148.

Wanner, C., E.L. Sonnenthal, X-M Liu, 2014. Seawater δ7Li: A direct proxy for global CO2 consumption by continental silicate weathering? *Chemical Geology*, 381: 154-167.

Werner, S.L., and Olson, L.J. (1970) Geothermal wastes and the water resources of the Salton Sea area. California Department of Water Resources Bulletin 143-7, 123 p.

Wolery T., Jove-Colon C., Rard., J., and A. Wijesinghe., 2004, Pitzer Database Development: Description of the Pitzer Geochemical Thermodynamic Database data0.ypf. Appendix I in In- Drift Precipitates/Salts Model (P. Mariner) Report ANL-EBS-MD-000045 REV 02. Las Vegas, Nevada: Bechtel SAIC Company.

Xu, T., & Pruess, K. (2001). Modeling multiphase non-isothermal fluid flow and reactive geochemical transport in variably saturated fractured rocks: 1. Methodology. *American Journal of Science*, *301*(1), 16-33.

Xu, T., K. Pruess, and G. Brimhall, 1999. An improved equilibrium-kinetics speciation algorithm for redox reactions in variably saturated flow systems, *Computers & Geosciences,* v. 25, p. 655-666.

Xu, T., E. Sonnenthal, N. Spycher, K. Pruess, G. Brimhall, and J.A. Apps, 2001. Modeling multiphase fluid flow and reactive geochemical transport in variably saturated fractured rocks: 2. Applications to supergene copper enrichment and hydrothermal flows. American Journal of Science, 301:34-59.

Xu, T., E. Sonnenthal, N. Spycher, and K. Pruess, 2006. TOUGHREACT: A simulation program for non-isothermal multiphase reactive geochemical transport in variably saturated geologic media: Applications to geothermal injectivity and CO_2 geological sequestration. Computers & Geosciences. 32:145-156.

Xu, T., N. Spycher, E. Sonnenthal, G. Zhang, L. Zheng, and K. Pruess, 2011. TOUGHREACT Version 2.0: A simulator for subsurface reactive transport under non-isothermal multiphase flow conditions. *Computers & Geosciences* 37, 763–774.

Yeh, G. T., and V.S. Tripathi, 1991. A model for simulating transport of reactive multispecies components: model development and demonstration*, Water Resour. Res*., v. 27, p. 3075-3094.

Zhang, G., N. Spycher, E. Sonnenthal, C. Steefel, and T. Xu, 2008. Modeling reactive multiphase flow and transport of concentrated solutions. Nuclear Technology, 164:180-195.

Chapter 7

Ajami, H. (2021). "Chapter 2: Watershed Hydrology - Hydrology and Water Resources in the Salton Sea Watershed" in Crisis at the Salton Sea: Vital Role of Science. In UNIVERSITY OF CALIFORNIA RIVERSIDE SALTON SEA TASK FORCE (Ed.). https://www.saltonseataskforce.ucr.edu/_files/ugd/0d73bf_965128e5688948918ff4af26a5f85fac.pdf

AQUAOSO. (2021). California Agricultural Water Prices by Water District. *Water Trends*. https://aquaoso.com/water-trends/california-agricultural-water-prices/#:~:text=According%20to%20the%20Water%20Market,to%20%24686%20per%20acre%2Dfoot.

Becker, R. (2022). California offers to reduce imports to Colorado River water. *Cal Matters*. https://calmatters.org/environment/2022/10/california-colorado-river-water/

Black Rock Geothermal LLC. (2023). *Black Rock Geothermal Project Application for Certification Volume 1*. https://efiling.energy.ca.gov/GetDocument.aspx?tn=249752&DocumentContentId=84391

Breuer, R., Eccles, R., Hunt, T., Mielke, E., Molnar, R., & Shikaze, S. (2021). *Standard Lithium Ltd. SW Arkansas Lithium Project*.

California Department of Water Resources, (2004), Imperial Valley Groundwater Basin. https://water.ca.gov/-/media/DWR-Website/Web-Pages/Programs/Groundwater-Management/Bulletin-118/Files/2003-Basin-Descriptions/7_030_ImperialValley.pdf

CEC (California Energy Commission), (2021). "2021 Total System Electric Generation." from https://www.energy.ca.gov/data-reports/energy-almanac/california-electricity-data/2021-total-system-electric-generation

Chakrabarti, D., Singh, S. K., Rashid, M. H., & Rahman, M. M. (2019). Arsenic: Occurrence in Groundwater. In *Encyclopedia of Environmental Health* (pp. 153-168). https://doi.org/10.1016/b978-0-12-409548-9.10634-7

Chambers Group Inc. (2021). Draft Environmental Impact Report For The Energy Source Mineral Atlis Project Imperial County, California [Environmental Impact Report].

Childress, A., Giammar, D., Jiang, S., Breckenridge, R., Howell, A., Macknick, J., Plata, S., Sedlak, D., & Stokes-Draut, J. (2021). *Power Sector Technology Roadmap*.

City of Brawley. (2015). *City of Brawley 2015 Urban Water Management Plan*. http://www.brawley-ca.gov/cms/kcfinder/upload/files/public_works/Brawley%202015%20UWMP%20Final%20Report.pdf

City of El Centro. (2020). 2020 Urban Water Management Plan. https://cityofelcentro.org/publicworks/wp-content/uploads/sites/6/2021/06/FINAL-DRAFT-2020-El-Centro-UWMP.pdf

Clark, C. E., Harto, C. B., Sullivan, J. L., & Wang, M. Q. (2011). *Water use in the development and operation of geothermal power plants*.

County of Imperial. (2022). *Hell's Kitchen PowerCo 1 and LithiumCo 1 Project*. https://files.ceqanet.opr.ca.gov/277330-1/attachment/umqX2ZYUYgPDPnQmJ1zkDyRyVLAng5T8MBZGSmrgzFDiB8GLtk0M8WcbNQvXIZ8U6A4g_EZEGzbWm6l_0

Dieter, C.A., Maupin, M.A., Caldwell, R.R., Harris, M.A., Ivahnenko, T.I., Lovelace, J.K., Barber, N.L., and Linsey, K.S., 2018, Estimated use of water in the United States in 2015: U.S. Geological Survey Circular 1441, 65 p., https://doi.org/10.3133/cir1441. [Supersedes USGS Open-File Report 2017–1131.]

Elmore North Geothermal LLC. (2023). *Elmore North Geothermal Project Application for Certification Volume 1*. https://efiling.energy.ca.gov/GetDocument.aspx?tn=249737&DocumentContentId=84377

Energy Source. (2012). Hudson Ranch Power II Geothermal Plant/Simbol Calipatria II Plant Project [EIR - Draft EIR].

Environmental Science Associates. (2022). *Salton Sea Monitoring Implementation Plan*. https://saltonsea.ca.gov/wp-content/uploads/2022/02/00_SaltonSeaMIP_508-Final.pdf

Flavelle, C. (2023). Biden Administration Proposes Evenly Cutting Water Allotments From Colorado River. *The New York Times*. https://www.nytimes.com/2023/04/11/climate/colorado-river-water-cuts-drought.html

Fogel, M., Nye, J. W., Ajami, H., Lyons, T. W., Bahreini, R., Porter, W., Aronson, E., Hung, C., McKibben, M. A., Raju, A. S., Elders, W., Lo, D. D., & Schwabe, K. (2021). *Crisis at the Salton Sea: Vital Role of Science*.

GEI Consultants Inc. (2012). *Imperial Integrated Regional Water Management Plan*. https://imperialirwmp.org/document-library-2/final-imperial-irwmp-volumes-1-2/

Hanak, E., Mount, J., Gray, B., Schwabe, K., Colby, B., Kenney, D., Bradley, T., Escriva-Bou, A., Jezdimirovic, J., & Fleck, J. (2018). *"Colorado River" Public Policy Institute of California (PPIC) Water Policy Center, November*. https://www.ppic.org/wp-content/uploads/californias-water-the-colorado-river-november-2018.pdf

IID (Imperial Irrigation District). (2023). *Water Rate Schedules*. https://www.iid.com/water/rules-and-regulations/water-rate-schedules

Jain, C. K., & Singh, R. D. (2012). Technological options for the removal of arsenic with special reference to South East Asia. *J Environ Manage*, *107*, 1-18. https://doi.org/10.1016/j.jenvman.2012.04.016

Kaspereit, D., Mann, M., Sanyal, S., Rickard, B., Osborn, W., & Hulen, J. (2016). *Updated Conceptual Model and Reserve Estimate for the Salton Sea Geothermal Field, Imperial Valley, California* GRC Annual Meeting, Sacramento, CA.

Kelly, J. C., Wang, M., Dai, Q., & Winjobi, O. (2021). Energy, greenhouse gas, and water life cycle analysis of lithium carbonate and lithium hydroxide monohydrate from brine and ore resources and their use in lithium ion battery cathodes and lithium ion batteries. *Resources, Conservation and Recycling*, *174*. https://doi.org/10.1016/j.resconrec.2021.105762

Kenny, J. F., Barber, N. L., Hutson, S. S., Linsey, K. S., Lovelace, J. K., & Maupin, M. A. (2009). *Estimated use of water in the United States in 2005: U.S. Geological Survey Circular 1344*.

Loeltz, O. J., Robison, J. H., & Omsted, F. H. (1975). Geohydrologic reconnaissance of the Imperial Valley, California.

MacKnick, J., Newmark, R., Heath, G., & Hallet, K. C. (2011). *A review of operational water consumption and withdrawal factors for electricity generating technologies*. https://www.nrel.gov/docs/fy11osti/50900.pdf

Marston, C., & Garska, M. (2022). Process for Selective Adsorption and Recovery of Lithium from Natural and Synthetic Brines (United States Patent No. (IS THIS MISSING A NUMBER?)

Maupin, M. A., Kenny, J. F., Hutson, S. S., Lovelace, J. K., Barber, N. L., & Linsey, K. S. (2014). *Estimated use of water in the United States in 2010: U.S. Geological Survey Circular 1405*. https://doi.org/https://dx.doi.org/10.3133/cir1405

Moran, B. J., Boutt, D. F., McKnight, S. V., Jenckes, J., Munk, L. A., Corkran, D., & Kirshen, A. (2022). Relic Groundwater and Prolonged Drought Confound Interpretations of Water Sustainability and Lithium Extraction in Arid Lands. *Earth's Future*, *10*(7). https://doi.org/10.1029/2021ef002555

Morton Bay Geothermal LLC. (2023). *Morton Bay Geothermal Project Application for Certification Volume 1*. https://efiling.energy.ca.gov/GetDocument.aspx?tn=249723&DocumentContentId=84361

NRC (National Research Council), (1999). Arsenic in Drinking Water. N. A. Press. Washington, DC, National Research Council.

OEHHA (Office of Environmental Health and Hazard Assessment), (2023). *Public Health Goals (PHGs)*. https://oehha.ca.gov/water/public-health-goals-phgs#:~:text=What%20Is%20a%20Public%20Health,PHGs%20are%20not%20regulatory%20standards.

Overpeck, J. T., & Udall, B. (2020). Climate change and the aridification of North America. *Proc Natl Acad Sci USA*, *117*(22), 11856-11858. https://doi.org/10.1073/pnas.2006323117

Partlow, J. (2023). As the Colorado River dries up, states can't agree on saving water. *The Washington Post*. https://www.washingtonpost.com/climate-environment/2023/01/31/colorado-river-states-water-cuts-agreement/

Paz, S. C., Kelley, R. E. V. C., Castaneda, S., Colwell, R., Dolega, R., Flores, M., Hanks, J. C., Lopez, A., Olmedo, L., Reynolds, A., Ruiz, F., Scott, M., Soto, T., & Weisgall, J. (2022). *Report of the Blue Ribbion Commission on Lithium Extraction in California*.

Robins, J. C., Kolker, A., Flores-Espino, F., Pettitt, W., Schmidt, B., Bekcers, K., Pauling, H., & Anderson, B. (2021). *2021 U.S. Geothermal Power Production and District Heating Market Report*.

Shields, T. (2022). In J. Stokes-Draut (Ed.).

Spang, E. S., Moomaw, W. R., Gallagher, K. S., Kirshen, P. H., & Marks, D. H. (2014). The water consumption of energy production: an international comparison. *Environmental Research Letters*, *9*(10). https://doi.org/10.1088/1748-9326/9/10/105002

SWRCB. (2018a). *Federal and State MCLs*. https://www.waterboards.ca.gov/drinking_water/certlic/drinkingwater/documents/ccr/mcls_epa_vs_dwp.pdf

SWRCB. (2018b). econdary Drinking Water Standards. https://www.waterboards.ca.gov/drinking_water/certlic/drinkingwater/documents/ddw_secondary_standards.pdf

SWRCB. (2020). *Groudwater Fact Sheet*. https://www.waterboards.ca.gov/publications_forms/publications/factsheets/docs/groundwater_fs.pdf

Tompson, A., Demir, Z., Moran, J., Mason, D., Wagoner, J., Mansoor, K., & McKereghan, P. (2008). *Groundwater Availability Within the Salton Sea Basin*. https://www.osti.gov/servlets/purl/932394

USBR (U.S. Bureau of Reclamation), (2023). *Near-term Colorado River Operations: Draft Supplemental Environmental Impact Statement*. https://www.usbr.gov/ColoradoRiverBasin/documents/NearTermColoradoRiverOperations/20230400-Near-termColoradoRiverOperations-DraftEIS-508.pdf

U.S. EPA. (2023a). *National Primary Drinking Water Regulations*. Retrieved 06/07/2023 from https://www.epa.gov/ground-water-and-drinking-water/national-primary-drinking-water-regulations

U.S. EPA. (2023b). *Secondary Drinking* Water *Standards: Guidance for Nuisance Chemicals*. Retrieved 06/07/2023 from https://www.epa.gov/sdwa/secondary-drinking-water-standards-guidance-nuisance-chemicals

USGS. (2015). *USGS Water Use Data for California*. Retrieved 2/28/2023 from https://waterdata.usgs.gov/ca/nwis/water_use?format=html_table&rdb_compression=file&wu_area=State+Total&wu_year=2015

USGS. (2018). *Health-Based Screening Levels for Evaluating Water-Quality Data*. Retrieved 04/05/2023 from https://water.usgs.gov/water-resources/hbsl/#:~:text=Health%2DBased%20Screening%20Levels%20(HBSLs,found%20in%20surface%2Dwater%20or

Vera, M. L., Torres, W. R., Galli, C. I., Chagnes, A., & Flexer, V. (2023). Environmental impact of direct lithium extraction from brines. *Nature Reviews Earth & Environment*, *4*(3), 149-165. https://doi.org/10.1038/s43017-022-00387-5

Vulcan Energy. (2021). Vulcan Energy Zero Carbon Lithium: Industry-leading Life Cycle Assessment results.

Werner, S. L., & Olson, L. J. (1970). Geothermal Wastes and the Water Resources of the Salton Sea Area.

Wietelmann, U., & Steinbild, M. (2014). In *Ullmann's Encyclopedia of Industrial Chemistry* (7th ed.). Wiley-VCH Verlag GmbH & Co. KGaA.

Chapter 8

Arnórsson, S. (1995). "Geothermal systems in Iceland: Structure and conceptual models—II. Low-temperature areas." Geothermics **24**(5-6): 603-629.

Bahreini, R., W. C. Porter and E. Aronson (2021). Particulate Matter, Pollutant Gases and Atmospheric Transport at the Salton Sea. Crisis at the Salton Sea: The Vital Role of Science, UC Riverside**:** 46-55.

Bayer, P., L. Rybach, P. Blum and R. Brauchler (2013). "Review on life cycle environmental effects of geothermal power generation." Renewable and Sustainable Energy Reviews **26**: 446-463.

Behera, S. N., R. Betha, P. Liu and R. Balasubramanian (2013). "A study of diurnal variations of PM2.5 acidity and related chemical species using a new thermodynamic equilibrium model." Sci Total Environ **452-453**: 286-295.

Bishop, H. K. and J. R. Bricarello (1978). "Scaling and Corrosion in an Experimental Geothermal Power Plant." Journal of Petroleum Technology **30**(09): 1240-1242.

Breuer, R., R. Eccles, T. Hunt, E. Mielke, R. Molnar and S. Shikaze (2021). Standard Lithium Ltd. SW Arkansas Lithium Project. Vancouver, BC, Canada, NORAM Engineering and Constructors Ltd.

CEC (California Energy Commission), (2021). "2021 Total System Electric Generation." from https://www.energy.ca.gov/data-reports/energy-almanac/california-electricity-data/2021-total-system-electric-generation.

CPUC (California Public Utilities Commission) (2021). DECISION REQUIRING PROCUREMENT TO ADDRESS MID-TERM RELIABILITY (2023-2026) Decision 21-06-035.

CARB. (2017). "2017 Estimated Annual Average Emissions: Salton Sea Air Basin." Emissions by Air Basin, from https://ww2.arb.ca.gov/applications/emissions-air-basin.

CARB, 2019: http://ww2.arb.ca.gov/sites/default/files/auction-proceeds/ccc_energycorps_userguide_101019.pdf

CARB. (2023a). "Ambient Air Quality Monitoring - Regulatory." 2023, from https://ww2.arb.ca.gov/our-work/programs/ambient-air-monitoring-regulatory.

CARB. (2023b). "Hydrogen Sulfide & Health." Retrieved May 10, 2023, 2023, from https://ww2.arb.ca.gov/resources/hydrogen-sulfide-and-health.

CARB. (2023c). "Standard Operating Procedures for Ambient Air Monitoring." 2023, from https://ww2.arb.ca.gov/resources/documents/standard-operating-procedures-ambient-air-monitoring.

CARB, Imperial County Air Pollution Control District and U.S. EPA. (2023). "Imperial Valley Air Quality." from http://www.imperialvalleyair.org/.

Chambers Group Inc. (2021). Draft Environmental Impact Report For The Energy Source Mineral Atlis Project Imperial County, California. San Diego, CA.

Chou, S., J. M. Ogden, H. R. Pohl, F. Scinicariello, L. Ingerman, L. Barber and M. Citra (2016). Toxicological profile for hydrogen sulfide and carbonyl sulfide, U.S. Department of Health and Human Services.

Collins, J. and D. Lewis (2000). Hydrogen Sulfide: Evaluation of Current California Air Quality Standards with Respect to Protection of Children, California Office of Environmental Health Hazard Assessment.

Elmore North Geothermal LLC (2023). Elmore North Geothermal Project Application for Certification Volume 1, BHER.

Ermak, D. L., R. A. Nyholm and P. H. Gudiksen (1980). "POTENTIAL AIR QUALITY IMPACTS OF LARGE-SCALE GEOTHERMAL ENERGY DEVELOPMENT IN THE IMPERIAL VALLEY." Atmospheric Environment **14**: 1321-1330.

ESMAP (2016). Greenhouse Gases from Geothermal Power Production: Interim Technical Note. Washington DC, USA, The World Bank.

Formation Environmental LLC. (2020). 2018/2019 Annual Report and PM10 Emissions Estimates. Salton Sea Emissions Monitoring Program, Imperial Irrigation District.

Gallup, D. L. (1992). 'Biox'- a new hydrogen sulfide abatement technology for the geothermal industry. Transactions - Geothermal Resources Council.

Gallup, D. L. (1996). `BIOX' hydrogen sulfide abatement process - application analysis. Transactions - Geothermal Resources Council.

Gallup, D. L. (1998). "Geochemistry of geothermal fluids and well scales, and potential for mineral recovery." Ore Geology Reviews **12**(4): 225-236.

Gill, J. S. and G. T. Jacobs (2018). "Cost effective technology to help geothermal power plants reduce hydrogen sulfide emissions by 98+%." GRC Transactions **42**: 1-6.

Gunnarsson, I., B. Sigfússon, A. Stefánsson, S. Arnórsson, S. W. Scott and E. Gunnlaugsson (2011). Injection of H2S from Hellisheiði power plant, Iceland. Thirty-Sixth Workshop on Geothermal Resevoir Engineering.

Hill, F. B. (1972). Atmospheric Sulfur and its Links with the Biosphere. Upton, NY, Brookhaven National Lab.

Hoyer, D., K. Kitz and D. Gallup (1991). "SALTON SEA UNIT 2: INNOVATIONS AND SUCCESSES." Geothermal Resources Council TRANSACTIONS **15**(October 1991).

IC-APCD (2017). IMPERIAL COUNTY 2017 STATE IMPLEMENTATION PLAN FOR THE 2008 8-HOUR OZONE STANDARD.

IC-APCD (2018). IMPERIAL COUNTY 2018 REDESIGNATION REQUEST AND MAINTENANCE PLAN FOR PARTICULATE MATTER LESS THAN 10 MICRONS IN DIAMETER (2018 PM10 PLAN). Imperial County.

IEA (2021). The Role of Critical Minerals in Clean Energy Transitions. 8th Annual Global Conference on Energy Efficiency.

Imperial County Department of Toxic Substance and Comité Cívico del Valle. (2023). "IVAN Imperial." 2023, from https://www.ivan-imperial.org/.

Kagel, A., D. Bates and K. Gawell (2005). Clearing the Air: Air Emissions from Geothermal Electric Power Facilities Compared to Fossil-Fuel Power Plants in the United States, GRC Bulletin.

Kaspereit, D., M. Mann, S. Sanyal, B. Rickard, W. Osborn and J. Hulen (2016). Updated Conceptual Model and Reserve Estimate for the Salton Sea Geothermal Field, Imperial Valley, California. GRC Annual Meeting. Sacramento, CA, GRC Transactions. **40**.

Matek, B. (2013). Promoting Geothermal Energy: Air Emissions Comparison and Externality Analysis. Washington, DC, Geothermal Energy Association.

Mazzini, A., H. Svensen, G. Etiope, N. Onderdonk and D. Banks (2011). "Fluid origin, gas fluxes and plumbing system in the sediment-hosted Salton Sea Geothermal System (California, USA)." Journal of Volcanology and Geothermal Research **205**(3-4): 67-83.

McKibben, M., J. Humphreys, M. Brounce, N. Planavsky and P. F. Dobson (2023). The Promise and Challenges of Geothermal Lithium, Lithium Resource Research and Innovation Center.

Muffler, L. P. and D. E. White (1968). "Origin of CO2 in the Salton Sea Geothermal System, Southeastern California, U.S.A.".

Reese, B. K., M. A. Anderson and C. Amrhein (2008). "Hydrogen sulfide production and volatilization in a polymictic eutrophic saline lake, Salton Sea, California." Sci Total Environ **406**(1-2): 205-218.

Robertson-Tait, A., W. Harvey, S. Hamm and L. Boyd (2021). The United States of America Country Update 2020 – Power Generation. Proceedings World Geothermal Congress 2020, Reykjavik, Iceland.

Robins, J. C., A. Kolker, F. Flores-Espino, W. Pettitt, B. Schmidt, K. Bekcers, H. Pauling and B. Anderson (2021). 2021 U.S. Geothermal Power Production and District Heating Market Report, NREL.

Rodríguez, E., W. S. Harvey and E. J. Ásbjörnsson (2014). Review of H_2S abatement methods in geothermal plants. Thirty-Eighth Workshop on Geothermal Reservoir Engineering, Stanford University, Stanford, CA.

Rodríguez, E., W. S. Harvey and E. J. Ásbjörnsson (2015). Review of H2S Abatement Methods in Geothermal Plants. Proceedings World Geothermal Congress 2015, Melbourne, Australia.

Roskill (2020). Roskill: CO2 emissions from lithium production set to triple by 2025.

S&P Global (2021). New lithium supply chains could slash sector emissions by nearly a third: Roskill.

Shukla, S. P. and M. Sharma (2010). "Neutralization of rainwater acidity at Kanpur, India." Tellus B: Chemical and Physical Meteorology **62**(3).

State of California. (2020). "Traffic Census Program | Caltrans." Retrieved 03/16/2023, 2023, from https://dot.ca.gov/programs/traffic-operations/census.

Svensen, H., D. A. Karlsen, A. Sturz, K. Backer-Owe, D. A. Banks and S. Planke (2007). "Processes controlling water and hydrocarbon composition in seeps from the Salton Sea geothermal system, California, USA." Geology **35**(1).

Tardiff, G. E. (1977). Using Salton Sea Geothermal Brines for Electrical Power: A Review of Progress in Chemistry and Materials Technology - 1976 Status, Lawrence Livermore Laboratory.

Tratt, D. M., S. J. Young, P. D. Johnson, K. N. Buckland and D. Lynch, K. (2016). Multi-year study of remotely-sensed ammonia emission from fumaroles in the Salton Sea Geothermal Field. 2016 8th Workshop on Hyperspectral Image and Signal Processing: Evolution in Remote Sensing (WHISPERS), IEEE**:** 1-5.

U.S. EPA (2012). Benzene

U.S. EPA (2001). Introduction to Stationary Point Source Emission Inventory Development. Emissions Inventory Improvement Program (EIIP). Eastern Research Group. **2.**

U.S. EPA. (2015a). "Emissions Inventory System (EIS) Gateway." from https://www.epa.gov/air-emissions-inventories/emissions-inventory-system-eis-gateway.

U.S. EPA. (2015b). "Regulatory Actions - Final Mercury and Air Toxics Standards (MATS) for Power Plants." Retrieved 3/31/2023, from https://www.epa.gov/mats/regulatory-actions-final-mercury-and-air-toxics-standards-mats-power-plants.

U.S. EPA (2016). Toxicological Review of Ammonia (Noncancer Inhalation): Executive Summary.

U.S. EPA (2017). 2017 National Emissions Inventory (NEI) Data.

U.S. EPA (2020). The Emissions & Generation Resource Integrated Database: eGRID Technical Guide with Year 2020 Data.

U.S. EPA. (2022, September 9, 2022). "Scope 1 and Scope 2 Inventory Guidance." EPA Center for Corporate Climate Leadership Retrieved June 28, 2023, from https://www.epa.gov/climateleadership/scope-1-and-scope-2-inventory-guidance.

Vulcan Energy. (2020). "Zero Carbon Lithium®." from https://v-er.com/wpcontent/uploads/2020/11/2020AGMPresentation.pdf.

Vulcan Energy (2021). Vulcan Energy Zero Carbon Lithium: Industry-leading Life Cycle Assessment results, Vulcan Energy.

WHO (2003). Hydrogen Sulfide: Human Health Aspects. Geneva.

Xue, J., A. K. H. Lau and J. Z. Yu (2011). "A study of acidity on PM2.5 in Hong Kong using online ionic chemical composition measurements." Atmospheric Environment **45**(39): 7081-7088.

Chapter 9

Baba, A., Demir, M. M., Koç, G. A., & Tuğcu, C. (2015). Hydrogeological properties of hyper-saline geothermal brine and application of inhibiting siliceous scale via pH modification. *Geothermics*, *53*, 406-412. https://doi.org/https://doi.org/10.1016/j.geothermics.2014.08.007

Barclays Official California Code of Regulations. (2015). *22 CA ADC § 66261.24 Characteristic of Toxicity*. Westlaw.com. https://govt.westlaw.com/calregs/Document/I8430AAA95B6111EC9451000D3A7C4BC3?viewType=FullText&originationContext=documenttoc&transitionType=CategoryPageItem&contextData=(sc.Default)

Besseling, E. (2018). *Lithium Recovery From Geothermal Brine CEC Workshop and Discussion,* (Docket Number: 17-GRDA-01). Geothermal Grant and Loan Program Workshops and Discussions). California Energy Comission. https://www.energy.ca.gov/data-reports/california-power-generation-and-power-sources/geothermal-energy/lithium-valley

Bhave, R. R., Harrison, S., Moyer, B. A., & Paranthaman, M. P. (2019). *Lithium extraction composite for recovery of lithium from brines, and process of using said composition* US Patent Application 2019/0275473 A1).

BHER Minerals. (2020). "Salton Sea Geothermal Lithium Recovery Demonstration Project." California Energy Commission Agreement EPC-019-020. https://www.energy.ca.gov/filebrowser/download/293

Bishop, H. K., & Bricarello, J. R. (1978). Scaling and Corrosion in an Experimental Geothermal Power Plant. *Journal of Petroleum Technology*, *30*(09), 1240-1242. https://doi.org/10.2118/6612-PA

BRG Consulting Inc. (2021). *Desert Valley Company Monofill Expansion Project, Cell 4, Draft Environmental Impact Report, vol. 1*. Prepared for: County of Imperial Planning & Development Services Dept.

Brown, K. (2013). Mineral scaling in geothermal power production, Report 39.

Burba, J. L., Stewart, R. F., Viani, B. E., Harrison, S., Vogdes, C. E., & Lahlouh, J. G. S. (2014). *Sorbent for lithium extraction (Patent 8,753,594)* US Patent 8,753,594).

Burrtec Waste Industries Inc. (2020). *Joint Technical Document (JTD), Salton City Solid Waste Site, Amended 8/20*. Prepared by: Geo-Logic Associates.

Burrtec Waste Industries Inc. (2022). *Joint Technical Document (JTD), Salton City Solid Waste Site, Amended 1/22*. Prepared by: Geo-Logic Associates.

CalGEM. (2023a). *GeoSteam - Search Geothermal Well Records, Production and Injection Data*. California Geologic Energy Management Division (CalGEM). https://geosteam.conservation.ca.gov/

CalGEM. (2023b). *WellFinder: CalGEM GIS*. California Geologic Energy Management Division (CalGEM). https://maps.conservation.ca.gov/doggr/wellfinder/#/

California DTSC. (2022). *Defining Hazardous Waste*. California Department of Toxic Substances Control,. Retrieved April 26 from

California DTSC. (2023a). *California Hazardous Waste Classification Training*. https://dtsc.ca.gov/california-hazardous-waste-classification-training/

California DTSC. (2023b). *Hazardous Waste Tracking System*. California Department of Toxic Substances Control (DTSC). https://hwts.dtsc.ca.gov/

California DTSC. (2023c). *Hazardous Waste Tracking System*. California Department of Toxic Substances Control. Retrieved April from https://hwts.dtsc.ca.gov/

California DTSC. (2023d). *Kettleman Hills Facility*. Retrieved April from https://dtsc.ca.gov/kettleman-hills-facility/

California RWQCB Colorado River Basin Region. (2013a). *Monitoring and Reporting Program R7-2013-0059 for John L. Featherstone Geothermal Power Plant*. California Regional Water Quality Control Board (RWQCB) Colorado River Basin Region.

California RWQCB Colorado River Basin Region. (2013c). *Waste Discharge Requirements for John L. Featherstone Geothermal Power Plant, Order R7-2013-0059*. California Regional Water Quality Control Board (RWQCB) Colorado River Basin Region.

California RWQCB Colorado River Basin Region. (2015a). *Monitoring and Reporting Program R7-2015-0020 for Leathers Power Plant*. California Regional Water Quality Control Board (RWQCB) Colorado River Basin Region.

California RWQCB Colorado River Basin Region. (2015b). *Waste Discharge Requirements for Leathers Power Plant, Order R7-2015-0020*. California Regional Water Quality Control Board (RWQCB) Colorado River Basin Region.

California RWQCB Colorado River Basin Region. (2016a). *Monitoring and Reporting Program R7-2016-0016 for Desert Valley Monofill Class II Solid Waste Management Facility*. California Regional Water Quality Control Board (RWQCB) Colorado River Basin Region.

California RWQCB Colorado River Basin Region. (2016b). *Waste Discharge Requirements For Desert Valley Monofill Class II Solid Waste Management Facility, Order R7-2016-0016*. California Regional Water Quality Control Board (RWQCB) Colorado River Basin Region.

California RWQCB Colorado River Basin Region. (2021a). *Monitoring and Reporting Program R7-2021-0008 for Region 1 Salton Sea Power Plant Units 1-5*. California Regional Water Quality Control Board (RWQCB) Colorado River Basin Region.

California RWQCB Colorado River Basin Region. (2021b). *Waste Discharge Requirements for Region 1 Salton Sea Power Plant Units 1-5, Order R7-2021-0008*. California Regional Water Quality Control Board (RWQCB) Colorado River Basin Region.

California RWQCB Colorado River Basin Region. (2022a). *Monitoring and Reporting Program R7-2022-0011 for "Region 2" Vulcan and Del Ranch (Hoch) Power Plants*. California Regional Water Quality Control Board (RWQCB) Colorado River Basin Region.

California RWQCB Colorado River Basin Region. (2022b). *Waste Discharge Requirements for "Region 2" Vulcan and Del Ranch (Hoch) Power Plants, Order R7-2022-0011*. California Regional Water Quality Control Board (RWQCB) Colorado River Basin Region.

California RWQCB Colorado River Basin Region. (2023a). *Monitoring and Reporting Program R7-2023-0011 for J.J. Elmore Geothermal Power Plant*. California Regional Water Quality Control Board (RWQCB) Colorado River Basin Region.

California RWQCB Colorado River Basin Region. (2023b). *Tentative - Waste Discharge Requirements for Hudson Ranch Power 1 LLC, Order R7-2023-0012*. California Regional Water Quality Control Board (RWQCB) Colorado River Basin Region.

California RWQCB Colorado River Basin Region. (2023c). *Waste Discharge Requirements for J.J. Elmore Geothermal Power Plant, Order R7-2023-0011*. California Regional Water Quality Control Board (RWQCB) Colorado River Basin Region.

California SWRCB. (2023). *GeoTracker*. California State Water Resources Control Board (SWRCB). https://geotracker.waterboards.ca.gov/

CalRecycle. (2023). *Solid Waste Information System (SWIS) Home*. Department of Resources Recycling and Recovery (CalRecycle). https://www2.calrecycle.ca.gov/SolidWaste/

CDC (California Department of Conservation), (2023). *Geothermal Resources*. California Department of Conservation. https://www.conservation.ca.gov/calgem/geothermal

CEC (California Energy Commission), (2019). *New Agreement # EPC-19-020: Salton Sea Geothermal Lithium Recovery Demonstration Project*. California Energy Comission. https://www.energy.ca.gov/filebrowser/download/293

CEC (California Energy Commission), (2023a). *Black Rock Geothermal Project (BRGP)*. https://www.energy.ca.gov/powerplant/steam-turbine/black-rock-geothermal-project-brgp

CEC (California Energy Commission), (2023b). *Elmore North Geothermal Project (ENGP)*. Retrieved June from https://www.energy.ca.gov/powerplant/steam-turbine/elmore-north-geothermal-project-engp

CEC (California Energy Commission), (2023c). *Morton Bay Geothermal Project (MBGP)*. https://www.energy.ca.gov/powerplant/steam-turbine/morton-bay-geothermal-project-mbgp

CEC (California Energy Commission), (2023d). *Sonoma Geothermal Project - Unit 3*. California Energy Comission. https://www.energy.ca.gov/powerplant/steam-turbine/sonoma-geothermal-project-unit-3

Chambers Group Inc. (2021). Draft Environmental Impact Report for the Energy Source Mineral ATLiS Project Imperial County, California.

Clarke, R. (2022). *TCLP, STLC, TTLC… What Does It All Mean?* Enthalpy Analytical. Retrieved April 26 from https://enthalpy.com/blog/tclp-stlc-ttlc-what-does-it-all-mean/

Controlled Thermal Resources. (2023). *Community & Environmental Information. Hell's Kitchen Lithium and Power, Imperial Valley, California*. Controlled Thermal Resources. https://www.cthermal.com/resources

County of Imperial Planning & Development Services Department. (2020). *Initial Study & Environmental Analysis For: Hell's Kitchen PowerCo 1 and LithiumCo 1 Project*. County of Imperial Planning & Development Services Department.

County of Imperial Planning & Development Services Department. (2022). *Initial Study & Environmental Analysis For: Hell's Kitchen PowerCo 1 and LithiumCo 1 Project*. County of Imperial Planning & Development Services Department. https://ceqanet.opr.ca.gov/2022030704

Desert Valley Company. (2014). Desert Valley Company Class II Solid Waste Management Facility, Quarterly Detection Monitoring Report for July-September 2014, Regional Board WDID No. 7A 13 2197 001, Board Order No. R7-2016-0016. https://documents.geotracker.waterboards.ca.gov/esi/uploads/geo_report/6932151556/L10003472657.PDF

Desert Valley Company. (2015a). Desert Valley Company Class II Solid Waste Management Facility, Quarterly Detection Monitoring Report for April-June 2015, Regional Board WDID No. 7A 13 2197 001, Board Order No. R7-2016-0016. https://documents.geotracker.waterboards.ca.gov/esi/uploads/geo_report/4305357515/L10003472657.PDF

Desert Valley Company. (2015b). Desert Valley Company Class II Solid Waste Management Facility, Quarterly Detection Monitoring Report for January-March 2015, Regional Board WDID No. 7A 13 2197 001, Board Order No. R7-2016-0016. https://documents.geotracker.waterboards.ca.gov/esi/uploads/geo_report/3587495923/L10003472657.PDF

Desert Valley Company. (2015c). Desert Valley Company Class II Solid Waste Management Facility, Quarterly Detection Monitoring Report for July-September 2015, Regional Board WDID No. 7A 13 2197 001, Board Order No. R7-2016-0016. https://documents.geotracker.waterboards.ca.gov/esi/uploads/geo_report/5388891637/L10003472657.PDF

Desert Valley Company. (2015d). Desert Valley Company Class II Solid Waste Management Facility, Quarterly Detection Monitoring Report for October-December 2014, Regional Board WDID No. 7A 13 2197 001, Board Order No. R7-2016-0016. https://documents.geotracker.waterboards.ca.gov/esi/uploads/geo_report/8728476822/L10003472657.PDF

Desert Valley Company. (2016a). Desert Valley Company Class II Solid Waste Management Facility, Quarterly Detection Monitoring Report for April- June 2016, Regional Board WDID No. 7A 13 2197 001, Board Order No. R7-2016-0016. https://documents.geotracker.waterboards.ca.gov/esi/uploads/geo_report/5895865082/L10003472657.PDF

Desert Valley Company. (2016b). Desert Valley Company Class II Solid Waste Management Facility, Quarterly Detection Monitoring Report for January-March 2016, Regional Board WDID No. 7A 13 2197 001, Board Order No. R7-2016-0016. https://documents.geotracker.waterboards.ca.gov/esi/uploads/geo_report/9308943331/L10003472657.PDF

Desert Valley Company. (2016c). Desert Valley Company Class II Solid Waste Management Facility, Quarterly Detection Monitoring Report for July- September 2016, Regional Board WDID No. 7A 13 2197 001, Board Order No. R7-2016-0016. https://documents.geotracker.waterboards.ca.gov/esi/uploads/geo_report/3399534761/L10003472657.PDF

Desert Valley Company. (2016d). Desert Valley Company Class II Solid Waste Management Facility, Quarterly Detection Monitoring Report for October-December 2015, Regional Board WDID No. 7A 13 2197 001, Board Order No. R7-2016-0016. https://documents.geotracker.waterboards.ca.gov/esi/uploads/geo_report/7828947603/L10003472657.PDF

Desert Valley Company. (2017a). Desert Valley Company Class II Solid Waste Management Facility, Quarterly Detection Monitoring Report for April- June 2017, Regional Board WDID No. 7A 13 2197 001, Board Order No. R7-2016-0016. https://documents.geotracker.waterboards.ca.gov/esi/uploads/geo_report/1832708954/L10003472657.PDF

Desert Valley Company. (2017b). Desert Valley Company Class II Solid Waste Management Facility, Quarterly Detection Monitoring Report for January-March 2017, Regional Board WDID No. 7A 13 2197 001, Board Order No. R7-2016-0016. https://documents.geotracker.waterboards.ca.gov/esi/uploads/geo_report/9636483967/L10003472657.PDF

Desert Valley Company. (2017c). Desert Valley Company Class II Solid Waste Management Facility, Quarterly Detection Monitoring Report for July- September 2017, Regional Board WDID No. 7A 13 2197 001, Board Order No. R7-2016-0016. https://documents.geotracker.waterboards.ca.gov/esi/uploads/geo_report/5552170038/L10003472657.PDF

Desert Valley Company. (2017d). Desert Valley Company Class II Solid Waste Management Facility, Quarterly Detection Monitoring Report for October- December 2016, Regional Board WDID No. 7A 13 2197 001, Board Order No. R7-2016-0016. https://documents.geotracker.waterboards.ca.gov/esi/uploads/geo_report/9736106574/L10003472657.PDF

Desert Valley Company. (2018a). *2017 Annual Compliance Report for Desert Valley Company Monofill, Conditional Use Permit #05-0020*. https://documents.geotracker.waterboards.ca.gov/esi/uploads/geo_report/5091073095/L10003472657.PDF

Desert Valley Company. (2018b). Desert Valley Company Class II Solid Waste Management Facility, Quarterly Detection Monitoring Report for April- June 2018, Regional Board WDID No. 7A 13 2197 001, Board Order No. R7-2016-0016. https://documents.geotracker.waterboards.ca.gov/esi/uploads/geo_report/1415350794/L10003472657.PDF

Desert Valley Company. (2018c). Desert Valley Company Class II Solid Waste Management Facility, Quarterly Detection Monitoring Report for January-March 2018, Regional Board WDID No. 7A 13 2197 001, Board Order No. R7-2016-0016. https://documents.geotracker.waterboards.ca.gov/esi/uploads/geo_report/6313669025/L10003472657.PDF

Desert Valley Company. (2018d). Desert Valley Company Class II Solid Waste Management Facility, Quarterly Detection Monitoring Report for July - September 2018, Regional Board WDID No. 7A 13 2197 001, Board Order No. R7-2016-0016. https://documents.geotracker.waterboards.ca.gov/esi/uploads/geo_report/7970315039/L10003472657.PDF

Desert Valley Company. (2018e). Desert Valley Company Class II Solid Waste Management Facility, Quarterly Detection Monitoring Report for October- December 2017, Regional Board WDID No. 7A 13 2197 001, Board Order No. R7-2016-0016. https://documents.geotracker.waterboards.ca.gov/esi/uploads/geo_report/8995093226/L10003472657.PDF

Desert Valley Company. (2019a). *2018 Annual Compliance Report for Desert Valley Company Monofill, Conditional Use Permit #05-0020*. https://documents.geotracker.waterboards.ca.gov/regulators/deliverable_documents/9911904454/2018%20DVC%20CUP%20Annual%20Compliance%20Report%2005-0020.pdf

Desert Valley Company. (2019b). Desert Valley Company Class II Solid Waste Management Facility, Quarterly Detection Monitoring Report for July - Sept 2019, Regional Board WDID No. 7A 13 2197 001, Board Order No. R7-2016-0016. https://documents.geotracker.waterboards.ca.gov/esi/uploads/geo_report/6318605899/L10003472657.PDF

Desert Valley Company. (2019c). Desert Valley Company Class II Solid Waste Management Facility, Quarterly Detection Monitoring Report for October - December 2018, Regional Board WDID No. 7A 13 2197 001, Board Order No. R7-2016-0016. https://documents.geotracker.waterboards.ca.gov/esi/uploads/geo_report/1286124110/L10003472657.PDF

Desert Valley Company. (2019d). Revised Desert Valley Company Class II Solid Waste Management, Facility Quarterly Detection Monitoring Report for Apr - June 2019, Regional Board WDID No. 7A 13 2197 001, Board Order No. R7-2016-0016. https://documents.geotracker.waterboards.ca.gov/esi/uploads/geo_report/6940924525/L10003472657.PDF

Desert Valley Company. (2019e). Revised Desert Valley Company Class II Solid Waste Management, Facility Quarterly Detection Monitoring Report for Jan - Mar 2019, Regional Board WDID No. 7A 13 2197 001, Board Order No. R7-2016-0016. https://documents.geotracker.waterboards.ca.gov/esi/uploads/geo_report/4049123942/L10003472657.PDF

Desert Valley Company. (2020a). *2019 Annual Compliance Report for Desert Valley Company Monofill, Conditional Use Permit #05-0020*. https://documents.geotracker.waterboards.ca.gov/regulators/deliverable_documents/7749005973/2019%20DVC%20Annual%20Compliance%20Report%20CUP%2005-0020.pdf

Desert Valley Company. (2020b). Desert Valley Company Class II Solid Waste Management Facility, Quarterly Detection Monitoring Report for April - June 2020, Regional Board WDID No. 7A 13 2197 001, Board Order No. R7-2016-0016. https://documents.geotracker.waterboards.ca.gov/esi/uploads/geo_report/6440548241/L10003472657.PDF

Desert Valley Company. (2020c). Desert Valley Company Class II Solid Waste Management Facility, Quarterly Detection Monitoring Report for January - March 2020, Regional Board WDID No. 7A 13 2197 001, Board Order No. R7-2016-0016. https://documents.geotracker.waterboards.ca.gov/esi/uploads/geo_report/4189280629/L10003472657.PDF

Desert Valley Company. (2020d). Desert Valley Company Class II Solid Waste Management Facility, Quarterly Detection Monitoring Report for July - September 2020, Regional Board WDID No. 7A 13 2197 001, Board Order No. R7-2016-0016. https://documents.geotracker.waterboards.ca.gov/esi/uploads/geo_report/1297890424/L10003472657.PDF

Desert Valley Company. (2020e). Desert Valley Company Class II Solid Waste Management Facility, Quarterly Detection Monitoring Report for October - December 2019, Regional Board WDID No. 7A 13 2197 001, Board Order No. R7-2016-0016. https://documents.geotracker.waterboards.ca.gov/esi/uploads/geo_report/7536520838/L10003472657.PDF

Desert Valley Company. (2021a). *2020 Annual Compliance Report for Desert Valley Company Monofill, Conditional Use Permit #05-0020*. https://documents.geotracker.waterboards.ca.gov/regulators/deliverable_documents/7353910148/2020%20DVC%20CUP%20Annual%20Compliance%20Report%2005%20-0020%20Finalred_asrev.pdf

Desert Valley Company. (2021b). Desert Valley Company Class II Solid Waste Management Facility, Quarterly Detection Monitoring Report for April - June 2021, Regional Board WDID No. 7A 13 2197 001, Board Order No. R7-2016-0016. https://documents.geotracker.waterboards.ca.gov/esi/uploads/geo_report/2977108299/L10003472657.PDF

Desert Valley Company. (2021c). Desert Valley Company Class II Solid Waste Management Facility, Quarterly Detection Monitoring Report for January - March 2021, Regional Board WDID No. 7A 13 2197 001, Board Order No. R7-2016-0016. https://documents.geotracker.waterboards.ca.gov/esi/uploads/geo_report/4749398291/L10003472657.PDF

Desert Valley Company. (2021d). Desert Valley Company Class II Solid Waste Management Facility, Quarterly Detection Monitoring Report for July - September 2021, Regional Board WDID No. 7A 13 2197 001, Board Order No. R7-2016-0016. https://documents.geotracker.waterboards.ca.gov/esi/uploads/geo_report/1454646229/L10003472657.PDF

Desert Valley Company. (2021e). Desert Valley Company Class II Solid Waste Management Facility, Quarterly Detection Monitoring Report for October - December 2020, Regional Board WDID No. 7A 13 2197 001, Board Order No. R7-2016-0016. https://documents.geotracker.waterboards.ca.gov/esi/uploads/geo_report/9111377179/L10003472657.PDF

Desert Valley Company. (2022a). *2021 Annual Compliance Report for Desert Valley Company Monofill, Conditional Use Permit #05-0020*. https://documents.geotracker.waterboards.ca.gov/regulators/deliverable_documents/7617032706/2021%20DVC%20CUP%20Annual%20Compliance%20Report%2005%20-0020.pdf

Desert Valley Company. (2022b). Desert Valley Company Class II Solid Waste Management Facility, Quarterly Detection Monitoring Report for October - December 2021, Regional Board WDID No. 7A 13 2197 001, Board Order No. R7-2016-0016. https://documents.geotracker.waterboards.ca.gov/esi/uploads/geo_report/3746813774/L10003472657.PDF

Ecolab USA Inc. (2018). *Unique technology helps geothermal power plant reduce hydrogen sulfide emissions by 98+%. CASE STUDY - POWER. CH-1889*. https://www.ecolab.com/-/media/Widen/Nalco-Water/Power-Generation/CH1889Uniquetechnologyhelpsgeothermalpowerplantreducehydrogensulfideemissionsby98percentpdf.pdf

Eggleton, R. A., & Tilley, D. B. (1998). Hisingerite: A Ferric Kaolin Mineral with Curved Morphology. *Clays and Clay Minerals*, *46*(4), 400-413. https://doi.org/10.1346/CCMN.1998.0460404

Energy Information Agency. (2023). *California State Profile and Energy Estimates*. U.S. Department of Energy. Retrieved June from https://www.eia.gov/state/analysis.php?sid=CA

EnergySource. (2012). *Hudson Ranch/Simbol II FEIR Final Environmental Impact Report*. I. C. P. D. Services. https://www.icpds.com/planning/environmental-impact-reports/final-eirs/hudson-ranch-simbol-ii-feir

EnergySource Minerals. (2020). *Technology: ILiAD*. Retrieved 4 August from https://www.esminerals.com/

EnergySource Minerals. (2021). *Project ATLiS*. EnergySource Moinerals. Retrieved 4 August from https://www.esminerals.com/project

Eramet. (2021). *EuGeLi Project: Extracting European Lithium for Future Electric Vehicle Batteries*. Retrieved 10 September from: https://www.eramet.com/en/activities/innovate-design/eugeli-project

Ermak, D. L., Nyholm, R. A., & Gudiksen, P. H. (1980). Potential air-quality impacts of large-scale geothermal-energy development in the Imperial Valley [Article]. *Atmospheric Environment*, *14*(11), 1321-1330. https://doi.org/10.1016/0004-6981(80)90233-4

Featherstone, J., Butler, S., & Bonham, E. (1995). Comparison of crystallizer reactor clarifier and pH MOD process technologies used at the Salton Sea Geothermal Field. World Geothermal Congress, Salton Sea, CA.

Featherstone, J. L., Hanson, P. J., Garska, M. J., & Marston, C. R. (2019). *System and process for recovery of lithium from a geothermal brine (application)* US 2019/0248667 A1).

Featherstone, J. L., Van Note, R. H., Pawlowski, B. S. (1979). A cost effective treatment system for the stabilization of spent geothermal brines. *Geothermal Resources Council TRANSACTIONS*, *3*, 201-204.

Finster, M., Clark, C., Schroeder, J., & Martino, L. (2015). Geothermal produced fluids: Characteristics, treatment technologies, and management options. *Renewable and Sustainable Energy Reviews*, *50*, 952-966. https://doi.org/https://doi.org/10.1016/j.rser.2015.05.059

Gallup, D. L. (1989). Iron silicate scale formation and inhibition at the salton sea geothermal field. *Geothermics*, *18*(1), 97-103. https://doi.org/https://doi.org/10.1016/0375-6505(89)90015-1

Gallup, D. L. (1992). BIOX - a new hydrogen sulfide abatement technology for the geothermal industry. *Geothermal Resources Council TRANSACTIONS*, *16*(October), 591-596. https://www.scopus.com/inward/record.uri?eid=2-s2.0-0026998125&partnerID=40&md5=74385430de5e7677be7a3e03f26f86e2

Gallup, D. L. (1996a). BIOX hydrogen sulfide abatement process - application analysis. *Geothermal Resources Council TRANSACTIONS*, *20*, 11-17. https://doi.org/Conference: Annual meeting of the Geothermal Resources Council, Portland, OR (United States), 29 Sep - 2 Oct 1996; Other Information: PBD: 1996; Related Information: Is Part Of Geothermal development in the Pacific rim. Transactions, Volume 20; PB: 886 p.

Gallup, D. L. (1996b). Brine pH modification scale control technology. *Geothermal Resources Council Transactions*, *20*, 749-755.

Gallup, D. L. (1998). Geochemistry of geothermal fluids and well scales, and potential for mineral recovery. *Ore Geology Reviews*, *12*(4), 225-236. https://doi.org/https://doi.org/10.1016/S0169-1368(98)00004-3

Gallup, D. L. (2002). Investigations of organic inhibitors for silica scale control in geothermal brines. *Geothermics*, *31*(4), 415-430. https://doi.org/https://doi.org/10.1016/S0375-6505(02)00004-4

Gallup, D. L. (2009). Production engineering in geothermal technology: A review. *Geothermics*, *38*(3), 326-334. https://doi.org/https://doi.org/10.1016/j.geothermics.2009.03.001

Gallup, D. L. (2011, May 25-27). pH modification scale control technology. International Workshop on Mineral Scaling, Manila, Philippines.

Gallup, D. L., & Featherstone, J. L. (1995). Control of NORM deposition from Salton Sea geothermal brines. *Geothermal Science & Technology*, *4*(4), 215-226.

Geo-Logic Associates. (2021). Final Design Report Phase 2A Cell Construction, Salton City Solid Waste Site, Imperial County, California. https://documents.geotracker.waterboards.ca.gov/regulators/deliverable_documents/2933698356/Salton%20City%20Phase%202A%20Design%20Report_FINAL_081321%20W-APPENDICES.pdf

Gill, J. S., & Jacobs, G. T. (2018). Cost effective technology to help geothermal power plants reduce hydrogen sulfide emissions by 98+%. *GRC Transactions*, *42*, 1-6. https://www.geothermal-library.org/index.php?mode=pubs&action=view&record=1033956

Gritters, G. A., Dunes, B., Featherstone, J. L., & Reverente, J. P. (1988). *Process for treating geothermal brine in two phase brine separators* (U.S. Patent No. 4,776,961).

Harrar, J. E., Otto, J., C. H., Deutscher, S. B., Ryon, R. W., & Tardiff, G. E. (1979a). Studies of brine chemistry, precipitation of solids, and scale formation at the Salton Sea geothermal field (UCRL-52640) (UCRL-52640).

Harrar, J. E., Otto, J., C. H., Deutscher, S. B., Ryon, R. W., & Tardiff, G. E. (1979b). Studies of brine chemistry, precipitation of solids, and scale formation at the Salton Sea geothermal field, UCRL 52640.

Hell's Kitchen Power Co. (2021). *Hell's Kitchen Power Co 1 Project and Hell's Kitchen Lithium Co 1 Project-Conditional Use Permit Applications*. Imperial County Planning & Development Services. https://www.icpds.com/assets/CUP21-0020-RFP-EIR-WEB-12-17-21.pdf

Hoyer, D., Kitz, K., & Gallup, D. (1991). Salton Sea Unit 2: innovation and successes. *Geothermal Resources Council TRANSACTIONS*, *15*.

Iranpour, R., Coxa, H. H. J., Deshusses, M. A., & Schroeder, E. D. (2005). Literature review of air pollution control biofilters and biotrickling filters for odor and volatile organic compound removal [Review]. *Environmental Progress*, *24*(3), 254-267. https://doi.org/10.1002/ep.10077

Jacobs, G., Castanieto, H., Butler, S. J., & Featherstone, J. L. (2017). *Hydrogen sulfide abatement in geothermal facilities* (US Patent No. 9828264). https://patents.google.com/patent/US9828264B2/en

Jamero, J., Zarrouk, S. J., & Mroczek, E. (2018). Mineral scaling in two-phase geothermal pipelines: Two case studies [Article]. *Geothermics*, *72*, 1-14. https://doi.org/10.1016/j.geothermics.2017.10.015

Jost, J. W., & Gallup, D. L. (1985). *Inhibiting scale precipitation from high temperature brine* (U.S. Patent No. 4,500,434).

Kaspereit, D., Mann, M., Sanyal, S., Rickard, B., Osborn, W., & Hulen, J. (2016). Updated conceptual model and reserve estimate for the Salton Sea Geothermal Field, Imperial Valley, California. *Geothermal Research Council (GRC) Transactions*, *40*(1), 57-66.

Lue, A. (2015, Sept. 6). *CalEnergy, Approval Requested for Use of Bromine Oxidant in Fresh Water System*. CalEnergy Operating Corporation. https://geotracker.waterboards.ca.gov/esi/uploads/geo_report/4331651210/T10000006248.PDF

Lue, A. (2016, Jan. 2). *CalEnergy, Approval Requested for Nalco Replacement Water Treatment Products*. CalEnergy Operating Corporation. https://geotracker.waterboards.ca.gov/esi/uploads/geo_report/5479041755/T10000006248.PDF

Lue, A. (2018, Jan. 19). *CalEnergy, Chemical Approval Request*. CalEnergy Operating Corporation. https://geotracker.waterboards.ca.gov/esi/uploads/geo_report/8093866705/T10000006248.PDF

Lue, A. (2019a, Jul. 2). CalEnergy Power Plants, Approval Requested for ChemTreat water treatment products ChemTreat GS5810, ChemTreat CT788, ChemTreat CL456, ChemTreat 4822, ChemTreat 5832 and ChemTreat CT709. CalEnergy Operating Corporation. https://geotracker.waterboards.ca.gov/regulators/deliverable_documents/3011391758/Chem%20treat%20State%20Water%20Board%20Request_7-2-2019.pdf

Lue, A. (2019b, Oct. 19). *CalEnergy Power Plants, Approval Requested for Nalco GEO 912*. CalEnergy Operating Corporation. https://geotracker.waterboards.ca.gov/esi/uploads/geo_report/5220385074/L10003292609.PDF

Lue, A. (2019c, Dec. 20). *CalEnergy Power Plant, Approval Requested for ChemTreat Water Treatment Product CL2065 and CL2155*. CalEnergy Operating Corporation. https://geotracker.waterboards.ca.gov/esi/uploads/geo_report/6598994374/T10000006248.PDF

Lue, A. (2020, Feb. 14). CalEnergy Power Plants, Approval Requested for ChemTreat Product CL453, CL2115, CL2150, CL2250, CL4520, CL1495, CL5788, CT790, P8000L, and Sodium Hydroxide (54%) and Hydrogen Peroxide (20 - <35%). CalEnergy Operating Corporation. https://geotracker.waterboards.ca.gov/esi/uploads/geo_report/5236415028/T10000006248.PDF

Maimoni, A. (1982). Minerals recovery from salton-sea geothermal brines - a literature-review and proposed cementation process. *Geothermics*, *11*(4), 239-258. https://doi.org/10.1016/0375-6505(82)90031-1

Materials Research LLC. (2020). *Pilot Scale Recovery of Lithium from Geothermal Brines*. C. E. Comission. https://www.energy.ca.gov/filebrowser/download/296

MidAmerican Energy Holding Co. (2003). *Mineral Recovery from Geothermal Brine, Final Report (GEO-99-001)* (GEO-99-001 Final Report). C. E. Commission.

Morris, W. F., & Stephens, F. B. (1981). *Characterization of Geothermal Solid Wastes*.

Nagl, G. J. (1999). Controlling H2S emissions in geothermal power plants. *Bulletin d'Hydrogeologie*, *17*, 393-402.

Nalco-Ecolab. (2018). *Unique technology helps geothermal power plant reduce hydrogen sulfide emissions by 98+%. Case Study - Power CH-1889*. https://www.ecolab.com/-/media/Widen/Nalco-Water/Power-Generation/CH1889Uniquetechnologyhelpsgeothermalpowerplantreducehydrogensulfideemissionsby98percentpdf.pdf

Nardini, G., Paglianti, A., & Petarca, L. (1995). An analysis on the BIOX process to hydrogen sulfide abatement. *Geothermal Resources Council TRANSACTIONS*, *19*(October), 457 - 461.

Pambudi, N. A., Itoi, R., Yamashiro, R., Css Syah Alam, B. Y., Tusara, L., Jalilinasrabady, S., & Khasani, J. (2015). The behavior of silica in geothermal brine from Dieng geothermal power plant, Indonesia [Article]. *Geothermics*, *54*, 109-114. https://doi.org/10.1016/j.geothermics.2014.12.003

Pardelli, P. T., Tempesti, C., Mannelli, A., Kravos, A., Sabard, A., Fanicchia, F., Paul, S., Şengun, R., Sahiller, H. A., Halaçoğlu, U., Pekdüz, I., Stefansson, A., & Galeczka, I. M. (2021). Design of a scaling reduction system for geothermal applications. *E3S Web Conf.*, *238*, 01014. https://doi.org/10.1051/e3sconf/202123801014

Paz, S., Kelley, R. E., Castaneda, S., Colwell, R., Dolega, R., Flores, M., Hanks, J. C., Lopez, A., Olmedo, L., Reynolds, A., Ruiz, F., Scott, M., Soto, T., & Weisgall, J. (2022). *Report of the Blue Ribbon Commission on Lithium Extraction in California. California Energy Commission. Publication Number: CEC-300-2022-009-F*. C. E. Commission.

Pudi, A., Rezaei, M., Signorini, V., Andersson, M. P., Baschetti, M. G., & Mansouri, S. S. (2022). Hydrogen sulfide capture and removal technologies: A comprehensive review of recent developments and emerging trends. *Separation and Purification Technology*, *298*, 121448. https://doi.org/https://doi.org/10.1016/j.seppur.2022.121448

Rasmussen, P. (2020, May 26). *Approval to Use ChemTreat Water Treatment Products, CalEnergy Calipatria, Imperial County*. Colorado River Basin Water Quality Control Board. https://geotracker.waterboards.ca.gov/view_document?docurl=/regulators/deliverable_documents/2882611930/5%2E26%2E2020%5FCalEnergy%5FChemtreat%20Approval%5Fzo%2Epdf

Rodríguez, E., Harvey, W. S., & Ásbjörnsson, E. J. (2014, February 24-26, 2014). Review of H_2S abatement methods in geothermal plants. Thirty-Eighth Workshop on Geothermal Reservoir Engineering, Stanford University, Stanford, CA.

RWQCB. (2015). *Waste Discharge Requirements for Leathers Power Plant, Order R7-2015-0020*. California Regional Water Quality Control Board (RWQCB) Colorado River Basin Region.

RWQCB. (2021). *Waste Discharge Requirements for Region 1 Salton Sea Power Plant Units 1-5, Order R7-2021-0008*. California Regional Water Quality Control Board (RWQCB) Colorado River Basin Region.

RWQCB. (2022). Waste Discharge Requirements for "Region 2" Vulcan and Del Ranch (Hoch) Power Plants, Order R7-2022-0011. California Regional Water Quality Control Board (RWQCB) Colorado River Basin Region.

RWQCB. (2023a). *Tentative - Waste Discharge Requirements for Hudson Ranch Power 1 LLC, Order R7-2023-0012*. California Regional Water Quality Control Board (RWQCB) Colorado River Basin Region.

RWQCB. (2023b). *Waste Discharge Requirements for J.J. Elmore Geothermal Power Plant, Order R7-2023-0011*. California Regional Water Quality Control Board (RWQCB) Colorado River Basin Region.

Sanopoulos, D., & Karabelas, A. (1997). H2S abatement in geothermal plants: Evaluation of process alternatives. *Energy Sources*, *19*(1), 63-77. https://doi.org/10.1080/00908319708908833

Schiavon, M., Ragazzi, M., Rada, E. C., & Torretta, V. (2016). Air pollution control through biotrickling filters: a review considering operational aspects and expected performance [Review]. *Critical Reviews in Biotechnology*, *36*(6), 1143-1155. https://doi.org/10.3109/07388551.2015.1100586

Schultze, L., & Bauer, D. (1982a). Operation of a Mineral Recovery Unit on Brine From the Salton Sea Known Geothermal Resourze Area (RI 8680) (RI 8880). U. B. o. M. U.S. Department of the Interior.

Schultze, L. E., & Bauer, D. J. (1982b). Comparison of lime and sulfide precipitation of metal values from geothermal brine. *Abstracts of Papers of the American Chemical Society*, *183*(MAR), 104-INDE.

SCS Engineers. (2022). *Title V Permit Renewal Application for the Copper Mountain Landfill*. https://static.azdeq.gov/pn/aq_coppermtn_app.pdf

Sizemore, T. (2023). Personal communication May 16th. In.

Stringfellow, W. T., & Dobson, P. F. (2021). Technology for the Recovery of Lithium from Geothermal Brines. *Energies*, *14*, 6805. https://doi.org/https://doi.org/10.3390/en14206805

U.S. Department of the Interior. (2018). *Final List of Critical Minerals 2018, 83 Fed. Reg. 23295*. https://www.federalregister.gov/documents/2018/05/18/2018-10667/final-list-of-critical-minerals-2018

U.S. EIA. (2023). *U.S. Energy Information Administration (EIA)*. U.S. Energy Information Administration (EIA). https://www.eia.gov/

U.S. EPA (Environmental Protection Agency), (2000). *Soil Screening Guidance for Radionuclides: User's Guide, EPA/540-R-00-007*. Office of Radiation and Indoor Air / Office of Solid Waste and Emergency Response. https://semspub.epa.gov/work/HQ/175428.pdf

U.S. EPA (Environmental Protection Agency) (2023a). *Basic Information about Landfills*. https://www.epa.gov/landfills/basic-information-about-landfills

U.S. EPA (Environmental Protection Agency), (2023b). *Resource Conservation and Recovery Act (RCRA) Laws and Regulations*. U.S. Environmental Protection Agency,. https://www.epa.gov/rcra

von Hirtz, P. (2016). Chapter 16 - Silica scale control in geothermal plants—historical perspective and current technology. In R. DiPippo (Ed.), *Geothermal Power Generation* (pp. 443-476). Woodhead Publishing. https://doi.org/https://doi.org/10.1016/B978-0-08-100337-4.00016-4

Warren, I. (2021). Techno-Economic Analysis of Lithium Extraction from Geothermal Brines. NREL/TP-5700-79178. N. R. E. Laboratory. https://www.nrel.gov/docs/fy21osti/799178.pdf

Zarrouk, S. J., & Purnanto, M. H. (2015). Geothermal steam-water separators: Design overview. *Geothermics*, *53*, 236-254.

Zukin, J. G., Hammond, D. E., Teh-Lung, K., & Elders, W. A. (1987). Uranium-thorium series radionuclides in brines and reservoir rocks from two deep geothermal boreholes in the Salton Sea Geothermal Field, southeastern California. Geochimica Et Cosmochimica Acta, 51(10), 2719-2731.

Chapter 10

Brodsky, E. E. & Lajoie, L. J. Anthropogenic Seismicity Rates and Operational Parameters at the Salton Sea Geothermal Field. Science 341, 543–546 (2013).

Brown, R. L., Durbin, J. & Evans, J. M. Techniques for Testing the Constancy of Regression Relationships Over Time. Journal of the Royal Statistical Society: Series B (Methodological) 37, 149–163 (1975).

Cleveland, R. B., Cleveland, W. S., McRae, J. E. & Terpenning, I. STL: A Seasonal-Trend Decompostion Procedure Based on Loess. Journal of Official Statistics 6, 3–73 (1990).

Galis, M., Ampuero, J. P., Mai, P. M. & Cappa, F. Induced seismicity provides insight into why earthquake ruptures stop. Science Advances 3, eaap7528 (2017).

Gutenberg, B., C. F. Richter; Frequency of earthquakes in California. Bulletin of the Seismological Society of America 1944; 34 (4): 185–188. doi: https://doi.org/10.1785/BSSA0340040185

Hauksson, E., Stock, J. M. & Husker, A. L. Seismicity in a weak crust: the transtensional tectonics of the Brawley Seismic Zone section of the Pacific–North America Plate Boundary in Southern California, USA. Geophysical Journal International 231, 717–735 (2022).

Hauksson, E., Yang, W. & Shearer, P. M. Waveform Relocated Earthquake Catalog for Southern California (1981 to June 2011) Short Note. Bulletin of the Seismological Society of America 102, 2239–2244 (2012).

Hutton, K., Woessner, J. & Hauksson, E. Earthquake Monitoring in Southern California for Seventy-Seven Years (1932–2008). Bulletin of the Seismological Society of America 100, 423–446 (2010).

Ikari, M. J., Saffer, D. M. & Marone, C. Frictional and hydrologic properties of clay-rich fault gouge. Journal of Geophysical Research: Solid Earth 114 (2009).

Lohman, R. B. & McGuire, J. J. Earthquake swarms driven by aseismic creep in the Salton Trough, California. Journal of Geophysical Research: Solid Earth (1978–2012) 112 (2007).

Martínez-Garzón, P., Zaliapin, I., Ben-Zion, Y., Kwiatek, G. & Bohnhoff, M. Comparative Study of Earthquake Clustering in Relation to Hydraulic Activities at Geothermal Fields in California. Journal of Geophysical Research: Solid Earth 123, 4041–4062 (2018).

McGarr, A. Maximum magnitude earthquakes induced by fluid injection. Journal of Geophysical Research: Solid Earth 119, 1008–1019 (2014).

Morrow, C. A., Shi, L. Q. & Byerlee, J. D. Permeability of fault gouge under confining pressure and shear stress. Journal of Geophysical Research: Solid Earth 89, 3193–3200 (1984).

Ogata, Y. Statistical Models for Earthquake Occurrences and Residual Analysis for Point Processes. Journal of the American Statistical Association 83, 9–27 (1988).

Trugman, D. T., Shearer, P. M., Borsa, A. A. & Fialko, Y. A comparison of long-term changes in seismicity at The Geysers, Salton Sea, and Coso geothermal fields. Journal of Geophysical Research: Solid Earth 121, 225–247 (2016).

van der Elst, N. J., Page, M. T., Weiser, D. A., Goebel, T. H. & Hosseini, S. M. Induced earthquake magnitudes are as large as (statistically) expected. Journal of Geophysical Research: Solid Earth 121, 4575–4590 (2016).

White, M. C. A., Ben-Zion, Y. & Vernon, F. L. A Detailed Earthquake Catalog for the San Jacinto Fault-Zone Region in Southern California. Journal of Geophysical Research: Solid Earth 124, 6908–6930 (2019).

Zaliapin, I. & Ben-Zion, Y. Earthquake Declustering Using the Nearest-Neighbor Approach in Space-Time-Magnitude Domain. Journal of Geophysical Research: Solid Earth 125 (2020).

Chapter 11

Bielak, A. T., Campbell, A., Pope, S., Schaefer, K., & Shaxson, L. (2008). From Science Communication to Knowledge Brokering: the Shift from 'Science Push' to 'Policy Pull.' In D. Cheng, M. Claessens, T. Gascoigne, J. Metcalfe, B. Schiele, & S. Shi (Eds.), *Communicating Science in Social Contexts: New models, new practices* (pp. 201–226). Springer Netherlands.

Calpine. (n.d.). *Seismic Monitoring Advisory Committee(SMAC)*. The Geysers. Retrieved June 28, 2023, from https://geysers.com/smac

CEC (California Energy Commission), (2022). *Lithium Valley Fact Sheet*. https://www.energy.ca.gov/filebrowser/download/4041

Cheney, A. M., Ortiz, G., Trinidad, A., Rodriguez, S., Moran, A., Gonzalez, A., Chavez, J., & Pozar, M. (2023). Latinx and Indigenous Mexican Caregivers' Perspectives of the Salton Sea Environment on Children's Asthma, Respiratory Health, and Co-Presenting Health Conditions. *International Journal of Environmental Research and Public Health*, *20*(11). https://doi.org/10.3390/ijerph20116023

Collins, S. E., Clifasefi, S. L., Stanton, J., The Leap Advisory Board, Straits, K. J. E., Gil-Kashiwabara, E., Rodriguez Espinosa, P., Nicasio, A. V., Andrasik, M. P., Hawes, S. M., Miller, K. A., Nelson, L. A., Orfaly, V. E., Duran, B. M., & Wallerstein, N. (2018). Community-based participatory research (CBPR): Towards equitable involvement of community in psychology research. *The American Psychologist*, *73*(7), 884–898.

Elmallah, S., Reames, T. G., & Spurlock, C. A. (2022). Frontlining energy justice: Visioning principles for energy transitions from community-based organizations in the United States. *Energy Research & Social Science*, *94*, 102855.

Hacker, K. (2013). *Community-Based Participatory Research*. SAGE Publications.

Harvard Catalyst. (n.d.). *Translation Guidelines for Equity in Research*. Harvard Catalyst Community Engagement Program. Retrieved June 28, 2023, from https://catalyst.harvard.edu/community-engagement/translation-guidelines-for-equity-in-research/

Illingworth, S. (2017). Delivering effective science communication: advice from a professional science communicator. *Seminars in Cell & Developmental Biology*, *70*, 10–16.

Johnston, J. E., Razafy, M., Lugo, H., Olmedo, L., & Farzan, S. F. (2019). The disappearing Salton Sea: A critical reflection on the emerging environmental threat of disappearing saline lakes and potential impacts on children's health. *The Science of the Total Environment*, *663*, 804–817.

Key, K. D., Furr-Holden, D., Lewis, E. Y., Cunningham, R., Zimmerman, M. A., Johnson-Lawrence, V., & Selig, S. (2019). The Continuum of Community Engagement in Research: A Roadmap for Understanding and Assessing Progress. *Progress in Community Health Partnerships: Research, Education, and Action*, *13*(4), 427–434.

Larkin, A. (2023, April 20). *2023 Aspen Prize for Community College Excellence Awarded to Amarillo College & Imperial Valley College*. The Aspen Institute. https://www.aspeninstitute.org/news/2023-aspen-prize-amarillo-college-imperial-valley-college/

Madrigal, D., Claustro, M., Wong, M., Bejarano, E., Olmedo, L., & English, P. (2020). Developing Youth Environmental Health Literacy and Civic Leadership through Community Air Monitoring in Imperial County, California. *International Journal of Environmental Research and Public Health*, *17*(5). https://doi.org/10.3390/ijerph17051537

Mancini, L., & Sala, S. (2018). Social impact assessment in the mining sector: Review and comparison of indicators frameworks. *Resources Policy*, *57*, 98–111.

McCauley, D., & Heffron, R. (2018). Just transition: Integrating climate, energy and environmental justice. *Energy Policy*, *119*, 1–7.

McKibben, M. A., Elders, W. A., & Raju, A. S. K. (2020). Lithium and other geothermal mineral and energy resources beneath the Salton Sea. *Crisis at the Salton Sea: Research Gaps and Opportunities, Salton Sea Task Force, The EDGE Institute, UC Riverside*, 107–122.

Muhammad, M., Wallerstein, N., Sussman, A. L., Avila, M., Belone, L., & Duran, B. (2015). Reflections on Researcher Identity and Power: The Impact of Positionality on Community Based Participatory Research (CBPR) Processes and Outcomes. *Critical Sociology*, *41*(7–8), 1045–1063.

Newman, S. D., Andrews, J. O., Magwood, G. S., Jenkins, C., Cox, M. J., & Williamson, D. C. (2011). Community advisory boards in community-based participatory research: a synthesis of best processes. *Preventing Chronic Disease*, *8*(3), A70.

Schulz, A. J., Israel, B. A., & Lantz, P. (2003). Instrument for evaluating dimensions of group dynamics within community-based participatory research partnerships. *Evaluation and Program Planning*, *26*(3), 249–262.

Slattery, M., Kendall, A., Helal, N., & Whittaker, M. L. (2023). What do frontline communities want to know about lithium extraction? Identifying research areas to support environmental justice in Lithium Valley, California. *Energy Research & Social Science*, *99*, 103043.

Spicer, S. (2017). The nuts and bolts of evaluating science communication activities. *Seminars in Cell & Developmental Biology*, *70*, 17–25.

SQM monitor en línea. (n.d.). Retrieved June 28, 2023, from https://www.sqmsenlinea.com/

Viswanathan, M., Ammerman, A., Eng, E., Garlehner, G., Lohr, K. N., Griffith, D., Rhodes, S., Samuel-Hodge, C., Maty, S., Lux, L., Webb, L., Sutton, S. F., Swinson, T., Jackman, A., & Whitener, L. (2004). Community-based participatory research: Assessing the evidence: Summary. In *AHRQ Evidence Report Summaries*. Agency for Healthcare Research and Quality.

What are ArcGIS StoryMaps? (2019, June 10). Esri. https://storymaps.arcgis.com/stories/9a500acb526f4be8b0a3c66ffa8e53fa

Williams, A., September, & Pierce, G. (2022). Lithium Extraction Policy in the Salton Sea and Thacker Pass: A Critical Analysis of Emerging Regulatory and Multi-Sectoral Complexities. The Nature Conservancy. https://innovation.luskin.ucla.edu/wp-content/uploads/2022/09/Lithium-Extraction-Policy-in-the-Salton-Sea-and-Thacker-Pass.pdf

Related References

Ambrose, H., and Kendall, A., 2020, Understanding the future of lithium: Part 1, resource model: Journal of Industrial Ecology, v. 24, no. 1, p. 80–89.

Chordia, M., Wickerts, S., Nordelöf, A., and Arvidsson, R., 2022, Life cycle environmental impacts of current and future battery-grade lithium supply from brine and spodumene: Resources, Conservation and Recycling, v. 187, p. 106634.

Dobson, P., McKibben, M. A., 2023, Salton Sea Li Brine Resource Estimate Information. This Report.

Kumar, S., Dumas, P., and Garabetian, T., 2022, Geothermal lithium: Unlocking the door to climate-proofed industrial and energy strategies: European Geothermal Congress 2022, Berlin, Germany, 17-21 October.

Liu, W., and Agusdinata, D.B., 2020, Interdependencies of lithium mining and communities sustainability in Salar de Atacama, Chile: Journal of Cleaner Production, v. 260, p. 120838**.**

Olivetti, E.A., Ceder, G., Gaustad, G.G., and Fu, X., 2017, Lithium-Ion Battery Supply Chain Considerations: Analysis of Potential Bottlenecks in Critical Metals: Joule, v. 1, no. 2, p. 229–243.

Oskin, M., and Stock, J., 2003, Pacific–North America plate motion and opening of the Upper Delfín basin, northern Gulf of California, Mexico: Geological Society of America Bulletin, v. 115, no. 10, p. 1173–1190.

Sonnenthal, E., Spycher, N., Araya, N., Dobson, P., O'Sullivan, P., McKibben, M. A., Humphreys, J., and Brounce, M., 2023, Constraints on Lithium Evolution and Reservoir Sustainability in the Salton Sea Geothermal Field from Reactive-Transport Modeling, this report

Sun, X., Hao, H., Zhao, F., and Liu, Z., 2017, Tracing global lithium flow: A trade-linked material flow analysis: Resources, Conservation and Recycling, v. 124, p. 50–61.

USGS, 2022, U.S. Geological Survey releases 2022 list of critical minerals.: https://www.usgs.gov/news/national-news-release/us-geological-survey-releases-2022-list-critical-minerals, accessed at https://www.usgs.gov/news/national-news-release/us-geological-survey-releases-2022-list-critical-minerals.

USGS (United States Geological Survey), (2022). 2022 Final List of Critical Minerals. Federal Register, Vol. 87, No. 37, Thursday, February 24. Department of the Interior.

Dorsey, R.J., Fluette, A., McDougall, K., Housen, B.A., Janecke, S.U., Axen, G.J., and Shirvell, C.R., 2007, Chronology of Miocene–Pliocene deposits at Split Mountain Gorge, Southern California: A record of regional tectonics and Colorado River evolution: Geology, v. 35, no. 1, p. 57.

McKibben, M.A., Andes, J.P., and Williams, A.E., 1988b, Active ore formation at a brine interface in metamorphosed deltaic lacustrine sediments; the Salton Sea geothermal system, California: Economic Geology, v. 83, no. 3, p. 511–523.

CalGEM. "GeoSteam: Geothermal Well Records, Production and Injection Data [Data Files]." (2022). https://geosteam.conservation.ca.gov/

CDC (California Department of Conservation). "Geothermal Production and Injection Data [Salton Sea]." (2022). https://www.conservation.ca.gov/calgem/geothermal/manual

Meidav, T., West, R., Katzenstein, A., and Rostein, Y. "An Electrical Resistivity Survey of the Salton Sea Geothermal Field, Imperial Valley California." *Lawrence Livermore Laboratory*, UCRL-13690, (1976).

McKibben, M.A., Williams, A.E., Elders, W.A., and Eldridge, C.S. "Saline brines and Metallogenesis in a Modern Sediment-filled Rift: the Salton Sea Geothermal system, California, U.S.A." *Applied Geochemistry*, 2, (1987), 563-578.

California RWQCB Colorado River Basin Region. (2013b). *Waste discharge requirements for Hudson Ranch power I LLC (Order R7-2013-0059)* (ORDER R7-2013-0059). California Regional Water Quality Control Board (RWQCB) Colorado River Basin Region.

Schulz, K. J., DeYoung, J. H., Seal, R. R., & Bradley, D. C. (2018). *Critical Mineral Resources of the United States: Economic and Environmental Geology and Prospects for Future Supply*. Geological Survey. https://doi.org/https://doi.org/10.3133/pp1802K

Benson, T.R., Coble, M.A., Rytuba, J.J., Mahood, G.A., 2017. Lithium enrichment in intracontinental rhyolite magmas leads to Li deposits in caldera basins. Nat. Commun. 8, 1–9. https://doi.org/10.1038/s41467-017-00234-y

Babcock, E.A., 1974, Geology of the Northeast Margin of the Salton Trough, Salton Sea, California: Geological Society of America Bulletin, v. 85, no. 3, p. 321–332.

Brothers, D.S., Driscoll, N.W., Kent, G.M., Baskin, R.L., Harding, A.J., and Kell, A.M., 2022, Seismostratigraphic analysis of Lake Cahuilla sedimentation cycles and fault displacement history beneath the Salton Sea, California, USA: Geosphere, v. 18, no. 4, p. 1354–1376.

Chan, L.-H., Alt, J.C., and Teagle, D.A.H., 2002, Lithium and lithium isotope profiles through the upper oceanic crust: a study of seawater-basalt exchange at ODP Sites 504B and 896A: Earth and Planetary Science Letters, v. 201, no. 1, 187–201.

Chan, L.-H., Gieskes, J.M., Chen-Feng, Y., and Edmond, J.M., 1994, Lithium isotope geochemistry of sediments and hydrothermal fluids of the Guaymas Basin, Gulf of California: Geochimica et Cosmochimica Acta, v. 58, no. 20, p. 4443–4454.

Charles, R.W., Janecky, D.R., Goff, F., and McKibben, M.A., 1988, Chemographic and Thermodynamic Analysis of the Paragenesis of the Major Phases in the Vicinity of the 6120-Foot (1866 m) Flow Zone, California State Well 2-14: Journal of Geophysical Research: Solid Earth, v. 93, no. B11, p. 13145–13157.

Cho, M., Liou, J.G., and Bird, D.K., 1988, Prograde Phase Relations in the State 2-14 Well Metasandstones, Salton Sea Geothermal Field, California: Journal of Geophysical Research: Solid Earth, v. 93, no. B11, p. 13081–13103.

Coffey, D.M., Munk, L.A., Ibarra, D.E., Butler, K.L., Boutt, D.F., and Jenckes, J., 2021, Lithium Storage and Release From Lacustrine Sediments: Implications for Lithium Enrichment and Sustainability in Continental Brines: Geochemistry, Geophysics, Geosystems, v. 22, no. 12.

Coplen, T., 1976, Cooperative geochemical resource assessment of the Mesa Geothermal system: Final Report Univ. California Riverside, IGPP-UCR-76-1, 97 p.

Coplen, T.B., 2002, Compilation of Minimum and Maximum Isotope Ratios of Selected Elements in Naturally Occurring Terrestrial Materials and Reagents: U.S. Geological Survey Water- Resources Investigations Report 01-4222.

Dellinger, M., Gaillardet, J., Bouchez, J., Calmels, D., Louvat, P., Dosseto, A., Gorge, C., Alanoca, L., and Maurice, L., 2015, Riverine Li isotope fractionation in the Amazon River basin controlled by the weathering regimes: Geochimica et Cosmochimica Acta, v. 164, p. 71–93.

Desaulty, A.-M., Monfort Climent, D., Lefebvre, G., Cristiano-Tassi, A., Peralta, D., Perret, S., Urban, A., and Guerrot, C., 2022, Tracing the origin of lithium in Li-ion batteries using lithium isotopes: Nature Communications, v. 13, no. 1, p. 4172.

Dorsey, R.J., Fluette, A., McDougall, K., Housen, B.A., Janecke, S.U., Axen, G.J., and Shirvell, C.R., 2007, Chronology of Miocene–Pliocene deposits at Split Mountain Gorge, Southern California: A record of regional tectonics and Colorado River evolution: Geology, v. 35, no. 1, p. 57.

Dyar, M., Guidotti, C., Harper, G., McKibben, M., and Saccocia, P., 1992, Controls on ferric iron in chlorite: Geological Society of America, Abstracts with Programs, v. 24, A130.

Elders, W.A., and Sass, J.H., 1988, The Salton Sea Scientific Drilling Project: Journal of Geophysical Research: Solid Earth, v. 93, no. B11, p. 12953–12968.

Elders, W.A., Rex, R.W., Robinson, P.T., Biehler, S., and Meidav, T., 1972, Crustal Spreading in Southern California: The Imperial Valley and the Gulf of California formed by the rifting apart of a continental plate.: Science, v. 178, no. 4056, p. 15–24.

Elliott, T., Thomas, A., Jeffcoate, A., and Niu, Y., 2006, Lithium isotope evidence for subduction-enriched mantle in the source of mid-ocean-ridge basalts: Nature, v. 443, no. 7111, p. 565–568.

Ellis, B.S., Szymanowski, D., Harris, C., Tollan, P.M.E., Neukampf, J., Guillong, M., Cortes-Calderon, E.A., and Bachmann, O., 2022, Evaluating the Potential of Rhyolitic Glass as a Lithium Source for Brine Deposits: Economic Geology, v. 117, no. 1, p. 91–105.

Fan, J.-J., Tang, G.-J., Wei, G.-J., Wang, H., Xu, Y.-G., Wang, Q., Zhou, J.-S., Zhang, Z.-Y., Huang, T.-Y., and Wang, Z.-L., 2020, Lithium isotope fractionation during fluid exsolution: Implications for Li mineralization of the Bailongshan pegmatites in the West Kunlun, NW Tibet: Lithos, v. 352–353, p. 105236.

Garcia, M.G., Borda, L.G., Godfrey, L.V., López Steinmetz, R.L., and Losada-Calderon, A., 2020, Characterization of lithium cycling in the Salar De Olaroz, Central Andes, using a geochemical and isotopic approach: Chemical Geology, v. 531, p. 119340.

Godfrey, L., and Álvarez-Amado, F., 2020, Volcanic and Saline Lithium Inputs to the Salar de Atacama: Minerals, v. 10, no. 2, p. 201.

Godfrey, L.V., Chan, L.-H., Alonso, R.N., Lowenstein, T.K., McDonough, W.F., Houston, J., Li, J., Bobst, A., and Jordan, T.E., 2013, The role of climate in the accumulation of lithium-rich brine in the Central Andes: Applied Geochemistry, v. 38, p. 92–102.

Han, L., Hole, J.A., Stock, J.M., Fuis, G.S., Williams, C.F., Delph, J.R., Davenport, K.K., and Livers, A.J., 2016, Seismic imaging of the metamorphism of young sediment into new crystalline crust in the actively rifting Imperial Valley, California: Geochemistry, Geophysics, Geosystems, v. 17, no. 11, p. 4566–4584.

He, M.-Y., Luo, C.-G., Yang, H.-J., Kong, F.-C., Li, Y.-L., Deng, L., Zhang, X.-Y., and Yang, K.-Y., 2020, Sources and a proposal for comprehensive exploitation of lithium brine deposits in the Qaidam Basin on the northern Tibetan Plateau, China: Evidence from Li isotopes: Ore Geology Reviews, v. 117, p. 103277.

Helgeson, H.C., 1968, Geologic and thermodynamic characteristics of the Salton Sea geothermal system: American Journal of Science, v. 266, p. 129–166.

Herzig, C.T., and Elders, W.A., 1988, Nature and Significance of Igneous Rocks Cored in the State 2-14 Research Borehole: Salton Sea Scientific Drilling Project, California: Journal of Geophysical Research: Solid Earth, v. 93, no. B11, p. 13069–13080.

Herzig, C.T., and Jacobs, D.C., 1994, Cenozoic volcanism and two-stage extension in the Salton trough, southern California and northern Baja California: Geology, v. 22, no. 11, p. 991.

Herzig, C.T., Mehegan, J.M., and Stelting, C.E., 1988, Lithostratigraphy of the State 2-14 Borehole: Salton Sea Scientific Drilling Project: Journal of Geophysical Research: Solid Earth, v. 93, no. B11, p. 12969–12980.

Huh, Y., Chan, L.-H., Zhang, L., and Edmond, J.M., 1998, Lithium and its isotopes in major world rivers: implications for weathering and the oceanic budget: Geochimica et Cosmochimica Acta, v. 62, no. 12, p. 2039–2051.

Huh, Y., Chan, L.-H., and Edmond, J.M., 2001, Lithium isotopes as a probe of weathering processes: Orinoco River: Earth and Planetary Science Letters, v. 194, nos. 1–2, p. 189–199.

Humphreys, J, Brounce, M., McKibben, M. A., Dobson, P., Planavsky, N., & Kalderon-Asael, B., 2023, SS-GF Mineral Major Elements and Li Concentration. United States. https://gdr.openei.org/submissions/1515

Jochum, K.P., Dingwell, D.B., Rocholl, A., Stoll, B., Hofmann, A.W., Becker, S., Besmehn, A., Bessette, D., Dietze, H.-J., Dulski, P., Erzinger, J., Hellebrand, E., Hoppe, P., Horn, I., et al., 2000, The Preparation and Preliminary Characterisation of Eight Geological MPI-DING Reference Glasses for In-Situ Microanalysis: Geostandards and Geoanalytical Research, v. 24, no. 1, p. 87–133.

Kelley, K.A., Plank, T., Ludden, J., and Staudigel, H., 2003, Composition of altered oceanic crust at ODP Sites 801 and 1149: Geochemistry, Geophysics, Geosystems, v. 4, no. 6, 8910.

Kelly, J.C., Wang, M., Dai, Q., and Winjobi, O., 2021, Energy, greenhouse gas, and water life cycle analysis of lithium carbonate and lithium hydroxide monohydrate from brine and ore resources and their use in lithium ion battery cathodes and lithium ion batteries: Resources, Conservation and Recycling, v. 174, p. 105762.

Kısakűrek, B., James, R.H., and Harris, N.B.W., 2005, Li and δ7Li in Himalayan rivers: Proxies for silicate weathering? Earth and Planetary Science Letters, v. 237, nos. 3–4, p. 387–401.

Lemarchand, E., Chabaux, F., Vigier, N., Millot, R., and Pierret, M.-C., 2010, Lithium isotope systematics in a forested granitic catchment (Strengbach, Vosges Mountains, France): Geochimica et Cosmochimica Acta, v. 74, no. 16, p. 4612–4628.

Liu, X.-M., Wanner, C., Rudnick, R.L., and McDonough, W.F., 2015, Processes controlling δ7Li in rivers illuminated by study of streams and groundwaters draining basalts: Earth and Planetary Science Letters, v. 409, p. 212–224.

Lonsdale, P., 1989, Geology and tectonic history of the Gulf of California, in Winterer, E.L., Hussong, D.M., and Decker, R.W. eds., The Eastern Pacific Ocean and Hawaii: The Geology of North America, v. N, Geological Society of America, p. 499–521.

Lynton, S.J., Walker, R.J., and Candela, P.A., 2005, Lithium isotopes in the system Qz-Ms-fluid:An experimental study: Geochimica et Cosmochimica Acta, v. 69, no. 13, p. 3337–3347.

MacDougal, D.T., 1914, The Salton Sea: A Study of the Geography, the Geology, the Floristics, and the Ecology of a Desert Basin: Carnegie Institution of Washington.

Magenheim, A.J., Spivack, A.J., Alt, J.C., Bayhurst, G., Chan, L.-H., Zuleger, E., and Gieskes, J.M., 1995, 13. Borehole fluid chemistry in hole 504B, LEG 137: formation water or in-situ reaction? Proceedings of the Ocean Drilling Program, Ocean Drilling Program.

Magna, T., Novák, M., Cempírek, J., Janoušek, V., Ullmann, C.V., and Wiechert, U., 2016, Crystallographic control on lithium isotope fractionation in Archean to Cenozoic lithium-cesium-tantalum pegmatites: Geology, v. 44, no. 8, p. 655–658.

Maimoni, A., 1982, Minerals recovery from Salton Sea geothermal brines: a literature review and proposed cementation process: Geothermics, v. 11, no. 4, p. 239–258.

Marschall, H.R., and Tang, M., 2020, High-temperature processes: Is it time for lithium isotopes?: Elements, v. 16, p. 247–252.

McDowell, S.D., and Elders, W.A., 1980, Authigenic layer silicate minerals in borehole Elmore 1, Salton Sea Geothermal Field, California, USA: Contributions to Mineralogy and Petrology, v. 74, no. 3, p. 293–310.

McKibben, M., and Hardie, L., 1997, Ore-forming brines in active continental rifts: Geochemistry of hydrothermal ore deposits, v. 3, p. 877–935.

McKibben, M.A., and Elders, W.A., 1985, Fe-Zn-Cu-Pb mineralization in the Salton Sea geothermal system, Imperial Valley, California: Economic Geology, v. 80, no. 3, p. 539–559.

McKibben, M.A., Williams, A.E., and Okubo, S., 1988a, Metamorphosed Plio-Pleistocene evaporites and the origins of hypersaline brines in the Salton Sea geothermal system, California: Fluid inclusion evidence: Geochimica et Cosmochimica Acta, v. 52, no. 5, p. 1047–1056.

McKibben, M.A., Andes, J.P., and Williams, A.E., 1988b, Active ore formation at a brine interface in metamorphosed deltaic lacustrine sediments; the Salton Sea geothermal system, California: Economic Geology, v. 83, no. 3, p. 511–523.

Millot, R., Guerrot, C., and Vigier, N., 2004, Accurate and High-Precision Measurement of Lithium Isotopes in Two Reference Materials by MC-ICP-MS: Geostandards and Geoanalytical Research, v. 28, no. 1, p. 153–159.

Millot, R., Scaillet, B., and Sanjuan, B., 2010, Lithium isotopes in island arc geothermal systems: Guadeloupe, Martinique (French West Indies) and experimental approach: Geochimica et Cosmochimica Acta, v. 74, no. 6, p. 1852–1871.

Moriguti, T., and Nakamura, E., 1998, Across-arc variation of Li isotopes in lavas and implications for crust/mantle recycling at subduction zones: Earth and Planetary Science Letters, v. 163, nos. 1–4, p. 167–174.

Muffler, L.P., and White, D.E., 1969, Active metamorphism of upper Cenozoic sediments in the Salton Sea geothermal field and the Salton Trough, southeastern California: Geological Society of America Bulletin, v. 80, no. 2, p. 157–181.

Munk, L., Jochens, H., Jennings, M., Bradley, D., Hynek, S., and Godfrey, L., 2011, Geochemistry of lithium-rich brines in Clayton Valley, Nevada, USA: Biennial Meeting of SGA, Antofagasta, Chile.

Munk, L.A., Boutt, D.F., Hynek, S.A., and Moran, B.J., 2018, Hydrogeochemical fluxes and processes contributing to the formation of lithium-enriched brines in a hyper-arid continental basin: Chemical Geology, v. 493, p. 37–57.

Nishio, Y., Nakai, S., Ishii, T., and Sano, Y., 2007, Isotope systematics of Li, Sr, Nd, and volatiles in Indian Ocean MORBs of the Rodrigues Triple Junction: Constraints on the origin of the DUPAL anomaly: Geochimica et Cosmochimica Acta, v. 71, no. 3, p. 745–759.

Pearce, N.J.G., Perkins, W.T., Westgate, J.A., Gorton, M.P., Jackson, S.E., Neal, C.R., and Chenery, S.P., 1997, A Compilation of New and Published Major and Trace Element Data for NIST SRM 610 and NIST SRM 612 Glass Reference Materials: Geostandards and Geoanalytical Research, v. 21, no. 1, p. 115–144.

Penniston-Dorland, S., Liu, X.-M., and Rudnick, R.L., 2017, Lithium Isotope Geochemistry: Reviews in Mineralogy and Geochemistry, v. 82, no. 1, p. 165–217.

Philibosian, B., Fumal, T., and Weldon, R., 2011, San Andreas Fault Earthquake Chronology and Lake Cahuilla History at Coachella, California: Bulletin of the Seismological Society of America, v. 101, no. 1, p. 13–38.

Plank, T., 2014, The Chemical Composition of Subducting Sediments, in Treatise on Geochemistry: Elsevier, p. 607–629.

Pogge Von Strandmann, P.A.E., and Henderson, G.M., 2015, The Li isotope response to mountain uplift: Geology, v. 43, no. 1, p. 67–70.

Pogge Von Strandmann, P.A.E., Burton, K.W., James, R.H., Van Calsteren, P., Gíslason, S.R., and Mokadem, F., 2006, Riverine behaviour of uranium and lithium isotopes in an actively glaciated basaltic terrain: Earth and Planetary Science Letters, v. 251, nos. 1–2, p. 134–147.

Pogge Von Strandmann, P.A.E., Burton, K.W., James, R.H., Van Calsteren, P., and Gislason, S.R., 2010, Assessing the role of climate on uranium and lithium isotope behaviour in rivers draining a basaltic terrain: Chemical Geology, v. 270, nos. 1–4, p. 227–239.

Pogge Von Strandmann, P.A.E., Kasemann, S.A., and Wimpenny, J.B., 2020, Lithium and lithium isotopes in Earth's surface cycles: Elements, v. 16, no. 4, p. 253–258.

Rex, R., 1983, The origin of the brines of the Imperial Valley, California: Trans. Geotherm. Resour. Counc, v. 7, p. 321–324.

Robinson, P.T., Elders, W.A., and Muffler, L.J.P., 1976, Quaternary volcanism in the Salton Sea geothermal field, Imperial Valley, California: Geological Society of America Bulletin, v. 87, no. 3, p. 347.

Rockwell, T.K., Meltzner, A.J., Haaker, E.C., and Madugo, D., 2022, The late Holocene history of Lake Cahuilla: Two thousand years of repeated fillings within the Salton Trough, Imperial Valley, California: Quaternary Science Reviews, v. 282, p. 107456.

Sanjuan, B., Millot, R., Ásmundsson, R., Brach, M., and Giroud, N., 2014, Use of two new Na/Li geothermometric relationships for geothermal fluids in volcanic environments: Chemical Geology, v. 389, p. 60–81.

Sanjuan, B., Millot, R., Innocent, Ch., Dezayes, Ch., Scheiber, J., and Brach, M., 2016, Major geochemical characteristics of geothermal brines from the Upper Rhine Graben granitic basement with constraints on temperature and circulation: Chemical Geology, v. 428, p. 27–47.

Sanjuan, B., Gourcerol, B., Millot, R., Rettenmaier, D., Jeandel, E., and Rombaut, A., 2022, Lithium-rich geothermal brines in Europe: An up-date about geochemical characteristics and implications for potential Li resources: Geothermics, v. 101, p. 102385.

Sass, J.H., Priest, S.S., Duda, L.E., Carson, C.C., Hendricks, J.D., and Robison, L.C., 1988, Thermal Regime of the State 2-14 Well, Salton Sea Scientific Drilling Project: Journal of Geophysical Research: Solid Earth, v. 93, no. B11, p. 12995–13004.

Sauzéat, L., Rudnick, R.L., Chauvel, C., Garçon, M., and Tang, M., 2015, New perspectives on the Li isotopic composition of the upper continental crust and its weathering signature: Earth and Planetary Science Letters, v. 428, p. 181–192.

Schauble, E.A., 2004, Applying stable isotope fractionation theory to new systems. Reviews in Mineralogy and Geochemistry, v. 55, p. 65−111

Schmitt, A.K., and Hulen, J.B., 2008, Buried rhyolites within the active, high-temperature Salton Sea geothermal system: Journal of Volcanology and Geothermal Research, v. 178, no. 4, p. 708–718.

Schmitt, A.K., Perrine, A.R., Rhodes, E.J., and Fischer, C., 2019, Age of Obsidian Butte in Imperial County, California, Through Infrared Stimulated Luminescence Dating of Potassium Feldspar from Tuffaceous Sediment: California Archaeology, v. 11, no. 1, p. 5–20.

Skinner, B.J., White, D.E., Rose, H.J., and Mays, R.E., 1967, Sulfides associated with the Salton Sea geothermal brine: Economic Geology, v. 62, no. 3, p. 316–330.

Stock, J., and Hodges, K., 1989, Pre-Pliocene extension around the Gulf of California and the transfer of Baja California to the Pacific plate: Tectonics, v. 8, no. 1, p. 99–115.

Sturz, A., 1989, Low-temperature hydrothermal alteration in near-surface sediments, Salton Sea Geothermal Area: Journal of Geophysical Research: Solid Earth, v. 94, no. B4, p. 4015–4024.

Teng, F.-Z., McDonough, W.F., Rudnick, R.L., Dalpé, C., Tomascak, P.B., Chappell, B.W., and Gao, S., 2004, Lithium isotopic composition and concentration of the upper continental crust: Geochimica et Cosmochimica Acta, v. 68, no. 20, p. 4167–4178.

Tomascak, P.B., Hemming, N.G., and Hemming, S.R., 2003, The lithium isotopic composition of waters of the Mono Basin, California: Geochimica et Cosmochimica Acta, v. 67, no. 4, p. 601–611.

Tomascak, P.B., Langmuir, C.H., Le Roux, P.J., and Shirey, S.B., 2008, Lithium isotopes in global mid-ocean ridge basalts: Geochimica et Cosmochimica Acta, v. 72, no. 6, p. 1626–1637.

Tompson, A.F.B., 2016, Born from a flood: The Salton Sea and its story of survival: Journal of Earth Science, v. 27, no. 1, p. 89–97.

Van De Kamp, P.C., 1973, Holocene Continental Sedimentation in the Salton Basin, California: A Reconnaissance: Geological Society of America Bulletin, v. 84, no. 3, p. 827.

Vigier, N., Gislason, S.R., Burton, K.W., Millot, R., and Mokadem, F., 2009, The relationship between riverine lithium isotope composition and silicate weathering rates in Iceland: Earth and Planetary Science Letters, v. 287, nos. 3–4, p. 434–441.

Waters, M.R., 1983, Late Holocene Lacustrine Chronology and Archaeology of Ancient Lake Cahuilla, California: Quaternary Research, v. 19, no. 03, p. 373–387.

Wilke, P.J., 1976, Late Prehistoric Human Ecology at Lake Cahuilla, Coachella Valley, California: University of California, Riverside.

Williams, A.E., and McKibben, M.A., 1989, A brine interface in the Salton Sea Geothermal System, California: Fluid geochemical and isotopic characteristics: Geochimica et Cosmochimica Acta, v. 53, no. 8, p. 1905–1920.

Williams, A.E., 1997, Fluid density distribution in a high temperature, stratified thermohaline system: implications for saline hydrothermal circulationEarth and Planetary Science Letters 146, 12, 1- 136.

Winker, C.D., and Kidwell, S.M., 1986, Paleocurrent evidence for lateral displacement of the Pliocene Colorado River delta by the San Andreas fault system, southeastern California: Geology, v. 14, no. 9, p. 788–791.

Wright, H.M., Vazquez, J.A., Champion, D.E., Calvert, A.T., Mangan, M.T., Stelten, M., Cooper, K.M., Herzig, C., and Schriener, A., 2015, Episodic Holocene eruption of the Salton Buttes rhyolites, California, from paleomagnetic, U-Th, and Ar/Ar dating: Salton Buttes rhyolites: Geochemistry, Geophysics, Geosystems, v. 16, no. 4, p. 1198–1210.

Wunder, B., Meixner, A., Romer, R.L., Feenstra, A., Schettler, G., and Heinrich, W., 2007, Lithium isotope fractionation between Li-bearing staurolite, Li-mica and aqueous fluids: An experimental study: Chemical Geology, v. 238, nos. 3–4, p. 277–290.

Li, H.C., You, C.F., Ku, T.L., Xu, X.M., Buchheim, H.P., Wan, N.J., Wang, R.M., Shen, M.L., 2008. Isotopic and geochemical evidence of palaeoclimate changes in Salton Basin, California, during the past 20 kyr: 2. 87Sr/86Sr ratio in lake tufa as an indicator of connection between Colorado River and Salton Basin. Palaeogeogr. Palaeoclimatol. Palaeoecol. 259, 198–212. https://doi.org/10.1016/j.palaeo.2007.10.007

Takahashi, N., Tsujimori, T., Chang, Q., Kimura, J.I., 2018. In-situ lithium isotope geochemistry for a veined jadeitite from the New Idria serpentinite body, California: Constraints on slab-derived fluid and fluid-rock interaction. Lithos 318–319, 376–385. https://doi.org/10.1016/j.lithos.2018.08.015

Teichert, Z., Bose, M., Williams, L.B., 2020. Lithium isotope compositions of U.S. coals and source rocks: Potential tracer of hydrocarbons. Chem. Geol. 549. https://doi.org/10.1016/j.chemgeo.2020.119694

Wimpenny, J., Colla, C.A., Yu, P., Yin, Q.Z., Rustad, J.R., Casey, W.H., 2015. Lithium isotope fractionation during uptake by gibbsite. Geochim. Cosmochim. Acta 168, 133–150. https://doi.org/10.1016/j.gca.2015.07.011

Xu, T., and K. Pruess, 1998. Coupled modeling of non-isothermal multiphase flow, solute transport and reactive chemistry in porous and fractured media: 1. Model development and validation, Lawrence Berkeley National Laboratory Report LBNL-42050, Berkeley, California, 38 pp.

Berthold, C. E., Hadzeriga, P., Christopher, D. H., Applegate, T. A., & Gillespie, D. M. (1975). *Process technology for recovering geothermal brine minerals (BuMines OFR 35-75)* (BuMines OFR 35-75).

Crane, C. H. (1982). Experience with minerals recovery from geothermal and other brines. *Geothermal Resources Council, TRANSACTIONS*, *6*.

Defense Logistics Agency. (2023). *DLA Strategic Materials: Materials of Interest*. U.S. Defense Logistics Agency. https://www.dla.mil/Strategic-Materials/Materials/

Gallup, D. L., & Barcelon, E. (2005). Investigations of organic inhibitors for silica scale control from geothermal brines–II. *Geothermics*, *34*(6), 756-771. https://doi.org/https://doi.org/10.1016/j.geothermics.2005.09.002

Gallup, D. L., & Reiff, W. M. (1991). Characterization of geothermal scale deposits by Fe-57 Mössbauer spectroscopy and complementary X-ray diffraction and infra-red studies. *Geothermics*, *20*, 207-224.

Geo-Logic Associates. (2022). Report of Geotechnical and Geosynthetic Construction Quality Assurance (CQA), Phase 2A Liner Construction, Salton City Solid Waste Site, Imperial County, California. https://documents.geotracker.waterboards.ca.gov/esi/uploads/geo_report/9271563529/L10005850536.PDF

Harrison, S. (2015). Selective removal of silica from silica containing brines US Patent 9,051,827).

Harrison, S., & Burba, J. (2015). Treated geothermal brine compositions with reduced concentrations of silica, iron and lithium US Patent Application 2015/0152309 A9).

Harrison, S., Sharma, C. V. K., & Conley, M. S. (2019). *Porous Activated Alumina Based Sorbent for Lithium Extraction* (USA Patent No. US Patent 10,328,424 B2). U.S.P. Office.

Kavanagh, L., Keohane, J., Cabellos, G. G., Lloyd, A., & Cleary, J. (2018). Global Lithium Sources-Industrial Use and Future in the Electric Vehicle Industry: A Review. *Resources-Basel*, *7*(3), Article 57. https://doi.org/10.3390/resources7030057

Manceau, A., Ildefonse, P., Hazemann, J. L., Flank, A. M., & Gallup, D. (1995). Crystal chemistry of hydrous iron silicate scale deposits at the Salton Sea Geothermal Field. *Clays and Clay Minerals*, *43*(3), 304-317. https://doi.org/10.1346/CCMN.1995.0430305

Mohr, S., Mudd, G., & Giurco, D. (2010). Lithium Resources and Production: a critical global assessment (Cluster Research Report No. 1.4) (Cluster Research Report No. 1.4).

Neupane, G., & Wendt, D. S. (2017). Potential economic values of minerals in brines of identified hydrothermal systems in the US. *Geothermal Resources Council TRANSACTIONS*, *41*(1), 1938-1956.

The National Institute for Occupational Safety and Health. (2011). *Hydrogen Sulfide*.

Wendt, D. S., Neupane, G., Davidson, C. L., Zheng, R., & Bearden, M. A. (2018). GeoVision Analysis Supporting Task Force Report: Geothermal Hybrid Systems, INL/EXT-17-42891, PNNL-27386. I. N. Laboratory.

Nakata, N., Gualtieri, L. & Fichtner, A. Seismic Ambient Noise 370 (Cambridge Univ. Press, 2019).

Taira, T., Nayak, A., Brenguier, F. & Manga, M. Monitoring reservoir response to earthquakes and fluid extraction, Salton Sea geothermal field, California. Science Advances 4, e1701536. http://advances.sciencemag.org/ (2018).

Back Cover Photo: Mud volcanoes and mudpots next to the Featherstone power plant at the edge of the Salton Sea. Photo credit: Michael McKibben/UC Riverside

BERKELEY LAB
Bringing Science Solutions to the World

U.S. DEPARTMENT OF ENERGY
Office of ENERGY EFFICIENCY & RENEWABLE ENERGY